WOODHEAD PUBLISHING IN MATERIALS

Nanotechnology in eco-efficient construction

Edited by F. Pacheco-Torgal, M. V. Diamanti, A. Nazari and C-G. Granqvist

WP
WOODHEAD PUBLISHING

Nanotechnology in eco-efficient construction

Related titles:

Eco-efficient concrete (ISBN 978-0-85709-424-7)
Understanding the tensile properties of concrete (ISBN 978-0-85709-045-4)
Handbook of recycled concrete and demolition waste (ISBN 978-0-85709-682-1)

Details of these books and a complete list of titles from Woodhead Publishing can be obtained by:

- visiting our web site at www.woodheadpublishing.com
- contacting Customer Services (e-mail: sales@woodheadpublishing.com; fax: +44 (0) 1223 832819; tel.: +44 (0) 1223 499140 ext. 130; address: Woodhead Publishing Limited, 80 High Street, Sawston, Cambridge CB22 3HJ, UK)
- in North America, contacting our US office (e-mail: usmarketing@woodhead-publishing.com; tel.: (215) 928 9112; address: Woodhead Publishing, 1518 Walnut Street, Suite 1100, Philadelphia, PA 19102-3406, USA

If you would like e-versions of our content, please visit our online platform: www.woodheadpublishingonline.com. Please recommend it to your librarian so that everyone in your institution can benefit from the wealth of content on the site.

We are always happy to receive suggestions for new books from potential editors. To enquire about contributing to our Materials series, please send your name, contact address and details of the topic/s you are interested in to francis.dodds@woodheadpublishing.com. We look forward to hearing from you.

The Woodhead team responsible for publishing this book:
Commissioning Editor: Francis Dodds
Publications Coordinator: Lucy Beg
Project Editor: Cathryn Freear
Editorial and Production Manager: Mary Campbell
Production Editor: Richard Fairclough
Cover Designer: Terry Callanan

Nanotechnology in eco-efficient construction

Edited by
F. Pacheco-Torgal, M. V. Diamanti, A. Nazari and C-G. Granqvist

Oxford Cambridge Philadelphia New Delhi

Published by Woodhead Publishing Limited,
80 High Street, Sawston, Cambridge CB22 3HJ, UK
www.woodheadpublishing.com
www.woodheadpublishingonline.com

Woodhead Publishing, 1518 Walnut Street, Suite 1100, Philadelphia,
PA 19102-3406, USA

Woodhead Publishing India Private Limited, G-2, Vardaan House,
7/28 Ansari Road, Daryaganj, New Delhi – 110002, India
www.woodheadpublishingindia.com

First published 2013, Woodhead Publishing Limited

British Library Cataloguing in Publication Data
A catalogue record for this book is available from the British Library.

Library of Congress Control Number: 2013931614

ISBN 978-0-85709-544-2 (print)
ISBN 978-0-85709-883-2 (online)

The publisher's policy is to use permanent paper from mills that operate a sustainable forestry policy, and which has been manufactured from pulp which is processed using acid-free and elemental chlorine-free practices. Furthermore, the publisher ensures that the text paper and cover board used have met acceptable environmental accreditation standards.

Typeset by Toppan Best-set Premedia Limited, Hong Kong
Printed by the UK by MPG Books Group

Contents

Contributor contact details

(* = main contact)

Editors

Dr Eng. F. Pacheco-Torgal
Sustainable Construction Group
C-TAC Research Centre
University of Minho
Campus de Azurem
4800-058 Guimarães
Portugal

E-mail: torgal@civil.uminho.pt

Maria Vittoria Diamanti
Politecnico di Milano
Department of Chemistry, Materials and Chemical Engineering 'Giulio Natta'
Via Mancinelli 7
20131 Milan
Italy

E-mail: mariavittoria.diamanti@polimi.it

A. Nazari
Islamic Azad University
Iran

Professor Claes G. Granqvist
Department of Engineering Sciences
The Ångström Laboratory
Uppsala University
P.O. Box 534
SE-75121 Uppsala
Sweden

E-mail: claes-goran.granqvist@angstrom.uu.se

Chapter 1

Dr Eng. F. Pacheco-Torgal
Sustainable Construction Group
C-TAC Research Centre
University of Minho
Campus de Azurem
4800-058 Guimarães
Portugal

E-mail: torgal@civil.uminho.pt

Chapter 2

Dr Georgios Constantinides
Research Unit for Nanostructured Material Systems
Department of Mechanical Engineering and Materials Science and Engineering
Cyprus University of Technology
Lemesos, 3041
Cyprus

E-mail: g.constantinides@cut.ac.cy

Chapter 3

Dr Eng. F. Pacheco-Torgal*
Sustainable Construction Group
C-TAC Research Centre
University of Minho
Campus de Azurem
4800-058 Guimarães
Portugal

E-mail: torgal@civil.uminho.pt

S. Miraldo
University of Aveiro
Portugal

Y. Ding
State Key Laboratory of Coastal and Offshore Engineering
Dalian University of Technology
Dalian
China

J. A. Labrincha
Ceramics and Glass Engineering Department
University of Aveiro and CICECO
Campus Universitário de Santiago
3810-193 Aveiro
Portugal

Chapter 4

Zhipei Chen and Yining Ding
Institute of Structure Engineering
Dalian University of Technology
Dalian 116024
China

E-mail: ynding@hotmail.com

Dr Eng. F. Pacheco-Torgal*
Sustainable Construction Group
C-TAC Research Centre
University of Minho
Campus de Azurem
4800-058 Guimarães
Portugal

E-mail: torgal@civil.uminho.pt

Yulin Zhang
Centre of Mathematics
University of Minho
4700-052
Portugal

Chapter 5

Xianming Shi*
Corrosion and Sustainable Infrastructure Laboratory
Western Transportation Institute
Montana State University
P.O. Box 174250
Bozeman, Montana, 59717-4250
USA

E-mail: xianming.shi@gmail.com

Zhenjian Xiao
Shenzhen Jinzhou Precision Technology Corporation
Longgang High-Tech Industry Park
Shenzhen 518116
China

E-mail: dearxiaozj@sina.com

Jianlin Wu
School of Civil Engineering and Architecture
Wuhan Polytechnic University
Wuhan 430023
China

E-mail: forestwjl@yahoo.com.cn

Chapter 6

Dr Saeed Ghaffarpour Jahromi
Department of Civil Engineering
Shahid Rajaee Teacher Training University
Tehran
Iran

E-mail: Saeed_ghf@srttu.edu

Chapter 7

Melissa Spitzmiller and Shaily Mahendra
Department of Civil & Environmental Engineering
University of California, Los Angeles (UCLA)

Dr Robert Damoiseaux*
California NanoSystems Institute
Molecular Screening Shared Resource
University of California, Los Angeles (UCLA)
570 Westwood Plaza
Los Angeles, CA 90095-7277
USA

E-mail: Rdamoiseaux@mednet.ucla.edu

Chapters 8 and 11

Professor Claes G. Granqvist
Department of Engineering Sciences
The Ångström Laboratory
Uppsala University
P.O. Box 534
SE-75121 Uppsala
Sweden

E-mail: claes-goran.granqvist@angstrom.uu.se

Chapter 9

Ruben Baetens
Building Physics Section
Department of Civil Engineering
Faculty of Engineering
KU Leuven
Kasteelpark Arenberg 40 bus 2447
BE-3000 Leuven
Belgium

E-mail: ruben.baetens@bwk.kuleuven.be

Chapter 10

Professor Eng. Cinzia Buratti* and Dr Eng. Elisa Moretti
Department of Industrial Engineering
University of Perugia
Via G. Duranti 67
06125 Perugia
Italy

E-mail: cburatti@unipg.it; elisa.moretti@unipg.it

Chapter 12

Dr Lisa Ann Lamont
Transmission and Distribution Division
Mott MacDonald Ltd
1 Atlantic Quay
Broomielaw
Glasgow G2 8JB
UK

E-mail: Lisa.Lamont@mottmac.com

Chapter 13

Maria Vittoria Diamanti* and MariaPia Pedeferri
Politecnico di Milano
Department of Chemistry, Materials and Chemical Engineering 'Giulio Natta'
Via Mancinelli 7
20131 Milan
Italy

E-mail: mariavittoria.diamanti@polimi.it

Chapter 14

Damian Synnott, Nicholas Nolan, Darragh Ryan, John Colreavy and Suresh C. Pillai*
Centre for Research in Engineering Surface Technology (CREST)
FOCAS Institute
Dublin Institute of Technology
Kevin Street
Camden Row
Dublin 8
Republic of Ireland

E-mail: suresh.pillai@dit.ie

Chapter 15

Carmen del Cacho*
Department of Analytical Chemistry
Faculty of Science
Palacky University in Olomouc
17, Iistopadu 12
CZ-77146 Olomouc
Czech Republic

E-mail: ccacho@quim.ucm.es

Otmar Geiss, Paolo Leva, Salvatore Tirendi and Josefa Barrero-Moreno
European Commission
Joint Research Centre
Institute for Health and Consumer Protection
Ispra (VA)
Italy

Chapter 16

Soumitra Kar* and Professor P. K. Tewari
Desalination Division
Bhabha Atomic Research Centre
Trombay, Mumbai – 400085
India

E-mail: soubiswa@barc.gov.in; soumitra.1stmay@gmail.com; pktewari@barc.gov.in

1

Introduction to nanotechnology in eco-efficient construction

F. PACHECO-TORGAL, University of Minho, Portugal

DOI: 10.1533/9780857098832.1

Abstract: This chapter provides a brief overview of some important aspects of nanotechnology starting with its earlier steps and how countries are trying to establish an advantageous position in this field. China deserves a special mention because it is already the second largest producer of nanotechnology papers after the United States. The need for nanotechnology in the construction sector is emphasized. An outline of the book is given.

Key words: nanotechnology, eco-efficient construction, UN Millennium Goal, concrete, energy efficiency.

1.1 Introduction

Nanotechnology is a hot topic in current research, defined by Drexler (1981) as the manufacture of products using dimensions and precision of between 0.1 and 100 nm (1 nm = 1×10^{-9} m). It should be noted, however, that two decades prior to Drexler's work, the physicist Richard Feynman made a speech entitled 'There's plenty of room at the bottom' at a 1959 meeting of the American Physical Society at Caltech; this is considered to be the beginning of the era of nanotechnology era (Feynman, 1960).

In 1981 an expert group appointed by the European Commission was not able to agree on a firm definition of nanotechnology, but did arrive at a working definition for nanoscience and nanotechnology (NST) as 'the manipulation, precision placement, measurement, modeling or manufacture of sub-100 nanometer scale matter' (Glänzel *et al.*, 2003). The rapid evolution of research in this area is demonstrated by the growth rate of papers published with the 'nano-' prefix in the title in the period between 1992 and 2001, which increased exponentially with a doubling time of 2 years (Glänzel *et al.*, 2003). Economic estimates regarding advances in nanotechnology are still more striking: it is predicted that products and services related to nanotechnology could reach several hundred billion euros by the end of the decade (NSF, 2001; Compañó and Hullmann, 2002).

Dozens of countries already have national strategies in place and have begun to implement national nanotechnology plans (Rieke and Bachmann, 2004; Soltani *et al.*, 2011). According to Arnall and Parr (2005), countries

are trying to establish an advantageous position 'so that when nanotech applications begin to have a significant impact in the world economy, countries are able to exploit these new opportunities to the full'. Europe has assigned 4.865 billion euros to 'Nanosciences, Nanotechnologies, Materials and New Production Technologies' as part of the 7th Framework Programme for the 2007–2013 period. In the United States, a dedicated nanotechnology act was signed into law, which set aside 3.679 billion dollars of funding for the 2005–2008 period (Salerno *et al.*, 2008). China has identified nanotechnology as a priority area in its national agenda of science and technology development, and has increased R&D investment in the field. China has consequently emerged as one of the key global players in nanotechnology, producing the second largest number of nanotechnology papers after the United States (Wang and Guan, 2010, 2012).

Of course, nanotechnology is not entirely risk-free, with issues already raised with regard to the potential toxicity of nanoparticles and a new problem of the disposal of nanowastes (Bystrzejewska-Piotrowska *et al.*, 2009; Tyshenko, 2010). Despite these risks, however, Arnall and Parr (2005) quote Mihail Roco, the senior advisor for nanotechnology to the NSF, who stated that 'early payoffs will come in electronics and IT, and medicine and health'. Malanowski and Zweck (2007) also report that although almost all fields of industry are expected to be affected by nanotechnology by 2015, the areas most affected will be 'chemistry, life sciences and electronics'.

1.2 The need for nanotechnology in the construction sector

Very few nanotech applications are currently used in the construction sector, which in fact seems to have been somewhat neglected by nanotech research to date. A search for the terms 'nanotechnology' and 'eco-efficient construction' in journals listed in Scopus revealed only five papers, all related to cement and concrete. Of course, many more papers examining the role of nanotechnology in cement and concrete have been published; however, the number is very low compared to other major areas of current research. Moreover, much more work on standardization is required to ensure that high quality investigations into the use nanotechnology in cement and concrete applications can reach the global market (Sanjuan *et al.*, 2011).

It is understandable that nanotech research in today's economically driven society has so far been focused mainly on high profit areas such as those mentioned above. It is rather strange, however, that the same society so easily forgets the economics of environmental problems such as the probable meltdown of the world economy associated with global warming (Stern, 2006). Nanotechnology priorities should therefore be driven by

'higher' goals; in particular, the 7th UN Millennium Goal related to environmental sustainability should be a major focus of attention. Consequently, the construction industry should also be at the core of the R&D efforts in nanotechnology: as one of the largest and most active sectors in the world, it will continue to grow at a rapid pace over the coming decades, and most importantly, it has a very high environmental impact, being responsible for the depletion of large amounts of non-renewable resources and for carbon dioxide gas emissions.

Concrete is the most widely-used construction material on Earth, currently used at a level of about 10 km^3/year (Gartner and Macphee, 2011), compared to 2 km^3 for fired clay, 1.3 km^3 for timber, and 0.1 km^3 for steel (Flatt *et al.*, 2012). These astonishing figures show the importance of concrete in the context of material efficiency (Allwood *et al.*, 2011). The main binder of concrete, Portland cement, is responsible for almost 80% of the total CO_2 emissions from concrete, which in turn make up around 6–7% of the planet's total CO_2 emissions (Shi *et al.*, 2011). This is particularly serious in light of current concerns around climate change and, more worryingly still, demand for Portland cement is expected to increase by almost 200% between 2010 and 2050, reaching a level of 6000 million tons/year (Pacheco-Torgal and Jalali, 2011). Nanotech research is therefore crucial in helping to identify methods to make concrete more environmentally friendly.

Another relevant aspect of the high environmental impact of the construction industry relates to the high energy consumption in buildings (accounting for approximately one third of the world's energy consumption) which is responsible for a significant proportion of global greenhouse gas emissions. In Europe, buildings are responsible for more than 40 percent of energy consumption and greenhouse gas emissions (Lechtenbohmer and Schuring, 2011), and energy efficiency is an issue of crucial importance. The recasting of the Energy Performance of Buildings Directive (EPBD) was adopted by the European Parliament and the Council of the European Union on 19 May 2010. The recast set 2020 as the deadline for all new buildings to be 'nearly zero energy'; for public buildings, the deadline is even sooner – the end of 2018. Technologies and methods to improve energy efficiency (Clements-Croome, 2011) are therefore required to ensure eco-efficient construction.

1.3 Outline of the book

The key role that nanotechnology has to play in the development of a more eco-friendly type of concrete is the basis for several chapters in the first part of the book, which looks at infrastructural applications (Chapters 2–7). Chapter 2 covers the experimental and theoretical advancements in the field of nanotechnology; these should allow a greater understanding of the

nature of concrete, which in turn will create the scientific basis for the development of more eco-efficient concrete. In Chapter 3, the use of nanoparticles to produce concrete with high strength and high durability is discussed, while Chapter 4 looks at the development of self-sensing concrete with nanomaterials. This feature enables the assessment of strain or stress variations in concrete structures. This not only allows savings in terms of structure inspections but also removes the requirements for conservation processes which are rather expensive. Chapter 5 deals with the use of nanotechnology to improve the bulk and surface properties of steel, which is the most widely used metallic alloy in modern industry, for structural applications. In Chapter 6, nanoclay-modified asphalt mixtures are discussed, showing the importance of nanoclay in improving the stability, resilient modulus and indirect tensile strength of asphalt mixtures. The use of nanoclay allows a superior performance compared to that of unmodified bitumen to be obtained. Finally in Part I, in Chapter 7 safety issues related to nanomaterials are reviewed; this chapter highlights some crucial issues relevant not only to construction industry practitioners but also to health professionals. It covers the potential health hazards of the nanomaterials utilized in construction, describes the lifecycle of nano-enabled structures, and analyses toxicity profiling for nanomaterials.

The importance of energy efficiency in buildings is the subject of Part II (Chapters 8–12). This section opens with Chapter 8 which reviews techniques for producing thin films and nanostructured coatings for energy applications. Chapter 9 covers high performance thermal insulators, namely nanoporous thermal insulators and partial vacuum thermal insulators, while Chapter 10 reviews the use of silica nanogel to produce highly energy-efficient windows and skylights. Switchable glazing technology is the subject of Chapter 11, which also reviews progress in electrochromics and thermochromics. Switchable glazing technology refers to 'materials and devices [that] make it possible to construct glazings whose throughput of visible light and solar energy can be switched to different levels depending on the application of an electrical voltage or on the temperature', which is an important feature in energy efficiency technologies. Chapter 12 closes Part II, and looks at the importance of photovoltaic technology for energy efficiency. It reviews the advantages and limitations of first and second generation photovoltaic cells and also examines the third generation and, most importantly, the role of nanotechnology in the development of highly efficient low cost photovoltaic cells.

Part III (Chapters 13–16) looks at photocatalytic applications. Chapter 13 concerns the photocatalytic capability of concrete, mortar and plaster that contain semiconductor nanoparticles, and reviews their self-cleaning, air depollution, antibacterial and anti-vegetative properties. This chapter describes existing patents and standards relating to photocatalytic cementi-

tious materials as well as pilot projects and field tests, while Chapter 14 looks at self-cleaning and antibacterial tiles and glass. Photocatalytic paints are discussed in Chapter 15 along with an analysis of strategies for the preparation of photocatalytic paints activated by indoor light, and the potential formation of by-products from photocatalytic paints. Finally, Chapter 16 covers the use of nanotechnology for domestic water purification. As the authors of this chapter put it, water 'is the single most essential commodity responsible for the existence and sustenance of life on the planet earth . . . Unfortunately, the most coveted natural resource was already scarce, and is becoming increasingly scarce day by day . . . As emphasized in one of the UN Millennium Development Goals, water scarcity calls for strengthened international cooperation in the fields of technologies for enhanced water productivity'.

I hope that all of those involved in the construction industry can benefit from the knowledge contained in the present book, which was kindly assembled by a number of international experts. Special gratitude goes to my three co-editors whose contributions to the book have greatly enhanced its quality.

1.4 References

Allwood, J., Ashby, M., Gutowski, T. and Worrell, E. (2011) Material efficiency: A white paper. *Resources, Conservation and Recycling* 55, 362–81.

Arnall, A. and Parr, D. (2005) Moving the nanoscience and technology (NST) debate forwards: short-term impacts, long-term uncertainty and the social constitution. *Technology in Society* 27, 23–38.

Bystrzejewska-Piotrowska, G., Golimowski, J. and Urban, P. (2009) Nanoparticles: their potential toxicity, waste and environmental management. *Waste Management* 29, 2587–95.

Clements-Croome, D. (2011) Sustainable intelligent buildings for people: a review. *Intelligent Buildings International* 3, 67–86.

Compañó, R. and Hullmann, A. (2002) Forecasting the development of nanotechnology with the help of science and technology indicators. *Nanotechnology* 13, 243–7.

Drexler, K. (1981) Molecular engineering: an approach to the development of general capabilities for molecular manipulation. *Proc Natl Acad Sci USA* 78, 5275–8.

Feynman R. (1960) There's plenty of room at the bottom (reprint from the speech given at the annual meeting of the West Coast section of the American Physical Society). *Eng Sci* 23, 22–36.

Flatt, R., Roussel, N. and Cheeseman, C.R. (2012) Concrete: an eco-material that needs to be improved. *Journal of the European Ceramic Society* 32, 2787–98.

Gartner, E. and Macphee, D. (2011) A physico-chemical basis for novel cementitious binders. *Cement and Concrete Research* 41, 736–49.

Glänzel, W., Meyer, M., du Plessis, M., Thijs, B., Magerman, T., Schlemmer, B., Debackere, K. and Veugelers, R. (2003) *Nanotechnology: Analysis of an Emerging Domain of Scientific and Technological Endeavour*. Steunpunt O& O Statistieken, Leuven.

Lechtenbohmer, S. and Schuring, A. (2011) The potential for large-scale savings from insulating residential buildings in the EU. *Energy Efficiency* 4, 257–70.

Malanowski, N. and Zweck, A. (2007) Bridging the gap between foresight and market research: integrating methods to assess the economic potential of nanotechnology. *Technological Forecasting and Social Change* 74, 1805–22.

NSF (2001) *Societal Implications of Nanoscience and Nanotechnology*. National Science Foundation, Arlington, VA.

Pacheco-Torgal, F. and Jalali, S. (2011) *Eco-efficient Construction and Building Materials*. Springer Verlag, London.

Rieke, V. and Bachmann, G. (2004) German innovation initiative for nanotechnology. *Journal of Nanoparticle Research* 6, 435–46.

Salerno, M., Landoni, P. and Verganti, R. (2008) Designing foresight studies for nanoscience and nanotechnology (NST) future developments. *Technological Forecasting and Social Change* 75, 1202–23.

Sanjuan, M., Zaragoza, A. and Agui, J. (2011) Standardization for an innovative world. *Cement and Concrete Research* 41, 767–74.

Shi, C., Fernández Jiménez, A. and Palomo, A. (2011) New cements for the 21st century: the pursuit of an alternative to Portland cement. *Cement and Concrete Research* 41, 750–63.

Soltani, A., Tabatabaeian, S., Hanafizadeh, P. and Soofi, J. (2011) An evaluation scheme for nanotechnology policies. *Journal of Nanoparticle Research* 13, 7303–12.

Stern, N. (2006) *Stern Review on Economics of Climate Change*. Cambridge University Press, Cambridge.

Tyshenko, M. (2010) Nanotechnology innovation as a *deus ex machina* and potential effects on sustainability in a global context. *International Journal of Nanotechnology* 7, 209–23.

Wang, G. and Guan, J. (2010) The role of patenting activity for scientific research: a study of academic inventors from China's nanotechnology. *Journal of Informetrics* 4, 338–50.

Wang, G. and Guan, J. (2012) Modeling the dynamic relation between science and technology in nanotechnology. *Scientometrics* 90, 561–79.

2

Nanoscience and nanoengineering of cement-based materials

G. CONSTANTINIDES, Cyprus University of Technology, Cyprus

DOI: 10.1533/9780857098832.1.9

Abstract: Concrete is the most widely used construction material and given the current population growth, economic development, and need for repair/replacement of aging infrastructure, its consumption is expected to increase. Unfortunately though, the production of one of its major constituents, cement, is associated with approximately 5–10% of the global anthropogenic carbon dioxide emissions and therefore the industry and the specific material is in urgent need for reevaluation. The chemical reactions and resulting products that are produced when cement is mixed with water create a material that is highly complex. The dominant component, C-S-H gel, has a local structure of a precipitate with nanoscale features that are difficult to model and understand. Consequently, the development of the material relied primarily on empirical knowledge obtained through macroscopic experimentation and little is known about the underlying mechanisms that control the response of the material when employed in engineering applications. Recent experimental and theoretical advancements in the field of nanoscience and nanotechnology provide optimistic expectations for a refined understanding of the material that will create the scientific basis for a more sustainable and eco-efficient construction.

Key words: concrete nanoscience, concrete nanoengineering, C-S-H nanomechanics, concrete nanocomposites.

2.1 Introduction

2.1.1 Macroscale: cement and concrete

Cement is a pulverized fine powder which develops into a strong binder when mixed with water. The best known hydraulic cement[1] is ordinary Portland cement (OPC). Current production of cement (the main component of concrete and all other cement-based materials) is approximately over 3 billions tonnes per year which makes it the most widely used solid on earth (Fig. 2.1). This quantity is sufficient to produce over 30 billions tonnes of concrete or over 4 tonnes for every person currently alive. Given

[1] By the term 'hydraulic cement', we refer to those materials whose products are stable in aqueous environments.

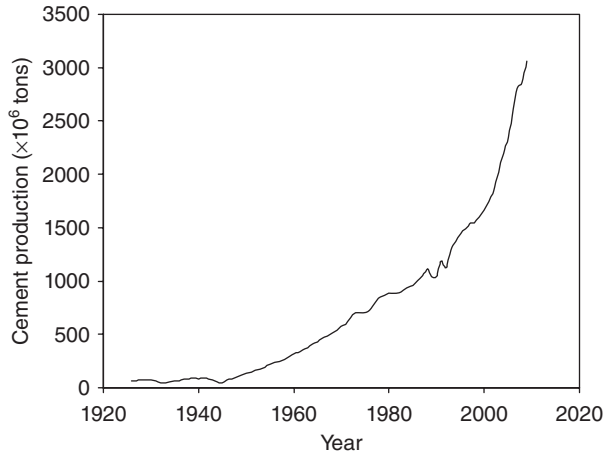

2.1 Worldwide annual cement production for the period 1925–2009. Data from Kelly and van Oss (2010).

Table 2.1 Chemical formulae and cement nomenclature for major constituents of Portland cement. Cement chemistry abbreviation: C = CaO, S = SiO_2, A = Al_2O_3, F = Fe_2O_3. Also water is abbreviated as H = H_2O. (Hewlett, 2004)

Mineral	Chemistry	Oxide composition	Abbreviation	%
Tricalcium silicate (alite)	Ca_3SiO_5	$3CaO.SiO_2$	C3S	50–70
Dicalcium silicate (belite)	Ca_2SiO_4	$2CaO.SiO_2$	C2S	15–30
Tricalcium aluminate	$Ca_3Al_2O_4$	$3CaO.Al_2O_3$	C3A	5–10
Tetracalcium aluminoferrite	$Ca_4Al_nFe_{2-n}O_7$	$4CaO.Al_nFe_{2-n}O_3$	C4AF	3–8

the abundance of its major natural constituents (calcium and silica) in the earth's crust (responsible for its current low price), and technical advantages over other construction materials (timber, steel, composites, etc.), it is highly unlikely that any other material will displace concrete from the construction industry, at least in the foreseeable future.

Concrete is essentially a composite consisting of a binding matrix (cement paste) with embedded particles (aggregates). Cement paste is the resulting product of the complex chemical reactions that take place between cement (see Table 2.1 for typical compositions) and water (Double and Hellawell, 1976). Aggregates could be sand, gravel, crushed stone, crushed blast-furnace slag, or demolition waste and are usually separated by their size.

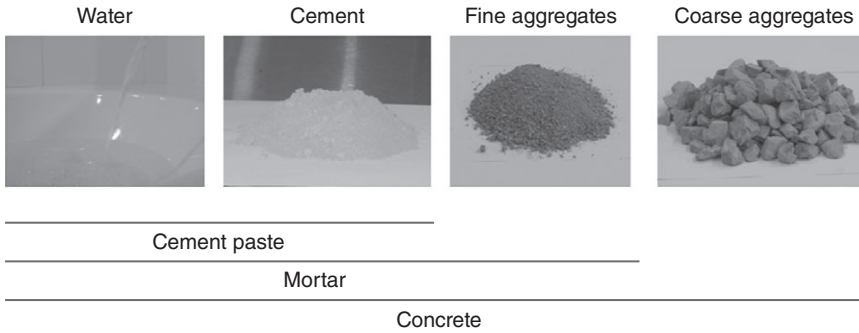

2.2 Schematic of the composition of cement paste (water + cement), mortar (cement paste + fine aggregates) and concrete (mortar + coarse aggregates).

Aggregates with diameters larger than 4.75 mm (No. 4 sieve) are referred to as coarse, whereas particles with diameter in the range of 75 μm–4.75 mm (No. 200 to No. 4 sieve) are referred to as fine (Mehta and Monteiro, 2006). When fine aggregates are added to the initial mix, we term the resulting product as mortar (cement + water + fine aggregates), whereas concrete is created with the further addition of coarse aggregates (cement + water + fine/coarse aggregates), as illustrated in Fig. 2.2.

2.1.2 Nanoscale: C-S-H

Cementitious materials are the product of complex chemical reactions that take place when cement (primarily tricalcium and dicalcium silicates) reacts with water to form various hydration products with nanoscale features that are arranged in a multi-scale fashion in a three-dimensional space (Feldman and Sereda, 1968; Taylor, 1990, 1993; Nonat, 2004; Richardson, 2008). As alite and belite (C_3S and C_2S) comprise over 80% of most cements, their hydration products dominate in terms of volume. Both silicate phases react with water to form a hydrated version of calcium silicates (C-S-H) and calcium hydroxide (CH or Portlandite):

$$C_3S/C_2S + H \rightarrow C\text{-}S\text{-}H + CH \qquad [2.1]$$

The main constituent phase, C-S-H, which dominates in terms of volumetric proportions (>70%) and as a consequence governs the macroscopic response, manifests itself in the nm to μm length scale (Nonat, 2004; Jennings, 2008; Richardson, 2008). The poorly crystalline, highly porous and non-conductive nature of the material makes it difficult to study and as a result the actual mechanisms that govern the formation and its properties remain unidentified to date. In fact, the hyphens in C-S-H reflect its uncer-

tain stoichiometry. Furthermore, this constituent phase cannot be recapitulated effectively *ex-situ*; one has to, therefore, access the properties of C-S-H *in-situ* at the length scale where it naturally occurs. Experimental data report C/S-ratios in the 1.2–2.1 range with an average around 1.75, while the H content fluctuates even more. The recent advent of innovative and powerful experimental techniques provides the cement and concrete community with an unprecedented opportunity to probe this phase in its natural environment, understand its behavior, and transfer these ideas to higher levels through multi-scale models that can deliver the composite concrete response.

2.1.3 Call for innovation

Despite the ubiquitous presence and extreme importance of concrete for modern societies, its development over the past decades has had a largely empirical basis. On one hand, the construction industry is characterized by risk aversion as the use of materials is dictated by codes or standards, and therefore it is difficult for new products to be introduced into the industry. On the other hand, the industry itself is highly fragmented[2] and as a consequence very little effort and money is invested by companies on fundamental research and development. As a result, our knowledge of this very important material has remained largely on an empirical basis, and any fundamental research for understanding and innovation is developing from isolated efforts primarily in research and educational institutions.

The low cost and wide availability of the material, coupled with its excellent properties such as ability to be shaped, resistance to water and fire, and good mechanical properties, have been sufficient to maintain concrete as the most used material in the construction industry. Recent environmental publications, however, raise concerns over the ecological footprint of cement and as a consequence cement-based materials like concrete. Compared to steel, aluminum, plastics and other manufactured materials, Portland cement concrete is generally considered as environmentally friendly (Fig. 2.3). However, the large volumes of the material produced every year consume 2–3% of the global energy (Juenger *et al.*, 2011) and approximately 12–15% of the industrial energy (Ali *et al.*, 2011). Furthermore, there is a growing awareness that concrete production and construction practices of today are not sustainable (Worrell *et al.*, 2001; Gartner, 2004; Phair, 2006; Damtoft *et al.*, 2008; Mehta, 2009).

The production of cement involves heating clay and limestone to 1450°C which involves the burning of fossil fuels to generate such heat releasing in

[2] According to (Mann, 2006) about 97% of EU construction companies employ fewer than 20 people.

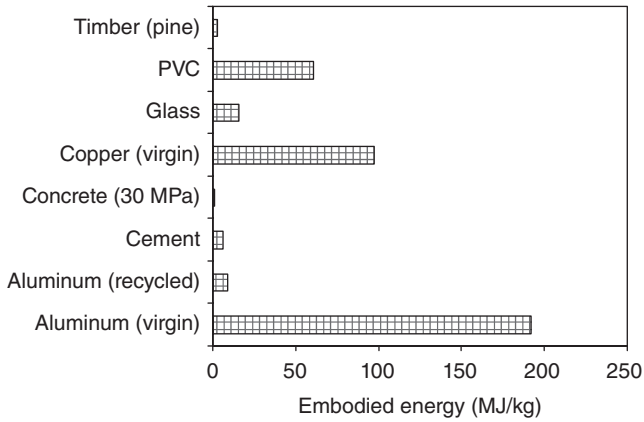

2.3 Embodied energy consumption of some common construction materials. Data from Alcorn (2003).

the process significant amounts of CO_2 into the atmosphere. It is estimated that for every tonne of cement produced, approximately a tonne of CO_2 is released in the atmosphere. About 60% of that is allocated to the chemical reactions that occur when limestone is heated in the kiln (calcination) with the remaining 40% admitted to energy generation through fossil fuels usage for kiln heating and clinker grinding. As a result, cement production is one of the major carbon dioxide contributors in the Earth's atmosphere. Estimates suggest that the industry is responsible for approximately 7% of global CO_2 emissions. Furthermore, while concrete structures are generally thought to be 'eternal', they have life-spans that range between 50 and 100 years, depending on the material quality and environmental conditions in use. As a result, the durability performance of the majority of the world's infrastructure is gradually decaying, posing significant sustainability concerns for various governments.

These recent sustainability concerns provide important drivers for the further understanding and development of this very important material. Recent advances in experimental and theoretical nanomechanics provide new avenues for material decoding (nanoscience) and material optimization for specific applications (nanoengineering). The fundamental idea of the efforts that have been in effect over the last decade or so is to develop the material science approach that will link the initial synthesis and processing conditions with the evolving microstructure and the resulting macroscopic response. An elegant scientific methodology equivalent to the one used in industrial metals and ceramics is currently lacking. The microstructure-property approach is adopted such as to provide scientific interpretations for the macroscopic mechanical, physical, and chemical responses observed in practice.

2.1.4 Chapter outline

This chapter provides an overview of the recent contributions of nanotechnology to the cement and concrete industry. Space constraints dictate that we explore promising ideas and contributions in a non-exhaustive way, while the reader is directed throughout the text to journal publications for a more detailed exposition. Some recent reviews can also serve as introduction to the topic (Mann, 2006; Scrivener and Kirkpatrick, 2008; Sanchez and Sobolev, 2010; Black *et al.*, 2010; Raki *et al.*, 2010; Jennings and Bullard, 2011; Pacheco-Torgal and Jalali, 2011). The content is presented in two main parts:

1. Section 2.2, 'Nanoscience of cement-based materials', deals with the fundamental understanding recently obtained through the application of novel techniques that probe the nanoscale structure of concrete (C-S-H). This refined understanding provides opportunities for more delicate modeling that can transfer nanoscale knowledge to the level where the material is applied to engineering applications.
2. Section 2.3, 'Nanoengineering of cement-based materials', is devoted to recent attempts to modify the nanoscale of cementitious materials utilizing advances in nanoscale synthesis, chemistry, and manufacturing in order to develop a stronger, more durable, and environmentally friendly material.

2.2 Nanoscience of cement-based materials

2.2.1 Experimental micro/nano-mechanics

In the past few decades the scientific community has experienced a rapid advancement in the availability of experimental tools for monitoring, manipulating and synthesizing nanoscale features. This provided an unprecedented opportunity for revisiting ubiquitous materials like cementitious systems and refining our fundamental understanding of the underlying mechanisms that control their macroscopic response while at the same time opening avenues for science-based innovation and materials optimization. Several new techniques have been developed, some of which have already been exploited on cementitious materials and some of which remain unexplored. These include atomic force microscopy (AFM), nuclear magnetic resonance (NMR), X-ray microscopy, focused ion beam (FIB), scanning electron microscopy (SEM/ESEM), transmission electron microscopy (TEM), small angle neutron scattering (SANS), small angle X-ray scattering (SAXS). The application of some of these techniques to the benefit of cement and concrete nanoscience is presented below.

Atomic force microscopy (AFM)

Seeing the nanoscale of cementitious materials has been challenging primarily because the C-S-H matrix is highly porous and thus non-conducting. The advent of AFM has provided an opportunity to 'visualize' the nanoscale of this important material as it relies on contact rather than any other conduction-related mechanism. AFM, which is generally considered the successor of scanning tunnelling microscopy (STM), was developed by Gerd Binnig and Heinrich Rohrer[3] in the early 1980s at IBM Research Labs. The technique, which works by scanning a very sharp metal wire tip over the surface of interest, is utilizing quantum mechanical effects of tunneling and piezoelectric effects to develop a nanoscale image of the material surface. AFM was introduced a few years later in 1985 by Binnig *et al.* (1986) mainly to overcome the main drawback of STM, its requirement for conductive surfaces. The technique which utilizes interatomic van der Waals forces as monitoring mechanism consists of a sharp tip, usually sharp silicon with nanoscale curvatures, to scan the surface and provide a digital three-dimensional morphological profile. Through the contact interaction mechanism, the technique can be applied on virtually any type of surface, these being polymers, metals, ceramics, biomaterials, composites or concrete.

Early attempts (to the best of the author's knowledge) to apply nanotechnology tools to cementitious materials date back to 1996 when Mitchell *et al.* (1996) applied AFM to study the physicochemical changes that occur during the hydration process of cement. The ability to image in a liquid environment was found to be beneficial for this material system whose formation is the resulting product of a chemical reaction. This innovative approach presented for the first time the morphological details of the main hydration product, the C-S-H phase. It was observed that C-S-H forms nanocrystalline domains of the order of a few nanometers that agglomerate into a larger porous domain, the main connecting matrix of all cementitious composites. This nanogranular microstructural arrangement was suggested by several other subsequent publications (Lesko *et al.*, 2001; Nonat, 2004). Plassard *et al.* (2005) managed to isolate atomically smooth domains of recrystallized C-S-H nanoparticles through long-term exposure to saturated calcium hydroxide solution specimens with various C/S ratios. The atomic scale characteristics and nanomechanical responses (elastic modulus) via AFM indentation have been studied by Plassard *et al.* (2004). Other AFM studies have concentrated on the origin of C-S-H strength and cohesion which remains unresolved. Interaction forces between C-S-H and probes have been measured (Finot *et al.*, 1999; Lesko *et al.*, 2001; Plassard *et al.*, 2005) and the growth process has been monitored (Garrault *et al.*, 2005) shedding some light on this intriguing material system.

[3]The two researchers were awarded a Nobel Prize in Physics in 1986 for their development.

The technique further contributed to the study of other chemical constituents of cement paste as well as their chemomechanical stability in time. The carbonation of calcium hydroxide crystals, prepared using the mica-replication method, exposed to various environments (combinations of N_2, O_2, H_2O, and CO_2), has been studied using AFM images. Spherules of $CaCO_3$, the chemical product of the carbonation reactions, have been observed and the necessary conditions for their formation have been recorded (Yang *et al.*, 2003). The technique currently provides reliable means of seeing at the nanoscale of C-S-H and assists in the quantification of either modification attempts (e.g., Weiguo *et al.*, 2011) or in the fundamental understanding of chemical formation or degradation phenomena.

Nanoindentation

The advent of instrumented indentation enabled fundamental studies of the nanomechanical response of metals, ceramics, polymers, and composites (see, e.g., Oliver and Pharr, 1992, 2004; Fischer-Cripps, 2011). Current technology allows for contact-based deformation of nanoscale load and displacement resolution and has been leveraged for both general mechanical characterization of small materials volumes and unprecedented access to the physics and deformations processes of materials. While nanoindentation was originally developed for homogeneous metals and ceramics, it was quickly appreciated that nanoscale resolution can be of significant use to the decoding of C-S-H structure, the binding phase of all cementitious materials (Constantinides *et al.*, 2003; Constantinides and Ulm, 2004). However, accurate nanomechanical analysis of composites requires advanced analysis that takes into consideration the multi-phase, multi-scale nature of the material and its pressure-sensitive mechanical response (Constantinides *et al.*, 2003; Constantinides and Ulm, 2004, 2007; Ulm *et al.*, 2005, 2007, 2010; Ganneau *et al.*, 2006; Trtik *et al.* 2009; Randall *et al.*, 2009).

A typical nanoindentation test consists of establishing contact between an indenter (typically diamond) and a smooth sample (Miller *et al.*, 2008), while continuously measuring the load, P and the penetration depth h (Plate I between pages 162 and 163). Analysis of the P-h response proceeds by applying a continuum scale model (Fischer-Cripps, 2011) to derive the indentation modulus M, $M = \frac{\sqrt{\pi}}{2}\frac{S}{\sqrt{A_c}}$, and indentation hardness H, $H = \frac{P_{\max}}{A_c}$, where S is the unloading slope at maximum depth $h_{\max}$, $P_{\max}$ is the maximum indentation force, and A_c is the projected contact area at $h_{\max}$. Several empirical means to estimate A_c exist, either through post-indentation inspection, geometric idealizations of the probe, or more commonly through analysis of the indentation response for a material of

ostensibly known E and H to determine this area as a function of $A_c = A(h_c)$. Equations for M and H rely on the assumption of a semi-infinite half-space and therefore caution should be exercised when testing highly heterogeneous materials. In particular, the number of tests should be significantly increased and the choice of indentation depth should be carefully made (Constantinides *et al.*, 2006; Ulm *et al.*, 2007). The two indentation properties measured during a test (M and H) can then be linked to the elastic $M = M(E, \nu)$ and plastic $H = H(c, \varphi)$ properties of the indented materials, through advanced continuum scale models (Ganneau *et al.*, 2006). The extracted mechanical properties of the two types of C-S-H measured on hundreds of specimens where found to be intrinsic to all cement-based materials E = 20–30 GPa and H = 400–1000 MPa, where the range relates to the local density variations (nanoscale porosity) observed in cement-based materials.

Instrumented indentation provides mechanical access to the C-S-H phases and has been exploited apart from fundamental studies (Constantinides *et al.*, 2003; Constantinides and Ulm, 2004, 2007; Mondal *et al.*, 2007, 2008; Vandamme and Ulm, 2009; Vandamme *et al.* 2010; Chen *et al.*, 2010; Ulm *et al.*, 2010; Xu and Yao, 2011; Song *et al.*, 2011) but also for the evaluation of chemical degradation phenomena (Constantinides and Ulm, 2004; DeJong and Ulm, 2007), and the nanomechanical quality of various cement-based systems like alkali activated aluminosilicates (Nemecek *et al.*, 2010), ultra high performance concrete (Sorelli *et al.*, 2008), fiber reinforced systems (Wang *et al.*, 2009; Sakulich and Li, 2011), nanosilica concrete (Zyganitidis *et al.*, 2011), and carbon nanotube reinforced concrete (Sáez de Ibarra *et al.*, 2006; Konsta-Gdoutos *et al.*, 2010a). The technique can potentially serve as a nanomechanical screening tool in the search for a more durable and environmentally friendly material.

Small angle neutron and x-ray scattering (SANS/SAXS)

Small angle neutron and X-ray scattering (SANS/SAXS) are powerful techniques for characterizing the micro- and nanostructures of disordered heterogeneous materials on the 1–100 nm length scale (Winslow and Diamond, 1974; Winslow *et al.*, 1994, 1995; Allen *et al.*, 1982, 1987; Volkl *et al.*, 1987; Allen, 1991; Eichhorn *et al.*, 1993; Beddoe and Lang, 1994; Allen and Thomas, 2007). Macro structures like polymers, precipitates in metallurgical specimens, biological molecules, micelles and magnetic systems like ferrofluids can be identified. The drawback, however, is that SANS requires a neutron source which is expensive and available only in a handful of laboratories around the world associated with research nuclear reactors. Around 37 neutron sources exist, the majority of which (>60%) are in Europe. Neutron scattering has an advantage over X-ray scattering (SAXS) due to selective

absorption and scattering cross section of neutrons across the periodic table. SAS is particularly suitable for cement-based materials as it does not require drying and can be conducted *in situ* during hydration. Furthermore, it circumvents the need for specimen preparation and any associated interference that might be incorporated, as with microscopy techniques.

The technique involves measuring the intensity of neutron or X-ray scattered (due to heterogeneities) through small angles, usually less than 1°. By employing a suitable model for data interpretation, one can determine information on the geometrical characteristics like size distribution, volume fractions, surface area, fractal characteristics, etc. In general, and owing to their neutrality, neutrons can penetrate the specimen far better than X-ray scattering techniques, thus probing the material on higher length-scales. In fact, recent instrument modifications, namely ultrasmall-angle scattering (USANS and USAXS), allow through crystal diffraction optics material data to be received from much lower scattering vectors, thus enabling microstructure characterization to extend to larger domains, i.e. >1 μm for USAXS and >10 μm for USANS. The combination of all these techniques suggest that C-S-H is a nanogranular material with a fundamental unit on the order of 5 nm in the vertical direction, a chemical formula of $(CaO)_{1.7}(SiO_2)(H_2O)_{1.8}$ and a density of 2604 kg/m^3 (Allen *et al.*, 2007; Jennings *et al.*, 2007). This unit appears to agglomerate, possibly with fractal characteristics, into larger domains with local spatial variability in particle packing and therefore densities. Information on the larger CH crystals can be obtained through inelastic neutron scattering (INS), whereas the different states of free and bound water found in cement systems can be probed when employing quasielastic neutron scattering techniques (QENS). Apart from a fundamental understanding of the C-S-H phase, the techniques have been employed for monitoring the hydration mechanism and its alteration through accelerators or decelerators, the effect of cement additives and cement replacement materials, and the effect of calcium leaching.

The microstructure of concrete revisited

It is now clear that at the centimeter scale, concrete or mortar can be considered as a two-phase composite with a (usually) weak interface generated by the local packing of the cement particles during hydration that generates what is known as an interfacial transition zone (ITZ). While this macroscopic visualization is quite accurate at that level, it cannot capture all the peculiarities that cement-based materials exhibit, e.g., access to aggressive ions, time-dependent deformation, sensitivity to humidity, response to low and high temperatures, pressure sensitivity of strength, and many more. All these require understanding of the percolated C-S-H phase which controls the macroscopic response. The very nature of C-S-H has been the subject

of many experimental and theoretical attempts over the last 100 years. It is now well accepted that it is a colloidal network gel with local density variability (Scherer, 1999; Jennings, 2000, 2008; Tennis and Jennings, 2000). While C-S-H continues to be the subject of significant research towards its fundamental understanding, there is now ample experimental data on which to build preliminary predictive models. The models aim to rationalize as many experimental data reported as possible. Among the many reported over the years, we refer to the models by Feldman and Sereda, and Jennings (Fig. 2.4).

The Feldman and Sereda model suggests that C-S-H, similar to clay particles, forms a three-dimensional assemblage of layer silicate sheets which locally tend to form parallel network groups with entrapped water and pore space (Fig. 2.4a). The Jennings nanoscale model for the structure of C-S-H rationalizes the differences in the density and surface area values obtained from different experimental techniques. The smallest distinct units of C-S-H are 'globules' just under 5 nm in the smallest dimension, which pack together into two distinct structures, called high density (HD) C-S-H and low density (LD) C-S-H. The average packing density of the HD structure is 74%, while the LD C-S-H structure is more complex, with a packing density that varies with scale such that the structure is fractal over length scales up to a maximum of about 60 nm. The LD C-S-H structure was found to vary with the curing conditions, aging, load, and environment. The mechanical response of these two phases (LD and HD C-S-H) has been measured by nanoindentation (Constantinides and Ulm, 2004) and serves as the input of multi-scale micromechanical models.

Fundamental questions remain regarding the physics of C-S-H that need to be decoded to aid significant advancements. One such nagging question is the very nature of water in nanoconfined spaces and how this contributes to the strength of this material (Kalinichev *et al.*, 2007; Pellenq *et al.*, 2008; Xu *et al.*, 2009).

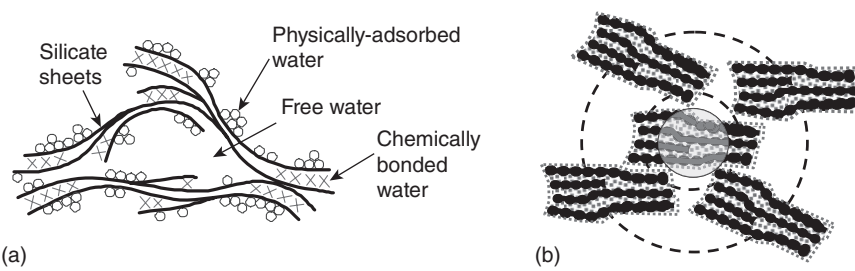

2.4 Two of the many C-S-H models proposed in the literature: (a) Feldman and Sereda layered model and (b) Jennings colloidal model.

2.2.2 Theoretical nano/micro-mechanics

Atomistic simulations

The exponential growth of computer power over the past decades has springboarded the development of computational methods and code interfaces that provide the potential of material simulations for a variety of scientific problems. The community of concrete science and engineering was reluctant to employ these techniques primarily because the important characteristics of C-S-H were poorly understood.

A realistic molecular model of hydrating cement has recently been presented in Pellenq *et al.* (2009). Starting from a monoclinic periodic computational cell of dry Tobermorite and subtracting SiO_2 groups, they created a defected silicate chain that achieve C/S ratios close to the experimentally obtained values from NMR (Cong and Kirkpatrick, 1996). The resulting molecular model was then enriched, using grand canonical Monte Carlo simulations, with water molecules to reach a crystal structure of $(CaO)_{1.65}(SiO_2)(H_2O)_{1.75}$ and a density of 2.56 g/cm^3 which are in close agreement with the experimental values reported through SANS/SAXS by Allen *et al.* (2007) of $(CaO)_{1.7}(SiO_2)(H_2O)_{1.8}$ and 2.6 g/cm^3, respectively. The model was then contrasted to experimental data on hydrated cement, namely fine structures X-ray absorption spectroscopy signals, X-ray diffraction intensities, nanoindentation results, and vibrational density from infrared spectroscopy with very good agreement.

The studies that have already been presented in the literature include the calculation of elastic and chemical bonding properties of the most common cement analoges, Tobermorite and Jennite (Churakov, 2008, 2009; Shahsavari *et al.*, 2009), the atomistic modeling of the major hydration products of cement (Manzano *et al.*, 2006, 2007, 2009), the development of an empirical force field (CSH-FF) for calcio-silicate hydrates (Shahsavari *et al.*, 2011), the impact of chemical impurities on the hydration/structure/mechanical performance of alite (Ca_3SiO_5 or in short C_3S) and belite (Ca_2SiO_4 or in short C_2S) clinker phases (Manzano *et al.*, 2011), and the chloride binding on the various hydration products (Kalinichev and Kirkpatrick, 2002), to name a few. The development of a robust computational model at the nanoscale will allow scientists and engineers to fine-tune and optimize the nanostructure of material through cost-effective virtual simulations. Proper benchmarking against detailed nanoscale experiments will be an essential part of the development process.

Continuum micromechanical modeling

There have been significant developments in the field of micromechanics over the last 50 years (i.e., Torquato, 2001; Dormieux *et al.*, 2006). As the

tools of nanoscale synthesis and manipulation became available, there was a pressing need for concurrent development of the predictive modeling techniques. Continuum micromechanics represent the systematic approach for upscaling properties (mechanical, physical, etc.) of composite materials based on the constituents' properties that compose the heterogeneous microstructure. Typical models incorporate the fundamental mechanical properties of C-S-H together with estimates of the volumetric proportions (f_i) of all constituent phases (i) in a multi-scale homogenization scheme that can predict the composite macroscopic elastic (E_{hom}, $\nu_{hom} = F(E_i,\nu_i,f_i)$) (Constantinides and Ulm, 2004; Ulm *et al.*, 2004; Sanahuja *et al.*, 2007) and strength (c_{hom}, $\varphi_{hom} = F(c_i,\varphi_i,f_i)$) behavior (Pichler *et al.*, 2009; Pichler and Hellmich, 2011), where the only input requirements are the elastic (E_i, ν_i) and plastic (c_i, φ_i) properties of the individual constituents and their volumetric proportions (f_i). The morphological arrangement of the phases in space is taken into consideration in the choice of the continuum micromechanical models. It has been found that for cementitious materials, a combination of Mori–Tanaka and self-consistent schemes appears to deliver robust results (Constantinides, 2006). Figure 2.5 demonstrates the predictive capabilities of continuum-based micromechanical models, suggesting

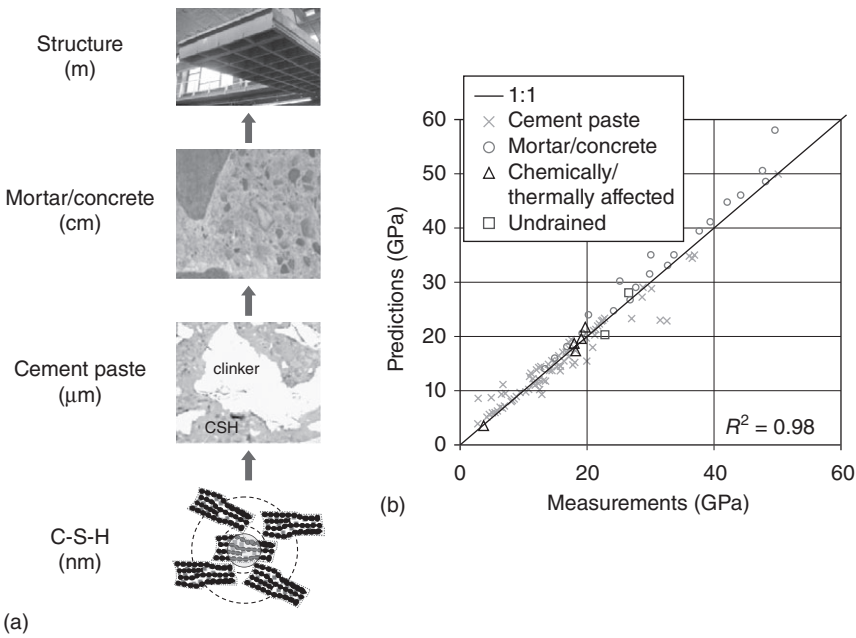

2.5 (a) Multi-scale think model for cement-based materials. (b) Micromechanical predictions vs. macroscopic experimental data for the elastic properties of cementitious materials.

that they can effectively transfer the information across several orders of magnitude in length scale starting from the atomistic C-S-H level to the decimeter level of concrete structures. While the above described approaches rely on analytical formulation of the problem, numerical schemes are also employed which provide more powerful possibilities to tackle with non-linear phenomena, like strength, creep, permeability, etc. (Hain and Wriggers, 2008; Smilauer and Bazant, 2010).

2.2.3 Concluding remarks: a framework for science-based innovation

The field of experimental and theoretical nanomechanics is advancing at a rapid pace. As the tools of experimentation and the resulting theoretical frameworks of data analysis are developing, new opportunities for understanding and characterization of materials arise. This provides an unprecedented opportunity to probe long-used ubiquitous construction materials, like concrete, that have not been rigorously characterized and modeled in the past and create a science-based platform for material optimization. Some ideas and recent developments in the field of cement-based materials are presented below.

2.3 Nanoengineering of cement-based materials

The process of tailoring the microstructure of cementitious materials to achieve desirable properties for specific applications is termed materials engineering. When nanoscale features are involved, we refer to this process as nanoengineering. From the above discussion it becomes apparent that cement-based materials, which essentially depend on the performance of C-S-H, are nanoscale materials. Nanoengineering can occur by modifying this nanoscale phase directly, through some macroscopic synthesis and processing means, or by introducing nanoscale additives that can either be inert or chemically interact with the material in certain ways. Recent developments in nanotechnology provide ample routes for concrete nanoengineering, some of which are discussed below.

2.3.1 Empirical routes for material development

When reviewing the historical evolution of cementitious materials, it can be identified that much of their development relied on empirical knowledge that was achieved through trial and error experimentation. In retrospect, the degree of optimization that has been achieved in this fashion is rather impressive. Traditionally, the most used variable for the material characterization has been the mass ratio of water to cement in the initial mix. It has

been argued that this ratio is ultimately related to the spacing achieved within cement particles (Bentz and Aitcin, 2008) and as a result of the amount of porosity and all related parameters. It is common knowledge in the concrete community that the lower the w/c ratio the higher the elasticity, strength, and durability. Of course the process cannot be continued indefinitely: as the distance between particles is reduced, the particles tend to agglomerate with a subsequent loss of workability. To circumvent this problem, a higher particle packing can be achieved by playing with the particle size distribution of the dry mix (Fig. 2.6). Furthermore, the development of superplasticizers that could create workable mixes for low w/c ratios resulted in high strength and performance materials. As for most materials, the stronger they become, the more brittle they tend to be. The development of fiber reinforcements (steel, polymeric, etc.) added ductility to the system and created a material as attractive as metallic systems. Cementitious materials with strength as great as that of mild steel have been reported in the literature (e.g., Richard and Cheyrezy, 1995). Other empirical techniques that alleviated some of the problems associated with these high performance systems, like heat treatment, etc., have been proposed.

2.3.2 Cementitious nanocomposites

Nanoparticles have sizes with at least one of their dimensions in the 1–100 nm range. As the particle size decreases, a larger proportion of atoms is situated on the free surface compared to those atoms in the bulk, resulting

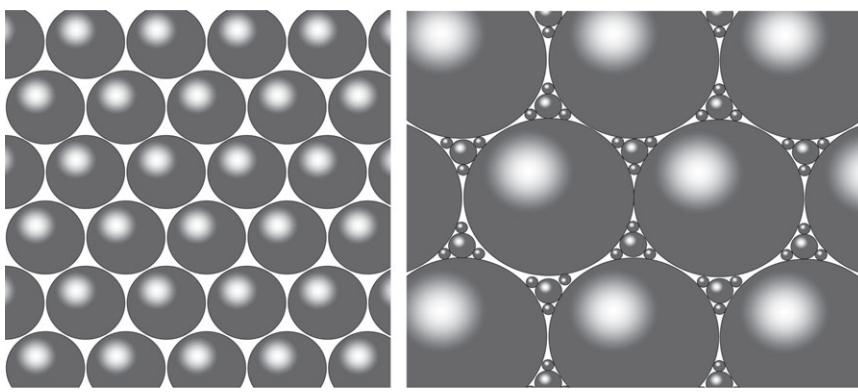

2.6 (a) Packing of mono-sized spheres. (b) The packing density of the system can be significantly increased by using an initial mix with a particle size distribution.

in properties which can be significantly different from their larger scale counterparts. Several nanoscale particles are currently being considered as nanoscale additives with the aim of improving macroscopic performance or adding functionality to the material. Among the candidates are nanosilica, titanium dioxide, carbon nanotube, nanoscale limestone, haematite nanoparticles, pigments, clay particles, etc. (Meng *et al.*, 2008; Sato and Diallo, 2010; Tregger *et al.*, 2010a,b; Sato and Beaudoin, 2011).

Micro- and nanosilica (μ/n-SiO_2)

Silica fume, also known as microsilica, is an amorphous polymorph of silicon dioxide, silica. It is a by-product of the carbothermic reduction of high purity quartz in electric arc furnaces in the production of silicon and ferrosilicon alloys. The resulting product is a grey powder of surface area on the order of 20 m^2/g and particle sizes in the 100–200 nm range, approximately one hundredth of the cement particles. When silica fume is added to Portland cement concrete, it increases its compressive strength, tensile strength and abrasion resistance. These improvements stem from the closed packing achieved in the cement paste system that reduces the overall porosity and improves the interfacial transition zone. Furthermore, the material is involved in the pozzolanic reaction (Lin *et al.*, 2011) with the calcium hydroxide crystals producing additional cementing material (C-S-H) and eliminating areas of stress concentrations and prone to failure initiation ($Ca(OH)_2$ crystals). The reduction of porosity produces at the same time a material more durable and resistant to chemical degradation processes like chloride ion diffusion, alkali silica reaction and calcium leaching, which preserves the material from mechanical degradation and protects reinforcing steel from corrosion (Zhang and Li, 2011). Several recent publications report on the significant advantages of nano-SiO_2 as compared to microsilica (Jo *et al.*, 2007; Ye *et al.*, 2007; Senff *et al.*, 2010).

The already reported benefits persist in an amplified fashion. The highly reactive and large surface area provided by colloidal silica accelerates cement hydration and has a significant impact on the hydration process at early ages (Bjornstrom *et al.*, 2004). The high surface area, however, decreases the amount of lubricating water and interferes with the flowing characteristics of fresh concrete. It is therefore essential to ensure proper workable conditions, i.e., with the use of superplasticizers, so as to avoid air entraining in the fresh system and benefiting from the above described performance (Senff *et al.*, 2009). The use of silica reinforced cementitious materials might find applications in a variety of systems ranging from oil well cement (Choolaei *et al.*, 2012) to pavement (Zhang and Li, 2011) and high performance compacting applications (Nazari and Riahi, 2011).

Carbon nanotubes

Carbon nanotubes (CNT) are the strongest and stiffest material known to date[4] and hold great promise for reinforcing cement-based composites (Makar and Beaudoin, 2004; Makar *et al.*, 2005; Nasibulin *et al.*, 2009; Chaipanich *et al.*, 2010; Konsta-Gdoutos *et al.*, 2010b; Manzur and Yazdani, 2010; Metaxa *et al.*, 2010; Wille and Loh, 2010; Kumar *et al.*, 2012). They are allotropes of carbon with a cylindrical-tubular geometry of diameter that ranges from 1 to 100 nm and lengths up to a few millimeters. Aspect ratios (length-to-diameter ratio) beyond 100,000,000:1 have been reported in the literature which allows crack-bridging capabilities at finer scales. Owing to their geometry and covalent sp^2 bonds formed between the individual carbon atoms, they exhibit superb mechanical, electrical, and thermal properties (among others) coupled with impressive deformation characteristics which makes them excellent candidates for additives to various structural materials, including concrete (Salvetat *et al.*, 1999). It is in fact impressive that with only a tiny portion of reinforcement the composite system can potentially influence the mechanical response. CNTs can occur as a single layer of graphite rolled in a tubular shape (SWCNT) or multiple wall concentric tubes (MWCNT, also known as CNF, whereas F stands for fiber). SWCNT have reported values of 1 TPa for elasticity and 60 GPa for strength whereas the respective values for CNF are in the order of 400 GPa and 7 GPa respectively. The mechanical reduction of MWCNTs is due to the weak shear interactions between adjacent tubes. This limitation has recently been addressed by applying high-energy electron irradiation, which crosslinks inner shells and tubes, and can effectively increase the strength of these materials to ~60 GPa.

In order to harness the real benefits of the filler, any fiber-reinforced composite should ensure the efficient transfer of the stresses between the hosting matrix and the reinforcing material. To ensure this condition, two requirements should be met: (a) the fibers should be uniformly dispersed in the matrix thus avoiding possible agglomeration of particles, through van der Waals forces, in the system, and (b) the fiber–matrix interface should be strong enough such as to avoid pull-out phenomena during service. The selection of chemicals that will ensure proper dispersion and bonding is complicated by the requirement to comply with the chemical system, i.e., not to interfere in a negative way with the hydration process. As a result, many of the well-known surfactants that have been used effectively to disperse CNTs in other systems have been discarded for use in concrete. While the actual protocol that will allow proper dispersion of CNT in the matrix and good bonding qualities is still the subject of intense research,

[4]The recent invention of graphene, an allotrope of carbon, might relegate CNT to second in rank.

some preliminary results have already been reported in the literature (Gay and Sanchez, 2010; Yazdanbakhsh *et al.*, 2010; Collins *et al.*, 2012). Approaches to disperse the fibers include their surface modification through functionalization usually in conjunction with sonication (Cwirzen *et al.*, 2008). Surface treatment with ozone gas (Chung, 2005), sulphuric and nitric acids (Li *et al.*, 2005), use of gum Arabic (Sáez de Ibarra *et al.*, 2006), polyacrylic acid and polyallylamine hydrochloride (Grunlan *et al.*, 2008), growing CNTs on cement particles (Nasibulin *et al.*, 2009; Nasibulina *et al.*, 2010) and polymer grafting on CNT (Li *et al.*, 2005) have also been suggested.

Admixtures that are commonly used in cementitious materials have also been tested with the polycarboxylate and lignosulfate to show good results (Collins *et al.*, 2012). Cwirzen *et al.* (2008) demonstrated that stable and homogeneous water dispersions of MWCNTs can be obtained by using functionalized CNTs with COOH and additional treatment with polyacrylic acid polymers. The mixing method included stirring combined with sonication at 50 Hz. The cement paste specimens produced revealed an increase in compressive strength values in comparison with the reference pure cement paste specimens. The highest increase in the compressive strength was nearly 50% in cement paste incorporating only 0.045% of the polyacrylic acid polymer-treated MWCNTs. These results indicate the existence of chemical bonds between the OH groups and probably the C-S-H phase of the cement matrix which enabled the stress transfer.

The quality of the interface characteristics is an even more complicated field and is still in its infancy. CNTs have been treated using a H_2SO_4/HNO_3 mixture solution which potentially leads to the formation of carboxyl acid groups on their surfaces (Li *et al.*, 2005). The presence of carboxylic acid groups enhances the interface efficiency through a series of chemical reactions. In general, when properly dispersed and well bonded, CNTs enhance compressive, tensile, and flexural performance by creating bridging mechanisms between the fibers and matrix, thus capturing microcracks and causing more material to go into plastic deformation prior to failure. Furthermore, there appears to be a densification of the C-S-H matrix. Through nanoindentation experiments, it has been suggested that CNT promote the formation of the HD C-S-H (Shah *et al.*, 2009). The CNT can potentially be employed in any cement-based material ranging from fly-ash mix (Chaipanich *et al.*, 2010) to ultra high performance composites (Sáez de Ibarra *et al.*, 2006). Finally the exploitation of CNTs in the matrix for monitoring and sensing properties is currently under investigation (Wansom *et al.*, 2006; Li *et al.*, 2007; Han *et al.*, 2011).

Titanium dioxide

Titanium dioxide nanoparticles in the form of anatase have received considerable attention in the construction industry in recent years due to their

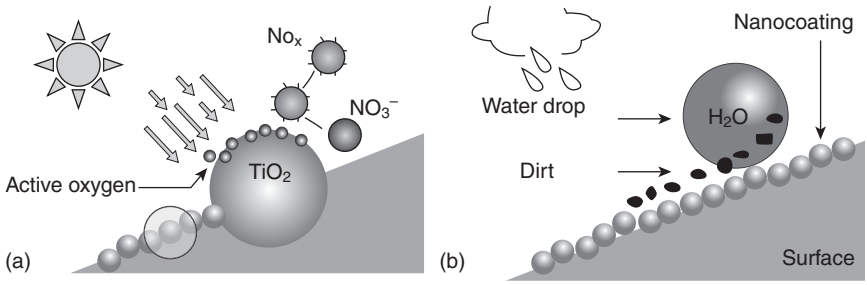

2.7 (a) Photocatalytic and (b) self-cleaning mechanisms of TiO_2 nanocomposites.

potential to add new functionalities to infrastructures, i.e., self-cleaning properties and the ability to remove air pollutants through photocatalysis (Fig. 2.7). TiO_2 are semiconductors that behave as photocatalysts when irradiated by ultraviolet (UV) light in the presence of gas or liquid (Serpone and Pelizzetti, 1989). When mixed with cement, it can photocatalytically degrade organic pollutants that are, after neutralization, washed away through the hydrophilic nature of the surface, maintaining at the same time the aesthetic characteristics of concrete structures, particularly those constructed with white cement (Cassar, 2004; Ruot *et al.*, 2009). TiO_2 has proven very efficient in the removal of pollutants such as NOx, aromatics, aldehydes, and ammonia, and currently finds applications in various infrastructure projects like pavements, tunnels, buildings, etc. (Guerrini, 2012). A more detailed exposition of photocatalytic applications is provided in a separate chapter of this book.

Cement-polymer nanocomposites

While considerable research effort has been devoted to the study of organic composites with small amounts of inorganic reinforcements, like polymer-clay systems, little is known about the consequences of adding small amounts of organic material in an inorganic matrix, like the C-S-H/polymer system. This approach constitutes a rather recent and alternative route for concrete nanocomposites which stems from biomimicry approaches (synthesis of composites from aqueous routes like many natural biocomposites, e.g., tooth, bone, and shells) and relates to the attempt to modify the nanoscale C-S-H material through organic hybridization (Matsuyama and Young, 1999a,b; Minet *et al.*, 2006, Franceschini *et al.*, 2007; Alizadeh *et al.*, 2011; Fan *et al.*, 2012). The process, which has been verified computationally (Pellenq *et al.*, 2008), involves grafting organic moieties on the silica layers through controlled hydrolysis of organo-silane precursor mixtures or by hydration of anhydrous silicates in silanized polymer solutions. Additional benefits are expected when the organic molecules intercalate the interlayer

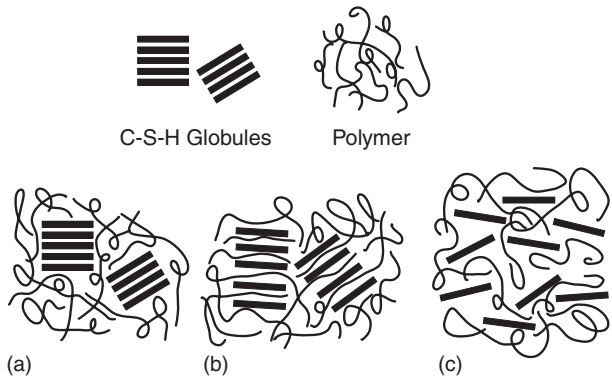

2.8 Schematic representation of the potential microstructures of C-S-H/polymer composites, analogous to clay/polymer composites: (a) conventional nanocomposites, (b) intercalated nanocomposites, (c) exfoliated nanocomposites.

C-S-H spaces (Fig. 2.8). The real breakthrough, however, is expected when (and if) an exfoliation of the C-S-H layer is achieved within the organic matrix. The actual chemistries and processing conditions involved are the topic of extreme importance for cement chemists. Recently, a few promising articles have presented experimental data on organic–inorganic hybrid composites that have been synthesized through the sol-gel method. Intercalations has been reported for specific polymers and C-S-H stoichiometric conditions suggesting that the initial chemistry of the inorganic material can act as a template for material tuning. The degree of modification of properties and actual structures involved remains to be quantified.

2.4 Conclusion

Over the last decade, the scientific community has witnessed rapid progress on available experimental, theoretical, and technological developments that allow revisiting this ubiquitous material and examining its environmental footprint. We have presented in this chapter some recent developments in the field of concrete science and engineering which provide a refined understanding, especially of the nanostructure that is responsible for what we experience in the macroscopic world of engineering applications, and allow us to devise methodologies for a stronger, more durable, and environmentally friendly material. While a lot has been achieved so far, even more has to be contributed until a sustainable and ecological, friendly construction material is developed. The necessary tools are being developed which makes us optimistic for the future. It is hoped that the construction industry

will invest in a scientific approach in order to utilize (or even invent) new technologies so as to lead concrete into a sustainable future.

2.5 References

Alcorn, A., 2003. Embodied energy and CO_2 coefficients for NZ building materials, Centre for Building Performance Research Report, Victoria University of Wellington, New Zealand.

Ali, M.B., Saidur, R. and Hossain, M.S., 2011. A review on emission analysis in cement industries. *Renewable and Sustainable Energy Reviews*, 15(5), 2252–2261.

Alizadeh, R., Beaudoin, J.J., Raki, L. and Terskikh, V., 2011. C-S-H/polyaniline nanocomposites prepared by *in situ* polymerization. *Journal of Materials Science*, 46(2), 460–467.

Allen, A.J., 1991. Time-resolved phenomena in cements, clays and porous rocks. *Journal of Applied Crystallography*, 24(5), 624–634.

Allen, A.J. and Thomas, J.J., 2007. Analysis of C-S-H gel and cement paste by small-angle neutron scattering. *Cement and Concrete Research*, 37(3), 319–324.

Allen, A.J., Windsor, C.G., Rainey, V.S., Pearson, D., Double, D.D. and Alfor, N.McN., 1982. A small-angle scattering study of cement porosities. *Journal of Physics D: Applied Physics*, 15(9), 1817–1833.

Allen, A.J., Oberthur, R.C., Pearson, D., Schofield, P. and Wilding, C.R., 1987. Development of the fine porosity and gel structure of hydrating cement systems. *Philosophical Magazine Part B*, 56(3), 263–288.

Allen, A.J., Thomas, J.J. and Jennings, M.H., 2007. Composition and density of nano scale calcium silicate hydrate in cement. *Nature Materials*, 35(6), 311–316.

Beddoe R.E. and Lang, K., 1994. Effect of moisture on fractal dimension and specific surface of hardened cement paste by small-angle X-ray-scattering. *Cement and Concrete Research*, 24(4), 605–612.

Bentz, D.P. and Aitcin, P.C., 2008. Hidden meaning of water-cement ratio. *Concrete International*, 30(5), 51–54.

Binnig, G.K., Quate, C.F. and Gerber, Ch., 1986. Atomic force microscope. *Physical Review Letters*, 56(9), 930–933.

Bjornstrom, J., Martinelli, A., Matic, A., Borjesson, L. and Panas, I., 2004. Accelerating effects of colloidal nano-silica for beneficial calcium-silicate-hydrate formation in cement. *Chemical Physics Letters*, 392(1–3), 242–248.

Black, L., Purnell, P. and Hill, J., 2010. Current themes in cement research. *Advances in Applied Ceramics*, 109(5), 253–259.

Cassar, L., 2004. Photocatalysis of cementitious materials: clean buildings and clean air. *MRS Bulletin*, 29(5), 328–331.

Chaipanich, A., Nochaiya, T., Wongkeo, W. and Torkittikul, P., 2010. Compressive strength and microstructure of carbon nanotubes–fly ash cement composites. *Materials Science and Engineering: A*, 527(4–5), 1063–1067.

Chen, J.J., Sorelli, L., Vandamme, M., Ulm, F.-J. and Chanvillard, G., 2010. A coupled nanoindentation/SEM-EDS study on low water/cement ratio Portland cement paste: evidence for C-S-H/$Ca(OH)_2$ nanocomposites. *Journal of the American Ceramic Society*, 93(5), 1484–1493.

Choolaei, M., Rashidi, A.M., Ardjmand, M., Yadegari, A. and Soltanian, H., 2012. The effect of nanosilica on the physical properties of oil well cement. *Materials Science and Engineering: A*, 538, 288–294.

Chung, D.D., 2005. Dispersion of short fibers in cement. *Journal of Materials in Civil Engineering*, 17(4), 379–383.

Churakov, S.V., 2008. Hydrogen bond connectivity in Jennite from *ab initio* simulations. *Cement and Concrete Research*, 38(12), 1359–1364.

Churakov S.V., 2009. Structure of the interlay in normal 11A Tobermorite from *ab initio* study. *European Journal of Mineralogy*, 21(1), 261–271.

Collins, F., Lambert, J. and Duan, W.H., 2012. The influences of admixtures on the dispersion, workability, and strength of carbon nanotube-OPC paste mixtures. *Cement and Concrete Composites*, 34(2), 201–207.

Cong, X.D. and Kirkpatrick, R.J., 1996. Si-29 MAS NMR study of the structure of calcium silicate hydrate. *Advanced Cement Based Materials*, 3(3–4), 144–156.

Constantinides, G., 2006. Invariant mechanical properties of calcium silicate hydrates (C-S-H) in cement-based materials: instrumented nanoindentation and microporomechanical modeling. PhD Thesis, MIT.

Constantinides, G. and Ulm, F.-J., 2004. The effect of two types of C-S-H on the elasticity of cement-based materials: results from nanoindentation and micromechanical modeling. *Cement and Concrete Research*, 34(1), 67–80.

Constantinides, G. and Ulm, F.-J., 2007. The nanogranular nature of C-S-H. *Journal of the Mechanics and Physics of Solids*, 55(1), 64–90.

Constantinides, G., Ulm, F.-J. and van Vliet, K.J., 2003. On the use of nanoindentation for cementitious materials. *Materials and Structures*, 36(205), 191–196.

Constantinides, G., Ravichandran, K.S., Ulm F.-J. and van Vliet, K.J., 2006. Grid indentation analysis of composite microstructure and mechanics: Principles and validation. *Materials Science and Engineering: A*, 430(1–2), 189–202.

Cwirzen, A., Habermehl-Cwirzen, K. and Penttala, V., 2008. Surface decoration of carbon nanotubes and mechanical properties of cement/carbon nanotube composites. *Advances in Cement Research*, 20(2), 65–73.

Damtoft, J.S., Lukasik, J., Herfort, D., Sorrentino, D. and Gartner, E.M., 2008. Sustainable development and climate change initiatives. *Cement and Concrete Research*, 38(2), 115–127.

DeJong, M.J. and Ulm, F.-J., 2007. The nanogranular behavior of C-S-H at elevated temperatures (up to 700 degrees C). *Cement and Concrete Research*, 37(1), 1–12.

Dormieux, L., Kondo, D. and Ulm F.-J., 2006. *Microporomechanics*. Wiley, New York.

Double, D.D. and Hellawell, A., 1976. The hydration of Portland cement. *Nature*, 261(10), 486–488.

Eichhorn, F., Haussler F. and Baumbach H., 1993. Structural studies on hydrating cement pastes. *Journal de Physique IV*, 03(C8), 369–372.

Fan, W., Stoffelbach, F., Rieger, J., Regnaud, L., Vichot, A., Bresson, B. and Lequeux, N., 2012. A new class of organosilane-modified polycarboxylate superplasticizers with low sulfate sensitivity. *Cement and Concrete Research*, 42(1), 166–172.

Feldman, R.F. and Sereda P.J., 1968. A model for hydrated Portland cement paste as deduced from sorption-length change and mechanical properties. *Materials and Structures*, 1(6), 509–520.

Finot, E., Lesniewska, E., Mutin, J.C. and Goudonnet, J.P., 1999. Investigations of surface forces between gypsum crystals in electrolytic solutions using microcantilevers. *Journal of Chemical Physics*, 111(14), 6590–6598.

Fisher-Cripps, A.C., 2011. *Nanoindentation*. Springer, New York.

Franceschini, A., Abramson, S., Mancini, V., Bresson, B., Chassenieux, C. and Lequeux, N., 2007. New covalent bonded polymer-calcium silicate hydrate composites. *Journal of Materials Chemistry*, 17(9), 913–922.

Ganneau, F.P., Constantinides, G. and Ulm F.-J., 2006. Dual-indentation technique for the assessment of strength properties of cohesive-frictional material. *International Journal of Solids and Structures*, 43(6), 1727–1745.

Garrault, S., Finot, E., Lesniewska, E. and Nonat, A, 2005. Study of C-S-H growth on C3S surface during its early hydration. *Materials and Structures*, 38(278), 435–442.

Gartner, E, 2004. Industrially interesting approaches to 'low-CO_2' cements. *Cement and Concrete Research*, 34(9), 1489–1498.

Gay, C. and Sanchez, F., 2010. Performance of carbon nanofiber-cement composites with a high-range water reducer. *Transportation Research Record*, 2142, 109–113.

Grunlan, C., Liu, L. and Regev, O., 2008. Weak polyelectrolyte control of carbon nanotube dispersion in water. *Journal of Colloid and Interface Science*, 317(1), 346–349.

Guerrini, G.L., 2012. Photocatalytic performances in a city tunnel in Rome: NO(x) monitoring results. *Construction and Building Materials*, 27(1), 165–175.

Hain, M. and Wriggers, P., 2008. Numerical homogenization of hardened cement paste. *Computational Mechanics*, 42(2), 197–212.

Han, B., Yu, X. and Ou, J., 2011. Multifunctional and smart carbon nanotube reinforced cement-based materials. In Gopalakrishnan, K., Birgisson, B., Taylor, P. and Attoh-Okine, N.O. (eds), *Nanotechnology in Civil Infrastructure*, Springer, Berlin, pp. 1–47.

Hewlett, P. (ed.), 2004. *Lea's Chemistry of Cement and Concrete*, 4th ed, Butterworth-Heinemann, London.

Jennings, H.M., 2000. A model for the microstructure of calcium silicate hydrate in cement paste. *Cement and Concrete Research*, 30(1), 101–116.

Jennings, M.H., 2008. Refinements to colloid model of C-SH in cement: CM-II. *Cement and Concrete Research*, 38(2), 275–289.

Jennings, M.H. and Bullard, J.W., 2011. From electrons to infrastructure: engineering concrete from the bottom up. *Cement and Concrete Research*, 41(7), 727–735.

Jennings, H.M., Gevrenov, J.S., Thomas, J.J., Constantinides, G. and Ulm, F.-J., 2007. A multi-technique investigation of the nanoporosity of cement paste. *Cement and Concrete Research*, 37(3), 329–336.

Jo, B.W., Kim, C.H., Tae, G.H. and Park, J.B., 2007. Characteristics of cement mortar with nano-SiO_2 particles. *Construction and Building Materials*, 21(6), 1351–1355.

Juenger, M.C.G, Winnefeld, F., Provis, J.L. and Ideker, J.H., 2011. Advances in alternative cementitious binders. *Cement and Concrete Research*, 41(12), 1232–1243.

Kalinichev, A.G. and Kirkpatrick, R.J., 2002. Molecular dynamics modeling of chloride binding to the surfaces of calcium hydroxide, hydrated calcium aluminate, and calcium silicate phases. *Chemistry of Materials*, 14(8), 3539–3549.

Kalinichev, A.G., Wang, J.W. and Kirkpatrick, R.J., 2007. Molecular dynamics modeling of the structure, dynamics and energetics of mineral–water interfaces: application to cement materials. *Cement and Concrete Research*, 37(3), 337–347.

Kelly, T.D. and van Oss, H.G., 2010. *Cement Statistics*, US Geological Survey, Reston, VA.

Konsta-Gdoutos, M.S., Metaxa, Z.S. and Shah, S.P., 2010a. Highly dispersed carbon nanotube reinforced cement based materials. *Cement and Concrete Research*, 40(7), 1052–1059.

Konsta-Gdoutos, MS, Metaxa, ZS and Shah, SP, 2010b. Multi-scale mechanical and fracture characteristics and early-age strain capacity of high performance carbon nanotube/cement nanocomposites. *Cement and Concrete Composites*, 32(2), 110–115.

Kumar, S., Kolay, P., Malla, S. and Mishra, S., 2012. Effect of multiwalled carbon nanotubes on mechanical strength of cement paste. *Journal of Materials in Civil Engineering*, 24(1), 84–91.

Lesko, S.I., Lesniewska, E., Nonat, A. and Mutin, J.C., 2001. Investigation by atomic force microscopy of forces at the origin of cement cohesion. *Ultramicroscopy*, 86(1), 11–16.

Li, G.Y., Wang, P.M. and Zhao, X., 2005. Mechanical behaviour and microstructure of cement composites incorporating surface-treated multi-walled carbon nanotubes. *Carbon*, 43(6), 1239–1245.

Li, G.Y., Wang, P.M. and Zhao, X., 2007. Pressure-sensitive properties and microstructure of carbon nanotube reinforced cement composites. *Cement and Concrete Composites*, 29(5), 377–382.

Lin, Q., Xu, Z.Z., Lan, X.H., Ni, Y.R. and Lu, C., 2011. The reactivity of nano silica with calcium hydroxide. *Journal of Biomedical Materials Research Part B: Applied Biomaterials*, 99B(2), 239–246.

Makar, J.M. and Beaudoin, J.J., 2004. Carbon nanotubes and their application in the construction industry. In Bartos, P.J.M., Hughes, J.J., Trtik, P. and Zhu, W. (eds), *Nanotechnology in Construction*. Royal Society of Chemistry, Cambridge, pp. 331–341.

Makar, J., Margeson, J. and Luh, J., 2005. Carbon nanotube/cement composites – Early results and potential applications. *Proceedings of the 3rd International Conference on Construction Materials: Performance, Innovations and Structural Implications*, Vancouver, BC, August 22–24, pp. 1–10.

Mann, S., 2006. *Nanoforum report on Nanotechnology and Construction*. Available at: www.nanoforum.org/dateien/temp/Nanotech and Construction Nanoforum report.pdf?09052012123958 (accessed November 2012).

Manzano, H., Dolado, J.S. and Ayuela, A., 2006. On the formation of cementitious C-S-H nanoparticles. *Journal of Computer Aided Material Design*, 14(1), 45–51.

Manzano, H., Dolado, J.S., Guerrero, A. and Ayuela, A., 2007. Mechanical properties of crystalline calcium-silicate-hydrates: comparison with cementitious C-S-H gels. *Physica Status Solidi A*, 204(6), 1775–1780.

Manzano, H., Dolado, J.S. and Ayuela, A., 2009. Elastic properties of the main species present in Portland cement pastes. *Acta Materialia*, 57(5), 1666–1674.

Manzano H., Durgun E., Abdulhosseine Quomi M.J., Ulm, F.-J., Pellenq, R. and Grossman, J., 2011. Impact of the chemical impurities on the crystalline cement

clinker phases determined by atomistic simulations. *Crystal Growth and Design*, 11(7), 2964–2979.

Manzur, T. and Yazdani, N., 2010. Strength enhancement of cement mortar with carbon nanotubes: early results and potential. *Transportation Research Record*, 2142(2), 102–108.

Matsuyama, H. and Young, J.F., 1999a. Intercalation of polymers in calcium silicate hydrate: a new synthetic approach to biocomposites? *Chemistry of Materials*, 11(1), 16–19.

Matsuyama, H. and Young, J.F., 1999b. Synthesis of calcium silicate hydrate/polymer complexes: Part II. Cationic polymers and complex formation with different polymers. *Journal of Materials Research*, 14(8), 3389–3396.

Mehta, P.K., 2009. Global concrete industry sustainability. *Concrete International*, 32(2), 45–48.

Mehta, P.K. and Monteiro P.J.M., 2006. *Concrete: Microstructure, Properties and Materials*, 3rd edn. McGraw-Hill, Maidenhead.

Meng, T., Qian, K.L., Qian, X.Q. and Zhan, S.L., 2008. Effect of the nano-$CaCO_3$ on hydrated properties and interface of cement paste. *Rare Metal Materials and Engineering*, 37(2), 667–669.

Metaxa, Z.S., Konsta-Gdoutos, M.S. and Shah, S.P., 2010. Carbon nanofiber-reinforced cement-based materials. *Transportation Research Record*, 2142, 114–118.

Miller, M., Bobko, C., Vandamme, M. and Ulm, F.-J., 2008. Surface roughness criteria for cement paste nanoindentation. *Cement and Concrete Research*, 38(4), 467–476.

Minet, J., Abramson, S., Bresson, B., Franceschini, A., Van Damme, H. and Lequeux, N., 2006. Organic calcium silicate hydrate hybrids: a new approach to cement based nanocomposites. *Journal of Materials Chemistry*, 16(14), 1379–1383.

Mitchell, L.D., Prica, M. and Birchall, J.D., 1996. Aspects of Portland cement hydration studied using atomic force microscopy. *Journal of Materials Science*, 31(16), 4207–4212.

Mondal, P., Shah, S.P. and Marks, L., 2007. A reliable technique to determine the local mechanical properties at the nanoscale for cementitious materials. *Cement and Concrete Research*, 37(10), 1440–1444.

Mondal, P., Shah, S.R. and Marks, L.D., 2008. Nanoscale characterization of cementitious materials. *ACI Materials Journal*, 105(2), 174–179.

Nasibulin, A.G., Shandakov, S.D., Nasibulina, L.I., Cwirzen, A., Mudimela, P.R., Habermehl-Cwirzen, K., Grishin, D.A., Gavrilov, Y.V., Malm, J.E.M., Tapper, U., Tian, Y., Penttala, V., Karppinen, M.J. and Kauppinen, E.I., 2009. A novel cement-based hybrid material. *New Journal of Physics*, 11, 023013.

Nasibulina L.I., Koltsova, T.S., Joentakanen, T., Nasibulin, A.G., Tolochko, O.V., Malm, J.E.M., Karppinen, M.J. and Kauppinen, E.I., 2010. Direct synthesis of carbon nanofibers on cement particles. *Transportation Research Record*, 2142, 96–101.

Nazari, A. and Riahi, S., 2011. The effects of SiO_2 nanoparticles on physical and mechanical properties of high strength compacting concrete. *Composites Part B: Engineering*, 42(3), 570–578.

Nemecek, J., Smilauer, V. and Kopecky, L., 2010. Nanoindentation characteristics of alkali-activated aluminosilicate materials. *Cement and Concrete Composites*, 33(2), 163–170.

Nonat, A., 2004. The structure and stoichiometry of C-S-H. *Cement and Concrete Research*, 34(8), 1521–1528.

Oliver, W.C. and Pharr, G.M., 1992. An improved technique for determining hardness and elastic modulus using load and displacement sensing indentation experiments. *Journal of Materials Research*, 7(6), 1564–1583.

Oliver, W.C. and Pharr, G.M., 2004. Measurement of hardness and elastic modulus by instrumented indentation: advances in understanding and refinements to methodology. *Journal of Materials Research*, 19(1), 3–20.

Pacheco-Torgal, F. and Jalali, S., 2011. Nanotechnology: advantages and drawbacks in the field of construction and building materials. *Construction and Building Materials*, 25(2), 582–590.

Pellenq, R.J.-M., Lequeux, N. and Van Damme, H., 2008. Engineering the bonding scheme in C-S-H: the iono-covalent framework. *Cement and Concrete Research*, 38(2), 159–174.

Pellenq, R.J.-M., Kushima, A., Shahsavari, R., Buehler, M.J., Van Vliet, K.J., Yip, S. and Ulm, F.-J., 2009. A realistic molecular model of cement hydrates. *Proceedings of the National Academy of Sciences of the United States of America*, 106(38), 16102–16107.

Phair, J.W., 2006. Green chemistry for sustainable cement production and use. *Green Chemistry*, 8(9), 763–780.

Pichler, B., Hellmich, C., 2011. Upscaling quasi-brittle strength of cement paste and mortar: a multi-scale engineering mechanics model. *Cement and Concrete Research*, 41(5), 467–476.

Pichler, B., Hellmich, C. and Eberhardsteiner, J., 2009. Spherical and acicular representation of hydrates in a micromechanical model for cement paste: prediction of early-age elasticity and strength. *Acta Mechanica*, 203(3–4), 137–162.

Plassard, C., Lesniewska, E., Pochard, I. and Nonat, A., 2004. Investigation of the surface structure and elastic properties of calcium silicate hydrates at the nanoscale. *Ultramicroscopy*, 100(3–4), 331–338.

Plassard, C., Lesniewska, E., Pochard, I. and Nonat, A., 2005. Nanoscale experimental investigation of particle interactions at the origin of the cohesion of cement. *Langmuir*, 21(16), 7263–7270.

Raki, L., Beaudoin, J., Alizadeh, R., Makar, J. and Sato, T., 2010. Cement and concrete nanoscience and nanotechnology. *Materials*, 3(2), 918–942.

Randall, N.X., Vandamme, M. and Ulm, F.-J., 2009. Nanoindentation analysis as a two-dimensional tool for mapping the mechanical properties of complex surfaces. *Journal of Materials Research,* 24(3), 679–690.

Richard, P. and Cheyrezy, M., 1995. Composition of reactive powder concretes. *Cement and Concrete Research* 25(7), 1501–1511.

Richardson, I.G., 2008. The calcium silicate hydrates. *Cement and Concrete Research* 38(1), 137–142.

Ruot, B., Plassais, A., Olive, F., Guillot, L. and Bonafous, L., 2009. TiO_2-containing cement pastes and mortars: measurements of the photocatalytic efficiency using a rhodamine B-based colourimetric test. *Solar Energy*, 83(10), 1794–1801.

Sáez de Ibarra, Y., Gaitero, J.J., Erkizia, E. and Campillo, I., 2006. Atomic force microscopy and nanoindentation of cement pastes with nanotube dispersions. *Physica Status Solidi (A)*, 203(6), 1076–1081.

Sakulich, A.R. and Li, V.C., 2011. Nanoscale characterization of engineered cementitious composites (ECC). *Cement and Concrete Research*, 41(2), 169–175.

Salvetat, J.-P., Bonard, J.-M., Thomson, N.H., Kulik, A.J., Forró L., Benoit, W. and Zuppiroli L., 1999. Mechanical properties of carbon nanotubes. *Applied Physics A*, 69(3), 255–260.

Sanahuja, J., Dormieux, L. and Chanvillard, G., 2007. Modelling elasticity of a hydrating cement paste. *Cement and Concrete Research*, 37(10), 1427–1439.

Sanchez, F. and Sobolev, K., 2010. Nanotechnology in concrete – a review. *Construction and Building Materials*, 24(11), 2060–2071.

Sato, T. and Beaudoin, J.J., 2011. Effect of nano-$CaCO_3$ on hydration of cement containing supplementary cementitious materials. *Advances in Cement Research*, 23(1), 33–43.

Sato, T. and Diallo, F., 2010. Seeding effect of Nano-$CaCO_3$ on the hydration of tricalcium silicate. *Transportation Research Record*, 2141, 61–67.

Scherer, G.W., 1999. Structure and properties of gels. *Cement and Concrete Research,* 29(6), 1149–1157.

Scrivener, K.L. and Kirkpatrick R.J., 2008. Innovation in use and research on cementitious materials. *Cement and Concrete Research*, 38(2), 128–136.

Senff, L., Labrinca, J.A., Ferreira, V.M., Hotza, D. and Repette, W.L., 2009. Effect of nano-silica on rheology and fresh properties of cement pastes and mortars. *Construction and Building Materials*, 23, 2487–2491.

Senff, L., Hotza, D., Repette, W.L., Ferreira, V.M. and Labrinca, J.A., 2010. Mortars with nano-SiO_2 and micro-SiO_2 investigated by experimental design. *Construction and Building Materials*, 24, 1432–1437.

Serpone, N., and Pelizzetti, E., 1989. *Photocatalysis: Fundamentals and Applications*. Wiley, NewYork.

Shah, S.P., Konsta-Gdoutos, M.S., Metaxa, Z.S. and Mondal, P., 2009. Nanoscale modification of cementitious materials. *Nanotechnology in Construction 3*, Part 2, 125–130.

Shahsavari, R., Buehler, M.J., Pellenq, R.J.M. and Ulm, F.-J., 2009. First-principles study of elastic constants and interlayer interactions of complex hydrated oxides: case study of Tobermorite and Jennite. *Journal of the American Ceramic Society*, 92(10), 2323–2330.

Shahsavari, R., Pellenq, R.J.M. and Ulm, F.-J., 2011. Empirical force fields for complex hydrated calcio-silicate layered materials. *Physical Chemistry Chemical Physics*, 13(3), 1002–1011.

Smilauer, V. and Bazant, Z.P., 2010. Identification of viscoelastic C-S-H behavior in mature cement paste by FFT-based homogenization method. *Cement and Concrete Research*, 40(2), 197–207.

Song, D., Yao, W., Liang, K. and He, L., 2011. Nanoindentation characterization of calcium-silicate-hydrate with different curing conditions. *Advanced Materials Research*, 177, 613–616.

Sorelli, L., Constantinides, G., Ulm, F.-J. and Toutlemonde, F., 2008. The nanomechanical signature of ultra high performance concrete by statistical nanoindentation techniques. *Cement and Concrete Research*, 38, 1447–1456.

Taylor, H.F.W., 1990. *Cement Chemistry*, Academic Press, London.

Taylor, H.F.W., 1993. Nano scale microstructure of C-S-H: current status. *Advanced Cement Materials*, 1(1), 38–46.

Tennis, P.D. and Jennings, H.M., 2000. A model for two types of C-S-H in the microstructure of Portland cement pastes. *Cement and Concrete Research*, 30(6), 855–863.

Torquato, S., 2001. *Random Heterogeneous Materials*. Springer, Berlin.

Tregger, N., Pakula, M. and Shah, S.P., 2010a. Influence of micro- and nanoclays on fresh state of concrete. *Transportation Research Record*, 2141, 68–74.

Tregger, N., Pakula, M. and Shah, S.P., 2010b. Influence of clays on the rheology of cement paste. *Cement and Concrete Research*, 40(3), 384–391.

Trtik, P., Münch, B. and Lura, P., 2009. A critical examination of nanoindentation on model materials and hardened cement pastes based on virtual experiments. *Cement and Concrete Composites*, 31(10), 705–714.

Ulm, F.-J., Constantinides, G. and Heukamp, F.H., 2004. Is concrete a poro-mechanics material? A multi-scale investigation of poro-elastic properties. *Materials and Structures*, 37(1), 43–58.

Ulm, F.-J., Delafargue, A. and Constantinides, G., 2005. Experimental microporomechanics. In Dormieux, L. and Ulm, F.-J. (eds), *Applied Microporomechanics of Porous Materials*, CISM Lecture notes no 580, Springer Wien, New York.

Ulm, F.-J., Vandamme, M., Bobko, C. and Ortega, J.A., 2007. Statistical indentation techniques for hydrated nanocomposites: concrete, bone, and shale. *Journal of the American Ceramic Society*, 90(9), 2677–2692.

Ulm, F.-J., Vandamme, M., Jennings, H., Vanzo, J., Bentivegna, M., Krakowiak, K., Constantinides, G., Bobko, C. and Van Vliet, K., 2010. Does microstructure matter for statistical nanoindentation techniques? *Cement and Concrete Composites,* 32(1), 92–99.

Vandamme, M. and Ulm, F.-J., 2009. Nanogranular origin of concrete creep. *Proceedings of the National Academy of Sciences of the United States of America*, 106(26), 10552–10557.

Vandamme, M., Ulm, F.-J. and Fonollosa, P., 2010. Nanogranular packing of C-S-H at substochiometric conditions. *Cement and Concrete Research*, 40(1), 14–26.

Volkl, J.J., Beddoe, R.E. and Setzer, M.J., 1987. The specific surface of hardened cement paste by small-angle X-ray-scattering – effect of moisture-content and chlorides. *Cement and Concrete Research*. 17(1), 81–88.

Wang, X.H., Jacobsen, S., He, J.Y., Zhang, Z.L., Lee, S.F. and Lein, H.L., 2009. Application of nanoindentation testing to study of the interfacial transition zone in steel fiber reinforced mortar. *Cement and Concrete Research*, 39(8), 701–715.

Wansom, S., Kidner, N.J., Woo, L.Y. and Mason, T.O. 2006. AC-impedance response of multi-walled carbon nanotube/cement composites. *Cement and Concrete Composites*, 28(6), 509–519.

Weiguo, S., Gejin, G., Rui, D., Yu, T., Hu, C. and Liqi, X., 2011. Fabrication and characterization of nano colloid surfaced concrete. *Materials and Structures*, 44(9), 1559–1564.

Wille K. and Loh, K.J., 2010. Nanoengineering ultra-high-performance concrete with multiwalled carbon nanotubes. *Transportation Research Record*, 2142, 119–126.

Winslow, D.N. and Diamond, S., 1974. Specific surface of hardened cement paste as determined by small-angle X-ray scattering. *Journal of the American Ceramic Society*, 57(5), 193–197.

Winslow, D.N., Bukowski, J.M. and Young, J.F., 1994. The early evolution of the surface of hydrating cement. *Cement and Concrete Research*, 24(6), 1025–1032.

Winslow, D., Bukowski, J.M. and Young, J.F., 1995. The fractal arrangement of hydrated cement paste. *Cement and Concrete Research*, 25(1), 147–156.

Worrell, E., Price, L., Martin, N., Hendriks, C. and Meida, L.O., 2001. Carbon dioxide emissions from the global cement industry. *Annual Review of Energy and the Environment*, 26, 303–329.

Xu, J. and Yao, W., 2011. Nano-scratch as a new tool for assessing the nano-tribological behavior of cement composite. *Materials and Structures*, 44(9), 1703–1711.

Xu, S.Y., Simmons, G.C., Mahadevan, T.S., Scherer, G.W., Garofalini, S.H. and Pacheco, C., 2009. Transport of water in small pores. *Langmuir*, 25(9), 5084–5090.

Yang, T., Keller, B., Magyari, E., Hametner, K. and Gunther, D., 2003. Direct observation of the carbonation process on the surface of calcium hydroxide crystals in hardened cement paste using an atomic force microscope. *Journal of Materials Science*, 38(9), 1909–1916.

Yazdanbakhsh, A., Grasley, Z., Tyson, B. and Al-Rub, R.K.A., 2010. Distribution of carbon nanofibers and nanotubes in cementitious composites. *Transportation Research Record*, 2142, 89–95.

Ye, Q., Zhang, Z.N., Kong, D.Y. and Chen, R.S., 2007. Influence of nano-SiO_2 addition on properties of hardened cement paste as compared with silica fume. *Construction and Building Materials*, 21(3), 539–545.

Zhang, M.H. and Li, H., 2011. Pore structure and chloride permeability of concrete containing nano-particles for pavement. *Construction and Building Materials*, 25(2), 608–616.

Zyganitidis, I., Stefanidou, M., Kalfagiannis, N. and Logothetidis, S., 2011. Nanomechanical characterization of cement-based pastes enriched with SiO_2 nanoparticles. *Materials Science and Engineering: B*, 176(19), 1580–1584.

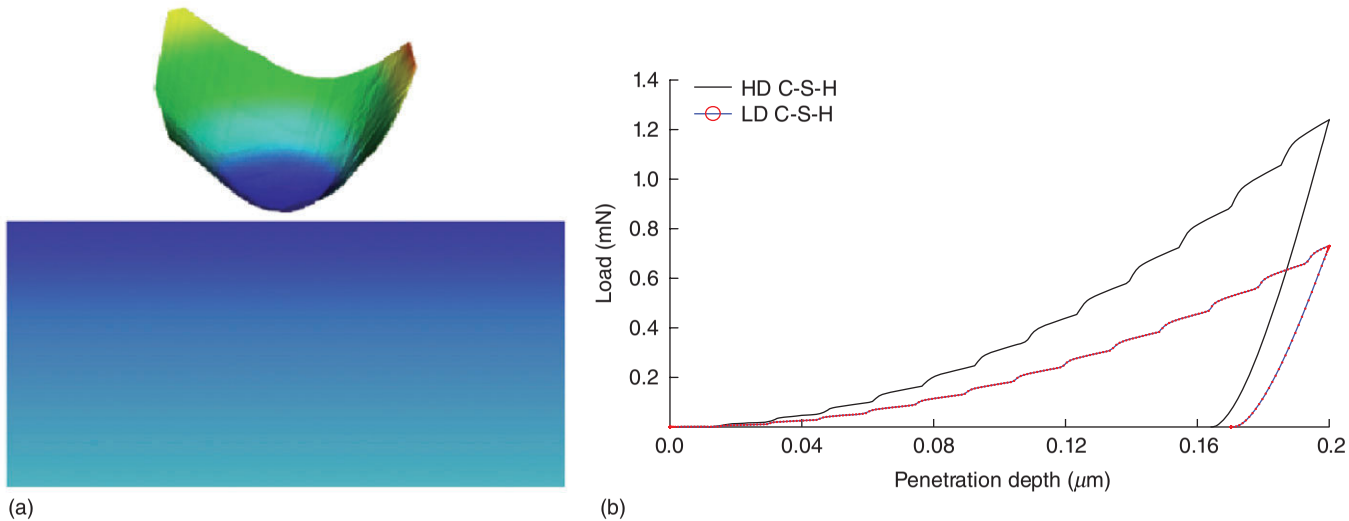

Plate I (a) Nanoindentation principle: a diamond nanoindenter is brought in contact with the material of interest and the force (*P*) and penetration depth (*h*) are monitored continuously. (b) Typical *P-h* curves for a low-density (LD) and a high-density (HD) version of C-S-H. Results are from finite element simulations.

3

Nanoparticles for high performance concrete (HPC)

F. PACHECO-TORGAL, University of Minho, Portugal, S. MIRALDO, University of Aveiro, Portugal, Y. DING, Dalian University of Technology, China and J. A. LABRINCHA, University of Aveiro & CICECO, Portugal

DOI: 10.1533/9780857098832.1.38

Abstract: According to the 2011 ERMCO statistics, only 11% of the production of ready-mixed concrete relates to the high performance concrete (HPC) target. This percentage has remained unchanged since at least 2001 and appears a strange choice on the part of the construction industry, as HPC offers several advantages over normal-strength concrete, specifically those of high strength and durability. It allows for concrete structures requiring less steel reinforcement and offers a longer serviceable life, both of which are crucial issues in the eco-efficiency of construction materials. Despite the growing importance of nanotechnology, investigations into the incorporation of nanoparticles into concrete are rare (100 out of 10,000 Scopus concrete-related articles published in the last decade). It therefore remains to be seen how research in this area will contribute to concrete eco-efficiency. This chapter summarizes the state of current knowledge in the field and considers the influence of nanoparticles on the mechanical properties of concrete and its durability. It also includes the control of calcium leaching. The problem of efficient dispersion of nanoparticles is analyzed.

Key words: Portland cement, nanoparticles, calcium leaching, concrete durability, high performance concrete (HPC).

3.1 Introduction

Concrete is the most widely used of all construction materials. Its production currently stands at around 10 km^3/year (Gartner and Macphee, 2011). For purposes of comparison, the amount of fired clay, timber, and steel used annually is around 2, 1.3 km^3 and 0.1 km^3, respectively (Flatt *et al.*, 2012). Portland cement, which acts as the main binder in concrete, represents almost 80% of the total CO_2 emissions associated with concrete, which contribute 6–7% of the planet's total CO_2 emissions (Shi *et al.*, 2011; Pacheco-Torgal *et al.*, 2012). This is of particular concern in the context of climate change.

The demand for Portland cement is expected to increase by almost 200% over 2010 levels by 2050, reaching 6,000 million tons per year. According

to the ERMCO 2011 statistics, ready-mixed concrete production lies essentially between C25/30 and C30/37. In addition, only 11% of the concrete production corresponds to the high performance concrete (HPC) strength class target. As ERMCO 2001 statistics showed a 10% figure for this type of concrete, it appears that high strength concrete demand has remained unchanged during the last decade. Normal strength concrete produces less durable structures which require frequent maintenance and conservation operations or even complete replacement, with the associated consumption of additional raw materials and energy. Many degraded concrete structures were built decades ago at a time when little attention was given to durability (Hollaway, 2011). It is not therefore surprising that worldwide concrete infrastructure rehabilitation costs are extremely high.

For example, in the USA, around 27% of all highway bridges are in need of repair or replacement. In addition, the cost of deterioration caused by deicing and sea salt is estimated at over US$150 billion (Davalos, 2012). In the European Union, nearly 84,000 reinforced and pre-stressed concrete bridges require maintenance, repair and strengthening. This results in an annual cost of £215 million, not including traffic management costs (Yan and Chouw, 2013). Beyond the durability problems caused by imperfect concrete placement and curing operations, the real problem with the durability of ordinary Portland cement concrete (OPC) is the intrinsic properties of the material which has a high degree of permeability. This allows the ingress of water and other aggressive elements, leading to carbonation and chloride ion attack, which ultimately result in corrosion (Bentur and Mitchell, 2008; Glasser *et al.*, 2008). The importance of durability for eco-efficiency in construction materials has been described by Mora (2007). The author stated that increasing concrete durability from 50 to 500 years would reduce its environmental impact by a factor of 10. It is also worth noting that according to Hegger *et al.* (1997), the increase of compressive strength in concrete would mean a reduction of as much as 50% in the use of reinforced steel. These are crucial issues in materials efficiency (Pacheco-Torgal and Jalali, 2011a; Allwood *et al.*, 2011), highlighting the need for investigation into the future production of concretes with high mechanical strength and high durability.

Nanotechnology involves study at the microcospic scale (1 nm= 1×10^{-9} m). Some estimates predict that products and services related to nanotechnology could reach 1,000,000 million euros per year beyond 2015 (Pacheco-Torgal and Jalali, 2011b). The use of nanoparticles to increase the strength and durability of cementitious composites was predicted by the report RILEM TC 197-NCM, 'Nanotechnology in construction materials' (Zhu *et al.*, 2004), as a research area with high nanotechnology potential. Since that time, several dozen papers have been published by the Society of Chemical Industry (SCI) in the field. However, the majority of these

publications were written by materials science investigators and were principally concerned with materials performance with a lesser focus on civil engineering short-term commercial applications. For instance, the 'bottom-up' multiscale modeling approach (Pellenq *et al.*, 2009), could be an excellent strategy which 'has been spectacularly successful in fields ranging from metallurgy to medicine' (Jennings and Bullard, 2011) but, unfortunately, relies on tools that 'require years of training and considerable computational expense to operate', neither of which are traditionally associated with the construction industry. The importance of the present review lies in the need to redirect future investigations in this field to a precise target capable of serving a clear short-term civil engineering goal.

3.2 Concrete with nanoparticles

Nanoparticles may be obtained either through high milling energy (Sobolev and Ferrada-Gutierrez, 2005) or by chemical synthesis (Lee and Kriven, 2005). They have a high surface area to volume ratio (Fig. 3.1) which provides high chemical reactivity. Most investigations use nano-silica (nano-SiO_2), and nano-titanium oxide (nano-TiO_2), while a few use nano-Fe_2O_3 (Sanchez and Sobolev, 2010).

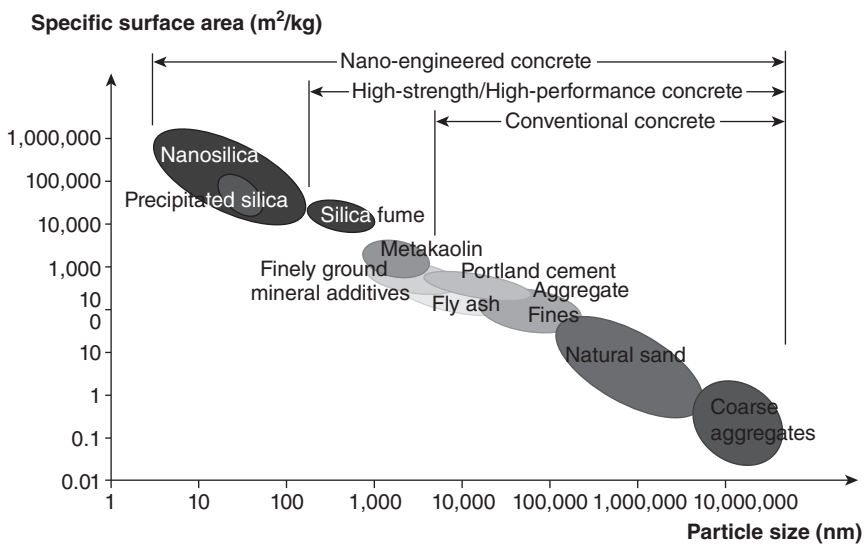

3.1 Particle size and specific surface area related to concrete materials (Sanchez and Sobolev, 2010).

3.2.1 Mechanical properties

Porro *et al.* (2005) refers to the use of nano-silica particles as increasing the compression strength of cement pastes. The same authors state that this phenomenon is not due to pozzolanic reaction, as the calcium hydroxide consumption is very low, but rather to the increase of silica compounds which contribute to a denser micro-structure.

According to Lin *et al.* (2008), the use of nano-silica on sludge/fly ash mortars, compensates for the negative effects associated with sludge incorporation in terms of the setting time and initial strength. Sobolev *et al.* (2008) reported that the addition of nano-silica produced an increase in strength of 15–20%. Other authors (Gaitero, 2008; Gaitero *et al.*, 2009) believe that nano-silica causes an increase in the C-S-H chain dimension and stiffness. Nasibulin *et al.* (2009) reported a twofold increase in strength. Chaipanich *et al.* (2010) records that 1% of carbon nano-fibers (by binder mass) can compensate for the strength reduction associated with the replacement of 20% fly ash. Konsta-Gdoutos *et al.* (2010a) also studied the effect of carbon nano-fibers on cement pastes (0.08% by binder mass) and observed an increase in strength.

Nazari and Riahi (2011a) used ZrO_2 nanoparticles with an average particle size of 15 nm and reported an improvement in the flexural strength of self-compacting concrete up to 4 wt%. Increasing the nanoparticle content caused a reduction in flexural strength because of the inadequate dispersion of nanoparticles within the concrete matrix. Givi *et al.* (2010) studied the effects of different particle sizes of nano-SiO_2 (15 and 80 nm) and reported that the optimal replacement level of nano-SiO_2 particles was gained at 1.0% and 1.5%, respectively. The effect of nanoparticle addition is threefold:

1. As the average diameter of C-S-H gel is approximately 10 nm, the nanoparticles fill the voids in the CHS structure, so producing a denser concrete.
2. The nanoparticles act as nucleation centers, contributing to the development of hydration in Portland cement.
3. Nanoparticles react with $Ca(OH)_2$ crystals and produce C-S-H gel. They also act as kernels in the cement paste which reduces the size of $Ca(OH)_2$ crystals.

3.2.2 Durability

Investigations carried out by Ji (2005) showed that concrete containing nano-silica particles has lower water permeability. This is due to the reduction of the amount of $Ca(OH)_2$ which produces a denser inter-facial transition zone (ITZ). A reduction of chloride ion permeability as a result of

using 1% of nanoparticles per cement mass was reported by He and Shi (2008). Li *et al.* (2006) showed that nanoparticles are more favorable to producing abrasion resistance in concrete than are polypropylene (PP) fibers. They also recorded that the abrasion resistance of concrete decreases with its nanoparticle content and that the abrasion resistance of concrete containing nano-TiO_2 is higher than that containing the same amount of nano-SiO_2. Chen and Lin (2009) used nano-silica particles to improve the performance of sludge/clay mixtures for tile production. The results show that nanoparticles improve the reduction of water absorption and lead to an increase in abrasion and impact strength. A reduction in water absorption was reported by Givi *et al.* (2011). Ozyildirim and Zegetosky (2010) used 4% nano-Fe_2O_3 per cement mass and reported a reduction in the permeability of the concrete. A reduction in permeability was also reported for concrete in which 45% Portland cement was replaced by GGBFS containing 4% nano-TiO_2 per cement mass (Khoshakhlagh *et al.*, 2012). Shekari and Razzaghi (2011) compared the mechanical performance and the durability of concretes containing 1.5% of distinct nanoparticles (nano-ZrO_2, nano-TiO_2, nano-Al_2O_3, nano-Fe_3O_4). They concluded that the nano-Al_2O_3 is the most effective, but offered no explanation for the finding.

Nazari and Riahi (2011b) studied the performance of concrete in which Portland cement was replaced by up to 2% nano-Al_2O_3, with an average particle size of 15 nm. They reported that the optimum level of nano-Al_2O_3 particle content was 1.0%. Jalal *et al.* (2012) showed that concretes containing 2% SiO_2 nanoparticles underperformed when compared to those prepared with a mixture of 2% SiO_2 nanoparticles with the addition of 10% micro-silica. This composition showed enhanced mechanical strength (Fig. 3.2) as well as improved durability. This was assessed by water absorption, capillary water absorption, Cl ion percentage and electric resistivity (Fig. 3.3). According to Zhang and Li (2011), the pore structure of concrete containing nano-TiO_2 is finer than that of concrete containing the same amount of nano-SiO_2. The resistance to chloride penetration of concretes containing nano-TiO_2 is higher than that of concretes containing the same amount of nano-SiO_2.

This is explained by the particle diameter of nano-SiO_2 being smaller than that of nano-TiO_2, and the specific surface area of nano-SiO_2 being much larger than that of nano-TiO_2. The water requirement of concrete containing nano-SiO_2 is therefore higher than that of concrete containing the same amount of nano-TiO_2. The authors also reported that the pore structure refinement increases with the content of nanoparticles (5% < 3% < 1%) while chloride penetration decreases (5% < 3% < 1%). These results partially confirm those previously obtained by Li *et al.* (2006). In their view, the increased content of nanoparticles weakens the refinement of the pore structure of concrete. This may be attributed to the reduction of the distance

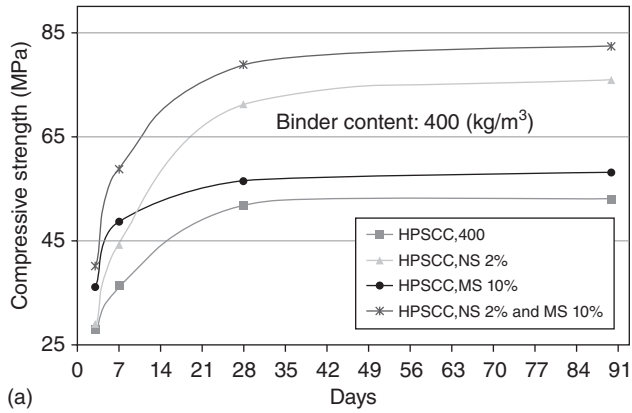

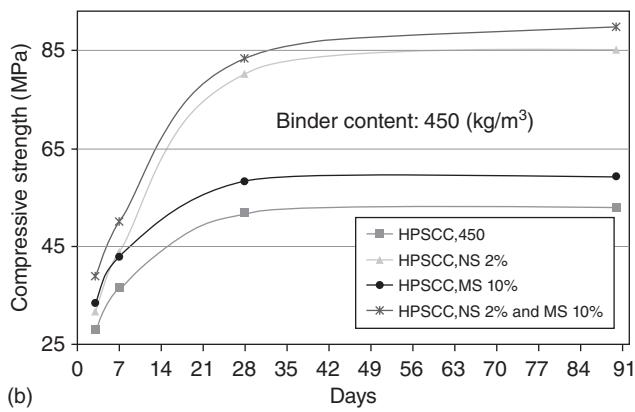

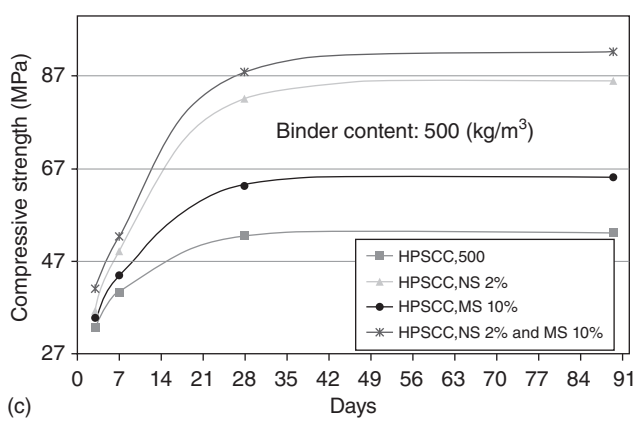

3.2 Compressive strength of HPSCC samples with binder contents of (a) 400, (b) 450, and (c) 500 (Nazari and Riahi, 2011b).

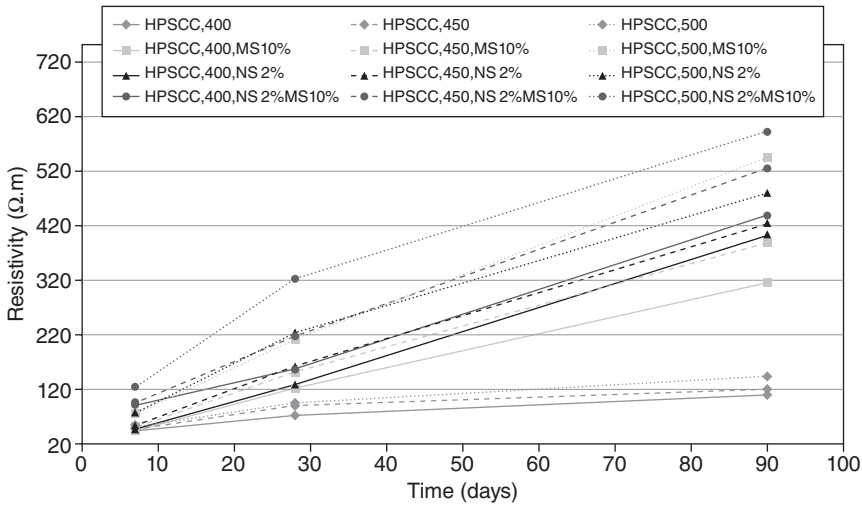

3.3 Resistivity versus time for different mixtures (Nazari and Riahi, 2011b).

between nanoparticles existing in higher concentration, so limiting the formation and growth of $Ca(OH)_2$ crystals due to space limitations. In this situation, the ratio of crystals to C–S–H gel is reduced and the shrinkage and creep of the cement matrix tend to increase. In consequence, the pore structure of the cement matrix is relatively more coarse (Zhang and Li, 2011).

3.2.3 Control of calcium leaching

High durability concrete requires the reduction of calcium leaching. This degradation process consists of a progressive dissolution of the cement paste caused by the migration of calcium atoms to the aggressive solution. Cement paste phases have different rates of degradation. While Portlandite dissolves completely in an aggressive solution, C-S-H gel undergoes only a slight increase in porosity (Carde *et al.*, 1996; Kamali *et al.*, 2003; Haga *et al.*, 2005; Gaitero *et al.*, 2012). Calcium leaching is responsible for an increase in concrete porosity and consequently in increased permeability. This allows water and other aggressive elements to enter the concrete which causes carbonation and corrosion problems. Gaitero *et al.* (2008) studied the influence of silica nanoparticles on the reduction of calcium leaching. Concrete mixtures containing 6% (by weight of cement) of four different types of commercial silica nanoparticles (Table 3.1) were used.

Figure 3.4 shows that the addition of silica nanoparticles to the cement paste favors the growth of silicate chains. This is advantageous as longer

Table 3.1 Main physico-chemical properties of the commercial additions used as stated by the manufacturer (Gaitero *et al.*, 2008)

Name	Particle size (nm)	pH	Stabilizing agent	SiO_2 content (wt%)	Presentation
CS1	30	10	Na_2O	45	Colloid
CS2	20	10	Na_2O	20	Colloid
CS3	120	9.5	NH_3	40	Colloid
ADS	1400	–	–	95	Powder

All the colloids were dispersed in water, being the amount of the stabilizing agents <0.1 wt%.

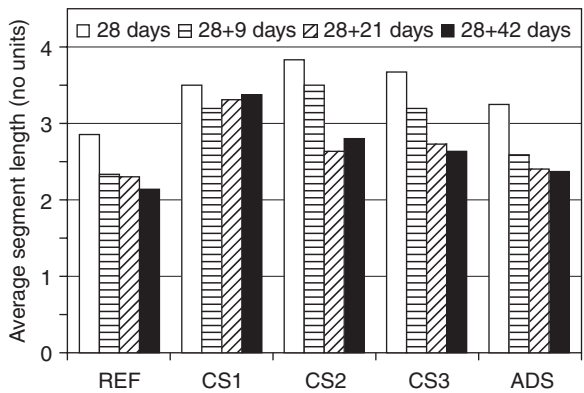

3.4 Evolution of the average segment length. The results were obtained from the relative areas of the ^{29}Si MAS-NMR spectra (Gaitero *et al.*, 2008).

chains correspond to greater C–S–H stability. The authors concluded that the addition of nano-silica to cement-based materials can control C–S–H degradation induced by calcium leaching. However, the benefits depend on the conditions under which nanoparticles are used. Colloidal dispersions proved much more effective than dry powders in reducing the effects of degradation.

3.3 The problem of efficient nanoparticle dispersion

The most significant issue in the use of nanoparticles is that of effective dispersion. Vera-Agullo *et al.* (2009) stated that the use of nanoparticles will cause a higher degree of hydration in cementitious compounds if higher nanoparticle dispersion can be achieved. Givi *et al.* (2010) recorded that a proper dispersion of nano-SiO_2 particles was achieved by stirring with part of the mixing water at high speed (120 rpm) for one minute and then adding

to the mixture. Zhang and Li (2011) used a water-reducing agent (UNF-5, a type of b-naphthalene sulfonic acid and formaldehyde condensates) to help disperse the nanoparticles in the cement paste and to achieve a good degree of workability in the concrete. A de-foamer (tributyl phosphate) was also used to decrease the number of air bubbles. To prepare concrete containing nanoparticles, a water-reducing agent was first mixed with water in a mortar mixer. The nanoparticles were then added and stirred at high speed for five minutes. A de-foamer was added during stirring. Following this, the cement, sand and coarse aggregate were mixed at low speed for two minutes in a centrifugal concrete blender. The mixture of water, water-reducing agent, nanoparticles, and de-foamer was then slowly added and stirred at low speed for a further two minutes to achieve good workability.

Dispersion difficulties also occur when carbon nanotubes or carbon nanofibers are used because of their strong Van der Waals self-attraction (Xie *et al.*, 2005). Sanchez and Ince (2009) confirmed that Van der Waals forces hold the carbon nanofibers together in clumps (Fig. 3.5).

These authors found that silica fume facilitated the dispersion of carbon nanofibers due to its small particle size when compared to that of anhydrous cement particles (around 100 times smaller). Figure 3.6 shows silica fume particles intermixed with carbon nanofibers. The authors recorded that even when carbon nanofiber dispersion was facilitated by silica fume, a significant number of carbon nanofiber pockets still remained. Konsta-Gdoutos *et al.* (2010b) used an aqueous surfactant and ultrasonic energy to achieve a high degree of carbon nanofiber dispersion. They found that a constant surfactant to carbon weight ratio of 4.0 achieved effective dispersion. Nochaiya and Chaipanich (2011) also found that homogeneous dispersion can be obtained if carbon nanotubes are mixed with water and then subjected to ultrasound for one hour. Nasibulina *et al.* (2012) suggest that high-quality dispersion of carbon nanotubes may be achieved by a two-step method:

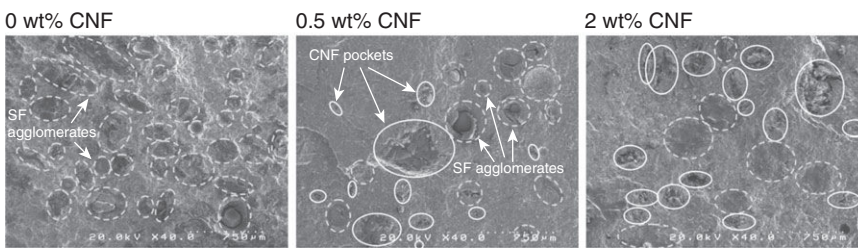

3.5 Scanning electron micrographs of the fracture surface of hybrid CNF/SF cement composites, revealing the presence and distribution of SF agglomerates and CNF pockets at a magnification of 40× (Sanchez and Ince, 2009).

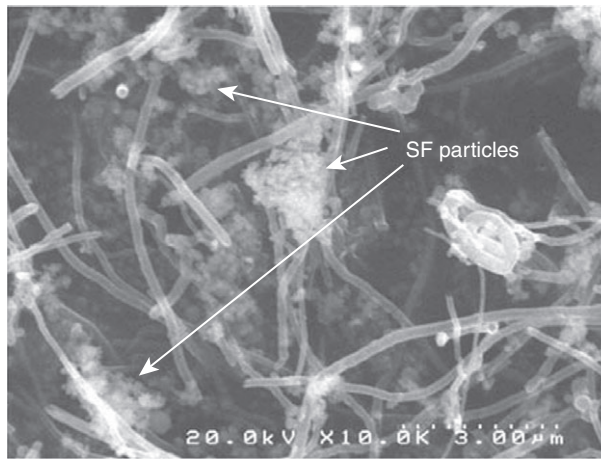

3.6 Scanning electron micrograph showing silica fume particles intermixed with carbon nanofibers after dry mixing (Sanchez and Ince, 2009).

1. Carbon nanotubes are functionalized in a mixture of nitric and sulfuric acids (70 wt% and 96 wt%, respectively) at 80°C.
2. Functionalized carbon nanotubes are washed with acetone to remove carboxylated carbonaceous fragments formed during oxidation of the nanotubes.

Metaxa *et al.* (2012) developed an ultracentrifugation concentration process for the production of highly concentrated suspensions of carbon nanotubes. Ultracentrifugation is used to reduce the amount of water in the nanotube water/surfactant suspension, thus increasing the concentration of nanotubes (Figs 3.7 and 3.8).

The process involves the dispersion of carbon nanotubes in an aqueous surfactant solution by ultrasonication and ultracentrifugation of the suspension, followed by decantation and ultrasonication of the remaining suspension. Absorbance spectroscopy results confirmed a fivefold increase in the concentration of carbon nanotubes in the suspensions. Another important issue in the dispersion of nanoparticles is its quantitative characterization. To date, three common methods have been used to analyze the dispersion of CNTs or CNFs in aqueous solutions. These are optical microscopy, electron microscopy (using both scanning electron microscopes (SEM) and transmission electron microscopes (TEM)), and ultraviolet–visible (UV–Vis) spectroscopy (Tyson *et al.*, 2011). These authors developed a method for quantifying the dispersion and agglomeration of both carbon nanofibers and carbon nanotubes within an aqueous solution. The dispersion quantity, D, is measured by the free-path spacing between particles; the agglomera-

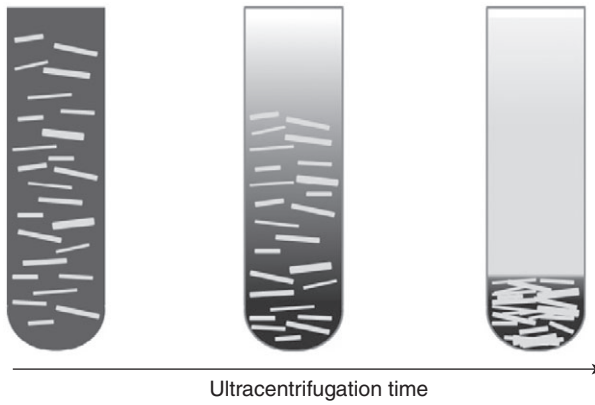

3.7 Schematic figure showing the progression of the sedimentation of nano-materials inside a tube during ultracentrifugation (Metaxa *et al.*, 2012).

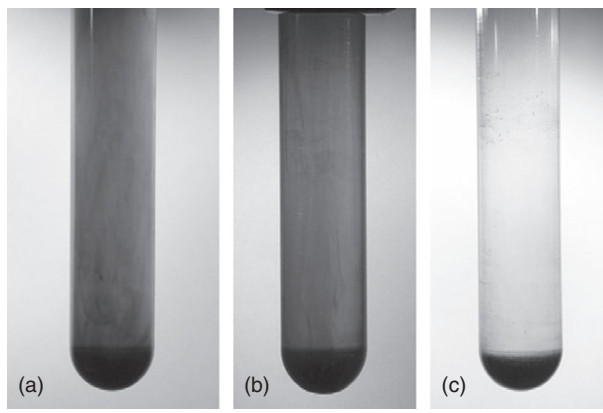

3.8 Suspensions of carbon nanotubes ultracentrifuged for (a) 30 min, (b) 45 min and (c) 60 min (Metaxa *et al.*, 2012).

tion quantity, A, is measured by the particle size. The agglomeration percentage is critical because, in certain cases, dispersion between two images can be identical, although the agglomeration percentage will have changed. In both cases, a quantifiable percentage is calculated based on the statistical probability that either the free-path spacing or particle size will fall within a certain percentage above and below l, where l is either the mean spacing or the particle size. A high value of D indicates a better dispersion. A lower value of A indicates a reduction in agglomeration.

3.4 Conclusions

A review of the literature on the contribution of nanoparticles in HPC shows the following.

- Nanoparticles may contribute to a dramatic increase in the mechanical strength of cementitious composites, thus helping the production of HPC. The related mechanisms are as follows:
  - The filling of voids in the C-H-S structure, so enabling the production of concrete of greater density.
  - Acting as nucleation centres and contributing to the development of hydration in Portland cement.
  - Reaction with $Ca(OH)_2$ crystals to produce C–S–H gel. The nanoparticles also act as kernels in the cement paste and reduce the size of the $Ca(OH)_2$ crystals.
- The optimal quantity of nanoparticles will depend upon their type and average dimension.
- Further investigations are needed to determine which nanoparticles are most effective in enhancing concrete durability.
- Nano-silica appears to control calcium leaching. Colloidal dispersions are more effective in reducing the effects of degradation than dry dispersions.
- One of the most significant issues in the use of nanoparticles is that of effective dispersion. Different authors have used different methods in order to achieve a high dispersion. However, there is still a need to search for improved methods. The tools used to assess uniformity of distribution are largely quantitative (optical microscopy, electron microscopy and transmission electron microscopy). The validity of the methods used to date must therefore be confirmed using quantitative characterization tools.

3.5 References

Allwood J, Ashby M, Gutowski T, Worrell E (2011) Material efficiency: a white paper. *Resources, Conservation and Recycling* 55, 362–381.

Bentur A, Mitchell D (2008) Material performance lessons. *Cement and Concrete Research* 38, 259–272.

Carde C, Franqois R, Torrenti J (1996) Leaching of both calcium hydroxide and C–S–H from cement paste: modeling the mechanical behaviour. *Cement and Concrete Research* 26, 1257–1268.

Chaipanich A, Nochaya T, Wongkeo W, Torkittikul P (2010) Compressive strength and microstructure of carbon nanotubes-fly ash cement composites. *Materials Science and Engineering A* 527, 1063–1076.

Chen L, Lin D (2009) Applications of sewage sludge ash and nano-SiO_2 to manufacture tile as construction material. *Construction and Building Materials* 23, 3312–3320.

Davalos, JF (2012) Advanced materials for civil infrastructure rehabilitation and protection. Seminar at The City College of New York, New York.

ERMCO (2001) *European Ready-mixed Concrete Industry Statistics, Year 2000*. European Ready Mixed Concrete Organization, Brussels.

ERMCO (2011) *Ready-mixed Concrete Industry Statistics, Year 2010*. European Ready Mixed Concrete Organization, Brussels.

Flatt R, Roussel R, Cheeseman CR (2012) Concrete: an eco-material that needs to be improved. *Journal of the European Ceramic Society* 32, 2787–2798.

Gaitero J (2008) Multi-scale study of the fibre matrix interface and calcium leaching in high performance concrete. PhD Thesis, Centre for Nanomaterials Applications in Construction of Labein-Tecnalia, Spain.

Gaitero J, Campillo L, Guerrero A (2008) Reduction of the calcium leaching rate of cement paste by addition of silica nanoparticles. *Cement and Concrete Research*, 38 1112–1118.

Gaitero J, Zhu W, Campillo I (2009) Multi-scale study of calcium leaching in cement pastes with silica nanoparticles. *Nanotechnology in Construction 3*, Springer, Berlin Heidelberg.

Gaitero J, Dolado J, Neuen C, Heber F, Koenders E (2012) Computational 3D simulation of calcium leaching in cement matrices. INS Preprint No. 1203, Institut für Numerische Simulation, Rheinische Friedrich-Wilhelms-Universität Bonn.

Gartner E, Macphee D (2011) A physico-chemical basis for novel cementitious binders. *Cement and Concrete Research* 41, 736–749.

Givi A, Rashid S, Aziz F, Salleh M (2010) Experimental investigation of the size effects of SiO_2 nanoparticles on the mechanical properties of binary blended concrete. *Composites: Part B* 41, 673–677.

Givi A, Rashid S, Aziz F, Salleh M (2011) The effects of lime solution on the properties of SiO_2 nanoparticles binary blended concrete. *Composites: Part B* 42, 562–569.

Glasser F, Marchand J. Samson E (2008) Durability of concrete – degradation phenomena involving detrimental chemical reactions. *Cement and Concrete Research* 38, 226–246.

Haga K, Sutou S, Hironaga M, Tanaka S, Nagasaki S (2005) Effects of porosity on leaching of Ca from hardened ordinary Portland cement paste. *Cement and Concrete Research* 35, 1764–1775.

Hegger J, Nitsch A, Burkhardt J (1997) Höchleistungbeton im Fertigteilbau. *Betonwerk Fertigteil-Technik* 2, 81–90.

He X, Shi X (2008) Chloride permeability and microstructure of Portland cement mortars incorporating nanomaterials. *Transportation Research Record* 2070, 13–21.

Hollaway LC (2011) Key issues in the use of fibre reinforced polymer (FRP) composites in the rehabilitation and retrofitting of concrete structure. In Karbhari VM and Lee LS (eds), *Service Life Estimation and Extension of Civil Engineering Structures*. Woodhead Publishing, Cambridge.

Jalal M, Mansouri E, Sharifipour M, Pouladkhan A (2012) Mechanical, rheological, durability and microstructural properties of high performance self-compacting concrete containing SiO_2 micro and nanoparticles. *Materials and Design* 34, 389–400.

Jennings H, Bullard J (2011) From electrons to infrastructure: engineering concrete from the bottom up. *Cement and Concrete Research* 41, 727–735.

Ji T (2005) Preliminary study on the water permeability and microstructure of concrete incorporating nano-SiO_2. *Cement and Concrete Research* 35, 1943–1947.

Kamali S, Gerard B, Moranville M (2003) Modeling the leaching kinetics of cement based materials – influence of materials and environment. *Cement and Concrete Composites* 25, 451–458.

Khoshakhlagh A, Nazari A, Khalaj G (2012) Effects of Fe_2O_3 nanoparticles on water permeability and strength assessments of high strength self-compacting concrete. *Journal of Materials Science & Technology* 28, 73–82.

Konsta-Gdoutos M, Metaxa Z, Shah S (2010a) Highly dispersed carbon nanotube reinforced cement based materials. *Cement and Concrete Research* 40, 1052–1059.

Konsta-Gdoutos M, Metaxa Z, Shah S (2010b) Multi-scale mechanical and fracture characteristics and early-age strain capacity of high performance carbon nanotube/cement nanocomposites. *Cement and Concrete Composites* 32(2), 110–115.

Lee S, Kriven W (2005) Synthesis and hydration study of Portland cement components prepared by organic steric entrapment method. *Materials and Structures* 38, 87–92.

Li H, Zhang M-H, Ou J-P (2006) Abrasion resistance of concrete containing nanoparticles for pavement. *Wear* 260, 1262–1266.

Lin D, Lin K, Chang W, Luo H, Cai M (2008) Improvements of nano-SiO_2 on sludge/fly ash mortar. *Waste Management* 28, 1081–1087.

Metaxa Z, Seo J-W, Konsta-Gdoutos M, Hersam M, Shah S (2012) Highly concentrated carbon nanotube admixture for nano-fiber reinforced cementitious materials. *Cement and Concrete Composites* 34, 612–617.

Mora E (2007) Life cycle, sustainability and the transcendent quality of building materials. *Building and Environment* 42, 1329–1334.

Nasibulin A, Shandakov S, Nasibulina L, Cwirzen A, Mudimela P, Habermehl-Cwirzen K, Grishin D, Gavrilov Y, Malm J, Tapper U, Tian Y, Penttala V, Karppinen M, Kauppinen E (2009) A novel cement-based hybrid material. *New Journal of Physics* 11, 023013.

Nasibulina LI, Anoshkin IV, Nasibulin AG, Cwirzen A, Penttala V, Kauppinen EI (2012) Effect of carbon nanotube aqueous dispersion quality on mechanical properties of cement composite. *Journal of Nanomaterials* 2012, 169262.

Nazari A, Riahi S (2011a) The effects of zinc dioxide nanoparticles on flexural strength of self-compacting concrete. *Composites: Part B* 42, 167–175.

Nazari A, Riahi S (2011b) Al_2O_3 nanoparticles in concrete and different curing media. *Energy and Buildings* 43, 1480–1488.

Nochaiya T, Chaipanich A (2011) Behavior of multi-walled carbon nanotubes on the porosity and microstructure of cement-based materials. *Applied Surface Science* 257(6), 1941–1945.

Ozyildirim C, Zegetosky C (2010) Laboratory investigation of nanomaterials to improve the permeability and strength of concrete. Virginia Transportation Research Council, Final Report VTRC 10-R18.

Pacheco-Torgal F, Jalali S (2011a) *Eco-efficient Construction and Building Materials*. Springer Verlag, London.

Pacheco-Torgal F, Jalali S (2011b) Nanotechnology: advantages and drawbacks in the field of building materials. *Construction and Building Materials* 25, 582–590.

Pacheco-Torgal F, Jalali S, Labrincha J, John VM (2012) *Eco-efficient Concrete*. Woodhead Publishing, Cambridge.

Pellenq R, Kushima A, Shahsavari R, Vliet K, Buehler M, Yip S, Ulm F (2009) A realistic molecular model of cement hydrates. *Proceedings of the National Academy of Sciences* 106(38), 16102–16107.

Porro A, Dolado J, Campillo I, Erkizia E, de Miguel Y, de Ybarra Y, Ayuela A (2005) Effects of nanosilica additions on cement pastes. *Proc International Conference on Applications of Nanotechnology in Concrete Design*, 87–96.

Sanchez F, Ince C (2009) Microstructure and macroscopic properties of hybrid carbon nanofiber/silica fume cement composites. *Composites Science and Technology* 69, 1310–1318.

Sanchez F, Sobolev K (2010) Nanotechnology in concrete – a review. *Construction and Building Materials* 24, 2060–2071.

Shekari A, Razzaghi M (2011) Influence of nanoparticles on durability and mechanical properties of high performance concrete. *Procedia Enginnering* 14, 3036–3041.

Shi C, Fernández Jiménez A, Palomo A (2011) New cements for the 21st century: the pursuit of an alternative to Portland cement. *Cement and Concrete Research* 41, 750–763.

Sobolev K, Ferrada-Gutierrez M (2005) How nanotechnology can change the concrete world: Part 2. *American Ceramic Society Bulletin* 84, 16–19.

Sobolev K, Flores I, Hermosillo R, Torres-Martinez L (2008) Nanomaterials and nanotechnology for high-performance cement composites. *American Concrete Institute, ACI Special Publication* 254, 93–120.

Tyson B, Abu Al-Rub R, Yazdanbakhsh A, Grasley Z (2011) A quantitative method for analyzing the dispersion and agglomeration of nanoparticles in composite materials. *Composites Part B: Engineering* 42, 1395–1403.

Vera-Agullo J, Chozas-Ligero V, Portillo-Rico D, Garcia-Casas M, Gutierrez-Martinez A, Mieres-Royo J, Gravalos-Moreno J (2009) Mortar and concrete reinforced with nanomaterials. *Nanotechnology in Construction 3*, Springer, Berlin.

Xie X-L, Mai Y-W, Zhou X-P (2005) Dispersion and alignment of carbon nanotubes in polymer matrix: a review. *Mater Sci Eng R* 49, 89–112.

Yan L, Chouw N (2013) Behavior and analytical modeling of natural flax fibre reinforced polymer tube confined plain concrete and coir fibre reinforced concrete. *Journal of Composite Materials* (in press).

Zhang M-H, Li H (2011) Pore structure and chloride permeability of concrete containing nanoparticles for pavement. *Construction and Building Materials* 25, 608–616.

Zhu W, Bartos P, Porro A (2004) Application of nanotechnology in construction. Summary of a state-of-the-art report. RILEM TC 197-NCM. *Materials and Structures* 37, 649–658.

4

Self-sensing concrete with nanomaterials

Z. CHEN and Y. DING, Dalian University of Technology, China, F. PACHECO-TORGAL and Y. ZHANG University of Minho, Portugal

DOI: 10.1533/9780857098832.1.53

Abstract: Conductive concrete containing nano carbon black (NCB) and carbon fibre (CF) to enable the self-diagnosis of strain and damage was studied. The effect of NCB and CF on workability, mechanical properties and fractional change in resistance (FCR) in fresh and hardened concrete was analysed. The relationship between the FCR, the strain of initial geometrical neutral axis (IGNA) and the degree of beam damage was established. The results showed that the relationship between the FCR and the IGNA strain can be described by the First Order Exponential Decay function, and that the slope of this function reflects the sensitivity of conductive concrete. Based on the above relationship and damage mechanics theory, internal damage to the concrete is indicated by the relationship between the degree of damage and resistance. This self-sensing of strain in conductive concrete can be applied in monitoring damage to flexible components.

Key words: conductive concrete, nano carbon black, carbon fibre, self-diagnosing of damage, fractional change in resistance, strain.

4.1 Introduction

Degradation, cumulative structural damage or material resistance are common reasons for the failure of conventional concrete structures such as dams and bridges which undergo differing levels of load, fatigue or corrosion. In order to prevent the possibility of sudden failure and to prolong the service life of concrete structures, the study of cumulative damage has concentrated on strain behaviour and fatigue process (Li and Ou, 2007; Ou, 1996). Monitoring is valuable for structural safety and the application of conductive cementitious composite materials was reported by Wen and Chung (2000, 2004, 2005, 2006, 2007), using electric resistance measurement to monitor strain and damage.

Over the last decade, nanomaterials have been used as smart fillers for a broad range of multifunctional composites as well as in strain or damage sensors (Li *et al.*, 2008; Chung, 2012). This chapter considers the addition of both nano carbon black (NCB) and carbon fibre (CF) as conductive phases which enhance electrical conductivity and produce diphasic electric conduc-

tive concrete. This enables resistivity measurements to be carried out and may be used to analyse variations of strain or stress in structural components, thus making possible the early evaluation of damage without the need to embed sensors. Conduction concrete also has a wide application in the electromagnetic shielding of vital equipment and de-icing of airfields and highways (Yehia and Tuan, 1999).

The addition of short CF to concrete creates continuous conductive pathways which transmit current, playing a fundamental role in the electrical transport process. The enhanced electrical conductivity of concrete with CF also decreases shrinkage and cracking, so improving durability and resistance to freezing. In addition, it does not require a large quantity of water. The addition of NCB reduces cost by improving electrical conductivity and the toughness of the aggregate interface within the concrete matrix. It also provides a filler effect which enhances the density of the matrix (Cai and Chung, 2007). Due to the extremely small size of NCB compared to traditional carbon fibre, it penetrates the matrix in carbon fibre reinforced composites. This connects the conductive pathways to form conductive networks which further improve electrical conductivity (Li *et al.*, 2006, 2008). Initial and evolving strain in concrete may cause damage which breaks conductive pathways or networks, resulting in a change of electric resistance. The combined use of NCB and short CF provides conductive concrete with effective mechanical properties.

Damage to cement-based material may change its electric resistance, as manifested in elastic tension, plastic deformation and cracking. Concrete components with coarse aggregate are often subjected to differences in loading (e.g., compression, tension and bending), and may also experience various stages of load-deformation, including pre- and post-cracking behaviour. Studies on strain sensing in carbon fibre reinforced geopolymer concrete under conditions of bending and compression have been reported. However, studies on concrete beams with diphasic electrical conduction admixtures for diagnosis of damage caused by bending are still very rare. There are several problems in the study of conductive concrete beams. The electric characteristics must be suitable for a particular application without degradation of the workability of fresh concrete or detriment to the mechanical behaviours of hardened concrete.

Based on investigations into the effect of NCB and CF on the workability, compression strength and flexural strength of concrete, a large number of concrete beams reinforced with conductive material were investigated experimentally to study the damage and FCR under varied loading levels. The purpose of this work was to analyse the effect of NCB or CF, and especially the hybrid use of NCB and short CF, as diphasic conductive materials on the FCR of concrete beams. It was also concerned with the relationship between FCR, strain and degree of damage in concrete beams

undergoing bending in the pre-cracking region. The relationship between FCR and the strain of initial geometrical neutral axis (IGNA) was established by regression analysis. Based on damage mechanics theory and the relationship mentioned above, the correlation between the degree of damage and the FCR was established. The results show that the relationship between FCR and the strain of the IGNA in concrete beams can be effectively described by the First Order Exponential Decay curve before cracking.

4.2 Studying conductive admixtures in concrete

4.2.1 Materials

The nano carbon black (Fig. 4.1) used in the experiments was a superconductive form of porous agglomerates of carbon particles with an average size of 60 nm and a density of 0.3–0.5 g/cm^3. The carbon fibre used (Fig. 4.2) in the conductive phase was asphalt base short carbon fibre with a diameter of 12–15 μm and a length of 6 mm. Its density was 1.55–1.60 g/cm^3. The properties of NCB and CF used are shown in Tables 4.1 and 4.2.

In order to analyse the effect of conductive admixtures on the concrete, plain concrete samples without CF and NCB were prepared as references. The design mixture of the plain concrete is shown in Table 4.3. The type of cement used was CEM I 42.5, the W/B was 0.45, and a water reducing agent (WR) was used in the amount of 1.0% by mass of binder. The 28d compressive strength was 43.6 MPa. The NCB content with a particle size of *ca.* 30–90 nm (Fig. 4.1) was between 0.1% and 0.4% by mass of binder (0.53–

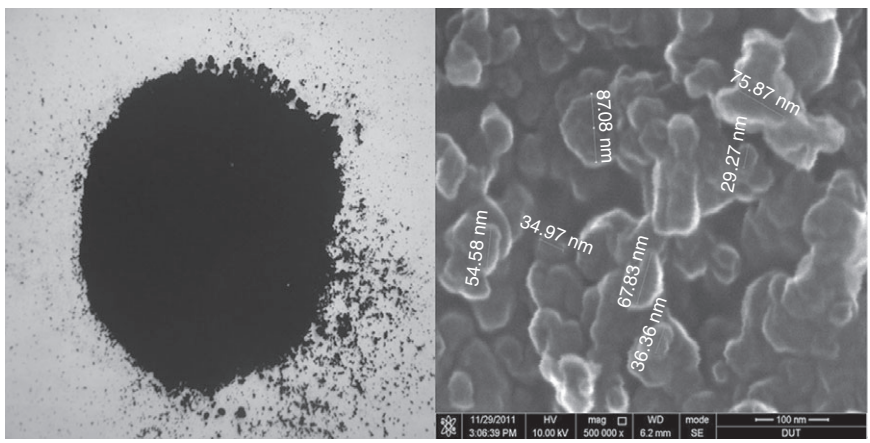

4.1 Nano carbon black and particle size using high resolution field emission SEM.

4.2 Carbon fibre.

Table 4.1 Properties of NCB

Particle size (nm)	Density (g/cm^3)	Volume resistance (Ω.cm)	Surface resistance (Ω)
30–90	0.3–0.5	2.3	30.6

Table 4.2 Properties of CF

Density (g/cm^3)	Diameter (10^{-6} mm)	Length (mm)	Tensile strength (N/mm^2)	Resistivity (mΩ.cm)
1.55–1.6	12–15	6	3000	3–7

Table 4.3 Design mixture of reference concrete

Cement (kg/m^3)	Fly ash (kg/m^3)	Fine aggregate 1–4 mm (kg/m^3)	Coarse aggregate 5–10 mm (kg/m^3)	Water (kg/m^3)	SP (kg/m^3)
370	160	733	733	240	5.33

Table 4.4 Comparison of the dosages of the conductive admixtures

Serial number		NCB (mass/binder %)	CF (mass/binder %)
Plain concrete (concrete without conductive admixture)	PC	0	0
Concrete containing NCB	NCB 01	0.1%	0
	NCB 02	0.2%	0
	NCB 03	0.3%	0
	NCB 04	0.4%	0
Concrete containing CF	CF 04	0	0.4%
	CF 08	0	0.8%
	CF 10	0	1.0%
	CF 13	0	1.3%
	CF 16	0	1.6%
Concrete containing BF (NCB and CF)	BF 14	0.1%	0.4%
	BF 18	0.1%	0.8%
	BF 24	0.2%	0.4%
	BF 28	0.2%	0.8%

2.12 kg/m^3). The carbon fibre content with a diameter of 12–15 μm and a length of 6 mm (Fig. 4.2) was between 0.4% and 1.6% by mass of binder (2.12–8.48 kg/m^3). Where CF was used (both alone and in combination with NCB), methyl-cellulose was used as a dispersing agent along with a defoamer to optimize the dispersion of carbon fibre in the concrete (Wen and Chung, 2007). Methyl-cellulose and defoamer were not used in the absence of carbon fibre. The defoamer dosage was 2.13 kg/m^3, and the methyl-cellulose content was between 2.13 and 8.52 kg/m^3. The series of electric conductive concrete samples (CF only, NCB only, hybrid use of CF and NCB) and different contents of conductive phases are listed in Table 4.4.

4.2.2 Specimen preparation and testing set-up

Mixing was carried out using a mechanical concrete mixer. Methyl-cellulose was dissolved in water and the defoamer and CF (if applicable) were added and stirred manually for around two minutes. The methyl-cellulose mixture, fine aggregate, coarse aggregate, cement, fly ash, water, NCB and superplasticizer were then mixed for five minutes. The mixture was poured into oiled moulds and an external electric vibrator was used to facilitate compaction and to decrease the quantity of air bubbles. The specimens were removed from the moulds after a day and four electrical contacts in the form of conductive adhesive tape were wrapped around the specimens. Based on

the four-pole method of electric resistance measurement, contacts A and D were used for passing the current while contacts B and C measured the voltage (Cai and Chung, 2006). Finally, carefully prepared specimens were cured at room temperature for 28 days. All the beams prepared for testing measured 100 mm × 100 mm × 400 mm. The dimensions and electrical contacts details of all beams are shown in Fig. 4.3. The result represents the average across three beams.

4.2.3 Test methods

The four-pole method was adopted for measuring resistance (Tian and Hu, 2012). A hydraulic servo testing machine (MTS Model 810) was used. The close-loop test was controlled by displacement and the deformation rate at the mid-span was 0.2 ± 0.02 mm per minute up to the specified end-point deflection which was 3 kN larger than that of the previous loading level. The two possibilities in loading and load–time relationships are illustrated in Fig. 4.4.

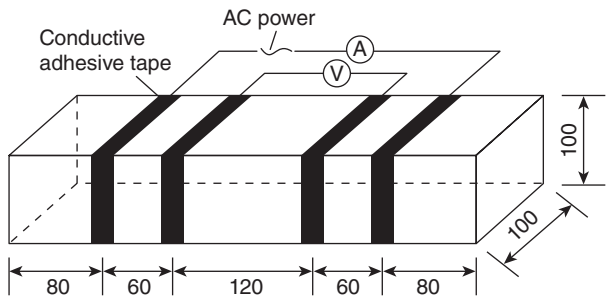

4.3 Specimen configuration for measuring resistance.

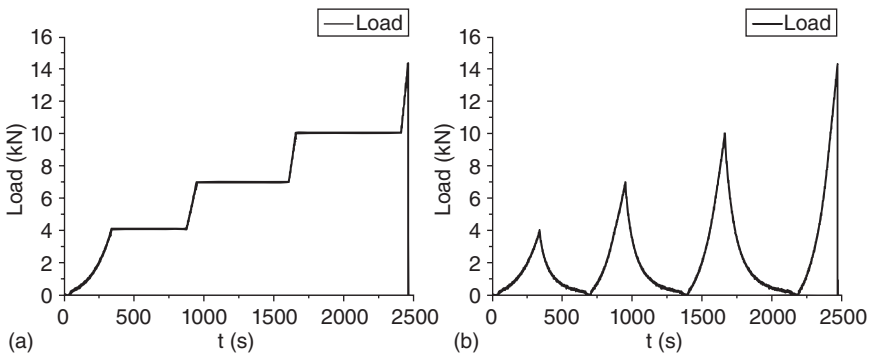

4.4 Loading histories of the beam: (a) load–time relationship I, (b) load–time relationship II.

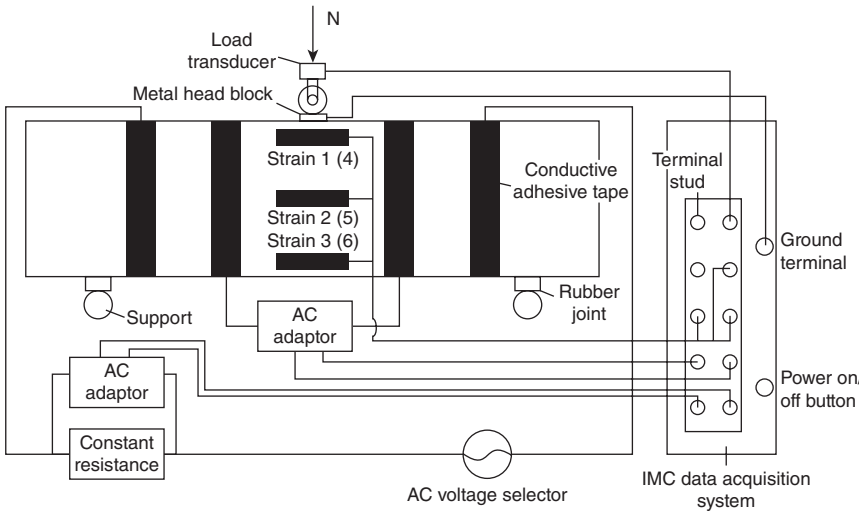

4.5 Arrangement of measuring points.

Six strain gauges were applied for measuring the longitudinal strain, two of which (Strain 2(5)) were used on each side of the two opposing surfaces to measure the strain of initial geometrical neutral axis (IGNA) under the externally applied load N.

During the loading process, the strain near the top of the concrete beam in the compression zone, the strain of IGNA and the tensile strain near the bottom of the beam were measured by strain gauges. The resistance of concrete beam was measured simultaneously. The IGNA strains were then obtained by strain gauges (2) and (5). The resistance of the beams was continuously measured during loading by using the four-pole method described above. Other experimental instruments included an AC stabilized voltage supply, IMC Intelligence Data Collecting System, a fixed resistor and an AC/DC converter. A schematic view of the beam under loading with current and voltage electrodes is illustrated in Fig. 4.5. Rubber joints were placed under the support points during the experiment (see Fig. 4.5) in order to isolate the concrete beam from the loading frame.

4.3 Influence of conductive admixtures on the mechanical properties of concrete

4.3.1 Influence on workability and compression strength

The workability of high flowable fresh concrete, with and without conductive admixture, has been evaluated by measuring the slump flow. The experimental results of workability are listed in Table 4.5. The factor *d* represents

Table 4.5 Content of conductive admixture, slump flow, compressive strength and flexural strength

Mixture/samples		Content of NCB (kg/m^3)	Content of CF (kg/m^3)	Slump flow, d (mm)	Compressive strength (f_{cu}) (MPa)	Flexural strength (σ_u) (MPa)
Plain concrete	PC	0	0	620	42.55	4.44
Concrete with NCB only	NCB01	0.3733	0	600	43.53	4.52
	NCB02	0.7467	0	540	43.67	4.71
	NCB03	1.1200	0	390	44.17	4.79
	NCB04	1.4933	0	330	45.45	4.83
Concrete with CF only	CF04	0	1.4933	590	43.49	5.10
	CF08	0	2.9866	570	44.37	5.19
	CF10	0	3.7333	550	45.10	5.22
	CF13	0	4.8533	520	44.6	5.30
	CF16	0	5.9733	500	44.76	5.31
Concrete with BF (NCB + CF)	BF14	0.3733	1.4933	590	43.78	4.90
	BF18	0.3733	2.9866	540	44.01	4.94
	BF24	0.7467	1.4933	480	43.54	5.02
	BF28	0.7467	2.9866	410	43.98	5.13

the average diameter in the slump flow test. It may be seen from Table 4.5 that fresh PC (plain concrete without any conductive admixtures) corresponds well to the requirements of self-compacting concrete. There is very good flowability and no segregation. However, the workability of fresh concrete declines with an increase in NCB or CF content. The slump flow of BF28 is only about 410 mm. This means that the content of diphasic conductive admixtures (0.747 kg/m^3 (NCB) + 2.99 kg/m^3(CF)) is less than the lower limit (450 mm) of the workability of highly flowable concrete. The flow behaviour of NCB03, NCB04, and BF28 is much less fluid than that of other mixtures due to the relatively high content of CF and NCB.

The average values of compressive strength f_{cu} and flexural strength σ_u after 28 days may be found in Table 4.5. The increment of compression strength ranges between 2.2% and 6.2%. This indicates that the addition of NCB, CF and BF shows some positive effect on the compressive strength of concrete, but does not amount to a significant trend of improvement.

4.3.2 Influence of conductive admixtures on flexural strength

When a beam is subjected to bending, strains are produced. These strains create compression stress at the top of the beam and tension at the bottom. The load is applied until a crack is imminent. If the beam section does not

crack, then the ordinary elastic beam theory applies. The effects of conductive admixtures on flexural strength $\sigma_u = M_u/W$ (where M_u is ultimate bending moment and W is the section modulus) are illustrated in Table 4.5. It may be seen that the flexural strength of a concrete beam increases with the addition of conductive admixtures. Amongst these, the samples containing only NCB show a smaller increment of flexural strength as the NCB dosages are increased (between 1.8% and 8.8%). However, there is a clear increase in flexural strength when both the CF and BF dosages are increased. When compared with a PC beam without any conductive admixture, the increment of flexural strength in beams containing CF and BF is between 10% and 19%.

4.4 Influence of conductive admixtures on the electrical properties of concrete beams

As described above, flexural strains are produced when a beam is subjected to bending. During the loading process, the strain near the top of the beam in the compression zone, the strain of initial geometrical neutral axis (IGNA) and the tensile strain near the bottom of the concrete beam (Fig. 4.5) are measured by strain gauges. The resistance of the beam is measured simultaneously. The strains of IGNA are obtained by strain gauges (2) and (5), and the FCR at each loading stage can also be measured. The relationship between the force and electrical fields is used to investigate stress and strain behaviour through analysis of physical quantities such as current, voltage and resistance (Wu, 2005).

4.4.1 Feasibility of relationship between force field and electric field

It is difficult to measure quantities such as stress or current density directly. However, there are some experimentally measurable physical quantities, such as resistance in the electric field and strain in the force field. The stress can be calculated by stress–strain curves, while current and current density can be calculated by Ohm's law. Once the resistance–strain correlations are established through experimentation, the relationship between the force and electric fields is determined, so making it possible to obtain the immeasurable quantities in the force field with the measurable voltage and resistance of the electric field. The corresponding parameters of the electric field and the force field are illustrated in Table 4.6.

The Laplace Equation [4.1] is satisfied for both the electric and force fields:

$$\frac{\partial^2 \varphi}{\partial x^2} + \frac{\partial^2 \varphi}{\partial y^2} + \frac{\partial^2 \varphi}{\partial z^2} = 0 \qquad [4.1]$$

Table 4.6 Comparison of electrical and mechanical parameters

Electric field variable	Force field variable
Current: I	Load: N
Voltage: V	Deformation: U
Current density: $i = I/A = Ce$	Stress: $\sigma = N/A = E\varepsilon$
Generated voltage: $e = V/L$	Strain: $\varepsilon = U/L$
Ohm's law: $I = V/R$	Hooke's law: $N = U/\delta = EA\varepsilon$
Resistivity: $\rho = RA/L$	Stiffness coefficient: $B = EA/L = 1/\delta$
Conductivity: $C = 1/\rho = L/RA$	Elastic modulus: $E = L/(A\delta)$
Sensitivity: $\lambda = \Delta R/(R\varepsilon)$	Damage degree: $D = \Delta E/E$

For the electric field:

$$\frac{\partial^2 V}{\partial x^2} + \frac{\partial^2 V}{\partial y^2} + \frac{\partial^2 V}{\partial z^2} = 0 \qquad [4.2]$$

For the force field:

$$\frac{\partial^2}{\partial x^2} + \frac{\partial^2}{\partial y^2} + \frac{\partial^2}{\partial z^2}(\sigma_x + \sigma_y + \sigma_z) = 0 \qquad [4.3]$$

where x, y and z are space coordinates; φ and σ are respectively the potential function and stress. The Laplace equations presented here are based on the assumption that both the electric field (see Fig. 4.6a) and the force field (see Fig. 4.6b) comply with the same boundary conditions. In the force field, the beam is subjected to three loading points (A and E are the support points, and C is the mid-span point with an applied external load N, see Fig. 4.5 and Fig. 4.6b). In the electric field, the beam is taken as being in a similar situation as voltage is provided through three points, B, C and D. As illustrated in Fig. 4.6a, electric potential points B and D are used to provide the same voltage, while point C at the mid-span is the ground terminal. Thus if the beam section does not crack (the ordinary elastic beam theory applies), the boundary condition of the electric field will be comparable with that of the force field.

The variation of strain on the IGNA, along with the load, is shown in Fig. 4.7 as a function of time during the loading process prior to cracking. Figure 4.8 shows the relationship between the resistance and strain of IGNA obtained simultaneously from the same specimen. It can be seen that the resistance decreases along with the strain of the IGNA due to the sensitivity of conductive concrete as previously reported. The relationship between the IGNA strain in the force field and the resistance in the electric field can therefore be established.

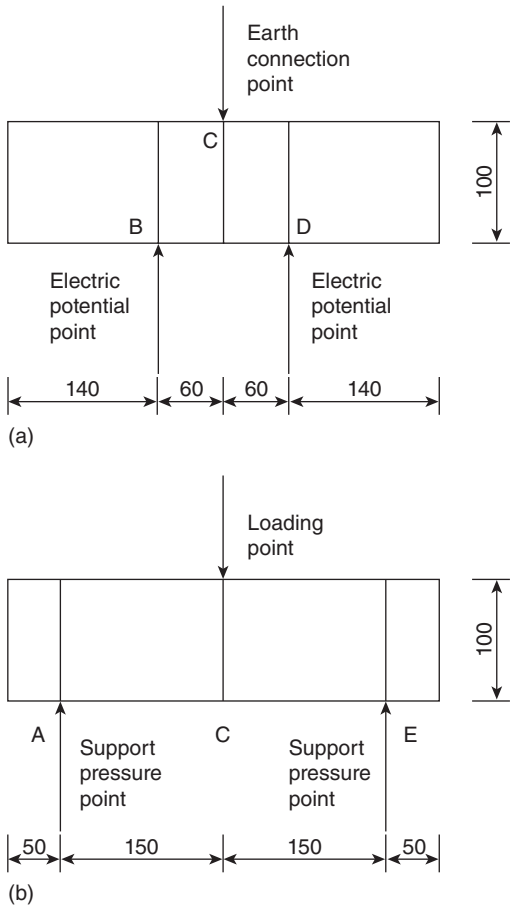

4.6 Comparison of loading boundary conditions between electric and force fields: (a) model of the electric field, (b) model of the force field.

4.4.2 Relationship between strain and FCR (Self-diagnosing of strain)

Figures 4.9–4.12 illustrate the relationship between FCR and the strain of IGNA (ε_2) in concrete beams. The effects of various conductive admixtures on these relationships can be also observed. It may be seen that the relationship between the FCR and the strain of IGNA corresponds well with the First Order Exponential Decay function, which may be expressed by:

$$Y = m\exp(-X/n + p) \qquad [4.4]$$

where m, n and p are constant parameters corresponding to the type and amount of the electric conductive phase and the variable X is the strain of

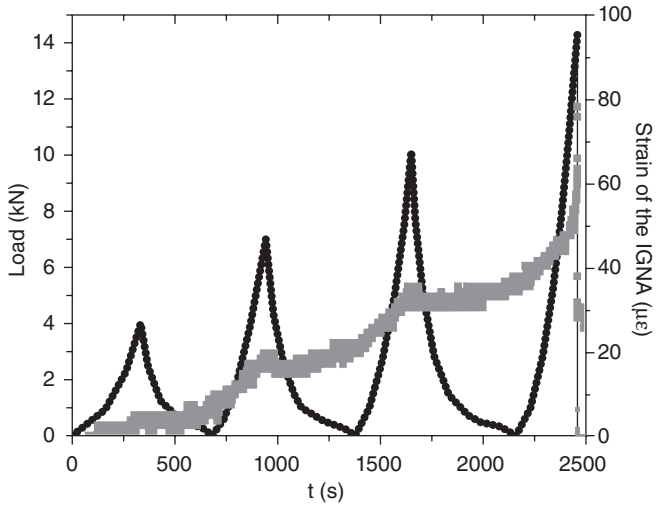

4.7 Variation of strain of IGNA (■) with load (•) vs time before cracking.

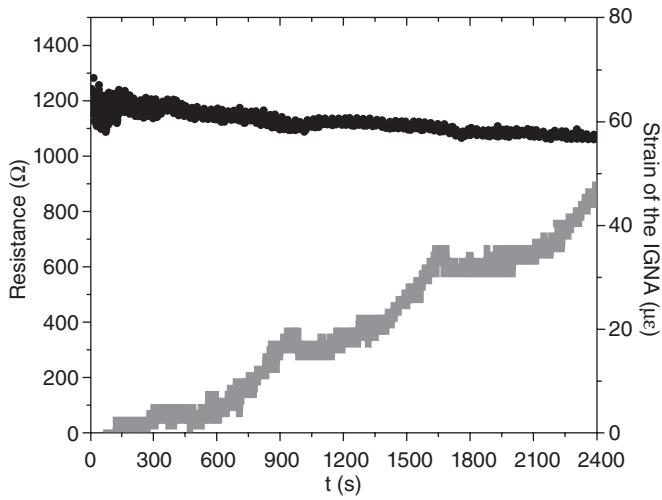

4.8 Resistance (•) vs strain of IGNA (■) and time.

IGNA; the unit of X is in $\mu\varepsilon$, and the FCR is the percentage of Y. The applied parameters and the correlation coefficient C_R^2 are illustrated in Table 4.7. The correlation coefficients of all beams in Table 4.7 range from 0.5 to 0.978. From Figs 4.9–4.12 and Table 4.7, it may be seen that:

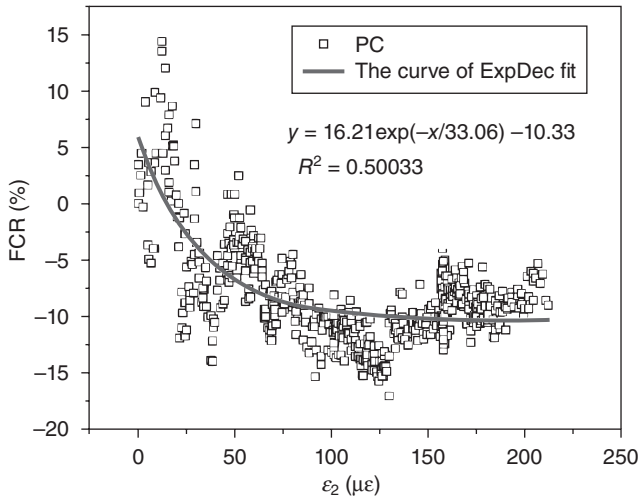

4.9 Relationship between FCR and $\varepsilon 2$ of PC.

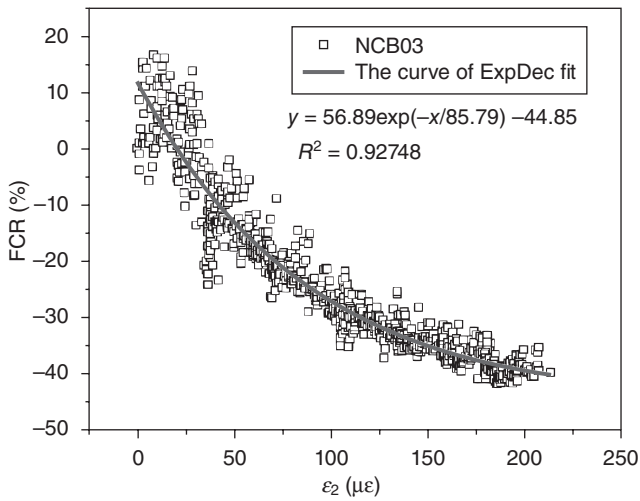

4.10 Relationship between FCR and $\varepsilon 2$ of NCB 03.

- The correlation coefficient C_R^2 of a plain concrete (PC) beam is only 0.50. This means that in a PC beam without conductive admixtures, the tested value is not strong in relation to the prediction in Eq. [4.4].
- The correlation coefficient C_R^2 of other beams with conductive materials such as NCB, CF or diphasic electric conductive materials (NCB + CF) is higher than 0.76. Hence, the relationship between FCR and strain of IGNA is quite strong when correlated with Eq. [4.4].

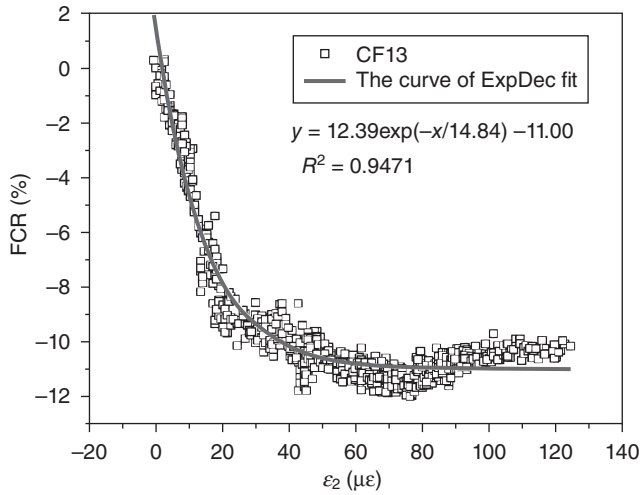

4.11 Relationship between FCR and $\varepsilon 2$ of CF 13.

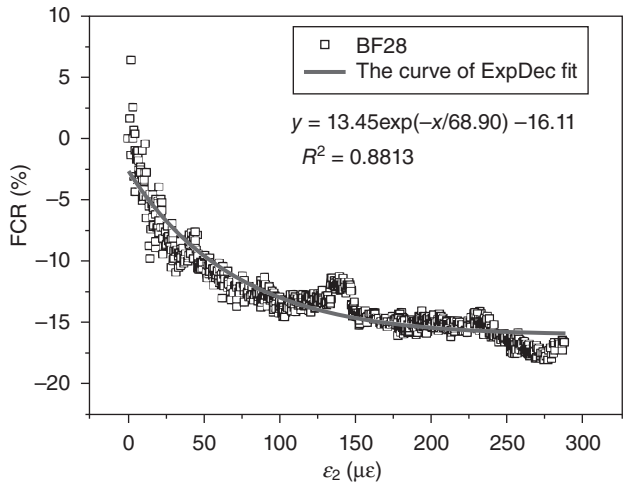

4.12 Relationship between FCR and $\varepsilon 2$ of BF 28.

- The correlation coefficient C_R^2 of NCB03, NCB04, CF10, CF13, BF14 and B24 is higher than 0.9. The relationship between FCR and the strain of IGNA is therefore very strong when correlated with Eq. [4.4], and the self-diagnosis of damage could be more effective, particularly in concrete components with the conductive admixtures suggested above.
- The curves in Figs 4.9–4.12 demonstrate a monotonically decreasing relationship between FCR and the strain of IGNA.

Table 4.7 Fitted parameters of regression equation

Serial number	Constant *m*	Constant *n*	Constant *p*	Correlation coefficient C_R^2
PC (NCB0% + CF0%)	16.21	33.06	–10.33	0.50033
NCB01 (NCB0.1% + CF0%)	32.31	47.48	–21.05	0.82466
NCB02 (NCB0.2% + CF0%)	34.57	5.21	–39.11	0.76742
NCB03 (NCB0.3%+ CF0%)	56.89	85.79	–44.85	0.92748
NCB04 (NCB0.4% + CF0%)	23.04	17.57	–25.56	0.90907
CF04 (NCB0% + CF0.4%)	27.87	13.00	–29.74	0.79566
CF08 (NCB0% + CF0.8%)	20.83	19.26	–21.25	0.83359
CF10 (NCB0% + CF1.0%)	25.55	12.39	–27.41	0.97752
CF13 (NCB0% + CF1.3%)	12.39	14.84	–11.00	0.9471
CF16 (NCB0% + CF1.6%)	42.96	15.75	–52.68	0.82598
BF14 (NCB0.1% + CF0.4%)	14.88	95.04	–12.56	0.95126
BF18 (NCB0.1% + CF0.8%)	106.63	83.70	–82.74	0.77459
BF24 (NCB0.2% + CF0.4%)	12.98	34.94	–15.24	0.90456
BF28 (NCB0.2% + CF0.8%)	13.45	68.90	–16.11	0.8813

4.4.3 Sensitivity of conductive concrete

The ability of a structural material to sense its own strain (i.e., sensitivity) is an attractive attribute of smart structures. The sensitivity of conductive concrete may be characterized by the gauge factor (λ) which is defined as the fractional change in resistance per unit strain (Chung, 2012; Tian and Hu, 2012). Hence λ is equal to the slope of Eq. [4.1] and may be expressed by:

$$\lambda = |0.01Y'| = \left|\frac{m}{100n}\exp(-X/n)\right| \qquad [4.5]$$

where m and n are both constant parameters and the variable X is the strain of the initial geometrical neutral axis (IGNA) as in Eq. [4.4].

It may be seen from Eq. [4.5] that the value of λ decreases in terms of exponential decay function as the strain IGNA increases, i.e., the development of strain leads to a degradation of sensitivity in electric conductive concrete.

4.5 Strain and damage in concrete beams (self-diagnosing of damage)

The damage done to a beam prior to the concrete cracking is discussed in this section and is based on the theory of damage mechanics (Cai and Cai, 1999). The problem may be simplified as uni-dimensional damage and only

the damage in the tension area is analysed. The effective tensile stress $\tilde{\sigma}_t$ in the tension area is expressed by:

$$\tilde{\sigma}_t = \frac{\sigma_t}{1-D} = E\varepsilon_t, (\sigma_t \geq 0, D \geq 0) \quad [4.6]$$

where D and E are respectively the degree of damage and the elastic modulus; ε_t and σ_t are respectively the strain and stress of the extreme tension fibre at the bottom of the concrete beam.

The effective compressive stress $\tilde{\sigma}_c$ in the compressive area is given by:

$$\tilde{\sigma}_c = \sigma_c = E\varepsilon_c, (\sigma_c \leq 0, D = 0) \quad [4.7]$$

where ε_c and σ_c are respectively the strain and stress of the extreme compression fibre at the top of the concrete beam.

When the effective stress $\tilde{\sigma} > 0$ (tension stress), we have $D = \frac{\tilde{\sigma}}{k}$, where k is the damage modulus. When $\tilde{\sigma} \leq 0$, we have $D = 0$. Based on the strain equivalence hypothesis, the following is obtained:

$$\sigma = (1-D)\tilde{\sigma} = (1-D)E\varepsilon = \left(1-\frac{\tilde{\sigma}}{k}\right)E\varepsilon = \left(1-\frac{E\varepsilon}{k}\right)E\varepsilon \quad [4.8]$$

where ε and σ are respectively the strain and stress of the concrete matrix.

If the beam is in the elastic stage, the degree of damage in the concrete $D = 0$, then $\sigma = E\varepsilon$. After the elastic stage, the stress state of the tension zone tends to be elasto-plastic due to the redistribution of stress before cracking. The correlation between ε and σ may be derived from Eq. [4.8] and expressed by:

$$\frac{d\sigma}{d\varepsilon} = E - \frac{2E^2\varepsilon}{k} \quad [4.9]$$

At the peak value of stress, the first derivative of stress should be equal to zero as described in Eq. [4.10]:

$$\frac{d\sigma}{d\varepsilon} = 0 \quad [4.10]$$

In this event, the critical cracking stress is σ_{cr} and the degree of damage D is equal to D_{cr}. From Eq. [4.9] and [4.10], we get $E\varepsilon = \frac{k}{2}$. Replacing $E\varepsilon$ in Eq. [4.8] gives the critical cracking stress $\sigma_{cr} = \frac{k}{4}$.

When $D = \frac{\tilde{\sigma}}{k}$, σ_{cr} can be evaluated as $\sigma_{cr} = \frac{k}{4} = (1-D_{cr})D_{cr}k$, from which $D_{cr} = 0.5$ is obtained. Therefore, the effective critical cracking stress $\tilde{\sigma}_{cr}$ may be expressed as:

$$\tilde{\sigma}_{cr} = D_{cr}k = \frac{k}{2} \quad [4.11]$$

The IGNA of the beam section may move up to the compression area as the tension area of the concrete beam is damaged and behaves in an approximately plastic manner. The depth of the beam section ($2h$) and the displacement of IGNA (the distance between the actual geometrical neutral axis and the initial geometrical neutral axis y_0) are illustrated in Fig. 4.13. The width of the beam section is b. During the loading process, the stress pattern in the compression zone changes continuously. Based on the plane section assumption, the relationship of stresses and strains may be described as follows:

$$\tilde{\sigma}_t = \frac{y - y_0}{h - y_0}\tilde{\sigma}_3 \quad [4.12a]$$

$$\tilde{\sigma}_1 = \frac{h + y_0}{y_0 - h}\tilde{\sigma}_3 \quad [4.12b]$$

$$\varepsilon_3 = \left(1 - \frac{h}{y_0}\right)\varepsilon_2 \quad [4.12c]$$

where ε_1, ε_2 and ε_3 are respectively the concrete strain at the top of the beam (outer fibre of the compression zone), the strain of the IGNA and the strain of the extreme tension fibre at the bottom, and $\tilde{\sigma}_1$, $\tilde{\sigma}_3$ are the corresponding effective stresses at the top and bottom of the beam section, respectively.

The resultant compression force N_c and the resultant tension force N_t in the cross section of the beam may be expressed as follows:

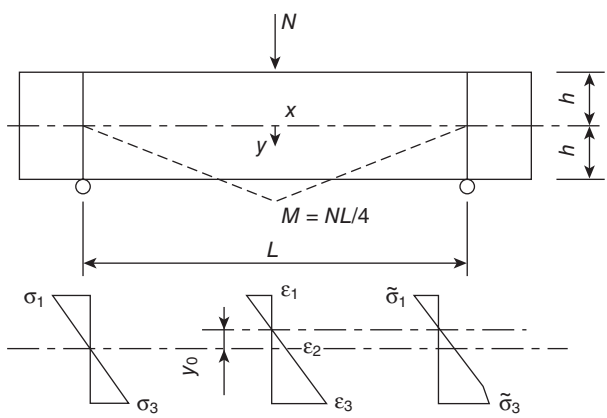

4.13 Flexural damage of rectangular concrete beam.

$$N_c = \frac{1}{2}b(h+y_0)\tilde{\sigma}_1 = \frac{b(h+y_0)^2}{2(y_0-h)}\tilde{\sigma}_3 \quad [4.13a]$$

$$N_t = \int_{y_0}^{h} dN_t = \frac{1}{6}b(h-y_0)\left(3-\frac{2\tilde{\sigma}_3}{k}\right)\tilde{\sigma}_3 \quad [4.13b]$$

The internal moment M_c caused by N_c and the internal moment M_t caused by N_t may be derived and expressed as follows:

$$M_c = -\frac{1}{6}b(h+y_0)(2h-y_0)\tilde{\sigma}_1 = \frac{b(h+y_0)^2(2h-y_0)}{6(h-y_0)}\tilde{\sigma}_3 \quad [4.14a]$$

$$M_t = \int_{y_0}^{h} ydN_t = \frac{1}{12}b(h-y_0)\left[4h+2y_0-\frac{\tilde{\sigma}_3}{k}(3h+y_0)\right]\tilde{\sigma}_3 \quad [4.14b]$$

Based on the equilibrium condition of the section, the following equations may be established:

$$N_c = N_t \quad [4.15a]$$

$$M = M_c + M_t = \frac{NL}{4} \quad [4.15b]$$

where M is the external bending moment.

From Eqs [4.12]–[4.15], the effective stress $\tilde{\sigma}_1$, $\tilde{\sigma}_3$ and degree of damage D of the extreme tension fibre at the bottom of the beam may be derived and expressed as follows:

$$\tilde{\sigma}_1 = \frac{6hy_0(h+y_0)}{(h-y_0)^3}k \quad [4.16]$$

$$\tilde{\sigma}_3 = \frac{-6hy_0}{(h-y_0)^2}k \quad [4.17]$$

$$D = \frac{\tilde{\sigma}_3}{k} = \frac{-6hy_0}{(h-y_0)^2} \quad [4.18]$$

As cracks form in the tensile zone of a concrete beam, failure occurs and the load bearing capacity of the beam will depend on the effective tensile stress $\tilde{\sigma}_3$. When the effective tension stress of concrete $\tilde{\sigma}_3$ reaches the critical cracking stress $\tilde{\sigma}_{cr}\left(\tilde{\sigma}_3 = \tilde{\sigma}_{cr} = \frac{k}{2}\right)$, then a beam without reinforcement will fail. From Eqs [4.13] and [4.14], the displacement of IGNA $(y_0)_{cr}$ and N_{cr} may also be described as follows:

$$(y_0)_{cr} = -0.102h \quad [4.19]$$

$$N_{cr} = \frac{0.944kbh^2}{L} \quad [4.20]$$

In the equations above, the factors such as strain (ε_1, ε_3) and the corresponding effective stress ($\tilde{\sigma}_1$ and $\tilde{\sigma}_3$) may be given as follows:

$$\varepsilon_1 = \frac{6N_{cr}Ly_0(h+y_0)}{0.944Ebh(h-y_0)^3} \quad [4.21]$$

$$\tilde{\sigma}_1 = \frac{6N_{cr}Ly_0(h+y_0)}{0.944bh(h-y_0)^3} \quad [4.22]$$

$$\varepsilon_3 = \frac{-6N_{cr}Ly_0}{0.944Ebh(h-y_0)^2} \quad [4.23]$$

$$\tilde{\sigma}_3 = \frac{-6N_{cr}Ly_0}{0.944bh(h-y_0)^2} \quad [4.24]$$

The relationship between the strain of IGNA (ε_2) and the degree of damage D may be written as follows:

$$\varepsilon_2 = \frac{N_{cr}L}{0.944Ebh^2} \cdot D\frac{1-\sqrt{1-\frac{2}{3}D}}{2} \quad [0 \le D \le 0.5] \quad [4.25]$$

It may be seen that the degree of damage D increases in a monotonic manner with an increase in the strain of IGNA ε_2.

Where R_0 denotes the initial electric resistance of a concrete beam before loading, R denotes the electric resistance of a beam subjected to external loading at different times and the First Order Exponential Decay function $Y = m\exp(-X/n) + p$, Y is replaced by $100\Delta R/R_0$ and X by ε_2, the relationship between the strain of IGNA (ε_2) and the FCR is obtained, which may be demonstrated as:

$$\varepsilon_2 = -n\ln\left[\frac{100(R-R_0)}{mR_0} - \frac{p}{m}\right] \Big/ 10^6 \quad [R \le R_0] \quad [4.26]$$

It may be seen that ε_2 increases with an increase in the absolute value of FCR.

The relationship between the degree of damage (D) and the FCR may be written as:

$$-n\ln\left[\frac{100(R-R_0)}{mR_0} - \frac{p}{m}\right] \Big/ 10^6 = \frac{N_{cr}L}{0.944Ebh^2} \cdot D\frac{1-\sqrt{1-\frac{2}{3}D}}{2} \quad [4.27]$$

It may be seen that the degree of damage D increases monotonically with an increase in the absolute value of FCR.

When the elastic modulus E, beam dimensions ($b, 2h, L$) and the cracking load (N_{cr}) are given, the electrical resistance (both the initial R_0 before loading and R under loading) can be measured. The stress–strain state

subjected to the cracking load may therefore be calculated according to Eqs [4.21]–[4.25]. The displacement of IGNA $(y_0)_{cr}$ under the cracking load is obtained from Eq. [4.19] and the degree of damage D of the concrete beam under the cracking load can be evaluated according to Eq. [4.27].

4.6 Diphasic electrical conductive materials

Specimen BF28 is taken as an example for diphasic electric conductive materials (the combination of NCB0.2% and CF0.8%). The beam dimensions are given as follows: section width (b) = 100 mm, section depth ($2h$) = 100 mm, beam length (L) = 300 mm. The loading history of the beam with BF28 is illustrated in Fig. 4.4b. The elastic modulus (E) is 3.0×10^4 N/mm^2; the cracking load (N_{cr}) is 14.5 kN; the parameters m (=13.45), n (=68.90) and p (= -16.11) may be obtained from Table 4.7 before the beam is subjected to loading N (at the beginning ($t = 0$)), R_0 = 1190 Ω; and $\varepsilon_2 = 0$, $y_0 = 0$, $D = 0$. When the beam is subjected to load N, concrete damage occurs and the resistance of the electric conduction concrete t $R(t)$, can be measured at any time. The values of the degree of damage D, the stresses and strains and the displacement of IGNA y_0 of diphasic electric conductive concrete beam BF28 at different load times are calculated using Eqs [4.21]–[4.27] and summarized in Table 4.8.

From Table 4.8 and Fig. 4.4, the following points may be observed:

- Prior to cracking in a flexural beam, the electrical resistance (R) usually declines with an increase in the loading magnitude and duration.
- The absolute value of the FCR in a flexural beam increases with an increase in the loading magnitude and duration.
- Both the degree of damage (D) and the strain of IGNA (ε_2) increase with an increase of the absolute value of FCR. At a time of 1655 seconds

Table 4.8 Results of measured resistance, calculated degree of damage, and the effective stress and strain of BF28

Variable factors	Calculation results		
Time t (s)	269	475	836
R (Ω, measured)	1142	1119	1095
|FCR| (%)	4	6	8
D (%)	26.00	42.18	49.53
ε_2 (10^{-6})	7.23	19.67	34.86
y_0 (mm)	–2.38	–4.12	–4.91
$\tilde{\sigma}_1$(N/mm^2)	–4.35	–6.58	–8.08
$\tilde{\sigma}_3$(N/mm^2)	4.78	7.76	10.18
ε_1 (10^{-6})	–144.98	–219.22	–269.42
ε_3 (10^{-6})	159.47	258.59	339.17

after loading, $D = 0.486$, which is close to $D_{cr} = 0.5$, indicating that the cracking load N_{cr} is almost reached.

- As the strain of IGNA (ε_2) increases with the loading magnitude, the FCR increases gradually with the increase of D. This provides convincing evidence that the suggested formula $Y = m\exp(-X/n) + p$ effectively meets the relationship between ε_2 and FCR.
- The absolute value of the displacement of IGNA (y_0) increases gradually with increased absolute values of FCR and D.
- Other factors such as $\tilde{\sigma}_1$ and $\tilde{\sigma}_3$, ε_1 and ε_3 increase with an increase in FCR and D.

4.7 Conclusions

A large number of experimental investigations have been carried out on the workability, electric properties and mechanical behaviour of concrete containing conductive materials. The effects of NCB, CF and diphasic BF on the relationship between fractional change in resistance, strain and degree of damage prior to cracking have been analysed. A relationship between the FCR and the strain of IGNA (ε_2) is suggested. The results have led to the following conclusions:

1. Concrete conductivity increases with an increase in dosages of NCB and CF. However, the workability of fresh concrete is an important precondition for selecting the types and content of the conductive materials.
2. Workability declines with an increase in NCB or CF content and the upper limit of conductive materials is determined mainly by workability, not by conductivity. This point had not been taken into consideration in previous investigations.
3. The flexural strength of a beam usually increases with an increase in CF and BF content. However, only the addition of NCB exerts any influence on the flexural strength.
4. The strain of IGNA (ε_2) is a function of FCR. Prior to the concrete cracking, the First Order Exponential Decay function agrees well with the relationship between ε_2 and |FCR| during the loading process of CFRC beams.
5. Both the degree of damage (D) and the strain of IGNA (ε_2) increase with an increase in FCR.
6. All the mechanical factors in concrete containing conductive admixtures decline with an increase in FCR and D.
7. Results from examples evaluating the effect of diphasic electric conductive materials on the capacity for the self-diagnosis of strain and damage have been validated.

4.8 References

Cai, S.W.; Cai, M. (1999), *Concrete Damage Fractures*. China Communications Press, Peking.

Cai, S.W.; Chung, D.D.L. (2006), Effects of strain and damage on strain-sensing ability of carbon fiber cement. *J. Mater. Civ. Eng.* 18, 355–360.

Cai, S.W.; Chung, D.D.L. (2007), Partial replacement carbon fiber by carbon black in multifunctional cement matrix composites. *Carbon* 45, 505–513.

Chung, D.D.L. (2012), Carbon materials for structural self-sensing, electromagnetic shielding and thermal interfacing. *Carbon* 50, 3342–3353.

Li, H.; Ou, J.P. (2007), Smart concrete and structures. In: *Proc. of 16th National Conference on Structural Engineering*, *Shanxi*, 58–76.

Li, H.; Xiao, H.G.; Ou, J.P. (2006), Effect of compressive strain on electrical resistivity of carbon black-filled cement-based composites. *Cement & Concrete Composites* 28, 824–828.

Li, H.; Xiao, H.G.; Ou, J.P. (2008), Electrical property of cement-based composites filled with carbon black under long-term wet and loading condition. *Composites Science and Technology* 68, 2114–2119.

Ou, J.P. (1996), Assessment of the accumulative damage and security for major engineering structure. In: *Chinese Mechanics towards the 21st Century – the Report of Young Scientists' Forum of the 9th Procession of the China Association for Science and Technology*. Tsinghua University Press, Peking.

Tian, X.; Hu, H. (2012), Test and study on electrical property of conductive concrete. *Procedia Earth and Planetary Science* 5, 83–87.

Wen, S.H.; Chung, D.D.L. (2000), Damage monitoring of cement paste by electrical resistance measurement. *Cement and Concrete Research* 30, 1979–1982.

Wen, S.H.; Chung, D.D.L. (2004), Effects of carbon black on the thermal, mechanical and electrical properties of pitch-matrix composites. *Carbon* 42, 2393–2397.

Wen, S.H.; Chung, D.D.L. (2005), Self-sensing characteristics of carbon fiber reinforced cement. *ACI Materials Journal* 102, 244–248.

Wen, S.H.; Chung, D.D.L. (2006), Self-sensing of flexural damage and strain in carbon fiber reinforced cement and effect of embedded steel reinforcing bars. *Carbon* 44, 1496–1502.

Wen, S.H.; Chung, D.D.L. (2007), Partial replacement of carbon fiber by carbon black in multifunctional cement–matrix composites. *Carbon* 45, 505–513.

Wu, X. (2005), Study on relations among electric conductivity, stress and strain under the whole loading process for conductible concrete. *J. Neu.* 7–19.

Yehia, S.; Tuan, C.Y. (1999), Conductive concrete overlay for bridge deck deicing. *ACI Materials Journal* 96, 382–390.

5

The use of nanotechnology to improve the bulk and surface properties of steel for structural applications

X. SHI, Montana State University, USA,
Z. XIAO, Shenzhen Jinzhou Precision Technology Corp., China
and J. WU, Wuhan Polytechnic University, China

DOI: 10.1533/9780857098832.1.75

Abstract: This chapter discusses the utilization of nanotechnology to greatly enhance the properties of steels, by modifying the chemical composition and/or microstructure of bulk material or surface layer. It starts with a brief discussion of the relevant knowledge base, including: microstructure and chemical composition of steel, influence of nano-modification and processing approaches, and modeling of nanocomposite steel. Then, it provides a review of technological advances in the use of nanotechnology to produce high performance steels with outstanding mechanical properties or corrosion resistance. The chapter concludes with a discussion of future developments expected on the subject.

Key words: plastic deformation, thermomechanical treatment, nanotechnology, nanostructured, nano/ultrafine grain size, high performance steel.

5.1 Introduction

Steel is a versatile material of technological importance and its outstanding recyclability and ease of manufacturing greatly contribute to eco-efficient construction. Steel is a type of widely used engineering material in many industries, e.g., transportation, construction, defense, healthcare, energy, aeronautics, manufacturing, and chemical processing. It has found diverse applications in transport vehicles and components, ships, buildings, civil structures, offshore structures, aircraft landing gears, bulletproof sheets and vests, household appliances, medical tools, pipelines, heat exchangers, solar panels, equipment, nuts and bolts, bearings, packaging, etc. Steel is the most widely used metallic alloy in modern industries, with its usage approximately 80% by weight of all alloys (Smith, 1981).

Over the last two decades, great strides have been made to improve the engineering properties of steels through research, development and implementation. In supporting such innnovative technological advances, nano-

technology has been playing an increasingly important role. For instance, Lesuer *et al.* (2010) reported the fabrication of Fe-C alloys with ultrahigh strength (4600 MPa) through quenching and severe plastic deformation (SPD). The strengthening was attributed to the nano-size effect of lath and plate martensite grains and the small interparticle spacing. As reviewed by Kolpakov *et al.* (2007), metallurgy approaches to the production of high performance steels with a fine-grain structure and/or self-organization of strengthening nanophases (carbides, nitrides, carbonitrides, intermetallides) have been burgeoning under the guide of nanotechnological principles, including nanoprocesses for steel smelting and microalloying, mechanical pressure treatment (e.g., SPD), and heat treatment (e.g., superfast quenching of melts). One such technology commercialized in the US produces high performance carbon steels that feature a 'three-phase microstructure consisting of grains of ferrite fused with grains that contain dislocated lath structures in which laths of martensite alternate with thin films of austenite' (Kusinski *et al.*, 2004).

Recent years have seen the fabrication of high performance steels desirable for light weight construction and other engineering applications. As detailed later, these steels typically feature an ultrafine or nano-grained microstructure, which leads to excellent properties in both strength and ductility. In addition, nanotechnology has been employed to enhance the durability of the steel bulk material or surface layer, in terms of resistance to wear, fatigue, and/or corrosion. This is made possible by achieving the desirable finely crystalline microstructure of steel (e.g., nanocrystallization) or by modifying its chemical composition at the nanometer scale. Formation of Cu nanoparticles at the steel grain boundaries (GBs) has been used to improve the corrosion resistance of steel. Addition of Cu nanoparticles has also been reported to mitigate the fatigue cracking of steel, by reducing the surface roughness of steel and associated stress risers (Mann, 2006).

This chapter synthesizes the findings of some of the major research efforts in this area and presents a discussion of utilizing nanotechnology to greatly enhance the properties of steels, by modifying the chemical composition and/or microstructure of bulk material or surface layer.

5.2 Research relating to nanocomposite steel

5.2.1 Microstructure and chemical composition of steel

While Fe is the main element in steels, other elements (e.g., C, alloying elements, and impurities) define the manifold properties of steels, including: tensile strength, fatigue strength, ductility, hardness, toughness, wear resistance, formability, weldability, fire resistance, corrosion resistance, etc. The

microstructure of steel is inherently heterogeneous, generally consisting of grains (or 'phases', considered to be homogeneous in physiochemical nature), dislocations, GBs, precipitates, and lattice defects. Figure 5.1 presents a portion of the equilibrium phase diagram of the Fe-C system under atmospheric pressure (Chipman, 1972), which illustrates the thermodynamics of three main phases in carbon steel, i.e., autensite (γ), ferrite (α), and cementite (Fe_3C), as a function of temperature and C content. Note that equilibrium phases tend to form when there is sufficient time to allow diffusion of atoms and molecules. In many cases, the processing of steel may include quenching or application of mechanical stress, which leads to the formation of non-equilibrium phases such as martensite (α'). For steels with a significant amount of alloying elements (e.g., stainelss steels), their microstructure may include many phases other than γ, α, and α' (Lo *et al.*, 2009).

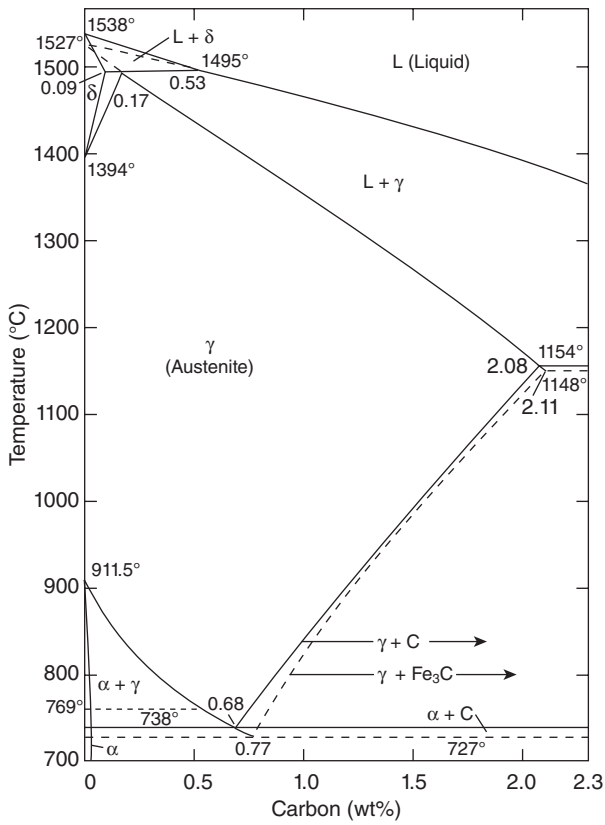

5.1 Portion of the phase diagram Fe-C relevant to carbon steel. Metastable γ-range and system Fe-Fe_3C shown by dashed lines. Curie temperature dotted (adopted from Chipman, 1972). *With kind permission from Springer Science and Business Media.*

High-strength steels are often martensitic; as the C content increases, their strength increases but ductility and weldability tend to decrease. Martensite can serve as an effective starting phase for acquiring ultrafine or nano-grained microstructure with small strains. For instance, Tsuji and Maki (2009) reported the formation of microstructure in steel characteristic of equiaxed α grains (~200 nm), by cold-rolling and annealing of a starting α' phase. Austenitic stainless steels (SS) generally have low yield strength (150–300 MPa) yet excel at corrosion and oxidation resistance, work-hardening rate, and formability. Their strengthening by grain refinement can be achieved via reverse α' transformation or SPD, and greatly enhances strength and resistance to wear, pitting, cavitation, cavitation-erosion, and radiation-induced damage (Lo *et al.*, 2009). The grain refinement of γ SS may compromise ductility and work-hardening. The strengthening of γ SS by martensite or dispersed precipitates can compromise their corrosion resistance, formability and ductility (Lo *et al.*, 2009).

Alloying elements in steel 'may change the transformation temperature, or form more stable special carbides instead of cementite, . . . (or) change the sequence of nucleation and growth processes by affecting the interface energies or the diffusion processes' (Eisenhüttenleute, 1992). In addition, the microstructure of steel can be controlled by manipulating the kinetics of its formation, via thermal and mechanical treatments. For instance, the following solid–solid state transformation can occur (Fig. 5.1): $\gamma \rightarrow \alpha + Fe_3C$ (Branagan *et al.*, 2006). Each phase may feature multiple allotropes, i.e., various structural forms of the same chemical composition. For instance, cementite can be in the form of 'pearlite, bainite, and/or tempered martensite, depending on steel composition and preceding cooling conditions' (Eisenhüttenleute, 1992). The ultimate microstructure of a steel with given alloy chemistry is often defined by the γ-state grain size and homogeneity, transformations induced by heat treatment (e.g., quenching and annealing), and physical interactions induced by mechanical processing (e.g., SPD).

5.2.2 Influence of nano-modification

In the last decades, grain refinement has been confirmed as an effective way to concurrently enhance strength and toughness of polycrystalline materials and has been used to remarkably improve the comprehensive mechanical properties of steels. Zhao *et al.* (2011) found the grain size of large-grain-size regions to be responsible for the ductile-to-brittle transition temperature of an ultrafine grained ferrite/cementite steel. As the average grain size or weighted average grain size decreases, the yield strength and hardness of polycrystalline materials (e.g., steels) are expected to increase greatly, according to the well-known Hall–Petch relation (Lo *et al.*, 2009). This can be attributed to the high concentration of GBs, which serve as barriers to

pin the motion of dislocations. Once the grain size is reduced to the nanometer range, an inverse Hall–Petch relation can be observed. This can be credited to the extremely high density of GBs in the microstructure of nano-grained steel, which leads to 'role-exchange of the grain bulk and the GB in the deforming mechanism' and 'a transition from intragranular to GB-mediated deformation' (Weertman, 1993; Song *et al.*, 1999; Frontán *et al.*, 2012). Nonetheless, as reviewed by Lesuer *et al.* (2010), the tensile strength of steels generally exhibits a negative linear relationship with the interparticle spacing, despite the significant variations in their chemical composition and thermomechanical history (Fig. 5.2). In other words, grain refinement has been the main pathway to achieve high strength for steels. The only exception was a case where a lath martensite nano-structure greatly enhanced the strength of the steel, thus deviating from this linear relation (Fig. 5.2).

One potential issue related to microstructure ultrafining of steels is that their heat affected zones (HAZ) tend to exhibit various degrees of embrittlement and localized softening as a result of localized grain coarsening. This can be addressed by inducing the nucleation of intragranular acicular ferrite around oxide inclusions, following the oxide-dispersed-strengthened (ODS) steel technology (Lei *et al.*, 2007). Another way to refine the HAZ

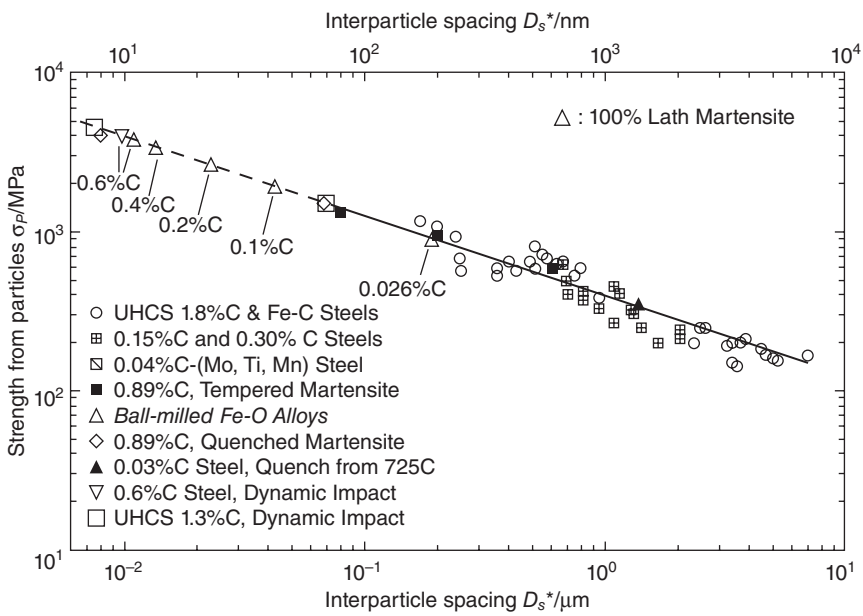

5.2 Tensile strength of steels as a function of interparticle spacing (adopted from Lesuer *et al.*, 2010). *With kind permission from Springer Science and Business Media.*

grains and improve weld toughness is to add Mg and Ca nanoparticles in the steel (Mann, 2006). Grain coarsening at elevated temperatures can be inhibited via GB segregation and various drag effects (Malow and Koch, 1997; Matsuia *et al.*, 2006), or via GB modification or manipulation of nanotwin boundaries inside the grains (Lu *et al.* 2009; Li *et al.* 2010). All of these mechanisms serve to preserve the ductility of high strength steel. Gonsalves *et al.* (1994) suggested that carbide particles a few microns in diameter may act as initiation sites of fatigue cracks. Lo *et al.* (2009) suggested that the precipitation of carbides at GBs can cause localized depletion of Cr content in SS and increase their risk of corrosion and sensitization They also reported the use of nitrogen to inhibit the formation of the $M_{23}C_6$ carbide so as to minimize its undesirable effects on GB serration and creep-fatigue resistance. As detailed in Table 5.1, the formation of nano-sized grains, twins, or inclusions can mitigate such risks of microstructure ultrafining.

Nanotechnology provides a potential solution to considerably enhancing the ductility of high strength steel, as the nanocomposite steels deform by GB mechanisms, e.g., sliding and diffusion, rather than dislocation motion. Grain refinement can be coupled with phase transformation induced plasticity (TRIP) to form γ grains of micron or nano-size, endowing the steel with outstanding synergy in strength, ductility, and work-hardening ability. While coarse MC carbides degrade creep-fatigue resistance and fracture resistance of SS, fine MC carbides can inhibit the growth of grains and greatly improve the impact property and strength of SS (Lo *et al.*, 2009). Often, a second phase or nanostructure can be uniformly dispersed in the relatively brittle bulk matrix in order to introduce plasticity. Alternatively, nano-grains or nanotwin boundaries inside the grains can be introduced to delocalize the micro- and nano-scale deformation and to improve toughness. Zhao *et al.* (2011) suggested high-angle GBs to be most effective in hindering the propagation of cleavage cracks. Manipulation of GB structures (i.e., GB engineering) can be utilized to enhance the bulk properties of steels, e.g., by reducing carbide precipitation at GBs (Lo *et al.*, 2009).

5.2.3 Influence of processing approaches

Conventionally, there are four main pathways to achieve a fine-grained microstructure (e.g., grain size of 1 mm): repetitive short austenitizing at low temperatures; 'deformation in the austenite range followed by recrystallization'; deformation of austenite at temperatures featuring a low recrystallization rate; or cooling to induce transformation at low temperatures (Eisenhüttenleute, 1992).

Recent decades have seen the increased use of metallurgical refining, SPD, thermomechanical treatment (TMT), and liquid-state treatments to produce steels with ultrafine grained microstructure. The reduction of grain

Table 5.1 Recent research on the utilization of nanotechnology to improve the mechanical properties of steel bulk

Reference	*Steel type*	*Production process*	*Microstructure of bulk material*	*Novel properties or phenomenon*	*Mechanism(s)*
Kusinski and Pollack (2008)	Carbon steel (≤0.35% C)	Heating into the austenite range + cooling to induce $\gamma \rightarrow \alpha$ and $\gamma \rightarrow \alpha'$ transformations + rolling or forging	Triple-phase: crystals featuring parallel α' laths with nano-γ films in between, fused with α crystals (2–100 μm)	High strength, toughness, corrosion resistance, and cold formability	Great toughness by the lath structure; ductility and formability by the retained-γ films
Eskandari *et al.* (2009)	301 SS	TMT: repetitive cold rolling + annealing	90 vol% of nano-crystal γ grains (30–40 nm)	High yield strength (up to 2000 MPa)	Strain inducing the formation of α' with lattice defects, followed by $\alpha' \rightarrow \gamma$ reverse transformation
Menapace *et al.* (2009)	Fe-1.5%Mo powder + SiC (1.5 wt.%, 30 nm) particles	Microalloying + spark plasma sintering	Multiphased nanostructure with 'elongated (bainitic α) lamellae separated by thin layers of retained-γ'; some equiaxed α-grains and α'	Yield strength of 550 MPa; uniform plastic strain (10%) at fracture (1020 MPa)	Transformation-induced plasticity (TRIP)
Guo *et al.* (2010)	Nb-microalloyed pipeline steel	Two-stage thermo-mechanical rolling + fast cooling	Mainly fine plate domains (~3.2 μm) featuring lath-bainite (~200 nm thick) and some acicular α	Yied strength of 900 MPa; low yield ratio of 0.84; El of 15%; impact toughness of 200 J at –20°C	Nano-precipitates of (Nb, Ti)(C,N) and NbC to inhibit grain growth; high dislocation density of microstructure

Table 5.1 Continued

Reference	*Steel type*	*Production process*	*Microstructure of bulk material*	*Novel properties or phenomenon*	*Mechanism(s)*
Du *et al.* (2010)	Microalloyed steels	Warm-rolling + deforming + quenching (repetitive)	Uniform and equiaxed α grains (100–300 nm)	'Deformation-induced transformation of ultrafine austenite (~1 μm) to ferrite'	Nucleation of α along γ GBs, enhanced by the boundary slipping
Askari *et al.* (2010)	High-strength α-steel (0.08% Ti)	Microalloying	Dual precipitate microstructure: TiC (avg. 10 nm) in the matrix and coarse cubic $M_{23}C_6$ at GBs and inside grains	Yield strength 2–3 times higher than 'conventional Ti-bearing high-strength hot-rolled sheet steels'	Nano-precipitates destroy the dislocations or anchor against their movement
Wang *et al.* (2011)	High-strength low-alloy steel (low C, low Ti)	Microalloying + hot rolling	Polyganal α and granular bainite, a small amount of α'- α islands, and very small amounts of fine pearlite	Yield strength 640 MPa	Strengthening effect of nano-scale Fe_3C precipitates
Hodgson *et al.* (2011)	0.79C-1.5Si-1.98Mn-0.98Cr-0.24Mo-1.06Al-1.58Co steel	200°C/10 days	Bainitic α laths (average thickness of 60 ± 10 nm) with retained-γ films in between and high dislocation density (~4.7×10^{15} m^{-2})	Excellent strength-toughness-ductility balance	Dual microstructure that contributes to ultrahigh strength and toughness (by nanobainitic laths) as well as ductility (retained γ)

Zhang *et al.* (2011)	High-strength α-steel (2.49% Cu)	1000°C/1h + quenching by water + 500°C/200h	$(FeAl)_2B$ nanoparticles along α GBs and Cu-rich nano-clusters in matrix	B-doping led to larger elongation of the steel	B enhances the GB cohesion and inhibits the integranular fracture
Foroozmehr *et al.* (2011)	Low-carbon steels	Martensite process: quenching + cold rolling + annealing	Nano/sub-micron scale α grains (e.g., 142 nm)	Increasing the C content or imposing larger (rolling) reduction can lead to finer ferrite grains	C reduces the size of blocks and packets in lath α'
Hosseini *et al.* (2011)	Low-carbon steel (0.13% C)	Martensite process: quenching + plane strain compression + annealing		UTS of 1135 Mpa; El of 11.6%	Fragmentation of the initial α' to α grains
Xu *et al.* (2011)	Ti-bearing α'-steel	Tempering + reheat quenching	High density of nano-precipitates (1–10 nm) of TiC in α' grains (~8 μm)	High yield strength (1280 MPa) and impact toughness (El of 13% and impact energy of 32 J at −40°C)	Strenghthening and grain refining by nano-TiC precipitates and toughening by high % of high-angle GBs

Table 5.1 Continued

Reference	*Steel type*	*Production process*	*Microstructure of bulk material*	*Novel properties or phenomenon*	*Mechanism(s)*
Taneike *et al.* (2003)	ODS α'-steel (0.002C-9Cr-3W-3Co-0.2V-0.06Nb-0.05N)	Conventional processing techniques (including heat treatment)	High density of nano-precipitates (5–10 nm) 'along prior (γ GBs) as well as along lath, block, and packet boundaries'	Outstanding high-temperature creep resistance (at 923K, time-to-rupture two orders of magnitude higher than conventional creep-resistant steels); sufficient fracture toughness (100–150 J at room temperature)	Carbonitride nano-precipitates pin the GBs
Kim *et al.* (2003)	ODS 12YWT α-steel	MA	Uniform distribution of Ti and W; dispersion of nano-sized complex Ti-Y-O oxides	Outstanding high-temperature TS and creep rupture strength	Solid solution hardening by W; dispersion strengthening by nanoparticles
Klueh *et al.* (2005)	ODS 9Cr-1Mo α'-steels	TMT: austenitizing + cooling + hot rolling + annealing + normalizing + tempering	MX precipitates (30 nm) at 7–8 $\times$ 10^{18} m^{-3} and $M_{23}C_6$ (130-150 nm) at 3–6 $\times$ 10^{19} m^{-3}	Outstanding high-temperature tensile and creep strength (600–750°C or higher)	Strengthening effect of nano-scale MX precipitates (VN, NbC, or NbNC)
Ohtsuka *et al.* (2007)	ODS 9Cr α'-steels	MA + annealing	Hard grains (residual-α) and soft grains (tempered α')	Increasing [Ti] to 0.30–0.35% greatly improves creep strength	Ti increases residual-α grains that suppress the GB sliding

Sokolov *et al.* (2007)	ODS 12YWT α-steel (12Cr-2.5W-0.4Ti-0.25Y_2O_3)	MA	High density of nano-sized complex Ti-Y-O oxides (clusters) dispersed in α matrix	High yield (~1300 MPa) and ultimate (~1400 MPa) strengths at room temperature; good fracture toughness (93 MPa $m^{1/2}$ at 100°C)	Ultrafine particles and solute segregation to the dislocations constrain the dislocation movement
Abe *et al.* (2007)	ODS 9Cr α'-steels	TMT: normalizing + tempering	MX precipitates (5–20 nm) along GBs and in the matrix and $M_{23}C_6$ (100–300 nm)	Excellent creep strength at 650°C	V and Nb nitrides pin the lath and block boundaries; TiC nano-precipitates stabilize the microstructure during creep
Oksiuta *et al.* (2011)	ODS RAF steel	MA + hot isostatic pressing and annealing	Nanoclusters of Fe_2Y or Y_2O_3 dispersed with a mix of small and large α-Fe (bcc) grains (avg. 5 μm)	ODS Fe_2Y steel: an upper shelf energy of 8.8 J and a ductile-to-brittle temperature of –24°C	γ-fcc structure of Fe_2Y nanoclusters: coarsened by annealing
Karak *et al.* (2011)	ODS high-Cr α-steels	MA + hot isostatic pressing	'Uniform dispersion of 20–30 nm Y_2O_3 or $Y_2Ti_2O_7$ in higher volume fraction'	Extremely high compressive strength (3325 MPa), Young's modulus (295 GPa), fracture toughness (21.8 MPa $m^{1/2}$); but low ductility	Dispersion strengthening by nanoparticles

Table 5.1 Continued

Reference	*Steel type*	*Production process*	*Microstructure of bulk material*	*Novel properties or phenomenon*	*Mechanism(s)*
Hidaka *et al.* (2003)	Pure Fe and cementite (6.2% C)	SPD: mechanical milling of metallic powder	Nano-crystal α grains (~15 nm, for Fe-0.8C) transformed from the dislocation cells	Dynamic continous recrystallization	Added C facilitates grain refining by increasing the 'net stored strain energy' by dislocations
Khodabakhshi *et al.* (2010)	Low-carbon steel (0.05–0.06% C)	SPD: constrained groove pressing	α grains (200–300 nm) at cumulative grain of 4.64	UTS of 450 MPa; increased superplasticity	Work hardening and grain refining
Khodabakhshi and Kazeminezhad (2010)				Electrical resistivity improved by ~100%	Refined microstructure and high density of dislocations
Kozikowski *et al.* (2010)	Eurofer 97 RAFM steel	SPD: HE + annealing	Heavily deformed grains (~80 nm) after HE	Post-deformation annealing at high temperature improves impact strength: 108 J/cm^2 after 800°C/1h	Grain refinement by HE enhances TS and microhardness but reduces ductility
Ahmadabadi *et al.* (2011)	10Ni-7Mn steel	SPD: cold rolling + equal-channel angular pressing	Ultrafine α grains separated by nano-NiMn precipitate-hardened pancake grains	Substantially improved tensile properties at thickness reductions > 60%	Deformation-induced $\alpha' \rightarrow \gamma$ reverse transformation and grain refining; high % of high-angle GBs and saturated vacancies

Li *et al.* (2011)	Low-carbon steel (0.12% C)	SPD: tempering + reheat quenching + cold rolling (80% reduction)	Nano-level delaminated microstructure with α' lathes (average 100 nm thick)	Significantly improved high-cycle fatigue properties	'Micro-cracks form on the weak interface of the nano-grained steel under low-stress conditions' and inhibit the propagation of main cracks
Liu *et al.* (2010)	316 SS	SPD: dynamic plastic deformation + annealing	~20 vol% nanotwin bundles embedded in micro- and nano-γ grains	UTS of ~1 GPa; El of 23–27%	Nanotwins with twin boundaries that act as slip planes while resisting dislocation motion; low dislocation density
Yan *et al.* (2012)	316 SS				
Lu *et al.* (2012)	316 SS and 25Mn γ-steel		Single-phase hierachical microstructure with nanotwinned γ grains: 'elastically homogeneous but plastically heterogeneous'	Superior strength-ductility synergy (e.g., yield strength of a few GPa and very high work-hardening rates)	

BOF: basic oxygen furnace; CSP: compact strip production; HE: hydrostatic extrusion.
RAFM: reduced activation ferritic/martensitic; UTS: ultimate tensile strength.

size from millimeter scale to micron scale is achieved by increasing the rate of grain nucleation while reducing the rate of grain growth. The grain refinement in the liquid state, for instance, may involve the use of pulsed magnetic fields, pulsed current, or ultrasonic energy to induce refined microstructure of SS during its solidification (Lo *et al.*, 2009). Okamura *et al.* (1995) reported the formation of ultrafine grained bainite structure in new HT780 steels (0.05–0.06% C; B-free) by direct quenching and tempering. These steels exhibit outstanding mechanical properties: tensile strength (TS) of 825 MPa and total elongation (El) of 26% at fracture. They also exhibit excellent welding properties (e.g., low HAZ hardness) and good fatigue properties, attributable to precipitation hardening and grain refinement by Cu, Nb, and V. Some alloying elements (e.g., Tb, Ni, and V) can form nano-precipitates with the C or N in steel and greatly inhibit the growth of grains while forming a high concentration of non-uniform grains. There are also alloying elements (e.g., Mn and Cr) that can reduce the phase transformation temperature and refine the grains during or after the phase transformation. Lei *et al.* (2007) suggested that the best way of grain refining was to couple alloying with TMT or SPD.

While nano-grained or nano-amorphous steels may be synthesized by the 'bottom-up' approach such as gas condensation or chemical analysis (Averback, 1993; Gonsalves *et al.*, 1994), these production processes do not lend themselves to industrial manufacturing. In contrast, the 'top-down' approach such as mechanical alloying (MA), TMT and SPD can be readily implemented at large industrial scale. TMT can be as simple as the conventional cold rolling followed by annealing, or may consist of advanced treatment sequences. Bhadeshia (2008) reported the use of TMT to induce phase transformation, forming nanostructured bainitic α and γ plates (~20 nm) in steels with a high C concentration. In addition to phase transformation, TMT may induce other solid–solid reactions such as recrystallization and precipitation. SPD involves intensive straining processes. SPD can induce the formation of nanocrystalline grains in bulk material (with equal channel angular pressing – ECAP, high pressure torsion, accumulative roll bonding, repetitive corrugation and straightening, constrained groove rolling or pressing, etc.) or in surface layer (100 μm to 30 mm thick, with surface mechanical attrition treatment – SMAT, ball milling, slide wearing, wire brushing, ultrasonic or high-energy shot peening, supersonic fine particles bombardment – SFPB, severe cold drawing, ultrasonic cold forging – UCFT, etc.). SPD concurrently improves the strength and toughness of steels by substantially refining the microstructure of steel, increasing the density of dislocations, dislocation walls, and vacancies, forming non-equilibrium GBs, and stabilizing austensite phases (Valiev, 2004). Tsuji and Maki (2009) demonstrated that nanostructures in steel can be produced by different ways of combining phase transformation and plastic deformation. They also revealed

the effective role of plastic deformation in increasing nucleation sites for subsequent phase transformation.

5.2.4 Modeling of nanocomposite steel

Modeling can be used as a powerful tool to advance the fundamental knowledge pertinent to nanocomposite steel, especially when integrated with or validated by experimental investigation. Thermodynamic modeling can provide insights into phase stability and transformations. For instance, a Pourbaix diagram (potential–pH diagram) can be used to predict and guide the synthesis and application of steels under given working conditions (Kaufman *et al.*, 2009). Molecular dynamics modeling can shed light on mechanisms underlying mechanical properties of steels, by simulating the interactions between dislocations with GBs, twins, precipitates and other barriers during deformation (Li *et al.*, 2010; Wu *et al.*, 2009, 2011). Mechanistic models have also been established for predicting the fatigue life of SS under various conditions (Lo *et al.*, 2009). In addition, improved understanding of corrosion and inhibition mechanisms has been continually achieved through characterization and modeling of the steel surface and corrosion products at various length scales down to the nanometer scale (Murayama *et al.*, 2008).

5.3 Properties of nanocomposite steel

5.3.1 Nanotechnology to improve mechanical properties of steel bulk

Nanotechnology has been employed to enhance the mechanical properties of the steel bulk itself, by achieving the desirable finely crystalline microstructure of steel or by modifying its chemical composition or morphology at the nano- or micro-scale. Table 5.1 summarizes recent research on this subject, involving various classes of steel: carbon steel (≤2.1% C, low alloy), SS (≥10.5% Cr), alloy steel, ODS steel, etc. A wide variety of processing approaches have been investigated for producing nanocomposite steels. TMT, MA, and SPD have been used individually or synergistically, to induce nanostructure via phase transformation and deformation processes. There is also a high level of diversity in the resulting microstructure of nanocomposite steel, ranging from single-phase, dual-phase, to multi-phase and ranging from nano-grains of α or γ, to α' laths or bainitic α lamellae with nano-γ films in between, to nano-precipitates/clusters in or along nano- or micro-grains of α' or α. These nano-modified steel bulk feature novel mechanical properties, characteristic of considerable improvements in strength (e.g., TS up to 2000 MPa) alone or in strength as well as toughness

(e.g., El of 15%; impact toughness of 200 J at –20°C) and high-temperature creep resistance (e.g., at 923K, time-to-rupture 2 orders of magnitude higher than conventional creep-resistant steels), etc. There are multiple mechanisms underlying the outstanding strength–ductility synergy of nanocomposite steels. Often the toughness is introduced by the lath or lamella structure or high percentage of high-angle GBs; ductility and formability are introduced by the retained γ films or tempered α'; and strength is enhanced by the nano-grains, nano-precipitates of carbides, nitrides, or carbonitrides, or other nano-inclusions.

One recent advance in this field is the use of dynamic plastic deformation (DPD) followed by annealing to produce SS and alloy steels with superior strength–ductility synergy, such as TS of 1 GPa, El of 27%, and very high work-hardening rates (Liu *et al.*, 2010; Lu *et al.*, 2012; Yan *et al.*, 2012). These nanocomposite steels feature a unique single-phase hierachical microstructure with ~20 vol% nanotwin (NT) bundles embedded in micro- and nano-γ grains and low dislocation density. Their mechanical behavior is 'elastically homogeneous but plastically heterogeneous'. It was hypothesized that the NT boundaries act as slip planes while resisting dislocation motion. Figure 5.3 presents typical bright-field transmission electron microscopy (TEM) images of 316 SS after DPD and annealing, showing the early-stage static recystallization (SRX) in shear bands between NT bundles. The SRX grains and NT bundles introduce a great amount of ductility into the steel bulk, while enhancing its strength simultaneously (Yan *et al.*, 2012).

5.3.2 Nanotechnology to improve mechanical properties of steel surface

Nanotechnology has also been employed to enhance the mechanical properties of the steel surface layer, by achieving the desirable finely crystalline microstructure of steel or by modifying its chemical composition and morphology at the nano- or micro-scale (Lo *et al.*, 2009). Table 5.2 summarizes recent research on this subject, involving various classes of steel: carbon steel, SS, alloy steel, etc. A variety of processing approaches have been investigated for producing a nanocomposite surface on steels, typically via surface SPD or SPD coupled with TMT. While there tends to be a gradient microstructure from the treated surface to the bulk of steel, there is also a high level of diversity in the resulting surface microstructure, ranging from nano-grains of α or α and cementite, to nano-scale retained γ grains embedded in the fine bainite and α', to net-shape pearlite along the nano-grains of α, to nano-twinned ultrafine crystals. These nano-modified steel surfaces feature novel mechanical properties, characteristic of considerable improvements in strength (e.g., TS by 91% and fatigue strength by 13%), hardness (by 100%), wear resistance (by 97%), and fatigue strength (by 25%), and

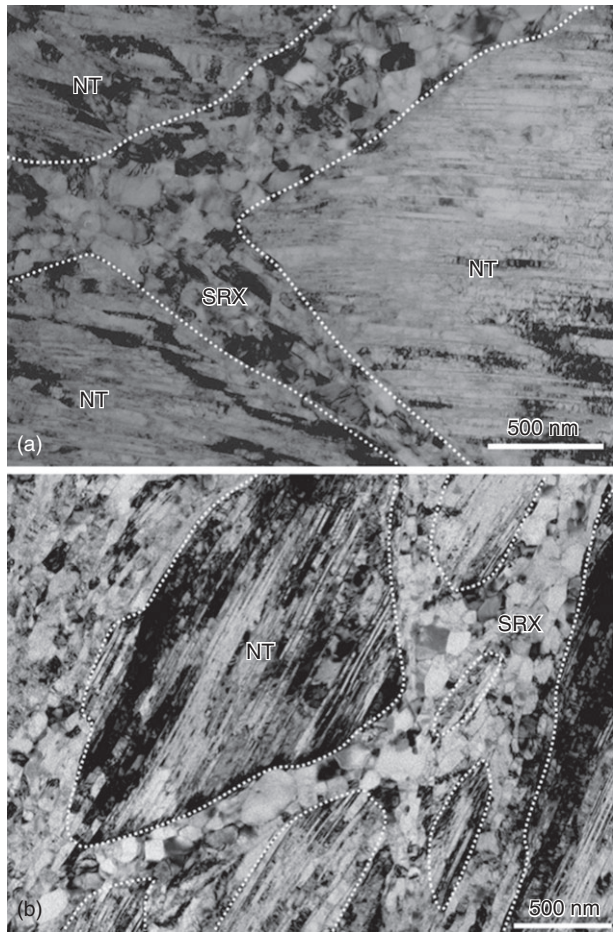

5.3 Typical bright-field TEM images (a and b) of 316 SS with DPD $\varepsilon = 1.6$, annealing @ 730°C / 20 min, showing the early-stage SRX in shear bands between NT bundles (Yan *et al.*, 2012). *With kind permission from Elsevier Science.*

toughness (e.g., El of 27.5%) and reduced friction coefficient (by 50%). There are multiple mechanisms underlying the outstanding strength–stiffness–ductility synergy of the nanocomposite surface. Often the toughness and ductility are introduced by phase transformation and dislocation distribution, whereas strength and stiffness are enhanced by surface nanocrystallization and/or nano-precipitation and change in the dominant deformation or wear mechanics.

One recent advance in this field is the use of SMAT to produce 304 SS with outstanding strength–stiffness–ductility synergy, by forming hard

Table 5.2 Recent research on the utilization of nanotechnology to improve the mechanical properties of steel surface

Reference	*Steel type*	*Production process*	*Microstructure of surface layer*	*Novel properties or phenomenon*	*Mechanism(s)*
Suh *et al.* (2007)	Tool steel (SKD-61/ equivalent H13)	UCFT	Gradient microstructure with nano-grains (average 50 nm) from the surface to 100 μm depth	Improved hardness (37%), compressive residual stress (83%), wear resistance (97%), and fatigue strength (25%). Reduced friction coefficient (50%)	Mixed nano-crystals and amorphous phase
Xu *et al.* (2008)	Carbon steel (0.7–0.75% C)	Severe cold drawing	Nano-grains of α and cementite	UTS increased from 1352 to 2586 MPa at a true strain of 3.58; outstanding wear resistance	Strain-induced α transformation (from cementite flakes) and nano-crystallization
Liu *et al.* (2009)	Low carbon steel (#45)	Added pressure shot peening	Uniformly distributed equiaxed grains (~65 nm) in the top surface	Doubled the hardness of the 30-μm thick surface layer; enhanced wear resistance	Nanocrystallization
Kwon *et al.* (2010)	Extra-AHSS™	Adding Mn and C to retain sufficient austenite	Nano-scale retained γ grains (200–500 nm) embedded in the fine bainite and α'	Extremely high strength-ductility balance, e.g., TS > 1033 MPa, El > 27.5%, and TS × El > 28,408 MPa.%	Partial reverse transformation during continuous annealing and transformation induced plasticity
Ba *et al.* (2007)	Cr-Si alloy steel	Quenching + tempering + SFPB	Uniformly distributed equiaxed α grains (5–65 nm) in the top surface	Greatly enhanced hardness and wear resistance and reduced friction coefficient	Nanocrystallization and change in the dominant wear mechanics

Ba *et al.* (2011)			Gradient microstructure with Lamellar-type dislocation cells with dense dislocation walls	Surface nanocrystallization: decomposing the cementite granules	Dislocation activities
Kim *et al.* (2009)	Low-carbon steel (0.15% C)	ECAP	α–α' dual phase microstructure with ultrafine grains	Enhanced hardness and strength but reduced wear resistance	'Lack of strain hardening due to unstable and non-equilibrium (GBs) and the cracking at the interface of α–α' phases'
Huang *et al.* (2011)	Low-carbon steel (≤ 0.2% C)	Quenching + tempering + ECAP	Net-shape pearlite along the GBs of α (~500 nm)	Enhanced strength, stronger surface passivation, and reduced adhesive bond shear strength, friction coefficient and wear rate	Grain refinement induced by SPD
Verezub *et al.* (2011)	Low-alloy steel (105WCr6)	*In situ* laser melt injection + heat treatment	20–30 vol% nano-sized $(Fe,W)_6C$ particles and ~56 vol% (W,Ti)C microparticles in the steel matrix	Enhanced microhardness and wear resistance at the 1 mm top layer	Strenghening by nano- and micro-precipitates

Table 5.2 Continued

Reference	*Steel type*	*Production process*	*Microstructure of surface layer*	*Novel properties or phenomenon*	*Mechanism(s)*
Li *et al.* (2009)	Low-carbon steel (0.17% C)	SMAT	Uniformly distributed equiaxed α grains (~13 nm) and cementite nanoparticles in the top surface	More than doubled the surface microhardness; 13% improvement in fatigue strength (302 Mpa based on fatigue life 5×10^6 cycles)	Surface nanocrystallization
Chen *et al.* (2011)	304 SS	SMAT	Hard nanocrystalline α' layer, α'-γ ultrafine layer, twinning layer, and compliant coarse-grained layer from outer to inner	Outstanding strength-stiffness-ductility synergy	Synergy of multiple deformation mechanisms and nano/micro-scale toughening
Frontán *et al.* (2012)	304 SS	SMAT + plasma nitriding or SMAT	Nanocrystalline or nanotwinned ultrafine crystals	Lower energy absorption and 40% less impact deformation than coarse-grained steel under ballistic loading	-
Wang *et al.* (2012)	Fe-9Cr steel	SMAT + annealing	Gradient microstructure with α grains (~14 nm) and smaller carbide particles dispersed along GBs	Annealing-induced grain refinement	$\alpha\rightarrow\gamma\rightarrow\alpha$ phase transformations

nanocrystalline α' layer, α'–γ ultrafine layer, twinning layer, and compliant coarse-grained layer from outer to inner of the stainless steel. This bio-inspired design aims to benefit from the synergy of multiple deformation mechanisms and nano/micro-scale toughening. Figure 5.4 presents typical TEM images of 304 SS after SMAT and its corresponding selected area electron diffraction (SAED) patterns at four different depths (Chen *et al.*, 2011).

Another advance in this field deals with the use of surface-modified nano-Cu as effective lubrication additive (at 10 vol% in oil). It works by 'forming a chemical reaction film on the steel' surfaces, thus improving their

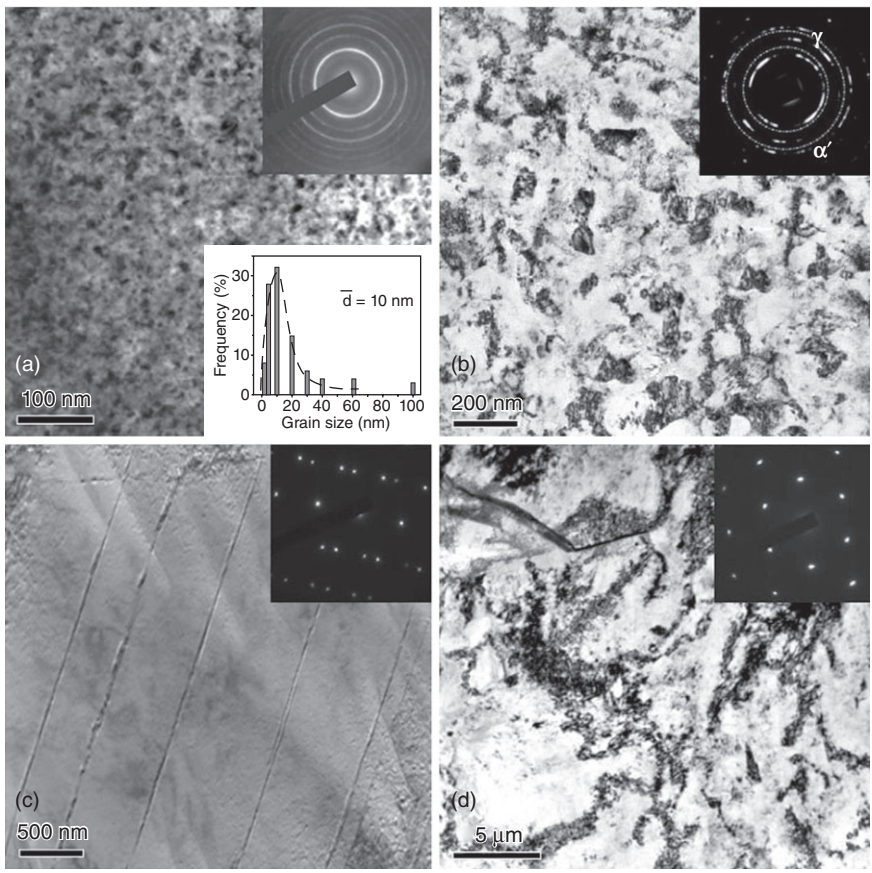

5.4 Typical TEM images of 304 SS after SMAT and its corresponding selected area electron diffraction (SAED) patterns at four different depths: 5, 100, 250, and 400 μm for (a)-(d) respectively. The lower inset of (a) is the grain size distribution (Chen *et al.*, 2011). *With kind permission from Elsevier Science.*

wear resistance and anti-fatigue performance of carbon steel (Zhang *et al.*, 2010).

5.3.3 Nanotechnology to improve corrosion resistance of steel

The corrosion of steel as a result of chemical or electrochemical reaction with its service environment is a spontaneous process, which can compromise the integrity of the materials and impact assets, environment, and people if no measures are taken to prevent or control it. The corrosion of steel is generally electrochemical in nature, and may take many forms such as uniform corrosion, galvanic corrosion, pitting corrosion, crevice corrosion, underdeposit corrosion, dealloying, stress corrosion cracking (SCC), corrosion fatigue, corrosion wear, and microbially influenced corrosion (MIC).

Nanotechnology has also been employed to enhance the corrosion resistance of the steel bulk or surface layer. Table 5.3 provides a snapshot of recent research on this subject, involving various classes of steel: weathering steel, SS, and alloy steel, whereas the following sections review recent inventions on this subject. The improved resistance to pitting corrosion, corrosion, wear, or corrosion wear can be derived from nano-phases in the passive film, high density of GBs as nucleation sites for growing passive film, hardening by nano-precipitates or nano-grains, etc. As summarized by Lo *et al.* (2009), laser surface melting (LSM) can reduce the size of carbides and impurities (e.g., MnS) and alter the microstructure in the surface layer of SS, often leading to improved resistance to intergranular corrosion and pitting.

It should be cautioned that some production processes of steels may alter their microstructure and increase their susceptibility to cavitation erosion and hydrogen embrittlement (Lo *et al.*, 2009). Amarnath and Namboodhiri (2003) revealed that for a high strength low alloy steel, heating followed by normalizing (air cooling) coarsened the grain sizes and lowered the dislocation density, which in turn decreased the number of hydrogen trap sites and increased the risk of hydrogen embrittlement. Relative to the as-received steel, its water quenching followed by tempering also led to higher risk of hydrogen embrittlement. It is hypothesized that a microstructure with high dislocation density and high concentration of GBs and other interfaces would be less prone to hydrogen embrittlement in steel. Addition of Mo and V nanoparticles has been reported to mitigate the delayed fracture of steel, by reducing the intergranular cementite and associated hydrogen embrittlement (Mann 2006). Addition of some alloying elements (e.g., Cu, Cr, Ni, Mo, W) can improve the corrosion resistance of steels.

Table 5.3 Recent research on the utilization of nanotechnology to improve the corrosion resistance of steel

Reference	*Steel type*	*Production process*	*Microstructure of surface or bulk*	*Novel properties or phenomenon*	*Mechanism(s)*
Zhang *et al.* (2001)	Tool steel (0.35C-5Cr-1.5Mo-1V)	Metal vapor vacuum arc ion implantation	Fe_2Mo, FeMo, Fe_2MoC, Mo_2C, MoC, MoC_x nano-precipitates in surface layer	Greatly improved resistance to pitting corrosion and corrosion	Nano-(Mo+C) phases improve the passive film
Wang and Li (2003)	304 SS	Sandblasting + annealing	Uniformly distributed nanocrystalline grains (~20 nm) in the top surface	Greatly improved resistance to corrosion, wear and corrosive wear	Nanocrystallization and change in the dominant wear mechanics
Kwok *et al.* (2006)	316 SS	Cavitation + low-temperature annealing	fcc γ-grains (91 nm)	Improved resistance to pitting corrosion and enhanced ability to repassivate	High density of GBs as nucleation sites for growing a uniform Cr-rich passive film
Vaynman *et al.* (2002)	NUCu weathering steel (ASTM A710B, 0.06% C)	Microalloying + hot-rolling + normalizing	Equaxed ferritic microstructure, with some dispersed pearlite bands	Outstanding mechanical, welding and anti-corrosion properties, e.g., TS of 567 MPa, El of 32.2%	Hardening by nano-Cu precipitation; solid solution strengthening by Ni; grain refinement by Nb

First, nanotechnology has been utilized in endowing the steel bulk materials with excellent corrosion resistance, mainly by refining their crystal grains to nano-scale. The steel substrate with a nano-phased grain structure tends to have less defects or inhomogeneities where corrosion attack traditionally initiates and/or propagates. Miura *et al.* (2010) disclose a steel with an improved corrosion resistance and ultra-hardness and toughness, comprising an aggregate of α nano-crystal grains containing a solid-solution type N (0.1–2.0% by mass). The steel is prepared by MA of fine powders of α steel-forming components (e.g., Fe, Cr, Ni, Mn, and C) and an N-containing substance (e.g., N_2, NH_3, and nitride of Fe, Cr, and Mn), followed by forming-by-sintering treatment and subsequent annealing. The crystal grains are more finely divided on a nanometer scale by mixing a particle dispersant (e.g., AlN, NbN, TaN, Si_3N_4, or TiN) or mixing a metal oxide or a semimetal oxide in the MA process. Furthermore, an oxide, nitride, carbide, silicide, or boride of a metal or semimetal exists as a crystal grain growth inhibitor between and/or in the nano-crystal grains. Such SS, having a high N concentration (in place of expensive Ni or Mn), were reported to feature much improved resistance to corrosion and particularly to pitting corrosion as well as significantly reduced sensitivity to SCC.

Buck (2008) discloses the use of TMT to create a fine-grained microstructure imparting the steel good corrosion resistance, high strength, and high toughness. In one example, a 15 cm thick steel slab was first soaked at 1230°C for 2 h 'such that the structure is mostly face-centered-cubic (fcc) γ throughout the alloy', before being hot-worked on a reversing rolling mill at a temperature between 1230°C and 1150°C. During the forming process, a true strain of 0.22–0.24 per pass was utilized to induce recrystallization. The resulting plate was then air-cooled to room temperature with or without further heat treatment, ultimately transformed into a fine-grained α' SS.

Wright and Jung (2006) disclose the invention of Cr-Ni-Co-Mo-Ti-Al SS with an excellent combination of strength, toughness, and corrosion resistance across a variety of strength levels. The SS feature 'a predominantly lath-α' microstructure essentially without topologically close packed intermetallic phases and strengthened primarily by a dispersion of intermetallic particles primarily of the η-Ni_3Ti phase'. The Ti and C levels are controlled 'such that C can be dissolved during a homogenization step and subsequently precipitated during forging to provide a grain-pinning dispersion' of carbides of Ti, V, Nb, or Ta.

Second, nanotechnology has been utilized in surface treatments to improve the performance and service life of steels in oxidizing and corrosive environments. A recent invention (Kerber, 2007) is directed to nanoparticle surface treatments and methods of providing such treatments for forming a thin oxide coating on alloys, thereby providing the substrate with

enhanced corrosion and oxidation resistance. The disclosed method relates to such nanoparticles as CeO_2, nanoceria, or an oxide of an element selected from the group consisting of Al, Si, Ti, Y, Nb, Zr, and other rare earth elements. One possible mechanism is that these elements exhibit a reactive element effect that decreases the oxide scale growth rate and reduces scale spallation by improving the scale–alloy adhesion. The invention suggests exemplary applications of this technology in protecting SS and Ni or Al alloys at high temperatures and in steam environments. The effectiveness of nanoparticle surface treatments in managing metallic oxidation and corrosion was demonstrated. For instance, the steel samples were dip-coated with nanoparticles in their respective solutions once or several times with intermediate drying at 200°C. After heating to 1000°C for 34 h, the 316 SS treated with nanoceria had a self-protective, thin, and adherent oxide film formed on its surface, whereas the sample without the nanoparticle treatment had thick, spalled oxide scale on its surface. Similarly, beneficial effects of nanoceria surface treatment for 430 and 410 SS were observed after heating to 800°C in air for some time. Tests of nanocrystalline-coated and uncoated SS confirmed the corrosion resistance of the self-protective surfaces to humid air, to direct contact with liquid in the temperature range of 150°C to 350°C, to submerged service in high salinity solutions, and to the vapor phase above these solutions.

Another invention in this category (Sugama, 2009) presents methods of endowing the alloy surfaces with outstanding corrosion resistance by forming an ultrathin (preferably less than 10 nm), Cr-free film comprising an at least partially crosslinked amido-functionalized silanol component and nanoparticles of rare-earth metal oxide. The formed coatings were reported to provide better coverage of the substrate metal and similar or superior corrosion resistance than Cr-based coatings. For instance, one such coating demonstrated to extend the lifetime of the steel substrate under salt-fog test at 35°C from approximately 10 h to approximately 768 h.

Third, nanotechnology has been utilized in decorative and protective coatings that provide the steel substrate with superior abrasion resistance and good corrosion resistance. Chen (2008) discloses the use of cathodic arc evaporation (CAE) for physical vapor deposition (PVD). For Zr, the resulting strike layer exists either as amorphous to nano-size crystals up to 50 nm or as preferentially-oriented crystals up to 80 nm in size, with a small percentage of amorphous refractory oxide acting as precipitation hardening particles. By maintaining the flow ratio of oxygen to argon into the vacuum chamber during CAE, a stoichiometric ZrO_2 layer (preferably between 10 and 30 nm thick) is then deposited on the strike layer, which provides another non-conductive barrier layer to improve resistance to corrosion and pitting.

Chan (2006) discloses novel methods of depositing a nanocomposite coating of SS and a metallic carbide or metallic nitride onto a solid metallic substrate (e.g., SS) to increase its surface hardness. Unlike the continuous deposition process, very thin layers (e.g., 5–10 nm per layer) of such nanocomposite coating are deposited by reactive sputtering in a C or N_2 gas plasma, using pure SS and Cr targets or their alloy targets. When the substrate is away from the deposition locations, the deposited SS and CrC (or CrN) phases were reported to relax into 'their most thermodynamically suitable sites'. The hardness improvement was achieved by forming the nanocomposite structure in which the CrC nanophases precipitated along the SS GBs. This method features a clean process for obtaining a hard, wear-resistant, and corrosion-resistant coating with an SS-like appearance.

Namavar (2006) discloses an invention that provides metallic components (e.g., SS) with integrally formed, homo-metallic protective coatings on their surfaces. The deposited substance and the bulk substrate have at least one metallic constituent element in common; and the formed coatings feature crystalline grains preferably in a range of about 10–200 nm and thus an enhanced hardness and a high degree of resistance to corrosion and wear. To improve the adhesion of the coating to the substrate, the average crystalline grain size can decrease continuously from the substrate to the coating within the transition zone.

Detor and Schuh (2006) disclose the use of bipolar pulsed current (BPP) to produce alloy deposits with a specified nanocrystalline average grain size and thus superior macroscopic quality and/or resistance to corrosion and abrasion. Polarity ratio (characterized by the amplitude and/or duration of the negative pulse relative to those of the positive pulse) was used to enable 'grading and layering of nanocrystalline crystal size and/or composition within a deposit' without introducing voids and cracks. Relative to traditional microcrystalline metals, the nanocrystalline metal coatings with nano-grains are expected to show exceptional combination of properties such as excellent corrosion and wear resistance, enhanced yield strength and ductility, and desirable magnetic properties.

Finally, nanotechnology has been employed to alter the steel/electrolyte interface, by forming nano-modified polymeric coating on steel. The incorporation of nano-sized particles (e.g., SiO_2, Fe_2O_3, and halloysite clay) into conventional polymer coatings can significantly enhance the anti-corrosive performance of such coatings on steel substrates (Shi *et al.*, 2009). A comprehensive review on this subject, however, is beyond the scope of this chapter. A recent review in 2007 by Saji and Thomas discussed the incorporation of nanoparticles in ceramic coatings, polymer coatings, and hybrid sol-gel systems for improved properties (e.g., resistance to corrosion and high-temperature oxidation, self-cleaning, and anti-fouling).

5.4 Future trends

The use of nanotechnology has led to remarkable improvements in the mechanical properties and corrosion resistance of steels, by achieving the desirable microstructure of steels via phase transformation or deformation kinetics or by controlling the key chemistry down to the nanometer scale. By controlling the grain size and distribution and the heterogeneity and gradation of microstructure (e.g., quantity, morphology, and distribution of nano-phases), strength/toughness synergy and other properties of steels could be greatly enhanced. One interesting research need is to optimize the distribution and motion of dislocations in nanocomposite steels. Many of the R&D efforts detailed in previous sections will undoubtedly continue and more cost-effective solutions will emerge as a result of the advanced knowledge base and continuous improvements in R&D and in production technologies (e.g., high N-content SS). The great potential of nanotechnology in this field has not yet been fully achieved and in the near future new techniques and new applications can be expected along with new products to be introduced into the market. Multi-scale modeling of nanocomposite steels under mechanical or chemical stresses is crucial to unravel the role of dislocations, GBs, precipitates, and lattice defects and their interactions at various length scales. Continued developments in design and processing technologies can be expected to address needs in long-term durability, minimized maintenance, environmental sustainability, and/or competitive performance (e.g., high strength-to-weight ratio). To maximize the sustainability of using steels for construction, it is important to match the steel type to the working conditions and user requirements.

Nanotechnology has demonstrated its clear benefits and will continue to play a key role in the production of high performance steels. Future developments will be centered on furthering the understanding of why and how superior properties of steels can be achieved by the design and control of their chemical composition and morphology at the micro- and nanometer scales. Progress in steel production technology will open up the possibility of rapid change in steel metallurgy and increase the competitiveness of nano-enabled products. More research is needed to advance the knowledge base relevant to using nanotechnology to modify the surface layer or bulk material of steels and to shed light on the mechanisms and pathways defining the cause-and-effect relations that link metallurgy and production processes with microstructure and properties of steels.

The research in this domain is ongoing and the interdisciplinary nature of nanotechnology requires experts from a variety of disciplines working together to produce viable solutions. While the authors anticipate many evolutionary and revolutionary developments in this specific field, the ultimate market share of nanocomposite steels will depend on continued

investment and efforts in R&D as well as market-driven product strategies (Osman *et al.*, 2006). A multitude of technical and cost barriers remain for many of the inventions. For instance, concerns have surfaced about the responsible development, production, use, and disposal of some nanomaterials and related technologies. These are generally sparked by the nanosize effect and present unique challenges to be addressed before the successful commercialization of nanocomposite steels in some applications. For instance, Khettabi *et al.* (2008) indicated that the formation of nano- and micro-sized particles during metal cutting may pose a health risk.

5.5 References

Abe, F.; Taneike, M.; Sawada, K. (2007), Alloy design of creep resistant 9Cr steel using a dispersion of nano-sized carbonitrides. *International Journal of Pressure Vessels and Piping* 84, 3–12.

Ahmadabadi, M.N.; Shirazi, H.; Ghasemi-Nanesa, H.; Nedjad, S.H.; Poorganji, B.; Furuhara, T. (2011), Role of severe plastic deformation on the formation of nanograins and nano-sized precipitates in Fe-Ni-Mn steel. *Materials and Design* 32, 3526–3531.

Amarnath, G.A.N.; Namboodhiri, T.K.G. (2003), Effect of heat treatments on the hydrogen embrittlement susceptibility of API X-65 grade line-pipe steel. *Bulletin of Materials Science* 26(4), 435–439.

Askari, H.A.; Shen, Y.F.; Wang, C.M.; Sun, X.; Zbib, H.M. (2010), The effect of nano-precipitates on strength in a micro-alloyed ferritic steel. *MRS Proceedings* 1296, mrsf10-1296-o05-04 doi:10.1557/opl.2011.1463.

Averback, R.S. (1993), Sintering and deformation of nano-grained materials. *Zeitschrift für Physik D: Atoms, Molecules and Clusters* 26, 84–88.

Ba, D.M.; Ma, S.N.; Meng, F.J.; Li, C.Q. (2007), Friction and wear behaviors of nano-crystalline surface layer of chrome-silicon alloy steel. *Surface and Coatings Technology* 202, 254–260.

Ba, D.M.; Ma, S.N.; Meng, F.J. (2011), The effect of initial microstructure on surface nanocrystallization of quenched and tempered steel. *Advanced Materials Research* 148–149, 778–782.

Bhadeshia, H.K.D.H. (2008), Properties of fine-grained steels generated by displacive transformation. *Materials Science and Engineering A* 481–482, 36–39.

Branagan, D.J.; Sergueeva, A.V.; Mukherjee, A.K. (2006), Towards the development of a new Iron Age. *Advanced Engineering Materials* 8(10), 940–943.

Buck, R.F. (2008), Method of producing fine-grained martensitic stainless steel. US patent 7,470,336.

Chan, W.S.Y. (2006), Method of forming a nanocomposite coating. US patent 7,001,675.

Chen, A.Y.; Ruan, H.H.; Zhang, J.B.; Liu, X.R.; Lu, J. (2011), Introducing a hierarchical structure for fabrication of a high performance steel. *Materials Chemistry and Physics* 129, 1096–1103.

Chen, G. (2008), Decorative and protective coating. US patent 20080206580A1.

Chipman, J. (1972), Thermodynamics and phase diagram of the Fe-C system. *Metallurgical and Materials Transactions B* 3(1), 55–64.

Detor, A.J.; Schuh, C.A. (2006), Method for producing alloy deposits and controlling the nanostructure thereof using negative current pulsing electro-deposition, and articles incorporating such deposits. US patent 20060272949A1.

Du, L.; Yao, S.; Xiong, M.; Liu, X.; Wang, G. (2010), Austenite grain ultrarefinement and the formation of nanocrystallized structure through transformation of low carbon steels. *Materials and Manufacturing Provesses* 25, 26–32.

Eisenhüttenleute, V.D. (1992), *Steel: A Handbook for Materials Research and Engineering. Volume 1: Fundamentals*. Springer-Verlag, New York.

Eskandari, M.; Kermanpur, A.; Najafizadeh, A. (2009), Formation of nano-grained structure in a 301 stainless steel using a repetitive thermal-mechanical treatment. *Materials Letters* 63, 1442–1444.

Foroozmehr, F.; Najafizadeh, A.; Shafyei, A. (2011), Effects of carbon content on the formation of nano/ultrafine grained low-carbon steel treated by martensite process. *Materials Science and Engineering A* 528, 5754–5758.

Frontán, J.; Zhang, Y.; Dao, M.; Lu, J.; Gálvez, F.; Jérusalem, A. (2012), Ballistic performance of nanocrystalline and nanotwinned ultrafine crystal steel. *Acta Materialia* 60, 1353–1367.

Gonsalves, K.E.; Xiao, T.D.; Chow, G.M.; Law, C.C. (1994), Synthesis and processing of nanostructured M50 type steel. *NanoStructured Materials* 4(2), 139–147.

Guo, A.; Misra, R.D.K.; Xu, J.; Guo, B.; Jansto, S.G. (2010), Ultrahigh strength and low yield ratio of niobium-microalloyed 900 MPa pipeline steel with nano/ultrafine bainitic lath. *Materials Science and Engineering A* 527, 3886–3892.

Hidaka, H.; Kawasaki, K.; Tsuchiyama, T.; Takaki, S. (2003), Effect of carbon on nano-crystallization in steel during mechanical milling treatment. *Materials Transactions* 44(10), 1912–1918.

Hodgson, P.; Timokhina, I.; Xiong, X.; Adachi, Y.; Beladi, H. (2011), Understanding of the banite transformation in a nano-structured bainitic steel. *Solid State Phenomena* 172–174, 123–128.

Hosseini, S.M.; Najafizadeh, A.; Kermanpur, A. (2011), Producing the nano/ultrafine grained low carbon steel by martensite process using plane strain compression. *Journal of Materials Processing Technology* 211, 230–236.

Huang, S.-J.; Semenov, V.I.; Shuster, L., Lin, P.-C. (2011), Tribological properties of the low-carbon steels with different micro-structure processed by heat treatment and severe plastic deformation. *Wear* 271(5–6), 705–711.

Karak, S.K.; Chudoba, T.; Witczak, Z.; Lojkowski, W.; Manna, I. (2011), Development of ultra high strength nano-Y_2O_3 dispersed ferritic steel by mechanical alloying and hot isostatic pressing. *Materials Science and Engineering A* 528, 7475–7483.

Kaufman, L.; Perepezko, J.H.; Hildal, K.; Farmer, J.; Day, D.; Yang, N.; Branagan, D. (2009), Transformation, stability and Pourbaix diagrams of high performance corrosion resistant (HRCRM) alloys. *CALPHAD: Computer Coupling of Phase Diagrams and Thermochemistry* 33, 89–99.

Kerber, S.J. (2007), Nanoparticle surface treatment. US patent 20070141370A1.

Khettabi, R.; Songmene, V.; Masounave, J.; Zaghbani, I. (2008), Understanding the formation of nano and micro particles during metal cutting. *International Journal of Signal System Control and Engineering Application* 1(3), 203–210.

Khodabakhshi, F.; Kazeminezhad, M. (2010), The effect of constrained groove pressing on grain size, dislocation density and electrical resistivity of low carbon steel. *Materials and Design* 32, 3280–3286.

Khodabakhshi, F.; Kazeminezhad, M.; Kokabi; A.H. (2010), Constrained groove pressing of low carbon steel: nano-structure and mechanical properties. *Materials Science and Engineering A* 527, 4043–4049.

Kim, I.-S.; Kchoi, C.-Y.; Kang, C.-Y.; Okuda, T.; Maziasz, P.J.; Miyahara, K. (2003), Effect of Ti and W on the mechanical properties and microstructure of 12% Cr base mechanical-alloyed nano-sized ODS ferritic alloys. *ISIJ International* 43(10), 1640–1646.

Kim, Y.-S.; Yu, H.-S.; Shin, D.-H. (2009), Low sliding wear resistance of ultrafine grained Al alloys and steel having undergone severe plastic deformation. *Intl. J. Mater. Res.* 6, 871–874.

Klueh, R.L.; Hashimoto, N.; Maziasz, P.J. (2005), Development of new nano-particle-strengthened martensite steels. *Scripta Materialia* 53, 275–280.

Kolpakov, S.V.; Parshin, V.A.; Chekhovoi, A.N. (2007), Nanotechnology in the metallurgy of steel. *Steel in Translation* 37(8), 716–721.

Kozikowski, P.M.; Krawczynska, A.T.; Kulczyk, M.; Lewandowska, M.; Kurydlowski, K.J. (2010), Tailoring mechanical properties of nano-structured Eurofer 97 steel for fusion applications. *Physica Status Solidi C: Current Topics in Solid State Physics* 7(5), 1388–1390.

Kusinski, G.J.; Pollack, D. (2008), Triple-phase nano-composite steels. International patent application PCT/US2002/040126.

Kusinski, G.J.; Pollack, D.; Thomas, G. (2004), Process for making triple-phase nano-composite steels. US patent 6,827,797.

Kwok, C.T.; Cheng, F.T.; Man, H.C.; Ding, W.H. (2006), Corrosion characteristics of nanostructured layer on 316L stainless steel fabricated by cavitation-annealing. *Materials Letters* 60, 2419–2422.

Kwon, O.; Lee, K.; Kim, G.; Chin, K.-G. (2010), New trends in advanced high strength steel developments for automotive application. *Materials Science Forum* 638–642, 136–141.

Lei, Y.; Yu, X.; Yu, S.; Liu, Z. (2007), Present status and development direction of high performance structural material-oriented ultra-fine grained steel. *Journal of China University of Petroleum* 31(2), 155–162.

Lesuer, D.; Syn, C.; Sherby, O. (2010), Nano-scale strengthening from grains, sub-grains and particles in Fe-C alloys. *Journal of Materials Science* 45, 4889–4894.

Li, D.; Chen, H.N.; Xu, H. (2009), The effect of nanostructured surface layer on the fatigue behaviors of a carbon steel. *Applied Surface Science* 255, 3811–3816.

Li, X.; Wei, Y.; Lu, W.; Lu, K.; Gao, H. (2010), Dislocation nucleation governed softening and maximum strength in nano-twinned metals. *Nature* 464(8), 877–880.

Li, X.; Jing, T.F.; Lu, M.M.; Xu, R.; Liang, B.Y.; Zhang, J.W. (2011), Fatigue property of nano-grained delaminated low-carbon steel sheet. *Journal of Materials Science and Technology* 27(4), 364–368.

Liu, G.Z.; Tao, N.R.; Lu, K. (2010), 316L austenite stainless steels strengthened by means of nano-scale twins. *Journal of Materials Science and Technology* 26(4), 289–292.

Liu, L.; Jie, X.; Yu, N.; Mai, Y. (2009), Study on surface nano-crystallization by adding pressure shot peening and its effect on wear resistance. *Hot Working Technology* 38(14), 124–126.

Lo, K.H.; Shek, C.H.; Lai, J.K. (2009), Recent developments in stainless steels. *Materials Science and Engineering R* 65, 39–104.

Lu, K.; Lu, L.; Suresh, S. (2009), Strengthening materials by engineering coherent internal boundaries at the nanoscale. *Science* 324(5925), 349–352.

Lu, K.; Yan, F.K.; Wang, H.T.; Tao, N.R. (2012), Strengthening austenitic steels by using nanotwinned austenitic grains. *Scripta Materialia* 66(11), 878–883.

Malow, T.R.; Koch, C.C. (1997), Grain growth in nanocrystalline iron prepared by mechanical attrition. *Acta Materialia* 45(5), 2177–2186.

Mann, S. (2006), *Nanotechnology and Construction*. European Nanotechnology Gateway – Nanoforum Report, Institute of Nanotechnology, 2–10.

Matsuia, K.; Ohmichi, N.; Ohgai, M.; Yoshida, H.; Ikuhara, Y. (2006), Effect of alumina-doping on grain boundary segregation-induced phase transformation in yttria-stabilized tetragonal zirconia polycrystal. *Journal of Materials Research* 21, 2278–2289.

Menapace, C.; Lonardelli, I.; Tait, M.; Molinari, A. (2009), Nanostructured/ultrafine multiphase steel with enhanced ductility obtained by mechanical alloying and spark plasma sintering of powders. *Materials Science and Engineering A* 517, 1–7.

Miura, H.; Miyao, N.; Ogawa, H.; Oda, K.; Katsumura, M.; Mizutani, M. (2010), Nano-crystal austenitic steel bulk material having ultra-hardness and toughness and excellent corrosion resistance, and method for production thereof. US patent 7,662,207.

Murayama, M.; Nishimura, T.; Tsuzaki, K. (2008), Nano-scale chemical analysis of rust on a 2% Si-bearing low alloy steel exposed in a coastal environment. *Corrosion Science* 50(8), 2159–2165.

Namavar, F. (2006), Nano-crystalline, homo-metallic, protective coatings. US patent 7,048,767.

Ohtsuka, S.; Ukai, S.; Sakasegawa, H.; Fujiwara, M.; Kaito, T.; Narita, T. (2007) Nano-mesoscopic structural characterization of 9Cr-ODS martensitic steel for improving creep strength. *Journal of Nuclear Materials* 367–370, 160–165.

Okamura, Y.; Okushima, M.; Tamehiro, H.; Kasuya, T.; Tanaka, M.; Yamaba, R.; Inoue, H.; Seto, A. (1995), Development of copper precipitation-hardened 780 N/mm^2 high-strengh steel with lower preheating temperature characteristics. *Nippon Steel Technical Report* 66(7), 65–76.

Oksiuta, Z.; Lewandowska, M.; Unifantowicz, P.; Baluc, N.; Kurzydlowski, K.J. (2011), Influence of Y_2O_3 and Fe_2Y additions on the formation of nano-scale oxide particles and the mechanical properties of an ODS RAF steel. *Fusion Engineering and Design* 86, 2417–2420.

Osman, F.M.; Rardon, D.E.; Friedman, L.B.; Vega, L.F. (2006), The commercialization of nanomaterials: today and tomorrow. *JOM* (4), 21–24.

Saji, V.S.; Thomas, J. (2007), Nanomaterials for corrosion control. *Current Science* 92(1), 51–55.

Shi, X.; Nguyen, T.A.; Suo, Z.; Liu, Y.; Avci, R. (2009), Effect of nanoparticles on the anticorrosion and mechanical properties of epoxy coating. *Surface and Coatings Technology* 204(3), 237–245.

Smith, W.F. (1981), *Structure and Properties of Engineering Alloys*. McGraw-Hill, New York.

Sokolov, M.A.; Hoelzer, D.T.; Stoller, R.E.; McClintock, D.A. (2007), Fracture toughness and tensile properties of nano-structured ferritic steel 12YWT. *Journal of Nuclear Materials* 367–370, 213–216.

Song, H.W.; Guo, S.R.; Hu, Z.Q. (1999), A coherent polycrystal model for the inverse Hall-Petch relation in nanocrystalline materials. *NanoStructured Materials* 11(2), 203–210.

Sugama, T. (2009), Corrosion-resistant metal surfaces. US patent 7,507,480.

Suh, C.-M.; Song, G.-H.; Suh, M.-S.; Pyoun, Y.-S. (2007), Fatigue and mechanical characteristics of nano-structured tool steel by ultrasonic cold forging technology. *Materials Science and Engineering A* 443, 101–106.

Taneike, M.; Abe, F.; Sawada, K. (2003), Creep-strengthening of steel at high temperatures using nano-sized carbonitride dispersions. *Nature* 424, 294–296.

Tsuji, N.; Maki, T. (2009), Enhanced structural refinement by combining phase transformation and plastic deformation in steels. *Scripta Materialia* 60, 1044–1049.

Valiev, R.Z. (2004), Materials science: nanomaterial advantage. *Nature Materials* 3, 511–516.

Vaynman, S.; Fine, M.E.; Asfahani, R.I.; Bormet, D.M.; Hahin, C. (2002), High performance copper-precipitation-hardened steel. In: *Microalloyed Steels 2002: Proceedings of the International Symposium on Microalloyed Steels*, Columbus, OH, 43–48.

Verezub, O.; Kálazi, Z.; Sytcheva, A.; Kuzsella, L.; Buza, G.; Verezub, N.V.; Fedorov, A.; Kaptay, G. (2011), Performance of a cutting tool made of steel matrix surface nano-composite produced by *in situ* laser melt injection technology. *Journal of Materials Processing Technology* 211, 750–758.

Wang, J.; Li, G.; Xiao, A.; Fu, J. (2011), Nano-scaled Fe_3C precipitation strengthening in hot rolled low carbon high strength titanium microalloyed steel. *Advanced Materials Research* 146–147, 838–843.

Wang, L.; Wang, Z.; Guo, S.; Lu, K. (2012), Annealing-induced grain refinement in a nanostructured ferritic steel. *Journal of Materials Science and Technology* 28(1), 41–45.

Wang, X.Y.; Li, D.Y. (2003), Mechanical, electrochemical and tribological properties of nano-crystalline surface of 304 stainless steel. *Wear* 255(7), 836–845.

Weertman, J.R. (1993), Hall-Petch strengthening in nanocrystalline metals. *Materials Science and Engineering A* 166, 161–167.

Wright, J.A.; Jung, J.-W. (2006), Martensitic stainless steel strengthened by Ni_3Ti h-phase precipitation. WO patent 2006/081401A3.

Wu, Z.X.; Zhang, Y.W.; Srolovitz, D.J. (2009), Dislocation-twin interaction mechanisms for ultrahigh strength and ductility in nanotwinned metals. *Acta Materialia* 57, 4508–4518.

Wu, Z.X.; Zhang, Y.W.; Srolovitz, D.J. (2011), Deformation mechanisms, length scales and optimizing the mechanical properties of nanotwinned metals. *Acta Materialia* 59, 6890–6900.

Xu, L.; Shi, J.; Cao, W.Q.; Wang, M.Q.; Hui, W.J.; Dong, H. (2011), Improved mechanical properties in Ti-bearing martensitic steel by precipitation and grain refinement. *Journal of Materials Science* 46, 6384–6389.

Xu, Y.H.; Peng, J.H.; Fang, L. (2008), Nano-crystallization of steel wire and its wear behavior. *Materials Science and Engineering A* 483–484, 688–691.

Yan, F.K.; Liu, G.Z.; Tao, N.R.; Lu, K. (2012), Strength and ductility of 316L austenitic stainless steels strengthened by nano-scale twin bundles. *Acta Materialia* 60, 1059–1071.

Zhang, T.; Wu, Y.; Yi, Z.; Zhang, X.; Wang, X. (2001), Nano-phases and corrosion resistance of C + Mo dual implanted steel. *Science in China E* 44(4), 383–388.

Zhang, Y.D.; Yan, J.S.; Yu, L.G.; Zhang, P.Y. (2010), Effect of nano-Cu lubrication additive on the contact fatigue behavior of steel. *Tribology Letters* 37, 203–207.

Zhang, Z.W., Liu, C.T.; Guo, S.; Cheng, J.L.; Chen, G.; Fujita, T.; Chen, M.W.; Chung, Y.-W.; Vaynman, S.; Fine, M.E.; Chin, B.A. (2011), Boron effects on the ductility of a nano-cluster-strengthened ferritic steel, *Materials Science and Engineering A* 528, 855–859.

Zhao, M.-C.; Zeng, T.-Y.; Li, J.-L.; Huang, X.; Zhao, Y.-C.; Atrens, A. (2011), Identification of the effective grain size responsible for the ductile to brittle transition temperature for steel with an ultrafine grain size ferrite/cementite microstructure with a biomodal ferrite grain size distribution. *Materials Science and Engineering A* 528, 4217–4221.

6

Nanoclay-modified asphalt mixtures for eco-efficient construction

S. GHAFFARPOUR JAHROMI, Shahid Rajaee Teacher Training University, Iran

DOI: 10.1533/9780857098832.1.108

Abstract: Polymeric nanocomposites are among the most exciting and promising classes of materials discovered recently. A number of physical properties are successfully enhanced when a polymer is modified with small amount of nanoclay on condition that the clay is dispersed at nanoscopic level. In this research, comparative rheological tests on binders and mechanical tests on asphalt mixtures containing unmodified and nanoclay modified bitumen were carried out. Two types of nanoclay were used: Nanofill-15 and Cloisite-15A. Rheological tests on binder were penetration, softening point, ductility and aging effect. Mechanical tests on asphalt mixture were Marshall stability, indirect tensile strength, resilient modulus, diametric fatigue and dynamic creep tests. Test results show that nanoclay can improve properties such as stability, resilient modulus and indirect tensile strength and result in superior performance compared to that of unmodified bitumen under dynamic creep. Nanoclays do not seem to have beneficial effects on fatigue behaviour at low temperatures. Optimum binder content and void in total mixture (VTM) increase by adding nanoclay to bitumen.

Key words: asphalt mixture, modified bitumen, nanoclay, engineering properties.

6.1 Introduction

Temperature susceptibility characteristics and physical properties of asphalt binder at high and low field operating temperatures can affect final performance of the mixture. To improve the performance of bitumen and asphalt concrete mixtures, addition of modifiers such as polymers has become popular in recent years. Polymeric nanocomposites are one of the most exciting materials discovered recently and physical properties are successfully enhanced when a polymer is modified with small amounts of nanoclay on the condition that the clay is dispersed at nanoscopic level (Pinnavaia and Beall, 2000).

Many research studies have been undertaken on nanoclay modified polymers; however, relatively little published information is available about nanoclay modified bitumen. Material variables which can be controlled and can have a profound influence on the nature and properties of the final

nanocomposite include the type of clay, the choice of clay pre-treatment, the selection of polymer component and the way in which the polymer is incorporated into the nanocomposites (Pinnavaia and Beall, 2000).

Common clays are naturally occurring minerals and are thus subject to natural variation in their constitution. The purity of the clay can affect final nanocomposite properties. Many types of clay are alumina-silicates, which have a sheet-like (layered) structure, and consist of silica SiO_4 tetrahedron bonded to alumina AlO_6 octahedron in a variety of ways. A 2:1 ratio of the tetrahedron to the octahedron results in mineral clays, the most common of which is montmorillonite (Fig 6.1). The thickness of the montmorillonite layers (platelets) is 1 nm and aspect ratios are high, typically 100–1500 (Grim, 1959). The degree of expansion of montmorillonite is determined

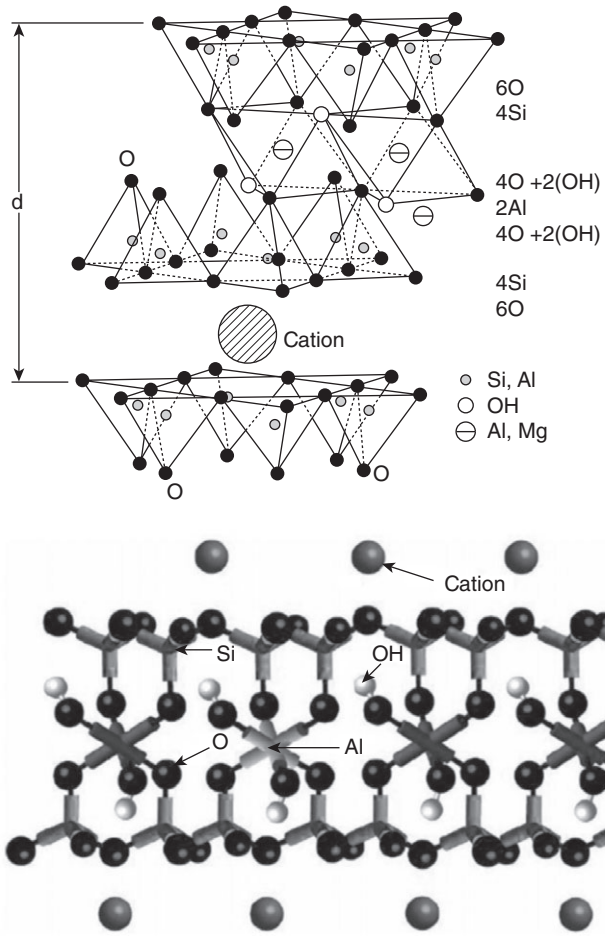

6.1 Structure of montmorillonite.

by their ion (e.g., cation) exchange capacities, which can vary widely. A characteristic number of these types of clay is the cation exchange capacity (CEC), which is a number for the amount of cations between the surfaces. The CEC of montmorillonite ranges from 80 to 120 meq/100 g (milli-equivalents per 100 grams), whereas kaolinite has CEC values ranging from 3 to 5.

The expansion pressure of montmorillonite in which sodium ions constitute the majority of the adsorbed cations (called Na-montmorillonite) is very high, leading to the exfoliation and dispersion of the crystal in the manner of fine particles or even single layers. When Ca^{2+}, Mg^{2+} and ammonium are the dominant exchangeable cations, the dispersion is relatively low and the size of the particle is relatively large. Separation of the clay discs from each other will result in a nanoclay with an enormous large active surface area (it can be as high as 700–800 m^2 per gram). This helps to have an intensive interaction between the nanoclay and its environment (bitumen in our case). The process to realize the separation (surface treatment) is dependent on the type of material to be mixed (Lan *et al.*, 1995).

A necessary prerequisite for successful formation of polymer-clay nanocomposite is therefore alteration of the clay polarity to make the clay 'organophilic'. To achieve fine dispersion, mechanical forces alone are not enough; there should be a thermodynamic driving force as well to separate the layers into the primary silicate sheets. This thermodynamic driving force is introduced by inserting a certain coating of surfactants (an agent such as detergent which reduces surface tension) on each individual layer (Theng, 2012). These surfactant molecules increase the layer distance, improve the compatibility with the polymer and can give an increase in entropy because they can mix with the polymer. Organophilic clay can be produced from normally hydrophilic clay by ion exchange with an organic cation. The organic reagents are quaternary ammonium salt with alkyl chains such as 12-aminododecanoic acid (ADA), octadecanoic alkyl trimethyl quaternary ammonium salt. The reaction process is described as:

$$\text{M-CLAY} + \text{CH}_3(\text{CH}_2)_n\,\text{NR}_3\text{X} \rightarrow \text{CH}_3(\text{CH}_2)_n\,\text{NR}_3\text{-Clay} + \text{MX}$$
$$(\text{R} = \text{-H}, \text{-CH}_3;\ \text{X} = \text{-Cl}, \text{-Br}, \text{-I};\ \text{M} = \text{Na}^+, \text{Ca}^{2+}, \text{Mg}^{2+}) \qquad [6.1]$$

Addition of a positively loaded surface active material, a kind of ADA, will in this case form an ADA layer around each clay disc. The clay disc in this case changes from a hydrophilic disc into a hydrophobic disc. These modified clay discs will separate automatically in water and can be used as nanoparticles. The correct selection of modified clay is essential to ensure effective penetration of the polymer into the interlayer spacing of the clay and result in the desired exfoliated or intercalated product. In intercalate structure, the organic component is inserted between the layers of the clay

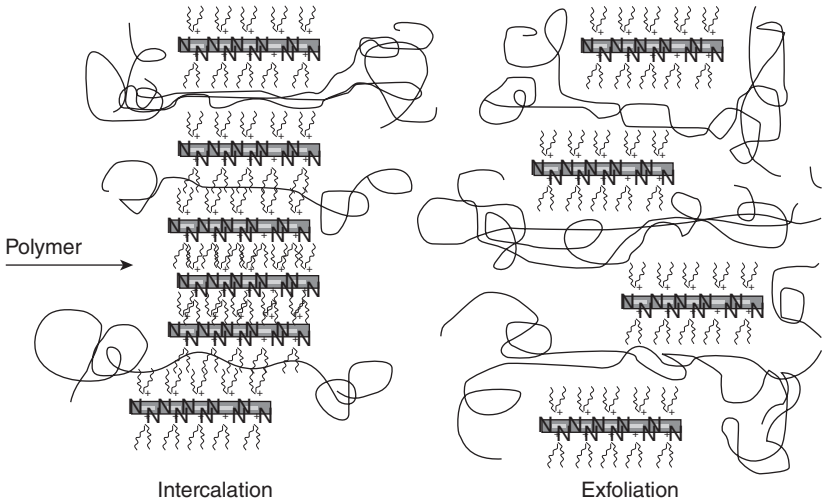

6.2 Intercalated and exfoliated nanocomposite.

such that the interlayer spacing is expanded, but the layers still bear a well-defined spatial relationship to each other. In an exfoliated structure (Fig. 6.2), the layers of the clay have been completely separated and the individual layers are distributed throughout the organic matrix (Nguyen and Baird, 2007).

With dispersing nanoclay in a thermoplastic material (a material that is plastic or deformable, melts to a liquid when heated, and freezes to a brittle, glassy state when cooled sufficiently), stiffness and tensile strength, tensile modulus, flexural strength and thermal stability will increase (Manias, 2001).

The Structures of bitumen and polymers are different as bitumen is a very complex polymer and not stable. The structure of asphaltenes on bitumen depends on the chemical composition of the binder and on temperature. In gel type, the asphaltenes are highly associated to each other, but in sol type, they are not associated to each other and have poor network and lower asphaltenes proportions and need a different approach to clay and bitumen interaction which probably limits the successes obtained in bitumen-nanoclay modifications.

6.2 Research on nanoclay-modified asphalt mixtures

Many studies have been carried out on nanoclay-modified polymers, but little published information is available about nanoclay-modified bitumen. Many research studies have been performed on bitumen modification by polymer materials such as SBS (styrene butadiene styrene block copolymer), SBR (styrene butadiene rubber latex) and EVA (ethyl vinyl acetate).

Chen *et al.* (2002) showed that SBS improved the rheological properties of asphalt binder due to the formation of a polymer network in the binder. This network forms in two stages: at low polymer concentrations, the SBS acts as a dispersed polymer and does not significantly affect properties; at higher concentrations, local SBS networks begin to form and are accompanied by a sharp increase in the complex modulus, softening point temperatures, and toughness.

Radziszewski (2007) studied mechanical properties of asphalt mixtures containing elastomer, plastomer and fine rubber modified binders. His study showed that while being exposed to simulated short-term ageing and long-term ageing, asphalt mixtures behave differently in terms of rutting and creeping. Ageing causes higher stiffness with unmodified binder mixtures than with polymer or rubberized bitumen modified binder mixtures. Permanent deformation depends on the type of asphalt mixture and the type of binder used. Asphalt concrete with rubberized bitumen, asphalt concrete with 7% polymer modified binders and SMA and Superpave mixtures with unmodified binders appeared to be most resistant to permanent deformations after long-term laboratory ageing (Radziszewski, 2007).

Recently, nanoscale inorganic fillers have drawn increasing interest as it is theoretically possible to significantly improve the properties of pristine polymers such as bitumen with a relatively small percentage of additive (Lan and Pinnavaia, 1994; Lan *et al.*, 1995, Kornmann *et al.*, 2001; Zerda and Lesser, 2001; Becker *et al.* 2002, Liu *et al.*, 2003). Nanoclays are micro-scale fillers which would make polymers efficient as filler reinforcements. Ghile (2005) performed mechanical tests on asphalt mixture modified by Cloisite. The results showed that nanoclay modification can improve mechanical behaviour properties of the mixture such as indirect tensile strength, creep and fatigue resistance. Chow (2003) investigated surface modified montmorillonite nanoclay and compatibilizer, and found that the strength and stiffness of polyamide polypropylene nanocomposites improved due to the synergistic effect of surface modified montmorillonite nanoclay and compatibilizer. Yasmin *et al.* (2003) found that the addition of Nanomer I.28E and Cloisite 30B into some pure epoxy polymers produced materials with higher elastic modulus than that of the pure epoxy.

6.3 Material and methods

The aggregates used in this study were crushed limestone aggregates with gradation characterized by 12.5 mm nominal size (according to Pavement Guidelines in Iran) and limestone mineral filler. Physical properties of the aggregate, both coarse and fine, together with mineral filler are given in Table 6.1 and aggregate gradation shown in Fig. 6.3. The bitumen was a 60/70 penetration grade (AC-10) and its properties are shown in Table 6.2.

Table 6.1 Properties of aggregates

Coarse aggregate (ASTM C127)	
Bulk specific gravity, g/cm^3	2.698
Apparent specific gravity, g/cm^3	2.714
Absorption, %	0.33
Fine aggregate (ASTM C128)	
Bulk specific gravity, g/cm^3	2.683
Apparent specific gravity, g/cm^3	2.735
Absorption, %	0.62
Filler (ASTM D854)	
Apparent specific gravity, g/cm^3	2.743
Los Angeles Abrasion, % (ASTM C131)	23.57
Polishing value (BS813)	0.47

Table 6.2 Properties of bitumen

Softening point	54
Penetration grade at 5°C	63
Flash point	243
Penetration index	+ 0.4
Ductility at 25°C	>100 cm
Fraass breaking point	14
Loss of heating	0.05%
Density	1.035
Viscosity	
at 50°C	250,000
at 60°C	100,000
at 72°C	20,000
Maltens	75%
Asphaltenes	27.2%

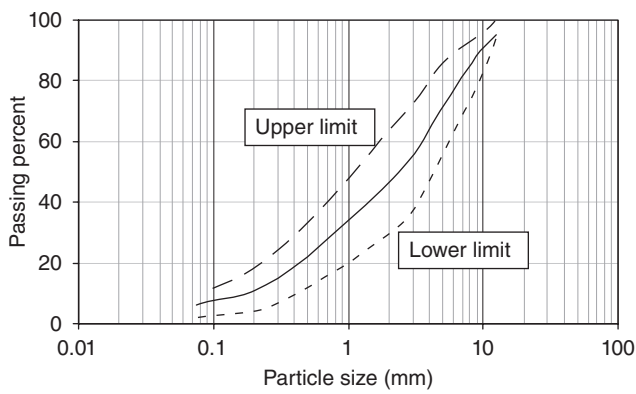

6.3 Aggregate grading.

Table 6.3 Properties of nanoclays

Treatment/properties	Cloisite-15A	Nanofill-15
Organic modifier	MT2ETOH (methyl, tallow, bis-2-hydroxyethyl, quaternary ammonium)	Nanodispers layered silicate, long chain hydrocarbon
Base	Montmorillonite	Montmorillonite
Modifier concentration	90 meq/100 g clay	75 meq/100 g clay
Moisture	<2%	<3%
Weight loss on ignition	43%	35%
Anion	Chloride	Ammonium chloride
Particle sizes		
10% less than	2 μm	5 μm
50% less than	6 μm	15 μm
90% less than	13 μm	25 μm
Colour	Off-white	cream
Loose bulk, kg/m^3	230	190
Packed bulk, kg/m^3	364	480
Density, gr/cc	1.66	1.88
X-ray results	d = 31.5 Å	d = 28 Å
Plastic index	88%	85%

Two types of common nanoclay used in this research were Cloisite-15A and Nanofill-15. Properties of nanoclays are shown in Tables 6.3.

Current test procedures used on modified and unmodified bitumen are empirical such as penetration, ductility, softening point. Marshall test and performance-based tests such as indirect tensile strength, resilient modulus test, fatigue resistance test and dynamic creep test were carried out on the mixture samples. Specimen preparation and compaction were conducted in accordance with ASTM D1559-89 (1994). All performance-based tests were done on Marshall-sized samples.

6.4 Rheological tests and results

Empirical rheological tests carried out on unmodified and modified bitumen with different nanoclay content were penetration, softening point and ductility tests. The modification of bitumen with nanoclay was performed at nanoscale level by thermodynamic driving force. The empirical tests were performed according to the standard test procedures. The nanoclay contents selected were 0.2%, 0.4% and 0.7% by weight of bitumen. The test results are shown in Fig. 6.4.

Nanofill-15 modification makes little change on penetration and softening point of the unmodified 60/70 pen bitumen. Addition of a few percent of Nanofill-15 increased penetration at 25°C, however, further increasing

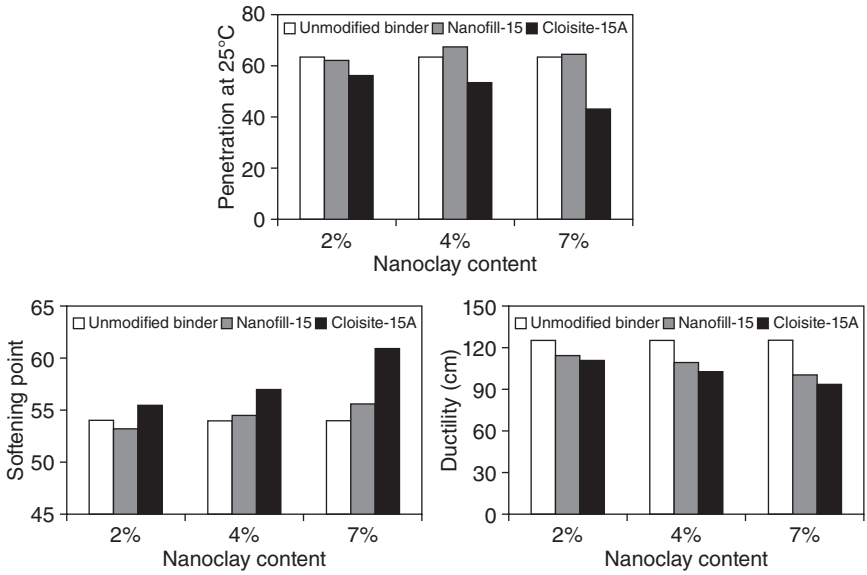

6.4 Rheological results test and nanoclay content.

Cloisite-15A content caused a decrease in penetration. Nanofill-15 has little effect on softening point; by adding 7% nanofill, softening point increased by only 3%. In contrast, Cloisite-15A has a relatively higher impact on penetration and softening point of bitumen. By increasing Cloisite-15A content, penetration decreases from 63 to 45 and softening point increases from 54 to 61. Also both nanoclays reduce ductility of binder but Cloisite-15A has a more pronounced effect in reducing ductility. This behaviour may be the result of chemical reaction and change in chemical structure, as pointed out by Ghile (2005).

When bitumen gets aged it becomes harder. Retained penetration (RP) and increase in softening point (ISP) values, as defined below, were used to find the ageing effect:

$$\text{RP}\,(\%) = \frac{\text{aged penetration}}{\text{unaged penetration}} \times 100$$

$$\text{ISP}\,(^{\circ}\text{C}) = (\text{aged softennig point} - \text{unaged softening point}) \qquad [6.2]$$

A lower RP value and higher ISP reflect more ageing of the binder. Long-term ageing was performed for 20 hours at 90°C and atmospheric pressure. The retained penetration and increase in softening point were computed and are presented in Fig. 6.5. It can be observed that there are some improvements in the resistance to ageing in the long term due to the Nanofill-15 modification and therefore it will probably suffer less when in contact with hot air or hot oxygen.

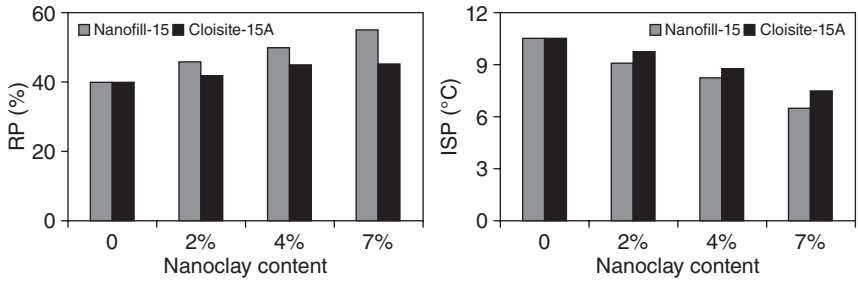

6.5 Retained penetration (RP) and increase in softening point (ISP) results.

6.5 Mechanical testing of asphalt mixtures

6.5.1 Specimen preparation

The specimens prepared for the different tests were Marshall tablets with an average height of 60–65 mm and 100–102 mm diameter (ASTM D1559-89, 1994). Dense mixture specimens were compacted by 75 blows applied on both sides. As mentioned before, Cloisite-15A reduces the viscosity of modified binder so that it is not fluid enough at the normal mixing temperature used for the standard binder (140°C). Hence, a high mixing temperature was needed for the preparation of the modified mixtures and so the temperature was increased to 155°C. The Cloisite-15A content was 0.2%, 0.4% and 0.7% by weight of bitumen.

During the preparation of the specimen, the modified binder had a different smell and became more viscous at 185°C. Modified binder was relatively less sticky to the mixing pan and to the moulds as compared to the specimens of the standard mixes. All tests were performed in closed temperature-controlled cabinets. In addition, all specimens selected for the different tests were stored in a temperature-controlled cabinet to the target temperature for a minimum of 3 h before commencing any test. The loading control and input parameters used in testing are given in Table 6.4.

6.5.2 Marshal stability, flow and VTM

To compare the effects of different nanoclays in the mixes, Marshall stability and VMA test results are shown in Figs 6.6 and 6.7. The results show that, by adding nanoclay, Marshall stability and VMA increase.

Nanoclay is an active filler that improves strength properties of bitumen. By adding 2% Cloisite-15A, stability increased by 15% but Nanofill-15 increased it by only 6%. Because of the large surface area, in the nanoclay modified mixture, the optimum binder increased. Even 1% nanoclay

Table 6.4 Loading properties and test temperatures

	Loading properties	Dimensions, (mm)			
		Diameter	Height	Duplication	Temperature
Marshal stability	Displacement controlled	100	65	3	60°C
Indirect tensile strength	Displacement controlled, 0.85 mm/s	100	40	3	5, 25, 40°C
Resilient modulus	Pulses number 5 Pulse form Half sine, 0.5 Hz, Loading period, 500 ms Recovery time, 1500 ms	100	40	3	5, 25, 40°C
Dynamic creep	Compressive stress controlled 100, 200, 300, 400 kPa Pulse form Half sine, 1 Hz Loading time, 200 ms Recovery Time, 800 ms	100	55	2	40, 60°C
Fatigue test	Stress controlled, varying between 150 and 1800 kPa Half sine pulse, Loading period, 150 ms at 5°C, without rest period at 25°C, with 50 ms rest period	100	40	2	5, 25°C

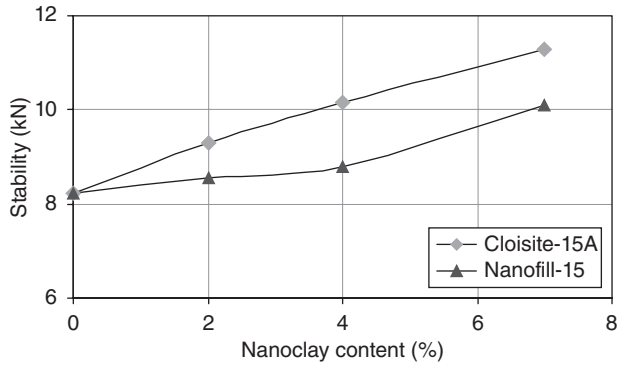

6.6 Stability and nanoclay content.

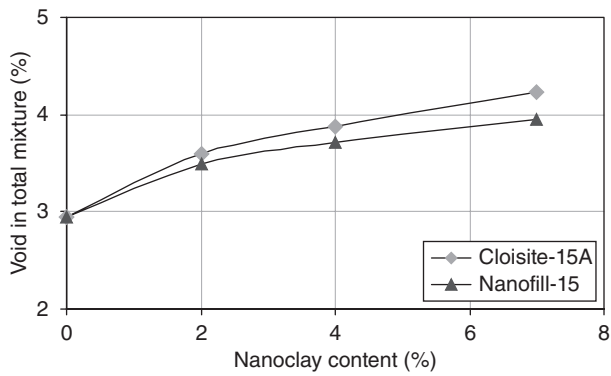

6.7 VTM and nanoclay content.

increased optimum binder by almost 0.3–0.35% as compared to unmodified mixtures. Cloisite-15A reduced viscosity of modified binder as compared to Nanofill-15, so in compaction process, nanofill modification compacted better than cloisite modification as the VTM increases in the cloisite-modified mixture.

6.5.3 Indirect tensile strength test

The tests were conducted at three different temperatures (5°C, 25°C and 40°). The indirect tensile strength is computed from the maximum compressive force measured during the test at failure. The results in Fig. 6.8 show an increase in strength at different temperatures for comparison. Results show that modified specimens have higher strength at all test temperatures. By increasing Cloisite-15A content from 2% to 7%, indirect tensile strength values increase from 8% to 40% and the percentage of increase is larger

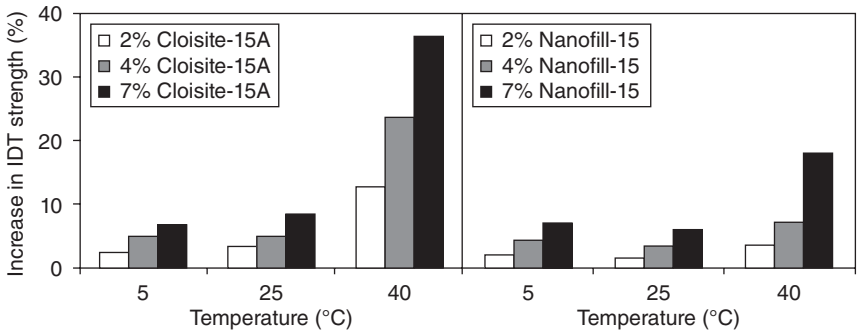

6.8 Increase in strength and temperature for Cloisite-15A.

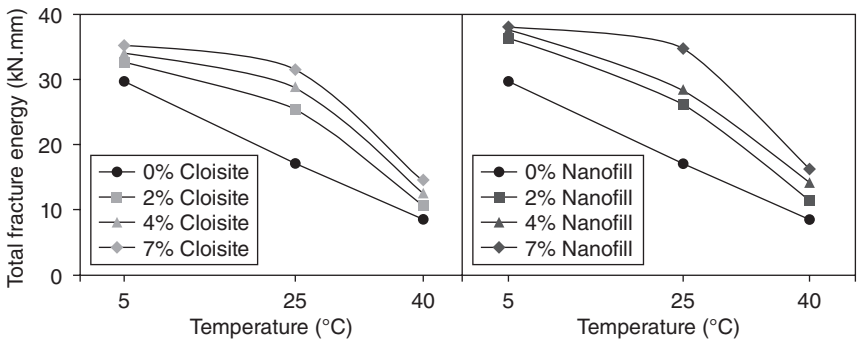

6.9 Total fracture energy results.

for the higher testing temperatures. There seems to be no major difference in the effects of adding nanofill and cloisite when tested at 5 or 25°C, but at 40°C and specially when 7% nanoclay is added, Cloisite-15A had increased the IDT almost twofold compared to Nanofill-15.

The area under force versus vertical displacement curve in the ITS test represents the dissipated energy to crack or fracture the specimen. Two fracture energy values can be defined: fracture energy until failure, which is the energy dissipated before the specimen starts failing, and total fracture energy, which is the total energy dissipated to completely destroy the specimen.

Figure 6.9 shows that addition of nanoclay increases the total energy as defined above. This increase in total energy ranges between 55 and 95% for nanofill and 26 and 72% for cloisite. It can be seen that, at low temperatures (5°C), modified mixtures need more energy to start the crack initiation as compared to standard mixture, but when the cracks gets started, less energy is required to destroy the specimen. At high temperatures (40°C), fracture energy decreases because of the visco-elasto-plastic behaviour of bitumen.

6.5.4 Resilient modulus test

The resilient modulus (Mr) test method detailed in ASTM D4123 was used in this study. The specimens were tested at 5, 25 and 40°C and the loading frequency applied at each temperature was 0.5 Hz. Pulse period and recovery time were set at 500 and 1500 ms, respectively. Resilient modulus depends on the test temperature and the loading frequency (ASTM D4123, 1995). Increase in modulus as plotted in Fig. 6.10 shows that nanoclay-modified mixture has a greater value than the unmodified mixture at all test temperatures. An increase in modulus due to the addition of 2–7% of nanoclay modification varies from 8% to 40% for Cloisite-15A and from 3% to 18% for Nanofill-15, depending on the test temperature.

6.5.5 Dynamic creep tests

Creep tests are used to evaluate the permanent deformation of the unmodified and modified mixtures at high temperatures. Accumulated permanent axial strain has three distinct stages with increasing number of cycles: primary stage, with a relatively large deformation during a short number of cycles; secondary stage, where the rate of accumulation of permanent deformation remains constant; and tertiary stage, which is the final stage where the rate of deformation accelerates until complete failure takes place. This stage is usually associated with the formation of cracks. The start of the tertiary stage is usually represented by the flow number, *FN*. This number is used as a rutting resistance indicator of asphalt mixtures (see Fig. 6.11).

In this test only modified mixture with 7% nanoclay was used and the results are compared to those of the unmodified mixture. The loading pulse was half sine with duration of 200 ms and a rest period of 800 ms. The specimens were tested at 40 and 60°C and the results are shown in Figs 6.12 and 6.13.

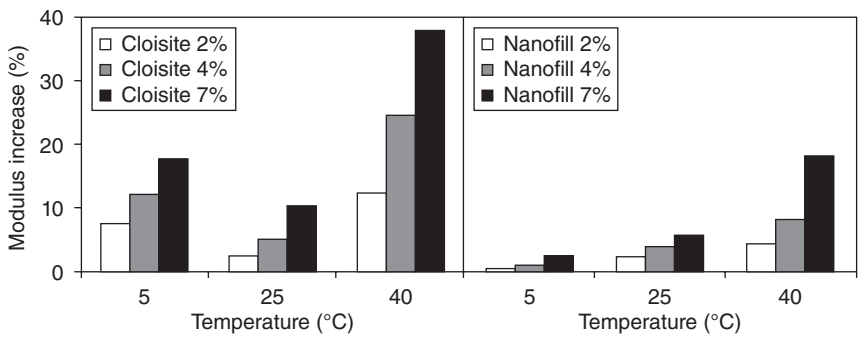

6.10 Modulus increment and temperature for nanoclays.

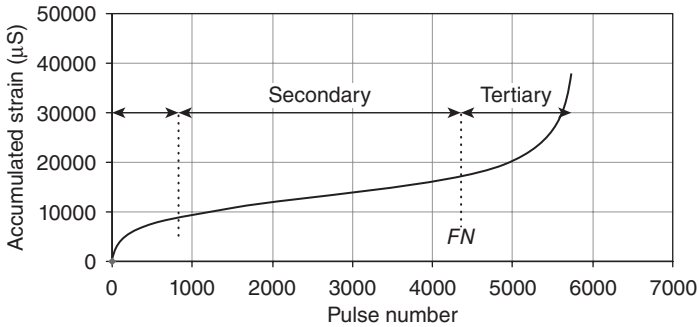

6.11 Cumulative permanent axial strain and number of loading cycles.

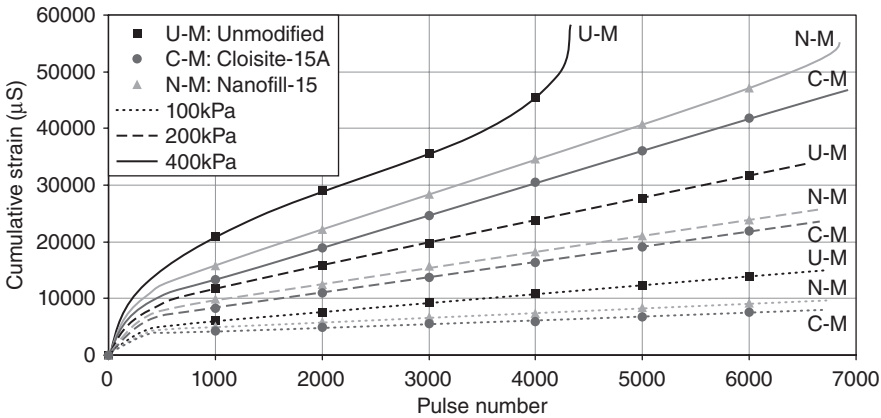

6.12 Dynamic creep test at 40°C.

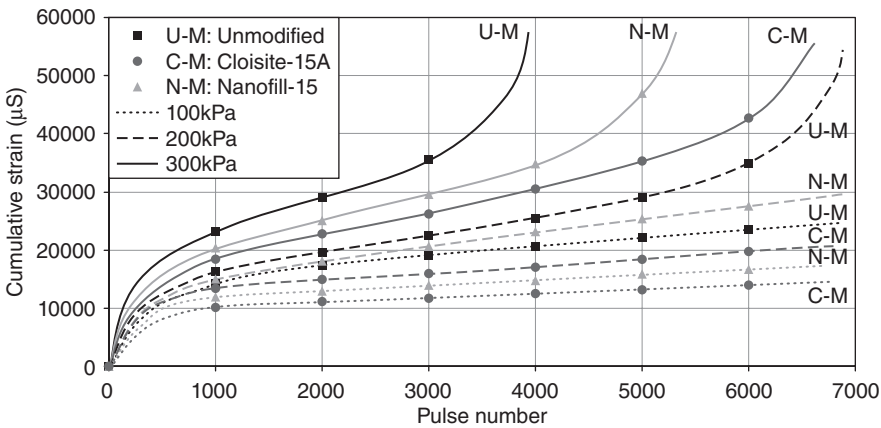

6.13 Dynamic creep test at 60°C.

At 40°C (Fig. 6.12), it can be seen that, for applied load levels of 100 kPa and 200 kPa, none of the modified and unmodified mixtures reached the tertiary stage before 6500 load repetitions. For applied load levels of 400 kPa, the unmodified mixture reached the tertiary stage at about 3200 pulses, whereas the modified mixture did not reach the tertiary stage before 6500 pulses. At 400 kPa, excessive deformation was shown in the unmodified mixture and specimens failed before the 6500 maximum pulse limit. The modified mixture did not show shear deformation failure till 6500 pulses and at all applied load levels, the primary deformations of unmodified mixture are bigger compared to those of the modified mixture samples.

At 60°C (Fig. 6.13), it can be seen that, after the 6500 pulses, none of the nanoclay modified mixtures reach the tertiary stage for applied load levels of 100 kPa and 200 kPa. All types of mixtures reached the tertiary stage if applied load was 300 kPa and the unmodified mixtures reached the tertiary stage after about 3000 pulses, whereas the Nanofill-15 modified mixtures reached the tertiary stage after about 4100 pulses, and Cloisite-15A modified mixtures reached the tertiary stage after about 5500 pulses. Unmodified mixture specimens had larger deformations in the primary stage and failed by excessive deformation at about 3800 pulse counts, whereas the Cloisite-15A and Nanofill-15-A modified mixture specimens did not fail completely at 5300 and 6500 pulse, counts respectively, at the 300 kPa loading.

6.5.6 Fatigue resistance test

Indirect tensile testing with diametric compressive loading was used to evaluate the fatigue resistance of unmodified and modified mixtures. A constant repetitive load was applied and the vertical deflection was measured in relation to pulse counts. The fatigue life is defined as the number of load repetitions at specimen fracture. As in the creep tests, only modified mixture with 7% nanoclay was used in this test to compare test results with those of the unmodified mixture. Fatigue resistance tests were performed at 5°C and 25°C. The results in Figs 6.14 and 6.15 show a linear fit between N_f and σ at 5 and 25°C. The R^2 values are very close to 1 for all mixture types. The slope of the fatigue line at 5°C is larger than the slope of the fatigue line at 25°C for the modified mixture and the unmodified mixture.

Based on the result, shown in Fig. 6.16, at low temperatures (5°C) and almost for all loading conditions, the unmodified mixture performed better under fatigue compared to nanoclay modified mixtures. The average fatigue life ratio between fatigue lives of the modified and unmodified mixtures is about 93% for Nanofill-15 and about 80% for Cloisite-15A. At a low loading stress, the fatigue life ratio for the modified mixture is about 100% and at a high loading stress, the fatigue life ratio decreased to 85% (Fig. 6.16). At high temperatures (25°C), for all loading conditions, the modified mixture

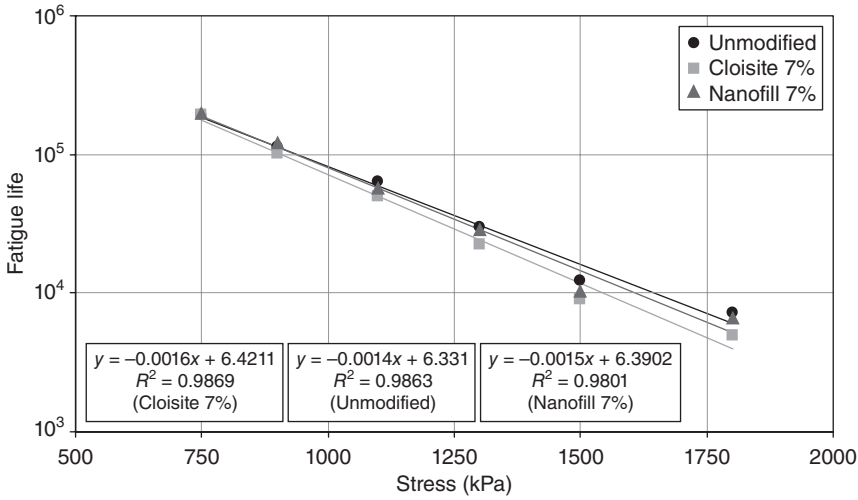

6.14 Fatigue test result at 5°C.

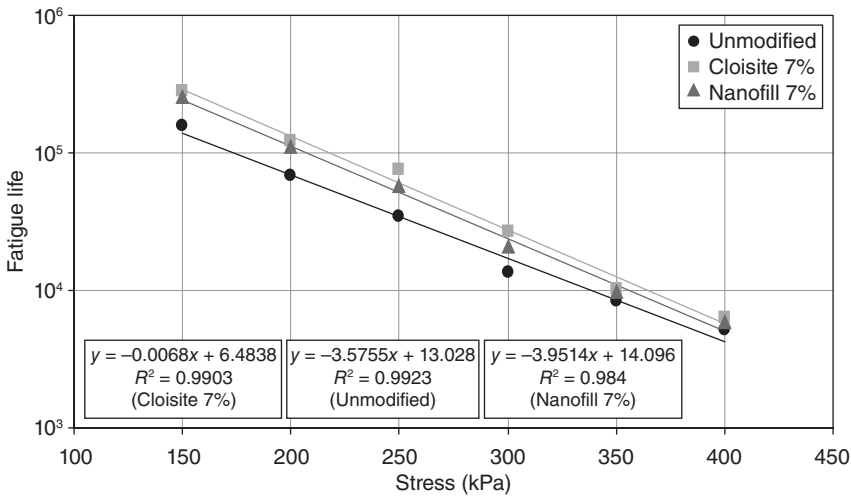

6.15 Fatigue test result at 25°C.

performed better under fatigue when compared to the unmodified mixtures (Fig. 6.17).

The average fatigue life ratio of modified mixtures is about 1.70 for Cloisite-15A and about 1.45 for Nanofill-15. The fatigue life ratio depends on the stress level. At high stress levels, the fatigue life ratio decreases (see Fig. 6.17). This can be due to the rest period of loading applied in the tests at 25°C.

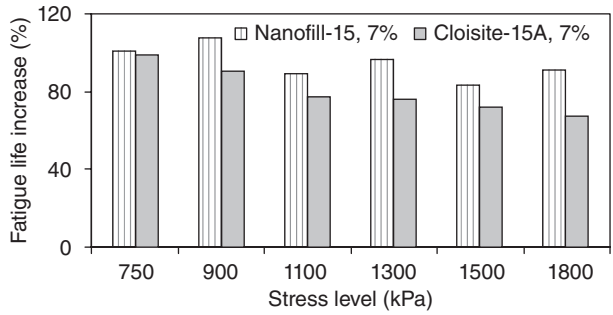

6.16 Percent life increase and stress levels at 5°C.

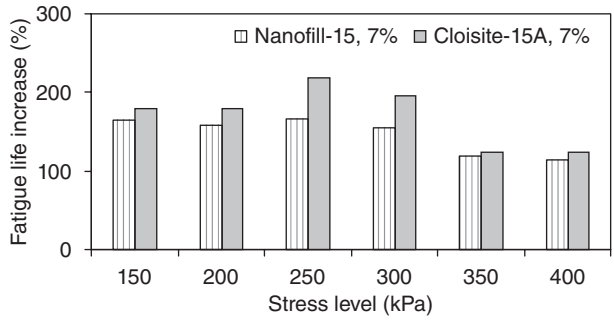

6.17 Percent life increase and stress levels at 25°C.

6.6 Conclusion

When bitumen is modified with small amounts of nanoclay, its physical properties are successfully enhanced on the condition that the clay is dispersed at nanoscopic level. Nanoclay materials have a larger aspect ratio and large surface area, and their particles are not uniform in size and arrangement. Nanofill-15 particles are smaller in size as compared to the Cloisite-15A particles. The plastic limit shows that nanoclay materials are the expansive type of clay. Adding low percentages of nanoclay to bitumen changes rheological properties, decreases penetration and ductility, and increases softening point and ageing. Tests performed on binders and dense asphalt mixtures show that the Cloisite-15A and Nanofill-15 modifications increase the stiffness and improve the rutting resistance, indirect tensile strength, resilient modulus and Marshall stability. However, fatigue performance decreases at low temperatures. Also optimum bitumen and VTM increase a little by adding nanoclay.

6.7 Future trends

Further investigations about nanoclay modification are needed in order to clarify several aspects, such as:

- use of different nanoclays on properties of bitumen mixture
- use of different nanomaterials and nanotubes on properties of bitumen mixture
- study of the effect of nanoclays on performance of different bitumen binders
- study of the effect of moisture and water on engineering properties of asphalt mixtures.

6.8 References

ASTM D1559-89 (1994) *Standard Test Method for Resistance to Plastic Flow of Bituminous Mixtures Using Marshall Apparatus*, American Society for Testing and Materials, West Conshohocker, PA.

ASTM D4123 (1995) *Standard Test Method for Indirect Tension Test for Resilient Modulus of Bituminous Mixtures*, American Society for Testing and Materials, West Conshohocker, PA.

Becker O.; Varley R.; Simon G. (2002) 'Morphology, thermal relaxations and mechanical properties of layered silicate nanocomposites based upon high-functionality epoxy resins', *Polymer* 43, 4365–4373.

Chen J.; Liao M.; Tsai H. (2002) 'Evaluation and optimization of the engineering properties of polymer-modified asphalt', *Practical Failure Analysis* 2(3), 75–83.

Chow W. (2003) *Development of Thermoplastic Nanocomposites Based on Blends of Polyamide and Polypropylene*, Material and Mineral Resources Engineering, University Sains Malaysia.

Ghile D. (2005) *Effects of nanoclay modification on rheology of bitumen and on performance of asphalt mixtures*, Delft University of Technology.

Grim R. (1959) 'Physic-chemical properties of soils: clay minerals', *Journal of the Soil Mechanics and Foundations Division, ASCE* 85 (SM2), 1–17.

Kornmann X.; Lindberg H.; Berglund LA. (2001) 'Synthesis of epoxy–clay nanocomposites: influence of the nature of the clay on structure', *Polymer* 42, 1303–1310.

Lan T.; Pinnavaia T. (1994) 'Clay-reinforced epoxy nanocomposites', *Chem Mater* 6, 2216–2219.

Lan T.; Kaviratna P.; Pinnavaia T. (1995) 'Mechanism of clay tactoid exfoliation in epoxy–clay nanocomposites', *Chem Mater* 7, 2144–2150.

Liu Y.; Hsu C.; Wei W.; Jeng R. (2003) 'Preparation and thermal properties of epoxy–silica nanocomposites from nanoscale colloidal silica', *Polymer* 44, 5159–5167.

Manias E. (2001) 'Origins of the materials properties enhancements in polymer/clay nanocomposites', *Focus on Polypropylene/Montmorillonite Hybrids. Proceedings of Nanocomposites, Delivering New Value to Plastics,* ECM Publications, IL, editor Amos Golovoy, vol. 1.

Nguyen Q.; Baird D. (2007) 'Process for increasing the exfoliation and dispersion of nanoclay particles into polymer matrices using supercritical carbon dioxide', PhD dissertation, Virginia Polytechnic Institute and State University.

Pinnavaia T.; Beall G. (2000) *Polymer–Clay Nanocomposites*, John Wiley & Sons, Chichester.

Radziszewski P. (2007) 'Modified asphalt mixtures resistance to permanent deformations', *Journal of Civil Engineering and Management*, XIII (4), 307–315.

Theng B. (2012), *Formation and Properties of Clay-Polymer Complexes*, 2nd edn Elsevier, Amsterdam.

Yasmin A; Luo J.J.; Abot J.L.; Daniel I.M. (2003) 'Mechanical and thermal behavior of clay/epoxy nanocomposites at room and elevated temperatures', *Proceedings of ASC*, 18th Annual Technical Conference.

Zerda A.; Lesser A. (2001) 'Intercalated clay nanocomposites: morphology, mechanics and fracture behavior', *Polymer Science, Part B, Polymer Physics* 39, 1137–1146.

7

Safety issues relating to nanomaterials for construction applications

M. SPITZMILLER, S. MAHENDRA and R. DAMOISEAUX, University of California, Los Angeles (UCLA), USA

DOI: 10.1533/9780857098832.1.127

Abstract: Nanotechnology holds great promise for advancements in medicine, basic science and engineering, not the least for the construction industry. Here, nanomaterials are used in a variety of eco-efficient applications including improved mechanical properties, interior light control, renewable energy harvesting, and advanced durability. However, the long-term safety aspects of these novel materials are poorly understood. While toxicological liabilities have been discovered in the laboratory for all known classes of nanomaterials, it is unclear how much toxic potential for humans and the environment various types of nanoscale materials pose. The number of manufactured nanomaterials (MNMs) keeps growing at an exponential pace and traditional *in vivo* toxicity approaches are unable to keep up with the sheer number of MNMs and MNM-composite materials that will be used in construction. Fortunately, the application of high-throughput *in vitro* methodologies allows insight to be gained into the underlying nanotoxicity paradigms, which in turn will enable an understanding of the nano-properties that cause the toxic effects of a given nanomaterial and thus informs on safe design features, enabling the safe employment of this powerful technology. This chapter aims to give a bird's eye view of nanomaterials used in construction, their potential toxicological liabilities, and high throughput methodologies that can be employed towards detecting nanotoxicity during the safety assessment of nanomaterials.

Key words: nanomaterials, green construction, high throughput screening, nanosafety, nanotoxicity, manufactured nanomaterial (MNM), engineered nanomaterial (ENM), nanotoxicology.

7.1 Introduction to nanotoxicity

Nanotechnology is at a critical juncture. Enough is known about the technology to see the enormous potential, but at the same time, the risk associated with this technology is not entirely clear (Damoiseaux *et al.*, 2011). While in the last two decades nanotechnology has been applied to many diverse fields and has been included in many consumer products (Gopel, 1991; Fahy, 1993; Murphy *et al.*, 1994; Ferrari, 2005), little is known about the long-term effects nanomaterials might have on health and the

environment. Manufactured nanomaterials (MNMs) have already played a critical role in the medical and electronic fields, while the construction industry has only recently been exploring nanotechnologies for means to advance traditional construction methods and materials (Zhu *et al.*, 2004; Ge and Gao, 2008; Alvarez *et al.*, 2010). The reason for the implementation of MNMs in construction lies in the unique physical and chemical properties of these nanomaterials that can lead to the improvement of numerous characteristics of construction materials (Tans *et al.*, 1998; Chan *et al.*, 2002; Daniel and Astruc, 2004; Arico *et al.*, 2005). It is the very same properties that make nanomaterials so unique that give rise to concern about their safety (Lee *et al.*, 2009).

The diversity of MNMs is staggering. On a broad scale MNMs can be subdivided into classes such as metals, metal oxides, metal chalcogenides ('quantum dots'), fullerenes, single-walled nanotubes (SWNT), multi-walled nanotubes (MWNT), dendrimers, etc. However, the members of these classes are typically fine-tuned toward their applications by the variation of properties, such as size, shape, aspect ratio, crystallinity, and surface modifications. At this point in time, we are only beginning to understand the interactions between nanomaterials and biomaterials that would enable us to rationally predict the positive or negative impact of MNMs. We are learning about the MNM properties that make an MNM safe or hazardous but are still forced to test each MNM for its safety profile empirically for the foreseeable future while over 1000 MNMs can be already found in consumer products – and the number is rising exponentially.

Traditional *in vivo* experiments have been performed to evaluate cytotoxicity of many MNMs using live organisms such as laboratory mammals. However, due to the sheer diversity of novel MNMs, this is not only financially unsustainable but time-consuming. More progressive methods employed are typically based on *in vitro* approaches or modeling of surface activity relationships. *In vitro* approaches allow for greater control over the experimental parameters, the assay readouts can be better tailored to answer specific questions regarding specific toxicity paradigms, and the process is generally less expensive. Most importantly, *in vitro* assays are amenable to high-throughput methodologies, which enable us to logistically manage the testing of this avalanche of novel MNMs in an effective manner, provide rapid feedback for the development of novel MNMs by enabling us to give the go-ahead to suitable MNMs and minimize hazardous MNMs.

Here, we discuss applications of MNMs in construction, review potential hazards of these materials and give an introduction to high-throughput nanotoxicology as an effective means toward the safety assessment of MNMs. We will also review an example of a safe design feature for zinc nanomaterials and review the current state of *a priori* prediction of nanotoxicity.

7.1.1 Naturally occurring nanomaterials

Nanomaterials are not necessarily manmade; many are created naturally through a variety of weather and geological phenomena. These include volcanic ash, ocean spray, forest fire smoke, and clouds (Goldman and Coussens, 2005). Some of these naturally occurring nanomaterials, such as nanoclays, are mined and have applications in composite building materials (Faruk and Matuana, 2008; Basak *et al.*, 2010). Many nanoparticles (NPs) can also be found in biological systems such as lipoprotein particles (German *et al.*, 2006) and biogenic magnetite in the human brain (Kirschvink *et al.*, 1992). Generally, these nanomaterials are created incidentally, like in the case of volcanic ash, or for an evolutionary purpose, such as the transport of fat molecules by lipoproteins.

7.1.2 Engineered nanomaterials and their use in construction

Unlike naturally occurring nanomaterials, engineered nanomaterials are typically manufactured for specific properties. MNMs can be tailored for application to a wide range of products including personal care products, medical devices, and electrical conductors (Derno *et al.*, 1995). For example, nano-TiO_2 has been used in sunscreens and lotions as a UV absorber (Contado and Pagnoni, 2008). Other consumer products such as toys and clothing use Ag NPs as an antimicrobial agent (Benn *et al.*, 2010). In the medical field, numerous advances in imaging and drug-delivery systems have been made using MNMs (Sosnik *et al.*, 2010; Parveen *et al.*, 2012). Quantum dots (QDs) are unique metallic nanomaterials with advanced electronic properties used in transistors and solar cells (Leobandung *et al.*, 1995; Nozik, 2002).

In the construction industry, MNMs have been used to improve the mechanical strength of concrete and steel, fireproofing of windows, electricity generation, and corrosion resistance (Zhu *et al.*, 2004; Mann, 2006; Abraham *et al.*, 2008). Manufactured nanomaterials are used in a wide range of construction applications from concrete and steel to glass windows and paint (Irie *et al.*, 2004; Sobolev and Gutierrez, 2005; Ge and Gao, 2008; Kumar *et al.*, 2008; Rana *et al.*, 2009; Raki *et al.*, 2010). There are several distinct categories of potential benefits that may be gained from the use of these materials such as improved safety, user convenience, enhanced lifetime of the structure, and increased ease of construction. It is also possible for one nanomaterial to provide various benefits spanning multiple benefit categories. For example, SiO_2-NPs incorporated in window glass confer flame resistance, anti-reflection, and self-cleaning, thus improving both safety and auxiliary properties (Mann, 2006; Rana *et al.*, 2009).

Carbon-based MNMs, such as carbon nanotubes, are some of the strongest materials currently known (Hayashi *et al.*, 2007). For this reason, they are often used in concrete and ceramics to improve the mechanical strength and durability (Becher, 1991; Luo *et al.*, 2004; Sobolev and Gutierrez, 2005; de Ibarra *et al.*, 2006; Ge and Gao, 2008; Raki *et al.*, 2010). In addition, carbon nanotubes help to prevent cracks by strongly binding together cement and aggregates. Similarly, these materials are incorporated into ceramics to also prevent crack propagation, and improve strength and thermal properties. Alternate uses include nano- and micro-sensors and actuators implanted into the structure to monitor real-time health and environmental conditions such as overall wear, moisture content, and temperature (Zhang *et al.*, 2006). These devices are known as nano- or micro-electro-mechanical systems (NEMS/MEMS). Carbon-based MNMs are capable of enhanced electron shuttling and can be used to harvest renewable energy in solar cells (Girishkumar *et al.*, 2005; Brown and Kamat, 2008).

In addition to carbon-based nanomaterials, metallic, non-metallic, and alloyed MNMs also have beneficial uses in the construction industry. Metal oxide NPs are used to reinforce the mechanical and compressive strength of concrete, generate non-utility electricity in solar cells, provide flame resistance to ceramics and windows, and increase the hydration ability of cement. Common metal oxide NPs used in construction are TiO_2, SiO_2, and Fe_2O_3. Often, SiO_2 and Fe_2O_3 are used as filling materials in the pores of concrete to prevent weakening from road deicers, such as salt, that react with the concrete constituents. When incorporated into concrete, these NPs also enhance the mechanical strength.

Nano-scale TiO_2 and SiO_2 are also utilized in windows, pavements, walls, and roofs to gain several useful benefits. Layers of nano-silica between glass window panels can provide fireproofing, where antireflective coatings of SiO_2 nanoparticles will control exterior light to improve energy conservation via reduction of air conditioning usage (Mann, 2006; Rana *et al.*, 2009). Reactive oxygen species (ROS) can be generated through reactions between TiO_2 and UV wavelengths from artificial or natural light, making TiO_2 an excellent antimicrobial agent and dirt-repellent (Paz *et al.*, 1995; Irie *et al.*, 2004). By coating windows with TiO_2, bacterial films and dirt buildup will be eliminated by these 'self-cleaning' windows. Titanium dioxide is also superhydrophilic, which aids in the prevention of hydrophobic dust accumulation. Similar results can be obtained on pavements, walls, and roofs, as TiO_2 will also act as an antifouling agent under solar irradiation. Additionally, light-mediated TiO_2 surface hydroxylation provides glass windows with antifogging properties (Irie *et al.*, 2004; Kontos *et al.*, 2007). Electricity generation is possible through the use of TiO_2 and silicon-based flexible solar cells applied to roofs and windows (Zhu *et al.*, 2004).

Popular metallic MNMs used in construction include copper and silver. The most common use for Cu NPs is incorporation into steel to improve weldability and provide resistance to corrosion (Ge and Gao, 2008). Like TiO_2, Ag NPs are also strong antimicrobials and can be used in paints and wall coatings to inactivate pathogenic microbes (Kumar *et al.*, 2008). Silver NPs can also be utilized indoors since their antimicrobial activity is not photo-assisted. This is particularly useful in hospitals and childcare facilities. Copper and CuO have been shown to have antimicrobial properties as well, but this may be a species-specific phenomenon (Ruparelia *et al.*, 2008). Nonetheless, Cu and CuO are sometimes used as a biocide instead of silver.

Many MNM alloys also have a niche in construction. These materials include metallic carbon or nitrogen compounds, QDs, and nanoclays. When uniformly dispersed through a steel matrix, metallic carbonitrides increase strength against creep by two orders of magnitude (Taneike *et al.*, 2003). Similar to metal oxide NPs like TiO_2 and SiO_2, QDs can also be used in windows to control interior light by being translucent in the visible spectrum to increase intensity and being reflective in the infrared spectrum to impede thermal transfer (Anikeeva *et al.*, 2009). A variety of non-metal polymeric NPs are used in matrices as constituents in windows, antibacterial coatings, and nano-clay composites (Chauhan *et al.*, 2006). Incorporation of polymeric MNMs can increase tensile strength and flexibility of construction materials (Podsiadlo *et al.*, 2007). Nanoclays and polymer-clay nanocomposites are used as filler materials or to increase compressive strength (Podsiadlo *et al.*, 2007). When nanoclays are incorporated into wood/plastic composites, the resulting material gains enhanced mechanical properties and improved rot-resistance (Faruk and Matuana, 2008).

7.2 Potential nano-hazards of manufactured nanomaterials (MNMs) utilized in construction

The unique characteristics of MNMs that allow them to enhance construction are frequently the very source of their hazardous properties. Carbon-based, metal-containing, and non-metallic MNMs, including carbon fullerenes, metal oxide and metallic NPs, quantum dots, and nanoclays, have been shown to have toxic effects in a variety of studies (Shiohara *et al.*, 2004; Lam *et al.*, 2006; Buzea *et al.*, 2007; Hagens *et al.*, 2007; Karlsson *et al.*, 2008; Xia *et al.*, 2009; Zolnik *et al.*, 2009). It has been further suggested that MNMs have the potential to modulate the immune system in unpredictable ways (Dobrovolskaia and McNeil, 2007; Dwivedi *et al.*, 2011). It is useful to know that a given class of nanomaterials frequently shares its toxicological traits with many of its members. Table 7.1 shows the properties of each MNM class that are frequently associated with their toxic effects. Table 7.2 gives the reverse view: shown are the nano-hazards of MNMs frequently utilized

Table 7.1 Overview of MNM classes and examples of properties which are associated with toxicity responses to the respective MNM class and the observed phenomenon or mode of action

MNM class	MNM property associated with toxicity	Toxicological phenomenon observed/mode of action
Metal	Shedding heavy metal (e.g., Ag, Cu, Pt)	DNA cleavage and damage leading to genotoxicity and mutation; heavy metal ions induced oxidative stress and inflammatory responses
	Surface chemistries that affect the structure and function of proteins (e.g., Au)	Protein denaturation that may lead to inactivation of hormones or proteins, opening of cryptic epitopes that could lead to autoimmune diseases, protein fibrillation and accumulation of misfolded protein could lead to disease conditions such as Alzheimer's
Metal oxide	Dissolution and heavy metal release (e.g., ZnO)	Heavy metal ions induced oxidative stress and inflammatory responses
	Electron hole pair generation during photoactivation (e.g., TiO_2)	Electron hole pair generation during photoactivation leading to free radical generation
Silica particles	Surface defects (e.g., SiO_2)	Blood platelet, vascular endothelial and clotting abnormalities
Metal chalcogenide	Heavy metal release (e.g., CdSe quantum dots)	ROS generation, lipid peroxidation, DNA damage
Fullerenes and CNTs	Heavy metal contamination, aspect ratio >5	Fibrogenesis and tissue remodeling injury, oxygen radical production, GSH depletion, bio-catalytic mechanisms
Polymer	Cationic charge density	Membrane damage/leakage/thinning; protein binding or unfolding responses/denaturation of proteins or fibrillation, lysosomal damage through proton pump inactivation or lysis of lysosomes

Table 7.2 Observed toxicological effects of nanomaterials used in the construction industry

Nanomaterial	Observed toxicological effects
Carbon nanotubes	ROS generation and damage to DNA and cell membranes Mechanical cell piercing Antibacterial Apoptosis/necrosis Respiratory inhibition in mitochondria Liver damage Granulomas and athereosclerotic lesions Inhibition of bacterial clearance from lungs
C_{60} (aqueous colloid)	Antibacterial ROS and ROS-independent oxidative stress Human cell cytotoxicity Enter human keratinocytes Proteins stabilizations Lipid peroxidation
C_{60} derivatives	Bactericidal for Gram-positive bacteria Cell wall/membrane damage Oxidative cytotoxicity Apoptosis/necrosis Accumulation in liver Gliomas and sarcomas in mice and human cells
TiO_2 nanoparticles	Bactericidal for Gram-positive bacteria Suppression of photosynthesis Acute lethality Growth inhibition ROS generation and oxidative damage Cell damage via ion release DNA damage Reduction in metabolic and mitochondrial activities
Cu and CuO nanoparticles	Toxic to freshwater algae Toxic to yeast Lipid peroxidation Inhibition of biogas production Single-strand breaks in DNA Acute toxicity to liver, kidneys, and spleen Necrosis of hepatocytes
Ag nanoparticles	Antibacterial DNA damage Cytotoxicity of mammalian cells Apoptosis Membrane damage Decrease in cellular metabolic activity Inflammation Genotoxicity Developmental toxicity Enhanced venous thrombus formation

Continued

Table 7.2 Continued

Nanomaterial	Observed toxicological effects
SiO_2 nanoparticles	Antibacterial ROS toxicity Cell enlargement in microorganisms Reduction in photosynthetic pigment content Inflammatory and immune responses Apoptosis Up-regulation of tumor necrosis factor (alpha genes)
Nanoclays	Intracellular ROS formation in human cells Cell membrane damage Enhanced numbers of multinucleated macrophage-agglomerates
Quantum dots	Bacterial toxicity due to metal release Lipid peroxidation Oxidative stress Transmembrane activity and proteolysis involving proteasome activation and ubiquitin-mediated processes Particle uptake DNA damage Multiple organelle damage Metal accumulation in liver, kidneys, and spleen

in construction. The reader should keep in mind that the field is very much in flux and thus our tables are unlikely to be comprehensive. We discuss some of the nanotoxicological issues of individual classes of MNMs in order to demonstrate the range of different toxicity paradigms that can be encountered when dealing with different MNM classes.

7.2.1 Carbon-based nanomaterials

Frequently used MNMs containing primarily carbon atoms enclosing a hollow interior include carbon nanotubes (CNTs) and fullerenes such as C_{20}, C_{60}, and C_{60} derivatives. Specifically, carbon nanotubes, C_{60} fullerenes, and C_{60} derivatives are currently raising health concerns as they have been shown to have adverse effects on bacterial, mammal and human cells (Jia *et al.*, 2005; Park *et al.*, 2010). CNTs are frequently contaminated with heavy metals, which is due to their particular production process. This brings up a common issue of MNMs: MNMs can be contaminated with other elements that might have toxicological relevance. Stringent quality control of the nanomaterials for such contaminations is essential.

Carbon nanotubes

Available in both single-walled (SWCNT) and multi-walled (MWCNT) forms, carbon nanotubes have been shown to exert bacterial toxicity via direct cell wall damage or oxidative stress (Kang *et al.*, 2007, 2008a, 2008b, 2009). More relevantly, however, studies have shown that both types can cause pulmonary inflammation, fibrosis, and epithelioid granulomas in mammalian cells when respired (Ding *et al.*, 2005; Jia *et al.*, 2005; Wei *et al.*, 2007). CNTs are likely to enter unprotected lungs because they are of breathable size and weight (Soto *et al.*, 2008; Herzog *et al.*, 2009). In a study performed on rats, it was concluded that MWCNTs pose a carcinogenic threat, inducing mesothelioma in exposed organisms (Basak *et al.*, 2010). Other toxicological implications include damage to mitochondrial DNA (Derno *et al.*, 1995), cellular apoptosis and necrosis (Hoffmann *et al.*, 1995, Hoffmann, 1995), and reproductive toxicity (Hansen *et al.*, 2008).

Additionally, heavy metal ions often become imbedded in the CNTs during the production phase. A common method for nanotube synthesis is chemical vapour deposition, which employs the use of a metal or alloyed catalyst such as iron, cobalt, or nickel. Ions from these metals will incidentally become bound within the CNTs. These metallic impurities can lead to toxic effects, which are not specifically 'nano' in nature; they still contribute to overall toxicological liability of CNTs (Vecitis *et al.*, 2010).

C_{60} fullerenes and their derivatives

C_{60} fullerenes may be respired during the preparation process, causing lung inflammation (Park *et al.*, 2010). In addition to their use as raw nanomaterials, these fullerenes are often suspended as water-stable aggregates. The resulting fullerene solution has been shown to have broad antimicrobial potential (Lyon *et al.*, 2005, 2006). While there have been hypotheses that this cytotoxicity is mediated by oxidative stress from ROS, recently it has been shown that direct cell membrane oxidation from C_{60} contact is likely responsible (Lyon and Alvarez, 2007; Lyon *et al.*, 2008). In eukaryotes, this oxidative stress is also responsible for cell death, leading to lipid peroxidation (Oberdörster, 2004; Sayes *et al.*, 2005). Derivatives of C_{60} fullerenes, such as fullerol and carboxyfullerene, can cause cytotoxicity by physical membrane damage (Tsao *et al.*, 2002) as well as by oxidative routes (Faruk and Matuana, 2008).

7.2.2 Metal-containing nanoparticles

Metals and metalloids are common components in manufactured nanomaterials and include titanium, copper, silver, iron, and zinc. These elements

can be used in pure nanoparticle form as with copper and silver, or as metal oxides like titanium dioxide and copper oxide.

Titanium dioxide nanoparticles

Titanium dioxide (TiO_2) NPs can cause cell death, inflammation, and DNA damage in mammalian cells by producing ROS under the presence of sunlight or UV light (Oberdorster *et al.*, 1995; Zhang *et al.*, 1998; Sayes *et al.*, 2006; Park *et al.*, 2007; Handy *et al.*, 2008; Karlsson *et al.*, 2008; Reeves *et al.*, 2008; Zhu *et al.*, 2008). While this irradiation gives TiO_2 its antibacterial property, it can potentially damage human cells by direct chemical oxidation (Dunford *et al.*, 1997). Additionally, TiO_2 NPs inhibit growth and suppress photosynthetic activity in algal cells. For these reasons, TiO_2 NPs are considered to be acutely lethal to microorganisms. In mammalian cells, a reduction in metabolic and mitochondrial activities has been observed when exposed to TiO_2 NPs.

Copper and copper oxide nanoparticles

Copper and CuO nanoparticles are shown to induce oxidative stress and cause damage to DNA via single strand breaks in a variety of organism and mammalian cells including bacteria, algae, yeast, as well as mouse and humans cell lines. In the mouse model, acute toxicity to the spleen, liver, and kidneys was observed (Chen *et al.*, 2006). Additional effects include lipid peroxidation and necrosis of hepatocytes. Studies indicate that the toxic effects resulting from exposure to Cu NPs are most likely mediated by ion release.

Silver nanoparticles

Silver NPs have been used in a wide range of applications as an antimicrobial agent. These NPs are known to have cytotoxic effects in algae, bacteria, mammalian, and yeast cells. Additionally, the extent of toxicity, including developmental toxicity and genotoxicity, has been observed to be dependent on cell type and particle size (Park *et al.*, 2011). *In vitro* studies show that oxidative stress from the production of ROS is likely the largest contributor to the Ag NP toxic effects. Like Cu NPs, ions released from Ag NPs are the facilitators of these toxic effects, including the aforementioned ROS generation.

7.2.3 Non-metal nanoparticles

Like many other nanomaterials, both silicon dioxide (SiO_2) and nanoclays have been shown to produce toxic effects in microorganisms and

mammalian cells. While these particular nanomaterials do not contain heavy metals, toxic effects have nonetheless been associated with them, as demonstrated by several studies: bacteria, algae, and mammalian cells are all targets of its ROS mediated cytotoxicity and membrane damage and carcinogenic effects have been observed.

Silicon dioxide nanoparticles

Studies indicate that exposure to SiO_2 NPs can cause lipid peroxidation and membrane damage to human lung cell lines (Lin *et al.*, 2006). In the rodent model, experiments indicate that these particles may induce tumor necrosis genes and might have carcinogenic activity. The generation of ROS appears to be a large contributor to the toxicity of SiO_2. Interestingly, the relative surface area of the particles is related to the toxicity effects in as much as a larger surface area caused stronger cytotoxicity effects in mammalian and algal cells. In microorganisms, experiments suggest that the direct interactions of SiO_2 particles attached to cell membranes are related to the mechanism of cellular toxicity. Additionally, the cell division of microalgae is hindered by the presence of SiO_2 NPs.

Nanoclay particles

Nanoclays are an umbrella term for a diverse group of MNMs and range in chemical makeup and crystalline structure. These particles are often used in polymer matrices to increase flexibility, durability, and strength but can be found as well as filler materials in construction nanocomposites. Studies in the rodent model indicate toxic effects via cell membrane damage. Specifically, sepiolite nanoclays have been found to elicit multinucleated macrophage agglomerates. *In vitro* studies on human cell lines demonstrate intracellular ROS generation, leading to oxidative stress and cell death.

7.2.4 Bimetallic alloys

In construction, this category of nanomaterials consists of semiconducting alloys in a core/shell configuration called quantum dots, which usually contain toxic heavy metals like cadmium. These quantum dots can dissolve in the digestive tract of rats upon ingestion and release these toxic components (Karabanovas *et al.*, 2008).

Quantum dots

Quantum dots may be toxic due to a variety of mechanisms depending on their composition. Most common is the release of toxic ions from the heavy

metals contained within the QDs core. These heavy metals may include cadmium, lead, and zinc and are extremely toxic to both mammalian cells and bacteria. Experiments performed on human cells indicate that cytotoxicity results from ROS damage to organelles and inflammation caused by the release of cytokines. Quantum dots can accumulate in the spleen, liver, and kidneys in mice, creating localized toxic effects. In microorganisms, other toxicity mechanisms include growth inhibition, lipid peroxidation, oxidative stress. In addition to the cellular toxicity caused by the heavy metal core, some shell materials have also been identified as toxic. Gene expression studies in algae show that toxic responses to intact QDs differ significantly from responses to internal ions: in eukaryotic cells, oxidative stress, damage to nucleic acids contribute to cytotoxicity independently of the release of internal heavy metal ions from their core. Additionally, QD toxicity experiments on mice neural cells demonstrate impaired calcium influx and exocytotic mechanisms.

7.3 Lifecycle of nano-enabled structures

Manufactured nanomaterials may be released into the environment over the entire lifecycle of the structure, from the time of construction, throughout the use of the structure, and after demolition and disposal. It is important to realize that these materials may transform over time via physical, chemical, or biological processes.

It is important to recognize that much research needs to be conducted to fill in the knowledge gaps regarding aging MNMs in structures. Few studies currently published have investigated long-term physical and chemical changes of imbedded MNMs and the associated hazards. For example, if an MNM is imbedded into a concrete floor or pavement, continual traffic and abrasion will inevitably cause the release of nanomaterials.

7.3.1 Manufacturing of nanomaterials and use in construction

One of the common human exposure routes for nanomaterials is through inhalation. This threat is prevalent largely during the periods of manufacturing and construction due to the high levels of airborne or aerosolized particles. Though unintentional, carbon fullerenes may be aerosolized during the aqueous suspension process, which might require sonication. These and other types of nanomaterials can become airborne when exposed to open air for weighing. Sepiolite nanoclay, which may be used as filler in construction nanocomposites, is lost to the air during mining, transportation, and the manufacturing process.

The most vital step to ensure exposure prevention is an accurate assessment of potential chemical or physical reactions that may occur during the lifecycle of the MNM. In other words, it is the responsibility of the manufacturing and construction industries to prevent any transformations of the MNM so that the creation of hazardous byproducts can be avoided. In addition, it is undesirable to incidentally modify the unique properties of the MNMs being used since this will likely make them behave less efficiently than design has intended, and perhaps cause more adverse structural or health effects than if they were not incorporated at all.

Since there are many factors involved in determining the relationships between the structure and the MNM, thorough physicochemical studies should be made by the manufacturer during the development process to identify any unfavorable conditions and reactions. Here, the fate, behavior, and environmental reactions such as adsorption and desorption, particle aggregation, reduction-oxidation reactions, deposition, or ion dissolution should be investigated for each MNM. Similarly, the construction companies using these new materials should consider the findings provided by the manufacturer and determine the safest way to incorporate the MNMs into the structure without taking away from their desired benefits. This may include encapsulation or coatings to reduce dangerous interactions with other structural components. Contractors should also consider minimizing the amount of MNMs used in a project when one material may do the work of many. It may be safer to use the same MNM for a variety of purposes than to use a different MNM for each purpose so that potential damaging reactions may be minimized and an increase in adverse health effects is kept low.

7.3.2 Useful life of the structure

Throughout the use of the structure, MNMs may still be released even when proper construction practices have been used. Unanticipated environmental conditions, weather phenomena, vandalizing, and wear and tear can cause cracks to form, paint to peel, and internal structural components to be exposed. When such damage occurs, MNMs may be released into the environment to be taken up by users via inhalation or ingestion, or they may be chemically/physically transformed by new unfavorable conditions. In addition to allowing MNMs to release from the construction, structural flaws also permit water and other reactants to enter through openings to transform the MNMs. Depending on the material used, hazardous byproducts may be created or unveiled, reducing the usefulness of the nanomaterial.

7.3.3 Demolition, disposal, and recycling

To reduce the consumption of raw MNMs and minimize waste, recycling and reusing MNMs from construction materials is a safe alternative. Demolition must be controlled and monitored to prevent the release of MNMs into the environment and community. As with the manufacturing and construction phases, MNMs are capable of becoming airborne during deconstruction and disposal, posing potential health risks for workers. Dust can contain MNMs that may be inhaled, ingested, or cause eye irritation.

Prior to demolition, efficient strategies for collecting the used MNMs from complex media should be developed so that the unique properties of the MNMs remain intact and human or environmental exposure is minimized. The MNMs should be characterized and evaluated for their ability to be reactivated and reused. The ease and costs of extraction should also be considered in determining the recycling potential of an MNM. The remaining MNM-containing construction wastes must be disposed of properly to prevent release and/or transformation of MNMs (Bystrzejewska-Piotrowska *et al.*, 2009). Each MNM may have special disposal requirements according to the manufacturer or other regulatory frameworks so a thorough investigation of these procedures should be performed in advance. Reinforcement barriers in landfills are recommended to prevent MNM leachate from contaminating groundwater and underlying aquifers. Once the appropriate disposal measures have been taken, continual interception and remediation methods must be developed to monitor secondary MNM release into the environment.

7.4 Toxicity profiling for nanomaterials

Currently, there is considerable debate about how to proceed with engineered nanomaterials (ENM) toxicity testing, with the major discussion points centering around which toxicological endpoints to screen for, the rigor of the screening effort, the correct balance of *in vitro* (cellular and molecular) versus *in vivo* (animal or whole organism) testing, the cost of the effort, and who should be responsible for overseeing this nano-EHS development. Attempts to use traditional toxicological assays and models have resulted in some advancement of our knowledge about nanotoxicology but we are still experiencing at times conflicting results and we are far away from the implementation of a generally accepted screening platform. While much of the knowledge about MNM toxicity has been generated using fairly straightforward single read-out plate reader based screening assays, each chosen assay represents typically only a single specific reaction to a toxic stimulus and thus is of limited predictive value. Since toxic effects are always a function of the presence or absence of targets for a given toxic

stimulus in the organism in question, toxic effects of MNMs can differ between species. For comprehensive MNM toxicity testing, it is thus necessary to consider the analysis of multiple species such as, e.g., human, fish, bacteria, algae, etc.

The biggest challenge for the evaluation of nanomaterial toxicity and hazard is the sheer number of different materials – we can expect in excess of 100,000 MNM enabled products in the next decade (Service, 2008). A solution to the bottleneck in MNM testing is high throughput screening (HTS). HTS became the leading paradigm in drug discovery in the late 1980s and early 1990s and generated many more lead compounds (Pereira and Williams, 2007) than the labor-intensive 40–50-year-old descriptive toxicology platforms used up to this point could handle. The toxicology departments had to adopt HTS methodologies (Dimasi, 2001) to keep up with the number of chemical candidates that came out of HTS campaigns. The resulting arsenal of HTS toxicology assays and platforms is large and much of it can be transferred to ENM toxicity screening. It is interesting to note that the National Academy of Sciences (NAS) has recognized the need for novel methodologies which can support carrying out a large number of toxicological tests without relying primarily on animal testing and put forth a vision and strategy paper in which HTS methodologies are prominently featured as one feasible approach for turning the vision into reality (Gibb, 2008). Similarly, the European Union has enacted the REACH program under which all chemicals have to undergo toxicology testing and takes notes from the EPA ToxCast program in which HTS toxicology methods are applied towards screening chemicals for their toxicological properties according to the NAS vision paper (Judson *et al.*, 2010).

7.4.1 Characterization of MNMs before toxicity screening

Before the actual toxicity testing, a thorough characterization of the MNMs in 'dry' and 'as dispersed' form is necessary (see Table 7.3 for an overview of MNM properties and frequently used techniques): while MNMs are typically delivered as a dry powder, when they come into contact with a living entity and exert their toxicity, they will be in aqueous phase – be this now in, e.g., a waste water matrix, or the lung fluid of a mammal. While the 'dry' characterization typically includes assessment of important metrics such as size and shape as well as phase and crystallinity, one has to bear in mind that MNMs can change quite drastically in aqueous phase: aggregation, changes in surface charge, absorption of, e.g., proteins present in the aqueous phase are quite common and influence the nano-toxicity. Hence, it is important to determine not only the properties of an MNM 'as produced' in dry powder form but also, e.g., the size, size distribution, state of dispersal/aggregation, stability and the zeta-potential of the MNM in aqueous phase,

Table 7.3 Overview characterization of ENMs. While Class 1 properties are intrinsic to a nanomaterial itself, the Class 2 properties are dependent on the interplay between ENM and assay system

Nanomaterial property	Available analytical techniques
Class 1: 'As produced' – morphology and structure	
Primary particle size, shape, and size distribution	TEM, SEM, AFM, ESEM, FIB-SEM, cryo-TEM
Fractal structure	TEM, SAXS, SANS
Pore size, porosity, and surface area	BET, SAXS, SANS
Crystallinity, framework structure, and crystal size	XRD, Raman, SAXS, NMR
Chemical composition	Raman, NMR, EDAX, FTIR, XPS, ICP
Elemental speciation and redox state	Raman, XAFS, XANES, NMR
Electronic, magnetic, and photonic properties	SAXS, Mossbauer, ESR, Raman, UV-Vis
'Dustiness' or tendency to aerosolize	EMPS, SMPS
Class 2: 'As dispersed' – interfacial properties	
Dispersed size and size distribution	DLS, EMPS, SMPS, laser diffraction
Aggregate size	DLS, electroacoustics
Charge density, pKa, PZC, ionization fraction	Direct titration in various suspending media
Surface (zeta) potential and IEP	EPM measurements in various suspending media
Surface tension components (LW, g +, g –)	Multiple probe liquid contact angle/ tensiometry
Roughness and chemical heterogeneity	AFM, CFM, FTIR, XPS, NMR, Raman

as these important parameters are dependent on the media matrix they are in.

For example, ions play an important role for the aggregation behaviour of MNMs (Jin *et al.*, 2010). Moreover, the MNM dispersions are typically not stable and much effort has been put into the discovery of suitable dispersal agents, which are compatible with the biological system in which they are to be tested. In this context it has to be mentioned that dispersion agents used for the stabilization during testing of MNMs do modify the surface of the material and may therefore interfere in toxicity screening: for example, DPPC in relatively high doses has been shown to completely suppress the cytotoxicity and pro-apoptotic effects of quartz nanoparticles (Gao *et al.*, 2001). In this context it should be noted that, although nanoparticle dispersion has been extensively researched, only a few studies have addressed the stability of the resulting dispersions and only limited information is available from systematic studies on the effect of proteins and other chemical surfactants on nanoparticle stability in assay media such as cell culture

media. A methodic approach is imperative when performing nanotoxicology in any assay system to exclude false results. Therefore, it becomes urgent to develop standard protocols for evaluating nanomaterial stability during *in vitro* or *in vivo* nanotoxicity studies.

We will now review existing approaches for small molecule HTS toxicology screening as many of these approaches and workflows currently used in drug discovery can be potentially adapted towards ENM toxicology screening.

7.4.2 General considerations for MNM toxicity profiling using HTS

HTS approaches for toxicology typically utilize microtiter plates of the 96 or 384 well plate format. These plate formats are formalized by the Society of Biomolecular Screening and all existing equipment is compatible with the plate formats.

The screening approaches themselves are either plate reader or high content screening (HCS) based. Plate reader based assays rely on one of the classic standard readouts such as luminescence, fluorescence, absorption, time-resolved fluorescence and fluorescence polarization and measure the whole well at once. TR-FRET and fluorescence polarization (FP) are readouts that are less commonly used for toxicity screening as their cost is higher than the other three assay readouts mentioned and especially FP is very sensitive to interference from contaminants and temperature variations. While plate reader based assays typically have a single parameter, which is measured at a point in time, HCS offers a complementary approach, which can be understood as automated microscopy coupled with image analysis software. It enables the measurement of multiple parameters with cellular resolution in the same well at the same time and offers a more detailed view. Moreover, HCS enables the detection of rare cellular events, segregation of sub-populations of cells from a single well and has the potential to be more sensitive and also pick up sub-lethal effects. Another important factor is that HCS enables phenotypic screening, which can be based on, e.g., cell morphology or translocation event of a given protein.

HCS-based toxicity screening has significant advantages over classical plate reader based assays. In a 2006 study (O'Brien *et al.*, 2006), conventional single plate reader based readouts were compared to a five parameter HCS assay for toxicology prediction power on a set of reference compounds: the single parameter readouts had a very limited sensitivity (<25%) but high specificity (about 90%), but HCS had a sensitivity of 93% and a specificity of 98%. What is more interesting is the fact that although hepatocyte HepG2 cells were used, 92% of the toxic drugs, which had other organ toxicities, but no hepatotoxic properties, were detected.

While many assays are available for toxicity screening of small organic molecules, it remains to be seen whether all possible toxicology paradigms can be covered with already existing assays as ENM-triggered toxicity has the potential to follow different paradigms than small molecule toxicity. Another argument in favor of custom development of novel assays is their usability for testing the hypothesis of the mode of action of ENM toxicity. To accomplish this, novel assay platforms are needed for the evaluation of ENMs in environmentally relevant systems such as, e.g., algae or other aquatic species, which will require tailoring of assays to ENM toxicity. The strength of plate reader based assays is their speed. HCS-based assays can be slow to read on the imaging systems, so at times a balance between information required and the needed acquisition speed has to be found.

Importantly, it has to be noted that each assay has its artifacts and other liabilities. This is especially true for nanotoxicology where it is very common for, e.g., dyes used in an assay to interact with a given MNM leading to unreliable or even false results. Table 7.4 gives an overview of MNM toxicity paradigms, corresponding assays/readouts as well as possible interference of the MNM with the assay readout. Typically, it is advisable to confirm results on toxic MNMs with another assay, which uses a different readout paradigm in order to exclude artifacts.

While, for example, some toxicity assays rely on cell-free systems such as detection of ROS generation (Gabriel *et al.*, 1997) by the MNM using a fluorescent dye or co-incubation of an MNM with an enzyme and subsequent measurement of enzymatic activity, it is the cell-based assays which offer the most insight into MNM toxicity as a living cell contains all potential targets for MNM toxicity (Damoiseaux *et al.*, 2011).

As the lowest functional unit of an organism, cells represent the ultimate target for an intruding MNM and from a biochemical perspective the cells respond to foreign materials in essentially similar ways to that of the whole organism. Although primary cell lines are ideal candidates for toxicity screening, the cells are frequently not available in sufficient quantities for use in HTS, hence cell lines are used. A cell-based assay in the context of nanotoxicity can be regarded as an analytical procedure that assesses the biological outcome resulting from the interaction of nanomaterials with a given cell. However, the manifestation of biological outcome is generally faster in a cell-based *in vitro* system (often in the order of minutes to hours) than *in vivo*, thus providing a rapid readout of MNM toxicity. In order to achieve the true toxicological significance of a cellular injury response, it is necessary to correctly pick the cell line type and *in vitro* end point/readout in order to generate high quality information about the potential impact of the nanomaterial.

The toxicity profile of NMs may vary from one cell type to another because of the possible difference in the cellular uptake and processing of

Table 7.4 Examples of toxicity paradigms, possible analytes, readout modes and potential problems when using various readouts for MNM toxicity screening

Toxicity type or paradigm	Analyte	Probes	Readout mode	Utility	Potential problem
Cytotoxicity	Cell number/ proliferation	Hoechst 33342/ DAPI	Fluorimetry/ High content assay	Cell quantification, nuclear content	Background signal from NPs with blue fluorescence
	Membrane leakage	Propidium Iodide/Syto 9	Fluorimetry/ High content assay	Compromised cell membrane integrity	Background signal from NPs with red fluorescence (e.g., QDs)
	Membrane integrity	LDH assay	Absorbance at 490 nm	Cell viability	NPs may inhibit enzyme and/ or absorb at 490 nm (CNTs, Ag)
	ATP	ATPlite™	Luminescence	Mitochondrial activity and viability status of cells	Not appropriate for NPs that may inhibit enzyme and/or absorb light (e.g., CNTs)
	Mitochondrial membrane potential	JC1/TMRM/ chloromethyl-X-rodhamine	Fluorimetry/ High content assay	Loss of MMP	Background signal from NPs with red or green fluorescence
	Metabolic activity	MTT, WST-1, XTT.	Absorbance	Mitochondrial activity and viability status of cells	NPs may inhibit enzyme and/ or absorb light or substrates
	Intracellular calcium flux	Fluo-4/ Fura 2-AM/Rho 2-AM	Fluorometry/ High content assay	Increased Intra-cellular calcium level	Background signal from NPs with green fluorescence
	Apoptosis	Calcein-AM	Fluorometry/ High content assay	Mitochondrial membrane permeability transition (MPT)	Background signal from NPs with green fluorescence

Table 7.4 Continued

Toxicity type or paradigm	Analyte	Probes	Readout mode	Utility	Potential problem
Genotoxicity	DNA cleavage	Micro-nuclei assay (HCS), BrDU incorporation	High content screening	Chromosome damage	Background signal from NPs with blue fluorescence
Inflammation	IL-1, IL-8, TNF-α	Antibody based ELISA or TR-FRET	Luminescence/ TR-FRET	Expression level of inflammatory markers	Not appropriate for NPs that interfere with TR-FRET (e.g., absorb protein) or luminescence reactions
	NF-kB and AP-1 activation	Reporter genes	Luminescence	Activation of inflammatory pathways	Not appropriate for NPs that may inhibit enzyme and/or absorb light
Oxidative stress	GSH, ROS	Absorbance/HCS using fluoresence probes	Fluorometry/ High content assay	Free radical generation, Glutathione depletion	Not appropriate for NPs that may interfere with fluorescence output
Fibrogenesis	TGF-1b, Collagen 1&3, MMPs	Fluorescence probe coupled antibody	Fluorometry/ High content assay	Induction of fibrogenesis	Not appropriate for NPs that may interfere with fluorescence output

nanomaterials. A simple solution to this liability is to incorporate more than one cell type (often different cell lineage) and to conduct multiple cytotoxicity assays simultaneously for a range of reasonable doses and durations of exposure. Recently, Shaw *et al.* (2008) demonstrated that the predictive power of an *in vitro* assay could be greatly improved by including multiple cell lines (4 different cell lines) and multiple doses of nanomaterials. It should be emphasized that the data quality from cell-based HTS assays is to a strong degree dependent on the equipment and the experimental conditions. Special attention has to be paid to artifacts stemming from the use of microtiter plates such as edge effects due to the evaporation of culture media or irregularities arising from liquid handling errors. Hence, any cell-based assay has to be thoroughly optimized for HTS, validated on the equipment used for the toxicity screening and it is necessary to standardize the experimental conditions employing appropriate negative and positive controls on each microtiter plate. We will now review in detail HTS approaches toward three of the most important nanotoxicity paradigms: mutagenicity, cytotoxicity, and oxidative stress.

7.4.3 HTS for mutagenicity, cytotoxicity and oxidative stress effects of MNMs

The first *in vitro* toxicology assay was the Ames test, which dates back to the 1970s and it is still in use today. In this test, several strains of bacteria – *Salmonella typhimurium* with various mutations in the histidine production pathway – are being exposed to a mutagenic material in question. Mutations resulting in a frame shift mutation or reversing a point mutation results in a restoration of the respective histidine production pathway gene and results in the production of histidine. The readout is growth on histidine deficient media. Several commercial HTS versions of this test exist for plate readers. For example, damaging effects of MNMs on DNA can be detected, triggering using a reporter gene assay system in which luciferase is put under the recN promoter which gets triggered by the SOS DNA repair response. The commercial name of this test is 'VitoTox' test (Verschaeve *et al.*, 1999).

Care should be taken when comparing the results from assays: while the Ames test detects mutagenicity, the VitoTox test detects genotoxicity. GreenScreen is another assay similar in principle to the VitoTox test. In GreenScreen (Van Gompel *et al.*, 2005), the RAD54 promotor drives green fluorescent protein (GFP) expression in yeast. RAD54 is involved in DNA double strand breakage response and the activation of the repair pathway by a genotoxic MNMs leads to GFP expression. In the commercial product RadarScreen, the GFP is replaced with β-galactosidase. Galactosidase can be read on a plate reader using various colorigenic or luminogenic

substrates. Going up in the evolutionary chain, the GreenScreen HC assay relies on a TK6 lymphoblastoma cell line with a growth arrest and damage gene promoter GADD45α in driving the luciferase reporter.

It is interesting to note that drugs, which are normally tested in these assays, are exposed to liver enzymes that metabolize the compound in question before their use in these assays. The reasoning is that frequently the metabolites are more toxic than the parent compound. At this point it is frequently unclear where and how MNMs are processed or broken down in an organism and it is unclear if exposure to liver enzyme will be useful for MNM toxicity testing. While results from assays for mutagenicity testing are quite universally applicable since the carrier of genetic information, DNA, is universal, this is not the case for cytotoxicity. Cytotoxicity is very dependent on the presence of a target mediating the cytotoxic effect. Hence precise knowledge of the mode of action (MOA) is necessary to fully understand and appreciate the cytotoxic potential of any given MNM.

For drugs, dyes allowing for measuring DNA content such as Hoechst 33342 are frequently used for the detection of, e.g., pro-mitotic effects using HCS approaches. Cell cycle analysis using various dye combinations can be very useful as well for the detection of hazardous MNMs and are best executed using HCS. Membrane integrity can be assessed using propidium iodide (PI) and/or Calcein-AM dyes. While the nucleic acid dye PI does not pass intact membranes, Calcein AM is a conjugated membrane permeable, fluorogenic fluoresceine derivative that once in the cell and processed by esterases can no longer leave the cell – except if the membrane integrity is compromised. This assay can be performed in a plate reader or HCS system.

Cytotoxicity of an MNM can show itself as well in the collapse of the gluthathion level of a cell or radical oxygen species (ROS) formation, which can be detected in the presence or absence of cells. Gluthathione depletion can be easily assessed using monochloimane and ROS formation can be easily measured using dichlorofluoresceine. Both of these dyes can be used in a plate reader format. The redox potential of a cell – i.e. gluthathion level – can be followed using dyes such as MTT or Alamar Blue (Nakayama *et al.*, 1997). While these dyes are relatively cheap, the fluorescent character of the nanomaterials might interfere with their detection. Hence the use of CytoLite (measures NADH) (Chan *et al.*, 2001), ATP-Lite or CellTiter Glo (measure ATP) might be preferable (Hannah *et al.*, 2001). A combination of these three assays should enable a first picture of the MOA of the toxicity of any given nanomaterial.

An interesting twist on apoptosis detection, which is a frequent liability of toxic MNMs, is the use of Z-DEVD-aminoluciferin for Caspase 3/7 and LETD-aminoluciferin for Caspase 8/9 (O'Brien *et al.*, 2005). Both substrates have in common that upon activation of the Caspases in question,

the peptide part is cleaved off the aminoluciferin hence making it convertible by firefly luciferase. While Capase 3/7 would indicate mitochondrial impairment, Caspase 8/9 activity might point more at inflammation and activation of TNFα and interleukin-1β secretion.

Injury responses due to oxidative stress from MNM exposure have been documented extensively in the literature and oxidative stress is one of the best-understood mechanisms of MNM mediated toxicity (Oberdorster *et al.*, 2005; Nel *et al.*, 2006, 2009). MNM induced oxidative stress can be divided into three tiers: antioxidant defense, pro-inflammatory effects and cytotoxicity. MNM toxicity is typically mediated by ROS generation which can be extra- or intracellular and in both cases depletes the gluthathion redox-equilibrium of the living cell. Each of these response tiers is initiated by specific biological sensors and activation mechanisms. In Tier 1, the transcription factor Nrf2 is activated to enhance the expression of phase II enzymes, which attempts to restore redox equilibrium. If the level of oxidant injury cannot be recovered by phase II enzymes, Tier 2 response commences, signaling pathways such as the mitogen-activated protein kinase (MAPK), and nuclear factor kappa B (NF-κB) cascades are activated and cells express proinflammatory cytokines. These inflammatory effects contribute to disease processes such as asthma and atherosclerosis.

At the highest level of oxidative stress (Tier 3), the mitochondrial integrity is compromised and a resulting drop in ATP synthesis and release of calcium and other pro-apoptotic factors ultimately leads to cell death. Cytotoxicity (Tier 3 response) is the most extreme response to particle effects involving ROS production. Modes of action can involve the shedding of toxic metal ions that trigger intracellular ROS generation or cationic nanoparticles or dissolved transition metal interference with the mitochondrial electron transduction. As is evident, it is necessary to select multiple readouts to capture cellular events specific to Tiers 1–3.

Oxidative stress can be detected very easily using HCS. For example, a cocktail of Hoechst 33342 and the mitochondrial membrane potential dye JC1 detects Tier 2 responses based on mitochondrial membrane depolarization. A dye cocktail of Hoechst 33342, fluo-4 (detecting cytosolic Ca^{2+}) and propidium iodide (detecting membrane damage) is very useful for the detection of Tier 3 responses in which the mitochondrial membrane loses integrity, calcium enters the cytosol and the cell membrane disintegrates. In the oxidative stress paradigm, *in vitro* and *in vivo* are correlated extremely well: for example, ZnO nanoparticles elicit responses *in vitro* that are analogous to a disease called 'metal fume fever' (Duffin *et al.*, 2007). Metal fume fever is an acute inflammatory condition of the lung in welders who are exposed to aerosolized metal oxide nanoparticles. In the workers, one finds the expression of Tier 2-like responses in macrophages and epithelial cells as demonstrated by the detection of secreted interleukin 8 (IL-8) and

TNF-α in the lungs and bronchoalveolar lavage fluid of exposed workers (Xia *et al.*, 2008).

7.5 Future trends and conclusions

With increased attention on MNM health hazards, there has been a need to develop new methods for toxicity profiling, safer manufacturing procedures, and 'greener' MNMs as alternatives to more harmful materials. While engineered nanomaterials provide many benefits to 'green' construction, uncertainty remains about the long-term effects of nano-enhanced structures. In this context, it will be important to ensure MNMs are not released into the environment until these MNMs are proven harmless. Or course, the ultimate goal is to use safe, next generation MNMs for future construction projects. Ultimately, methods for predicting MNM toxicity *a priori* must be explored. Since no definitively hazard-free nanomaterial presently exists, there is much work to be done in this area to alleviate public concern and move forward with new nano-enabled construction.

7.5.1 Nanomaterial toxicity and green nanomaterials

Our ability to generate safer MNMs will depend on our understanding of the toxicological liabilities of current MNMs, our ability to tie toxicological liabilities to MNM properties, and design of greener MNM, which are devoid of any toxicological liability while building on our conclusions. A prime example of this approach is the design of environmentally friendlier, 'greener' metal oxide MNMs (Meng *et al.*, 2009). One of the main toxicity paradigms of metal oxide MNMs is oxidative stress (Xia *et al.*, 2006). For example, it has been shown that the overlap of conduction band energy ($E(c)$) levels with the cellular redox potential (–4.12 to –4.84 eV) is strongly correlated to the ability of various nanoparticles to induce oxygen radicals, oxidative stress, and inflammation (Zhang *et al.*, 2012).

Iron doping is one way to tune down the toxicity of ZnO particles, which are notorious for their ability to generate ROS through ion shedding. The addition of 1–10% iron results in ZnO particles which are less soluble, which in consequence are less toxic in the rodent lung and towards zebrafish embryos. We can be hopeful that we will see many more examples of greener MNMs in the years to come.

Taking MNM production from 'green by trial and error' to 'green by design' requires us to be able to predict MNM toxicity *a priori*. Such a prediction of MNM toxicity will depend on our ability to generate a nanostructure activity relationship (nano-SAR) (Liu *et al.*, 2012) in which MNM toxicity properties are correlated with MNM descriptors (Zhang *et al.*, 2012). This nano-SAR will provide models of the toxicity profile of an MNM

at the design stage without actually having to test the material in the laboratory. Liu *et al*. have succeeded in generating such a nano-SAR for metal oxides. A set of 14 descriptors for MNMs was used in order to correlate the toxicity of a set of nine metal oxide MNMs on BEAS-2B lung epithelial cells measured as membrane degradation in a high content screening assay using propidium iodide. The best-performing nano-SAR model resulted in a 100% classification accuracy. This model was based on three descriptors: atomization energy of the metal oxide, period of the nanoparticle metal, and nanoparticle primary size, in addition to nanoparticle volume fraction (in solution). While the sample library of MNM was very small, the results are very encouraging and we may hope that the integration of much larger datasets will eventually yield universal design rules for green MNMs.

The nano revolution has tremendous potential to address some of the world's most pressing needs and it is our obligation to implement this disruptive technology safely. High throughput screening will play a decisive role, as it is the only technology which enables us to test a multitude of nanomaterials in various doses, time points and assay systems in a very short period at a reasonable cost. The necessary HTS infrastructure is accessible at centers such as the Molecular Screening Shared Resource (MSSR), which is part of the NSF/EPA sponsored multi-disciplinary University of California Center for the Environmental Impact of Nanotechnology (UC-CEIN) at the University of California, Los Angeles.

To work toward creating safe nanomaterials, it is important to coordinate research on nanotoxicology and cooperate on the development of new nanotechnology materials and applications. Rather than working independently, these areas must be closely collaborative to begin identifying health hazards during the developmental phase before new nanomaterials are used commercially. This research network will also facilitate the creation of nanomaterials with fewer environmental and health impacts and ways to better maintain their stability throughout their lifecycle. The future of the nanotechnology revolution and 'green' construction lies in the ability to understand potential hazards and mitigate these hazards before use. The answer is in a tightly cooperative network of researchers equally interested in advancing nanotechnology applications and the associated health concerns.

7.6 References

Abraham, V. C., Towne, D. L., Waring, J. F., Warrior, U. & Burns, D. J. (2008) Application of a high-content multiparameter cytotoxicity assay to prioritize compounds based on toxicity potential in humans. *J Biomol Screen*, 13, 527–537.

Alvarez, P. J. J., Lee, J. & Mahendra, S. (2010) Nanomaterials in the construction industry: a review of their applications and environmental health and safety considerations. *ACS Nano*, 4, 3580–3590.

Anikeeva, P. O., Halpert, J. E., Bawendi, M. G. & Bulovic, V. (2009) Quantum dot light-emitting devices with electroluminescence tunable over the entire visible spectrum. *Nano Letters*, 9, 2532–2536.

Arico, A. S., Bruce, P., Scrosati, B., Tarascon, J. M. & Van Schalkwijk, W. (2005) Nanostructured materials for advanced energy conversion and storage devices. *Nature Materials*, 4, 366–377.

Basak, G. C., Kumar, K. D., Bandyopadhyay, A. & Bhowmick, A. K. (2010) Elegant way of strengthening polymer-polymer interface using nanoclay. *ACS Applied Materials & Interfaces*, 2, 2933–2943.

Becher, P. F. (1991) Microstructural design of toughened ceramics. *J Am Ceram Soc*, 74, 255–269.

Benn, T., Cavanagh, B., Hristovski, K., Posner, J. D. & Westerhoff, P. (2010) The release of nanosilver from consumer products used in the home. *J Environ Qual*, 39, 1875–1882.

Brown, P. & Kamat, P. V. (2008) Quantum dot solar cells. Electrophoretic deposition of CdSe-C_{60} composite films and capture of photogenerated electrons with nC_{60} cluster shell. *J Am Chem Soc*, 130, 8890–8891.

Buzea, C., Pacheco Blandino, I. I. & Robbie, K. (2007) Nanomaterials and nanoparticles: sources and toxicity. *Biointerphases*, 2, MR17–172.

Bystrzejewska-Piotrowska, G., Golimowski, J. & Urban, P. L. (2009) Nanoparticles: their potential toxicity, waste and environmental management. *Waste Manag*, 29, 2587–2595.

Chan, J. H., Dua, H. S., Powell-Richards, A., Jones, D. R. & Harris, I. M. (2001) Effect of ABO blood group mismatching on corneal epithelial cells: an *in vitro* study. *Br J Ophthalmol*, 85, 1104–1109.

Chan, J., Bayliss, P. E., Wood, J. M. & Roberts, T. M. (2002) Dissection of angiogenic signaling in zebrafish using a chemical genetic approach. *Cancer Cell*, 1, 257–267.

Chauhan, R. S., Chaturvedi, R. & Gutch, P. K. (2006) Polymer-clay nano composites. *Defence Sci J*, 56, 649–664.

Chen, Z., Meng, H. A., Xing, G. M., Chen, C. Y., Zhao, Y. L., Jia, G. A., Wang, T. C., Yuan, H., Ye, C., Zhao, F., Chai, Z. F., Zhu, C. F., Fang, X. H., Ma, B. C. & Wan, L. J. (2006) Acute toxicological effects of copper nanoparticles *in vivo*. *Toxicol Lett*, 163, 109–120.

Contado, C. & Pagnoni, A. (2008) TiO_2 in commercial sunscreen lotion: flow field-flow fractionation and ICP-AES together for size analysis. *Anal Chem*, 80, 7594–7608.

Damoiseaux, R., George, S., Li, M., Pokhrel, S., Ji, Z., France, B., Xia, T., Suarez, E., Rallo, R., Madler, L., Cohen, Y., Hoek, E. M. & Nel, A. (2011) No time to lose – high throughput screening to assess nanomaterial safety. *Nanoscale*, 3, 1345–1360.

Daniel, M. C. & Astruc, D. (2004) Gold nanoparticles: assembly, supramolecular chemistry, quantum-size-related properties, and applications toward biology, catalysis, and nanotechnology. *Chem Rev*, 104, 293–346.

De Ibarra, Y. S., Gaitero, J. J., Erkizia, E. & Campillo, I. (2006) Atomic force microscopy and nanoindentation of cement pastes with nanotube dispersions. *Phys Stat Sol A – Appl Mater Sci*, 203, 1076–1081.

Derno, M., Jentsch, W. & Hoffmann, L. (1995) Effect of long-time exposure to different environmental temperatures on heat-production of growing pigs. *Livestock Production Science*, 43, 149–152.

Dimasi, J. A. (2001) Risks in new drug development: approval success rates for investigational drugs. *Clin Pharmacol Ther*, 69, 297–307.

Ding, L. H., Stilwell, J., Zhang, T. T., Elboudwarej, O., Jiang, H. J., Selegue, J. P., Cooke, P. A., Gray, J. W. & Chen, F. Q. F. (2005) Molecular characterization of the cytotoxic mechanism of multiwall carbon nanotubes and nano-onions on human skin fibroblast. *Nano Lett*, 5, 2448–2464.

Dobrovolskaia, M. A. & McNeil, S. E. (2007) Immunological properties of engineered nanomaterials. *Nat Nanotechnol*, 2, 469–478.

Duffin, R., Tran, L., Brown, D., Stone, V. & Donaldson, K. (2007) Proinflammogenic effects of low-toxicity and metal nanoparticles *in vivo* and *in vitro*: highlighting the role of particle surface area and surface reactivity. *Inhal Toxicol*, 19, 849–856.

Dunford, R., Salinaro, A., Cai, L. Z., Serpone, N., Horikoshi, S., Hidaka, H. & Knowland, J. (1997) Chemical oxidation and DNA damage catalysed by inorganic sunscreen ingredients. *FEBs Letters*, 418, 87–90.

Dwivedi, P. D., Tripathi, A., Ansari, K. M., Shanker, R. & Das, M. (2011) Impact of nanoparticles on the immune system. *J Biomed Nanotechnol*, 7, 193–194.

Fahy, G. M. (1993) Molecular nanotechnology. *Clin Chem*, 39, 2011–2016.

Faruk, O. & Matuana, L. M. (2008) Nanoclay reinforced HDPE as a matrix for wood-plastic composites. *Compos Sci Technol*, 68, 2073–2077.

Ferrari, M. (2005) Cancer nanotechnology: opportunities and challenges. *Nat Rev Cancer*, 5, 161–171.

Gabriel, C., Camins, A., Sureda, F. X., Aquirre, L., Escubedo, E., Pallas, M. & Camarasa, J. (1997) Determination of nitric oxide generation in mammalian neurons using dichlorofluorescin diacetate and flow cytometry. *J Pharmacol Toxicol Methods*, 38, 93–98.

Gao, N., Keane, M. J., Ong, T., Ye, J., Miller, W. E. & Wallace, W. E. (2001) Effects of phospholipid surfactant on apoptosis induction by respirable quartz and kaolin in NR8383 rat pulmonary macrophages. *Toxicol Appl Pharmacol*, 175, 217–225.

Ge, Z. & Gao, Z. (2008) Applications of nanotechnology and nanomaterials in construction. *First Inter Confer Construc Develop Countries*, 235–240.

German, J. B., Smilowitz, J. T. & Zivkovic, A. M. (2006) Lipoproteins: when size really matters. *Curr Op Colloid & Interface Sci*, 11, 171–183.

Gibb, S. (2008) Toxicity testing in the 21st century: a vision and a strategy. *Reprod Toxicol*, 25, 136–138.

Girishkumar, G., Rettker, M., Underhile, R., Binz, D., Vinodgopal, K., McGinn, P. & Kamat, P. (2005) Single-wall carbon nanotube-based proton exchange membrane assembly for hydrogen fuel cells. *Langmuir*, 21, 8487–8494.

Goldman, L. & Coussens, C. (2005) *Implications of Nanotechnology for Environmental Health Research*, Washington, DC, The National Academies Press.

Gopel, W. (1991) Chemical sensing, molecular electronics and nanotechnology – interface technologies down to the molecular scale. *Sensors and Actuators B-Chemical*, 4, 7–21.

Hagens, W. I., Oomen, A. G., De Jong, W. H., Cassee, F. R. & Sips, A. J. (2007) What do we (need to) know about the kinetic properties of nanoparticles in the body? *Regul Toxicol Pharmacol*, 49, 217–229.

Handy, R. D., Henry, T. B., Scown, T. M., Johnston, B. D. & Tyler, C. R. (2008) Manufactured nanoparticles: their uptake and effects on fish – a mechanistic analysis. *Ecotoxicology*, 17, 396–409.

Hannah, R. B. M., Moravec, R. & Riss, T. (2001) CellTiter-Glo™ luminescent cell viability assay: a sensitive and rapid method for determining cell viability. *Promega Cell Notes*, 11–13.

Hansen, S. F., Michelson, E. S., Kamper, A., Borling, P., Stuer-Lauridsen, F. & Baun, A. (2008) Categorization framework to aid exposure assessment of nanomaterials in consumer products. *Ecotoxicology*, 17, 438–447.

Hayashi, T., Kim, Y. A., Natsuki, T. & Endo, M. (2007) Mechanical properties of carbon nanomaterials. *Chem Phys Chem*, 8, 999–1004.

Herzog, E., Byrne, H. J., Casey, A., Davoren, M., Lenz, A. G., Maier, K. L., Duschl, A. & Oostingh, G. J. (2009) SWCNT suppress inflammatory mediator responses in human lung epithelium *in vitro*. *Toxicol Appl Pharmacol*, 234, 378–390.

Hoffmann, K. D. (1995) Population-growth poverty and environmental destruction in the third-world. *Gegenwartskunde Gesellschaft Staat Erziehung*, 44, 393–425.

Hoffmann, M. R., Martin, S. T., Choi, W. Y. & Bahnemann, D. W. (1995) Environmental applications of semiconductor photocatalysis. *Chem Rev*, 95, 69–96.

Irie, H., Sunada, K. & Hashimoto, K. (2004) Recent developments in TiO_2 photocatalysis: novel applications to interior ecology materials and energy saving systems. *Electrochem*, 72, 807–812.

Jia, G., Wang, H. F., Yan, L., Wang, X., Pei, R. J., Yan, T., Zhao, Y. L. & Guo, X. B. (2005) Cytotoxicity of carbon nanomaterials: single-wall nanotube, multi-wall nanotube, and fullerene. *Environ Sci Technol*, 39, 1378–1383.

Jin, X., Li, M., Wang, J., Marambio-Jones, C., Peng, F., Huang, X., Damoiseaux, R. & Hoek, E. M. (2010) High-throughput screening of silver nanoparticle stability and bacterial inactivation in aquatic media: influence of specific ions. *Environ Sci Technol*, 44, 7321–7328.

Judson, R. S., Houck, K. A., Kavlock, R. J., Knudsen, T. B., Martin, M. T., Mortensen, H. M., Reif, D. M., Rotroff, D. M., Shah, I., Richard, A. M. & Dix, D. J. (2010) *In vitro* screening of environmental chemicals for targeted testing prioritization: the ToxCast project. *Environ Health Perspect*, 118, 485–492.

Kang, S., Pinault, M., Pfefferle, L. D. & Elimelech, M. (2007) Single-walled carbon nanotubes exhibit strong antimicrobial activity. *Langmuir*, 23, 8670–8673.

Kang, S., Herzberg, M., Rodrigues, D. F. & Elimelech, M. (2008a) Antibacterial effects of carbon nanotubes: size does matter. *Langmuir*, 24, 6409–6413.

Kang, S., Mauter, M. S. & Elimelech, M. (2008b) Physicochemical determinants of multiwalled carbon nanotube bacterial cytotoxicity. *Environ Sci Technol*, 42, 7528–7534.

Kang, S., Mauter, M. S. & Elimelech, M. (2009) Microbial cytotoxicity of carbon-based nanomaterials: implications for river water and wastewater effluent. *Environ Sci Technol*, 43, 2648–2653.

Karabanovas, V., Zakarevicius, E., Sukackaite, A., Streckyte, G. & Rotomskis, R. (2008) Examination of the stability of hydrophobic (CdSe)ZnS quantum dots in the digestive tract of rats. *Photochem Photobiol Sci*, 7, 725–729.

Karlsson, H. L., Cronholm, P., Gustafsson, J. & Moller, L. (2008) Copper oxide nanoparticles are highly toxic: a comparison between metal oxide nanoparticles and carbon nanotubes. *Chem Res Toxicol*, 21, 1726–1732.

Kirschvink, J. L., Kobayashi-Kirschvink, A. & Woodford, B. J. (1992) Magnetite biomineralization in the human brain. *Proc Nat Acade Sci USA*, 89, 7683–7687.

Kontos, A. I., Kontos, A. G., Tsoukleris, D. S., Vlachos, G. D. & Falaras, P. (2007) Superhydrophilicity and photocatalytic property of nanocrystalline titania sol-gel films. *Thin Solid Films*, 515, 7370–7375.

Kumar, A., Vemula, P. K., Ajayan, P. M. & John, G. (2008) Silver-nanoparticle-embedded antimicrobial paints based on vegetable oil. *Nature Mater*, 7, 236–241.

Lam, C. W., James, J. T., McCluskey, R., Arepalli, S. & Hunter, R. L. (2006) A review of carbon nanotube toxicity and assessment of potential occupational and environmental health risks. *Crit Rev Toxicol*, 36, 189–217.

Lee, J., Mahendra, S. & Alvarez, P. J. J. (2009) Potential environmental impacts of nanomaterials used in the construction industry. In Bittnar, Z., Zeman, J., Nemecek, J., Smilauer, V. & Bartos, P. J. M. (eds) *Nanotechnology in Construction – 3*. Springer Verlag, Berlin.

Leobandung, E., Guo, L. J. & Chou, S. Y. (1995) Single hole quantum-dot transistors in silicon. *Appl Phys Lett*, 67, 2338–2340.

Lin, W. S., Huang, Y. W., Zhou, X. D. & Ma, Y. F. (2006) Toxicity of cerium oxide nanoparticles in human lung cancer cells. *Int J Toxicol*, 25, 451–457.

Liu, R., Rallo, R., George, S., Ji, Z., Nair, S., Nel, A. E. & Cohen, Y. (2012) Classification NanoSAR development for cytotoxicity of metal oxide nanoparticles. *Small*, 7, 1118–1126.

Luo, T. Y., Liang, T. X. & Li, C. S. (2004) Addition of carbon nanotubes during the preparation of zirconia nanoparticles: influence on structure and phase composition. *Powder Technology*, 139, 118–122.

Lyon, D. Y. & Alvarez, P. J. (2007) How a fullerene water suspension kills bacteria: exploring three possible mechanisms. *Chem Res Toxicol*, 20, 1991.

Lyon, D. Y., Fortner, J. D., Sayes, C. M., Colvin, V. L. & Hughes, J. B. (2005) Bacterial cell association and antimicrobial activity of a C_{60} water suspension. *Environ Toxicol Chem*, 24, 2757–2762.

Lyon, D. Y., Adams, L. K., Falkner, J. C. & Alvarez, P. J. J. (2006) Antibacterial activity of fullerene water suspensions: effects of preparation method and particle size. *Environ Sci Technol*, 40, 4360–4366.

Lyon, D. Y., Brunet, L., Hinkal, G. W., Wiesner, M. R. & Alvarez, P. J. J. (2008) Antibacterial activity of fullerene water suspensions (nC(60)) is not due to ROS-mediated damage. *Nano Letters*, 8, 1539–1543.

Mann, S. (2006) Nanotechnology and Construction. *Nanoforum Report*, May 30.

Meng, H., Xia, T., George, S. & Nel, A. E. (2009) A predictive toxicological paradigm for the safety assessment of nanomaterials. *ACS Nano*, 3, 1620–1627.

Murphy, J., Carr, B. & Atkinson, T. (1994) Nanotechnology in medicine and the biosciences. The UK National Symposium on Nanotechnology in Medicine and the Biosciences, London, UK, 16–18 March l994. *Trends Biotechnol*, 12, 289–290.

Nakayama, G. R., Caton, M. C., Nova, M. P. & Parandoosh, Z. (1997) Assessment of the alamar blue assay for cellular growth and viability *in vitro*. *J Immunol Methods*, 204, 205–208.

Nel, A., Xia, T., Madler, L. & Li, N. (2006) Toxic potential of materials at the nanolevel. *Science*, 311, 622–627.

Nel, A. E., Madler, L., Velegol, D., Xia, T., Hoek, E. M. V., Somasundaran, P., Klaessig, F., Castranova, V. & Thompson, M. (2009) Understanding biophysicochemical interactions at the nano-bio interface. *Nat Mater*, 8, 543–557.

Nozik, A. J. (2002) Quantum dot solar cells. *Physica E – Low-Dimensional Systems & Nanostructures*, 14, 115–120.

O'Brien, M. A., Daily, W. J., Hesselberth, P. E., Moravec, R. A., Scurria, M. A., Klaubert, D. H., Bulleit, R. F. & Wood, K. V. (2005) Homogeneous, bioluminescent protease assays: caspase-3 as a model. *J Biomol Screen*, 10, 137–148.

O'Brien, P. J., Irwin, W., Diaz, D., Howard-Cofield, E., Krejsa, C. M., Slaughter, M. R., Gao, B., Kaludercic, N., Angeline, A., Bernardi, P., Brain, P. & Hougham, C. (2006) High concordance of drug-induced human hepatotoxicity with *in vitro* cytotoxicity measured in a novel cell-based model using high content screening. *Arch Toxicol*, 80, 580–604.

Oberdörster, E. (2004) Manufactured nanomaterials (fullerenes, C_{60}) induce oxidative stress in the brain of juvenile largemouth bass. *Environ Health Perspectives*, 112, 1058–1062.

Oberdorster, G., Gelein, R. M., Ferin, J. & Weiss, B. (1995) Association of particulate air-pollution and acute mortality – involvement of ultrafine particles. *Inhal Toxicol*, 7, 111–124.

Oberdorster, G., Oberdorster, E. & Oberdorster, J. (2005) Nanotoxicology: an emerging discipline evolving from studies of ultrafine particles. *Environ Health Perspectives*, 113, 823–839.

Park, K., Park, E. J., Kim, H., Kim, Y., Yi, J. & Choi, K. (2010) Carbon fullerenes (C60s) can induce inflammatory responses in the lung of mice. *Toxicol Appl Pharmacol*, 244, 226–233.

Park, M. V. D. Z., Neigh, A. M., Vermeulen, J. P., De La Fonteyne, L. J. J., Verharen, H. W., Briede, J. J., Van Loveren, H. & De Jong, W. H. (2011) The effect of particle size on the cytotoxicity, inflammation, developmental toxicity and genotoxicity of silver nanoparticles. *Biomaterials*, 32, 9810–9817.

Park, S., Lee, Y. K., Jung, M., Kim, K. H., Chung, N., Ahn, E. K., Lim, Y. & Lee, K. H. (2007) Cellular toxicity of various inhalable metal nanoparticles on human alveolar epithelial cells. *Inhal Toxicol*, 19, 59–65.

Parveen, S., Misra, R. & Sahoo, S. K. (2012) Nanoparticles: a boon to drug delivery, therapeutics, diagnostics and imaging. *Nanomed – Nanotechnol Biol Med*, 8, 147–166.

Paz, Y., Luo, Z., Rabenberg, L. & Heller, A. (1995) Photooxidative self-cleaning transparent titanium-dioxide films on glass. *J Mater Res*, 10, 2842–2848.

Pereira, D. A. & Williams, J. A. (2007) Origin and evolution of high throughput screening. *Br J Pharmacol*, 152, 53–61.

Podsiadlo, P., Kaushik, A. K., Arruda, E. M., Waas, A. M., Shim, B. S., Xu, J. D., Nandivada, H., Pumplin, B. G., Lahann, J., Ramamoorthy, A. & Kotov, N. A. (2007) Ultrastrong and stiff layered polymer nanocomposites. *Science*, 318, 80–83.

Raki, L., Beaudoin, J., Alizadeh, R., Makar, J. & Sato, T. (2010) Cement and concrete nanoscience and nanotechnology. *Materials*, 3, 918–942.

Rana, A. K., Rana, S. B., Kumari, A. & Kiran, V. (2009) Significance of nanotechnology in construction engineering. *Int J Recent Trends in Engineering*, 1, 46–48.

Reeves, J. F., Davies, S. J., Dodd, N. J. F. & Jha, A. N. (2008) Hydroxyl radicals (•OH) are associated with titanium dioxide (TiO_2) nanoparticle-induced cytotoxicity and oxidative DNA damage in fish cells. *Mutat Res*, 640, 113–122.

Ruparelia, J. P., Chatteriee, A. K., Duttagupta, S. P. & Mukherji, S. (2008) Strain specificity in antimicrobial activity of silver and copper nanoparticles. *Acta Biomaterialia*, 4, 707–716.

Sayes, C. M., Gobin, A. M., Ausman, K. D., Mendez, J., West, J. L. & Colvin, V. L. (2005) Nano-C-60 cytotoxicity is due to lipid peroxidation. *Biomaterials*, 26, 7587–7595.

Sayes, C. M., Wahi, R., Kurian, P. A., Liu, Y. P., West, J. L., Ausman, K. D., Warheit, D. B. & Colvin, V. L. (2006) Correlating nanoscale titania structure with toxicity: a cytotoxicity and inflammatory response study with human dermal fibroblasts and human lung epithelial cells. *Toxicol Sci*, 92, 174–185.

Service, R. (2008) Nanotechnology – can high-speed tests sort out which nanomaterials are safe? *Science*, 321, 1036–1037.

Shaw, S. Y., Westly, E. C., Pittet, M. J., Subramanian, A., Schreiber, S. L. & Weissleder, R. (2008) Perturbational profiling of nanomaterial biologic activity. *Proc Nat Acad Sci USA*, 105, 7387–7392.

Shiohara, A., Hoshino, A., Hanaki, K., Suzuki, K. & Yamamoto, K. (2004) On the cyto-toxicity caused by quantum dots. *Microbiol Immunol*, 48, 669–675.

Sobolev, K. & Gutierrez, M. F. (2005) How nanotechnology can change the concrete world. *Am Ceram Soc Bull*, 84, 16–20.

Sosnik, A., Carcaboso, A. M., Glisoni, R. J., Moretton, M. A. & Chiappetta, D. A. (2010) New old challenges in tuberculosis: potentially effective nanotechnologies in drug delivery. *Adv Drug Deliv Rev*, 62, 547–559.

Soto, K. F., Garza, K. M., Shi, Y. & Murr, L. E. (2008) Direct contact cytotoxicity assays for filter-collected, carbonaceous (soot) nanoparticulate material and observations of lung cell response. *Atmos Environ*, 42, 1970–1982.

Taneike, M., Abe, F. & Sawada, K. (2003) Creep-strengthening of steel at high temperatures using nano-sized carbonitride dispersions. *Nature*, 424, 294–296.

Tans, S. J., Verschueren, A. R. M. & Dekker, C. (1998) Room-temperature transistor based on a single carbon nanotube. *Nature*, 393, 49–52.

Tsao, N., Luh, T., Chou, C., Chang, T., Wu, J., Liu, C. & Lei, H. (2002) *In vitro* action of carboxyfullerene. *J Antimicrob Chemotherapy*, 49, 641–649.

Van Gompel, J., Woestenborghs, F., Beerens, D., Mackie, C., Cahill, P. A., Knight, A. W., Billinton, N., Tweats, D. J. & Walmsley, R. M. (2005) An assessment of the utility of the yeast GreenScreen assay in pharmaceutical screening. *Mutagenesis*, 20, 449–454.

Vecitis, C. D., Zodrow, K. R., Kang, S. & Elimelech, M. (2010) Electronic-structure-dependent bacterial cytotoxicity of single-walled carbon nanotubes. *ACS Nano*, 4, 5471–5479.

Verschaeve, L., Van Gompel, J., Thilemans, L., Regniers, L., Vanparys, P. & Van Der Lelie, D. (1999) VITOTOX bacterial genotoxicity and toxicity test for the rapid screening of chemicals. *Environ Mol Mutagen*, 33, 240–248.

Wei, W., Sethuraman, A., Jin, C., Monteiro-Riviere, N. A. & Narayan, R. J. (2007) Biological properties of carbon nanotubes. *J Nanosci Nanotechnol*, 7, 1284–1297.

Xia, T., Kovochich, M., Brant, J., Hotze, M., Sempf, J., Oberley, T., Sioutas, C., Yeh, J. I., Wiesner, M. R. & Nel, A. E. (2006) Comparison of the abilities of ambient and manufactured nanoparticles to induce cellular toxicity according to an oxidative stress paradigm. *Nano Letters*, 6, 1794–1807.

Xia, T., Kovochich, M., Liong, M., Madler, L., Gilbert, B., Shi, H., Yeh, J. I., Zink, J. I. & Nel, A. E. (2008) Comparison of the mechanism of toxicity of zinc oxide and cerium oxide nanoparticles based on dissolution and oxidative stress properties. *ACS Nano*, 2, 2121–2134.

Xia, T., Li, N. & Nel, A. E. (2009) Potential health impact of nanoparticles. *Annu Rev Public Health*, 30, 137–150.

Zhang, H., Ji, Z., Xia, T., Meng, H., Low-Kam, C., Liu, R., Pokhrel, S., Lin, S., Wang, X., Liao, Y. P., Wang, M., Li, L., Rallo, R., Damoiseaux, R., Telesca, D., Madler, L., Cohen, Y., Zink, J. I. & Nel, A. E. (2012) Use of metal oxide nanoparticle band gap to develop a predictive paradigm for oxidative stress and acute pulmonary inflammation. *ACS Nano*, 6, 4349–4368.

Zhang, Q. W., Kusaka, Y., Sato, K., Nakakuki, K., Kohyama, N. & Donaldson, K. (1998) Differences in the extent of inflammation caused by intratracheal exposure to three ultrafine metals: role of free radicals. *J Toxicol Environ Health – Part a – Current Issues*, 53, 423–438.

Zhang, W., Suhr, J. & Koratkar, N. (2006) Carbon nanotube/polycarbonate composites as multifunctional strain sensors. *J Nanosci Nanotechnol*, 6, 960–964.

Zhu, W., Bartos, P. J. M. & Porro, A. (2004) Application of nanotechnology in construction – summary of a state-of-the-art report. *Mater Struct*, 37, 649–658.

Zhu, X. S., Zhu, L., Duan, Z. H., Qi, R. Q., Li, Y. & Lang, Y. P. (2008) Comparative toxicity of several metal oxide nanoparticle aqueous suspensions to Zebrafish (*Danio rerio*) early developmental stage. *J Environ Sci Health Part A*, 43, 278–284.

Zolnik, B. S., Gonzalez-Fernandez, A., Sadrieh, N. & Dobrovolskaia, M. A. (2009) Nanoparticles and the immune system. *Endocrinology*, 151, 458–465.

8

Thin films and nanostructured coatings for eco-efficient buildings

C. G. GRANQVIST, Uppsala University, Sweden

DOI: 10.1533/9780857098832.2.161

Abstract: Thin films and nanostructured coatings are becoming of increasing importance for eco-efficient construction. This chapter discusses the underlying reasons why this is so and then introduces the major technologies. They are subdivided into those requiring vacuum or plasmas – with focus on evaporation and sputtering – and a range of other techniques. Nanoparticle-based coatings are discussed separately, with an emphasis on advanced gas deposition, deposition of carbon-based structures, and microbial fabrication. Large-scale deposition is treated in particular detail, and some views are given on future developments.

Key words: thin film, surface coating, nanostructure, deposition technique, evaporation, sputtering, large-scale manufacturing, resource availability.

8.1 Introduction

Thin films and nanostructured coatings are essential for a number of eco-efficient technologies. We first discuss why this is the case and start by contemplating the world's population, which has grown from some one billion in the year 1800 to about 2.5 billion in 1950 and is currently (2012) around seven billion. The growth is not expected to stabilize until around the year 2100, and then the population has reached a stunning ten billion or more. In parallel to this population explosion, there has been an increase in general standards of living, and people in the poorer countries expect – as they rightly should – to have the same amenities and qualities of life that people in the more affluent countries are accustomed to. This means that the demands on the world's resources are growing very rapidly and that we at present make an unsustainable use of resources of every kind: water, fuels, minerals, etc.

The dangers to humanity are not only direct and related to the exhaustion of essential resources but also indirect, such as the burning of fossil fuels (coal oil and gas) and firewood leading to carbon dioxide emission and thereby to global warming, rising sea levels, harsher weather, increased risks for the spreading of diseases, mass migrations, shifts of species' distributions, etc. (IPCC, 2007, 2011; Chen *et al.*, 2011; de Sherbinin *et al.*, 2011a,b). The

sea-level rise, to take one particularly well recorded property, is 3.3 ± 0.4 mm per year, almost half of which is due to melting glaciers and ice caps (Nerem *et al.*, 2010; Jacob *et al.*, 2012). Furthermore, the geographically uneven distribution of most of the natural resources has huge macroeconomic effects and is also prone to yield political unrest and human disasters. The only sustainable way forward is through changes in life-style and the adoption of more eco-efficient technologies – also known as 'green' technologies or 'cleantec' – which are affordable and operate in harmony with nature's energy flows rather than in opposition to them, as discussed in some depth in a recent book by Smith and Granqvist (2010).

Thin films and nanostructured coatings are at the heart of the eco-efficient technologies because they allow one to do a lot with a little. We consider two cases, and as a first example we imagine a block of aluminium that is small enough that it can easily be carried by hand. By use of a thin film technology, such as vacuum evaporation or sputtering, one can deposit this material so that it produces a reflecting surface over a square kilometer. In full sunlight, this surface reflects of the order of a Gigawatt that otherwise might have been absorbed by the earth. Then, as a second example, imagine that this aluminium surface is covered with an equally thin nanostructured coating with tiny metallic particles embedded in an oxide host. Now the surface is no longer visibly reflecting but is dark and can serve as an excellent 'selective' solar absorber that not only picks up the energy but retains it and avoids strong thermal re-emission.

There are a great many analogous examples of thin films and nanostructured coatings that can be used to obtain not only energy efficiency, as in the two examples above, but also human comfort and security. In many cases, these films and coatings must be used in conjunction with other, perhaps bulk, materials to achieve a certain desired function. A full discussion of these options is neither possible nor desirable here, and many more examples are given elsewhere (Smith and Granqvist, 2010). However, we note that thin films and nanostructured coatings are of much interest for many of the eco-efficient technologies discussed in other chapters in this book. Thus photocatalytic oxide films require well-defined nanostructures in order to have maximum efficiency (Fujishima *et al.*, 2008; Henderson, 2011), windows with high thermal insulation must incorporate a transparent thin film with low thermal emittance to avoid radiative heat transfer, and photovoltaic cells – irrespectively of their being of first, second or third generation – normally contain thin films serving as current collectors. In particular, switchable glazing technology relying on thin films and nanostructured coatings is discussed elsewhere in this book.

The films that are of concern in this chapter have thicknesses that typically lie between 10 nm and 10 μm; they may be metallic, semiconducting or dielectric and deposited onto rigid substrates of metal, plastic or glass

and onto flexible foils of metal or plastic. There are many ways to make such thin films, and thin film science and technology are huge fields of very large importance not only for eco-efficient applications but for almost all modern technologies. It should not come as a surprise that there are numerous books and tutorial presentations on the subject. Some standard texts are by Maissel and Glang (1970), Vossen and Kern (1978, 1991), Bunshah *et al.* (1982), Smith (1995), Pulker (1999), Gläser (2000), Mahan (2000), Ohring (2002) and Mattox (2003, 2010). A general, popular survey of materials for many different eco-efficient constructions appeared recently (Ginley and Cahen, 2012).

This chapter gives a brief survey over the most important technologies for making thin films and nanostructured coatings and includes a number of specific examples. We consider films made by vacuum-based and non-vacuum-based techniques as well as nanoparticle-based coatings. For the vacuum-based techniques we look specifically at the possibilities to construct nanostructures by judicially chosen incidence of the deposition species and by moving the substrate. We then discuss large-scale deposition and round off the presentation by some concluding remarks. Nano-aspects – and there are many (Messier, 2008) – remain in focus throughout the exposition. This chapter can be viewed as an adaptation and significant extension of earlier presentations (see Appendix 1 in the book by Smith and Granqvist (2010) as well as a 'primer' by Granqvist (2012)).

8.2 Major thin film technologies and some illustrative examples

Table 8.1 gives an overview of the most important thin film technologies. They are classified according to the depositing species being atomistic (or molecular), particulate or in bulk form, or whether the surface of a material is modified in order to produce a layer with properties that are distinctly different from those of the underlying material. Atomistic deposition is most commonly used for eco-efficient constructions.

8.2.1 Vacuum- and plasma-based techniques: basics of evaporation and sputtering

Evaporation is a very well-known technique for making thin films. It is in constant use in research laboratories all over the world and has been so for 60 years or more. It is widespread also industrially today. This technique entails that the raw material of the film is heated in vacuum so that a vapour comprising atoms or molecules transfers material to the substrate at a sufficient rate (Holland, 1956; Glang, 1970). The energy of the impinging species is typically a fraction of an electron volt. The heating can be

Table 8.1 Survey of thin film deposition technologies

Atomistic deposition	Particulate deposition	Bulk coating	Surface modification
Vacuum environment • Evaporation • Molecular beam epitaxy • Ion beam deposition *Plasma environment* • Sputter deposition • Ion plating • Plasma polymerization • Glow discharge deposition *Electrolytic environment* • Electroplating • Electroless deposition *Chemical vapour environment* • Chemical vapour deposition • Spray pyrolysis *Liquid phase epitaxy*	*Thermal spraying* • Plasma spraying • Flame spraying • Detonation gun *Fusion coating* • Enameling • Electrophoresis	*Wetting processes* • Printing • Dip coating • Spin coating *Printing* *Cladding* • Explosive • Roll-binding *Weld coating*	*Chemical conversion* • Anodic oxidation • Nitridation *Leaching* *Thermal surface treatment* *Ion implantation* *Laser glazing*

produced by drawing current through a resistive coil or boat, often of tungsten, in contact with the substance to be evaporated or by thermionic emission from a wire and focusing of the electron beam onto the substance to be evaporated from a water-cooled 'electron gun'. The latter technique is referred to as electron-beam, or e-beam, evaporation.

Sputter deposition is very generally employed to make uniform coatings on glass, polymers, metals, etc. In essence, a plasma is set up in a low pressure of inert and/or reactive gases, and energetic ions in the plasma dislodge material from a solid plate or cylinder of the raw material of the film (known as the 'target') and deposit these atoms as a uniform film on an adjacent surface (called the 'substrate'). The technology is discussed in detail in books by Chapman (1980), Cuomo *et al.* (1989), Konuma (1992), Wasa and Hayakawa (1992) and Depla and Mahieu (2008). The sputter plasma can be inert, typically consisting of argon ions, in which case the target and the thin film have the same composition. Alternatively the plasma can be reactive and contain for example oxygen so that an oxide film can be formed by sputtering from a metallic target; an additional admixture of water vapour can yield an entire cocktail of metastable and highly reactive species in the plasma (Liu *et al.*, 2011). Analogously, nitrides can be made by sputtering in the presence of nitrogen, etc. The great versatility of the reactive sputtering technique should be obvious.

The plasma is normally confined to the target area by magnets placed behind the target, and one then refers to the deposition technique as 'magnetron sputtering'. Rotating targets can be used for maximum utilization of the deposition material. The deposition species typically have energies of some electron volts, i.e., the energies are higher than in the case of evaporation and are large enough to remove contaminants from the substrate. This self-cleaning feature is conducive to a good adherence between substrate and film, which is an advantage for sputtering when compared with evaporation as a thin film technology.

Evaporation and sputtering are often referred to jointly as 'physical vapour deposition' or PVD. What do thin films made by these techniques look like at the nano level? We consider the growth of metal films on dielectric substrates, such as glass or polymer. Figure 8.1 illustrates a series of scanning electron micrographs taken on gold films with the shown thicknesses and deposited by sputtering onto glass at room temperature (Lansåker *et al.*, 2009). The initial deposition is seen to yield tiny metallic nuclei at certain sites on the substrate, and continued deposition makes these nuclei grow, which is expected to occur via diffusion of atoms or molecules over the substrate surface as well as by direct impingement of atoms or molecules. The discrete metal 'islands' that are then formed have shapes that somewhat resemble ellipsoids. Continued deposition makes some of the 'islands' touch and rearrange into larger and more irregular objects; this is conventionally referred to as 'coalescence growth'. The growing film then passes through what can be called 'large-scale coalescence', meaning that a contiguous and meandering metallic network of macroscopic extent is formed. Only then can metallic conduction be detected along the film. The evolution of electromagnetic properties in a growing metal film is a topic of continued interest and is highly dependent on the prevailing nanostructures (Earp and Smith, 2011).

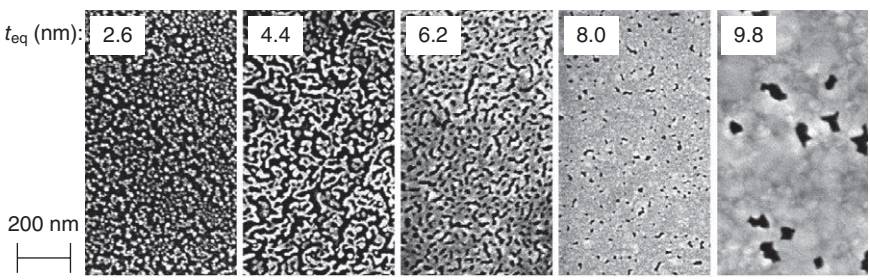

8.1 Scanning electron micrographs of gold films made by sputtering onto glass to the shown equivalent thickness t_{eq} (i.e., the thickness a corresponding metallic slab would have). The gold appears bright and the uncoated parts of the substrate look dark. From Lansåker *et al.* (2009).

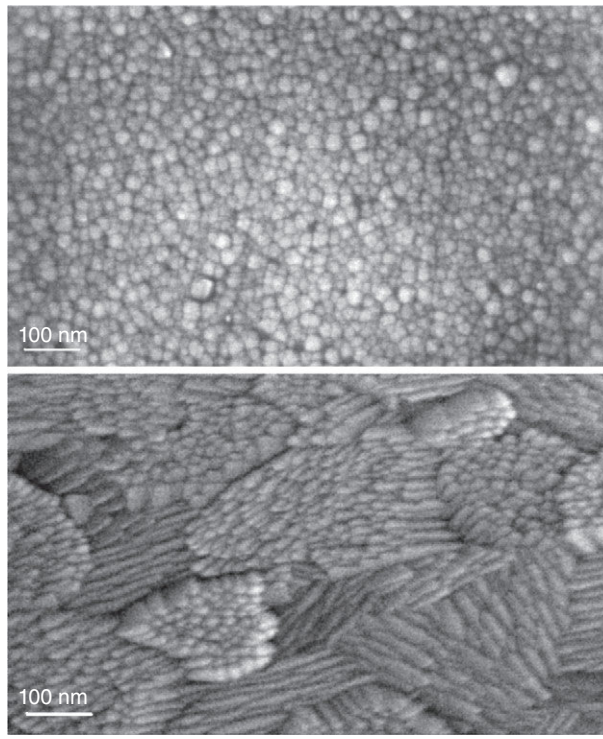

8.2 Scanning electron micrographs of an In_2O_3:Sn film sputter deposited at ambient temperature and annealing post-treated at 200°C (top) and for an analogous film sputter deposited onto a substrate maintained at 200°C (bottom). From Betz *et al.* (2006).

The development of the structure depends critically on deposition and post-treatment parameters, to an extent that might seem surprising. Thus, for example, depositing a gold film at room temperature and then heating it to a certain temperature is not equivalent to direct deposition onto a substrate at the same elevated temperature, as shown in a sequel to the work from which Fig. 8.1 was reproduced (Lansåker *et al.*, 2012). Another example of this sensitivity to the film preparation conditions is shown in Fig. 8.2 for the case of sputter deposited films consisting of In_2O_3:Sn (Betz *et al.*, 2006), which is a transparent and electrically conducting material of very large importance in energy technology and for transparent electronics of different kinds. The top panel illustrates a scanning electron micrograph for a film deposited onto a substrate at room temperature and then annealing post-treated at 200°C and the bottom panel pertains to a film that was sputtered onto a substrate at 200°C. Clearly the two films display striking differences.

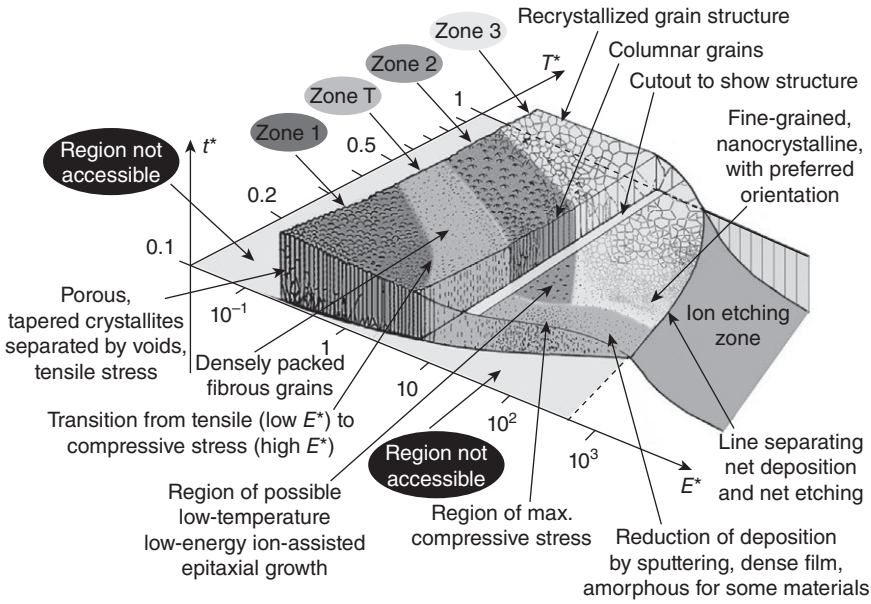

8.3 Schematic diagram showing nanostructures of thin films made by sputter deposition as a function of generalized temperature T^* and energy flux E^*, and with t^* denoting film thickness. Ion etching can take place at high energy flux. From Anders (2010).

A film that is thicker than those in Fig. 8.1 develops a characteristic nanostructure also over its cross section. Figure 8.3 is a recent extension (Anders, 2010) of a well-known structure zone diagram, known as a 'Thornton diagram' (Thornton, 1977), and illustrates what happens. The figure applies to sputtering and shows that the film typically exhibits a columnar structure oriented perpendicular to the substrate, and that this structure depends critically on the deposition parameters, especially on the energy of the sputtered species (in its turn related to the pressure in the sputter plasma, typically comprised of argon) and the substrate temperature. The structure of an evaporated film is found in the limit of a small argon pressure; it was described already in the 1960s (Movchan and Demchishin, 1969) and the modelling was subsequently refined (Barna and Adamik, 1998; Hultman and Sundgren, 2001).

For many thin film applications, there is a requirement for high durability, which means that compact films are wanted, and historically the sputter-based technology was developed to prepare films that were more durable than those made by evaporation. Parameters leading to films belonging to 'zone T' in the 'Thornton diagram' are then preferred. For other applications, however, it is desirable to make films with a carefully chosen

nanoporosity, and then one should make use of low substrate temperatures and high plasma gas pressures in order to reach 'zone 1'. Films of the latter kind are required for a number of eco-efficient technologies such as for energy efficient and comfort enhancing electrochromic 'switchable glazings' in buildings, for gas sensors devised for air quality assessment, and for photocatalytic surfaces capable of cleaning air and water (Granqvist, 1995; Smith and Granqvist, 2010); electrochromics is discussed further in Chapter 11.

Multilayer films are readily made by sequential evaporation or sputtering from more than one source and a practical deposition unit can incorporate a large number of sources which the substrate is transported past in a more or less continuous process which we return to below for the case of sputtering. Composite films can be prepared by deposition from one source of a compound material (as long as decomposition of this material does not take place) or from simultaneous deposition from two or more sources. Mixed metal-dielectric films can be deposited reactively, for example in the presence of a small amount of oxygen, so that the deposit comprises a random mixture of metallic and oxidized parts (known as a 'cermet' film). The underlying processes for reactive sputtering can be modelled very accurately (Berg and Nyberg, 2005).

Chemical post-treatment of thin films can modify the properties and lead to novel properties. Figure 8.4 shows one example where a sputter deposited film of ZnO:Al – a transparent conductor – is roughened by etching in dilute hydrochloric acid (Ruske *et al.*, 2007). The treated film exhibits significant light scattering. Chemical etching of some alloy films can yield highly nanoporous conducting layers (Maaroof *et al.*, 2005; Cortie *et al.*, 2006). An example is shown in Fig. 8.5, which reports on a sputter deposited $AuAl_2$ film after etching so that nothing but the gold remains.

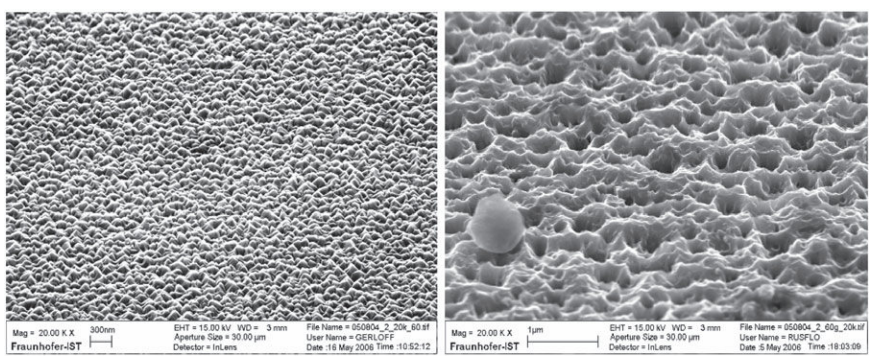

(a) (b)

8.4 Scanning electron micrographs of a sputter deposited ZnO:Al film (a) before and (b) after etching in 0.5% HCl. From Ruske *et al.* (2007).

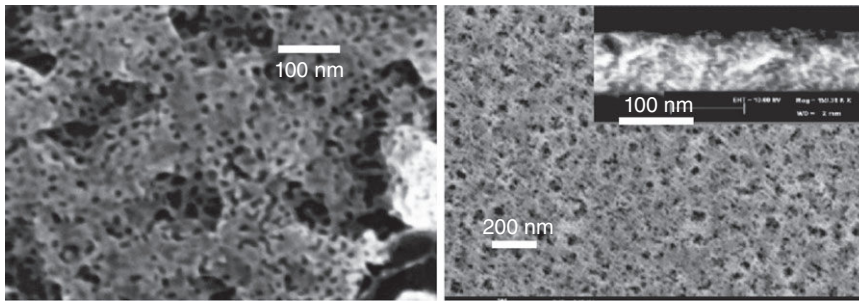

8.5 Nanoporous thin gold layer seen from the top at two magnifications (largest magnification on the left). The inset in the right-hand panel is a cross-section view of the film's nanostructure.

8.2.2 Vacuum- and plasma-based techniques: effects of glancing angle incidence and substrate rotation

For the deposition techniques discussed above, it was tacitly implied that the incidence of the deposition species is more or less perpendicular to the substrate. If this is not the case, it is possible to build up coatings with inclined nanostructures and, if a rotation of the substrate is invoked as well, one can arrive at an entire zoo of nanostructures. The pertinent deposition techniques are sometimes referred to as 'glancing angle deposition' or 'GLAD'.

Figure 8.6 shows the build-up of a film with an inclined columnar structure (Brett, 1989). It is based on calculations from a model wherein 'atoms' are depicted as two-dimensional hard discs which travel with a well-defined direction but otherwise randomly towards a 'substrate'. The 'atoms' stick wherever they hit the substrate or an earlier deposited 'atom'. Columns are then formed for the simple reason that a randomly formed protrusion tends to shade whatever is behind it from further deposition. 'Self-shadowing' is a term that is used to describe this. The character of the columns as well as the density of the nanostructure depends on the energy given to the 'atoms', i.e., to the mobility they attain. Figure 8.6 describes the structures that form when 'atoms' are injected at an off-normal angle of 50° and arriving from the upper right. The column orientation typically does not coincide with the direction of the incident species. Films of this type are sometimes referred to as 'sculptured thin films' and are theoretically well understood (Lakhtakia and Messier, 2004; Wakefield and Sit, 2011). Figure 8.7(a) shows a scanning electron micrograph of a film made by GLAD (Steele and Brett, 2007). The resemblance to the simulated structure is striking. Films of this type are known to exhibit angular-selective optical properties (Mbise *et al.*, 1997). By changing the direction of the incident species, it is possible to create a zig-zag pattern, as seen in Fig. 8.7(b).

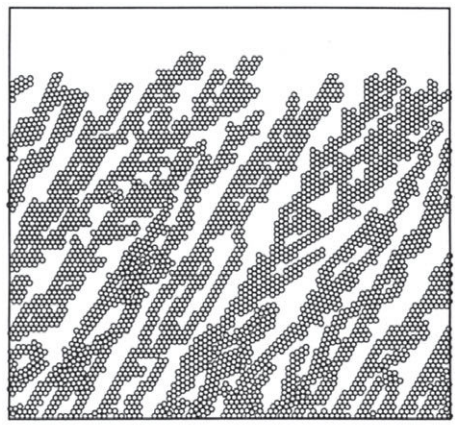

(a)

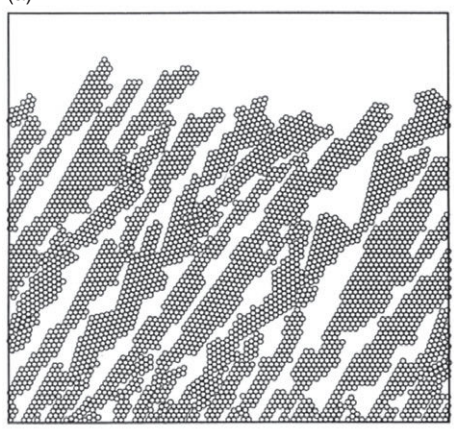

(b)

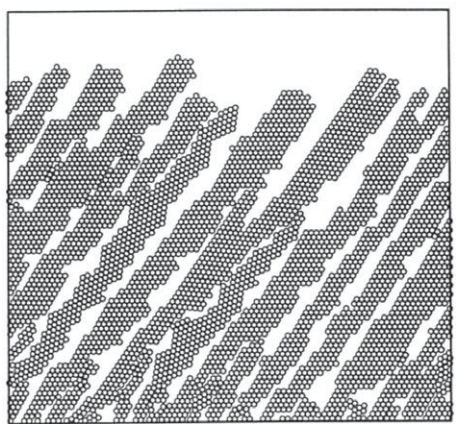

(c)

8.6 Simulated thin films grown with 'atoms' impinging from an off-normal angle and having (a) low, (b) medium and (c) high mobility. From Brett (1989).

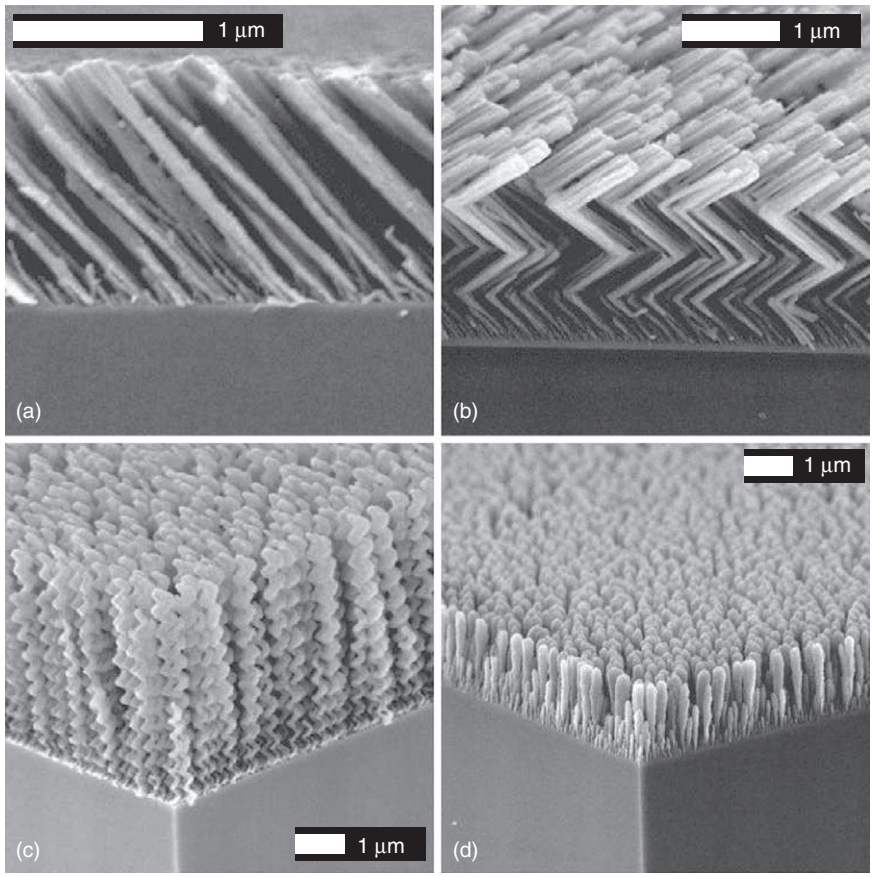

8.7 Nanostructured thin films made by 'glancing angle deposition' and, in parts (b) and (c), simultaneous rotation of the substrate in order to make 'nanochevrons' and a helical nanostructure ('nanotortiglioni'). From Steele and Brett (2007).

Still larger possibilities to produce nanostructured coatings are obtained if the substrate is rotated while the incident deposition species have an oblique angle of incidence. Figure 8.7(b) and (c) shows two striking examples using slow substrate rotation. With more rapid rotation, it is possible to obtain 'penniform' structures, as illustrated in Fig. 8.8 for the case of a titanium dioxide-based structure made by sputter deposition under conditions so that 'zone 1' films are to be expected (Rodríguez *et al.*, 2000).

8.2.3 Non-vacuum- and non-plasma-based techniques

There are many thin film technologies that do not require low pressures. For example, coatings can be prepared by dipping a substrate in a solution

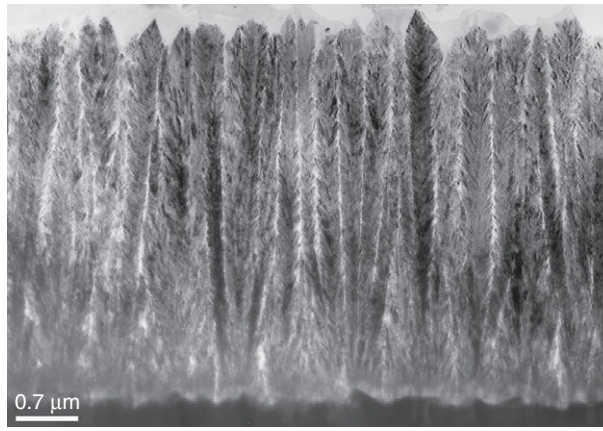

8.8 Cross section through a 'penniform' TiO_2 thin film made by sputter deposition and simultaneous substrate rotation at 50 rpm. From Rodríguez *et al.* (2000).

containing the species to be incorporated in the film, withdrawing at a controlled rate, and heating to remove volatile components in the solution; an alternative technique suitable for coating small objects is to apply the solution in the form of drops, then spin the substrate at a controlled speed in order to make an even layer, and finally heat treat. In either case the deposition can be repeated over and over in order to make a thicker film. As an alternative to dipping and spinning, the chemical solution can be applied by spraying. Film deposition processes of dipping, spinning and spraying are often referred to jointly as 'sol-gel deposition' (Klein, 1994; Frenzer and Maier, 2006). Figure 8.9 illustrates a cross section of a multi-layer coating made by dip coating (Boström *et al.*, 2011). It has two layers of nickel particles in alumina, with different compositions, and a top layer of silica. The coating is backed by metallic aluminium. This coating is an example of a solar-absorbing surface that avoids thermal re-emission and is thus of the kind mentioned as the second example in Section 8.1.

Chemical vapor deposition (CVD) uses heat to decompose a vapour of a 'precursor' substance in order to make a thin film of a desired composition (Morosanu, 1990; Pierson, 1999). This deposition technique can be made more efficient by combining it with plasma treatment in what is denoted 'plasma enhanced CVD' or 'PECVD'. A variety of the CVD technique is referred to as 'spray pyrolysis'; a fluid containing the precursor is then sprayed onto a hot substrate.

Electrochemical techniques embrace cathodic electroplating from a chemical solution (Lowenheim, 1978) and anodic conversion of a metallic surface to form a porous oxide. Anodization is most common in the case of

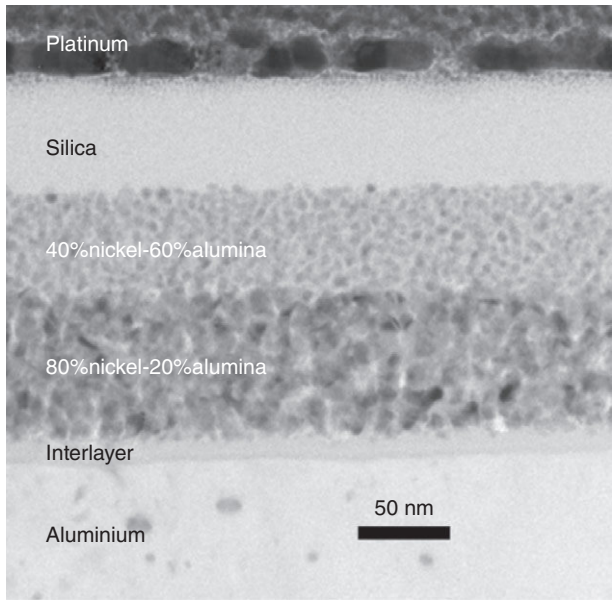

8.9 Scanning electron micrograph of the cross section of a sol-gel-produced multilayer coating of Ni-Al_2O_3 and SiO_2 deposited onto an Al substrate (with an interlayer to boost the adhesion to the substrate). The top layer of platinum was applied by sputter deposition in order to allow the imaging. From Boström *et al.* (2011).

aluminium (Wernick *et al.*, 2001), but other metals – such as titanium (Diamanti and Pedeferri, 2007) and tantalum (El-Sayed and Birss, 2011) – can be used too. Numerous alternative techniques exist as well. The anodization of aluminium can be carried out following several different strategies. Thus 'mild' anodization can lead to a self-ordered pore structure at the nanoscale, but this technique is slow and confined to a limited set of process parameters; 'hard' anodization, on the other hand, is a fast and industrially viable process leading to thick layers with a disordered pore arrangement. The latter technique is applied routinely for aluminium surfaces exposed to air. It was recently realized that a combination of 'mild' and 'hard' anodization in what is known as 'pulse' anodization can yield particularly interesting nano-features, such as those depicted in Fig. 8.10 (Lee *et al.*, 2008), which shows alternate layers with well developed nanostructures.

8.2.4 Nano-particle-based coatings

Vacuum-based coating methods, as discussed extensively above, had an important historical role for making films based on nanoparticles. In fact, vacuum-based techniques provided some of the first insights into approaches

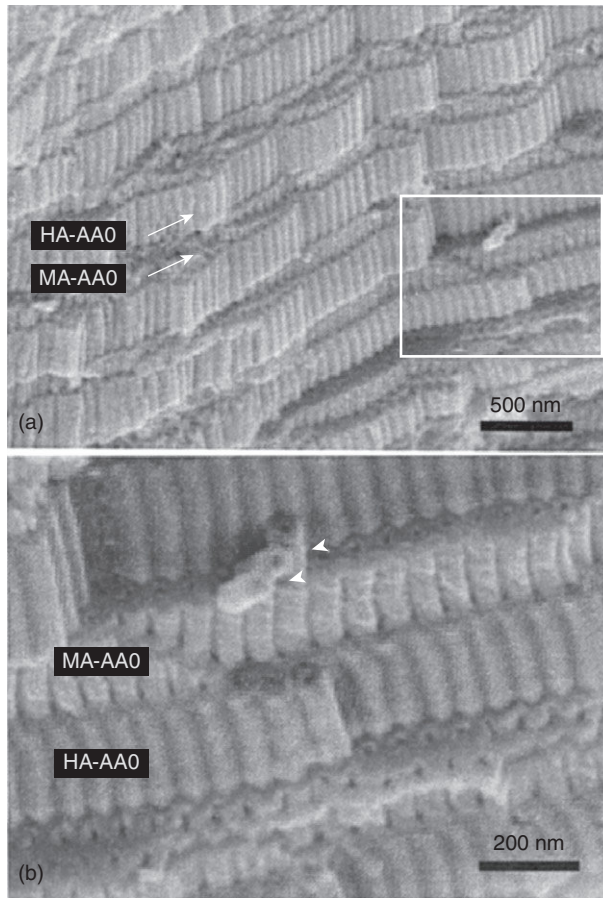

8.10 Panel (a) shows alternate layers of anodic aluminum oxide (AAO) prepared by 'pulse' anodization; the layers are representative of 'hard' anodization (HA) and 'mild' anodization (MA). Panel (b) is a magnification of the displayed rectangular area. From W. Lee *et al.* (2008).

to prepare nanoparticles under controlled conditions, specifically in the manufacture of 'gold blacks' for darkening of thermocouples by gold nanoparticles prepared by evaporation at pressures high enough to yield nanoparticle nucleation and growth of fractal aggregates in the gas phase (Harris *et al.*, 1948; Granqvist and Hunderi, 1977; Sotelo *et al.*, 2002).

A major step forward for the latter technique was taken when it was realized that the mean particle diameter and the size distribution could be understood and accurately modelled provided that the vapour source was equipped with accurate temperature control (Granqvist and Buhrman, 1976). This led to the 'advanced gas deposition' (AGD) technique, which is

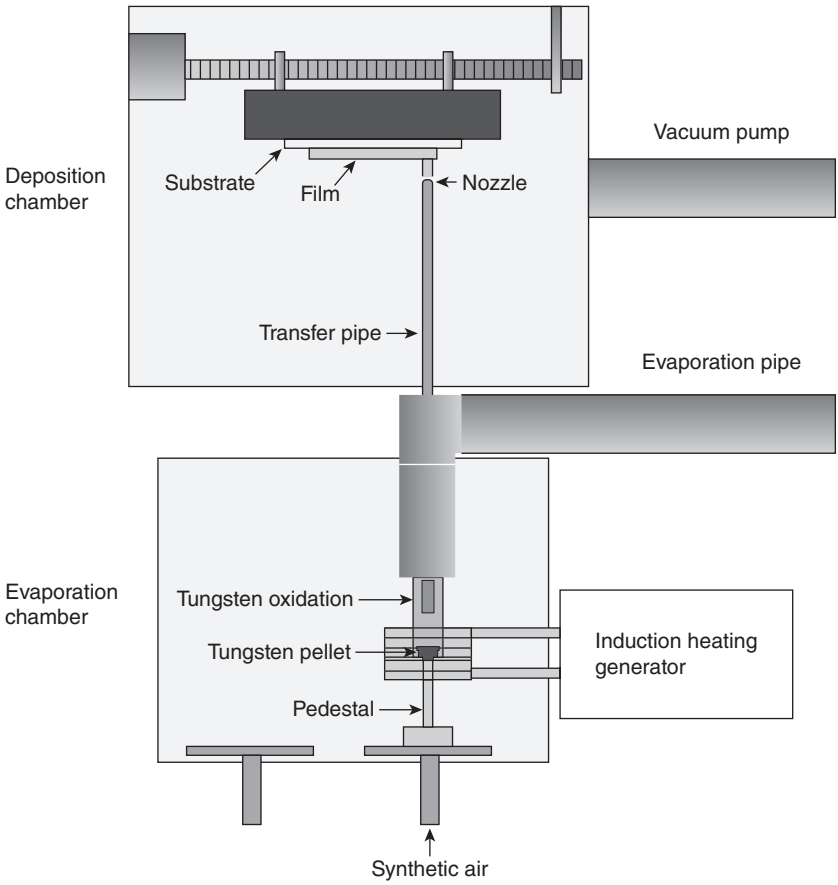

8.11 Schematic image of a unit for advanced gas deposition arranged for making tungsten oxide nanoparticles. From Reyes *et al.* (2004).

now used to mass-produce nanoparticles that can be collected for later use or for coating directly onto substrates. The technique and its implementation are described in detail in a book by Hayashi *et al.* (1997).

Figure 8.11 illustrates an AGD unit; as shown, it is arranged for tungsten oxide nanoparticle production (Reyes *et al.*, 2004) but the technique can be used reactively or non-reactively to make nanoparticles of a large variety of pure metals, oxides, nitrides, etc. Evaporation takes place in the lower chamber into a laminar gas flow surrounding the vapour source. The vaporized species are then cooled via collisions with gas molecules so that they form tiny nuclei that subsequently grow in the gas flow. A thin transfer pipe collects nanoparticles in a region at a controlled distance from the vapour source and transports them in a gas stream that ends in the upper deposition chamber, which is maintained at good vacuum. A separate evacuation

pipe removes nanoparticles outside the growth region. The nanoparticles are then deposited via a nozzle in order to gain momentum onto a substrate that can be moved so that they form a uniform film comprised of nanoparticles. The technique can be implemented with multiple vapour sources and transfer pipes in order to prepare materials consisting of mixed or layered nanoparticles. Figure 8.12 shows some typical nanoparticle deposits for the case of as-deposited tungsten oxide and WO_3:Pd sintered at 600°C (Hoel *et al.*, 2005). The particle size distribution is seen to be narrow. Evidently the sintering has caused significant grain growth.

A distinctive advantage of the AGD technique is that it separates nanoparticle formation and growth from thin film deposition. This feature makes it possible to fine-tune particle interaction within the film, at least to some extent, which is beneficial for devices that require well-controlled electrical contact between adjacent nanoparticles such as conductometric gas sensors for determining and surveying air quality. Gas phase synthesis of nanoparticles also can use high-temperature processes, since particles can form in a flame or plasma. The reader is referred to the book by Granqvist *et al.* (2004) for detailed coverage of this subject.

Chemical approaches are now widely used to grow and precipitate metallic, inorganic and semiconducting nanoparticles from solution and have been refined so as to limit size ranges, create elongated particles as well as spheres, and to overcoat nanoparticles or microparticles with nanoshells in 'core-shell' structures which enable new or improved functionality. These aspects have been discussed in detail in the literature (Cushing *et al.*, 2004). Thick layers incorporating nanoparticles can effectively function as thin ones provided that metal flakes are included and serve as 'artificial substrates' (Kunič *et al.*, 2009). Layers or coatings containing previously prepared nanoparticles are usually made by first dispersing them in a paint

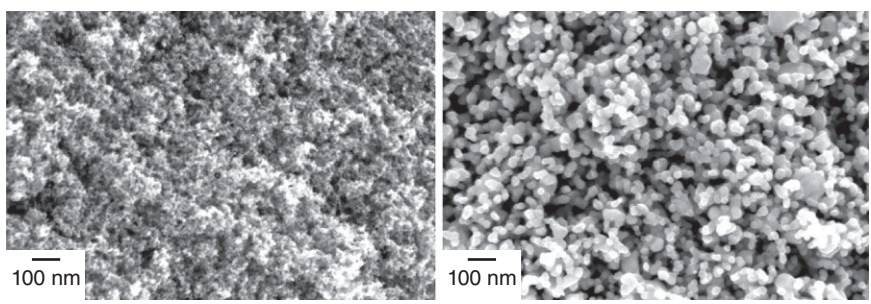

8.12 Scanning electron micrographs of (a) an as-deposited film of WO_3 and (b) a WO_3:Pd film sintered at 600°C. Both films were prepared by advanced gas deposition. Horizontal bars are 100 nm in length. From Hoel *et al.* (2005).

binder, a polymer coating solution, or a monomer solution prior to polymerization. The latter process can be used to produce master batches of concentrated nanoparticles in resin, which can subsequently be mixed with clear resin to prepare thin polymer foils doped with nanoparticles by extrusion. These foils can then be stuck onto surfaces or positioned between clear sheets. Nanoparticle-doped polymer sheets and other shapes of plastic can also be made by injection moulding and extrusion from suitable resins. If dilute coatings are needed, it is important to make sure that the particles are dispersed, which usually requires a surfactant (i.e., a 'soap' type molecule) on their surface to ensure that they do not stick together.

Carbon-based nanomaterials deserve particular attention and have undergone phenomenal development during recent years. Figure 8.13 illustrates how different nanostructures can be created from a two-dimensional arrangement of carbon atoms to yield C_{60} units (known as 'buckminsterfullerene molecules' or 'buckyballs'), long nanotubes with metallic and semiconducting properties, and graphene (two-dimensional graphite-like sheaths) (Geim and Novoselov, 2007).

Long nanoparticles can be prepared not only from carbon, as indicated in Fig. 8.13, but from many materials. Figure 8.14 illustrates an example of Ag nanowires that can be made from potentially inexpensive reduction of liquid silver nitrate to make electrically conducting and transparent

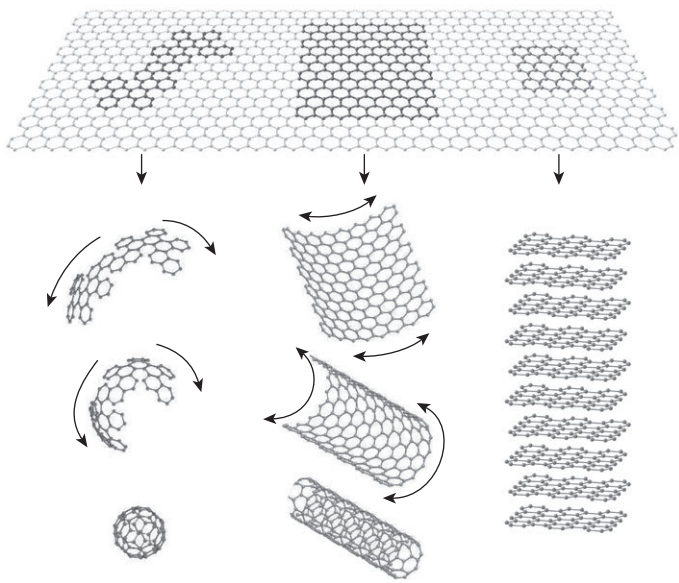

8.13 Schematic rendition of carbon-based nanostructures and of their formation. From Geim and Novoselov (2007).

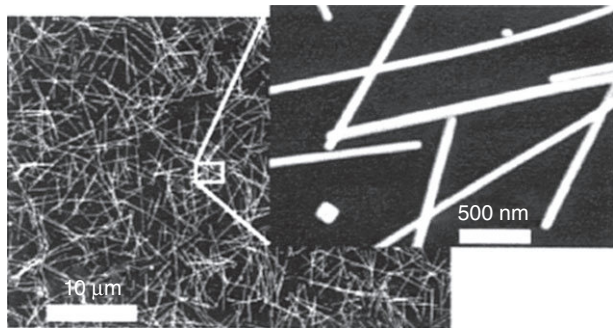

8.14 Scanning electron micrographs of Ag nanowire meshes. A magnification of the rectangle is shown in the upper right-hand panel. From J.-Y. Lee *et al.* (2008).

coatings with some degree of optical scattering ('haze') (J.-Y. Lee *et al.*, 2008; Hu *et al.*, 2010).

The final example of nanoparticle production for coatings is one where work has only recently begun and for which the potential is great though not yet easy to assess: microbiological preparation. Plate II (between pages 162 and 163) illustrates the growth of silver nanoparticles inside bacteria of *Pseudomonas stutzeri* (Klaus *et al.*, 1999; Klaus-Joerger *et al.*, 2001). It is remarkable that particles of this kind can be single-crystalline. They can be used, for example, to make selectively solar absorbing coatings (Joerger *et al.*, 2000). In fact, there seems to be a vast number of organisms that can serve as eco-efficient 'nanofactories' and produce inorganic nanoparticles either intra- or extracellularly, including magnetotactic bacteria, diatoms, fungi and others (Mandal *et al.*, 2006; Olenin and Lisichkin, 2011; Rai and Duran, 2011).

The marriage of biotechnology and materials science to make new eco-efficient constructions – as exemplified above – is a particularly exciting line of development, and recent work has demonstrated how viruses can be harnessed for making nanobatteries (Lee *et al.*, 2009) and nanostructured solar cells (Dang *et al.*, 2011).

8.3 Large-scale manufacturing

The cost of making thin films and nanostructured coatings is often of the greatest importance for judging whether they can be used in eco-efficient technologies or for other practical applications. The cost inherent in thin film manufacturing is a complicated issue and depends critically on the production scale. Thus large-scale manufacturing is essential. One example where this issue has been developed almost to perfection is for the coating

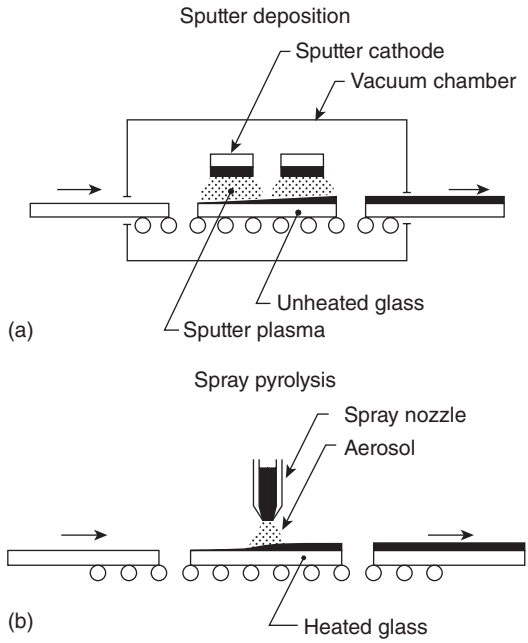

8.15 Principles for sputter deposition (a) and for spray pyrolysis (b) to coat surfaces of glass transported as indicated by the horizontal arrows. From Granqvist (1991).

of sheet glass in order to make thin films that can give low thermal emission and thereby good thermal insulation in a double-glazed window, or thin films that control the throughput of solar energy so that the need for air conditioning is diminished. Figure 8.15 shows two principles of how this is done (Granqvist, 1991): panel (a) illustrates sputtering onto moving sheet glass in a continuous process wherein panes are entering though a load lock at one end of a deposition unit and exiting at the other end, and panel (b) demonstrates another technique based on spray deposition of a metal-containing solution onto hot glass, most conveniently as the sheet glass emerges from the leer during float glass production. More detailed discussions of glass coating are given elsewhere, in particular in books and papers by Gläser (2000, 2008) and by Bach and Krause (2003). The practical deposition systems – particularly for sputter deposition – can be very large and involve a multitude of sputter targets mounted along a production line that is more than 100 m in length; Fig. 8.16 is a photograph of a system of this kind.

'Web coating' of flexible substrates (Schiller *et al.*, 2000; Fahlteich *et al.*, 2012) is a well-developed technology with possibilities for excellent process control. It can be used to make thin films cost-effectively on very large

8.16 Photograph of a manufacturing plant for making multilayer coatings on full-size glass panes.

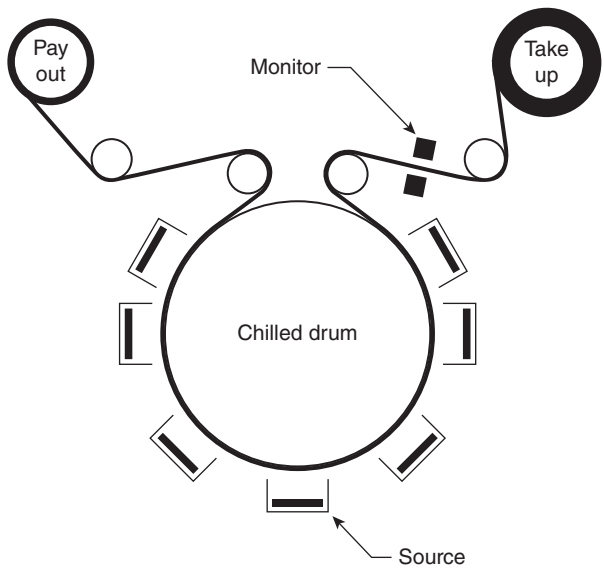

8.17 Schematic diagram of the internal components of a roll-to-roll coater with several sputter cathodes. From Meyer (1989).

surfaces as discussed in detail by Bishop (2010, 2011). Figure 8.17 illustrates one variety in which the web is transferred to a chilled drum, where the deposition takes place by sputtering or any other suitable technique (Meyer, 1989). The coated web is collected on a take-up roll. The whole process can take place inside a vacuum chamber. High-rate deposition may lead to thin

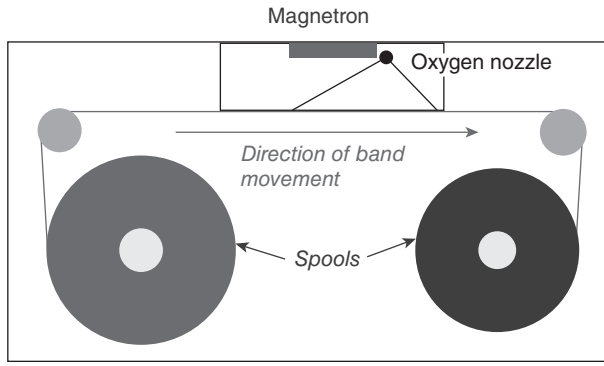

8.18 Schematic diagram of a roll-to-roll coating unit for continuous production of magnetron sputter-deposited films with graded cross-sectional composition. From Zhao (2007).

films with somewhat inclined columnar structures, which are formed by the processes outlined in Section 8.2.2.

It is even possible to use large-scale sputter deposition to make films whose composition varies in a highly controlled manner over the cross section. This latter possibility can be accomplished as illustrated in Fig. 8.18, showing continuous deposition onto a long metallic band. As the band moves past the sputter cathode, the initial deposition is in argon so that the film is metallic. Closer to the asymmetrically positioned oxygen inlet, the films get increasingly oxidized and – with properly adjusted parameters – the top layer can be almost purely comprised of oxide implying that it serves to anti-reflect the underlying material. This innovative technology has been used to make sputter-deposited surfaces for efficient conversion of solar energy into heat, i.e., conforming to the second example mentioned in Section 8.1 (Zhao, 2007). Large-scale deposition of films with inclined columnar structures, employing the GLAD technique discussed in Section 8.2.2, is another possibility (Motohiro *et al.*, 1989).

Cost issues are often misunderstood in scientific papers. Thus it is common to read statements implying that sol-gel deposition is 'cheap' because inherently expensive vacuum equipment is not needed. However, the necessary thermal post-deposition treatments of the sol-gel coatings lead to slow manufacturing, which may be disastrous for mass fabrication.

8.4 Conclusion and future trends

This chapter has given a survey over the manufacturing of thin films and nanostructured coatings for eco-efficient constructions. It has been demonstrated that there are a great many techniques with distinctive features and

specific pros and cons. These techniques allow the manufacturing of thin coatings of virtually any material and material combination either as a single layer or in a multilayer configuration.

It should be noted that the techniques that have been described are best suited for coating non-patterned surfaces. However, masking is possible in order to produce desired patterns and, alternatively, etching or some other subtractive technique can be used to obtain a certain configuration. Rather than obscuring or subtracting material, it is also possible to use an additive process such as printing with an appropriate ink containing nanoparticles, normally followed by heat treatment for some time to remove undesired binder residues. Recent advances in printing technology, as well as the great amount of contemporary work on large-scale fabrication of nanoparticles, nanorods and 'nano-anything' – referred to briefly in Section 8.2.4 – make it probable that printing-related techniques will gain increased popularity in the future.

As emphasized in Section 8.1, thin films use little material to reach large effects, and hence – generally speaking – the materials that can be employed in thin films are many more than those that can be used in the case of bulk-like materials. Nevertheless, clearly the least common elements should be avoided (Tao *et al.*, 2011). Plate III (between pages 162 and 163) gives an overview of the elemental abundance and shows that elements such as ruthenium, rhodium, tellurium, rhenium, osmium and iridium occur with a mass fraction around 10^{-9} or below (Berry, 2010). The data in the figure should be regarded with some caution, though, and the fact that an element is not rare does not make it cheap. One example may be indium oxide (Schwarz-Schampera and Herzig, 2002), which is often the premier choice for a transparent electrical conductor and is used in many modern information and communication technologies as well as for energy-related applications. This element is normally obtained as a small byproduct in zinc refining, which makes it much more costly than transparent conductors based on zinc oxide or tin oxide.

The technologies for making thin films and nanostructured coatings have been undergoing rapid development at least since the 1950s. This development still continues today, and does so at a stunning pace, and it is a safe bet that thin films and coating technologies will be of ever increasing importance as the burden on nature's resources becomes even more acute in the future.

8.5 References

Anders A (2010), 'A structure zone diagram including plasma-based deposition and ion etching', *Thin Solid Films*, 518, 4087–4090.

Bach H and Krause D (eds) (2003), *Thin Films on Glass*, Springer, Berlin.

Barna P B and Adamik M (1998), 'Fundamental structure forming phenomena of polycrystalline films and the structure zone models, *Thin Solid Films*, 317, 27–33.
Berg S and Nyberg T (2005), 'Fundamental understanding and modeling of reactive sputtering processes', *Thin Solid Films*, 476, 215–230.
Berry J J (2010), Private communication.
Betz U, Kharrazi Olsson M, Marthy J, Escolà M F and Atamny F (2006), 'Thin films engineering of indium tin oxide: large area flat panel displays application', *Surf Coating Technol*, 200, 5751–5759.
Bishop C A (2010), *Roll-to-Roll Deposition of Barrier Coatings*, Wiley, Hoboken, NJ.
Bishop C A (2011), *Vacuum Deposition onto Webs, Films, and Foils*, 2nd edn, William Andrew, Waltham, MA.
Boström T, Valizadeh S, Lu J, Jensen J, Westin G and Wäckelgård E (2011), 'Stucture and morphology of nickel-alumina/silica solar thermal selective absorbers', *J Non-Cryst Solids*, 357, 1370–1375.
Brett M J (1989), 'Simulation of structural transitions in thin films', *J Mater Sci*, 24, 623–626.
Bunshah R F, Blocher Jr J M, Bonifield T D, Fish J G, Ghate P B, Jacobson B E, Mattox D M, McGuire G E, Schwartz M, Thornton J A and Tucker Jr R C (1982), *Deposition Technologies for Films and Coatings*, Noyes, Park Ridge, NJ.
Chapman B (1980), *Glow Discharge Processes*, Wiley, New York, NY.
Chen I-C, Hill J K, Ohlemüller R, Roy D B and Thomas C D (2011), 'Rapid range shifts of species asociated with high levels of climate warming', *Science*, 333, 1024–1026.
Cortie M B, Maaroof A, Smith G B and Ngoepe P (2006), 'Nanoscale coatings of $AuAl_x$ and $PtAl_x$ and their mesoporous elemental derivatives', *Current Appl Phys*, 6, 440–443.
Cuomo J J, Rossnagel S M and Kaufman H R (eds) (1989), *Handbook of Ion Beam Process Technology*, Noyes, Park Ridge, NJ.
Cushing C, Kolesnichenko V L and O'Connor C J (2004), 'Recent advances in liquid-phase synthesis of inorganic nanoparticles', *Chem Rev*, 104, 3893–3946.
Dang X, Yi H, Ham M-H, Qi J, Yun D S, Ladewski R, Strano M S, Hammond P T and Belcher A M (2011), 'Virus-templated self-assembled single-walled carbon nanotubes for highly efficient electron collection in photovoltaic devices', *Nature Nanotechnol*, 6, 377–384.
Depla D and Mahieu S (eds) (2008), *Reactive Sputter Deposition*, Springer Series in Materials Science, Vol. 109, Springer, Berlin.
de Sherbinin A, Warner K and Ehrhart C (2011a), 'Casualties of climate change: shifts in rainfall patterns and shorelines will contribute to mass migrations on a scale never seen before', *Sci Am* (January), 64–70.
de Sherbinin A, Castro M, Gemenne F, Cernea M M, Adamo S, Fearnside P M, Krieger G, Lahmani S, Oliver-Smith A, Pankhurst A, Scudder T, Singer B, Tan Y, Wannier G, Boncour P, Erhart C, Hugo G, Pandey B and Shi G (2011b), 'Preparing for resettlement associated with climate change', *Science*, 334, 456–457.
Diamanti M V and Pedeferri M P (2007), 'Effect of anodic oxidation parameters on the titanium oxides formation', *Corrosion Sci*, 49, 939–948.
Earp A A and Smith G B (2011), 'Evolution of plasmonic response in growing silver thin films with pre-percolation non-local conduction and emittance drop', *J Phys D: Appl Phys*, 44, 255102.

El-Sayed H A and Birss V I (2011), 'Versatile fabrication of self-assembled metallic nanoparticle arrays', *J Mater Chem*, 21, 18431–18438.

Fahlteich J, Schiller N, Fahland M, Straach S, Günther S and Brantz C (2012), 'Vacuum roll-to-roll technologies for transparent barrier films', *Soc Vacuum Coaters Bull*, Spring, 40–45.

Frenzer G and Maier W F (2006), 'Amorphous porous mixed oxides: sol-gel ways to a highly versatile class of materials and catalysts', *Ann Rev Mater Res*, 36, 281–331.

Fujishima A, Zhang X and Tryk D A (2008), 'TiO_2 photocatalysis and related surface phenomena', *Surf Sci Rep*, 63, 515–582.

Geim A K and Novoselov K S (2007), 'The rise of graphene', *Nature Mater*, 6, 183–191.

Ginley D S and Cahen D (2012), *Fundamentals of Materials for Energy and Environmental Sustainability*, Cambridge University Press, Cambridge.

Glang R (1970), 'Vacuum evaporation', in *Handbook of Thin Film Technology*, ed. by Maissel L I and Glang R, McGraw-Hill, New York, pp. 1.3–1.130.

Gläser H J (2000), *Large Area Glass Coating*, von Ardenne Anlagentechnik GmbH, Dresden.

Gläser H J (2008), 'History of the development and industrial production of low thermal emissivity coatings for high heat insulating glass units', *Appl Opt*, 47, C193–C199.

Granqvist C G (1991), 'Energy efficient windows: present and forthcoming technology', in *Materials Science for Solar Energy Conversion Systems*, ed. by Granqvist C G, Pergamon, Oxford, pp. 106–167.

Granqvist C G (1995), *Handbook of Inorganic Electrochromic Materials*, Elsevier, Amsterdam.

Granqvist C G (2012), 'Preparation of thin films and nanostructured coatings: a primer', *Solar Energy Mater Solar Cells*, 99, 166–175.

Granqvist C G and Buhrman R A (1976), 'Ultrafine metal particles', *J Appl Phys*, 47, 2200–2219.

Granqvist C G and Hunderi O (1977), 'Optical properties of ultrafine gold particles', *Phys Rev B*, 16, 3513–3534.

Granqvist C G, Kish L B and Marlow W H (eds) (2004), *Gas Phase Nanoparticle Synthesis*, Kluwer, Dordrecht.

Harris L, McGinnies R T and Siegel B M (1948), 'The preparation and optical properties of gold blacks', *J Opt Soc Am*, 38, 582–589.

Hayashi C, Uyeda R and Tasaki A (eds) (1997), *Ultra-Fine Particles: Exploratory Science and Technology*, Noyes, Park Ridge, NJ.

Henderson M A (2011), 'A surface science perspective on TiO_2 photocatalysis', *Surf Sci Rep*, 66, 185–297.

Hoel A, Reyes L F, Saukko S, Heszler P, Lantto V and Granqvist C G (2005), 'Gas sensing with films of nanocrystalline WO_3 and Pd made by advanced reactive gas deposition', *Sensors Actuators B: Chem*, 105, 283–298.

Holland L (1956), *Vacuum Deposition of Thin Films*, Chapman & Hall, London.

Hu L, Kim H S, Lee J-Y, Peumans P and Cui Y (2010), 'Scalable coating and properties of transparent, flexible, silver nanowire electrodes', *ACS Nano*, 4, 2955–2963.

Hultman L and Sundgren J E (2001), 'Structure/property relationships for hard coatings', in *Handbook of Hard Coatings: Deposition Technologies and Applications*, ed. by Bunshah R F, Noyes, Norwich, NY, pp. 108–180.

IPCC (2007), in Metz B, Davidson O R, Bosch P, Dave R and Meyer L A (eds) *Climate Change 2007: Contribution to Working Group III to the Fourth Assessment Report of the Intergovernmental Panel on Climate Change*, Cambridge University Press, Cambridge.

IPCC (2011), in Field C B, Barros V, Stocker T F, Qin D, Dokken D, Ebi K L, Mastrandrea M D, Mach K J, Plattner G-K, Allen S K, Tignor M and Midgley P M (eds) *Intergovernmental Panel on Climate Change Special Report on Managing the Risks of Extreme Events and Disasters to Advance Climate Change Adaptation*, Cambridge University Press, Cambridge and New York.

Jacob T, Wahr J, Pfeffer W T and Swenson S (2012), 'Recent contributions of glaciers and ice caps to sea level rise', *Nature*, 482, 514–518.

Joerger R, Klaus-Joerger T, Olsson E and Granqvist C G (2000), 'Optical properties of biomimetically produced spectrally selective coatings', *Solar Energy*, 69 (Suppl), 27–33.

Klaus T, Joerger R, Olsson E and Granqvist C G (1999), 'Silver-based nanoparticles, microbially fabricated', *Proc Nat Acad Sci USA*, 23, 13611–13614.

Klaus-Joerger T, Joerger R, Olsson E and Granqvist (2001), 'Bacteria as workers in the living factory: metal-accumulating bacteria and their potential for materials science', *Trends Biotechnol*, 19, 15–20.

Klein L C (ed.) (1994), *Sol-Gel Optics: Processing and Applications*, Kluwer, Dordrecht.

Konuma M (1992), *Film Deposition by Plasma Techniques*, Springer, Berlin.

Kunič R, Koželj M, Šurca Vuk A, Vilčnik A, Slemenik Perše L, Merlini D and Brunold S (2009), 'Adhesion and thermal stability of thickness insensitive spectrally selective (TISS) polyurethane-based paint coatings on copper substrates', *Solar Energy Mater Solar Cells*, 93, 630–640.

Lakhtakia A and Messier R (2004), 'Sculptured thin films', in *Nanometer Structures: Theory, Modeling, and Simulation*, Lakhtakia A. (ed.) SPIE – The International Society for Optical Engineering, Bellingham, WA, pp. 5–44.

Lansåker P C, Backholm J, Niklasson G A and Granqvist C G (2009), 'TiO_2/Au/TiO_2 multilayer thin films: novel metal-based transparent conductors for electrochromic devices', *Thin Solid Films*, 518, 1225–1229.

Lansåker P C, Niklasson G A and Granqvist C G (2012), 'Thin gold films on SnO_2:In: temperature-dependent effects on the optical properties', *Thin Solid Films*, 520, 3688–3691.

Lee J-Y, Connor S T, Cui Y and Peumans P (2008), 'Solution-processed metal nanowire mesh transparent electrodes', *Nano Lett*, 8, 689–692.

Lee W, Schwirn K, Steinhart M, Pippel E, Scholz R and Gösele U (2008), 'Structural engineering of nanoporous anodic aluminium oxide by pulse anodization of aluminium', *Nature Nanotechnol*, 3, 234–239.

Lee Y J, Yi H, Kim W-J, Kang K, Yun D S, Strano M S, Ceder G and Belcher A M (2009), 'Fabricating genetically engineered high-power lithium-ion batteries using multiple virus genes', *Science*, 324, 1051–1055.

Liu D X, Iza F, Wang X H, Kong M G and Rong M Z (2011), '$He + O_2 + H_2O$ plasmas as a source of reactive oxygen species', *Appl Phys Lett*, 98, 221501.

Lowenheim F A (1978), 'Deposition of inorganic films from solution', in *Thin Film Processes*, ed. by Vossen J L and Kern W, Academic, New York, pp. 209–256.
Maaroof A I, Cortie M B and Smith G B (2005), 'Optical properties of mesoporous gold films', *J Opt A: Pure Appl Opt*, 7, 303–309.
Mahan J E (2000), *Physical Vapor Deposition of Thin Films*, Wiley, New York.
Maissel L I and Glang R (eds) (1970), *Handbook of Thin Film Technology*, McGraw-Hill, New York.
Mandal D, Bolander M E, Mukhopadhyay D, Sarkar G and Mukherjee P (2006), 'The use of microorganisms for the formation of metal nanoparticles and their detection', *Appl Microbiol Biotechnol*, 69, 485–492.
Mattox D M (2003), *The Foundations of Vacuum Coating Technology*, Noyes, Park Ridge, NJ.
Mattox D M (2010), *Handbook of Physical Vapor Deposition (PVD) Processing*, 2nd edn, Elsevier/William Andrew, Norwich, NY.
Mbise G W, Le Bellac D, Niklasson G A and Granqvist C G (1997), 'Angular selective window coatings: theory and experiments', *J Phys D: Appl Phys*, 30, 2103–2122.
Messier R (2008), 'The nano-world of thin films', *J Nanophotonics*, 2, 021995.
Meyer S F (1989), '*In situ* deposition monitoring for solar film production by roll coating', *J Vac Sci Technol A*, 7, 1432–1435.
Morosanu C E (1990), *Thin Films by Chemical Vapour Deposition*, Elsevier Science, Amsterdam.
Motohiro T, Yamadera H and Taga Y (1989), 'Angular-resolved ion-beam sputtering for large-area deposition', *Rev Sci Instrum*, 60, 2657–2665.
Movchan B A and Demchishin A V (1969), 'Structure and properties of thick condensates of nickel, titanium, tungsten, and aluminum oxides, and zirconium dioxide in vacuum', *Fiz Metal Metalloved*, 28, 653–660; English translation in *Phys Met Metallogr*, 28(4), 83–90.
Nerem R S, Chambers D P, Choe, C and Mitchum G T (2010), 'Estimating mean sea levels from the TOPEX and Jason altimeter missions', *Marine Geodesy*, 33 Suppl 1, 435–446.
Ohring M (2002), *The Materials Science of Thin Films: Deposition and Structure*, 2nd edn, Academic, New York.
Olenin A Yu and Lisichkin G V (2011), 'Metal nanoparticles in condensed media: preparation and the bulk and surface structural dynamics', *Usp Khim* 80, 635–662; English translation in *Russ Chem Rev* 80, 605–630.
Pierson H O (1999), *Handbook of Chemical Vapor Deposition: Principles, Technology, and Applications*, 2nd edn, Noyes, Park Ridge, NJ.
Pulker H K (1999), *Coatings on Glass*, 2nd edn, Elsevier, Amsterdam.
Rai M and Duran N (eds) (2011), *Metal Nanoparticles in Microbiology*, Springer, Berlin.
Reyes L F, Saukko S, Hoel A, Lantto V and Granqvist C G (2004), 'Structure engineering of WO_3 nanoparticles for porous film application by advanced reactive gas deposition', *J Eur Ceram Soc*, 24, 1415–1419.
Rodríguez J, Gómez M, Lu J, Olsson E and Granqvist C G (2000), 'Reactively sputter-deposited titanium oxide coatings with parallel penniform microstructure', *Adv Mater*, 12, 341–343.
Ruske F, Jacobs C, Sittinger V, Szyszka B and Werner W (2007), 'Large area ZnO:Al films with tailored light scattering properties for photovoltaic applications', *Thin Solid Films*, 515, 8695–8698.

Schiller S, Kirchhoff V, Schiller N and Morgner H (2000), 'PVD coatings of plastic webs and sheets with high rates on large areas', *Surf Coatings Technol*, 125, 354–360.
Schwarz-Schampera U and Herzig P (2002), *Indium: Geology, Mineralogy, and Economics*, Springer, Berlin.
Smith D L (1995), *Thin-Film Deposition*, McGraw-Hill, New York.
Smith G B and Granqvist C G (2010), *Green Nanotechnology: Solutions for Sustainability and Energy in the Built Environment*, CRC Press, Boca Raton, FL.
Sotelo J A, Pustovit V N and Niklasson G A (2002), 'Optical constants of gold blacks: fractal network models and experimental data', *Phys Rev B*, 65, 245113.
Steele J J and Brett M J (2007), 'Nanostructure engineering in porous columnar thin films: recent advances', *J Mater Sci: Mater Electron*, 18, 367–379.
Tao C S, Jiang J and Tao M (2011), 'Natural resource limitations to terawatt-scale solar cells', *Solar Energy Mater Solar Cells*, 95, 3176–3180.
Thornton J A (1977), 'High rate thick film growth', *Ann Rev Mater Sci*, 7, 239–260.
Vossen J L and Kern W (eds) (1978), *Thin Film Processes*, Academic, New York.
Vossen J A and Kern W (eds) (1991), *Thin Film Processes II*, Academic, New York.
Wakefield N G and Sit J C (2011), 'On the uniformity of films fabricated by glancing angle deposition', *J Appl Phys*, 109, 084332.
Wasa K and Hayakawa S (1992), *Handbook of Sputter Deposition Technology*, Noyes, Park Ridge, NJ.
Wernick S, Pinner R and Sheasby P G (2001), *The Surface Treatment and Finishing of Aluminium and Its Alloys*, vols 1 and 2, 6th edn, Finishing Publications Ltd, Stevenage.
Zhao S (2007), 'Spectrally selective solar absorbing coatings prepared by dc magnetron sputtering', PhD Thesis, Uppsala University, Sweden.

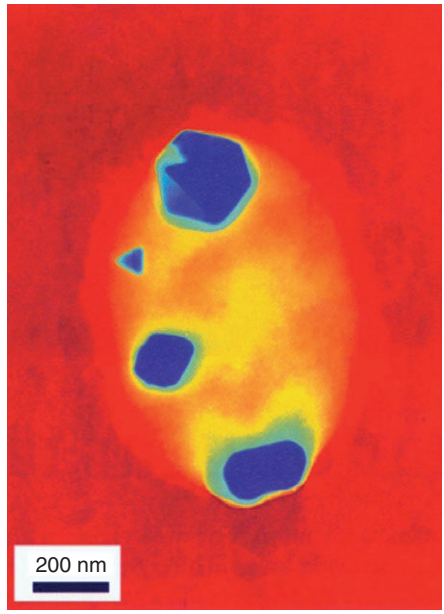

Plate II Transmission electron micrograph with artificial colouring showing silver-based crystalline nanoparticles grown inside *Pseudomonas* cells. From Klaus-Joerger *et al*. (2001).

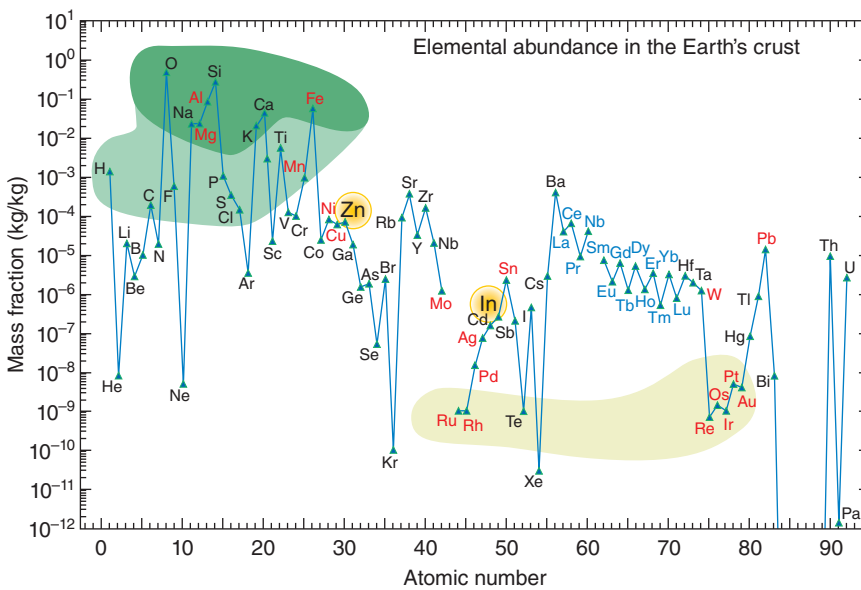

Plate III Elemental abundance in the Earth's crust. Greenish areas indicate the rock forming elements, and yellow areas denote the least common metals. The highlighted elements, zinc and indium, are discussed in the text. Data of this kind are found in many sources; this particular diagram was obtained from Berry (2010).

9

High performance thermal insulation materials for buildings

R. BAETENS, KU Leuven, Belgium

DOI: 10.1533/9780857098832.2.188

Abstract: Recent developments in high performance thermal insulators based on nanotechnology have enabled a strong drop in the effective thermal conductivity of insulation materials, down to 0.004–0.014 W/(mK). The reductions are achieved using the Knudsen effect, which describes the effect of pore size distributions and partial gas pressure in materials on the gaseous heat transfer. The resulting thermal insulation materials have specific properties of importance for the building industry, which should be considered in each project. Further exploitation and a similar approach to solid conduction may result in the next-generation high performance thermal insulators.

Key words: Knudsen, vacuum insulation, fumed silica, aerogel.

9.1 Introduction

The true origins of thermal insulation are difficult to identify. Prehistoric humans clothed themselves with wool and animal skin and built homes of wood, stone and earth, whereas the Romans as well as early inhabitants of Spain already used cork as an insulating material for roofs. Mineral fibers from volcanic deposits were first used by the Hawaiian natives to blanket their huts, but it was not until the first industrial revolution that commercial application of thermal insulation became common with Cabot's Quilt in 1891 as the earliest example. Since then, rock wool, fiberglass and extruded polystyrene have appeared commercially as thermal insulators in commercial and residential buildings (Close, 1947; Jester, 1995).

Recent progress in the development of high performance thermal insulators is due to progress in nanotechonolgy and material sciences, allowing the adaptation of known theoretical principles of thermal physics in practice. High performance thermal insulators (HPTIs) strongly differ from traditional insulators on base principles considering heat transfer. Traditional thermal isolators are distinguished by how they trap a gaseous material, i.e., in a fibrous material, in a cellular material, or in a granular material. These insulators have a thermal conductivity in the range of 0.025–0.040 W/(mK) and show a lower limit for their thermal conductivity close to the thermal conductivity of the trapped gas. As such, high performance thermal

insulators are generally defined as an insulator with a thermal conductivity below 0.02 W/(mK). Similarly to the distinction in traditional thermal insulators, current high performance thermal insulators are distinguished by how they achieve rarefaction of the gas, i.e., by a nanoporous solid structure, or by application of a partial vacuum, whereas the best results are achieved with a combination of both. The exploitation of the divergent physical theory of heat transfer in nanoporous materials is the reason why nanotechnology has produced a breakthrough in thermal insulators the last decade, as summarized in Fig. 9.1.

9.2 Heat transfer in thermal insulators

9.2.1 Macroscopic heat transfer

The macroscopic heat transfer in a material is described by Fourier's law relating the energy flux ø to the temperature gradient by its thermal conductivity k as

$$\phi = -k\nabla T \qquad [9.1]$$

The effective heat transfer ø for a porous insulator is a combination of four heat transfer mechanisms and can be approximated by their sum

$$\phi = \phi_{cd,s} + \phi_{rd} + \phi_{cd,g} + \phi_{cv}(+\phi_k) \qquad [9.2]$$

where $\phi_{cd,s}$ denotes heat conduction of the solid skeleton, ϕ_{rd} heat transfer by longwave radiation, $\phi_{cd,g}$ heat conduction of encapsulated gas molecules and ϕ_{cv} heat transfer by gas convection. The coupling term ϕ_k describing possible reciprocity between the different processes is generally neglected. Traditional thermal isolators use the inherently low conductivity $k_{cd,g}$ of a gas at standard temperature and pressure to achieve a low overall heat transfer. Convection in the gaseous material is avoided by reducing the pore sizes, and the impact of solid conduction $\phi_{cd,s}$ is reduced by means of a high porosity.

9.2.2 Rarefied gas regimes in current HPTIs

The traditional Fourier law is no longer valid if the materials characteristic time scale θ or length scale Λ has the same order of size as the natural time scale τ or length scale l of the physical problem, meaning that the physical process of heat transfer occurs at the same scale as the scale at which the basic solid properties of the materials are defined. Recent progress in the development of high performance insulators is based on this principle for the gaseous component $\phi_{cd,g}$ of the overall heat transfer. Here, the natural time or length scale denotes the distance traveled or time between two

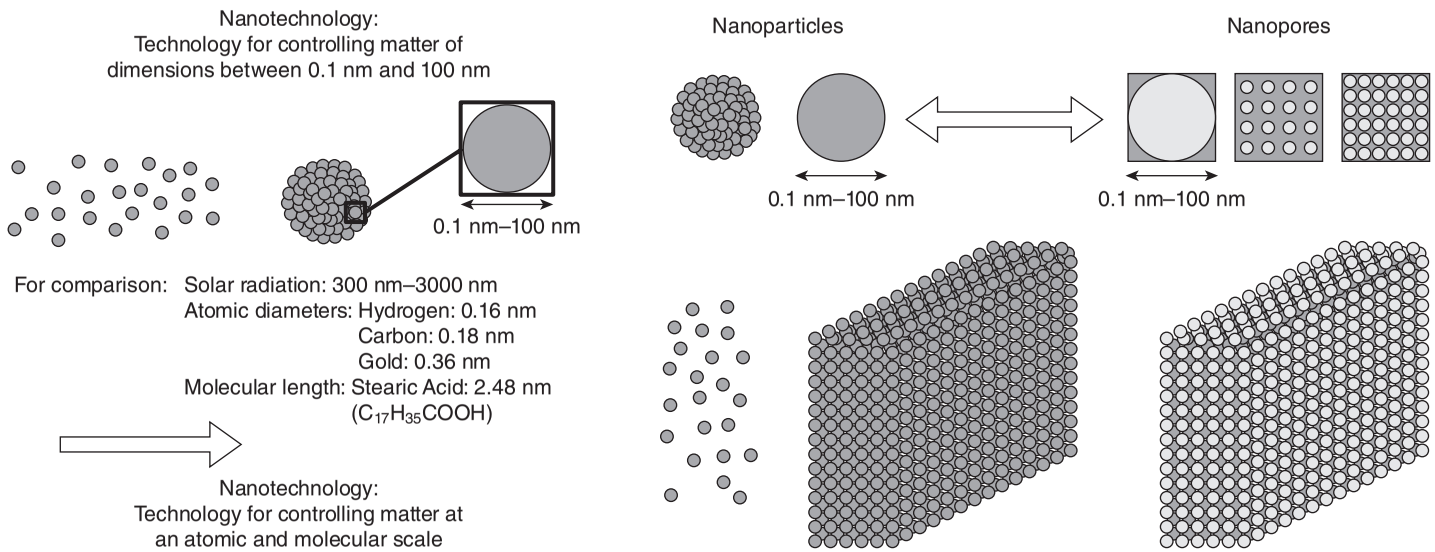

9.1 Nanotechnology and its application to high performance thermal insulation materials. (Jelle, 2011).

collisions of gaseous molecules, whereas the characteristic material scale denotes the size of pores in which the collisions occur.

The gas properties are described by definition of the velocity distribution function *f(r, v)* defining the number of gas molecule d*n* having a velocity in the range [*v*, *v* + d*v*] in the volume element *r* + d*r*. The resulting conductive heat transfer $\phi_{cd,g}$ is expressed as the transport of the particles kinetic energy (Volz, 2007), as:

$$\phi_{cd,g} = \frac{1}{2}\int m(\boldsymbol{v} - \langle \boldsymbol{v} \rangle)^3 f \cdot \boldsymbol{n} \mathrm{d}\boldsymbol{v} \quad \text{with} \quad \mathrm{d}n = f \, \mathrm{d}\boldsymbol{r} \, \mathrm{d}\boldsymbol{v} \qquad [9.3]$$

where *m* is the particle mass and ⟨*v*⟩ the local average velocity. The change of this one-particle distribution function *f* is described by the Boltzmann equation (Boltzmann, 1884) as:

$$\frac{\partial f}{\partial t} + v \cdot \frac{\partial f}{\partial \boldsymbol{r}} + \frac{\boldsymbol{F}}{L} \cdot \frac{\partial f}{\partial v} = \left.\frac{\partial f}{\partial t}\right|_{\text{coll}} \qquad [9.4]$$

where *F* is an applied external force field. The right-hand side describes the effect of collisions between particles and the walls of a container determined by the molecular chaos assumption depicting a binary collision of particles. The collision term is often approximated as $-[f - f^0] / \tau$ under the assumption that collisions in a gas from a non-equilibrium state will tend to an equilibrium state, with $\tau(v)$ the relaxation time to return to equilibrium within d*r* and f^0 the local equilibrium distribution. The resulting Boltzmann equation can be expressed by means of dimensionless parameters as:

$$\frac{\tau}{\theta}\frac{\partial f}{\partial t'} + \boldsymbol{v}' \cdot \frac{v\tau}{\Lambda}\frac{\partial f}{\partial \boldsymbol{r}'} + \boldsymbol{F}' \cdot \frac{v\tau}{\Lambda}\frac{\partial f}{\partial \boldsymbol{v}'} = -\left[f - f^0\right] \qquad [9.5]$$

where the accented parameters are dimensionless. One can notice that the changes in *f* are driven by $v\tau / \Lambda$, i.e., l / Λ in a stationary system, or by τ / θ in a homogeneous non-stationary system. This ratio expresses the ratio of the natural scale of the physical problem to that of the material, and is known as the Knudsen number Kn. Depending on this ratio, we can define two distinct regimes, i.e., a collisional regime with Kn << 1 as considered in the macroscopic laws with a system state close to f^0, and a rarefied regime with Kn >> 1 where inter-particle collisions are negligible and heat transfer is ruled by collisions with the walls. Here, the velocity distribution function evolves according to the Boltzmann equation with the collisional term equal to zero.

In contrast to the collisional regime, the heat transfer in a rarefied gas proceeds for the major part from the momentum exchange by collision between the gas molecules and the pore walls instead of by collision between

gas molecules. The resulting conductivity drop is described by the so-called Knudsen effect (Kennard, 1938). The heat transfer in rarefied gas regimes is generally expressed as derived from parallel surfaces by normalizing the heat transfer $\phi_{cd,g}$ by the heat transfer $\phi^*_{cd,g}$ denoting the apparent macroscopic heat transfer of the gas in the collisional regime. The resulting ratio $\phi_{cd,g} / \phi^*_{cd,g}$ depends only on the Knudsen number and a term $\beta(\alpha, \gamma)$ describing the heat transfer by collision between the gas molecule and the pore wall, depending on the thermal accommodation coefficient α and heat capacity ratio γ, expressed as:

$$\phi_{cd,g} = \frac{1}{1+\beta \cdot \mathrm{Kn}} \phi^*_{cd,g} \qquad [9.6]$$

and as shown graphically in Fig. 9.2, whereas the β is generally simplified as constant. The required Knudsen number can be determined based on the kinetic theory for an ideal gas as:

$$\mathrm{Kn} = \frac{l}{\Lambda} = \frac{1}{\sqrt{2} n \sigma} \frac{1}{\Lambda} \quad \text{with} \quad n = \frac{p}{k_B T} \qquad [9.7]$$

where σ is the collisional cross-sectional area equal to πd^2 with d the particle diameter, k_B the Boltzmann constant, T the average gas temperature, and p the total gas pressure.

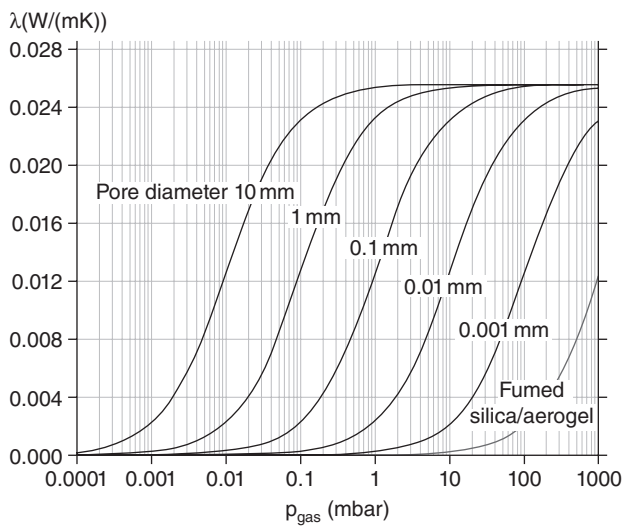

9.2 The thermal conductivity of air as a function of the air pressure and the average pore diameter of the medium.

9.2.3 Rarefied photon and phonon regimes for next-generation HPTIs

The Knudsen effect has shown that macroscopic laws of heat transport no longer apply at nanoscale. Convective heat transport at this level is well understood, but the background of solid conduction and radiative heat transfer at this characteristic length is a rather unexplored field for non-metallic materials.

Whereas the gas molecules are the energy carriers for gaseous conduction, the energy carriers of solid conduction and radiation are respectively photons and phonons. The behavior of phonons and photons is similar to gas molecules in several ways: they are treated as classical particles beyond a certain length scale, i.e., the coherence length for phonons and the wavelength for photons, and their propagation is described by a Boltzmann equation. As such, similar to strong reduction of the gaseous heat transfer $\phi_{cd,g}$ in the ballistic gas regime due to the so-called Knudsen effect, a reduction of the heat transfer by solid conduction $\phi_{cd,s}$ and radiative heat transfer ϕ_{rd} can be denoted in the ballistic regimes of their energy carriers.

Radiative heat transfer is described by definition of the specific intensity $L_\nu(u, r)$ in a frequency band $[\nu, \nu + \mathrm{d}\nu]$ depending on the direction u and the considered point r. This intensity can be interpreted as the product of the number of photons per unit volume $n_\nu(u, r)$ with the energy per photon $h\nu$ and the speed of propagation v_ν. The resulting radiative heat transfer ϕ_{rd} is expressed as:

$$\phi_{rd} = \iint L_\upsilon \boldsymbol{u}\, \mathrm{d}\Omega\, \mathrm{d}\omega \quad \text{with} \quad L_\upsilon = \frac{1}{4\pi} n_\upsilon h \upsilon v_\upsilon \qquad [9.8]$$

in the solid angle $\mathrm{d}\Omega$. The transport of specific intensity L_ν is described by the radiative transfer equation (Chandrasekhar, 1960) as:

$$\frac{1}{v_\upsilon}\frac{\partial L_\upsilon}{\partial t} + \boldsymbol{u}\cdot\nabla L_\upsilon = -(\mu_\upsilon + \sigma_\upsilon) L_\upsilon + \mu_\upsilon n^2 L_\upsilon^0(T) + \frac{\sigma_\upsilon}{4\pi}\int p_\upsilon L_\upsilon\, \mathrm{d}\Omega' \qquad [9.9]$$

stating the radiative energy balance of a beam, with negative terms from extinction by absorption and scattering, and positive terms from scattering and thermal emission, and where μ_υ is the monochromatic absorption coefficient, σ_ν is the scattering coefficient, n is the real part of the refraction index of the medium, T is the local temperature and p_ν is the fraction of the energy flux in direction u that is scattered in direction u'.

Analogous to radiative heat transfer, solid conduction can be described by definition of the phonon radiative intensity $I_\omega(u, r)$, interpreted as the product of the number of modes per unit volume $\mathrm{d}\Omega$ with the number of phonons per unit volume $n_\omega(u, r)$, with the energy per photon $\bar{\eta}\omega$ and the

group velocity v_ω. The resulting (solid) conductive heat transfer $\phi_{cd,s}$ is expressed as:

$$\phi_{cd,s} = \iint I_\omega \boldsymbol{u}\, \mathrm{d}\Omega\, \mathrm{d}\omega \quad \text{with} \quad I_\omega = \frac{1}{4} D(\omega) n_\omega \bar{\eta} \omega v_\omega \qquad [9.10]$$

in the solid angle dΩ. Also the transport of phonon radiative intensity $I\omega$ is described by a phonon radiative transfer equation (Srivastava, 1990) as:

$$\frac{1}{v_\omega}\frac{\partial I_\omega}{\partial t} + \boldsymbol{u}\cdot\nabla I_\omega = -\mu_\omega\left[I_\omega - I_\omega^0\right] \qquad [9.11]$$

stating the radiative phonon energy balance, with creation and destruction of phonons during collision, and where u_ω is the reciprocal of the mean free phonon path Λ_ω equal to $v_\omega\tau_\omega$.

Both the radiative transfer equation and the phonon radiative transfer equation denote that also radiative and conductive heat transfer has a ballistic regime with a characteristic length l_{ext} equal to respectively $(\mu_\upsilon + \sigma_\upsilon)^{-1}$ and μ_υ^{-1}. The characteristic length of radiation and solid conduction is, however, lower than the typical values for gaseous conduction and can be found in the range of 1–0.01 nm. This means that an equally strong reduction on $\phi_{cd,s}$ and ϕ_{rd} can be achieved as depicted by the Knudsen effect. Solid layers or structures with a thickness below this l_{ext} show a lower k due to ballistic phonon and photon transport. Here, the phonon radiative transfer equation is reduced to boundary scattering, whereas the radiative transfer equation for the ballistic regime can be obtained by inserting the decomposition of the specific intensity L_υ as $L_{\upsilon,bal}\cdot\delta(u - u_0)$ into the RTE, resulting in a ballistic component equal to

$$\frac{1}{v_\upsilon}\frac{\partial L_\upsilon}{\partial t} + \boldsymbol{u}\cdot\nabla L_\upsilon = -(\mu_\upsilon + \sigma_\upsilon) L_\upsilon \qquad [9.12]$$

denoting a strongly reduced ϕ_{rd} and resulting k-value. The reduction of both the solid conductive and radiative heat transfer component in ϕ can be used in two ways. Firstly, it could be used to reduced the effective thermal conductivity k of current state-of-the-art thermal insulators to values below 0.014 W/(mK) at ambient conditions. Secondly, it could be employed to develop more robust high performance thermal insulators with equal thermal properties to current state-of-the-art materials but without their drawbacks by reducing the importance of the gaseous conductive component $\phi_{cd,g}$ into the overal low heat transfer.

9.3 State-of-the-art insulators

As traditional thermal isolators are distinguished by how they trap a gaseous material, current high performance thermal insulators are distinguished by

how they achieve rarefaction of the gaseous material and its resulting high Knudsen number, i.e., by a nanoporous solid structure with a low pore size λ, such as fumed silica or aerogels (Baetens *et al.*, 2011; Dorchech & Abbasi, 2008; Hüsing & Schubert, 1998; Jelle *et al.*, 2010; Richter, 1995; Wang *et al.*, 2007), or by application of a partial vacuum such as for vacuum insulation panels (Alam *et al.*, 2011; Baetens *et al.*, 2010a; Jelle, 2011; Jelle *et al.*, 2010) with a low gas pressure p. The best results are achieved with a combination of both.

9.3.1 Nanoporous thermal insulators

As most thermal insulators that apply a partial vacuum use a material with nanoscale pores, nanoporous thermal insulators will be treated first. Within this context, the main nanoporous thermal insulators are aerogels (see Fig. 9.3) and microporous silica. Aerogels are used as a main thermal insulator on its own, whereas microporous silica is generally only used as core material for partial vacuum thermal insulators and will be treated later. Aerogels are essentially the solid framework of a gel isolated from its liquid medium and were discovered in the early 1930s by S.S. Kistler (Kistler, 1931). The main type of aerogels as high performance thermal insulators are silica aerogels, SiO_2. Aerogels have an extremely high porosity and a pore size distribution $f(\Lambda)$ below the mean free path for air molecules at standard temperature and pressure, making them a high performance thermal insulator.

The unique properties of aerogels are determined by its synthesis, which can be divided into three general steps: gel preparation, aging of the gel, and drying of the gel. A detailed comprehensive review on the synthesis of

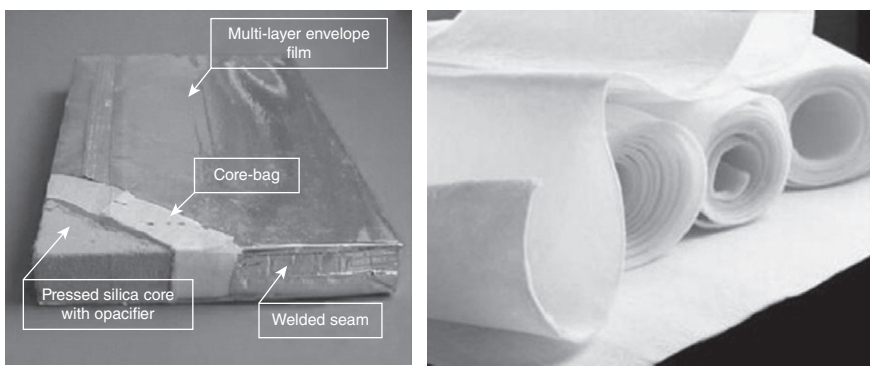

9.3 Typical VIP structure showing the main components and an example of aerogel as a high performance thermal insulation material for building applications (Baetens *et al.*, 2011; Jelle, 2011).

silica aerogels has recently been written by Dorcheh and Abbasi (2008) and the author would like to refer to this work for a more extensive analysis of the aerogel synthesis.

Gel preparation

Gel preparation happens by means of a sol-gel process (Brinker & Scherer, 1990; Dorchech & Abbasi, 2008), i.e., a process in which solid nanoparticles dispersed in a liquid agglomerate together to form a continuous three-dimensional network extending throughout the liquid. The main precursors for silica aerogels are silicon alkoxides. A simplified reaction based on tetramethoxysilane may be presented as

$$Si(OCH_3)_4 + 2\ H_2O \rightarrow SiO_2 + 4\ CH_3OH$$

The sol becomes a gel when the dispersed solid particles stick together during collision to form a network of particles spanning the entire liquid. Nanoparticles containing reactive surface groups stick by bonding or electrostatic forces, whereas others may require an additive. In general, acid hydrolysis and condensation results in weakly branched chains and microporous structures in silica sols and resulting long gelation times, whereas uniform particles are easily formed in base catalysis, leading to a broader distribution of larger pores which is less favorable for thermal insulation materials.

Aging of the gel

Aging of the gel in its mother solution is required to prevent the gel from shrinking during drying (Haereid *et al.*, 1996). The silica spine of the gel contains a significant number of unreacted alkoxide groups, and hydrolysis and condensation must continue a sufficient time for strengthening of the silica network. During this aging period, material transports to the spine neck region and small particles dissolve into larger ones. Common aging procedures involve ethanolsiloxane mixtures, adding new monomers to the solid SiO network, and increasing the degree of cross-linking. After aging, all water remaining within the pores must be removed before drying: any water left in the gel leads to an opaque and very dense aerogel.

Drying of the gel

Drying of the gel is the most critical stem in the production process and happens under special conditions to prevent the gel structure from collapsing due to shrinkage and possible capillary tension in the small pore sizes. If a liquid is held under pressure always greater than the vapor pressure,

and the temperature is raised, it will be transformed at the critical temperature into a gas without two phases having been present at any time (Kistler, 1932). As such, high temperature supercritical drying and low temperature supercritical drying from carbon dioxide is mostly used as drying process.

The unique structure of aerogels result in exceptional material properties: a bulk density typically of 70–150 kg/cm^3 due to a porosity of 85–95%, a specific surface area of 600–1000 m^2/g, a particle size below 5 nm, a $f(\Lambda)$ averaging 20 nm with maximum pore sizes of 100 nm close to the mean free path of 70 nm for air molecules at standard temperature and pressure, resulting in an effective thermal conductivity of 0.014 W/(mK) at atmospheric conditions. Also translucent aerogels can be achieved depending on water removal before the drying process, resulting in a transmittance between 0.8 and 0.95 in the visible and (near-)infrared spectrum for a layer of 1 cm and a low refraction index of around 1.0.

9.3.2 Partial vacuum thermal insulators

Vacuum insulation panels (VIP) (see Fig. 9.3) are defined as an evacuated foil-encapsulated open-porous material as thermal insulator. As such the insulator is no typical thermal insulation material, but consists of a system of three parts, each with their own specific purpose(s), i.e., the open-porous core material, the foil envelope and the applied vacuum. A perfect vacuum is the most effective reduction of the gas thermal conduction $\phi_{cd,g}$, achieving its limit value of 'zero'. This perfect vacuum is pure theoretically, but a low pressure P_g has a positive influence on the gaseous heat transfer. As such the core has a dual purpose, i.e., to withstand the pressure of the applied partial vacuum, and preferably to strengthen the thermal effect of this vacuum by its pore size distribution $f(\Lambda)$. This core material is typically a traditional open-porous thermal insulator, or a nanoporous high performance thermal insulator. The foil envelope only serves to maintain the applied partial vacuum in the core material and generally consists of an aluminum layer. Due to the relatively high thermal conductivity of such an envelope, the heat flux increases at the edges and corners. Furthermore, the foil envelope is not able to keep the applied vacuum constant at the pristine pressure due to gas and moisture mitigation through the foil and foil seams. The envelope choice is generally a compromise between the allowed pressure drop through time and the allowed thermal bridging at the panel edges.

Current state-of-the-art vacuum insulation panels consist of a core material of fumed silica with a bulk density of 160–220 kg/m^3, a specific surface area of 100–400 m^2/g and a $f(\Lambda)$ with maximum pore sizes around 300 nm close to the mean free path of 70 nm for air molecules at standard temperature and pressure, resulting in a effective thermal conductivity of 0.020 W/(mK) at atmospheric conditions. The applied partial vacuum is

around 5 mbar in pristine conditions, lowering the effective thermal conductivity of the fumed silica core material to 0.004 W/(mK). The multilayer films usable for VIP envelopes consist of different layers with an overall thickness of 100–200 μm. Two different film types are mainly being used for VIP envelopes: metal foils consisting of a central aluminum barrier layer laminated between an outer scratch-resistant polyethylene terephthalate layer and an inner polyethylene sealing layer, and metalized films made from up to three layers of aluminum-coated polyethylene terephthalate films and an inner polyethylene sealing layer.

9.4 Applications

Each of the mentioned materials has their specific application properties as thermal insulators in the building sector as summarized in Tables 9.1 and 9.2, and will be discussed below.

Thermal insulators for building constructions require a specific set of main functional requirements. The first requirement is, naturally, its resistance to heat transfer expressed in his low thermal conductivity k. Second, it must withstand degradation through time of its thermal properties, e, generally its resistance to radiation, its resistance to degradation by

Table 9.1 Summary of thermal properties for vacuum insulation and aerogel insulation (Baetens *et al.*, 2010b; Tenpierik & Cauberg, 2007)

	Initial k, 10^{-3} W/(mK)	k after 25 years, 10^{-3} W/(mK)	k after 100 years, 10^{-3} W/(mK)	ψ_e W/(mK)
Small 0.5 × 0.5 × 0.01 m^3 vacuum insulation panel with metalized envelope	4.0	9.2–9.9	14.0–15.5	0.18–0.26
Large 1.0 × 1.0 × 0.02 m^3 vacuum insulation panel with metalized envelope	4.0	7.2–7.7	10.0–10.8	0.20–0.24
Aerogel insulation	14			–

Table 9.2 Summary of advantages and disadvantages for vacuum insulation panels and aerogel insulation

	Advantages	Disadvantages
Aerogel insulation	• Relative low thermal conductivity • Possible transparency • On-site use similar to traditional materials	• Uncertain long-term physical properties • Energy-extensive and expensive production process • Uncertain health risks
Vacuum insulation panels	• Very low pristine thermal conductivity	• Aging and resulting increase of thermal conductivity • Limited robustness • No adaptation on-site • Thermal bridging at panel edges

moisture requiring a hydrophobic material, and its resistance to mechanical impact. The third requirement of importance is the possible ease of installation and its economic feasibility.

9.4.1 Nanoporous thermal insulators

The areas of application for aerogel insulation are strongly linked to their physical properties, and so these will be discussed first.

Properties

The main benefit of aerogel insulation is its low thermal conductivity at ambient conditions, while the material also shows exceptional properties concerning optical transmittance, sound absorption, and fire retardation.

Aerogel insulators have an overall thermal conductivity at ambient pressure down to 0.012 W/(mK) at ambient pressure and to 0.004 W/(mK) at a pressure of 50 mbar or less, whereas commercial aerogel thermal insulators for building purposes have a thermal conductivity of around 0.014 W/(mK) at ambient temperature and are very little affected up to a temperature of 200°C.

Silica aerogels have a high transmittance of radiation within the range of visible light, i.e., radiation with a wavelength between 380 and 780 nm. Monolith translucent silica aerogel in a 10 mm thick packed bed has a solar transmittance T_{sol} of 0.88 and a possible high transparency in the infrared spectrum T_{ir} of 0.85. Light reflected by silica aerogels appears bluish and transmitted light appears slightly reddened. This light scattering can be explained by λ^{-4}-type Rayleigh scattering caused by the interaction with inhomogeneities, and becomes more effective when the size of the particles

is similar to the wavelength of the incident light. The presence of pores within this range $f(\lambda)$ acts as scattering centers, and the efficiency of scattering will depend on the size of the scattering centers as well as the wavelength λ. Heat treatment of aerogels can increase their transparency, and the optical properties can be influenced further by selecting optimal synthesis parameters in the sol-gel process.

The sound absorption of a material increases with an increasing surface area facing the sound. As aerogels have a high porosity and a high specific surface area, sound waves are strongly absorbed and attenuated: monolith silica aerogels have a lower speed of sound than air. Sound velocities down to 40 m/s have been measured, whereas non-monolith commercial products claim to have a sound velocity of 100 m/s through the structure. Granular aerogels, on the other hand, are exceptional reflectors of audible sound, making excellent barrier materials. By combining multiple layers with different granular sizes, average attenuations of -60 dB have been found for a total thickness of only 0.07 m.

In contrast to combustible organic foam insulation that emits deadly fumes and smoke when burning, silica aerogel materials are non-combustible due to their non-organic SiO_2 structure and withstand heat up to 1400°C.

Due to their physical solid structure, aerogels show a low tensile strength and a brittle nature, whereas its porous structures make it very sensible to moisture due to high surface tensions.

Aerogel insulation sheets suffer from dust production. As most of the commercial aerogel insulation products consist of complete amorphous (and thus 0% crystalline) silica, exposure limits in the range of 5 mg/m^3 for respirable dust are set in the US by the Occupational Safety and Health Administration (OSHA). However, the International Agency for Research on Cancer (IARC) considers synthetic amorphous silica to be not classifiable as to its carcinogenicity to humans (i.e., belongs in group 3). No evidence of silicosis has been found from epidemiological studies of workers with long-term exposure to synthetic silica, whereas studies of various animal species show that amorphous silica can be completely cleared from the lungs (Merget *et al.*, 2002; Warheit, 2001).

Areas of application

Aerogel insulation panels have only recently been introduced to the market in small-scale production. The main building applications may be divided into two groups, i.e., as traditional thermal insulators by means of aerogel blankets, and in translucent form for high performance glazing.

Commercial manufacture of aerogel blankets began around the year 2000 and has been developed to meet various demands. An aerogel blanket

is a composite of a silica aerogel and fibrous reinforcement, turning the brittle structure of a silica aerogel into a durable, flexible, and hydrophobic material. The resulting blankets have a thermal conductivity k between 0.013 and 0.014 W/(mK). The aerogel insulation material consists of amorphous silica instead of crystalline silica, reducing possible health risks at exposure. Aerogel blankets can be used in the entire building industry similar to the use of traditional thermal insulators. However, their current high economic cost means that they are only used where limited space is available and where the use of vacuum insulation panels is not possible due to their drawbacks.

Aerogel is especially very interesting as a translucent or transparent insulation material because of its combination of a low thermal conductivity and a high transmittance of daylight and solar energy. At present, there are two commercial types of such aerogel-based daylight systems, i.e., Scoba-lit and Okagel windows. The aerogel product has a thermal conductivity of 0.018 W/(mK) and the fabricator offers skylights with a heat transmittance coefficient between 0.6 and 0.3 W/(m^{2}K) for layers of 30 and 60 mm Okagel respectively. The visible light transmission T_{vis} is 0.40 and the sound reduction is 52 dB. Research has been conducted in the last decade on the development of highly insulating windows based on both granular aerogel and monolithic aerogel. Two types of granular aerogel are used in prototype windows: semi-transparent spheres with a solar transmittance T_{sol} of 0.53 for a 10 mm packed bed and highly translucent granulates with a T_{sol} of 0.88. The granular aerogel is stacked in a polymethylmethacrylate double skin-sheet, between two gaps and glass panes. Increasing the aerogel thickness to 20.0 mm will lower the U-value further to approximately 0.5 W/(m^{2}K), while the solar transmittance will still stay above 0.75.

9.4.2 Partial vacuum thermal insulators

The areas of application of vacuum insulation panels are strongly linked to their physical properties and so these will be discussed first.

Properties

The main benefit of vacuum insulation panels is the reduction of the required thickness of the insulation layers. With a pristine center-of-panel thermal conductivity k of 0.004–0.005 W/(mK), equal thermal resistances are achieved within a thickness 5–8 times lower than traditional thermal insulators. The way this low thermal conductivity is achieved determines at the same time its main drawbacks, i.e., degradation through time of the thermal conductivity, thermal bridging at the panel edges, and strong limitations for installation and its resulting areas of application.

Degradation through time of the thermal resistance occurs mainly due to air and moisture intake through the panel envelope, and depends on the environmental conditions and the foil resistance for moisture and air transport. The intake results in an increase of the inner gas pressure $\delta p_g(\Gamma, \kappa)$, moisture pressure $\delta p_{wv}(\Gamma, \kappa)$ and water content $\delta_{uw}(\Gamma, \kappa)$, resulting in an increasing thermal conductivity $\delta k(p, u)$ through time strongly depending on the panel dimensions Γ, the permeability κ for air and moisture of the envelope material, and the environmental properties in the domain of application. Knowledge of the long-term thermal performance of vacuum insulation panels is still limited: predictions are based on calculations or short-term on-site measurements. General values for the thermal conductivity are 0.007 and 0.010 W/(mK) for large vacuum insulation panels after respectively 25 and 100 years, whereas higher values of 0.009 and 0.015 W/(mK) are depicted for small panels as shown in Table 9.1. The main differences between large and small panels is due to the envelope-to-volume and edge-to-volume ratio.

Thermal bridging at the panel edges occurs due to the metalized panel envelope. The edges reduce the effective overall thermal resistance of the insulation panel with a linear thermal transmittance coefficient $\psi_e(k_e, k)$, depending on the equivalent thermal conductivity k_e of the panel envelope and the center-of-panel thermal conductivity. In case of undamaged panels, the linear thermal transmittance measures 0.01 W/(mK) for metalized films and 0.04 W/(mK) for metal foils. Resulting from both degradation through time as well as thermal bridging of the panel edges, an equivalent thermal conductivity k_{eq} is generally used of 0.008 W/(mK), twice the center-of-panel thermal conductivity under pristine conditions.

Limitations of installation are due to the panel envelope which serves to maintain the inner vacuum of the panel, as this envelope may not be damaged. Vacuum insulation panels cannot be cut on-site into the required form, and much attention goes into the careful placing of the panels during construction and protection of the panels against mechanical damage during service life. When the vacuum is not maintained due to damage of the panel envelope, the thermal conductivity k increases to that of the core material under standard pressure conditions, i.e., 0.020 W/(mK) for a fumed silica core.

Areas of application

Vacuum insulation panels have already been introduced to the market in large-scale production, but manufacturing is still mainly hand-labor. In recent years, several building applications for VIPs have been proposed and/or tested, and a large-scale study has been carried out on the possibilities of vacuum insulation panels in insulated building envelopes. The main

building applications may be divided into several groups, i.e., for building envelope retrofitting, as main building envelope insulator, in sandwich elements, and in domestic appliances.

Retrofit insulation of the existing building envelope is an obvious application of vacuum insulation panels as this is the domain where its main advantage has most value, i.e., its highly limited thickness. As installing additional insulation on the inside results in a great loss of floor space, vacuum insulation panels are of great interest for renovations. However, special attention has to be paid to low surface temperatures and possible condensation damage at connections to surrounding compounds.

The use of vacuum insulation panels as main building envelope insulation for new buildings differs from retrofit solutions as the thickness is of less importance, i.e., the structure can be adapted for thicker insulation layers without loss of space. In such applications, it is always studied whether or not the complete envelope building components should be pre-assembled in advance, to ensure the proper handling of the vacuum insulation panels. As such, sandwich elements applying vacuum insulation panels as vacuum insulated sandwich elements in door frames, window frames, curtain walls (see Fig. 9.4) and in non-load bearing walls form a major part of this application.

Thermal insulation of household appliances, such as pipe insulation, insulation of thermal storage tank, insulation for underfloor heating, but also refrigerators form a last area of application. The strong reduction in required thickness is the main benefit with these cases, where the restriction of possible envelope damage forms a lower risk due to the possible protection of the panels.

9.5 Future trends

For further development and application of high performance thermal insulators based on nanotechnology, further progress is required in two domains: product and application development of the current products toward more durable solutions, and further exploitation of the (theoretical) physics of inhibited heat transfer, including radiation and solid conduction.

The reduced thermal conductivity k in the Knudsen regime is exploited in the nanoporous thermal insulators based on its $f(\Lambda)$ as well as in partial vacuum thermal insulators based on their reduced p. Neither silica aerogels nor vacuum insulation panels, however, form a durable solution for high performance thermal insulators (based on the Knudsen effect) due to their drawbacks, i.e., the very low pristine thermal conductivity k of 0.004 W/(mK) of vacuum insulation panels must be weighed against their strong aging through time and limited application possibilities, whereas the combination of a rather low thermal conductivity k of 0.014 W/(mK) with

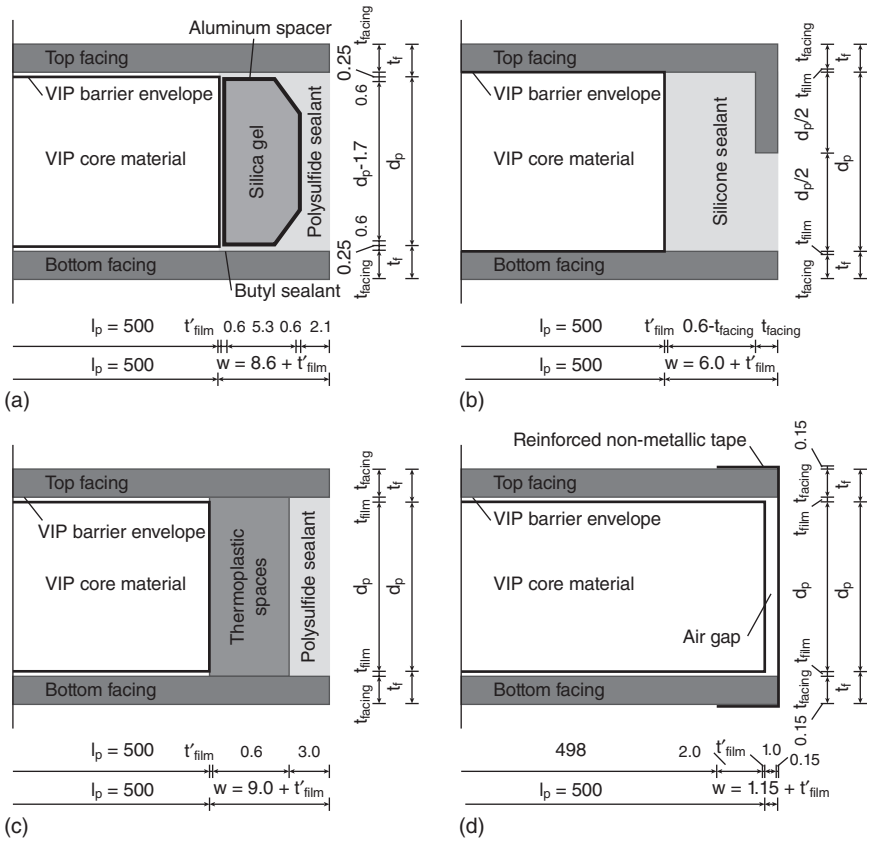

9.4 Four edge spacer construction types for vacuum insulated sandwich elements: (a) aluminum spacer of double glazing, (b) folded edge construction, (c) thermoplastic spacer and (d) reinforced non-metallic tape (Tenpierik *et al.*, 2008).

a possible high solar and visible transmittance of silica aerogels must be weighed against their fragile, brittle nature.

Aerogel insulation and vacuum insulation panels are today's best high performance thermal insulators. However, whereas traditional thermal insulators are 'cheap' and available in bulk, their specific properties and drawbacks compared to traditional thermal insulators require a shift in the way thermal insulators are applied in constructions.

A proper best practice of vacuum insulation panels in new constructions requires a shift of application toward prefabricated constructions, i.e., where the complete building process can be carried out under controlled circumstances, and to sandwich elements for curtain walls. Proper detailing of these constructions protects the panels from puncture during the period of

use and may also slow down aging of the panels. Also aerogels require protection due to their intrinsic vulnerability, i.e., low tensile strength. At material level this is solved by fibrous reinforcement in aerogel blankets, but this increases the effective thermal conductivity and results in non-translucent aerogel solutions. Also here, a proper best practice for aerogel insulation in new constructions requires a shift of application toward pre-fabricated construction elements, i.e., window fabrication, sandwich elements or as core material of vacuum insulation panels. Finally, due to their very low thermal conductivity k and as they are generally applied in thin layers, thermal bridging in constructions insulated with aerogel or vacuum insulation panels becomes more important.

Besides using current state-of-the-art thermal insulators the best possible way, one can envision the development of a thermal insulator combining the positive properties of aerogels and vacuum insulation panels but solving their specific drawbacks.

The basic required material properties could be stated based on the properties of the known nanoporous thermal insulators and the partial vacuum thermal insulators. First, a pore size distribution $f(\Lambda)$ completely below the mean free path of air at ambient conditions, i.e., 70 nm, which can be achieved based on aerogel synthesis technology. Secondly, an inner vacuum is desired without the need for a material envelope. As such, the thermal conductivity k of the material can be reduced further to the solid and radiative conductivity of 0.004 W/(mK) without the restriction of not being able to cut the material on site and without possible damage by puncture. This could be achieved by a closed porous structure instead of the classic open porous structure. However, the open porous solid structure is required in current vacuum insulation panels to enable a vacuum inside the material. As such, the vacuum pore structure must be created during the synthesis process of the material. One way to accomplish this is to envision a solid state material blowing itself up from within during the formation and subsequent expansion of an inner pore structure, or to create a grid structure which will efficiently and completely absorb the pore gas molecules, e.g., by a chemical reaction process.

9.6 References

Alam, M., Singh, H., & Limbachiya, M. C. (2011). Vacuum insulation panels (VIPs) for building construction industry – a review of the contemporary developments and future directions. *Applied Energy*, 88(11), 3592–3600.

Baetens, R., Jelle, B. P., Thue, J. V., Tenpierik, M. J., Grynning, S., Uvsløkk, S., & Gustavsen, A. (2010a). Vacuum insulation panels for building applications: a review and beyond. *Energy and Buildings*, 42(2), 147–172.

Baetens, R., Jelle, B. P., Gustavsen, A., & Roels, S. (2010b). Long-term thermal performance of vacuum insulation panels by dynamic climate simulations. In D.

Gawin & T. Kisilewicz (eds), *1st Central European Symp. on Building Physics*. Cracow, September 13–15, pp. A7–13.
Baetens, R., Jelle, B. P., & Gustavsen, A. (2011). Aerogel insulation for building applications: a state-of-the-art review. *Energy and Buildings*, 43(3), 761–769.
Boltzmann, L. (1884). Ableitung des Stefan'schen Gesetzes, betreffend die Abhängigkeit der Wärmestrahlung von der Temperatur aus der electromagnetischen Lichttheori.e., *Annalen der Physik und Chemie*, 22, 291–294.
Brinker, C. J., & Scherer, C. W. (1990). *Sol-Gel Science: The Physics and Chemistry of Sol-Gel Processing*. Los Angeles, CA: Academic Press.
Chandrasekhar, S. (1960). *Radiative Transfer*. New York: Dover Books.
Close, P. D. (1947). *Thermal Insulation of Buildings*. New York: Reinhold.
Dorchech, A. S., & Abbasi, H. (2008). Silica aerogel: synthesis, properties and characterization. *Journal of Materials Processing Technology*, 199, 10–26.
Haereid, S., Nilsen, F., & Einarsund, M. A. (1996). Properties of silica aerogel aged in TEOS. *Journal of Non-Crystalline Solids*, 204, 228–234.
Hüsing, N., & Schubert, U. (1998). Aerogels – airy materials: chemistry, structure and properties. *Angewandte Chemie International Edition*, 37(2), 22–45.
Jelle, B. P. (2011). Traditional, state-of-the-art and future thermal building insulation materials and solutions – Properties, requirements and possibilities. *Energy and Buildings*, 43, 2549–2563.
Jelle, B. P., Gustavsen, A., & Baetens, R. (2010). The path to the high performance thermal building insulation materials and solutions of tomorrow. *Journal of Building Physics*, 34(2), 99–123.
Jester, T. C. (1995). *Twentieth Century Building Materials*. New York: McGraw-Hill.
Kennard, E. H. (1938). *Kinetic Theory of Gases, with an Introduction to Statistical Mechanics*. New York: McGraw-Hill.
Kistler, S. S. (1931). Coherent expanded aerogels and jellies. *Nature*, 127, 741.
Kistler, S. S. (1932). Coherent expanded aerogels. *Journal of Physical Chemistry*, 32, 56.
Merget, R., Bauer, T., Küpper, H., Philippou, S., Bauer, H., Breitstadt, R., & Bruening, T. (2002). Health hazards due to the inhalation of amorphous silica. *Archives of Toxicology*, 75, 625–634.
Richter, K. (1995). Aerogels: applications, structure and heat transfer phenomena. *Annual Review on Heat Transfer*, 6, 61–114.
Srivastava, G. P. (1990). *The Physics of Phonons*. New York: Adam Hilger.
Tenpierik, M. J., & Cauberg, H. (2007). Analytical models for calculating thermal bridge effects caused by thin high barrier envelopes around vacuum insulation panels. *Journal of Building Physics*, 30(3), 185–215.
Tenpierik, M. J., van Der Spoel, W., & Cauberg, J. J. M. (2008). Analytical models for calculating thermal bridge effects in high performance building enclosure. *Journal of Building Physics*, 31, 361–388.
Volz, S. (2007). *Microscale and Nanoscale Heat Transfer*. Berlin: Springer.
Wang, X., Walliman, N., Ogden, R., & Kendrick, C. (2007). VIP and their applications in buildings: a review. *Construction Materials*, 160, 145–153.
Warheit, D. (2001). Inhaled amorphous silica particles: what do we know about their toxicological profiles? *Journal of Environmental Toxicology and Oncology*, 20, 133–141.

10

Silica nanogel for energy-efficient windows

C. BURATTI and E. MORETTI, University of Perugia, Italy

DOI: 10.1533/9780857098832.2.207

Abstract: This chapter discusses the utilization of silica nanogel to develop high energy-efficient windows and skylights. Silica aerogels are firstly discussed in terms of chemical structure, production process, and physical, mechanical, and thermal properties. The chapter then reviews their current applications in buildings as thermal and acoustic insulation materials. Finally, the potential of the nanogel windows for energy saving in buildings and the main future research trends are discussed.

Key words: silica aerogel, nanogel windows, highly energy-efficient windows.

10.1 Introduction

The global share of buildings in energy consumption has progressively increased, reaching a value of about 40% in developed countries. Because of the increasing demand for building services and comfort levels, the upward trend in energy consumption is expected to continue in the future (Pérez-Lombard *et al.*, 2008), above all in emerging economy nations (Southeast Asia, Middle East, South America and Africa). Energy policies at regional, national, and international level have therefore made energy saving one of the main objectives in residential and non-residential buildings (offices, public buildings, etc.), as shown by the recent directives of the European Parliament on building energy performance (European Parliament and the Council of the European Union, 2002). Moreover, according to data contained in a Pike Research report (2011), the total market for energy efficiency in buildings is rapidly increasing: from an estimated value of $67.9 billion in 2011, it is expected to pass $103.5 billion by 2017. In a building, the main total energy losses (up to 60%) can depend on the windows (Jelle *et al.*, 2012).

Windows have a double role in the building thermal envelope (Zanetti Freire *et al.*, 2011):

- thermal transmission properties have to be as low as possible in order to reduce energy consumption for heating and air conditioning;
- light transmission characteristics have to be as high as possible for visual comfort and electric energy saving in illuminating plants, thanks to natural lighting.

Moreover, windows should guarantee natural ventilation, above all in residential buildings. Finally, they have to also assure adequate acoustic insulation (Oral *et al.*, 2004). Highly energy-efficient windows such as nanogel windows (with silica aerogels in the interspace) could satisfy both these requirements, due to their high thermal insulation coefficient (thermal conductivity of silica aerogel is as low as 0.010 W/mK) and high light transmittance. A state-of-the-art market review of the best performing windows (AbuBakr *et al.*, 2008; Jelle *et al.*, 2012) showed that research has focused on lower thermal transmittance values of less than 0.5 W/(m^2K). Vacuum glazings, smart windows, solar cell glazing, electrochromic windows and finally aerogel windows were considered and investigated as the best solutions.

Aerogel windows, for which one of the lowest centre of glass U-values was found (0.30 W/m^2 K), seem to have the greatest potential for improving the thermal performance, daylight, and solar properties in the windows sector. Aerogel is a highly porous nanostructured and light material, with many particular properties that attracted the attention of researchers in various areas of science and technology, and also for building applications. The term 'aerogel' was first introduced over 80 years ago, marking gels in which the liquid was replaced with a gas, without collapsing the solid network of the gel (Kistler, 1931). Afterwards, the chemical composition of the material and the applications were progressively diversified, but a great part of applications was focused on the development of high-performance thermal insulation materials. The most promising applications in buildings involved granular translucent aerogels and transparent monolithic silica aerogels (Baetens *et al.*, 2011). Transparent monolithic panes were developed by a Swedish company in the 1990s, but advanced glazing systems with monolithic aerogel in the interspace are not yet used in mass production (Duer and Svendsen, 1998; Jensen *et al.*, 2004; Schultz and Jensen, 2008).

At the same time, granular translucent aerogels with an acceptable transparency were manufactured and, starting from 2005, many daylighting systems (polycarbonate panels, structural panels for continuous façades, insulated glasses) with translucent granular aerogel in the interspace appeared on the market (Rigacci *et al.*, 2004), offering excellent thermal performance, high quality of the diffused light, a good solar heat gain, and good sound insulation characteristics (Reim *et al.*, 2005). Nowadays, especially in the last two decades, the production of aerogels is localized in Europe (Sweden, Germany), USA, Japan, and Russia. This chapter investigates the utilization of silica aerogel in the interspace of highly energy-efficient windows. The production process of silica aerogels and the main physical, mechanical, and thermal properties are discussed first. Then, the current building applications of aerogels as thermal and acoustic transparent insulation material (TIM) in windows are discussed in more detail and

the performance of nanogel windows is underlined and compared with conventional glazing solutions. Finally, the main future research trends are discussed.

10.2 Aerogels for windows

Aerogels have a large number of applications and they differ from each other if the raw material is considered. They can be classified into:

- inorganic (silica-based and non-silicate aerogels);
- organic (natural and synthetic);
- composite (polymer crosslinked);
- exotic (based on metal chalcogenide).

For the purposes of the present chapter, inorganic silica-based aerogels will be considered, which are the most common as transparent insulating materials (TIM), both in the form monolithic and granular materials.

10.2.1 Synthesis and production of silica aerogels

Aerogels are light and transparent solid materials obtained from a gel by replacing the pore liquids with air and maintaining the network structure as it is in the gel state. Silica aerogels are manufactured by means of different processes; all them involve three general steps (Pierre and Pajonk, 2002; Dorcheh and Abbasi, 2008; Baetens *et al.*, 2011):

Gel preparation (sol-gel process)

The raw materials for the aerogel production are solid particles. In particular, silicon alkoxides are often used, such as tetramethoxysilane (TMOS, $Si(OCH_3)_4$), tetraethoxysilane (TEOS, $Si(OC_2H_5)_{4)}$, and polyethoxydisiloxane (PEDS-P_x, $SiO_n(OC_2H_5)_{4-2n}$). They are dispersed in a liquid where the solid nanoparticles collide and form a solid three-dimensional network, which can extend through the liquid (silica sols). Acidic or basic catalysts are usually added in the process. The gels are usually classified according to the dispersion medium used, e.g., hydrogel, alcogel and aerogel (for water, alcohol, and air, respectively). The following reaction may describe the synthesis of silica aerogels for insulation purposes (when the precursor is tetramethoxysilane, $Si(OCH_3)_4$):

$$Si(OCH_3)_4 + 2H_2O \leftrightarrow SIO_2 + 4CH_3OH \qquad [10.1]$$

The material resulting from the process is a cross-linked structure (Fig. 10.1) of silicon dioxide (SiO_2) chains (0.2–15% in volume, depending on the manufacturing method) with a large number of air-filled pores.

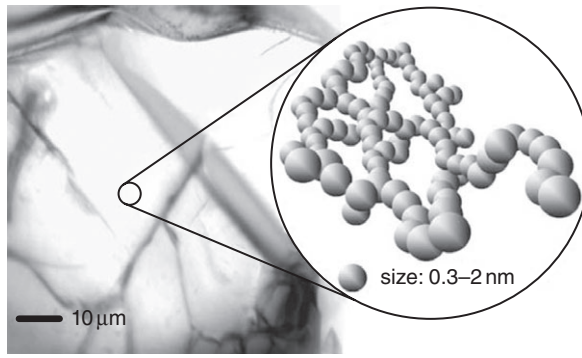

10.1 Structure of the nanoporous SiO_2 network of silica aerogel (Reim *et al.*, 2005).

Gel ageing

The gels are usually aged before drying, in order to increase stiffness and strength and to mechanically reinforce the tenuous solid skeleton generated during the sol-gel process. Different ageing techniques can be used. They are based on modifying the composition of the liquid phase contained in the pores by adding water and/or monomeric alkoxylanes. In fact, a significant number of the alcoxides contained in the liquid could be unreacted. The addition of these substances can enhance the surface reactions and allow supplementary condensation and re-precipitation of silica on the skeleton. The mechanisms operating during the ageing phase are the neck growth from reprecipitation of silica dissolved from particle surface onto necks between particles, and the dissolution of smaller particles and precipitation onto larger ones. The consequence is generally an increasing of the average pore size and of the apparent density of the gel. After ageing, the water still within the pores must be removed, by washing the gel with ethanol and heptanes. If water remains in the pores, it will not be removed with supercritical drying, therefore it will lead to an opaque and very dense gel.

Gel drying

Aerogels are the solid framework of the sol-gel isolated from liquid by means of the drying phase; it is the most critical step of the process, because it is governed by the capillary pressure which can cause fractures or collapse in the structure. Two different methods are usually used: ambient pressure drying (APD) and supercritical drying (SCD), where the capillary tension can be avoided by removing the liquid above the critical temperature and pressure. APD is generally carried out in two steps:

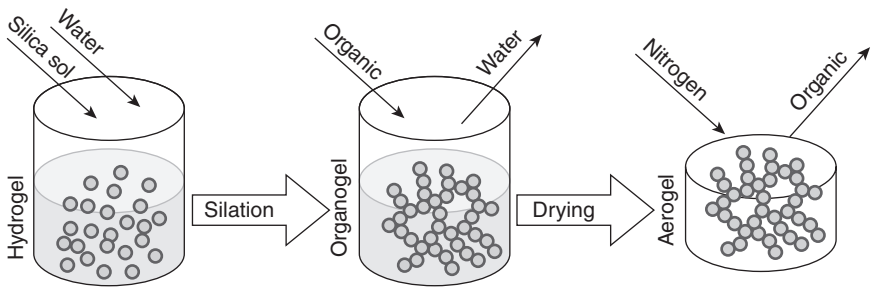

10.2 Manufacturing process of Cabot's aerogel (nanogel®).

- Firstly, the solvent is replaced with a water-free solvent and a silylating agent, so that the OH groups are silylated.
- Evaporation at ambient pressure is made in three steps: a warming period; a first drying period in which water moves to the external surface by capillary forces; a second drying period dominated by a diffusive vapour transport that allows liquid to escape slowly to the exterior.

SCD can be carried out by one of two methods:

- Light temperature supercritical drying (HTSCD), which occurs in three steps (the autoclave, half-filled with the aged gel, is sealed and heated slowly past the critical temperature and pressure, then it is isothermally depressurized, and finally, at ambient pressure, it is cooled to room temperature).
- Low temperature supercritical drying (LTSCD), similar to HTSCD and also carried out in three steps (the aged gel is placed in an autoclave and filled with CO_2 at 4–10°C and 100 bar, to replace the solvent in the pores, and it is heated to 40°C maintaining 100 bar; then it is isothermally depressurized and finally, at ambient pressure, it is cooled at room temperature).

For building applications, monolithic aerogels are manufactured with a LTSCD process. The APD process was nevertheless studied (Kim and Hyum, 2003) in order to lower the production costs and it is today the most promising technique. The production process of the commercial translucent granular aerogel, nanogel®, manufactured by Cabot Corporation (the main manufacturer of granular translucent aerogels), is schematized in Fig. 10.2. A water-based silica solution is destabilized and a gel is created (hydrogel); then, in the silation phase, an organic solvent replaces the water in the formulation. Finally, the solvent is removed by a drying process under ambient conditions. The innovative manufacturing process developed by Cabot allows production on a large scale, overcoming the problems that occur in the supercritical drying method, and it also allows careful control

of the material's properties, such as porosity (>90% air) and pores size (Aegerter *et al.*, 2011). A more detailed analysis of the synthesis process and of the recent developments can be found in the literature (Dorcheh and Abbasi, 2008; Aegerter *et al.*, 2011).

10.2.2 Physical, mechanical, and thermal properties of silica aerogels

The final physical, optical, and thermal properties of silica aerogels depend on both the starting silica source (TEOS, TMOS, PEDS-Px) and the process methodology, in particular on the catalyst and solvent used (Tajiri and Igarashi, 1998; Pajonk, 2003; Anderson *et al.*, 2009). Aerogels have unusual properties as solid materials, due to their structure. Furthermore, the physical, mechanical, and thermal characteristics can vary over a wide range, depending on the synthesis process.

Physical properties

Silica aerogels are amorphous materials; the skeleton density is about 2200 kg/m^3, but the material is extremely light (the bulk density is in the 50–200 kg/m^3 range), due to the very high porosity (the pore volume is above 90% of the total volume). The pore size is typically in the 5–100 nm range. Current aerogels for building applications have an overall density of 70–150 kg/m^3. The acoustic properties are very interesting: the acoustic propagation through aerogels depends on the nature and pressure of the interstitial gas, on the aerogel density, and more on the texture (Forest *et al.*, 1998), but the speed of sound in silica aerogels is lower than in air (down to about 40 m/s through monolithic aerogels and to about 100 m/s through granular ones). They can also improve the sound insulation in windows (see Section 10.4). The optical and scattering properties are discussed in the next paragraphs.

Mechanical properties

Aerogels are very fragile materials: the tensile strength is negligible, the compressive strength and the elastic modulus are very low, and they depend on the network connectivity and density. The compressive strength is in the 1–2 MPa range (Parmenter and Milstein, 1998; Luo *et al.*, 2006). The Young's modulus (E) is a function of the apparent density. It varies in the 10^{-3}–10 GPa range, when the apparent density varies in the 10^2–2×10^3 kg/m^3 (Woignier *et al.*, 1988; Hegde and Venkateswara Rao, 2007; Parmenter and Milstein, 1998); in Aegerter *et al.* (2011) an E value in the 2.7–8.6 MPa range was found, when the density is about 150–200 kg/m^3. The shear modulus G is in

the range 5–40 MPa when the density is in the 150–400 kg/m^3 range (Gross *et al.*, 1988; Pierre and Pajonk, 2002).

Moreover, contact with water must be avoided for monolithic aerogels: in commercial applications, aerogels may be used in vacuum conditions, with evident advantages in terms of thermal insulation. Nevertheless, the commercial granular aerogels (Cabot) are hydrophobic.

Thermal properties

Aerogel has the lowest thermal conductivity λ among solid materials: even if λ of the silica skeleton structure is relatively high (in the 1.3–1.4 W/mK range), the overall value is very low because of the high porosity, the low gas conductivity and the low radiative transmission in the infrared range up to a temperature of 200°C. Gas conduction in a porous media depends on the gas pressure and on the pore size (Baetens *et al.*, 2011), and it can be further reduced by decreasing the maximum pore size, by filling the aerogel with a low-conductive gas or by applying a vacuum: with a pressure of 50 mbar, the thermal conductivity can be reduced to 0.008 W/(mK). Commercially available aerogels for building purposes have a thermal conductivity between 0.013 and 0.018 W/(mK) at ambient temperature; moreover, the value is nearly constant up to a temperature of 200°C (Aspen Aerogels, Cabot Corporation, 2012).

Other properties

When considering safety, the material is not carcinogenic, non-flammable and non-reactive (Merget *et al.*, 2002).

10.3 Current applications of aerogels in buildings

Several applications of silica aerogels are reported in the literature (Pierre and Pajonk, 2002; Akimov, 2003; Aegerter *et al.*, 2011; Baetens *et al.*, 2011): microelectronics; electrical engineering; acoustics; oil and gas pipeline insulation, and space exploration (aerogel is in fact used as thermal insulation material in US spacecraft). Furthermore, of interest to us here are the building applications, as thermal and acoustic insulation material are nowadays the most considered.

In 2008, the share of aerogel technologies in the global insulation products market was about 0.3% ($83 million for aerogels products out of a total volume of $29 billion), but with the annual rate increasing at about 50% per annum (whereas the annual growth rate for conventional insulation products is only 5%), and the market volume is expected to reach 646 M$ by 2013. Silica aerogels are an innovative alternative to traditional insulation materials due to their thermal performance, although their costs are

still high for cost-sensitive industries such as the building one. In this field, opaque and transparent or translucent aerogels have been developed (Baetens *et al.*, 2011). In the translucent and monolithic form, they have interesting optical properties, such as high light and solar transmittance and excellent thermal insulation properties, when compared with conventional glass. Therefore they are used as transparent walls in solar collectors and in office buildings (Ackerman *et al.*, 2001; Reim *et al.*, 2002).

The opaque aerogels are flexible blankets obtained by adding fibres in the gel before the drying process (Cabot Corporation, Boston, MA, USA; Aspen Aerogels Inc., Northborough, MA, USA), in order to reduce their fragility. The thermal conductivity is about 0.13 W/(mK), but their cost is about 10 times higher than a conventional material with similar performance. Nanostructured materials as aerogels could be suitably employed in highly insulating windows and in the last 15 years windows based on translucent granular or monolithic aerogels were developed by companies in cooperation with researchers. Monolithic aerogel panes appear as a very transparent and lightweight material (Fig. 10.3), but they have a tendency to scatter the transmitted light, resulting in a hazy picture when objects are viewed through them.

Twenty years ago, thanks to the International Energy Agency Solar Heating and Cooling Programme, Task 18-Advanced Glazings and Associated Materials for Solar and Building Applications (Duer and Svendsen, 1998), several countries (Denmark, Finland, France, Germany, Japan, Norway, Sweden, United Kingdom) were involved in a project to develop and set up superinsulating glazings with monolithic aerogel. Five different samples were realized, characterized by different density, thickness and transparency: the light transmittance was in the 0.75–0.96 range. Depending

10.3 View through a monolithic aerogel sample (sample supplied by AIRGLASS, Sweden, 2010) (Buratti and Moretti, 2012b).

on the density of the sample, the measured thermal conductivity was in the 0.015–0.017 W/(mK) range and it decreased to 0.009–0.011 W/(mK) in evacuated conditions. Moreover, a first prototype of an evacuated double glazed window with aerogel in the interspace was manufactured in the 1990s (500 × 500 × 28 mm^3). A 20 mm thick aerogel pane was inserted between two glasses, sealing the sheet units and evacuating the interspace with the aerogel pane to a level below 5000 Pa. As expected, the same scattering of light was found in the aerogel glazings as in the aerogel samples, but excellent thermal performance was found and the thermal transmittance reached a value less than 0.5 W/(m^2K).

The very good results encouraged the research towards superinsulating clear windows with aerogel and within the European projects HILIT (Highly insulating and light transmitting aerogel glazing for window, EU Non-Nuclear Energy Programme JOULE III, Contract no. JOR3-CT97-0187, 1998–2001) and HILIT+ (Highly insulating and light transmitting aerogel glazing for super insulating windows, EU Energy, Environment and Sustainable Development Programme, Contract no. ENK6-CT-2002-00648, 2002–2005) transparent and insulating plane monolithic silica aerogel tiles (thickness of about 15 ± 1 mm) were manufactured at a pilot-scale since 2004, in collaboration with the Swedish company AIRGLASS (Jensen *et al.*, 2004). Several prototypes were made, following the optimized aerogel manufacturing process developed during the project (Fig. 10.4). A rim seal

10.4 An aerogel window manufactured by joining four optimized aerogel tile prototypes in a test frame (Jensen *et al.*, 2004).

was made, with the required barrier properties against atmospheric air and water vapour, in order to achieve a low thermal bridge effect and to ensure a theoretical lifetime of the glazing of about 30 years. The final assembly and evacuation process was set up and a final pressure in the aerogel of 500 Pa was reached. The solar and daylight transmittance of the aerogel glazing were optimized by means of low-iron glass covers, with an antireflection coating. The optical quality had a minimal disturbance in the view through, except if exposed to direct non-perpendicular radiation, when the diffusion of the light becomes significant. The centre U-value, measured by means of a hot-plate apparatus, was equal to 0.66 W/(m^2K), which corresponds to an estimated thermal conductivity of 0.010 W/(mK) for the aerogel pane (average aerogel thickness 14.8 mm) (Schultz *et al.*, 2005).

Granular silica aerogels were also investigated, in order to integrate them into highly-insulating translucent glazing (Reim *et al.*, 2002; 2004). Within the R&D project ISOTEG pursued by the ZAE Bayern (Bayerisches Zentrum für Angewandte Energieforschung, Germany), a daylighting system was developed by inserting aerogel granules between a double skin sheet made of polymethyl-methacrylate (PMMA). Two types of granular aerogel were used in prototype windows: semi-transparent, consisting of rather regular spheres, and highly translucent granulates, consisting of irregularly fractured spheres (Fig. 10.5). The optical properties (transmittance and reflectance) of the aerogel granulates between two highly transparent glass panes, for a 10 mm packed bed, were measured with an integrating sphere arrangement in the 400–2000 nm wavelength range. Scattering at structural inhomogeneities causes the decreasing of transmission with decreasing wavelengths below 600 nm (Fig. 10.6) and the investigated fractured aerogel samples show a higher transmittance than the more regular ones, both in the visible and solar range (see Section 10.4 for more details).

Different daylighting systems in PMMA were manufactured with a thickness less than 50 mm: in order to optimize the thermal insulation, the sheet was mounted between two low-e coated glass panes (emissivity equal to 0.03 or 0.08) and argon or krypton were used as filling gases (Fig. 10.7).

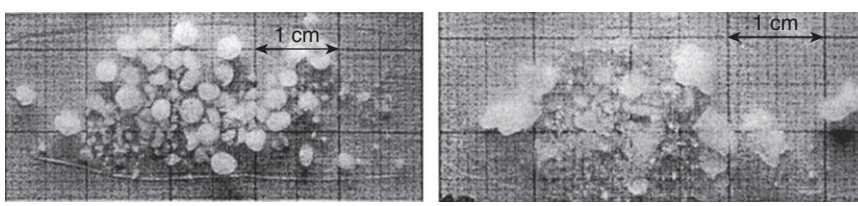

10.5 Granular aerogels: semi-transparent, consisting of regular aerogel granules (left) and highly translucent granulates, consisting of fractured aerogel pieces (right) (Reim *et al.*, 2002).

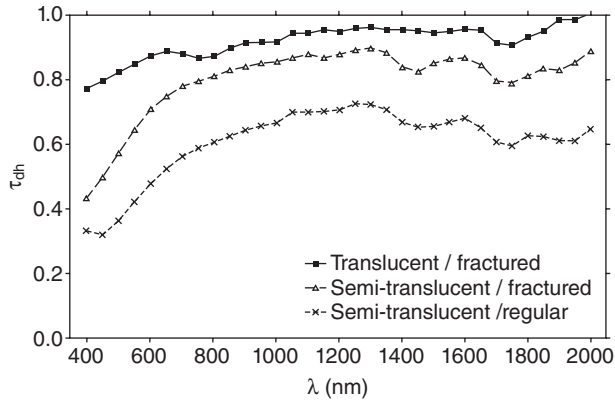

10.6 Spectral (normal-hemispherical) transmittance of different silica aerogel layers (translucent/fractured, semi-translucent/regular and semitranslucent/fractured), 10 mm thickness (Reim *et al.*, 2002).

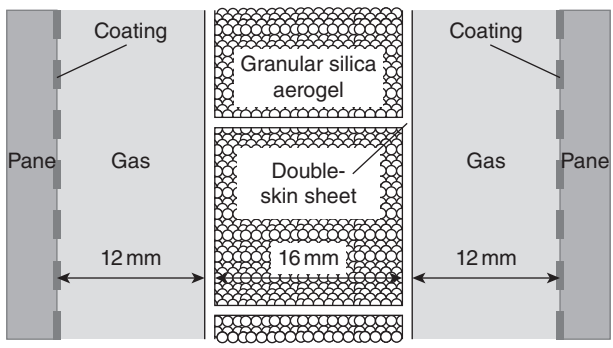

10.7 Granular aerogel window prototype consisting of two glass panes with low-e coating on the inside, two gas gaps and an aerogel-granulate filled PMMA double-skin sheet (Reim *et al.*, 2005).

Depending on the filling, the low-e coating emissivity and granular aerogel kind, an U-value in the 0.37–0.56 W/(m^{2}K) range and a total solar energy transmittance (solar factor, *g*) in the 17–45% range were obtained (Table 10.1, Reim *et al.*, 2005). The directional-hemispherical transmittance was in the 0.19–0.54 range if considering the visual properties.

Finally, for the German climate (Reim *et al.*, 2002), aerogel glazing mounted into a north-oriented façade shows the lowest thermal losses in the heating period if compared to a triple glazing window and to opaque insulation; in fact, the energetic balance of the aerogel glazing is significantly better than that of a triple glazing from 15 September to 15 April. Aerogel glazing offers the possibility to provide diffuse natural light inside

Table 10.1 Optical, thermal, and energy properties for daylighting systems developed with semi-translucent and highly translucent aerogel granulates (adapted from Reim *et al.*, 2005)

	Visual directional-hemispherical transmittance	Solar factor (*g*)	Centre U-value
Daylighting: glazing manufactured with two low-e glasses (emissivity equal to 0.08)	0.24 (semi-transparent) – 0.54 (translucent)	0.33 (semi-transparent) – 0.45 (translucent)	0.44 (90% krypton, 12 mm) – 0.56 (90% argon, 16 mm)
Sun control: glazing manufactured with two low-e glasses (emissivity equal to 0.03)	0.19 (semi-transparent) – 0.38 (translucent)	0.17 (semi-transparent) – 0.23 (translucent)	0.37 (90% krypton, 12 mm) – 0.47 (90% argon, 16 mm)

and, because of the low U-value, an inside surface temperature of the aerogel glazing equal to the inside air temperature, providing good thermal comfort conditions. During the project ISOTEG, a prototype of a new aerogel glazing with translucent granular aerogel (Reim *et al.*, 2005) was for the first time integrated into the façade of the ZAE (Bayerisches Zentrum für Angewandte Energieforschung) building in Wurzburg, Germany (2000).

At the moment, different commercial systems with translucent aerogels (polycarbonate panels, structural panels for continuous façades, insulated glasses) are available on the market, offering excellent thermal performance, a good solar heat gain and a good sound insulation, as described below. Aerogel glazing, together with vacuum glazing, new spacer materials and solutions, electrochromic windows, seem currently to have the largest potential in fenestration products (Jelle *et al.*, 2012).

One of the main manufacturers of opaque aerogels is Aspen Aerogels (USA). Cabot Corporation (USA) seems to be the main manufacturer of granular translucent aerogels and it has been producing its aerogel since 2003 at its plant in Frankfurt, Germany. The translucent product manufactured by Cabot, Lumira™ aerogel, formerly Nanogel® aerogel, gained wide acceptance across the USA and Europe for several kinds of highly insulated daylighting systems. The product is supplied to various partners in the USA and Europe, which developed different aerogel daylighting systems, such as: structural composite panels for skylights and façades, structural polycarbonate skylight systems, polycarbonate façade systems and U-channel glass (self-supporting systems of glass channels with an extruded metal perimeter frame). The Lumira™ aerogels are characterized by grain size in the

(a)

(b)

10.8 Application of Lumira™ aerogel in polycarbonate sheets, outer (a) and inner view (b) (courtesy of Roda, Germany).

0.5–3.5 mm range and the thermal conductivity is equal to about 0.018 W/(mK). EMB Products AG, Germany, developed an array of innovative façade systems with Lumira™ aerogel technology. A wide number of combinations is available for use in façades, separation walls and curtain walls; the thickness of the systems varies in the 10–50 mm range (Fig. 10.8).

Many daylighting systems with polycarbonate are proposed by TGP America, Advanced Glazings Ltd (Canada), and Xtralite (UK) (Dowson *et al.*, 2011). Glazing systems with nanogel are also developed by Okalux, Germany: the system okagel® consists of two glass layers filled with granular aerogel. The system is filled with granulate in a controlled and continuous process and the façade appears homogeneous and translucent; moreover, in order to avoid the settlement of the material during the service life of

the element, a hydrostatic stress state is applied to the material. Okagel can be used also in roof lights. The translucent material in the gap enables uniform lighting inside, avoiding glare problems, and exceptionally good thermal insulation, down to 0.3 W/(m^2K). An interesting example of the application of Okagel is the Halley VI research station in the Antarctic (temperatures of –60°C can be reached), where 72 m^2 Okagel façade elements with U-value of 0.3 W/m^2K were installed.

Finally, Nano High-tech Co. Ltd is the largest research and production company in China; it developed several aerogel products, including daylighting panels (TP), aerogel particles, and monoliths. Daylighting panels have a thermal conductivity equal to 0.025 W/mK and they can be used in large buildings such as theatres, airport terminals, exhibition centres, etc., both for daylighting and thermal insulation purposes. They are hydrophobic and the light transmittance is in the 40–70% range, depending on the panel thickness (10–30 mm). Further information about aerogel glazing systems (manufacturers and commercial products) is given in Table 10.2.

10.4 Performance of nanogel windows

The performance of innovative nanogel windows, when compared to conventional glazing systems, can be evaluated considering some important parameters:

- Light transmittance: the glazing system capacity to diffuse the natural light indoors is important since the natural light plays an active role in saving electric energy in the daytime and affects the general health of human beings; high values are required, in order to guarantee visual comfort and energy saving in lighting plants.
- Solar factor, *g*, and thermal transmittance, U-value influence the heat transferred through the glazing systems and the calculation of heating and cooling loads: low values are required, in order to guarantee thermal comfort and energy saving in HVAC plants.
- Sound reduction index, *R*, which influences the noise transmitted through the windows; high values are required in order to guarantee adequate acoustic comfort in buildings.

The optical transmission and the scattering properties of silica aerogels are widely discussed in the literature (Buratti, 2003; Jensen *et al.*, 2004; Reim *et al.*, 2005; Baetens *et al.*, 2011; Buratti and Moretti, 2011a, 2011b, 2012a, 2012b). Aerogels show very interesting optical properties for building applications and their transmittance is high in the whole solar spectrum, including the visible range, where it is similar to that of a 6 mm thick clear float glass. Values of the light transmittance τ_v equal to 0.78 and of the solar transmittance τ_e equal to 0.80 were found for an aerogel pane 14 mm thick;

Table 10.2 Nanogel window products: manufacturers and references

Manufacturer	Address/website	Products	Key properties	Image
Advanced Glazings Ltd	Sydney, NS, Canada, http://www.advancedglazings.com/nanogel	Insulated translucent glass units with Cabot nanogel® in interspace: Solera® + nanogel®	U = 0.31 W/m^{2}K (76.1 mm configuration)	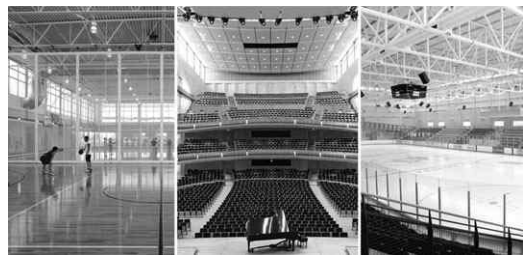
Airglass AB	Box 150, 245 22 Staffanstorp, Sweden, http://www.airglass.se/	Monolithic aerogel samples	Aerogel panes Density = 50–200 kg/m^3 λ = 0.010 W/(mK), in evacuated conditions	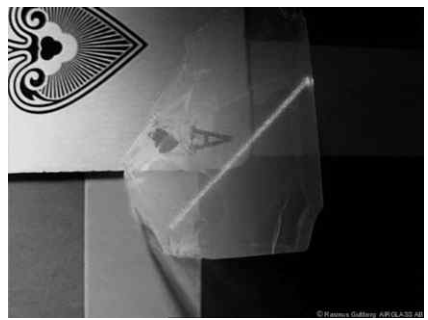

Table 10.2 Continued

Manufacturer	Address/website	Products	Key properties	Image
Cabot Corporation	USA: Cabot Aerogel, 157 Concord Road, Billerica, MA 01821, USA, http://www.cabot-corp.com/Aerogel Europe/Middle East/Africa, Interleuvenlaan, 15 i B-3001 Leuven Belgium	Lumira™ granular aerogel (previously called Nanogel® aerogel)	Hydrophobic granular aerogel produced as particles, λ = 0.018 W/(mK)	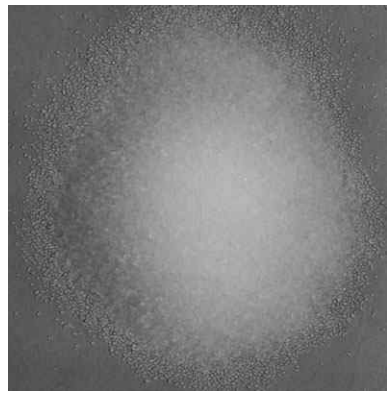
Kalwall Corporation	1111 Candia Road, PO Box 237, Manchester, NH, USA http://www.kalwall.com/aerogel.htm	Kalwall+ Nanogel® Translucent Daylighting Systems	U = 0.30 W/m^{2}K; light transmittance = 12–20% (total thickness = 70 mm)	

Nano High-Tech Co., Ltd	Chengdong Road Shanxi, 488, Shaoxing, Zhejiang 312000, China, http://www.nanuo.cn/english/product-3.htm	Daylighting panels (TP), aerogel particles (AP) and monoliths	For TP, $\lambda = 0.025$ W/(mK); light transmittance = 40% (30 mm)–70% (10 mm)	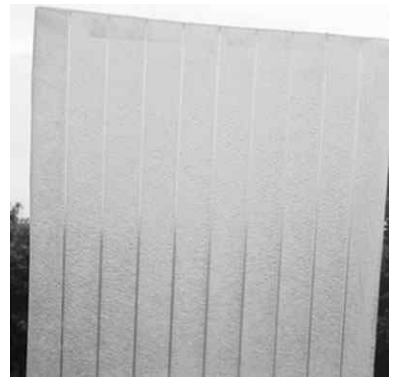
Okalux GmbH	Am Jöspershecklein 1 97828 Marktheidenfeld, Germany, http://www.okalux.com	Translucent façade elements filled with translucent granular aerogel (OKAGEL)	U = 0.30 (60 mm cavity)-0.6 (30 mm cavity) W/(m^2K) (4 mm thick low iron outer pane and 6 mm laminated low iron glass inner pane, 0.76 PVB foil).	

Table 10.2 Continued

Manufacturer	Address/website	Products	Key properties	Image
Roda	E.M.B. Products AG, Rudolf-Diesel-Straße 6,46446 Emmerich, Germany. http://www.roda.de/download_en_22.html	Daylight solutions in polycarbonate sheets with granular Lumira™ aerogel (thickness = 16–50 mm)	U = 0.48 (50 mm)–1.30 W/m^{2}K (16 mm); light transmittance = 20–64%	

Technical Glass Products	8107 Bracken Place SE, Snoqualmie, WA, USA, http://www.tgpamerica.com/structural-glass/pilkington-profilit/	Translucent linear channel glass systems Pilkington Profilit™ filled with Lumira™ aerogel.	U = 0.19 (low-e with 16 mm Lumira™)–0.21 W/m^{2}K (low-e with 25 mm Lumira™)	
Xtralite Rooflight	Spencer Road, Blyth Riverside Business Park, Blyth, Northumber land, NE24 STG.UK http://www.xtralite.co.uk/	Nanogel®-filled rooflights	U = 0.91 (25 mm thickness)–1.3 W/m^{2}K (16 mm)	

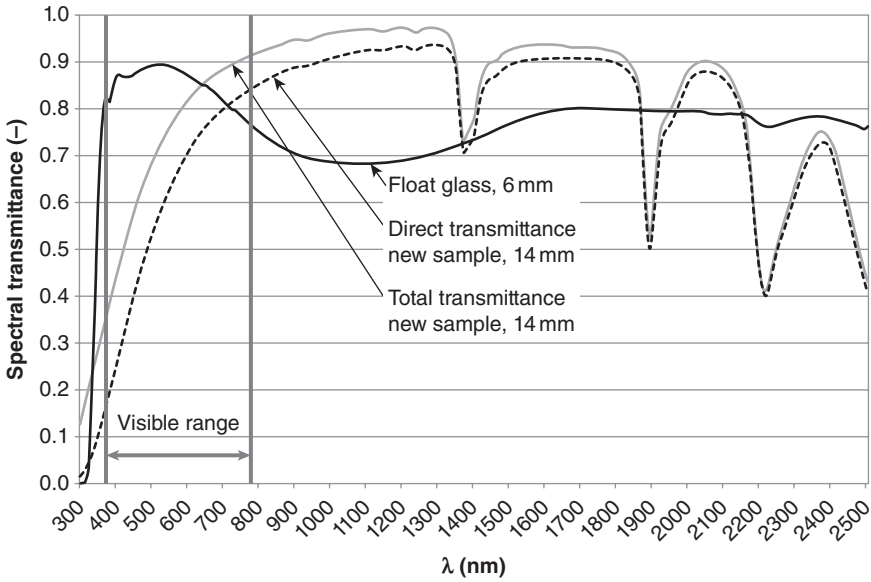

10.9 Aerogel pane transmission optical properties: direct and total solar spectral transmittance compared to a 6 mm thickness float glass (Buratti and Moretti, 2012b).

significant absorption bands in the NIR transmission spectrum are shown ($\lambda \cong 1350$ nm; $\lambda \cong 1900$ nm; $\lambda \cong 2200$ nm; $\lambda \cong 2500$ nm) (Fig. 10.9). Furthermore, if only direct and total transmittance are compared, it could be observed that a part of the radiation is scattered when transmitted through the material, according to the Rayleigh scattering theory (Fig. 10.9, Buratti and Moretti, 2012b). It causes reddening of the transmitted light, the bluish appearance of the reflected light and a possible blurred deformation of optical images (Duer and Svendsen, 1998). A decrease in the optical quality of the vision through the material is observed; nevertheless, this behaviour could be preferred in some situations, because the light penetrates very deeply in the room and it can reduce significantly glare problems in façade or skylight.

Using aerogel in clear windows can greatly affect the characteristics of the incoming light, modifying the colour appearance of surfaces and objects and contributing significantly to the comfort and visual satisfaction of human beings in indoor environments. The quality of the transmitted light can be usefully represented by the general colour rendering index R_a, which is calculated by applying the CIE standard procedure based on the differences in colour between eight test colours lighted directly by the reference illuminant D65 and by the same illuminant after the transmission through the glazing (EN 410, 2011); it is a normalized value in the 0–100 range. A

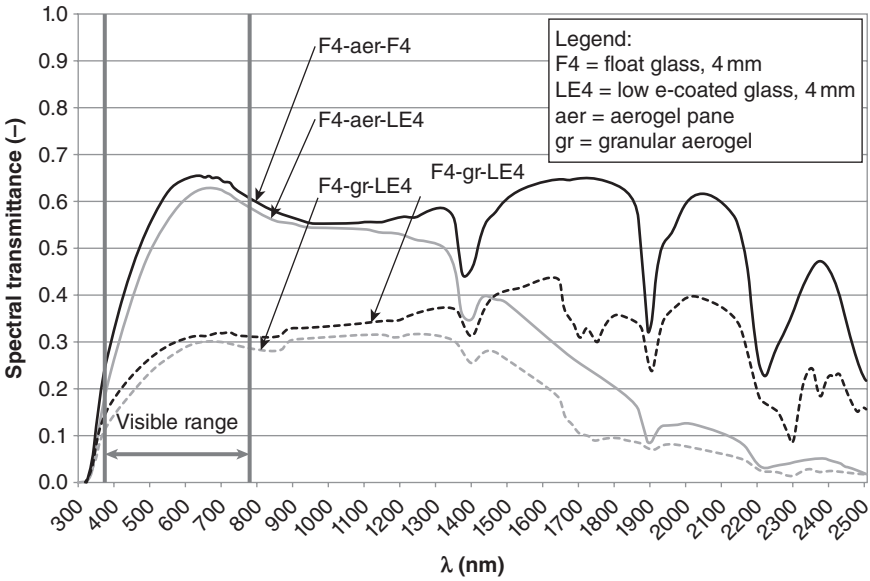

10.10 Spectral transmittance of different glazing samples with granular and monolithic aerogel in the interspace (Buratti and Moretti, 2012b).

value of 91 was found for 14 mm thickness aerogel panes, which is a good value if compared to the clear glass panes (R_a values of about 98). However, literature data (Buratti and Moretti, 2012b) showed a very good quality ($R_a > 90$) of the vision through the glazings with aerogel in the interspace: the colour rendering index is lower than those of the windows with air in the interspace ($R_a = 98$ with float glasses; $R_a = 94$ with one low-e glass), but it is equal to 93 for float glasses and granular aerogel (14 mm) and to 92 with monolithic aerogel. With low-e glasses, the R_a index reduces to 90–91.

As a final remark, the optical properties can be influenced furthermore by the production process, i.e. by selecting optimal synthesis parameters (Tajiri and Igarashi, 1998; Wagh *et al.*, 1999) and the transparency was improved in the last years.

Both monolithic and granular aerogels could be assembled in the interspace of different glasses or polycarbonates to give transparent glazings. Different transmission properties are found for glazing systems with monolithic and granular aerogel in the interspace (Fig. 10.10). Samples with float glasses have the same trend, but the spectral transmittance of the samples with granular aerogel is up to 50% lower than that of the monolithic, above all in the visible range. The curve trend is representative of aerogel behaviour, reproducing the selective absorption peaks. Samples with low-e glass show a different trend for wavelengths higher than 800 nm, due to the low-e

coating in the inner position. The solar transmittance, evaluated by means of the solar factor, is high for windows with monolithic translucent aerogels: the direct solar transmittance measured in the laboratory for a monolithic window prototype (15 mm aerogel) was higher than 75% (Jensen *et al.*, 2004) but, at the same time, the U-value was equal to the best triple-layered gas-filled glazing units ($U < 0.6$ W/m^{2}K). The net average energy balance on the window depends in fact on both the U-value and solar factor, in which case monolithic aerogel prototypes in evacuated conditions were better than the other highly insulating glazings (Fig. 10.11), especially in very cold climates such as in northern Europe: the improvements due to monolithic aerogel windows in a typical Danish single-family home were underlined by Schultz and Jensen (2008). A wide range of *g*-values can be found in the manufacturers' technical data for daylighting systems with granular translucent aerogels, depending on the external retaining layers (glasses, low-e glasses, PMMA, polycarbonate) and on the total thickness (see Tables 10.1 and 10.2).

Nanogel windows are excellent in the thermal insulation of buildings because of the very low thermal conductivity of transparent or translucent silica aerogel. As shown in Table 10.2, a wide range of U-values can be obtained for commercial products with translucent aerogels: the U-value can be as low as 0.48 W/(m^{2}K) for polycarbonate solutions (polycarbonate sheets with Lumira™ aerogel, thickness = 50 mm, RODA, Germany), whereas U-values in glass solutions can be about 0.20 W(m^{2}K) (translucent linear channel glass systems Pilkington Profilit™ filled with 25 mm Lumira™ aerogel, Technical Glass Products, USA). The energy consumptions with triple-layered argon-filled glazing and with aerogel glazing were

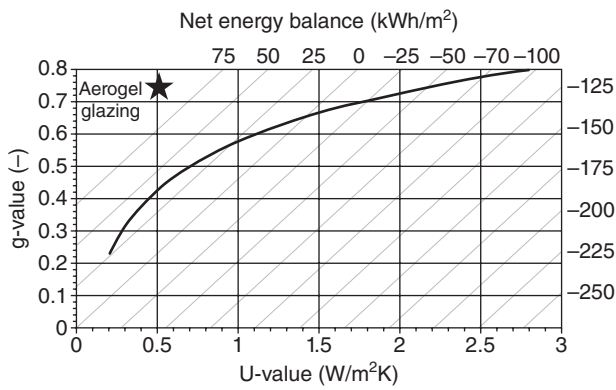

10.11 Energy balance (kWh/m^2) for window glazing as a function of U-value and solar factor. The curve represents the typical relationship for window glazing systems, the aerogel glazing position is shown by the star (Jelle *et al.*, 2012).

compared (Schultz and Jensen, 2008): the annual energy saving was about 1180 kWh/year (19%); in fact, in cold climates the increased heat insulation of triple glazing with respect to conventional double glazing can be thwarted by the *g* value decreasing (*g*-value is on the order of 0.4 for a argon-filled triple glazing). Considering a low-energy house, the savings become 700 kWh/year, which correspond to a 34% decrease in space heating demand.

Commercial applications with monolithic aerogels are not yet available, but U-values equal to 0.66 W/m^{2}K were measured for a prototype of an evacuated glazing with only 13.5 mm thick aerogel pane (see Section 10.3.2). Furthermore, translucent insulating materials in glazing can have a major advantage when they are used in roof applications: the U-values of glazing systems with adequate layers of translucent nanogel are not dependent on the inclination to the vertical, while the gas-filled glazing with air or gas (argon or krypton) have a worse behaviour than that expected when they are used in roofs. The U-value is in fact calculated or measured for a vertical position, according to the international standards, but when they are horizontal, the warm air meets the colder outer side more quickly when rising, so an accelerated flow arises. The thermal convection in the cavity becomes higher and the U-value can be more than 50% higher than that measured or calculated in the vertical, as shown in Fig. 10.12.

In order to characterize the acoustic properties of silica aerogels, the acoustic attenuation was measured according to the two-thickness method (Forest *et al.*, 2001) and it showed that the large granules of aerogels (mean

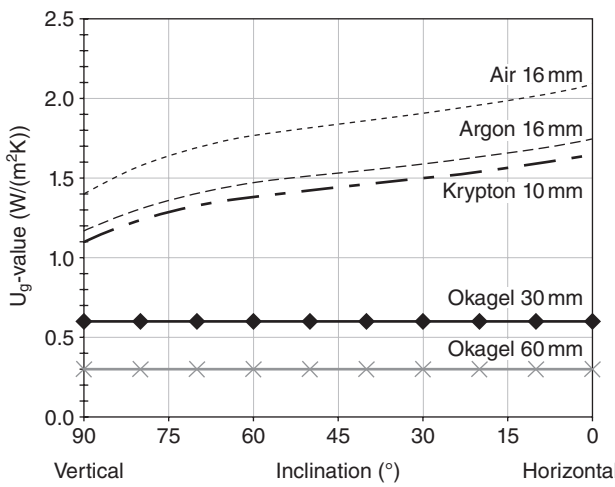

10.12 Dependence of U-value on the inclination for conventional glazing and glazing with translucent insulation materials (Okalux, 2012).

granule size: 3 mm) have a low attenuation (about 1 dB/cm), lower than that of a conventional insulating material, such as glass wool; nevertheless, in the small granules (mean granule size: about 80 μm) the attenuation values are in the 0–12 dB/cm range, depending on the frequency range: above 500 Hz, the values are higher than the glass wool ones (about 3 dB/cm). The efficiency of granular silica aerogels as sound insulators in the 100–2500 Hz frequency range was also demonstrated when they are used in multilayer (a fist layer (1 cm) made of large granules and the second one (3 cm) made of small granules): in the 300–1700 Hz range, the sound transmitted through the aerogel is 15 dB lower than that transmitted through glass wool with the same thickness.

Finally, the translucent insulating material in the interspace of glazing can improve the sound insulation of the building envelope, in comparison with systems with air, as shown in Buratti and Moretti (2012b). A prototype of an aluminium frame window with granular aerogel glazing was produced and tested: aerogel in granular form was put in a gap 15 mm in depth; indoor and outdoor layers were float glasses of 4 mm thickness (Fig. 10.13). Both the thermal and acoustic performance in the building façades of the window prototype were evaluated in terms of measured U-value (hot box method,

(a) (b)

10.13 Setting-up of the aerogel glazing system with nanogel® (a) and window prototype during the laboratory test (b) (Buratti and Moretti, 2012a).

ISO 12567-1) and sound reduction index (R, EN ISO 10140-2) and they were compared with conventional glazing with air interspace (same thickness). A U-value of 0.99 W/m^{2}K was found for the glazing with granular aerogel in the interspace. Furthermore, the presence of granular aerogel increases the sound reduction index values (Fig. 10.14) in all the frequency ranges (100–500 Hz), but above all in the central range (500–2000 Hz). Moreover, a weighted sound insulation index R_w (EN ISO 717-1, 2007) equal to 37 dB was obtained for the innovative prototype, 3 dB higher than that of the conventional window with air in the interspace (R_w = 34 dB), confirming good acoustic insulation properties.

10.5 Future trends

Further investigations about highly energy-efficient windows and skylights are needed in order to clarify several aspects and to improve some characteristics, such as:

- Aerogel glazings have the lowest potential U-values in the fenestration market, as low as 0.1 W/(m^{2}K) and, due to their very interesting

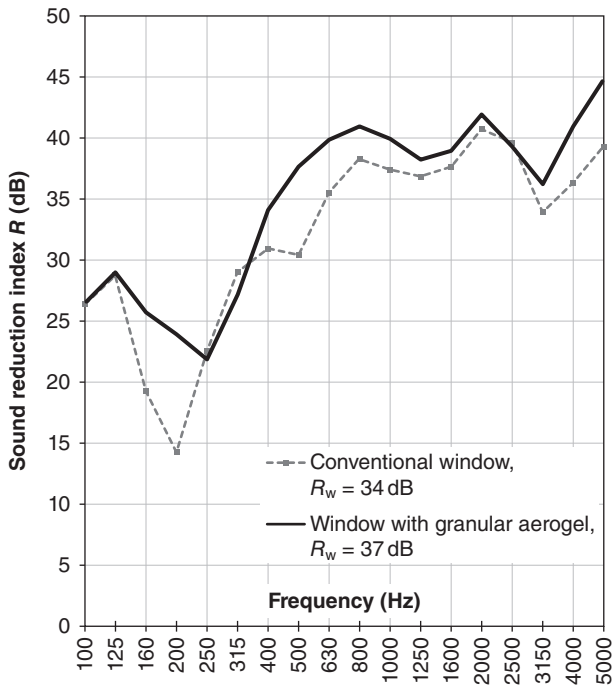

10.14 Sound reduction index (R) values vs. frequency for the conventional window and for the glazing prototype with aerogel in the interspace (Buratti and Moretti, 2012a).

properties (thermal and acoustic insulation, lightness), they allow novel architectural daylighting solutions, but further effort and work are required to improve the visible transmittance.

- Research should be finalized to solve some problems such as the phenomenon of light scattering, which gives a reduced optical quality of vision through the material; furthermore, the production process is very complex and it does not allow the use of very large sheets of monolithic aerogels, without altering performance.
- Nowadays, alternative high-performance glazing solutions, such as vacuum insulation panels (VIP), have technical limits and at the same time very high costs: in fact, a functional VIP with U-values of 0.1 W/m^2K is not available due to the problem of keeping the glazing gas-tight. Thus, the development of translucent or transparent aerogels, as a highly efficient insulating material to fill the glazing systems, seems at the moment the best possible thermal insulation system.
- Nanogel windows could become a decent alternative to conventional window solutions, above all in very cold climates, but aerogel manufacturers should put emphasis on cost reduction. A reference market price for silica aerogel (2008) is on the order of US$4000/$m^3$, but a price of US$1500/m^3 could be foreseen by 2020 with increasing commercialization. Concerning the applications in buildings, the price of commercial daylighting solutions with granular aerogel in polycarbonate sheets is on the order of €100–200/m^2 (frame excluded), depending on the thickness (10–25 mm).

10.6 References

AbuBakr Bahaj S, James PAB, Jentsch MF (2008), 'Potential of emerging glazing technologies for highly glazed buildings in hot arid climates', *Energy and Buildings*, 5, 720–731.

Ackerman WC, Vlachos M, Rouanet S, Fruendt J (2001), 'Use of surface treated aerogels derived from various silica precursors in translucent insulation panels', *Journal of Non-Crystalline Solids*, 285, 264–271.

Aegerter MA, Leventis N, Koebel MM (2011), *Aerogels Handbook,* Springer, Berlin.

Akimov YK (2003), 'Fields of application of aerogels (review)', *Instrument and Experiment Techniques*, 3, 287–299.

Anderson AM, Wattley CW, Carroll MK (2009), 'Silica aerogels prepared via rapid supercritical extraction: effect of process variables on aerogel properties', *Journal of Non-Crystalline Solids*, 2, 101–108.

Baetens R, Jelle BP, Gustavsen A (2011), 'Aerogel insulation for building applications: a state-of-the-art review', *Energy and Buildings*, 43, 761–769.

Buratti C (2003), 'Transparent insulating materials: experimental data and buildings energy savings evaluation', in *Proceedings of Energy & Environment 2003*, First International Conference on Sustainable Energy, Planning & Technology in Relationship to the Environment, Halkidiki, Greece.

Buratti C, Moretti E (2011a), 'Transparent insulating materials for buildings energy savings: experimental results and performance evaluation', in *Proceedings of Third International Conference on Applied Energy*, Perugia, Italy, 16–18 May 2011.

Buratti C, Moretti E (2011b), 'Lighting and energetic characteristics of transparent insulating materials: experimental data and calculation', *Indoor and Built Environment*, 20(4), 400–411.

Buratti C, Moretti E (2012a), 'Experimental performance evaluation of aerogel glazing systems', *Applied Energy*, 97, 430–437.

Buratti C, Moretti E (2012b), 'Glazing systems with silica aerogel for energy savings in buildings', *Applied Energy*, 98, 396–403.

Dorcheh AS, Abbasi H (2008). 'Silica aerogel: synthesis, properties and characterization', *Journal of Materials Processing Technology*, 199, 10–26.

Dowson M, Harrison D, Craig S, Gill Z (2011), 'Improving the thermal performance of single-glazed windows using translucent granular aerogel'. *International Journal of Sustainable Engineering*, 4(3), 266–280.

Duer K, Svendsen S (1998), 'Monolithic silica aerogel in superinsulating glazings', *Solar Energy*, 63, 259–267.

Europe Parliament and the Council of the European Union (2002), 'Directive 2002/91/EC of the European Parliament and of the Council of 16 December 2002 on the energy performance of buildings'. *Official Journal of the European Communities*, L1/65–L1/71.

EN 410 (2011), 'Glass in building – Determination of luminous and solar characteristics of glazing'.

EN ISO 10140-2 (2010), 'Acoustics – Measurement of sound insulation in buildings and of building elements. Part 2: Laboratory measurements of airborne sound insulation of building elements'.

EN ISO 717-1 (2007), 'Acoustics – Rating of sound insulation in buildings and of building elements. Part 1: Airborne sound insulation'.

Forest L, Gibiat V, Woignier T (1998), 'Biot's theory of acoustic propagation in porous media applied to aerogels and alcogels', *Journal of Non-Crystalline Solids*, 225, 287–292.

Forest L, Gibiat V, Hooley A (2001), 'Impedance matching and acoustic absorption in granular layers of silica aerogels', *Journal of Non-Crystalline Solids*, 285, 230–235.

Gross J, Reichenauer G, Fricke J (1988), 'Mechanical properties of SiO_2 aerogels', *Journal of Physics D:Applied Physics*, 21, 1447.

Hegde ND, Venkateswara Rao A (2007), 'Physical properties of methyltrimethoxysilane based elastic silica aerogels prepared by the two-stage sol–gel process', *Journal of Material Science*, 42, 6965–6971.

ISO 12567-1 (2010), 'Thermal performance of windows and doors – Determination of thermal transmittance by the hot-box method – Part 1: Complete windows and doors'.

Jelle BP, Hynd A, Gustavsen A, Arasteh D, Goudey H, Hart R (2012), 'Fenestration of today and tomorrow: a state-of-the-art review and future research opportunities', *Solar Energy Materials & Solar Cells*, 96, 1–28.

Jensen KI, Schultz JM, Kristiansen FH (2004), 'Development of windows based on highly insulating aerogel glazings', *Journal of Non-Crystalline Solids*, 350, 351–357.

Kim G-S, Hyun S-H (2003), 'Synthesis of window glazing coated with silica aerogel films via ambient drying', *Journal of Non-Crystalline Solids*, 320, 125–132.
Kistler SS (1931), 'Coherent expanded aerogels and jellies', *Nature*, 127, 741.
Luo L, Lu H, Leventis N (2006), 'The compressive behavior of isocyanate cross-linked silica aerogel at high strain rates', *Mechanical Time Depending Materials*, 10, 83–111.
Merget R, Bauer T, Küpper H, Philippou S, Bauer H, Breitstadt R, Bruening T (2002), 'Health hazards due to the inhalation of amorphous silica', *Archives of Toxicology,* 75, 625–634.
Oral GK, Yener AK, Bayazit NT (2004), 'Building envelope design with the objective to ensure thermal, visual and acoustic comfort conditions', *Building and Environment*, 3, 281–287.
Pajonk GM (2003), 'Some applications of silica aerogels', *Colloid and Polymer Science*, 281, 637–651.
Parmenter KE, Milstein F (1998), 'Mechanical properties of silica aerogels', *Journal of Non-Crystalline Solids*, 223, 3, 179–189.
Pérez-Lombard L, Ortiz J, Pout C (2008), 'A review on buildings energy consumption information', *Energy and Buildings*, 40, 394–398.
Pike Research (2011), 'Energy efficient buildings: global outlook', available at: http://www.pikeresearch.com/research/energy-efficient-buildings-global-outlook
Pierre AC, Pajonk GM (2002), 'Chemistry of aerogels and their applications', *Chemical Reviews*, 102, 4243–4265.
Reim M, Beck A, Körner W, Petricevic R, Glora M, Weth M, Schliermann T, Schmidtch, Pötter FJ, Fricke J (2002), 'Highly insulating aerogel glazing for solar energy usage', *Solar Energy*, 1, 21–29.
Reim M, Reichenauer G, Körner W, Manara J, Arduini-Schuster M, Korder S, Beck A, Fricke J (2004), 'Silica-aerogel granulate – structural, optical and thermal properties', *Journal of Non-Crystalline Solids*, 350, 358–363.
Reim M, Korner W, Manara J, Korder S, Arduini-Schuster M, Ebert HP, Fricke J (2005), 'Silica aerogel granulate material for thermal insulation and daylighting', *Solar Energy*, 2, 131–139.
Rigacci A, Einarsrud M, Nilsen E, Pirard R, Ehrburger-Dolle F, Chevalier B (2004), 'Improvement of the silica aerogel strengthening process for scaling-up monolithic tile production', *Journal of Non-Crystalline Solids*, 350, 196–201.
Schultz JM, Jensen KI (2008), 'Evacuated aerogel glazings', *Vacuum*, 82, 723–v729.
Schultz JM, Jensen KI, Kristiansen FH (2005), 'Super insulating aerogel glazing', *Solar Energy Materials and Solar Cells*, 89, 275–285.
Tajiri K, Igarashi K (1998), 'The effect of the preparation conditions on the optical properties of transparent silica aerogels', *Solar Energy Materials and Solar Cells*, 4, 189–195.
Wagh PB, Begar R, Pajonk GM, Venkateswara Rao A, Haranath D (1999), 'Comparison of some physical properties of silica aerogel monoliths synthesized by different precursors', *Materials Chemistry and Physics*, 57, 214–218.
Woignier T, Phalippou J, Sempere R, Pelous J (1988), 'Analysis of the elastic behaviour of silica aerogels taken as a percolating system', *Journal of Physics – France*, 49, 289–293.
Zanetti Freire R, Mazuroski W, Abadie O, Mendes N (2011), 'Capacitive effect on the heat transfer through building glazing systems', *Applied Energy*, 88, 4310–4319.

References websites

Advanced Glazings Ltd, Canada. http://www.advancedglazings.com/nanogel (last accessed on September 22, 2012).
Airglass AB, Sweden. http://www.airglass.se/ (last accessed on September 22, 2012).
Cabot Corporation, USA. http://www.cabot-corp.com/Aerogel (last accessed on September 22, 2012).
Kalwall Corporation, USA. http://www.kalwall.com/aerogel.htm (last accessed on September 22, 2012).
Nano High-Tech Co., Ltd, China. http://www.nanuo.cn/english/product-3.htm (last accessed on September 22, 2012).
Okalux GmbH, Germany. http://www.okalux.com (last accessed on September 22, 2012).
Roda E.M.B. Products AG, Germany. http://www.roda.de/download_en_22.html (last accessed on September 22, 2012).
Technical Glass Products, USA. http://www.tgpamerica.com/structural-glass/pilkington-profilit/ (last accessed on September 22, 2012).
Xtralite Rooflight, UK. http://www.xtralite.co.uk/products/specialist-glazing/lumira-technology/ (last accessed on September 22, 2012).

11

Switchable glazing technology for eco-efficient construction

C. G. GRANQVIST, Uppsala University, Sweden

DOI: 10.1533/9780857098832.2.236

Abstract: Electrochromic and thermochromic materials and devices make it possible to construct glazings whose throughput of visible light and solar energy can be switched to different levels depending on the application of an electrical voltage or on the temperature, respectively. These glazings are of much interest for eco-efficient buildings and are able to impart energy efficiency jointly with indoor comfort. The present chapter outlines the basics of the two technologies focusing on functional principles, relevant materials, device and manufacturing technology, as well as selected results from research and development.

Key words: electrochromism, thermochromism, chromogenic material, thin film, energy savings, energy-efficient buildings.

11.1 Introduction

Eco-efficient nanotechnologies offer many ways to diminish the energy that is used in buildings, as discussed in a recent book by Smith and Granqvist (2010). This energy amounts to as much as 30–40% of the world's primary energy (UNEP, 2007; Glicksman, 2008), and it follows that new and improved building technologies can have a very significant impact on global warming (Metz *et al.*, 2007), urban heat islands (Heisler and Brazel, 2010), and energy security. The potential energy savings are huge (McKinsey & Co, 2009) and, very importantly, can be accomplished without sacrificing the comfort and amenities that we rightly associate with good buildings (Richter *et al.*, 2008). The latter aspect is highly significant since we spend as much as 80–90% of our time indoors – in buildings and vehicles – in the most industrialized countries (Leech *et al.*, 2002). Furthermore, good energy performance can give financial advantages, and a recent study of market transactions in the USA showed that eco-efficient (also referred to as 'green') buildings can have higher rental rates and selling prices than comparable buildings without the eco-efficient attributes (Eichholtz *et al.*, 2010, 2011).

Windows are necessary in buildings in order to provide visual indoors–outdoors contact and daylight. However, it is frequently the case that the glazings let in or out too much energy which must be balanced by energy guzzling space cooling or space heating. An important step towards

energy efficiency can be taken if the glazings are 'switchable' (or 'smart'), i.e., are able to vary their throughput of visible light and solar energy (Lampert, 1984; Svensson and Granqvist, 1984). This functionality makes good use of the 'chromogenic' materials (Granqvist, 1990; Lampert and Granqvist, 1990; Smith and Granqvist, 2010) which are characterized by their ability to respond persistently and reversibly to external stimuli.

There are four kinds of chromogenic materials of primary interest for glazings in buildings. They are referred to as 'photochromic', 'thermochromic', 'electrochromic' and 'gasochromic'; their transmittance depends on irradiation intensity of ultraviolet light, temperature, application of an electrical voltage or current, and exposure to reducing and oxidizing gases, respectively. The largest energy savings can be accomplished with electrochromics (Selkowitz and Lampert, 1990; Granqvist *et al.*, 2010), and a recent report indicates that highly insulated electrochromic windows used in commercial as well as residential buildings would be able to save as much as 4.5 per cent on the annual energy use in the USA (Gillaspie *et al.*, 2010). The user acceptance of this technology appears to be very good (Clear *et al.*, 2006; Zinzi, 2006; Lee *et al.*, 2012). Thermochromics does not have an equally vast savings potential, but thermochromic devices can be based on a single thin layer or nanoparticle composite and are simpler than electrochromic devices which typically employ five superimposed layers (Granqvist, 1995). It should also be noted that electrochromic and thermochromic devices may be combined with optimized thermal insulation in future 'super fenestration' (Granqvist *et al.*, 2010).

Parts of this chapter are based on recent scientific papers by the author and his coworkers (Granqvist, 2012; Li *et al.*, 2012), but the text has been integrated and adapted. Throughout the text there are references to various coating technologies, and Chapter 8 of the present book, on the manufacturing of thin films and nanostructured coatings for eco-efficient constructions, can serve as a parallel source for some background material.

11.2 Electrochromics: materials and devices

Electrochromic materials are characterized by their ability to change their optical properties, reversibly and persistently, when a voltage is applied across them (Deb, 1973; Granqvist, 1995). This functionality clearly is of great interest for numerous applications, and device aspects rather than fundamental science have been leading the development of this technology ever since the discovery of electrochromism. Display devices were the focus during the early years, but applications to energy-efficient windows have been the driving force ever since the mid-1980s when it was realized that huge energy savings were feasible with electrochromic glazings (Lampert, 1984; Svensson and Granqvist, 1984; Granqvist, 2012).

Below we introduce the generic five-layer device technology in Section 11.2.1 and then survey some practical aspects of electrochromic glazings in Section 11.2.2. The subsequent parts, Sections 11.2.3 and 11.2.4, discuss the actual electrochromic films and the transparent conductors needed for applying the voltage, respectively. Finally Section 11.2.5 presents a case study of a particular type of electrochromic device with potential for very low-cost manufacturing.

11.2.1 Generic five-layer 'battery-type' device design

Figure 11.1 is a sketch of a standard electrochromic device (Granqvist, 1995) with five superimposed layers on a single transparent substrate or positioned between two such substrates. The optical functionality originates in the electrochromic film(s) which alter their optical absorption when ions are inserted or extracted from a centrally positioned electrolyte. This transport is easiest if the ions are small, in practice being protons (H^+) or lithium ions (Li^+). The electrolyte can be liquid, solid inorganic or comprised of a polymer. The ions are moved in an electrical field between two transparent electrical conductors, and the needed dc voltage is around 1–2 V. Except for very small devices, external metallic electrical contacts ('bus bars') must normally be put over at least part of the circumference of the device in order to achieve a reasonably fast and uniform colouring and bleaching.

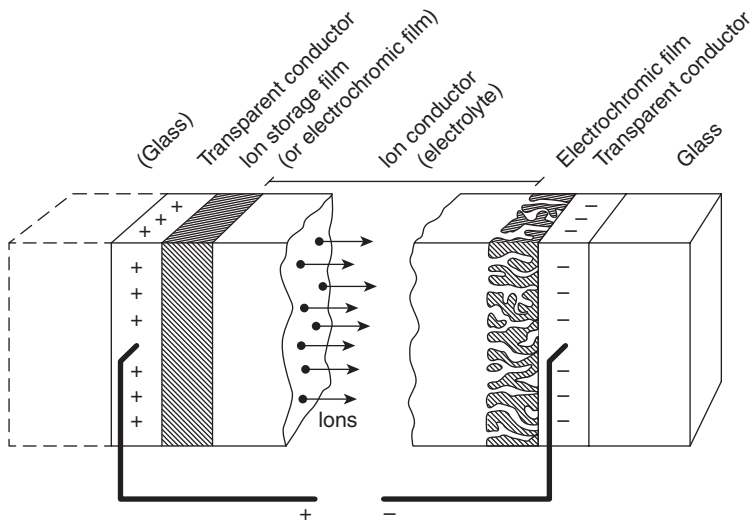

11.1 General electrochromic device design. Arrows signify ionic movement in an applied electric field. From Granqvist (1995).

There are three different kinds of layered materials in the device: The electrolyte is a pure ionic conductor and separates the two electrochromic films (or separates a single such film from an optically inactive ion storage film). The electrochromic films are mixed conductors of ions and electrons, whereas the transparent conductors conduct nothing but electrons. Optical absorption sets in when electrons are inserted into the electrochromic film(s) together with the ions from the electrolyte and are localized on metal ions. The valence of these ions is then changed, and when the 'extra' electrons interact with the incident light they can acquire enough energy to jump across a potential barrier to a neighbouring metal ion site. The absorption mechanism is conventionally referred to as 'polaron absorption' in physics and as 'intervalency absorption' in chemistry (a somewhat more detailed explanation is given in Section 11.2.3 below). This simplistic explanation of how the electrochromic devices work indicates that they can be viewed as thin-film batteries with a charging state that corresponds to the intensity of the optical absorption.

It is possible, already at this point, to introduce a number of interesting properties of electrochromic glazings which make them highly relevant to eco-efficient building technology (Granqvist, 2012):

- The devices have open circuit memory, like batteries, which means that they can keep their optical and charging properties for extended periods of time without drawing any current, depending on the quality of the electrical insulation of the electrolyte.
- The optical absorption can be set at any level between two extreme values.
- The optical changes are gradual and occur over times ranging from seconds to tens of minutes, depending on the size of the device; this time can be compared with the eyes' ability to adapt to changes in light, which takes minutes.
- The optical properties are founded on processes at the atomic scale, and hence an electrochromic glazing can be free of haze, which is an essential feature for most building-related applications.
- By combining two different electrochromic films it is possible to adjust the overall optical transmittance and achieve better colour neutrality than with a single electrochromic film.
- If the electrolyte is a solid and adhesive bulk-like polymer, the electrochromic glazing can combine its optical function with spall shielding, burglar protection, acoustic damping, near-infrared absorption, etc.

The electrochromic technology is not an easy one – which explains why it has taken so long to mature – and several more or less non-standard technologies must be mastered (Granqvist, 2008). Six challenges stand out for practical electrochromic glazings as listed below:

1. The electrochromic and counter electrode films must have well-defined nanoporosity over large areas, which requires non-conventional deposition technologies, which we return to in Section 11.2.3 below.
2. The transparent conductors must have excellent electrical conductivity jointly with optical transparency, which is demanding particularly for temperature-sensitive substrates; this part of the electrochromic device may be the most expensive one, so great care must be exercised in the choice of material and deposition technology, as further discussed in Section 11.2.4.
3. Describing the electrochromic device as a thin film battery points at the fact that insertion/extraction and charge balancing are vital processes; they may be based on controllable and industrially viable techniques such as gas treatments (Azens *et al.*, 2003a; Aydogdu *et al.*, 2010).
4. The electrolyte must combine good ion conductivity with excellent electrical insulation and high stability under ultraviolet irradiation; for laminated designs, it must also serve as a reliable adhesive.
5. Long-term cycling durability hinges on appropriate strategies for voltage and current control, just as in battery technology, and simple switching between two voltage levels, as is common in academic work on electrochromics, falls very short of an optimized strategy (Degerman Engfeldt *et al.*, 2011).
6. Large-scale manufacturing is the key to cost-effective electrochromic glazings and hence to their market acceptability. Obviously one must avoid time-consuming production steps such as extended thin film deposition, long post-treatment times, separate steps for electrochemical charge insertion/extraction, slow introduction of electrolytes, etc. Roll-to-roll coating of flexible substrates, followed by continuous lamination, offer particular advantages, and Section 11.2.5 below discusses the state-of-the-art for electrochromic devices based on such technologies.

11.2.2 Practical constructions of electrochromic glazings

The scientific and technical literature show many examples of electrochromic glazings of various sizes and has done so for decades, but few of these examples can be considered as products ready for the market or even prototypes. A number of those that are currently (2012) being delivered to customers on a very limited scale, or at least shown to customers, are introduced next (see also recent articles by Baetens *et al.*, 2010a, and Jelle *et al.*, 2012). All of these products or prototypes rely on electrochromic tungsten oxide films for at least some of the coloration.

- A five-layer 'monolithic' electrochromic device design on a single glass pane has been developed by several companies. The details are not

known, but it is evident that the electrolyte is a very thin layer. By this arrangement it is very hard to eliminate some leakage ('trickle') current between the electrochromic films via structural imperfections, and repeated electrical 'refresh pulses' are needed to maintain the window in a constant, darkened state; furthermore, coloration and bleaching may proceed unevenly over large areas.

- A laminated design with two parallel double-layer-coated glass panes joined by a polymer electrolyte is available on the market in limited quantities. Here the electrolyte is injected in fluid form in a millimeter-wide gap between two glass panes via vacuum filling, which is a time-consuming process (Xu *et al.*, 2009).
- A second laminated design (Kraft and Rottmann, 2009) makes use of an electrolyte based on polyvinyl buteral (PVB), which is a standard material for glass lamination, and transparent electrical conductors of fluorine-doped tin oxide made by low-cost spray pyrolysis in conjunction with float glass production. The ion storage film is of ferric hexacyanoferrate ('Prussian Blue'), which is possible to prepare via electro-deposition but, as far as is known, not by standard glass coating techniques such as magnetron sputtering; this film is a conductor for K^+ ions (de Tacconi *et al.*, 2003).
- Still another laminated design is different from the others in being based on flexible polyethylene terephthalate (PET) foil and hence allowing low-cost roll-to-roll web coating (Azens *et al.*, 2003b; Niklasson and Granqvist, 2007). One PET foil is coated with transparent and conducting indium-tin oxide (ITO) and electrochromic tungsten oxide, another PET foil is coated with ITO and an electrochromic nickel-based oxide, and the coated surfaces of the two foils are joined via an electrolyte applied by continuous lamination. The foil can be used as an add-on for upgrading existing windows, as a suspended electrochromic 'third pane' in an insulating glass unit, or as a lamination joining two glass panes. This type of electrochromic glazing is discussed further below in Section 11.3.5.

There are numerous alternative electrochromic device designs as well, both based on an oxide-based 'battery' approach as in Fig. 11.1 and others. Considering first the 'battery' type, one may note that there are non-oxide inorganic electrochromic materials, and 'Prussian Blue' (de Tacconi *et al.*, 2003) was mentioned above. Furthermore, electrochromism is a common phenomenon in organic materials, and a vast literature exists on this subject (Monk *et al.*, 2007). Their durability under irradiation is much less than for the oxides, but the coloration efficiency (the change in optical absorption per unit of charge exchange) can be much higher in organic materials than in oxides. Metal hydrides represent another option and can display variable

reflectance and can operate in conjunction with electrochromic thin films in devices; constructions with films based on nickel-magnesium hydride have been investigated in depth (Tajima *et al.*, 2010). Today's devices of this type tend to suffer from limitations in longevity, modulation span and high-temperature stability (Tajima *et al.*, 2011).

There are also several device designs that are distinctly different from the 'battery' type. One of these is the suspended particle device (often referred to as an 'SPD') which is rooted in the pioneering work on 'light valves' done by Land already in the 1930s (Marks, 1969). Essentially, a suspension of rod-like molecules, for example of herapathite (Kahr *et al.*, 2009), are aligned under an ac voltage of ~100 V (i.e., some two orders larger than for the electrochromic device illustrated in Fig. 11.1) and are randomly oriented in the absence of this field; the optical transmittance through suitably confined suspensions is then changed. The modulation can be strong for luminous radiation, but not for infrared light, and the devices exhibit some haze (Vergaz *et al.*, 2008). Alternatively, liquid crystals can be used in several different ways to create variable transmittance; the most common construction with regard to glazings uses polymer-dispersed liquid crystals (known as 'PDLCs') and suffers from significant haze (Cupelli *et al.*, 2009; Gardiner *et al.*, 2009). Another possibility is offered by some organic compounds, which can display optical absorption when a small current is drawn through them, and this phenomenon has been used very successfully for some two decades in 'self-dimming' rear view mirrors for automobiles. As a final possibility one may point at reversible electroplating, which in principle is able to give variable reflectance between very widely separated limits. This option has been investigated intensely (Ziegler, 1999; Laik *et al.*, 2001) but has not yet led to practically useful glazings.

11.2.3 Electrochromic thin films

There are two types of electrochromic metal oxides, which are referred to as 'cathodic' (colouring under ion insertion) and 'anodic' (colouring under ion extraction); they are discussed in detail in Granqvist (1995). The standard electrochromic device, such as the one shown in Fig. 11.1, embodies two electrochromic thin films and it is clearly advantageous to combine one 'cathodic' oxide (e.g., based on W, Mo, or Nb) and another 'anodic' oxide (e.g., based on Ni or Ir). Shuttling ions between the two electrochromic films one way makes both of these films colour, whereas shuttling ions the other way makes them both bleach; this is sometimes referred to as a 'rocking chair' operation. Coincidentally there are 'cathodic' and 'anodic' oxides which can work in tandem and jointly yield electrochromic glazings with a rather neutral visual appearance that is appropriate for general applications in architecture.

What is the origin of the electrochromism for these oxides? An approximate answer can be given by arguments based on the crystalline structure, and a detailed examination of the electrochromic oxides reveals that they can be represented as (defect) perovskites, rutiles, and having layer/block structures. All of these structures can be described as comprising 'ubiquitous' MeO_6 octahedra (where Me denotes metal) connected by sharing common corners and/or common edges. Edge-sharing is related to some degree of deformation of the octahedra. Only one electrochromic oxide falls outside this description and exhibits properties with both 'anodic' and 'cathodic' traits: this is vanadium pentoxide (V_2O_5) which can be viewed as built from square pyramidal VO_5 units. The octahedral coordination is very important for the electronic properties of the electrochromic oxides and leads to a qualitative model for the optical properties for all of the oxides mentioned above, as elaborated elsewhere (Granqvist, 1993, 1995).

The detailed mechanisms for the optical absorption in electrochromic oxides are often poorly understood. Generally speaking, the absorption is associated with charge transfer, and polaron absorption captures at the essential features (Granqvist, 1995; Niklasson and Granqvist, 2007). The electrons inserted together with the ions are localized on metal ions and, in the specific case of tungsten oxide, change some of the W^{6+} sites to W^{5+}. Transfer of electrons between sites designated i and j, say, then can be represented schematically as $W_i^{5+} + W_j^{6+} + \text{photon} \rightarrow W_i^{6+} + W_j^{5+}$. This mechanism operates only as long as transitions can take place from a state occupied by an 'extra' electron to one available to receive that electron, and if the ion and electron insertion is large enough this is no longer the case so that 'site saturation' (Denesuk and Uhlmann, 1996) becomes significant. Electron transfer then can occur also according to $W^{4+} \leftrightarrow W^{5+}$ and $W^{4+} \leftrightarrow W^{6+}$ (Berggren *et al.*, 2007). However, these latter kinds of charge transfer do not dominate since highly reversible electrochemical reactions limit the permissible insertion levels to those where $W^{5+} \leftrightarrow W^{6+}$ are prevalent.

Mixed electrochromic oxides can offer a number of advantages, and by having a large variety of sites available for charge transfer, it is possible to achieve an increasingly wavelength-independent absorption (i.e., a more neutral colour). Other advantages of mixed oxides are the possibility to widen the optical band gap in order to give a higher bleached-state transmittance in nickel-oxide-based (Avendaño *et al.*, 2004) and iridium-oxide-based (Azens and Granqvist, 2002) films, and to 'dilute' expensive iridium oxide without major effects on its electrochromism (Backholm and Niklasson, 2008; Harada *et al.*, 2011). Still another advantage is that the coloration efficiency can be increased by mixing suitable oxides, as shown in recent detailed work on mixed tungsten-nickel oxide films by Green *et al.* (2012).

The ubiquity of the MeO_6 octahedra is important not only for the optical properties but also for the possibilities to accomplish facile ion insertion

and extraction in the electrochromic oxides. This is so because the atomic arrangements give spaces – tunnels in three dimensions – that are large enough to serve as conduits for small ions. Furthermore, transition metal oxides can display many different types of crystallinity depending on temperature and pressure, and sub-stoichiometry can yield so called Magnéli phases (denoted W_mO_{3m-1}, with m being 1, 2, . . . for the case of tungsten oxide) with a combination of corner and edge sharing for the octahedral units.

Easy ion transport does not happen solely as a consequence of structures comprising MeO_6 octahedra but can occur as a result of film porosity ensuing from limited atomic movements during the thin film deposition process. In fact there is a large number of thin film technologies based on atomistic and particulate deposition, bulk coating and surface modification, as discussed elsewhere in this book (see Chapter 8). It seems that all of these technologies can be adapted, with greater or lesser difficulty, to the preparation of porous structures that are adequate for electrochromic oxide films.

11.2.4 Transparent conducting thin films

The transparent electrodes may be the single most expensive part in an electrochromic glazing and therefore they deserve particular attention. There are several categories of transparent conductors, each with its specific pros and cons (Granqvist, 2007; Ginley *et al.*, 2010; Smith and Granqvist, 2010). This section gives a bird's eye view of such films based on oxides, metals and carbon.

Heavily doped wide band gap oxides are commonly used as transparent conductors in electrochromic devices. The most pertinent materials are In_2O_3:Sn (ITO), ZnO:Al (AZO), ZnO:Ga (GZO), ZnO:In (IZO) and SnO_2:F (FTO), and the doping level is typically a few per cent. All of the materials can give a resistivity as low as ~1×10^{-4} Ωcm, a luminous absorptance of only a few per cent in a film with practically useful thickness (300 nm, say), and excellent durability. The optical properties are very well understood from basic theory, which means that detailed and trustworthy simulations of the optical properties can be made for devices (Hamberg and Granqvist, 1986; Jin *et al.*, 1988; Stjerna *et al.*, 1994). Films of ITO, AZO, GZO and IZO prepared by well-controlled reactive dc magnetron sputtering onto glass and PET typically have resistivities of ~2×10^{-4} and ~4×10^{-4} Ωcm, respectively. High-quality films of FTO are normally made by spray pyrolysis onto the hot glass emerging from the leer during float glass production. Depositions onto flexible substrates introduces risks for cracking and accompanying loss of electrical conductivity, but this effect is generally not a serious one unless the bending ratio is as small as a few centimeters

(Cairns *et al.*, 2000; Lan *et al.*, 2010). All of the mentioned oxides are transparent for most of the spectrum characterizing solar radiation.

ITO films can be expensive as a result of the high price of indium (despite the fact that this element is not uncommon in the earth's crust) and require careful process control for deposition; zinc oxide-based films can have similar optical and electrical properties but usually demand even more stringent process control; and good FTO apparently can only be made on very hot glass. Thus each of the transparent conducting oxide films has particular challenges and there is today no 'best' alternative for applications in electrochromic glazings. Health issues for the manufacturing of transparent conductors have been brought to attention recently, and it has been reported that the production of indium-containing oxides may lead to pulmonary disorders sometimes referred to as 'indium lung' (Taguchi and Chonan, 2006), which clearly can be an important concern for large-scale manufacturing.

Metal films can serve as excellent alternatives to the oxide-based transparent conductors. The coinage metals (Cu, Ag and Au) have conductivities that are some two orders of magnitude higher than for the best transparent conducting oxides so that comparative electrical properties can be achieved at about a hundredth of the film thickness; the luminous absorptance of the metal films can be of the order of 10%. The metal films are stretchable to a much larger degree than the oxide-based films (Graz *et al.*, 2009).

The relevant metal film thicknesses are extremely small, which means that details of the thin film growth are important. Continued deposition onto a dielectric substrate such as glass or PET causes the deposited metal to go through a number of distinct growth stages: tiny metallic nuclei are formed initially; they grow and create increasingly irregular 'islands'; these 'islands' interconnect and form a contiguous meandering network at a thickness corresponding to 'large-scale coalescence'; the network then transforms into a 'holey' film; and finally a well defined metallic film can be formed (Smith *et al.*, 1986; Lansåker *et al.*, 2009). The most interesting films have thicknesses only slightly above that for 'large-scale coalescence', in practice around 10 nm (Hövel *et al.*, 2010). Reflectance at the two interfaces of the metal film limits the luminous transmittance to ~50%, but the transmittance can be very significantly enhanced if the coinage metal films are positioned between high-refractive-index transparent layers that serve as antireflection coatings for the metal films.

There are several alternatives to the oxide-based and metal-based transparent conductors that are explored today (Hecht and Kaner 2011), and carbon-based transparent conductors may be of particular importance. Thus meshes of carbon nanotubes can combine high transmittance for luminous and solar radiation with good electrical conductivity (Hu *et al.*, 2010a; Niu, 2011). Another alternative – which currently enjoys intense interest – is

graphene, i.e., atomically thin layers of carbon atoms arranged in a honeycomb lattice (Geim and Novoselov, 2007; Eda and Chhowalla, 2010); these layers can be prepared via mechanical or chemical exfoliation of graphite into individual sheets as well as by chemical vapour deposition. Successful roll-to-roll production of graphene coatings was first demonstrated during 2010 (Bae *et al.*, 2010, 2012).

Metal-based nanowire meshes is another possibility, and it has been shown that silver nanowires with diameters of ~100 nm and lengths of ~10 μm can be produced in large amounts by inexpensive reduction of liquid silver nitrate (Hu *et al.*, 2010b, 2011). Suspensions of these nanowires can be deposited, and the conduction between adjacent wires can be improved by annealing. These coatings can have good electrical properties but suffer from some diffuse scattering which limits their applications in electrochromic glazings.

A final example may be poly(3,4-ethylenedioxytiophene), known as PEDOT, which cannot quite compete with regard to performance with most of the other options mentioned above, but which nevertheless is interesting since it can be prepared by printing at a very low cost (Elschner and Lövenich, 2011).

11.2.5 Flexible electrochromic foil

Tungsten oxide is the most extensively studied electrochromic material and was discussed in some detail above. It has cathodic coloration and needs to be combined with an appropriate anodic oxide to create an optimized device. Iridium oxide works very well in tandem with tungsten oxide but it is one of the rarest elements in the earth's crust and only found in abundance in a few places. An alternative is hence needed for large-scale applications, and hydrous nickel oxide is such a material as discovered in the 1980s by Svensson and Granqvist (1986).

A number of studies of electrochromic devices based on tungsten oxide and nickel oxide have been reported in the literature; they are either rigid and based on depositions onto glass (Mathew *et al.*, 1997; Subrahmanyam *et al.*, 2007; Huang *et al.*, 2011) or flexible and deposited onto PET foil (Azens *et al.*, 2003b; Niklasson and Granqvist, 2007). Figure 11.2 illustrates a specific device design that was mentioned in Section 11.2.2 above: one PET foil is coated with ITO and tungsten oxide, another PET foil is coated with ITO and nickel-based oxide, and the two electrochromic films are joined by an ion-conducting polymer adhesive. Figure 11.3 reports time-dependent transmittance at a mid-luminous wavelength of 550 nm for ten consecutive colouring/bleaching cycles. Colouring proceeds slower than bleaching and the values shown do not indicate the darkest state that can be reached. The highly repeatable properties should be noted, and the

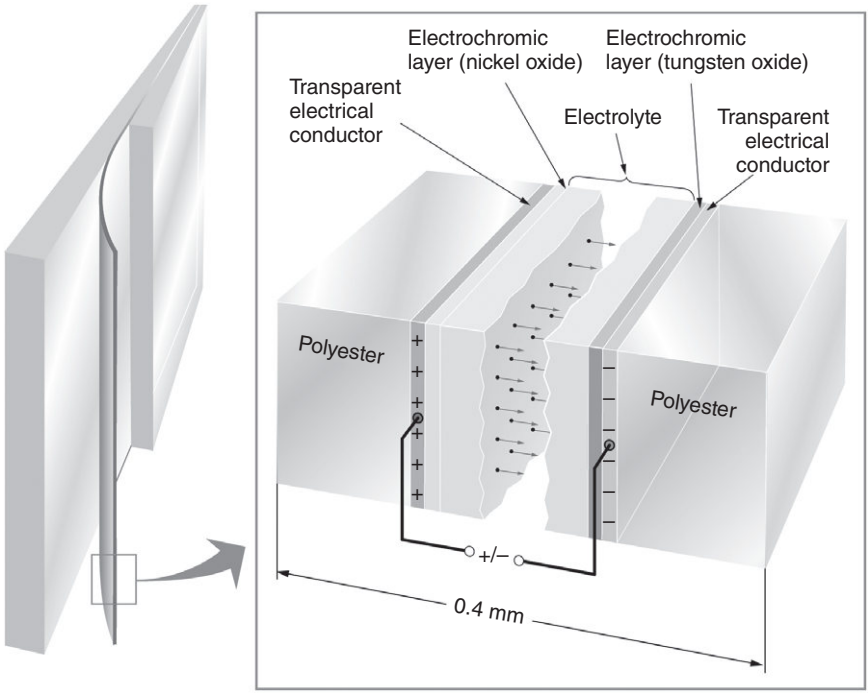

11.2 Construction principle for an electrochromic foil device. The entire foil can be used as a laminate between two glass panes.

cycling can be continued for tens of thousands of cycles without severe loss of performance.

The desired transmittance interval depends on the intended use of the electrochromic device. For architectural glazings one may emphasize a high bleached-state transmittance, and then low-cost antireflection coatings may be of interest (Jonsson and Roos, 2010; Jonsson *et al.*, 2010). However, other applications may require that a very dark state can be reached for the sake of glare control. A simple way to obtain a very small transmittance in the dark state is to put two or more electrochromic foils on top of each other (Granqvist, 2008). As a first approximation, the transmittance of a double-foil device is the square of the transmittance of a single-foil device. Figure 11.4 indicates that the transmittance at a mid-luminous wavelength can approach 1% in a double electrochromic foil, while the bleached-state transmittance is still appreciable.

It was emphasized above that low-cost manufacturing is the key to large-scale implementation of electrochromic glazings in buildings. Figure 11.5 shows some initial results on the transmittance modulation in an electrochromic foil-type device prepared by roll-to-roll deposition onto a ~1-km-long and 0.6-m-wide PET foil.

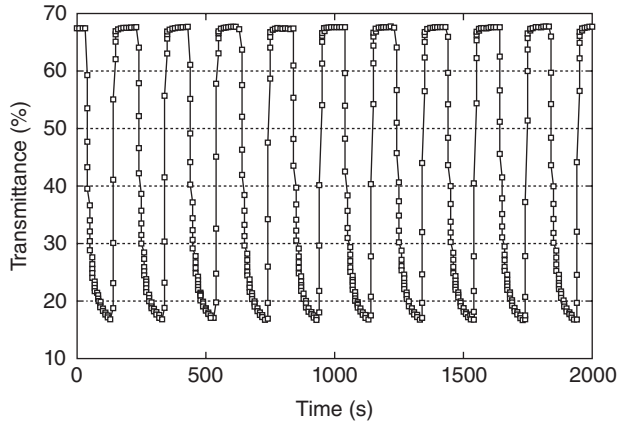

11.3 Mid-luminous transmittance vs. time during repeated colouring and bleaching of an electrochromic foil device of the type illustrated in Fig. 11.2.

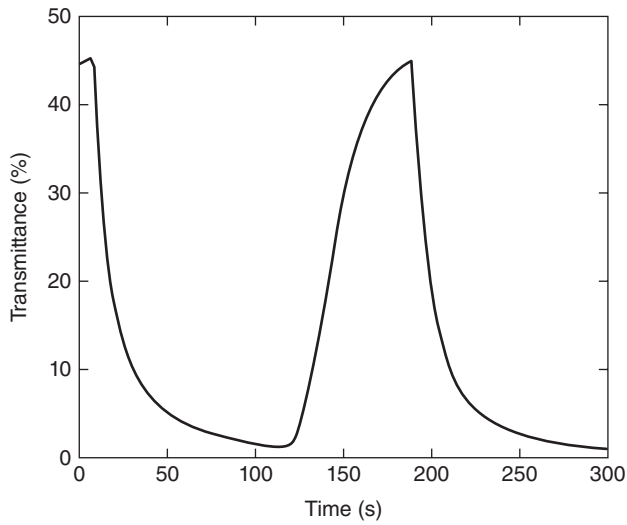

11.4 Mid-luminous transmittance vs. time for repeated colouring and bleaching of two superimposed electrochromic foils of the kind described in Fig. 11.2. From Granqvist (2008).

11.3 Thermochromics: materials and devices

Thermochromism is well known in a number of metal oxides and sulphides (Lampert and Granqvist, 1990; Smith and Granqvist, 2010). Vanadium dioxide, VO_2, stands out as the most interesting material with regard to eco-efficient technologies, and its thermochromism has been known for

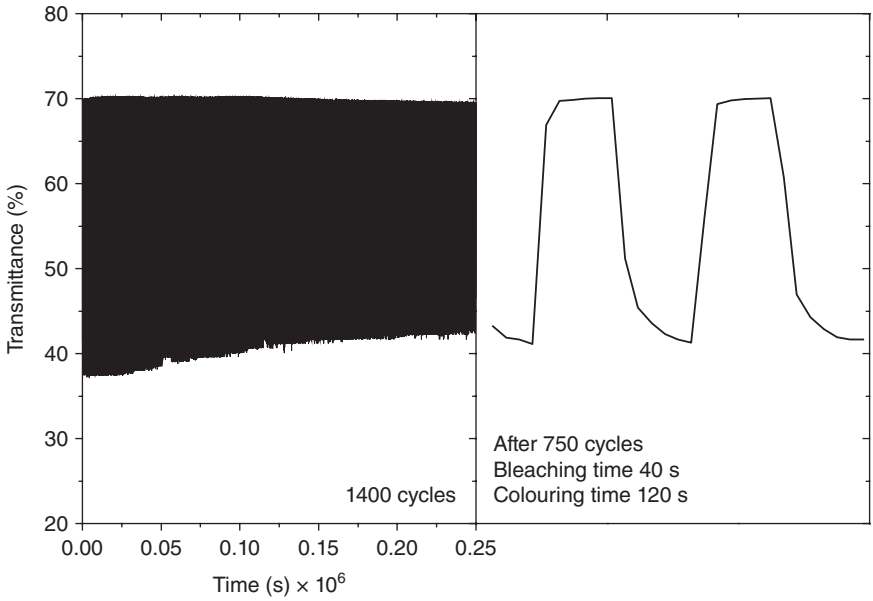

11.5 Initial data on transmittance modulation of luminous radiation in an electrochromic foil device made by roll-to-roll manufacturing and continuous lamination.

more than 50 years (Morin, 1959). However, vanadium dioxide is not directly applicable to glazings, and three particular challenges can be identified as elaborated in Section 11.3.1 below. In particular, the modulation of the solar energy throughput must be sufficiently large in order to have a significant impact on the buildings' energy expenditure, and this leads to the recently introduced concept of 'nanothermochromics' (Li *et al.*, 2010), which also is advantageous for yielding a large luminous transmittance as discussed in Section 11.3.2. The luminous transmittance can be further enhanced by doping of the VO_2, especially by magnesium, as discussed in Section 11.3.3. Finally, the modulation of the solar energy throughput must occur in the vicinity of a comfort temperature of about 25°C, which again can be accomplished by doping – in this case most expediently by tungsten – as elaborated in Section 11.3.4.

11.3.1 Vanadium dioxide-based thin films: three challenges

Vanadium dioxide is an interesting and complex material with at least seven different polymorphs among which rutile VO_2(R), monoclinic VO_2(M) (Morin, 1959), and triclinic VO_2(T) (Mitsuishi, 1967) phases are similar in structure, and there are also tetragonal VO_2(A) (Oka *et al.*, 1990),

monoclinic VO_2(B) (Théobald *et al.*, 1976), paramontroseite VO_2 (Wu *et al.*, 2008) and body centred cubic VO_2 (Wang *et al.*, 2008). The interesting thermochromic properties ensue from VO_2(R) and VO_2(M) which exhibit a reversible structural transformation and associated metal-insulator transition at a 'critical' temperature τ_c in the neighbourhood of a comfort temperature; VO_2(M) is semiconducting and reasonably infrared transparent at a temperature τ, so that $\tau < \tau_c$, whereas VO_2(R) is metallic and infrared reflecting for $\tau > \tau_c$.

The pioneering work on the thermochromism of VO_2 by Morin (1959) was performed on bulk specimens. However, it was soon realized that reactively sputter deposited and reactively evaporated thin films could exhibit a similar metal–insulator transition. Subsequently it has been found that virtually any thin film technology is capable of providing thermochromic VO_2. The reversibility of the metal-insulator transition can be excellent in films (Ko and Ramanathan, 2008), whereas bulk samples tend to deteriorate upon repeated thermal cycling around τ_c. The possibilities to create energy-efficient fenestration by letting solar energy into a building when there is a heating demand and rejecting solar energy when there is a cooling demand were pointed out already in the 1980s (Greenberg, 1983; Jorgenson and Lee, 1986; Babulanam *et al.*, 1987), and various aspects of this technology have been reviewed several times more recently (Granqvist, 2007; Parkin *et al.*, 2008; Saeli *et al.*, 2010a,b; Smith and Granqvist, 2010).

Figure 11.6 introduces the characteristic features of the thermochromism that can be seen in a thin VO_2 film. Spectral normal transmittance $T(\lambda)$ and spectral near-normal reflectance $R(\lambda)$ were recorded at 22 and 100°C, i.e., at $\tau < \tau_c$ and at $\tau > \tau_c$. The data were obtained for a 0.05-μm-thick film produced by reactive dc magnetron sputtering as reported elsewhere by Mlyuka *et al.* (2009a). Similar optical data – usually of spectral transmittance – have been reported many times in the scientific literature and are hence very well established (see the paper by Li *et al.* (2012) for references). It is clear from Fig. 11.6 that the short-wavelength optical properties are similar irrespective of the temperature, while the infrared reflectance for wavelengths beyond ~1 μm is higher for $\tau > \tau_c$ than it is for $\tau < \tau_c$, thus giving proof for the metal–insulator transition. The infrared transmittance at $\lambda > 1$ μm shows an analogous change.

Figure 11.6 also shows the spectral sensitivity of the light-adapted human eye, denoted φ_{lum} and lying in the $0.4 < \lambda < 0.7$ μm wavelength range (Wyszecki and Stiles, 2000) and the solar irradiance spectrum for air mass 1.5 (corresponding to the sun standing 37° above the horizon), denoted φ_{sol} and extending across the $0.3 < \lambda < 3$ μm interval (ASTM, 2003). One observes in particular that φ_{sol} drops sharply towards long wavelengths. Wavelength-integrated luminous and solar transmittance values are now introduced by

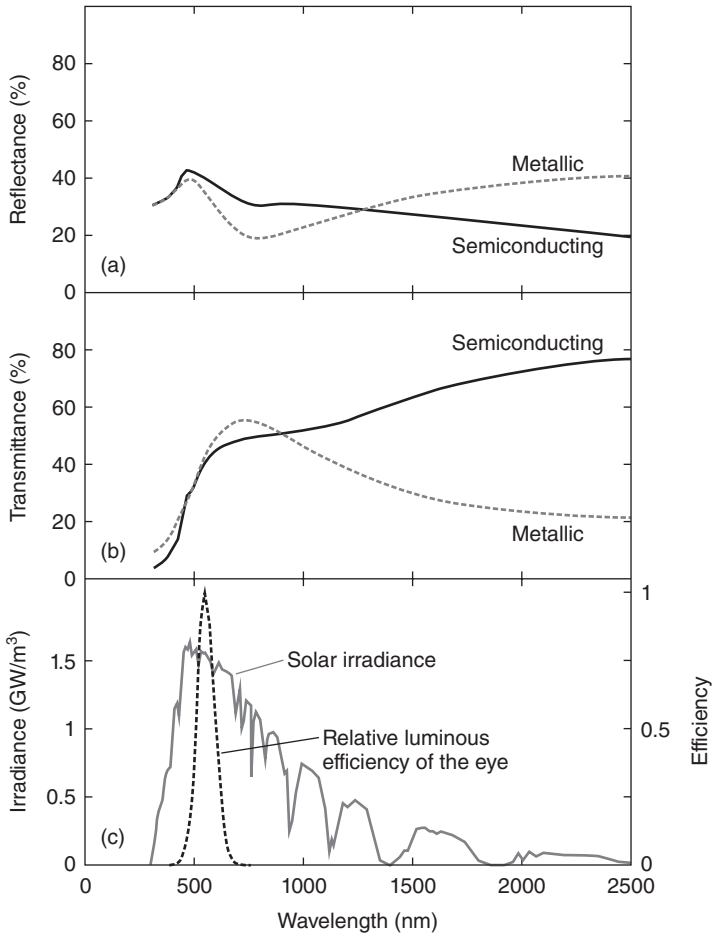

11.6 Spectral reflectance (upper panel) and transmittance (middle panel) for a 0.05-μm-thick thermochromic VO_2 film in semiconducting ($\tau < \tau_c$) and metallic ($\tau > \tau_c$) states. The lower panel illustrates typical spectra for the luminous efficiency of the human eye and for solar irradiance. After Mlyuka *et al.* (2009a).

$$T_{\text{lum,sol}}(\tau) = \int d\lambda\, \varphi_{\text{lum,sol}}(\lambda) T(\lambda, \tau) \Big/ \int d\lambda\, \varphi_{\text{lum,sol}}(\lambda). \qquad [11.1]$$

This equation was used to compute data, shown in Fig. 11.7, on $T_{\text{lum}}(\tau,t)$ and $T_{\text{sol}}(\tau,t)$ where t is the thickness of the VO_2 film (Li *et al.*, 2010). These computations used standard formulas for thin-film optics (Born and Wolf, 1999) together with optical constants n and k of VO_2 as evaluated before (Mlyuka *et al.*, 2009b). The discussion below will also make use of the corresponding dielectric constant, denoted $\varepsilon = \varepsilon_1 + i\varepsilon_2$, which is related to the optical constants via $\varepsilon_1 = n^2 - k^2$ and $\varepsilon_2 = 2nk$.

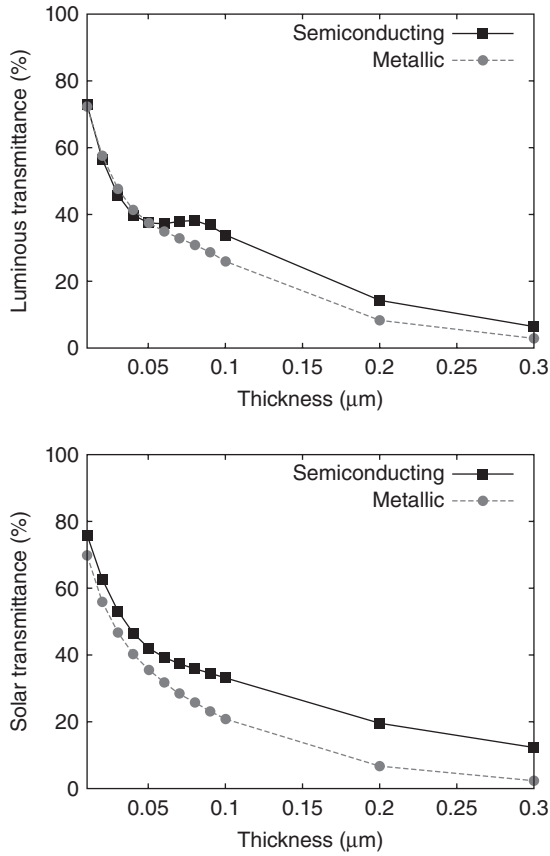

11.7 Computed data on luminous (upper panel) and solar (lower panel) transmittance as a function of the thickness of VO_2 films in semiconducting ($\tau < \tau_c$) and metallic ($\tau > \tau_c$) states. From Li *et al.* (2010).

The findings in Fig. 11.7 permit an identification of two properties of thermochromic VO_2 films that severely limit their applicability to energy-efficient fenestration:

- the modulation of solar energy, given by $\Delta T_{sol} \equiv T_{sol}(\tau < \tau_c) - T_{sol}(\tau > \tau_c)$, is no larger than ~10%, and
- T_{lum} is no higher than ~40% for films with a significant magnitude of ΔT_{sol}, which is too low for most applications to windows in real buildings (Wigginton 1996).

A third limitation, obviously, is that the change of the solar transmittance should take place in the vicinity of a comfort temperature of ~25°C, whereas

- $\tau_c \approx 68$°C for bulk VO_2 (Morin, 1959).

These linutations indicate three challenges that must be met for practical thermochromic glazings, and VO_2 has to be modified in order to achieve $\Delta T_{sol} >> 10\%$, $T_{lum} >> 40\%$, and $\tau_c \approx 25°C$.

A moderate boost of T_{lum} and/or T_{sol} can be obtained by straightforward optical design using high-refractive-index dielectric coatings, and data are available for a number of two-, three- and five-layer coatings with vanadium dioxide films between films of, for example, titanium dioxide and zirconium dioxide. The best properties were reached for $TiO_2/VO_2/TiO_2/VO_2/TiO_2$ (Mlyuka *et al.*, 2009a,b). However, these improvements are not sufficient for making thermochromic glazings of general practical interest. Fluorination is an alternative route to improve T_{lum} for VO_2 films to some extent (Khan *et al.*, 1988; Khan and Granqvist, 1989).

11.3.2 VO_2 nanoparticle composites with enhanced solar energy modulation and luminous transmittance

'Nanothermochromics' is a new concept that was introduced recently by the author of this chapter and his coworkers (Li *et al.*, 2010). It deals with VO_2 nanoparticles dispersed in a dielectric host and implies that the composite can be represented as an 'effective medium' with properties intermediate between those of the nanoparticles and their matrix. The particles are small enough not to cause optical scattering. The 'effective' dielectric function ε^{MG} is (Smith and Granqvist, 2010; Granqvist and Hunderi, 1977, 1978):

$$\varepsilon^{MG} = \varepsilon_m \frac{1 + \frac{2}{3} f\alpha}{1 - \frac{1}{3} f\alpha}, \qquad [11.2]$$

where ε_m accounts for the matrix and f is the 'filling factor', i.e., the volume fraction occupied by the particles. The calculations to be presented below employed $f = 0.01$ and a thickness of 5 μm (so that the VO_2 mass thickness was 0.05 μm, i.e., the same as for the VO_2 film reported on in Fig. 11.6).

Equation [11.2] is appropriate for the Maxwell-Garnett (*MG*) theory (Maxwell-Garnett, 1904), which pertains to nanoparticles in a continuous matrix (Niklasson *et al.*, 1981). There are many effective medium formulations – applicable to a multitude of nanotopologies – all of which coincide in the limit of a small filling factor; this implies that Eq. [11.2] can be used in the present case without any loss of generality.

The parameter α in Eq. [11.2] is given by

$$\alpha = \frac{\varepsilon_p - \varepsilon_m}{\varepsilon_m + L(\varepsilon_p - \varepsilon_m)}, \qquad [11.3]$$

where ε_p is the dielectric function of the particles and L is their depolarization factor. Spheres are characterized by $L = {}^1/_3$. A random distribution of ellipsoids can be represented by a sum over three components – corresponding to the symmetry axes – to yield α in the dilute limit (Niklasson and Granqvist, 1984). The calculations presented below pertain to prolate ('cigar-shaped') as well as oblate ('pancake-shaped') spheroids with depolarization factors obeying $\Sigma L_i = 1$. The depolarization factors can be expressed in terms of the major (a) and minor (c) axes of the spheroidal particles through known formulas (Landau *et al.*, 1984).

Wavelength-integrated transmittance values, specifically $T_{\text{lum}}(\tau,t)$ and $T_{\text{sol}}(\tau,t)$, were computed according to Eq. [11.1]. Data on ε_p were obtained from the literature (Mlyuka *et al.*, 2009b), and ε_m was set to 2.25 which is applicable to a matrix of a typical glass or polymer. Furthermore, the spheroids were taken to be oriented at random. The free electrons in the high-temperature phase of VO_2 have an exceedingly short mean free path (Allen *et al.*, 1993; Okazaki *et al.*, 2006; Gentle *et al.*, 2007) and, perhaps surprisingly, this innocent-looking oxide is not well understood in terms of fundamental theories. Notwithstanding this situation, the very small value of the mean free path makes it unnecessary to incorporate any size dependence on ε_p (as there is, for example, in coinage-metal nanoparticles (Granqvist and Hunderi, 1977) and for the non-uniform metal films mentioned above in Section 11.2.4 (Norrman *et al.*, 1978)).

The upper panel of Fig. 11.8 shows the experimental arrangement wherein light with photon energy $\hbar\omega$ (with $\hbar$ being Planck's constant divided by 2π and ω being angular frequency) is incident onto the nanoparticles; this panel also defines an 'aspect ratio' as a relationship between the axial lengths by $m = a/c$ for prolate spheroids and $m = c/a$ for oblate spheroids. The data in Fig. 11.8 can be directly compared with those for a VO_2 film with $t = 0.05$ μm in Fig. 11.7. The middle and lower panels of Fig. 11.8 prove that the nanoparticle composites have much higher values of ΔT_{sol} and T_{lum} than the films, which clearly shows the superior properties of the nanothermochromic composites. Spherical particles yield the highest transmittance. Still better properties can be obtained with VO_2 hollow nanoshells (Li *et al.*, 2011a). In terms of the underlying physics, the infrared optical absorption of the VO_2-based nanoparticles is governed by a plasmon resonance that is present in the metallic state at $\tau > \tau_c$ but absent in the insulating state at $\tau < \tau_c$ (Bai *et al.*, 2009; Li *et al.*, 2010).

Nanoparticles based on VO_2 can be produced in numerous ways as briefly reviewed in recent papers by Li *et al.* (2010, 2011a, 2012). More or less symmetrical particles can be prepared by wet chemical methods, molten salt synthesis, confined-space combustion, etc. There are also many methods to make nanorods (prolate spheroids with large aspect ratio) and nanosheets (oblate spheroids with small aspect ratio) by these techniques. A metastable

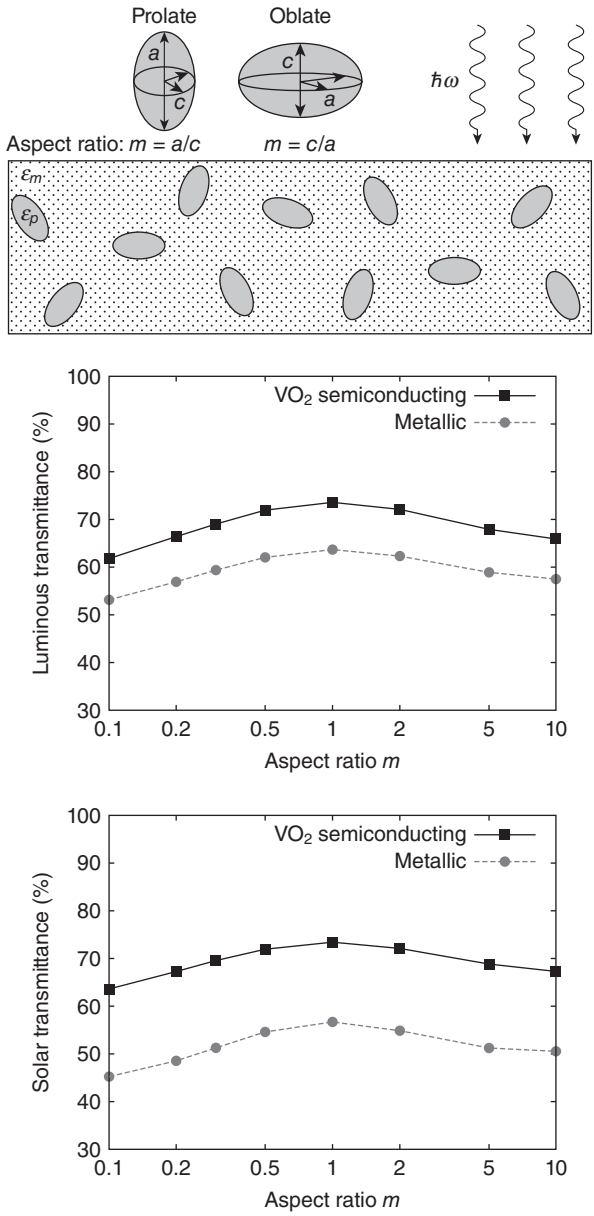

11.8 The upper panel depicts a structural model for a composite with randomly oriented nanoparticles having a dielectric function ε_p in a medium with the dielectric constant ε_m. Electromagnetic radiation with photon energy $\hbar\omega$ is indicated. The middle and lower panels show computed data on luminous and solar transmittance, respectively, vs. the aspect ratio m for VO_2-containing composites in semiconducting ($\tau < \tau_c$) and metallic ($\tau > \tau_c$) states. Prolate and oblate spheroids are characterized by $m > 1$ and $m < 1$, respectively. After Li *et al.* (2010).

form, generally referred to as VO_2(B), can be produced by chemical techniques and is of much contemporary interest for electrical batteries; this material can be transformed into thermochromic VO_2. Furthermore VO_2 can be made by oxidation of metallic vanadium and by reduction of V_2O_5. Recent data are available also for vanadium dioxide nanoparticles doped with tungsten (Ye *et al.*, 2010) and Mo (Chen *et al.*, 2010); the relevance of this doping will be explained in Section 11.3.4 below.

The nanoparticle composites can be useful in several ways and may be incorporated in polymer foils or laminates for practical low-cost thermochromic glazing as indicated in Fig. 11.9. Another possible application is in composites of VO_2 and an oxide such as ITO (see Section 11.2.4), where the latter component can impart a low thermal emittance (Li *et al.*, 2011b).

11.3.3 Mg-doped VO_2 films with enhanced luminous transmittance

The luminous absorptance of VO_2 is undesirably high, and Fig. 11.6 showed that $T(\lambda)$ dropped distinctly at $\lambda < 0.6$ μm for a film thickness as small as 0.05 μm. This property can be understood as an effect of band-to-band

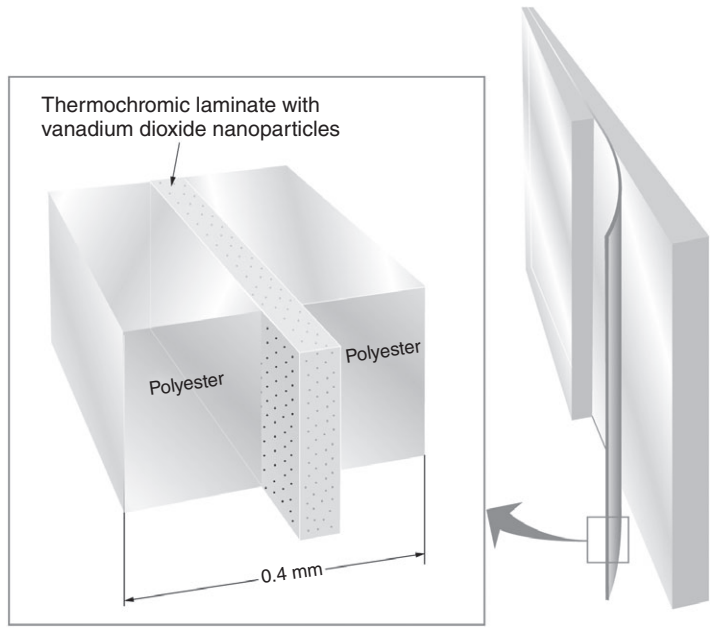

11.9 Conceptual sketch of a thermochromic foil incorporating a laminate with VO_2-based nanoparticles between two foils of polyethylene terephthalate (polyester, PET).

absorption and hence is inherent in the material. This problem with vanadium dioxide has been known for decades, and much effort has gone into finding ways to diminish its influence. The problem received an at least partial solution in recent work on sputter deposited films (Mlyuka *et al.*, 2009c), where it was shown that Mg doping could produce band gap widening, i.e., an enhancement of $T(\lambda)$ for $\lambda < 0.6\,\mu m$. The upper panel of Fig. 11.10 shows spectral data for a VO_2-based film containing 7.2 at% Mg at $\tau < \tau_c$ and $\tau > \tau_c$ and compares these results with corresponding ones for

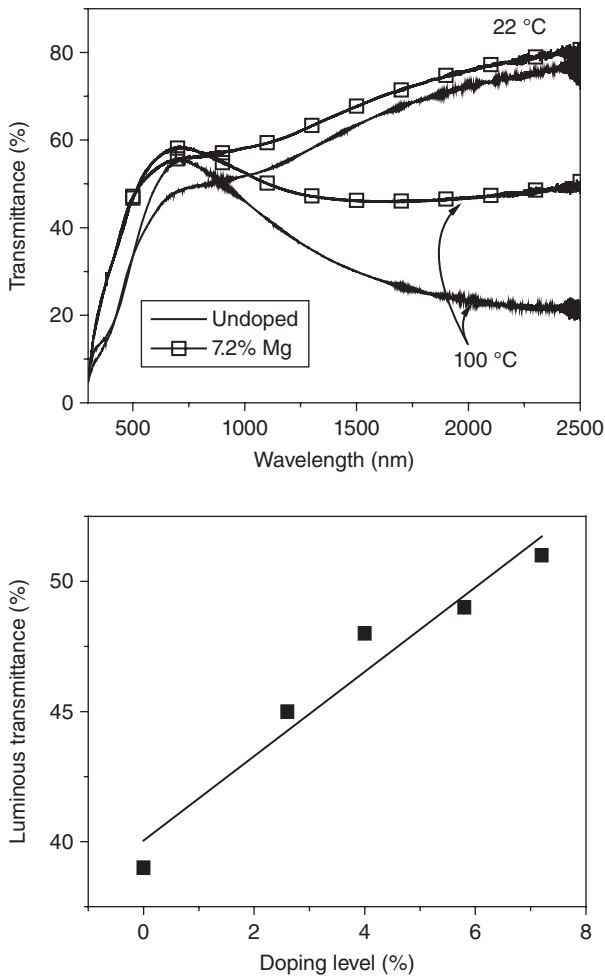

11.10 Upper panel shows the spectral transmittance at $\tau < \tau_c$ and $\tau > \tau_c$ and lower panel shows the luminous transmittance vs. doping level at $\tau < \tau_c$ for 0.05-μm-thick Mg-containing VO_2 films. The line in the lower panel was drawn for convenience. From Mlyuka *et al.* (2009c).

undoped VO_2. The lower panel of Fig. 11.10 elaborates the quantitative role of the Mg doping on T_{lum}, which is seen to go monotonically from ~40% to more than 50% when the Mg content is increased from zero to 7.2 at%. Some concomitant decrease of the distinctness of the thermochromism for $\lambda > 1$ μm is apparent from the upper panel of Fig. 11.10. Mg doping has a secondary beneficial effect as well, as it influences τ_c favourably, as mentioned briefly below.

A more detailed description of the band gap shifts in Mg-doped VO_2 films can be put forward via an evaluation of n and k for $0.3 < \lambda < 2.5$ μm and $\tau < \tau_c$. The absorption coefficient α was then derived from $\alpha = 4\pi k/\lambda$. Figure 11.11 shows an evaluation of $(\alpha\hbar\omega)^{1/2}$ versus $\hbar\omega$ (as is appropriate for indirect allowed band gaps; Wooten, 1972). Two band gaps appear: one shifting from ~1.6 to 2.3 eV for rising Mg doping and another lying at ~0.5 eV irrespective of the Mg doping. A preliminary interpretation of the two band gaps is feasible from the band structure in the proximity of the Fermi level for VO_2 at $\tau < \tau_c$ (Goodenough, 1971; Abe *et al.*, 1997) as elaborated elsewhere by Li *et al.* (2012).

11.3.4 Doped VO_2 films with thermochromic switching at room temperature

Doped VO_2, denoted $M_xV_{1-x}O_2$, can exhibit shifted values of their 'critical' temperature, and, at least for bulk specimens, M being W^{6+}, Mo^{6+}, Ta^{5+}, Nb^{5+} and Ru^{4+} yields a lowered τ_c, while M being Ge^{4+}, Al^{3+} and Ga^{3+} produces an increased τ_c (Goodenough, 1971). Thin films of doped VO_2 display the

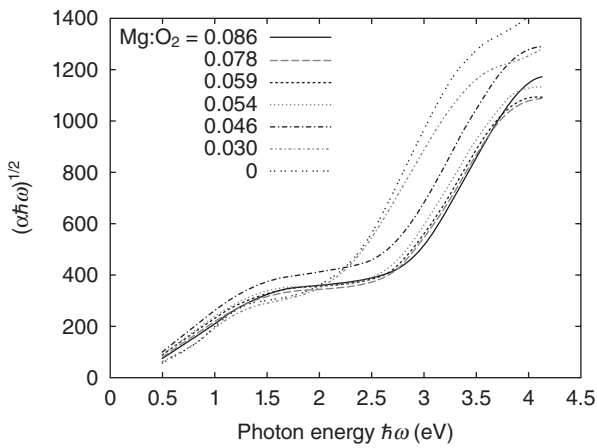

11.11 $(\alpha\hbar\omega)^{1/2}$ vs. $\hbar\omega$, where α is absorption coefficient and $\hbar\omega$ is photon energy, for Mg-doped VO_2 films at $\tau < \tau_c$.

same tendencies, but τ_c can also be influenced by several external parameters such as thickness, mechanical deformation, non-stoichiometry, small crystallite size, etc.

Tungsten is known to be the most efficient doping element for decreasing τ_c, i.e., it has the largest fall-off rate R as the amount of doping is increased. This material has been discussed in detail in the literature. For bulk crystals of $W_xV_{1-x}O_2$ it has been reported that $R = 27 \pm 1$°C/at%W (Goodenough, 1971; Hörlin *et al.*, 1972), while $R = 21$°C/at%W was stated in some subsequent work (Reyes *et al.*, 1976). It follows that as little as ~2 at% of tungsten is able to bring τ_c to a comfort temperature. Thin films of $W_xV_{1-x}O_2$ also have decreased values of τ_c, but the quantitative magnitudes of R have been found to lie between 7 and 26°C/at%W, i.e., differing by a factor of almost four; detailed data have been given elsewhere (Li *et al.*, 2012). Tungsten doping has only a very minor effect on the optical properties (Tazawa *et al.*, 1998).

There are two basic reasons why the data on τ_c for thin films are scattered, one being that the electrical properties depend strongly on crystallinity, grain size, and the conditions at the two interfaces of the films; the other reason is the difficulty of evaluating unique 'critical' temperatures from graded and hysteretic transitions of the resistance. Two experimental parameters of great significance are the substrate temperature during deposition and the post-deposition annealing temperature. Empirical data show that either of these temperatures must exceed ~450°C (Li *et al.*, 2012).

The films of $Mg_xV_{1-x}O_2$, discussed in Section 11.3.3 above, also have lowered values of their 'critical' temperatures, and $R \approx 3$°C/at%Mg describes the data (Mlyuka *et al.*, 2009c). This may be compared with measurements on bulk crystals of $Mg_xV_{1-x}O_{2-2x}F_{2x}$, which yielded $R \approx 6$°C/at%Mg (Akroune *et al.*, 1985).

11.4 Future trends in electrochromic and thermochromic glazing

This chapter has provided an introduction to oxide-based electrochromics and thermochromics and has discussed applications, device designs, and critical materials issues with regard to eco-efficient buildings. The discussion is now widened and includes a number of perspectives.

Beginning with applications, there have been numerous claims over the past decades that electrochromic glazings 'finally' are ready for implementation on a large scale. However, only prototypes and commercial products delivered to select customers or for very specific applications or markets have been presented so far. Is the situation going to change soon? The answer is almost certainly 'yes', and the basic reason is the worldwide awareness of the acute need for 'eco-efficient' or 'green' technologies,

particularly for the built environment as discussed by Smith and Granqvist (2010). There are several interesting electrochromic technologies with different pros and cons and a notion that *one* technology takes it all is most likely going to be false. One may compare this with the case of photovoltaics where a vast number of different device types and materials currently compete fiercely for market share.

What device types and materials will be dominating for electrochromic glazings? Again there is no obvious answer, but mass fabrication speaks in favour of low-cost roll-to-roll coating and continuous lamination, which definitely are applicable to electrochromics. Combinations of cathodic and anodic electrochromic oxides can be used to boost the coloration efficiency and obtain suitable luminous properties. These oxides are unlikely to be based on a single metal. Possibly the required transparent electrical conductors are getting ready for a revolution, and current work on metal-based and carbon-based materials may lead to radical cost cuts for electrochromic glazings.

Added functionality is of interest for electrochromic glazings devices. For example, should the infrared part of the solar radiation – with about half of the energy – be admitted or not when the devices are in their bright state? Near-infrared absorption can be accomplished by adding non-scattering nanoparticles to the polymer electrolyte; this was demonstrated for the case of ITO (Bayrak Pehlivan *et al.*, 2012), and LaB_6 (Schelm *et al.*, 2005) as well as Cs_xWO_3 (Guo *et al.*, 2011), which are other alternative nano-pigments. However, except under very cold climate conditions there is sometimes a need for heating, so that electrochromic glazing should transmit in the infrared, while at other times there is a need for cooling so that the infrared transmittance should be kept to a minimum. This functionality clearly calls for thermochromism.

Thermochromic glazings have a long history of unfulfilled promises regarding applications in buildings and automobiles. The first problem, that was obvious from the very beginning, was that the thermochromic switching has to take place around a comfort temperature of about 25°C. However, this was readily accomplished by tungsten doping of vanadium dioxide films. The film must be sufficiently crystalline which requires deposition or annealing temperatures of at least 400–500°C. Such temperatures are not any problem for coatings on float glass, but they are not compatible with deposition onto plastic web in a straightforward way.

Recent work has taken some steps towards thermochromic fenestration of practical interest. The first of these steps was the discovery (Mlyuka *et al.*, 2009c) of a doping element that was capable of widening the fundamental band gap of VO_2 so that the luminous transmittance was boosted. Another very significant step was the realization that VO_2-based nanoparticles could give a strong, broad and temperature-dependent plasma

absorption peak in the near infrared, which yields a much enhanced modulation of solar energy transmittance and a higher luminous transmittance (Li *et al.*, 2010). The next and obvious step, which has not yet been taken (in 2012), will be to explore the influence of Mg doping on VO_2 nanoparticles. Well crystallized VO_2-based nanoparticles – produced by some efficient high-temperature process – may be possible to embed in polymer foils and laminates (Ji *et al.*, 2011; Lu *et al.*, 2011), which opens interesting avenues towards low-cost implementation of thermochromic fenestration.

The recent advances in electrochromics and thermochromics make it interesting and timely to consider possibilities to develop 'super fenestration' in multiple-pane constructions with an electrochromic functionality on the outer panes – which may be dark or transparent depending on temperature or user preferences (Azens and Granqvist, 2003) – and thermochromic functionality on the inner panes which tends to follow the room temperature. The electrochromic and thermochromic components should be thermally decoupled, which can be done by vacuum insulation to cut down on conductive and convective heat transfer and a low-emittance coating to minimize radiative heat transfer (Baetens *et al.*, 2010b; Smith and Granqvist, 2010). The vacuum gap needs some spacer, such as tiny glass rods or silica aerogel. Figure 11.12 illustrates such 'super fenestration' with an electrochromic outer pane according to Fig. 11.2 and a thermochromic inner

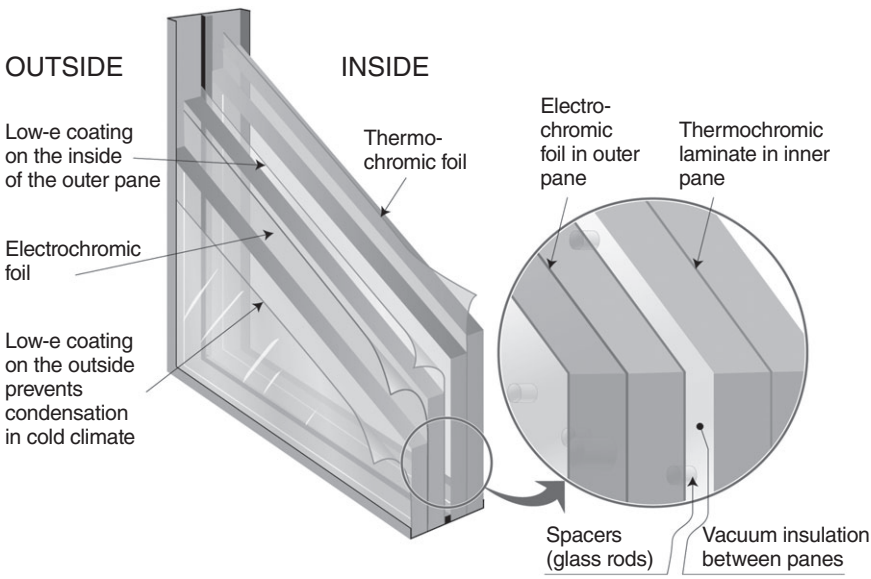

11.12 Conceptual sketch of 'super fenestration' combining electrochromic and thermochromic functionalities.

pane according to Fig. 11.9. Additional coatings may be used to improve the performance, such as a low-emittance coating on the innermost glass surface in order to prevent excessive thermal radiation into the building when the thermochromic foil is absorbing (not shown). A low-emittance coating on the outermost glass surface, as indicated in Fig. 11.12, may prevent condensation in cold climates (Smith and Granqvist, 2010).

Building skins with adjustable properties have been the architects' dream for decades (Wigginton, 1996; Campagno, 2002). Such skins will alter the very concept of a building into that of an entity which operates in harmony with nature rather than as, in most cases, in stark opposition to nature and requiring energy guzzling measures (such as air conditioning and artificial lighting) to create a livable indoor environment. Electrochromic foil technology, in particular, opens new avenues towards membrane architecture (Ishii, 1999; Koch, 2004; Fernández, 2007) and may make it possible to create climate shells and blurred zones between indoors and outdoors. The membranes can be based on ethylene tetrafluoroethylene (ETFE) with well-documented long-term durability as a building material (Robinson-Gayle *et al.*, 2001; LeCuyer, 2008).

As a final comment, we stress once again that a number of 'eco-efficient' or 'green' technologies are under intense development today (2012). They include thin film solar cells, light-emitting diodes of various types, polymer batteries, supercapacitors, electrochromics, and others. Advances in any one of these fields will be beneficial for the others, and this healthy co-evolution will speed up the progress for all of them.

11.5 References

Abe H, Terauchi M, Tanaka M, Shin S and Ueda Y (1997), 'Electron energy-loss spectroscopy of the metal-insulator transition in VO_2', *Jpn J Appl Phys*, 36, 165–169.

Akroune A, Claverie J, Tazairt A, Villeneuve G and Casalot A (1985), 'Propriétés structurales, magnétiques et electriques des oxyfluorures $V_{1-x}M_xO_{2-2x}F_{2x}$ (M = Mg, Ni)', *Phys Stat Sol A*, 89, 271–282.

Allen P B, Wentzcovitch R M, Schulz W W and Canfield P C (1993), 'Resistivity of the high-temperature metallic phase of VO_2', *Phys Rev B*, 48, 4359–4363.

ASTM (2003), 'G173-03 Standard Tables of Reference Solar Spectral Irradiances: Direct Normal and Hemispherical on a 37° Tilted Surface', *Annual Book of ASTM Standards*, Vol. 14.04, American Society for Testing and Materials, Philadelphia, PA, USA; http://rredc.nrel.gov/solar/spectra/am1.5.

Avendaño E, Azens A, Niklasson G A and Granqvist C G (2004), 'Electrochromism in nickel oxide films containing Mg, Al, Si, V, Zr, Nb, Ag, or Ta', *Solar Energy Mater Solar Cells*, 84, 337–350.

Aydogdu G H, Ruzmetov D and Ramanathan S (2010), 'Metastable oxygen incorporation into thin film NiO by low temperature active oxidation: influence on hole conduction', *J Appl Phys*, 108, 113702.

Azens A and Granqvist C G (2002), 'Electrochromism in Ir-Mg oxide films', *Appl Phys Lett*, 81, 928–929.

Azens A and Granqvist C G (2003), 'Smart windows: energy efficiency and device aspects', *J Solid State Electrochem*, 7, 64–68.

Azens A, Kullman L and Granqvist C G (2003a), 'Ozone coloration of Ni and Cr oxide films', *Solar Energy Mater Solar Cells*, 76, 147–153.

Azens A, Gustavsson G, Karmhag R and Granqvist C G (2003b), 'Electrochromic devices on polyester foil', *Solid State Ionics*, 165, 1–5.

Babulanam S M, Eriksson T S, Niklasson G A and Granqvist C G (1987), 'Thermochromic VO_2 films for energy-efficient windows', *Solar Energy Mater*, 16, 347–363.

Backholm J and Niklasson G A (2008), 'Optical properties of electrochromic iridium oxide and iridium–tantalum oxide thin films in different colouration states', *Solar Energy Mater Solar Cells*, 92, 1388–1392.

Bae S, Kim H, Lee Y, Xu X, Park J-S, Zheng Y, Balakrishnan J, Lei T, Kim H R, Song Y I, Kim Y-J, Kim K S, Özyilmaz B, Ahn J-H, Hong B H and Iijima S (2010), 'Roll-to-roll production of 30-inch graphene films for transparent electrodes', *Nature Nanotechnol*, 5, 574–578.

Bae S, Kim S J, Shin D, Ahn J-H and Hong B H (2012), 'Towards industrial applications of graphene electrodes', *Phys Scr*, T146, 014024.

Baetens R, Jelle B P and Gustavsen A (2010a), 'Properties, requirements and possibilities of smart windows for dynamic daylight and solar energy control in buildings: a state-of-the-art review', *Solar Energy Mater Solar Cells*, 94, 87–105.

Baetens R, Jelle B P, Thue J V, Tenpierik M J, Grynning S, Uvsløkk S and Gustavsen A (2010b), 'Vacuum insulation panels for building applications: a review and beyond', *Energy Buildings*, 42, 147–172.

Bai H, Cortie M B, Maaroof A I, Dowd A, Kealley C and Smith G B (2009), 'The preparation of a plasmonically resonant VO_2 thermochromic pigment', *Nanotechnology*, 20, 085607.

Bayrak Pehlivan İ, Runnerstrom E, Li S-Y, Niklasson G A, Milliron D J and Granqvist G A (2012), 'A polymer electrolyte with high luminous transmittance and low solar throughput: polyethyleneimine-lithium bis(trifluoromethylsulfonyl) imide with In_2O_3:Sn nanoparticles', *Appl Phys Lett*, 100, 241902.

Berggren L, Jonsson J C and Niklasson G A (2007), 'Optical absorption in lithiated tungsten oxide films: experiment and theory', *J Appl Phys*, 102, 083538.

Born M and Wolf E (1999), *Principles of Optics*, 7th edn, Cambridge University Press, Cambridge.

Cairns D R, Witte II R P, Sparacin D K, Sachsman S M, Paine D C, Crawford G P and Newton R R (2000), 'Strain-dependent electrical resistivity of tin-doped indium oxide on polymer substrates', *Appl Phys Lett*, 76, 1425–1427.

Campagno A (2002), *Intelligente Glasfassaden/Intelligent Glass Façades*, 5th edn, Birkhäuser, Basel, Switzerland.

Chen Y, Liang W D and Xu H (2010), 'Effect of Mo on phase transition of VO_2 nanopowders', *Mater Res Innovations*, 14, 173–176.

Clear R D, Inkarojrit V and Lee E S (2006), 'Subject reponses to electrochromic windows', *Energy Buildings*, 38, 758–779.

Cupelli D, Nicoletta F P, Manfredi S, Vivacqua M, Formoso P, De Filpo G and Chidichimo G (2009), 'Self-adjusting smart windows based on polymer-dispersed liquid crystals', *Solar Energy Mater Solar Cells*, 93, 2008–2012.

Deb S K (1973), 'Optical and photoelectric properties and colour centres in thin films of tungsten oxide', *Philos Mag*, 27, 801–822.

Degerman Engfeldt J, Georen P, Lagergren C and Lindbergh G (2011), 'Methodology for measuring current distribution effects in electrochromic smart windows', *Appl Opt*, 50, 5639–5646.

Denesuk M and Uhlmann D R (1996), 'Site-saturation model for the optical efficiency of tungsten oxide based devices', *J Electrochem Soc*, 143, L186-L188.

de Tacconi N R, Rajeshwar K and Lezna R O (2003), 'Metal hexacyanoferrates: *in situ* characterization, and applications', *Chem Mater*, 15, 3046–3062.

Eda G and Chhowalla M (2010), 'Chemically derived graphene oxide: towards large-area thin-film electronics and optoelectronics', *Adv Mater*, 22, 2392–2415.

Eichholtz P, Kok N and Quigley J M (2010), 'Doing well by doing good? Green office buildings', *Am Econ Rev*, 100, 2492–2500.

Eichholtz P, Kok N and Quigley J M (2011), 'The economics of green building', Report E^3 WP-002, University of California Center for Energy and Environmental Economics, Berkeley, CA.

Elschner A and Lövenich W (2011), 'Solution-deposited PEDOT for transparent conductive applications', *MRS Bull*, 36, 794–798.

Fernández E (2007), 'Materials for aesthetic, energy-efficient, and self-diagnostic buildings', *Science*, 315, 1807–1815.

Gardiner D J, Morris S M and Coles H J (2009), 'High-efficiency multistable switchable glazing using smectic A liquid crystals', *Solar Energy Mater Solar Cells*, 93, 301–306.

Geim A K and Novoselov K S (2007), 'The rise of graphene', *Nature Mater*, 6, 183–191.

Gentle A, Maaroof A I and Smith G B (2007), 'Optical and electrical switching in nanostructured coatings of VO_2', *Nanotechnology*, 18, 025202.

Gillaspie D T, Tenent R C and Dillon A C (2010), 'Metal-oxide films for electrochromic applications: present and future directions', *J Mater Chem* 20, 9585–9592.

Ginley D S, Hosono H and Paine D C (eds) (2010), *Handbook of Transparent Conductors*, Springer Science + Business Media, New York.

Glicksman L R (2008), 'Energy efficiency in the built environment', *Phys Today* (July), 35–40.

Goodenough J B (1971), 'The two components of the crystallographic transition in VO_2', *J Solid State Chem*, 3, 490–500.

Granqvist C G (1990), 'Chromogenic materials for transmittance control of large-area windows', *Crit Rev Solid State Mater Sci*, 16, 291–308.

Granqvist C G (1993), 'Electrochromic materials: microstructure, electronic bands, and optical properties', *Appl Phys A*, 57, 3–12.

Granqvist C G (1995), *Handbook of Inorganic Electrochromic Materials*, Elsevier, Amsterdam.

Granqvist C G (2007), 'Transparent conductors as solar energy materials: a panoramic review', *Solar Energy Mater Solar Cells*, 91, 1529–1598.

Granqvist C G (2008), 'Oxide electrochromics: why, how, and whither', *Solar Energy Mater Solar Cells*, 92, 203–208.

Granqvist C G (2012), 'Oxide electrochromics: an introduction to devices and materials', *Solar Energy Mater Solar Cells*, 99, 1–13.

Granqvist C G and Hunderi O (1977), 'Optical properties of ultrafine gold particles', *Phys Rev B*, 16, 3513–3534.

Granqvist C G and Hunderi O (1978), 'Optical properties of Ag-SiO_2 cermet films: a comparison of effective medium theories', *Phys Rev B*, 18, 2897–2906.

Granqvist C G, Green S, Niklasson G A, Mlyuka N R, von Kræmer S and Georén P (2010), 'Advances in chromogenic materials and devices', *Thin Solid Films*, 518, 3046–3053.

Graz I M, Cotton D P J and Lacour S P (2009), 'Extended cyclic uniaxial loading of stretchable gold thin-films on elastomeric substrates', *Appl Phys Lett*, 94, 071902.

Green S V, Pehlivan E, Granqvist C G and Niklasson G A (2012), 'Electrochromism in sputter deposited nickel-containing tungsten oxide films', *Solar Energy Mater Solar Cells*, 99, 339–344.

Greenberg C B (1983), 'Undoped and doped VO_2 films grown from $VO(OC_3H_7)_3$', *Thin Solid Films*, 110, 73–82.

Guo C, Yin S, Yan M and Sato T (2011), 'Facile synthesis of homogeneous Cs_xWO_3 nanorods with excellent low-emissivity and NIR shielding property by a water controlled-release process', *J Mater Chem*, 21, 5099–5105.

Hamberg I and Granqvist C G (1986), 'Evaporated Sn-doped In_2O_3 films: basic optical properties and applications to energy-efficient windows, *J Appl Phys*, 60, R123–R159.

Harada S, Yoshino K, Fukudome S, Kawano Y and Sei F (2011), 'Growth of IrO_x–SnO_x films deposited by reactive sputtering', *Jpn J Appl Phys*, 50, 05FB14 1–2.

Hecht D S and Kaner R B (2011), 'Solution-processed transparent electrodes', *MRS Bull*, 36, 749–755.

Heisler G M and Brazel A J (2010), 'The urban physical environment: temperature and urban heat islands', in Aitkenhead-Peterson J and Volder A (eds), *Urban Ecosystem Ecology*, Agronomy Monograph Series Vol. 55, American Society of Agronomy, Crop Science Society of America, Soil Science Society of America, Madison, WI, pp. 29–56.

Hörlin T, Niklewski T and Nygren M (1972), 'Electrical and magnetic properties of $V_{1-x}W_xO_2$, $0 \le x \le 0.060$', *Mater Res Bull*, 7, 1515–1524.

Hövel M, Gompf B and Dressel M (2010), 'Dielectric properties of ultrathin metal films around the percolation threshold', *Phys Rev B*, 81, 035402.

Hu L, Hecht D S and Grüner G (2010a), 'Carbon nanotube thin films: fabrication, properties and applications', *Chem Rev*, 110, 5790–5844.

Hu L, Kim H S, Lee J-Y, Peumans P and Cui Y (2010b), 'Scalable coating and properties of transparent, flexible, silver nanowire electrodes', *ACS Nano*, 4, 2955–2963.

Hu L, Wu H and Cui Y (2011), 'Metal nanogrids, nanowires, and nanofibers for transparent electrodes', *MRS Bull*, 36, 760–765.

Huang H, Tian J, Zhang W K, Gan Y P, Tao X Y, Xia X H and Tu J P (2011), 'Electrochromic properties of porous NiO thin film as a counter electrode for NiO/WO_3 complementary electrochromic window', *Electrochim Acta*, 56, 4281–4286.

Ishii K (ed.) (1999), *Membrane Designs and Structures in the World*, Shinkenchikusa-sha, Tokyo.

Jelle B P, Hynd A, Gustavsen A, Arasteh D, Goudey H and Hart R (2012), 'Fenestration of today and tomorrow: a state-of-the-art review and future research opportunities', *Solar Energy Mater Solar Cells*, 96, 1–28.

Ji S, Zhang F and Jin P (2011), 'Preparation of high performance pure single phase VO_2 nanopowder by hydrothermally reducing the V_2O_5 gel', *Solar Energy Mater Solar Cells*, 95, 3520–3526.

Jin Z-C, Hamberg I and Granqvist C G (1988), 'Optical properties of sputter-deposited ZnO:Al films', *J Appl Phys*, 64, 5117–5131.

Jonsson A and Roos A (2010), 'Visual and energy performance of switchable windows with antireflection coatings', *Solar Energy*, 84, 1370–1375.

Jonsson A, Roos A and Jonson E K (2010), 'The effect on transparency and light scattering of dip coated antireflection coatings on window glass and electrochromic foil', *Solar Energy Mater Solar Cells*, 94, 992–997.

Jorgenson G and Lee J C (1986), 'Doped vanadium oxide for optical switching films', *Solar Energy Mater*, 14, 205–214.

Kahr B, Freudenthal J, Phillips S and Kaminsky W (2009), Herapathite, *Science*, 344, 1407.

Khan K A and Granqvist C G (1989), 'Thermochromic sputter-deposited vanadium oxyfluoride coatings with low luminous absorptance', *Appl Phys Lett*, 55, 4–6.

Khan K A, Niklasson G A and Granqvist C G (1988), 'Optical properties at the metal-insulator transition in thermochromic $VO_{2-x}F_x$ thin films', *Appl Phys Lett*, 64, 3327–3329.

Ko C and Ramanathan S (2008), 'Stability of electrical switching properties in vanadium dioxide thin films under multiple thermal cycles across the phase transition boundary', *J Appl Phys*, 104, 086105.

Koch K-M (ed.) (2004), *Membrane Structures*, Prestel, Munich.

Kraft A and Rottmann M (2009), 'Propertes, performance and status of the laminated electrochromic glass of Gesimat', *Solar Energy Mater Solar Cells*, 93, 2088–2092.

Laik B, Carrière D and Tarascon J-M (2001), 'Reversible electrochromic system based on aqueous solution containing silver', *Electrochim Acta*, 46, 2203–2209.

Lampert C M (1984), 'Electrochromic materials and devices for energy efficient windows', *Solar Energy Mater*, 11, 1–27.

Lampert C M and Granqvist C G, eds (1990), *Large-Area Chromogenics: Materials and Devices for Transmittance Control*, SPIE Institutes for Advanced Optical Technologies, Vol. IS 4, SPIE – The International Society for Optical Engineering, Bellingham, WA.

Lan Y F, Peng W C, Lo Y H and He J L (2010), 'Durability under mechanical bending of the indium tin oxide films deposited on polymer substrate by thermionically enhanced sputtering', *Org Electr*, 11, 670–676.

Landau L D, Lifshitz E M and Pitaevskii L P (1984), *Electrodynamics of Continuous Media*, 2nd edn, Butterworth Heinemann, Oxford.

Lansåker P C, Backholm J, Niklasson G A and Granqvist C G (2009), 'TiO_2/Au/TiO_2 multilayer thin films: novel metal-based transparent conductors for electrochromic devices', *Thin Solid Films*, 518, 1225–1229.

LeCuyer A (2008), *ETFE: Design and Technology*, Birkhäuser, Basel, Switzerland.

Lee E S, Claybaugh E S and LaFrance M (2012), 'End user impacts of automated electrochromic windows in a pilot retrofit application', *Energy Buildings*, 47, 267–284.

Leech J A, Nelson W C, Burnett R T, Aaron S and Raizenne M E (2002), 'It's about time: a comparison of Canadian and American time–activity patterns', *J Expo Anal Environ Epidemiol*, 12, 427–432.

Li S-Y, Niklasson G A and Granqvist C G (2010), 'Nanothermochromics: Calculations for VO_2 nanoparticles in dielectric hosts show much improved luminous transmittance and solar energy transmittance modulation', *J Appl Phys*, 108, 063525.

Li S-Y, Niklasson G A and Granqvist C G (2011a), 'Nanothermochromics with VO_2-based core–shell structures: calculated luminous and solar optical properties', *J Appl Phys*, 109, 113515.

Li S-Y, Niklasson G A and Granqvist C G (2011b), 'A thermochromic low-emittance coating: calculations for nanocomposites of In_2O_3:Sn and VO_2', *Appl Phys Lett*, 99, 131907.

Li S-Y, Niklasson G A and Granqvist C G (2012), 'Thermochromic fenestration with VO_2-based materials: three challenges and how they can be met', *Thin Solid Films*, 520, 3823–3828.

Lu Z, Li C and Yin Y (2011), 'Synthesis and thermochromic properties of vanadium dioxide colloidal particles', *J Mater Chem*, 21, 14776–14782.

Marks A M (1969), 'Electrooptical characteristics of dipole suspensions', *Appl Opt*, 8, 1397–1412.

Mathew J G H, Sapers S P, Cumbo M J, O'Brien N A, Sargent R B, Rakhsha V P, Ladaherne R B and Hichwa B P (1997), 'Large area electrochromics for architectural applications', *J Non-Cryst Solids*, 218, 342–346.

Maxwell-Garnett J C (1904), 'Colours in metal glasses and in metallic films', *Philos Trans Roy Soc London*, 203, 385–420.

McKinsey & Co (2009), *Unlocking Energy Efficiency in the US Economy*, available at: http://www.mckinsey.com/clientservice/electricpowernaturalgas/downloads/US_energy_efficiency_full_report.pdf.

Metz B, Davidson O R, Bosch P, Dave R and Meyer L A (eds) (2007), *Climate Change 2007: Mitigation. Contribution to Working Group III of the Fourth Assessment Report of the Intergovernmental Panel on Climate Change*, Cambridge University Press, Cambridge.

Mitsuishi T (1967), 'On the phase transformation of VO_2', *Jpn J Appl Phys*, 6, 1060–1071.

Mlyuka N R, Niklasson G A and Granqvist C G (2009a), 'Thermochromic multilayer films of VO_2 and TiO_2 with enhanced transmittance', *Solar Energy Mater Solar Cells*, 93, 1685–1687.

Mlyuka N R, Niklasson G A and Granqvist C G (2009b), 'Thermochromic VO_2-based multilayer films with enhanced luminous transmittance and solar modulation', *Phys Stat Sol A*, 206, 2155–2160.

Mlyuka N R, Niklasson G A and Granqvist C G (2009c), 'Mg doping of thermochromic VO_2 film enhances the optical transmittance and decreases the metal-insulator transition temperature', *Appl Phys Lett*, 95, 171909.

Monk P M S, Mortimer R J and Rosseinsky D R (2007), *Electrochromism and Electrochromic Devices*, Cambridge University Press, Cambridge.

Morin F J (1959), 'Oxides which show a metal-to-insulator transition at the Neel temperature', *Phys Rev Lett*, 3, 34–36.

Niklasson G A and Granqvist C G (1984), 'Optical properties and solar selectivity of coevaporated Co-Al_2O_3 composite films, *J Appl Phys*, 55, 3382–3410.

Niklasson G A and Granqvist C G (2007), 'Electrochromics for smart windows: thin films of tungsten oxide and nickel oxide, and devices based on these', *J Mater Chem*, 17, 127–156.

Niklasson G A, Granqvist C G and Hunderi O (1981), 'Effective medium models for the optical properties of inhomogeneous materials', *Appl Opt*, 20, 26–30.

Niu C (2011), 'Carbon nanotube transparent conducting films', *MRS Bull*, 36, 766–773.

Norrman S, Andersson T, Granqvist C G and Hunderi O (1978), 'Optical properties of discontinuous gold films', *Phys Rev B*, 18, 674–695.

Oka Y, Yao T and Yamamoto N (1990), 'Powder X-ray crystal structure of VO_2(A), *J Solid State Chem*, 86, 116–124.

Okazaki K, Sugai S, Muraoka Y and Hiroi Z (2006), 'Role of electron-electron and electron-phonon interaction effects in the optical conductivity of VO_2', *Phys Rev B*, 73, 165116.

Parkin I P, Binions R, Piccirillo C, Blackman C S and Manning T D (2008), 'Thermochromic coatings for intelligent architectural glazing', *J Nano Res*, 2, 1–20.

Reyes J M, Sayer M and Chen R (1976), 'Transport properties of tungsten-doped VO_2', *Can J Phys*, 54, 408–412.

Richter B, Goldston D, Crabtree G, Glicksman L, Goldstein D, Greene D, Kammen D, Levine M, Lubell M, Savitz M, Sperling D, Schlachter F, Scofield J and Dawson J (2008), 'How America can look within to achieve energy security and reduce global warming', *Rev Mod Phys*, 80, S1–S107.

Robinson-Gayle S, Kolokotroni M, Cripps A and Tanno S (2001), 'ETFE foil cushions in roofs and atria', *Construction Building Mater*, 15, 323–327.

Saeli M, Piccirillo C, Parkin I P, Ridley I and Binions R (2010a), 'Nano-composite thermochromic thin films and their application in energy-efficient glazing', *Solar Energy Mater Solar Cells*, 94, 141–151.

Saeli M, Piccirillo C, Parkin I P, Binions R and Ridley I (2010b), 'Energy modeling studies of thermochromic glazing', *Energy Buildings*, 42, 1666–1673.

Schelm S, Smith G B, Garrett P D and Fisher W K (2005), 'Tuning the surface-plasmon resonance in nanoparticles for glazing applications', *J Appl Phys*, 97, 124314.

Selkowitz S E and Lampert C M (1990), 'Application of large-area chromogenics to architectural glazing', in Lampert C M and Granqvist C G (eds), *Large-Area Chromogenics: Materials and Devices for Transmittance Control*, SPIE Institutes for Advanced Optical Technologies, Vol. IS 4, SPIE – The International Society for Optical Engineering, Bellingham, WA, pp. 22–45.

Smith G B and Granqvist C G (2010), *Green Nanotechnology: Solutions for Sustainability and Energy in the Built Environment*, CRC Press, Boca Raton, FL.

Smith G B, Niklasson G A, Svensson J S E M and Granqvist C G (1986), 'Noble-metal-based transparent infrared reflectors: experiments and theoretical analyses for very thin gold films', *J Appl. Phys*, 59, 571–581.

Stjerna B, Olsson E and Granqvist C G (1994), 'Electrical and optical properties of RF sputtered tin oxide films doped with oxygen vacancies, F, Sb, or Mo', *J Appl Phys*, 76, 3797–3817.

Subrahmanyam A, Kumar C S and Karuppasamy K M (2007), 'A note on fast protonic solid state electrochromic device: $NiO_x/Ta_2O_5/WO_{3-x}$', *Solar Energy Mater Solar Cells*, 91, 62–66.

Svensson J S E M and Granqvist C G (1984), 'Electrochromic tungsten oxide films for energy efficient windows', *Solar Energy Mater*, 11, 29–34.

Svensson J S E M and Granqvist (1986), 'Electrochromic hydrated nickel oxide coatings for energy efficient windows: optical properties and coloration mechanism', *Appl Phys Lett*, 49, 1566–1568.

Taguchi O and Chonan T (2006), 'Three cases of indium lung', *J Jpn Respiratory Soc*, 44, 532–536.

Tajima K, Yamada Y, Bao S, Okada M and Yoshimura K (2010), 'Optical switching properties of all-solid-state switchable mirror glass based on magnesium-nickel thin film for environmental temperature', *Solar Energy Mater Solar Cells*, 94, 227–231.

Tajima K, Yamada Y, Okada M and Yoshimura K (2011), 'Polyvinyl chloride seal layer for improving the durability of electrochromic switchable mirrors based on Mg-Ni thin film', *Thin Solid Films*, 519, 8114–8118.

Tazawa M, Jin P and Tanemura S (1998), 'Optical constants of $V_{1-x}W_xO_2$ films', *Appl Opt*, 37, 1858–1861.

Théobald F, Cabala R and Bernard J (1976), 'Essai sur la structure de VO_2(B)', *J Solid State Chem*, 17, 431–438.

UNEP (2007), *Buldings and Climate Change: Status, Challenges and Opportunities*, United Nations Environment Programme, Paris.

Vergaz R, Sánchez-Pena J-M, Barrios D, Vázquez C and Contreras-Lallana P (2008), 'Modelling and electro-optical testing of suspended particle devices', *Solar Energy Mater Solar Cells*, 92, 1483–1487.

Wang Y, Zhang Z, Zhu Y, Li Z, Vajtai R and Ajayan P M (2008), 'Nanostructured VO_2 photocatalysts for hydrogen production', *ACS Nano*, 2, 1492–1496.

Wigginton M (1996), *Glass in Architecture*, Phaidon, London.

Wooten F (1972), *Optical Properties of Solids*, Academic Press, New York.

Wu C, Hu Z, Wang W, Zhang M, Yang J and Xie Y (2008), 'Synthetic paramontroseite VO_2 with good aqueous lithium-ion battery performance', *Chem Commun*, 3891–3893.

Wyszecki G and Stiles W S (2000), *Color Science: Concepts and Methods, Quantitative Data and Formulae*, 2nd edn, Wiley, New York.

Xu C, Ma C, Kong X and Taya M (2009), 'Vacuum filling process for electrolyte in enhancing electrochromic polymer window assembly', *Polymers Adv Technol*, 20, 178–182.

Ye J, Zhou L, Liu F, Qi J, Gong W, Lin Y and Ning G (2010), 'Preparation, characterization and properties of thermochromic tungsten-doped vanadium dioxide by thermal reduction and annealing', *J Alloys Compounds*, 504, 503–507.

Ziegler J P (1999), 'Status of reversible electrodeposition electrochromic devices', *Solar Energy Mater Solar Cells*, 56, 477–493.

Zinzi M (2006), 'Office worker preferences of electrochromic windows: a pilot study, *Building Environment*, 41, 1262–1273.

12

Third generation photovoltaic (PV) cells for eco-efficient buildings and other applications

L. A. LAMONT, Mott MacDonald Ltd, UK

DOI: 10.1533/9780857098832.2.270

Abstract: Solar technology has developed from a basic idea to a technology that could help support the world's increasing energy requirements. Currently, first and second generation panels are used widely in industry but do not offer the most efficient and cost effective product. It is hoped that the third generation can overcome these problems, either through multi-junction devices or the use of different materials/technologies. One area of interest is nanotechnology as this is something that could be used in photovoltaic panels and provide the higher efficiency levels demanded by industry at a reasonable cost; hence providing a feasible tool to support ever-expanding energy requirements. However, this is not yet commercially viable and a lot more research and development is needed.

Key words: photovoltaic, solar energy, renewable energy, nanotubes, quantum dots, first generation, second generation, third generation.

12.1 Introduction

The sun is a source of practically unlimited energy and is essential for life on earth. Currently the sunlight that reaches the earth in a single hour is equivalent to what we use in one year and hence it will comfortably meet our future worldwide energy needs. The amount of sun that each country receives varies, and the Middle East, one of the sunbelt regions, receives nearly double that of European countries, highlighting where the geographical future focus of this technology could lie. The energy from the sun is clean, free and continuous during daylight hours. Solar energy is caused by a fusion reaction of hydrogen molecules, which occurs between the hydrogen and helium gases contained in the sun's core. However, this reaction is not what provides our energy. It is the loss matter that is produced as a by-product of this reaction that provides the energy we use. As the saying goes, one man's waste is another man's gold, and the sun's waste – radiant energy – is what can be used freely as our ultimate power source.

The sun is known for its extreme temperatures and high pressure, but this is not harmful to humans as it is located far away from earth and it is this that makes it such a useful power source. The output of the nuclear

fusion that is harnessed for conversion into electricity is completed through a scientific innovation discovered in the nineteenth century. Previously we only optimized the heat and light from the sun, but this new innovation – the photovoltaic cell, which works using the principle of the photoelectric effect – also enables power to be harnessed. Explained in its simplest form, the photovoltaic cell is a device that enables the conversion of sunlight into electricity, which is known as solar power.

One question many people ask is whether all the radiation reaching the earth can be used for direct conversion. The simple answer is no, as primarily the human race does not currently need all the energy the sun provides (many thousand times daily more than we can cope with) and also the sun is used not only for producing electricity, but it also has many other functions. Nearly half of the radiation hitting the earth (which is already dramatically reduced due to filtering by the earth's atmosphere), is either reflected directly back into space or used for water evaporation, and the remaining amount is free energy to provide warmth and light, grow food, and potentially supply as much energy as mankind could ever want. It is a little known fact that all energy sources come from the sun, except for nuclear, and therefore for years humans have been using this power, although not for direct conversion. Even the world's current huge energy demand does not utilize all the potential energy provided and a lot of the sun's free energy goes unused.

Although there are many advantages of solar energy, there are also many negative factors, such as:

- restriction of generation to daylight hours
- efficiency of solar cells can be affected by pollution and weather
- harnessing solar energy on an industrial scale can be extremely expensive
- efficient long-term storage of solar energy is limited and this area needs to be further investigated.

Solar energy has been hailed as the development for the future of mankind, but whether it will eventually live up to this accolade is very much still to be proven. One thing is certain: with dwindling supplies of traditional fuel reserves, we must keep on searching for ways to harness solar energy for the generations to come.

12.2 History of photovoltaic (PV) cells

Solar energy has already been in development in various forms for well over 150 years and this will continue and increase for at least the next 150 years. Alexandre Edmond Becquerel's first discovery of the photoelectric effect in 1839 truly was the first step in relation to the development of solar

energy. In 1873 Willoughby Smith, although not directly researching into solar energy, found that selenium had sensitivity to light, hence opening an interesting area of research, using selenium to produce solar cells. This principle was separately verified by Richard Day and William Adams in 1876 with only a slight modification of a platinum intersection. Adams continued in 1877 to produce an initial selenium solar cell, with Charles Fritts in 1883 building another solar cell. The device had poor efficiency of approximately 1–2% and it was produced by forming a junction of gold on the semiconductor selenium. This was just the start, and levels of efficiency and performance could only improve from this point. However, it was not until 1888 that the first patent in the US was filed by Edward Weston for a 'Solar Cell' (Weston, 1888).

After the initial discovery, there was little progress for nearly 20 years, but in the early twentieth century Nikola Tesla filed his patents on 'Apparatus for the Utilization of Radiant Energy' (Tesla, 1901a) and 'Method of Utilizing Radiant Energy' (Tesla, 1901b). This started a revival and some further publications were produced with the most commonly known by Albert Einstein in 1905 entitled 'On a Heuristic Viewpoint Concerning the Production and Transformation of Light' (Einstein, 1905), discussing the photoelectric effect which in 1921 would gain him the Nobel Prize, and be further verified in 1916 by Robert Milliken. During the past century a great deal of work has been ongoing on the photoelectric effect on different materials and also photovoltaic cell structures.

Although Russell Ohl in 1946 patented the 'modern solar cell', the first research team to really bring photovoltaics to the general public was Pearson, Chapin and Fuller from Bell Laboratories, who in the 1950s worked on PV efficiency and patented their discoveries (Chapin *et al.*, 1954, 1957). The first practical use of a photovoltaic (PV) was in 1958 when the US Signal Corps powered the Vanguard 1 satellite with solar energy for an eight-year period. For many years the implementation of PVs was limited to the space industry before terrestrial panels became more cost-effective.

Now, in the twenty-first century, photovoltaics are widely accepted as an efficient form of energy supply and can be used for both on-grid and off-grid electrical applications. They are not limited to this usage but can also be successfully used to power cars like the General Motors Sunracer vehicle in 1997 or even airplanes such as the Solar Challenger in 1981 or the Icar Plane in 1996. Initially the US led the way in using solar panels but Europe quickly followed, expanding the technology worldwide. In 2011, although the countries of Europe were still extremely strong contenders in the race to be the top PV country, the Japanese were also successfully throwing their hat in the ring (Fig.12.1). Worldwide, the capacity has expanded from the 58% increase which occurred from 2006 to 74% in 2011, showing how worldwide PV capacity has, in 2011, reached 70 GW.

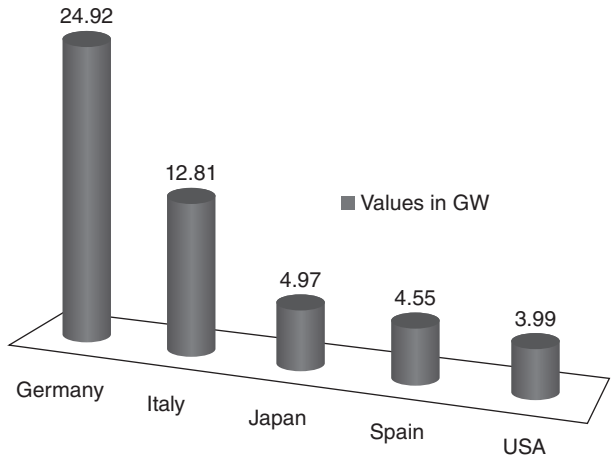

12.1 Top five global PV country producers in 2011.

However, the leader in total capacity as seen in Fig.12.1 is unlikely to change dramatically for the next few years due to its current extensive lead and addition of new projects. Surprisingly, one thing that did change in 2011 is that Italy jumped ahead of Germany in the amount of PVs added followed by a new player – China – which came in third, showing that the number of countries embracing solar energy is expanding. PV systems are now successfully used in more than 120 countries with 25% of the market being utility-scale. Currently most of the manufacturing process has moved from the US to Asia, with 61% of 2011 global production located in this area.

The drive to continue worldwide embracement of PVs has not slowed down. In 2011 the main leaps forward took place in Europe and China. Germany has continued its love for solar energy but it is now joined by Italy, both rising by 57%, asserting themselves by the amount of the electric energy produced by PVs in 2011 as market leaders in the utilization of this energy source. In relation to the manufacturing element, China has risen as the frontrunner, not only housing the largest manufacturing PV company, Suntech Power Holding, but also being given the title of the country producing most (650 panel manufacturing companies) of the world's PV panels. However, as the market expands, so does the interest in new utility-scale markets, which are emerging in Mali, China, Bulgaria, the United Arab Emirates, Egypt, Thailand and India, with the future being very much related to the regions of the Middle East, Africa, South America, India and China. Like many other countries that have embraced PVs, Europe has set some targets it wants to achieve in the next decade for the embracement of renewable energy. The continent states that by 2020 more than 33% of

electricity will be produced by renewable energy sources, with up to 12% of this being specifically related to PVs.

12.3 Functions of a photovoltaic (PV) cell

Although technology has branched out in relation to the combination of materials used and the production methods selected, the basic operating principles are the same as they all aim to take the range of intensities from daylight and absorb the photons from it to create an electric current, hence the reason it was named 'photovoltaic' as it produces electricity from light (Fig.12.2).

The structure of the cell as shown in Fig.12.3 outlines simply how in the basic first generation crystalline silicon solar cell the sunlight is transferred into electrical energy, which is really the only energy source with no limit to its potential. These cells are manufactured from similar materials to those used in semiconductor wafers which create an electric field with one side being negative and the reverse positive. However, a PV panel is not a single cell, but rather a combination of series and parallel cells, which creates an array and are connected and housed in a structure encapsulated by a glass surface. With the cells connected in series providing a larger voltage and

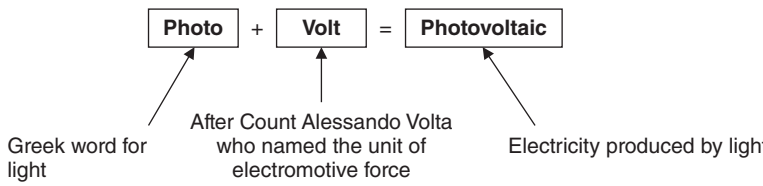

12.2 The origin of the word photovoltaic.

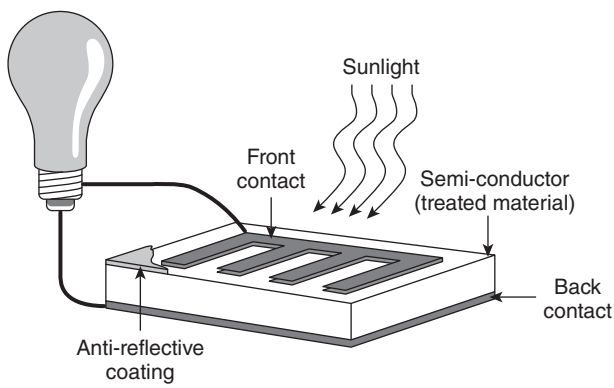

12.3 Operation of a basic first generation PV.

the increased current coming from parallel connections, although the cell voltage is not sensitive to light intensity, the current is affected. This structure enables a variety of voltage and current options to be available depending on the user's requirements. The steps (Table 12.1) of the process that is undertaken in the cell are highlighted below but it needs to be noted that when sunlight hits the panel not all energy is directly converted to direct current (DC) electricity, as the light can either be absorbed, reflected or move straight through the cell.

A common assumption by many is that this principle will only work on sunny days. This is incorrect; solar power works to its maximum when there are no clouds in the sky and the sun is in its optimum position, but it will also operate without maximum sun, albeit slightly less efficiently. Out of the many renewable energy technologies, it is suspected that solar power could have the brightest future, not only because of potential advancements in materials and production methods but also because of some basic engineering principles embedded in the technology. PV cells currently produce approximately 1.5 W, dependent on size, so when they are placed together in a matrix form on a frame covered in glass, this is referred to as a module raising possible output. Several modules can be furthermore connected together in an array to provide any power combination required; hence in this configuration output power is not an issue. As with all innovations, PVs have positive and negative points as outlined in Table 12.2; however, resear-

Table 12.1 Steps in producing electricity from the sun

Step	Description
1	Solar panel is struck by photons contained in sunlight
2	In the semiconductor material, negative electrons are knocked loose from their atoms
3	Enabling movement in a single direction in the material
4	Creating the possibility of an electric circuit from the electrons
5	Provided the negative and positive of the cell are connected, then DC electricity is generated

Table 12.2 Photovoltaic advantages and disadvantages

Advantages	Disadvantages
No moving parts	High costs
Operates quietly	Low efficiency
No operating emissions	More expensive than fossil fuels
Long term use	
Limited-maintenance	
Modular – enabling gradual expansion	

Table 12.3 Factors affecting efficiency

	Factors
1	Fill factor
2	Collection efficiency
3	Surface reflection losses
4	Shading of front metal contacts
5	Voltage factor
6	Issues with energy requirements to break bond to create free electrons
7	Loss of extra energy from the photons as it is split into thermal and one free electron
8	Losses due to incomplete absorption caused by the small thickness of the cell

chers are constantly working on remedying, improving and eliminating the negative factors.

One of the issues widely discussed in relation to the solar cell is that of efficiency. Initially the factors highlighted in Table 12.3 were defined as the most important elements reducing the efficiency of the solar cell, but it should be possible to address some of these in future generations of this technology. The efficiency ratio discussed considers the relationship between the output and optical powers of incident solar light and there are several factors that can affect this (especially the first generation PV) which are highlighted in Table 12.3.

Before it is identified which technology could potentially solve any of these issues, it is first important to have a broad understanding of the different technologies available and the differences between them.

12.4 Overview of photovoltaic (PV) technology: first, second and third generation cells

The PV industry started with one basic technology but has now expanded its search for the most optimal solution to convert solar energy into electricity. Currently there are three main areas that both the industrial and research communities are considering. The first and second generation PVs are more industry-focused, with some research being completed, and the third generation is still being heavily researched due to the drive from industry to develop a device that could be the solution to all our solar energy concerns. Although there have been many new innovations in materials over the years, the most common material for the production of solar cells to date is still silicon. Outlined below is an overview of the current technology used in solar modules, from the traditional mono-crystalline silicon to the second generation thin films, including the rest of the silicon

family, polycrystalline and amorphous, but also not forgetting the semiconductor PVs that are manufactured from compound materials and the new and promising third generation developments. This section gives an overview of how and why the technology moved from the first to the second generation, and how it is hoped that the best of both can be used to provide a third generation that might solve all previously acknowledged issues. Figure 12.4 outlines the efficiency levels of some of the first, second and third generation PVs, recorded in 2010 (Saari, 2010).

The following sections summarize where the technologies are now but also question how they got to this point and the historical steps that were taken to arrive at today's technology, before providing a glimpse of where it could go in the future.

12.4.1 First generation

The first generation had one simple task, with no limitations, which was split into two steps:

1. Absorb light energy so positive and negative charges can be generated.
2. Create a potential difference by separating the positive and negative charges.

This generation of solar cells is commonly known to have, on the positive side, high efficiency, but on the flip side it also has a higher cost, to be expected with any new technology. It is estimated that the maximum theoretical efficiency that these single junction silicon cells could hope to reach is approximately 33%, limited only by thermodynamics (Shockley and Queisser, 1961). To date, first generation PVs account for the largest market

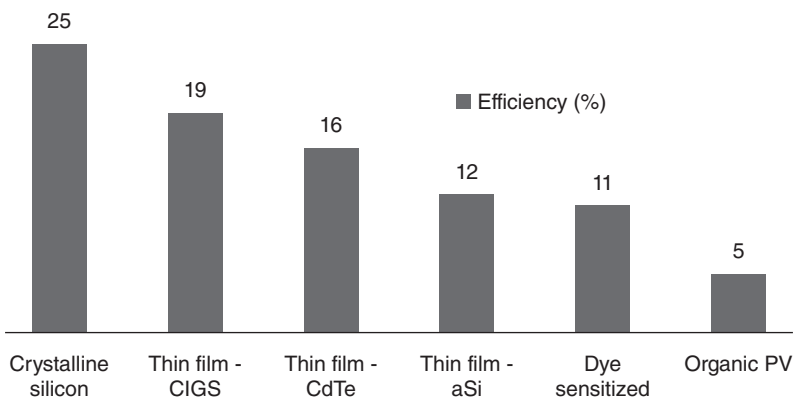

12.4 Energy levels achieved by PVs in 2010 (Saari, 2010).

Table 12.4 Photovoltaic first generation summary

Monocrystalline silicon (single crystalline)	
Efficiency	14–16%
Degradation	0.25–0.50% every year
Advantages	Due to the production process has a large possible output power Currently most commonly used technology Most commercially viable technology
Disadvantage	Cost is an issue due to their production technique
Polycrystalline silicon (semi- or multi-crystalline)	
Efficiency	10–11%
Degradation	0.25–0.50% every year
Advantages	Unlike monocrystalline, can be easily shaped Efficiency losses are not good but are being improved through R&D
Disadvantage	Uses a lower grade of silicon which is also lower in cost but less efficient

share, but this is changing (Brown and Wu, 2009). One of the issues with this technology is its manufacturing process, which is expensive and based on the same principles as the computer industry, with the two major elements being the requirement for pure silicon (with the higher purity providing greater possible efficiency), and the single-junction photon energy extraction. Crystalline silicon PVs have to their advantage the fact that there is an abundance of raw material, and, due to the maturity of this technology, they have a long life, high module reliability, and are nearly at their maximum theoretical efficiency. However, developers have discovered that silicon is not the optimal material for PV cells and it is considered highly unlikely that the cost of this generation will ever drop below the equivalent energy cost of fossil fuels. There is no clear solution to the high labour and energy required for the production, again providing a barrier to reduction in cost. Table 12.4 summarizes the efficiency, degradation and the advantages/disadvantages of this first generation PVs for two models.

12.4.2 Second generation

The middle member of the PV family, which has been under constant research since the late twentieth century, is the second generation solar panel. It is considered as the smaller but fastest growing division (Brown and Wu, 2009). It has opposite traits to the first generation, and has both lower cost and energy – essentially the two issues it was created to address, following the shortcomings of the first technology (Hamakawa, 2004). The main reason for the difference in the two technologies is related to the

smaller amounts of material, in addition to the lower manufacturing process cost. It was theorized that the ideal solar panel would not utilize the wafer principle as it uses a lot of material, hence the development of the thin film principle. The thin film was created by using various inexpensive deposition methods to produce thin layers of silicon, micrometres thick, which enable approximately 90–95% of the solar light spectrum to be absorbed, compared to the first generation which would need to be 200–400 μm thick for the same amount of absorption. The difference in this silicon material is it contains almost no crystal structure, hence can neither be referred to as crystalline nor multi-crystalline. Rather, it is named amorphous silicon (a-Si).

The main issue with this material is its low electrical properties, hence not improving overall efficiency. Many interesting structures and processes have enabled such PVs to reach approximately 10% efficiency, but this is anticipated to improve. One of the largest issues with the a-Si is the Staebler-Wronski phenomenon (Kolodziej, 2004), which basically causes degradation when the panel is exposed to sunlight. So, although this component of the second generation technology has good potential due to its low cost, more research and development is required to ensure a stable and efficient device. One of the most interesting principles associated with this technology is it has the ability to be either flexible or semi-transparent, leading the way to further installation options. If no flexibility is required, it is placed between two pieces of glass with no frame, but if flexibility is needed then it can be deposited onto plastic film. This thin film technology is normally connected with the second generation, but silicon is not the only material that can be linked with this group of PV technologies.

Panels are also commonly associated with materials that include cadmium telluride and cadmium sulphide layers (CdTe/CdS) or members of the chalcopyrite family, copper indium gallium selenide and copper indium diselenide (CIGS/CIS), which offer high-efficiency possibilities. As can be seen, the difference between these two initial types of PVs is the material used and the manufacturing methods, rather than a difference in the method of conversion.

One further technology that is sometimes considered under this second generation umbrella is the PVs made from organic materials, which currently (2012) have a very low efficiency of 1–8%, but have potential because, not only is the material accessible, but it is reasonably priced to further support easy and cheap manufacturing methods. These organic devices, which operate in a similar way to the photosynthesis process, could in the future offer an alternative to inorganic materials.

It has been anticipated that not only will this second generation technology have the market share by 2015 but also by this year it will be able to provide power at a lower cost than fossil fuel. It is only with time that we

Table 12.5 Photovoltaic second generation summary

a-Si (amorphous silicon)	
Efficiency	5–7%
Degradation	2% in the first initial months
Advantages	Cheap to produce
	Absorbs light better hence they are thinner and cheaper
	Can be applied as a thin layer to a variety of material both flexible and non-flexible
	Good for building integrated PVs
Disadvantages	Poor cell efficiency
	Fast degradation
	Low efficiency
	Larger surface area required for commercial installation
Compound semi-conductors	
Efficiency	CIS (copper indium gallium) – 12%
	GaAs (gallium arsenide) – up to 40%
	CIGS (copper indium gallium selenide) – 12–15%
	CdTe (cadmium telluride) – 10%
Degradation	Varying
Advantages	Has not seen the high degradation experienced by amorphous silicon
	Overall the initial development of the modules is impressive
	GaAs is good for high temperature performance and efficiency
	CdTe has a low cost production process
	CIGS and CIS have good efficiency and low cost production
Disadvantages	Requires thicker layers than amorphous silicon
	Indium is expensive
	Issues with toxic gases used in the production of CIS and CIGS
	GaAs both material and production is expensive
	Cadmium is toxic

will be able to assess if their lifetime will be proven compatible with first generation technology. Table 12.5 summarizes the efficiency, degradation and the advantages/disadvantages of second generation PVs for two models.

12.4.3 Third generation

Third generation PVs are still heavily under research. Although development of this technology has been ongoing for about 20 years, they are only now starting to emerge on to the market. It is expected that third generation photovoltaics will combine the best of both the first and second generation technologies; hence they should have high efficiency and low cost. The original definition of 'third generation' was that the technology had to have

Table 12.6 Third generation PV potential efficiencies (Green, 2009)

Solar conversion methods	Efficiency (%)
Circulators	74
Tandem (n = infinity)	68
Tandem (n = 6)	58
Thermal, thermo PV, thermionic	54
Tandem (n = 3)	50
Impurity PV & band, up-converters	49
Impact ionization	45
Tandem (n = 2)	44
Down-converters	39
Single cell (n = 1)	31

an intrinsically higher efficiency than a single junction device, had to use thin-film technology, as well as abundant, non-toxic, durable materials (Green, 2009). However, this has been developed as researchers have worked on this area and Table 12.6 outlines some of the third generation solar conversion methods and their approximate associated efficiency (Green, 2009).

Researchers expect that this generation will have the ability to overcome the Shockley–Queisser boundary of 31–41% efficiency which was seen by previous generations. The Shockley–Queisser limit is most simply put as a basic physics boundary on the maximum possible solar cell efficiency, and aims to maintain low production costs while trying to enhance performance. One of the options being considered through development of the second generation thin films is incorporating novel approaches to increase their efficiency range to 30–60%.

Figure 12.5 shows a multi-junction device with three layers, sometimes referred to as cascaded or tandem. Each of the three materials has three varying band gap energies which are normally formed from lowest to highest. The highest band gap energies (Eg) are stopped by Cell 2 with the rest flowing to this cell which stops the mid-energy photons as it has the middle Eg. Cell 3 is the final layer and it absorbs the photons with low energy. This type of technology has already proved interesting with a practical efficiency so far of 32%. This technology expands upon the developments of the second generation thin films as most of them are not only multi-junction but also thin film.

The reasoning behind the interest in this technology is that, although there is a wide spectrum range, most of this does not reach the PV panel. The two main types of light that are of interest are red and blue. The red light and silicon band gap are similar at approximately 1.1 eV. Unfortunately, the blue light, which has a higher band gap and approximately three

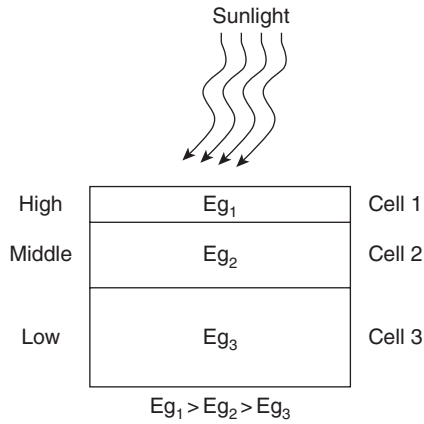

12.5 Operation of a three-layer multijunction PV.

Table 12.7 Multilayer PV layers

Layer	Band gap (eV)	Max theoretical power conversion efficiency (%)	Notes
1	1.13	33.7	Energy below and above red are lost
2	1.64 0.94	44	
3	1.83 1.16 0.71	48	
Infinity	Undefined	64	Estimation

times the energy, is not absorbed as the band gap is too low – this is an issue under research, hence the interest in multi-junctions. Table 12.7 outlines four different layers and the possible theoretical efficiency with each highlighting the band gaps that they include.

The second part of the third generation focuses on the development of nanostructures, which obviously are in the size of nanometres. It must be understood that there are vast differences between normal and nanostructures because at that small scale the quantum physical effect takes over the device. The most important feature of the nanostructure is that their optical features change as the size varies providing the option of changing the optical properties by optimizing the size of the nanostructure. This provides many more options with regard to how the capture of the photons can be optimized, enabling more of the energy of the solar spectrum to be used, thus providing maximum efficiency.

The market suggests that there is still some time to wait before this technology will be commercially viable, and it is likely it will be towards the end of the first quarter of the twenty-first century before it is achieved. It is anticipated that the third generation will shatter the current price of $1/W to around $0.20/W (Green, 2003).

12.5 The use of nanotechnology in photovoltaic (PV) technology

Nanotechnology is related to the direct control of matter on the atomic scale and it can also be used to describe material, devices or structures with one of their dimensions being between 1 and 100 nanometres. An atom is considered the basic building block and has a diameter of 0.1 nm with its nucleus being smaller at 0.00001 nm. It is difficult to actually picture this size – one nanometre (nm) is equal to one billionth or 10^{-9} of a metre. The size of atoms are not the only factor to consider – as with every industry, it has its own specific assembly methods and in nanotechnology it is split into two main areas, the bottom-up and top-down approaches, which are summarized in Table 12.8 (Rodger, 2006).

Currently, nanotechnology has been accepted for use in applications related to surface science, organic chemistry, semiconductor physics, modular biology and micro-fabrication, but in the future it is expected that this will expand to include electronics, medicine, biomaterials and energy production.

If PV technology is to become a good competitor to fossil fuels, it must be cost competitive. Currently, silicon-based PVs are actually more expensive per kilowatt hour, hence the search for another solution. The nanostructure configuration is known to enable control of the electronics, structural and optical factors, therefore providing it as a possible solution for PVs. With this under consideration, development of nanotechnology PVs (Anon., 2010) is expected to increase in the coming years and ameliorate the problems seen in the first and second generation aiming at lower cost (Anai *et al.*, 2010) by not only reducing material but also ensuring that the manufacturing process is efficient. Most importantly, the PV industry considers

Table 12.8 Approaches in nanotechnology

Approaches	Description
Bottom-up	Self-assembly by chemical principles of molecular components using the principle of molecular recognition
Top-down	No atomic-level control as objects are built from larger parts

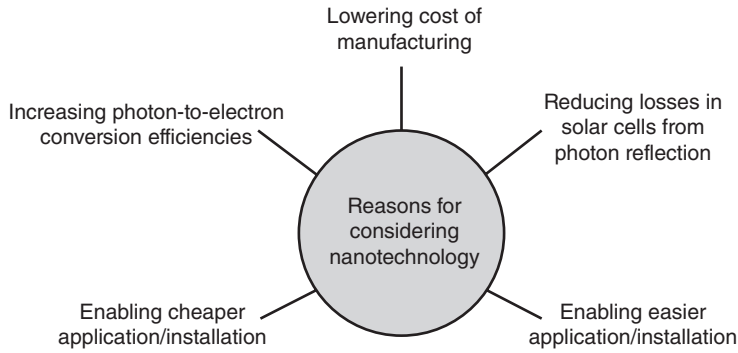

12.6 Reasons for considering nanotechnology.

that nanotechnology offers flexibility and also can overcome the limitations with band gap issues (Serrano *et al.*, 2009).

The main reasons for opting to try nanotechnology as a third generation solution (Fthenakis *et al.*, 2009) are shown in Fig. 12.6. Although it is currently known that it requires more energy for the material and manufacturing, it is hoped that solutions to these drawbacks can be found.

Nanotech PVs offer a solar option that not only could be more efficient (Hamakawa, 2004) but also 'greener' as the product offers the possibility of recycling at the end of its lifetime (Shockley and Queisser, 1961), something not often initially considered when assessing renewable energy technologies. Other advantages of nano-PVs are as follows:

- roll-to-roll manufacturing
- low cost substrate
- more than one band gap for absorption
- minimal material cost
- high mobility
- long lifetime
- more than one absorption mechanism.

One of the main issues that has been seen in this area relates to problems with PV cell design, but as the sector develops, it is hoped that this can be overcome.

Although nanotechnology is still primarily in the research and development phase there are some companies at the manufacturing stage. One of the benefits of nano-tech PV design is that the dimensions of the nanocrystals identify which part of the solar spectrum is absorbed with their specific band gap, hence solving some previous issues. Table 12.9 presents a nano-solar technology company example, briefly outlining some of the positive points of the product. It is expected that over the coming years many more companies producing this technology will emerge.

Table 12.9 Nanotechnology company example

Company	Nanosolar
Country	USA
Types	CIGS nanoparticles
Substrate	Metal foil or glass (low cost)
Manufacturing	Non-vacuum printing of nanoparticle ink to a substrate. These are transferred to electronic film of high quality using the rapid thermal processing (RTP) method
Efficiency	14%
Cell cost	$0.36 per watt
Panel cost	$0.99 per watt
Throughput	1 panel per 10 seconds

Currently PVs made from nanoscale materials are not suitable for large-scale installations because of issues not only with their efficiency – which it is hoped will be improved – but also with their long-term stability. These problems are due to the fact that there are some factors that are difficult to experimentally understand in the nanoscale range, hence high power computation is required, which until recently was a problem (Anai *et al.*, 2010). Currently, because of the development of high performance computing and advances in the calculation of electronic structures, it is easier to consider material properties using atomistics information, enabling researchers to develop more materials with specific properties through calculation.

The current nanotechnology PV research and development focus is on (Manna and Mahajan, 2007):

- quantum dots
- nanotubes.

The next sections will explain each of these areas in detail.

12.5.1 Quantum dots

The principle related to this technology was first discovered by Ekimov in the 1980s (Ekimov and Onushchenko, 1981) and the technology was initially applied to LED technology. The quantum dot, which was first defined by Reed *et al.* (1988), has properties between discrete modules and semiconductors (Norris, 1995; Bawendi *et al.*, 2000; Brus, 2007).

Quantum dots (QDs) are made up from nanostructures of semiconductor materials which are categorized by their confinement dimensions. Figure 12.7 (Nozik, 2010) outlines samples of quantization in nanoscale materials and where the quantum dot falls in this band. Quantum dots are normally in the range of 2–10 nanometres in diameter, containing hundreds to

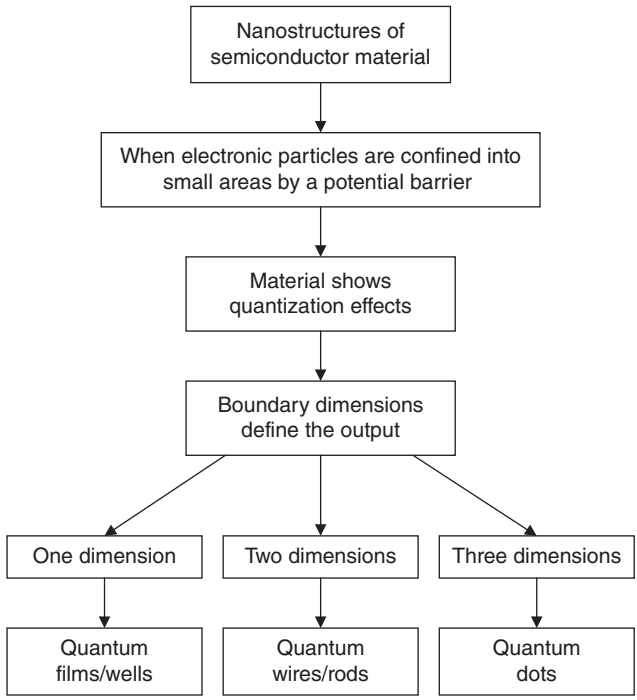

12.7 Nanostructures and their dimensions.

thousands of atoms. As defined in Fig.12.7, QD or nanoparticles are semiconducting nanometre-sized crystals (Manna and Mahajan, 2007). There is still a lot of research ongoing into the various shapes that nanocrystals come in, but for renewable energy currently the most focus is being placed on spheres, cubes, rods, wires, tubes and tetrapods. As with the traditional PV market, QD developers have also decided to consider semiconductor materials; however, it is not limited to this and research could be completed into metals or organic materials and they could be combined with porous films or dyes, but as semiconductors are currently the number one PV material, this is the obvious starting point. Semiconductor materials are made from the following mixture of periodic groups: II–VI, III–V and IV–VI.

QDs are expected to be ideal for use in solar panels as they can overcome one of the previously identified issues of the limited band gap (BG). The adjustable band gap they offer means that the larger and wider BG equals more light absorbed which in turn provides more output voltage. A smaller BG provides more current but less output voltage. Hence to optimize this phenomenon, ideally tuning the QD to different band gaps would enable absorption of different wavelengths (Manna and Mahajan, 2007), therefore removing the previous limited PV efficiency which is seen with the earlier

generations. This, however, is not the only reason for the use of QDs: the QD also enables material moulding into different forms as well as being cheaper due to the fact that they use basic chemical reactions (MIT, 2007) and they also reduce wasteful heat seen in the previous generations, in addition to maximizing the amount of light to electricity conversion.

Issues with non-utilization of PVs extra electron energy ('hot carrier' or 'hot excitation') have been previously highlighted. Normally it is kinetic free energy which is lost in pico or subpicoseconds through a process of electron-phonon scattering creating heat from the kinetic energy. Some of these issues have been previously solved by tandem PVs, but not all. A positive aspect is that the quantum dot holds on to the hot carrier for a longer time, thus enabling an extended period for it to cool, extending the lifetime of the hot electrons by as much as 1,000 times. Part of this is the three-dimensional array of the QD, which enables strong electronic coupling producing an extended lifetime for excitons. This provides more movement of hot carriers and the possibility of more electric generation, enabling more charge from one photon (Manna and Mahajan, 2007).

Quantum dots are very interesting and exciting as they have optical properties that are not seen in typical materials and enable a good spectrum control of emitted light, and these properties come from confinement of the electron-hole pairs. The QD offers a varied emission and absorption spectrum which is linked to the various particle sizes, although it is important to remember that the QDs will only stay in a confined space if their wavelengths are associated.

The relationship between the size of dot with wavelength and energy can be summarized as a smaller dot equalling shorter wavelength fit, also equalling higher energy of the electron, with the larger dots having the opposite relationship. Also different from traditional PVs is the QDs' photovoltaics' ability to obtain three electrons from one high energy photon of sunlight where normally it was only a maximum of one (Nozik, 2001; Ellingson *et al.*, 2005; ISIS Press Release, 2006). This is referred to as multiple exciton generation, or MEG for short.

Extended research is ongoing with regard to progression in QDs. Conibeer (2007) discusses a crystalline material tandem thin film QD which obviously enables the wider band gap (BG) and is constructed of silicon placed between layers of Si-based dielectric compound with a QD diameter of 2 nm and a BG of 1–7 eV. The process to produce this QD is as follows:

- Thin film is created by using either sputtering or chemical vapour deposition (CVD) methods.
- High temperature toughening of the crystallized QD.

This method means that issues with lattice mismatching are not suffered as the framework is lacking a definite shape. However, Conibeer (2007)

highlights that there is still work to be done on the creation of junctions, passivation of defects and connection to silicon cells. One of the real ongoing problems is linked to spectral sensitivity. Green (2009) also discusses silicon QD, defining the link between changing QD size to control the optical band gap. Also discussed in this reference is the research that is ongoing into increasing the voltage by increasing optical BG. The silicon option is expected to provide not only a higher efficiency but also a lower cost and it will also use material that is abundant and, most importantly in this era, environmentally friendly. More work on exciton splitting and collection of resulting free electrons and holes could further improve the devices.

An obvious factor also to consider is the materials that could be and are currently being used in the development of this technology. Materials used to date include, but are not limited to, cadmium selenide, cadmium sulphide, cadmium telluride, indium phosphide, indium arsenide, lead selenide and lead sulphide.

Another example of a QD is a lead selenide semiconductor compound combined with titanium oxide which is used to remove the hot carriers, hence enabling new electrons to be embraced. The issue with arrangement is linked with the fact that, although one wants to induce electronic transfer, no chemical interaction between the layer/material can be allowed.

In the next few years it is thought that the quantum dot efficiency could be increased by not only improving the electrode and layer structure but also by increasing the QD density. At the start of this century, Nozik predicted that the use of QDs in PVs would increase efficiency, enabling 65% of the sun's energy to be converted into electricity. There have been many predictions but only time and practical development will truly lay the building blocks to future technology.

The size of the QD as discussed previously is a consideration that can improve efficiency and so how the size is controlled is important and includes the following factors:

- medium in which they react
- reaction temperature
- reaction duration.

Therefore the method of QD fabrication is important and currently there are two main options. The first is the suspension in liquid of ultrafine particles, referred to as colloids. This colloidal chemistry is not expensive and does not require any expensive equipment; rather it only needs the proper chemicals and room temperature as a requirement to produce. Basically it is the linking of one metal ion with another. The second fabrication method is epitaxial growth. In this process, crystals are grown on a semiconductor material on the surface of another with the structural orientation being the same.

12.5.2 Carbon nanotubes (CNT)

Carbon nanotubes (CNTs), or nanotubes (NTs) as they are often referred to, are cylinders constructed of carbon atoms (nanostructure) and are not only organic but are good photosensitive material. Basically they consist of a single sheet of graphite with a hexagonal lattice (Manna and Mahajan, 2007) which is constructed from linked carbon rings forming the tube, capped at each end with a pentagonal carbon ring.

Nanotubes are made up of *n* rows and *m* columns and the link between them defines exactly how they are formed. The structure has a length-to-diameter ratio of 132,000,000:1 (Wang *et al.*, 2009), although this can vary, which is significantly larger than any other material. An NT is very thin, being approximately 10,000 times thinner than a human hair and hollow in the middle. Nanotubes are normally divided into two specific types, which are specifically related to the amount of walls contained in the structure; SWNTs (single-walled nanotubes) which have good light absorption properties and efficiency, and MWNTs (multi-walled nanotubes) which have slightly different properties. The SWNT, although any length, normally has a diameter of approximately 1 nm, as the structure is basically a one atom-thick layer of graphite which is wrapped until both ends meet, forming a tube. Obviously it is harder to define the size of the multi-walled nanotube as this depends on the amount of walls. The main reason that the solar industry is interested in nanotubes as a third generation PV is related to the properties associated with its materials and structure. The following points are interesting facts about nanotubes commonly known in the industry:

- They are as elastic as a rubber band.
- Impressive thermal conduction which is twice that of diamond.
- Withstand temperatures of 2700°C.
- Do not react with other atoms.
- Better electrical conductor than copper (100 times).
- Depending on their structure, their electrical properties will either be metallic or semiconductor.
- Conduct at 10^9 amperes per square cm.
- Thermal properties vary depending on the location – along the tube there are good thermal properties whereas other locations in the tube provide good insulation.
- Electrical properties change depending on what material is attached to them.

Although nanotubes have all these advantageous properties, their practical implementation is still ongoing, with research and development looking into ways to ensure they reach their maximum potential. Carbon nanotubes are of interest in nanotechnology but are not limited to this field; it is

expected that electronics, optics and material science amongst others would also be considered.

Currently, two main areas where nanotubes are being used which have been published are:

- NASA's decision to develop a composite material from NT and another material to be used in spacecraft.
- The delivery of medical drugs by attaching the drugs to the nanotubes.

Although these two examples are not in the photovoltaic field, they demonstrate how broad the use of nanotubes could be. However, this chapter is specifically interested in their relationship to support and enhance the development of the third generation PV and its continuous aim to develop a panel that uses materials that have a higher conversion efficiency rate.

Nanotubes are widely believed to be one of the forerunners in third generation PVs and it is expected that in the next decade their efficiency and cost will improve significantly (Anon., 2010). If this development happens, it will be due to several advancements that are linked together to provide the ideal material for photovoltaic panels. In the future, with these improvements it is expected that panels will not only withstand extended sunlight but also be able to be bent into any form due to their physical characteristics. They also accept high currents but withstand the effect of the heat generated. A very important point for any material being introduced into a system is that there should be no reaction with its surroundings and the NT complies with this. Finally, but importantly, it must provide good conduction without loss of energy to friction.

One of the most important environmental aspects is that the NT is both easy to reuse (Scharber, n.d.) and is biodegradable, hence it can be decomposed, answering one often-posed question about how to deal with the end-of-life cycle of renewable energy products. However, more pressing issues are related to problems and obstacles that need to be overcome to ensure that NT PV have a chance of succeeding in this industry. The issue of cost effectiveness needs to be addressed, as does the improvement of mass production to ensure quality products. In addition, the high temperature needed to produce the nanotubes could affect other components used in the solar cell/panel, hence this needs to be considered. One technical issue that needs more research is the problem with low fill factor which is only adding to the low energy conversion efficiency problem.

Carbon nanotubes are currently used in several areas of the PV device. One such area is the photoactive layers, which are expected to provide more efficient PV devices due to the nanotube and polymer junctions. The high electric field created here enables splitting up of the excitons and also in

this structure the SWNT allows a pathway for the electrons to travel along (Kymakis *et al.*, 2003). Unfortunately, this is currently very inefficient and issues with the combination of the NTs are still occurring, leaving the way open for further improvements.

Another approach is to use CNT as a transparent electrode to replace the currently used indium tin oxide (ITO) which could solve issues with its lack of compatibility with polymers, poor mechanical properties, expensive production costs and material cost and availability. Currently the option of ITO over CNT provides comparable efficiency but again more work is required to make it a practical option.

Finally, one further option to enhance the flow of current between the cells is to use graphene as a possible electrode, again as an alternative to ITO. Graphene offers an inexpensive, transparent and flexible omnipresent carbon substrate in a flat chicken-wire form with the major problem to date being the joining of the graphene to the panel due to it not accepting water solutions. However, it has been suggested by Park *et al.* (2010) that this issue could be overcome by doping the cell surface, hence including impurities, which in turn enables the graphene to be accepted. Added to this is the fact that the overall conductivity is improved and this could in theory solve some of the issues seen in the previous generation, offering a lightweight, flexible, transparent PV cell, thus leading the way to other PV installation options.

Research has discussed many aspects related to carbon nanotubes. Not only can they be combined with polymers and bucky balls, which is a hollow spherical module completely made of carbon, to form a painted PV product, the NT can also be coated by both p and n type semiconductors which provides a p-n junction for electricity generation. In 2002 SWNT and polymer PV devices were seen to provide a doubled photocurrent, but this was not the last advancement, rather the start of this development. Also the substrates which the CNT are placed on are currently polyethylene terephthalate, glass, polymethyl methacrylate and silicon, but this research is only in the primary stages and could be further expanded. A specific example is naphthalocyanine (NaPc) dye-sensitized nanotubes which use nanotubes as electrons and polymer as holes and provide increased absorption of both red and ultraviolet as well as larger short circuit current (Kymakis and Amaratunga, 2003). It is not only the quantum dot that enables more output from the electron; the NT also offers this possibility.

Work is ongoing and, in 2011, the University of Surrey Advanced Technology Institute published work on the combination of organic solar cells and MWNT, showing that both SWNT and MWNT are progressing (Miller *et al.*, 2006). Also the development of the CNT will include matching to the related solar spectrum, improved optical absorption and the reduction of carrier scattering. To date there are three main production methods for

nanotubes. The method that is currently used most is arc discharge (Iijima, 1991; Ebbesen and Ajayan, 1992) which basically consists of a high current being placed between two graphite electrodes in a helium atmosphere producing a nanotube that has a maximum length of 50 micrometres (Collins and Avouris, 2000) with a product yield of 30%.

The second is laser ablation, which is used for single- and multi-walled nanotubes (Guo *et al.*, 1995a, 1995b) but mostly SWNTs. In the basic process, the laser changes a graphite piece into vapour in a reactor, while at the same time gas is drawn into the chamber and the nanotube forms on the cold surfaces in the reactor. Although this yields 70%, which is more than arc discharge, it is also the most expensive method (Collins and Avouris, 2000). The final method, which was also mentioned in the quantum dot section, is CVD (chemical vapour deposition) (Bunch *et al.*, 2005). It is expected that CVD will probably be the most commonly used method in the commercial production of carbon nanotubes in the future and it is expected that it could reach industrial scale during this century.

In the future, with improved production, or by varying nanotubes, efficiency will improve (Landi *et al.*, 2005; Cataldo *et al.*, 2012), costs will reduce, the expected efficiency of 71% will be closer to reality (Anon., 2006) and properties such as lifetime can be realistically considered.

12.6 Future trends

The future development of PVs is principally split into three areas – countries' governments, the scientists/researchers, and consumers, with each of them having a varied amount of responsibility. Governments are responsible for encouraging and supporting the research, development and integration of its progression into each country and they could introduce subsidies and incentives as encouragement for consumers and companies. In developing countries specifically there are many options for the use of solar power in remote locations that could enable up to two billion more people to have electricity; for example, the kerosene lamps that are currently used in villages could be replaced by a 5 W system with a battery backup for approximately $500 per village.

In developed nations energy demands are high so solar energy is an additional power resource to support the traditional sources. In many large developed countries, power accessibility is not the problem, and rather the issue is the installation of distribution lines, which can cost up to $30,000 per km. Therefore, for remote locations, a PV array would be a more suitable and cheaper alternative.

Governments worldwide are definitely making plans for solar power to be part of future energy strategies, and this is supported by the fact that in the last five years the cost of this technology has reduced by about

one-third, and with all the research and development this can only improve. Europe is one of the leaders in this field and it is hoped that by 2020 it can produce 688 GW of power, with expectations nearly double this target by 2030. This would ensure that by 2020 Europe would produce 12% of its power from the sun, with the sunbelt countries potentially hitting the same target by 2030. Worldwide, 9% of all power could feasibly be provided by solar energy by 2030, with this increasing to 20% by 2050. However, it is not just about the energy produced; countries are also embracing it as a sustainable clean energy source, hence a way of cutting their carbon dioxide emissions and helping impact positively on climate change. If solar energy continues to increase, it is predicted that by 2050 4,047 million tonnes of CO_2 could be cut worldwide every year. The last but equally important factor, due to the global financial climate, is the added bonus of jobs using this technology and Fig. 12.8 shows the possibility for this over the next 20 years. All these compelling arguments should continue to drive governments to keep striving to enhance their implementation, research and development of solar technologies.

The most major obstacle to implementation of the technology is that, despite silicon being the second most abundant element in the earth's crust, for it to be used in PVs it must be purified to a high level to produce better efficiency. However, to achieve the correct purity the cost is $40 per kg. The simplest solution to this problem may be to use a lower purity of silicon but unfortunately to date this is not an option that has been researched to an acceptable level.

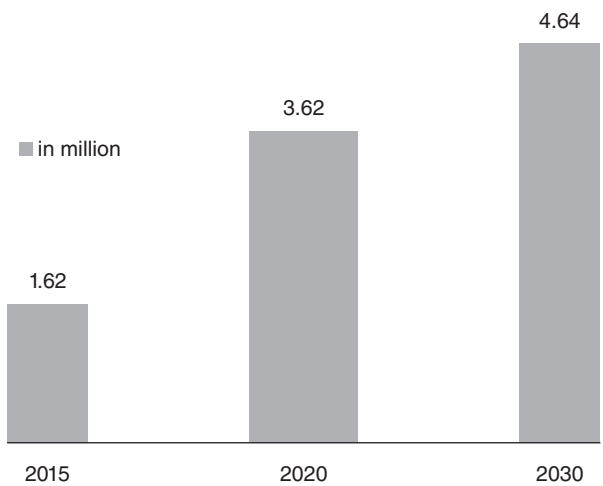

12.8 Job creation opportunities from PVs.

There is also a lot of work ongoing in the solar technology field to challenge other technologies in the race against thin film to beat the $1 per watt production cost. Rivalry is not always a bad thing. On the development side, advancements in other industries are having an impact on PVs; the flat screen TV has meant that larger sheets of glass are readily available and progress in the semi-conductor industry has provided second-hand machinery that can produce thicker cells. All these factors can help to reduce the cost of production, but we must also keep in the forefront of our minds that the real aim is about refining it to be more efficient.

The greatest advancement to date might be the emergence of screen printing on solar cells as it allows the option of PV roofing shingles that could easily be added to any current or future home. This new method will also enable different PV mounting frames and positions to be considered, a factor that has always impacted on the full PV system. However, in the future it is expected that the greatest advancements will be in third generation technology, specifically related to nanotechnology.

Finally, the consumer must be encouraged and educated in various ways such as advertising, literature, etc., to make the choice to embrace this clean source of energy, even if it is currently more expensive than traditional energy. Its use in devices such as a simple solar powered calculator or garden light is broad, but further devices that we use on a daily basis need to be considered to ensure less effect on the environment than in previous generations. More consumers purchasing PVs will obviously have an effect as it will introduce more competition in the market, thus not only lowering cost but also challenging further and new developments, which can only be a positive step forward for all.

12.7 References

Anai, Y., Neaton, J.B. and Grossman, J.C., 2010. Theory and simulation of nanostructured materials for photovoltaic applications. *Computing in Science & Engineering*, 12(2), 18–27.

Anon., 2006. 'How much does solar energy cost'. Facts-about-solar-energy.com. Available at: http://www.facts-about-solar-energy.com/solar-energy-cost.html accessed 10 January 2012.

Anon., 2010. 'Multijunction solar cells' REUK. Available at: http://www.reuk.co.uk/Multi-Junction-Solar-Cells.htm (Accessed 11 January 2012).

Bawendi, M.G., Murray, C.B. and Kagan, C.R., 2000. Synthesis and characterization of monodisperse nanocrystals and close-packed nanocrystal assemblies. *Annual Review of Material Research*, 30(1), 545–610.

Brown, G.F. and Wu, J., 2009. Third generation photovoltaics. *Lanser & Photonics Reviews*, 3(4), 394–405.

Brus, L.E., 2007. Chemistry and Physics of Semiconductor Nanocrystals. Available at: http://www.columbia.edu/cu/chemistry/fac-bios/brus/group/pdf-files/semi_nano_website_2007.pdf (accessed 27 January 2012).

Bunch, J.S., Yaish, Y., Brink, M., Bolotin, K. and McEuen, P.L., 2005. Coulomb oscillations and Hall effect in quasi-2D graphite quantum dots. *Nano Letters*, 5(2), 287–290.

Cataldo, S., Salice, P., Menna, P. and Pignataro, B., 2012. Carbon nanotubes and organic solar cells. *Energy Environ. Sci.*, 5(3), 5919–5940.

Chapin, D.M., Fuller, C.S. and Pearson, G.L., 1954. A new silicon p-n junction photocell for converting solar radiation into electrical power. *Journal of Applied Physics*, 25, 676–677.

Chapin, D.M., Fuller C.S. and Pearson, G.L., 1957. Solar Energy Converting Apparatus. US Patent No. 2780765.

Collins, P.G. and Avouris, P., 2000. Nanotubes for electronics. *Scientific American*, 283(6), 62–69.

Conibeer, G., 2007. Third-generation photovoltaics. *Materials Today*, 10(11), 42–50.

Ebbesen, T.W. and Ajayan, P.M., 1992. Large-scale synthesis of carbon nanotubes. *Nature* 358 (6383), 220–222.

Einstein, A., 1905. Über einen die Erzeugung und Verwandlung des Lichtes betreffenden heuristischen Gesichtspunkt. *Annalen der Physik*, 322(6), 132–148.

Ekimov, A.I. and Onushchenko, A.A., 1981. Quantum size effect in three-dimensional microscopic semiconductor crystals. *JETP Letters*, 35(6), 345–349.

Ellingson, R.J., Beard, M.C., Johnson, J.C., Yu, P., Micic, O.I., Nozik, A.J., Shabaev, A. and Efros, A.L., 2005. Highly efficient multiple exciton generation in colloidal PbSe and PbS quantum dots. *Nano Letters*, 5(5), 865–871.

Fthenakis, V., Kim, H.C., Gualtero, S. and Bourtsalas, A., 2009. Nanomaterials in PV manufacture: some life cycle environmental and health considerations. In: *Electron Devices Society – ED & Lasers and Electro-Optics Society – LEO, Photovoltaic Specialists Conference (PVSC)*, 7–12 June 2009, Philadelphia, PA: IEEE.

Green, M.A., 2003. *Third Generation Photovoltaics: Advanced Solar Energy Conversion*. New York: Springer.

Green, M.A, 2009. Third generation photovoltaics: assessment of progress over the last decade. In: *Electron Devices Society – ED & Lasers and Electro-Optics Society – LEO, Photovoltaic Specialists Conference (PVSC)*, 7–12 June 2009, Philadelphia, PA: IEEE.

Guo, T., Nikolaev, P., Rinzler, A.G., Tomanek, D., Colbert, D.T. and Smalley, R.E., 1995a. Self-assembly of tubular fullerenes. *J. Phys. Chem.*, 99(27), 10694–10697.

Guo, T., Nikolaev, P., Thess, A., Colbert, D. and Smalley, R., 1995b. Catalytic growth of single-walled nanotubes by laser vaporization. *Chemical Physics Letters*, 243, 49–54.

Hamakawa, Y., 2004. *Thin-film Solar Cells: Next Generation Photovoltaics and its Applications*. Berlin: Springer.

Iijima, S., 1991. Helical microtubules of graphitic carbon. *Nature* 354(6348), 56–58.

ISIS Press Release, 2006. http://www.i-sis.org.uk/index.php (accessed Jul 2011).

Kolodziej, A., 2004. Staebler-Wronski effect in amorphous silicon and its alloys. *Opto-Electronics Review*, 12(1), 21–32.

Kymakis, E. and Amaratunga, G.A.J., 2003. Photovoltaic cells based on dye-sensitisation of single-wall carbon nanotubes in a polymer matrix. *Solar Energy Materials and Solar Cells*, 80, 465–472.

Kymakis, E., Alexandrou, I. and Amaratunga, G.A.J., 2003. High open-circuit voltage photovoltaic devices from carbon-nanotube-polymer composites. *Journal of Applied Physics*, 93(3), 1764–1768.

Landi, B.J., Raffaelle, R.P., Castro, S.L. and Bailey, S.G., 2005. Single-wall carbon nanotube-polymer solar cells. *Progress in Photovoltaics: Research and Applications*, 13(2), 165–172.

Manna, T.K. and Mahajan, S.M., 2007. Nanotechnology in the development of photovoltaic cells. In *Int. Conf. on Clean Electrical Power, 2007. ICCEP '07*. Capri, Italy: IEEE.

Miller, A.J., Hatton, R.A. and Silva, S.R.P., 2006. Interpenetrating multiwall carbon nanotube electrodes for organic solar cells. *Applied Physics Letters*, 89(13), 133117–133117-3.

MIT, 2007. Nanocharging solar, technology review, [blog] March 12, 2007. Available at: http://www.technologyreview.com/read_article.aspx?ch=specialsection&sc=emerging&id=18285 (accessed 6 January 2012).

Norris, D.J., 1995. Measurement and Assignment of the Size-Dependent Optical Spectrum in Cadmium Selenide (CdSe) Quantum Dots, PhD thesis, MIT.

Nozik, A.J., 2001. Quantum Dot Solar Cells. NCPV Program Review Meeting, Lakewood, Colorado, October 14–17.

Nozik, A.J., 2010. Nanoscience and nanostructures for photovoltaics and solar fuels. *Nanoletters*, 10(8), 2735–2741.

Park, H., Rowehl, J.A., KangKim, K., Bulovic, V. and Kong, J., 2010. Doped grapheme electrodes for organic solar cells. *Nanotechnology*, 21, 505204–505210.

Reed, M.A., Randall, J.N., Aggarwal, R.J., Matyi, R.J., Moore, T.M., and Wetsel, A.E., 1988. Observation of discrete electronic states in a zero-dimensional semiconductor nanostructure. *Physical Review Letters*, 60(6), 535–537.

Rodger, P., 2006. Nanoelectronics: single file. *Nature Nanotechnology*, doi: 10.1038/nnano.2006.5.

Saari, J., 2010. Tekniikantie 14, FI02150 ESPOO: SPINVERSE

Scharber, M.C., n.d. Bulk heterojunction solar cells, perspectives and limitations. Available at: http://www.quantsol.org/pub/pub09_17.pdf (accessed 19 January 2012).

Serrano, E., Rus, G. and Garcia-Martinez, J., 2009. Nanotechnology for sustainable energy. *Renewable and Sustainable Energy Reviews*, 13(9), 2373–2384.

Shockley, W. and Queisser, H.J., 1961. Detailed balance limit of efficiency of p-n junction solar cells. *Journal of Applied Physics*, 32, 510–519.

Tesla, N.A., 1901a. Method of Utilizing Radiant Energy. US Patent No. 685958.

Tesla, N.A., 1901b. Apparatus for the Utilization of Radiant Energy. US Patent No. 685957.

Walker Jr., P.L., Rakszawski, J.F. and Imperial, G.R., 1959. Carbon formation from carbon monoxide-hydrogen mixtures over iron catalysts. I. Properties of carbon formed. *J. Phys. Chem.*, 63(2), 133–140.

Wang, X., Li, Q., Xie, J., Jin, Z., Wang, J., Li, Y., Jiang, K. and Fan, S., 2009. Fabrication of ultralong and electrically uniform single-walled carbon nanotubes on clean substrates. *Nano Letters* 9(9), 3137–3141.

Weston, E., 1888. Apparatus for Utilizing Solar Radiant Energy. US Patent No. 389124.

13

Concrete, mortar and plaster using titanium dioxide nanoparticles: applications in pollution control, self-cleaning and photo sterilization

M. VITTORIA DIAMANTI and M. P. PEDEFERRI,
Politecnico di Milano, Italy

DOI: 10.1533/9780857098832.3.299

Abstract: Many advances have been made in understanding the mechanisms of TiO_2 photoactivity and in developing its potential in addressing environmental issues. This chapter provides a short overview of these mechanisms, focusing on construction materials (mortar, plaster, concrete) modified through the addition of titanium dioxide nanoparticles. Examples will be given of laboratory experiments carried out in recent years, and of current applications in the built environment; attention will also be paid to the international standards that have been, and are still being, developed for this technology.

Key words: titanium dioxide, photocatalytic cement, self-cleaning, material ageing.

13.1 Introduction

TiO_2 has been used for centuries as white pigment in textiles and paints, well before the discovery of its photocatalytic properties. Curiously, alterations induced by TiO_2 pigments in supporting materials (degradation of paints and fabrics, or bleaching of dyes) had already been observed, but not understood. It was only in twentieth century that these alterations could be related to its photoactivation. The following list summarizes advances in research in the last 100 years in understanding mechanisms of TiO_2 photoactivation, and in developing and optimizing its properties:

- The first trace of scientific works on this subject is a paper published by Keidel in 1929, suggesting an active role of TiO_2 in the fading of paints.
- In 1938 the photobleaching of dyes caused by UV-irradiated TiO_2 was investigated by Goodeve and Kitchener, and ascribed to the presence of active oxygen species detected on TiO_2 surfaces.
- In 1964 Doerffler and Hauffe first proposed a research paper whose title contained the term 'heterogeneous photocatalysis': zinc oxide was used as photocatalyst.

- In the same year, Kato and Masuo reported the use of a TiO_2 suspension to photocatalyse the oxidation of tetralin, opening the way to similar processes proposed by McLintock and Ritchie on ethylene and propylene in 1965.
- In 1972 Fujishima and Honda for the first time reported the production of a TiO_2-based electrochemical cell for water splitting, which consisted of a single crystal rutile photoanode and a platinum counter electrode. This is now known as the 'Honda–Fujishima effect'.
- Frank and Bard (1977a, 1977b) first used TiO_2 as remedy to environmental pollution issues by studying the liquid phase reduction of cyanide ions in the presence of TiO_2 powders.
- This publication was followed in the same year by the development of nitrogen reducing solar cells – photocatalytic reduction of N_2 to ammonia – performed on pure and Fe-doped TiO_2 (Schrauzer and Guth, 1977).
- In 1978 TiO_2-catalysed organic synthesis was introduced by Kreutler and Bard (photosynthesis of methane from acetic acid).
- In 1985 TiO_2 was first applied successfully in biocide bacteria photokilling (Matsunaga *et al.*, 1985); this concept was then applied to tumour cells (Fujishima *et al.*, 1986).
- Matthews (1987) was the first to use TiO_2 powders immobilized on a substrate for liquid phase organic photocatalysis, to avoid filtration and resuspension.
- In 1991 O'Regan and Gratzel proposed the use of TiO_2 as anode in dye-sensitized photovoltaic cells.
- In 1995 the superhydrophilic effect was first noticed by Fujishima's research group, leading to the development of self-cleaning and antifogging surfaces (Wang *et al.*, 1997).
- The first photocatalytic TiO_2 products were delivered commercially in the late 1990s in the form of self-cleaning tiles and glass: in 1995, the Japanese company TOTO Ltd. started the manufacture of antibacterial Cu- or Ag-containing TiO_2 tiles, mainly for operating rooms (Watanabe *et al.*, 1995).
- The Marunouchi Building (or Marubiru), in Tokyo, opened in 2002, one of the first buildings featuring self-cleaning windows (Ohtani, 2010).
- Photoactivation was proved to induce a hardness modification in the surface of TiO_2, due to compressive stresses that are induced by volume increases connected with the onset of the superhydrophilic state (Shibata *et al.*, 2003).
- The church Dives in Misericordia (Rome, Italy), designed by Richard Meier for the Jubilee and finished in 2003, is one of the first examples of photocatalytic technology in Europe: it was built with TiO_2-modified

cement (former constructions: a school in Mortara, Italy, in 1999, and the Cité de la Musique in Chambéry, France, in 2000).
- 20,000 m^2 of self-cleaning windows were installed in the terminal building of Chubu International Airport (Japan), completed in 2005 (Fujishima and Zhang, 2006).
- The application of TiO_2 as cool material in energy-saving technologies for building was proposed: it exploits the latent heat flux generated by the evaporation of thin films of water on superhydrophilic surfaces (Irie *et al.*, 2004).

It is commonly assumed that the first studies on TiO_2 photoactivated properties date back to the early 1970s, when studies from Honda and Fujishima attracted the attention of the scientific community: the above list proves that other works had already been published, even though their findings clearly attracted less attention.

Photoinduced processes originate from the absorption of light by TiO_2, which causes an electron to be promoted to the conduction band (CB) leaving a hole in the valence band (VB). The electron-hole pair can be used to create electricity in photovoltaic solar cells, or to drive a chemical reaction: the latter action belongs to the category of heterogeneous photocatalysis. Trapping of holes at the TiO_2 surface also causes a dramatic increase in the surface wettability, which is defined as photoinduced superhydrophilicity. These phenomena will be explained in more detail in the following section.

13.2 Principles of heterogeneous photocatalysis

Many transition metal oxides are known to display a photocatalytic behaviour, i.e., these substances can act as catalysts and promote oxidation or reduction reactions when activated by electromagnetic radiation. Among these materials, titanium dioxide in its polymorphic structures (anatase, rutile and brookite) is undoubtedly the most relevant and studied, although other oxides and sulphides have attracted scientists' attention.

An ideal semiconductor for use in photocatalytic processes should have the following characteristics: chemical and biological inertia, ease of production and utilization, efficient solar light activation, high efficiency and low cost. Titanium dioxide possesses almost all the cited characteristics with the exception of the efficiency in solar light exploiting, since activation is promoted by UV light, which is less than 10% of solar light energy (Linsebigler *et al.*, 1995). But, how does heterogeneous photocatalysis work? The mechanism must be understood in order to explore its applications in everyday life, and especially as a complementary function of construction materials, as we will describe in the second part of this chapter.

13.2.1 Semiconductor activation

The initial process for semiconductor-supported heterogeneous photocatalysis of organic and inorganic compounds is the generation of electron-hole pairs, initiated by light absorption with energy equal to or greater than the band gap (Fig. 13.1). The process under irradiation can therefore be divided in four steps, as described by Schiavello (1988):

1. absorption of light, followed by the separation of the electron–hole couple,
2. adsorption of the reagents,
3. redox reaction,
4. desorption of the products.

Photoinduced charge transfer to other species (organic or inorganic molecules, water) relies on molecules migration and adsorption onto the semiconductor surface.

At its surface, the semiconductor can donate electrons to reduce an electron acceptor, given that the semiconductor CB bottom must be higher than the acceptor reduction energy, as a necessary condition. The acceptor in most cases is represented by oxygen, which forms a superoxide ion, $O_2^{\bullet -}$, or hydrogen peroxide, H_2O_2: they both have excellent reactivity and play important roles in photocatalytic reactions.

On the other side of the band gap, holes can combine with electrons provided by donor species adsorbed on the semiconductor surface, thus oxidizing the donor itself: in this case, the necessary condition is that the top of the semiconductor valence band must be lower than the donor oxidation energy. Typical oxidation reactions take place between semiconductor and water molecules to form hydroxyl radicals $OH^{\bullet}$, which are extremely active and tend to react easily due to their strong oxidizing power.

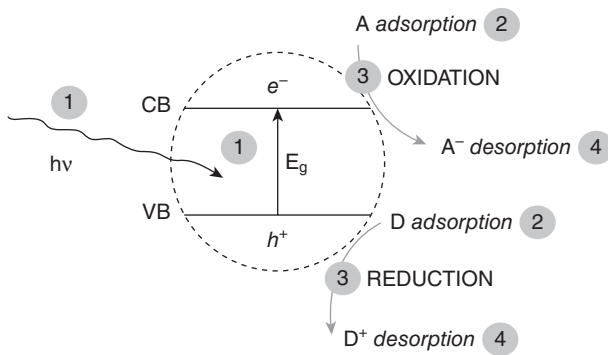

13.1 Schematic representation of photoactivation mechanism: $h\upsilon$ = incident radiation energy, E_g = semiconductor bandgap, A = acceptor, D = donor. Phases are numbered as in the related text.

In both cases, the rate of charge transfer is strongly influenced by the respective positions of conduction and valence band edges and the redox potential levels of adsorbate species: the greater the difference between semiconductor and adsorbate energy levels, the faster the redox reactions (Linsebigler *et al.*, 1995).

Charge transfer must compete with charge carrier recombination, which can take place in the volume of the semiconductor or at its surface and strongly decreases photocatalytic yield, i.e., the number of events occurring per absorbed photon. Charge carrier trapping can help increase the photogenerated species' lifetime. Localized energy surface states ascribed to irregularities and surface defects can act as charge traps, and thus reduce recombination effects; adsorbed oxygen usually acts as an electron scavenger for the trapped electrons, while trapped holes can react with oxygen ions or hydroxyl groups.

13.2.2 The most common photocatalyst: titanium dioxide

Titanium dioxide (TiO_2) is the most common among titanium minerals, and is extensively used in everyday life, specially as white pigment in painting, food and cosmetic industries, thanks to its high refractive index. It is found in nature in four polymorphs: anatase, which presents a distorted tetragonal crystal structure; rutile, which is also tetragonal; brookite, with orthorhombic crystal structure; and TiO_2(B), with monoclinic structure. Only two of the phases, anatase and rutile, are interesting for practical applications, as they are wide band gap semiconductors.

The E_g value for anatase is 3.20 eV, which corresponds to a wavelength absorption threshold of 384 nm. This means that its activation requires an irradiating source with wavelength lower than that indicated, that is, in the near-UV region, while visible light is not sufficiently energetic to induce photoactivity in this material (Fig. 13.2).

The parameters which mostly concur to determine photoactivation efficiency, and specifically photocatalysis, are the following, as defined by Carp *et al.* (2004):

- catalyst surface area, considering also specific surface (porosity) available
- initial concentration of the compound to be degraded (saturation regime) and formation of intermediate products competing for adsorption, even deactivating TiO_2
- reaction environment (oxygen, humidity, pH)
- wavelength and intensity of activating light source, which must provide enough energy to overcome the semiconductor band gap.

In Section 13.3 the main application fields of titanium dioxide will be described, as summarized in the well-known scheme of Fig. 13.3, together

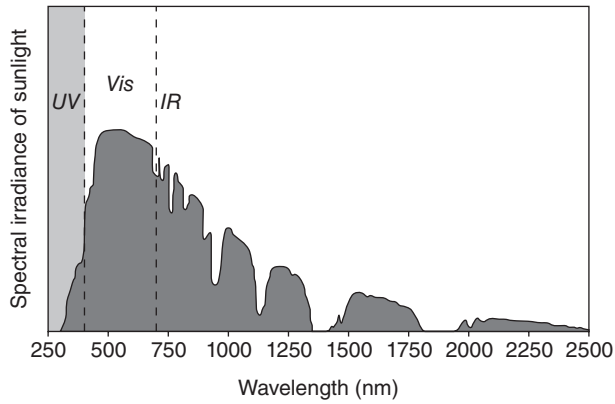

13.2 Spectral irradiance of sunlight as a function of wavelength, highlighting ultraviolect (UV), visible (Vis) and infrared (IR) fractions.

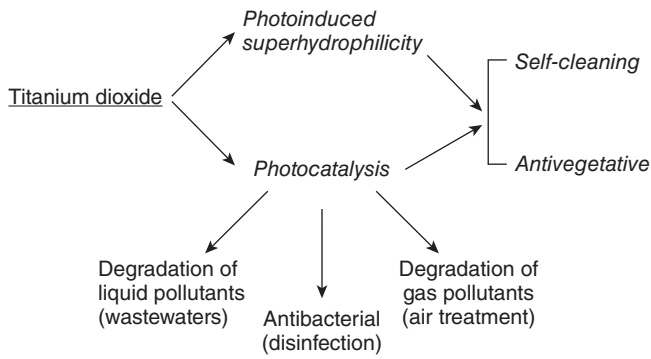

13.3 Main effects connected with TiO_2 photoactivity.

with the reasons for its success in such different environments. Before that, a brief look at other semiconductors that can be used as photocatalysts is required for a comprehensive treatise.

13.2.3 Other photocatalysts

Titanium dioxide is by far the most studied photocatalyst, but several works are also dedicated to the study of other transition metal oxides and to the evaluation of their semiconducting nature and consequent photocatalytic activity. Probably the most important reason for this broadening of the sector is the fact that titanium dioxide can only be activated by UV light, which occupies a very narrow percentage of natural light: the choice of a photocatalyst which is active under visible light would allow a wider slice of sunlight to be exploited, and therefore increase the material efficiency.

Moreover, UV light is also considered harmful to humans, as it can provoke skin and eye damage.

Possible alternative semiconductors that are susceptible to photoactivation are zinc oxide, ZnO (band gap 3.4 eV), mainly for the wide range of morphologies and properties achievable depending on the synthetic routes adopted, and tungsten oxide, WO_3, whose band gap of 2.7 eV is promising for applications in visible light conditions. Yet, few examples can be found of their use in photocatalytic construction materials. Studies on ZnO-modified cements usually deal with the related modification of mechanical properties, and controversial results have been proposed: the material strength was proved to increase by substituting a few percent of cement with zinc oxide (Riahi and Nazari, 2011), while Lackhoff *et al.* (2003) observed a set-retarding effect and a correlated decrease in mechanical resistance due to water losses during the prolonged dormant phase before setting. As for WO_3, tests were performed by Linkous *et al.* (2000) by coating a cement substrate with either WO_3 or TiO_2, and results indicated that the presence of WO_3 alone induced a lower photoactivity compared to TiO_2.

On the other hand, good photoactivation efficiencies were observed in hybrid oxides (mainly WO_3-TiO_2 and SiO_2-TiO_2): attention is now focusing on these composite systems as a means to improve the properties of photocatalytic materials. WO_3-TiO_2 hybrid nanoparticles were proved to exhibit photoactivity also under visible light activation (Chai *et al.*, 2006). Yet, no information is available on the interaction between the composite WO_3-TiO_2 nanoparticles and mortars or concrete, especially concerning possible influences on the setting properties of the material, or on its final mechanical behaviour.

SiO_2-supported TiO_2 materials have been extensively used as photocatalysts for a wide variety of reactions. The higher efficiency observed in a few works compared to pure titanium dioxide has been ascribed to different physicochemical properties, which depend on the possible interactions between the two oxides and on synthesis conditions (sol-gel, grafting of TiO_2 on SiO_2, coprecipitation, impregnation, chemical vapour deposition). The most interesting point about silica-supported TiO_2 is that silica itself is a common ingredient of cement-based materials, which makes the integration of these composite nanopowders easier (Bellardita *et al.*, 2010).

13.3 Applications of semiconductor photocatalysis

13.3.1 Photocatalytic degradation of pollutants

TiO_2 photocatalytic activity can be exploited to solve manifold purification issues arising not only from industrial uses or production of harmful substances, but also from heating and transportation. It exhibits good efficiency

in the degradation of organic pollutants as well as inorganic compounds, from nitrogen oxides to complex metal salts, in gas and liquid phase.

Several works on photocatalysis focus on the removal of organic pollutants from wastewaters, specially referring to dyes, which are toxic to microorganisms and aquatic life: as reported by Konstantinou and Albanis (2004), up to 20% of dyes used in manufacturing processes are dispersed in wastewaters, therefore efficient processes that avoid their release into natural water sources are vital to preserve the ecosystem. Several reviews can be found on TiO_2 effectiveness in dye degradation: we therefore suggest the reader refers to specific literature for further information (e.g., Akpan and Hameed, 2009; Han *et al.*, 2009).

However, in recent years the aspect of removing gas phase organic compounds has also attracted attention. Extensive studies have been carried out on the removal of outdoor and indoor pollutants, and more specifically volatile organic compounds (VOCs), by TiO_2 nanoparticles under UV illumination. These particles are often integrated in air purification devices, which are commercially available from several companies. VOCs are often responsible for malodorous air in buildings. They derive from several sources, such as cooking, cleaning products, furniture, etc.; in outdoor environments, they are usually part of combustion gases, industrial exhausts, cigarette smoke (Fujishima *et al.*, 2007). A long list of experimental studies is available in the scientific literature on this topic as well.

Photocatalysts are not only used for breaking down large volumes of soilage, they are also capable of destroying it as it accumulates, e.g., to prevent cigarette smoke residue stains, or unpleasant odours due to the presence of VOCs, of the order of 10 ppb by volume. At these concentrations, TiO_2 should be able to decompose such compounds even with scarce UV light (even as low as 1 $\mu W/cm^2$ according to some authors). Bright UV lamps are also used in city and highway tunnels to reduce pollution released by traffic, degrading both VOCs and nitrogen oxides, NO_x, as described by Demeestere *et al.* (2008), Toma *et al.* (2004), and many others.

13.3.2 Self-cleaning

Besides photocatalytic applications of TiO_2, another fascinating phenomenon arises from UV irradiation, that is, the alteration of TiO_2 wettability and formation of a highly hydrophilic surface state: this behaviour is defined as photoinduced superhydrophilicity (Wang *et al.*, 1997), and involves the reduction of Ti^{4+} to Ti^{3+} by electrons and simultaneous hole trapping at lattice sites. This reduces the bond strength between reduced titanium and the closest oxygen, which is then removed when another water molecule arrives in contact with the surface and adsorbs on it. This creates a highly hydroxylated surface layer, which is responsible for hydrogen bonds with

water and consequent increased hydrophilicity of the surface, as depicted in Fig. 13.4.

In this way, water can reach a contact angle close to zero on the surface of irradiated TiO_2 (Drelich *et al.*, 2011). Moreover, this surface is not solely hydrophilic: on the contrary, it presents an amphiphilic nature, with hydrophobic and hydrophilic domains of nanometre size alternating across the surface. This allows both oils and water to spread easily on the photoactivated TiO_2 surface (Fujishima and Zhang, 2006).

Regardless of the in-depth study of the chemical and photochemical mechanisms involved, this effect is of extreme practical importance, as it defines one of the most renowned abilities of titanium dioxide and the reason why it has found so many applications in building materials: the self-cleaning effect.

The formation of an amphiphilic domain network is accompanied by photocatalytic activity, as both have a common origin: UV irradiation. This double photoinduced phenomenon results in the self-cleaning effect: surface contaminants are first photomineralized, at least in part, and subsequently washed away by water, which spreads below them in tight contact with the TiO_2 surface. Moreover, drop formation on superhydrophilic surfaces is avoided, which in turn precludes stain formation due to slow water evaporation from the surface (Fig. 13.5). Another effect, anti-fogging, also arises from the same mechanism: no water droplets form on surfaces with a

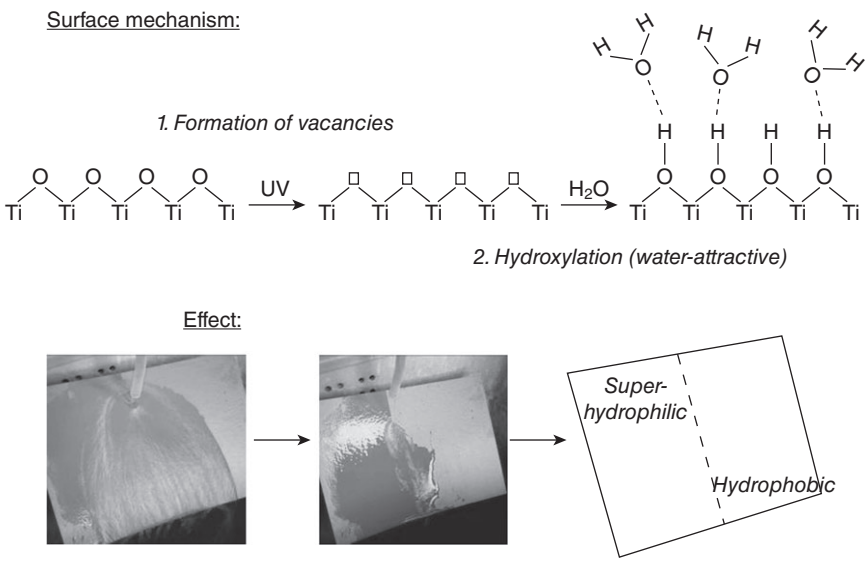

13.4 Theoretical mechanism and practical effect of photoinduced superhydrophilicity (photographs represent a plastic sheet covered on the left side with a TiO_2 layer).

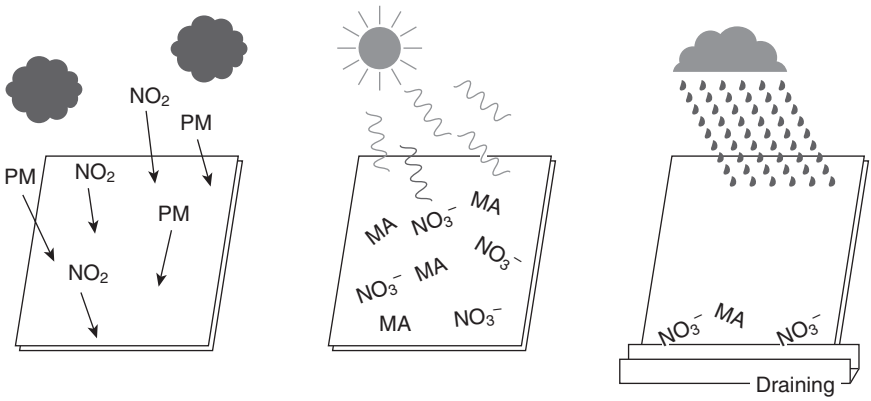

13.5 Schematic representation of self-cleaning on TiO_2 containing surfaces: PM = particulate matter, MA = mineral acids.

contact angle lower than 20°, as in the case of irradiated TiO_2 (Fujishima and Zhang, 2006).

To be precise, this property of self-cleaning should be referred to as 'easy cleaning': in fact, dirt and particles can adhere on the surface of titanium dioxide, even when irradiated; it is then extremely easy to remove them, as only UV light (available in natural sunlight) and water (that can be provided by rain) are required to remove stains and dirt.

Self-cleaning has become popular in a number of fields, even in clothing: some companies are producing self-cleaning cotton fabric, for an easier cleaning and deodorizing of clothes. Yet, their chief success is in the built environment, with the production of self-cleaning glass, tiles, paints, mortars and many other materials and components. In building façades, soiling is due to the adhesion of particulate matter on the surface of the materials they are made of, which are often porous (and therefore more prone to adsorbing such compounds). Particulate usually attaches to the surface through organic bonds, such as fatty acid chains and carboxylic groups. The twofold role of TiO_2 is then the photocatalytic degradation of such groups and the onset of superhydrophilicity, which drives rainwater in direct contact with the surface, removing particles which are at that point loosely adherent, thus reducing the need for maintenance.

13.3.3 Antibacterial and anti-vegetative properties

Another possible way of exploiting the photocatalytic properties of TiO_2 is its ability to mediate the destruction of bacteria, viruses and other biological materials. This function is often referred to as photosterilization, and it is of great interest for applications connected to air depuration – possibly of

private housing, but mainly of medical-related environments, such as operating theatres, common rooms and patient rooms – due to the chance to induce the death of bacteria, viruses, as well as allergens and fungi.

The mechanism is similar to that of photocatalytic degradation: active species are once again surface hydroxyl radical species produced by photogenerated holes, and superoxide ions produced by photogenerated electrons, which damage or destroy cell walls of biological materials (Mills and Lee, 2002; Gerrity *et al.*, 2008). A more detailed explanation is given by Hamal *et al.* (2009), who ascribe the photosterilization effect to the oxidation of complex proteins and to the inhibition of enzymatic functions of bacterial cells, which lead to ultimate cell death. In this respect, the employment of Ag-doped titanium dioxide is gaining much attention so as to achieve an easy decontamination and disinfection of common rooms and offices, as well as of medical equipment and operating theatres (Page *et al.*, 2007; Wysocka-Krol *et al.*, 2011).

Antibacterial activity was also described as a means to control biological growth on concrete surfaces and avoid unsightly stains. As described by Kurth *et al.* (2007), biofilm growth on concrete and mortar causes the triggering of undesirable chemical and aesthetical changes. The introduction of TiO_2 in the material does not explicate a strictly bactericidal activity in this frame, but more properly an anti-vegetative effect. Polo *et al.* (2011) investigated the possibility of using titanium dioxide as a control technology to counteract biofilm microorganism growth, and reported the photokilling effect of immobilized TiO_2 nanopowders on planktonic cells; conversely, no cell inactivation was observed on young biofilms, suggesting that possible applications of TiO_2 should focus on preventative measures rather than on the disaggregation of already existing biofilms. Linkous *et al.* (2000), and Linkous and Robertson (2006) also reported the inhibition of algae adhesion on cement substrates and on roofing membranes modified with TiO_2 (and WO_3).

13.4 TiO_2 in cement-based materials

Since their earliest appearance in Japan at the end of twentieth century, the diffusion of building materials modified with photocatalytic components has been constantly diffusing, spreading also to European countries. This is correlated with the increase in the generation of pollution and depletion of natural resources caused by intense and rapid industrial expansion, which pushes towards the development of sustainable materials, technologies and energy sources.

The widespread commitment inside the scientific community in the field of sustainability has focused much on purification devices, both for wastewater treatment and to improve the quality of air in industrial areas and

large urban centres. This has driven great improvements in advanced oxidation processes (AOPs), specifically considering heterogeneous photocatalysis as a substitute for older, less efficient or more expensive techniques (Palmisano *et al.*, 2007; Sievers, 2011).

In this field, a great number of scientific studies and patents deal with titanium dioxide nanopowder production and characterization (Paz, 2010; Shapovalov, 2010). Integrating TiO_2 in construction materials has gained much interest (Fujishima and Zhang, 2006; Hüsken *et al.*, 2007) in the attempt to meet air quality requirements promoted by several national and international committees, such as the quality standards introduced in early 1990s by the US Environmental Protection Agency (EPA), through the 1990 Clean Air Act Amendments which reported ozone, particulate matter, carbon monoxide, NO_x, SO_2 and lead as the most hazardous air pollutants causing severe concern for human health (Fig. 13.6).

As previously cited, several types of devices implementing the use of titanium dioxide have been designed and are currently commercialized. Examples of functionalized materials are photoactive paints for interior or exterior, tiles, self-cleaning fabrics for clothing; complete devices, like TiO_2-containing air purifiers, are also available. These examples, which list just some of the available photocatalytic materials, make clear the interest in active principles capable of solving the cited air quality issues, or at least to mitigate them.

Construction materials represent the most easily available medium to distribute photoactive substances over the widest surface area possible, gaining the maximum efficiency thanks to a versatile support for the photocatalyst and to a limited increase in material costs. The introduction of heterogeneous photocatalysis principles in building materials also allows the exploitation of the self-cleaning attitude conferred by the simultaneous

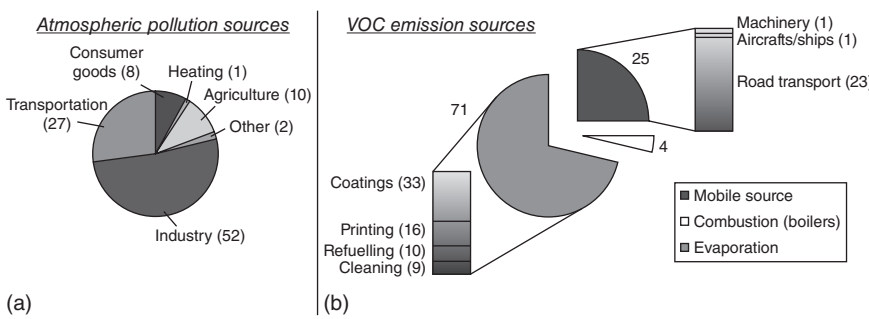

13.6 (a) Generic sources of emission of atmospheric pollutants and related percentages (source: Environment Canada website); (b) specific case: typical sources of VOC release (source: Tokyo Metropolitan Government website).

occurrence of (i) the degradation of greasy deposits accumulating on their surface and (ii) a state of photoinduced superhydrophilicity, with consequent washing away of reaction products, as reported by several authors including Mellott *et al.* (2006). The applications of these materials concern horizontal (cementitious tiles, pavings) and vertical structures (plasters, coatings, concrete structures) as well as galleries (cementitious paintings, concrete panels, asphalt coatings). Self-cleaning properties are mostly exploited in white concrete buildings: among the most representative examples, the Cité des Arts et de la Musique in Chambéry, France (Fig. 13.7a), completed in 2000, and the church Dives in Misericordia, built in Rome, Italy, by architect Richard Meier in 2003 (Fig. 13.7b).

Experimental works on TiO_2-containing construction materials were carried out by several research groups, usually performing the addition of titanium dioxide nanopowders or suspensions, with varying particle size, to cement pastes, plasters, mortars and concretes, generally characterized by a low water-to-cement ratio. On the other hand, little information is available on the actual behaviour of the photocatalyst integrated in the material, and particularly on its evolution in time. A summary of experimental works proposed on photoactive construction materials is reported in the following sections.

13.4.1 Interaction with hydraulic and non-hydraulic binders

The introduction of TiO_2 nanoparticles in building materials surely brings advantages, mainly from an economic point of view (i.e., the decrease in

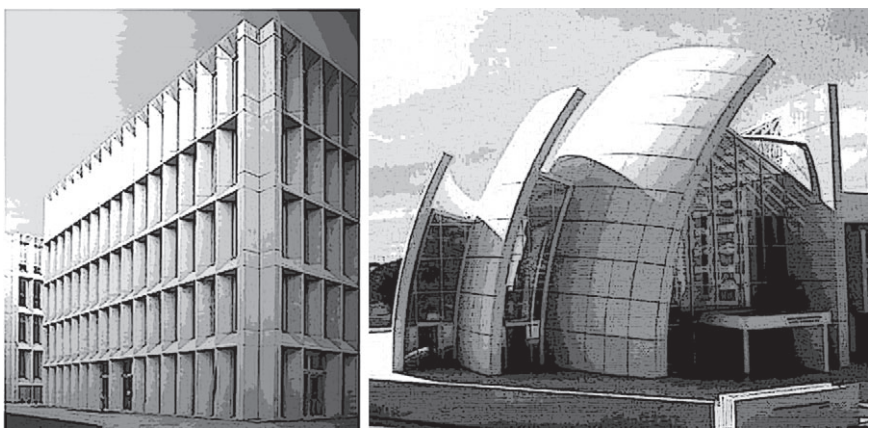

(a) (b)

13.7 Examples of buildings produced with TiO_2-containing cement: (a) Cité des Arts et de la Musique, Chambéry, (b) church Dives in Misericordia, Rome.

maintenance costs during the lifetime of the structure), and possibly an improvement of the surrounding air quality. The latter effect is actually connected with the extension of photocatalytic surfaces in relation with the volume of air to be depolluted: a limited space such as an indoor environment can benefit from this property, while a single building in a polluted city area will not be able to have a positive effect on the huge volume of air that comes into contact with it, this contact in most cases being very short due to wind.

Yet, the interaction of TiO_2 with such a complex hosting environment may also have negative consequences. In fact, materials based on either hydraulic (cement, hydraulic lime) and non-hydraulic (gypsum, lime) binders consist of a mixture of calcium-based inorganic compounds, mainly calcium oxide/hydroxide, carbonate, silicate and sulphate. These constituents do not occupy the whole volume of the material, and materials are typically porous at the micro- and also nano-scale: this porosity is where TiO_2 usually finds its collocation, acting as a further aggregate, or nano-filler. Therefore, all reaction products of cement hydration that remain unbounded in the material porosities can adsorb on the TiO_2 surface, if small (e.g., impurities, germs of calcium hydroxide crystals, etc.), thus 'stealing' active sites to external polluting substances that could be degraded in a mechanism of competitive adsorption. Furthermore, a side effect of increased electron-hole couple recombination can also occur on adsorbed species (Lackhoff *et al.*, 2003; Kwon *et al.*, 2006).

This is the most evident influence of the alkaline hosting material on TiO_2 photoactivated properties; it is then immediate to wonder whether TiO_2 itself may lead to changes in the material characteristics. Concerning the fresh state, the key modification induced by TiO_2 nanopowders is a decrease in workability: in fact, this is not correlated to the chemical nature of the particles, but to their nanometric size, which produces a drastic change in the rheological behaviour of the mix. This change is quite pronounced, and must be considered in order to assure a determined workability.

On the other hand, hardening properties are just slightly affected by TiO_2. Attention has been focused on the observed increase in the compressive resistance of the material: this was mainly ascribed to the already cited filling effect, which was addressed by several works and summarized in the review by Sanchez and Sobolev (2010). Yet, controversies arise when a possible active behaviour of TiO_2 is considered. Lackhoff *et al.* (2003) and Li *et al.* (2007) hypothesize a pozzolanic activity of TiO_2; while the former justify this as an indirect consequence of an accelerated cement hydration observed with NMR relaxometry, in the latter case no experimental validation is provided, and the assumption is probably made in the wake of the pozzolanic activity of silica nanopowders proved in previous works (Ji, 2005; Jo *et al.*, 2007). This was further supported by Nazari and Riahi in 2010, as

a consequence of observed reduction in setting time and final porosity of TiO_2-containing concrete, in spite of Chen and Poon's observations (2009a) rebutting any pozzolanic nature of TiO_2. Their experimental tests showed no TiO_2 mass change during hydration, which suggests an inert behaviour of the nanopowders, whose maximum effect is that of providing a wide surface for nucleation or clinging of hydration products. This issue is still open for discussion.

The majority of works in this field are related to hydraulic binder-based materials, as they represent the larger volume of products, especially concerning the realization of new structures; a few works are also available on non-hydraulic binders, focusing on the conservation of historical and contemporary structures. In this specific context, Karatasios *et al.* (2010) investigated the ageing of lime mortars, and specifically their carbonation. They attributed to the presence of TiO_2 an effect of CO_2 release, which accelerated carbonation reactions. In fact, TiO_2 presence would have caused the photocatalytic degradation of organic substances adsorbed on the material surface, releasing CO_2 as a reaction product. The process was considered beneficial since surface carbonation of these materials decreases the risks of calcium leaching by run-off water, one of the main causes of binder degradation, due to the lower solubility of calcium carbonate compared to calcium hydroxide (Hansen *et al.*, 2003).

13.4.2 Ageing of the material

Understanding the evolution of the material during its whole lifetime and the possible onset of negative interferences between TiO_2 and its hosting environment is just as important as studying its beneficial effects.

The alkaline material undergoes carbonation in time, which decreases capillary absorption and causes the precipitation of calcium carbonate inducing a solid volume increase of the material higher than 10% (Ceukelaire and Nieuwenburg, 1993; Castellote *et al.*, 2009). These precipitates tend to obstruct active sites, thus decreasing the photocatalytic efficiency of TiO_2 mainly for a shielding effect (Chen and Poon, 2009b). This effect builds up with the accumulation of contaminants on surfaces exposed to the environment, as noted in a report of the Hong Kong Environmental Protection Department (Yu, 2003) (Fig. 13.8).

Although some data are already available, the influence of carbonation on the photocatalytic and self-cleaning efficiency of TiO_2 embedded in construction materials has not been examined thoroughly yet. This can be a vital aspect to define the service life of such materials, as a careful design of the mix must take into account a possible decrease, and eventually the loss, of this functionality. This is true for any kind of element considered – mortar panels for cladding systems, repair plasters, and even more impor-

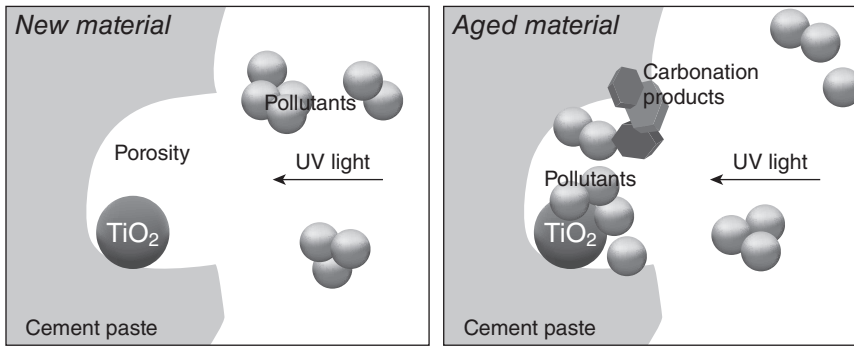

13.8 Scheme of possible progressive shielding of photocatalyst due to material ageing.

tantly if the whole structure is built with photocatalytic concrete, since its degradation cannot be easily overcome by substitution or re-application. A guideline dedicated to solving design issues with photocatalytic materials would therefore be a desirable target of further research.

13.5 Efficiency of TiO_2 in the built environment

Experimental works concerning the use of TiO_2 nanopowders in the construction field are variegated in terms of substrate material (bare cement pastes, mortars, concrete), composition (mix proportions with different binder, water/binder ratio, photocatalyst concentration, type and quantity of sand/aggregates, additives) and final application (precast panels, paving blocks, concrete pavements, cement-based tiles, indoor and outdoor walls, masonry blocks).

Characterization tests performed are also numerous, all involving a more or less intense and prolonged irradiation with UV light or simulated sunlight. Different experimental setups are applied in laboratory testing, depending on the property to be tested:

- photocatalytic activity: measurement of the extent of gas phase degradation of inorganic pollutants (NO_x) or volatile organic compounds (VOCs) at the material surface
- self-cleaning: introduction of the material in a closed chamber with soiling atmosphere, or impregnation with an organic dye, and monitoring of colour loss (colour recovery); analysis of chromatic changes during extended exposure of materials to the external environment
- superhydrophilicity: measurement of contact angle of water on the material surface
- antibacterial and anti-vegetative effect: inhibition of biofilm formation, algae adhesion and proliferation, and sterilization effects.

13.5.1 Air depollution

Investigations on photocatalytic activity of cement pastes, mortars and concrete containing TiO_2 nanopowders have been performed in most cases by flowthrough methods. Nitrogen monoxide, or directly a NO_x ($NO + NO_2$) mixture, are used as polluting source with typical concentration of approximately 1 ppmv (1 part per million in volume), and NO and NO_2 concentrations are compared in the inlet and outlet gas flow; a chemiluminescent NO_x analyser is used as measuring unit. Tests involve a first phase of gas flow in the absence of any irradiation, to reach an equilibrium of air composition in the reactor chamber and of the NO absorption in the cementitious material itself, which clearly must not be considered in the calculation of NO degradation. Afterwards, a UV light source (or solar spectrum lamp) is switched on and the outlet gas composition sampled at predefined time intervals: NO concentration usually drops immediately by some percent, and finally goes back to its initial value when the lamp is switched off and the test interrupted.

In NO_x degradation tests, it is important to keep in mind that the first chemical reaction taking place at the TiO_2 surface is the reduction of NO to NO_2. Therefore, after a rapid decrease of NO_x concentration, a slight increase in its value can be observed in the steady state of reaction, since the drop of NO concentration is accompanied by the formation of NO_2. Finally, NO_2 is reduced as well, by the following reactions:

$$NO + OH^{\cdot} \rightarrow NO_2 + H^+ \quad [13.1]$$

$$NO_2 + OH^{\cdot} \rightarrow NO_3^- + H^+ \quad [13.2]$$

Degradation efficiencies of laboratory specimens range from approximately 50–60% in flow conditions to the total degradation of pollutants in batch conditions, depending on gas concentration, flux and irradiation time. Humidity was observed in many cases to slightly reduce photocatalytic activity when above a certain threshold, as the adsorption of water molecules on the surface of TiO_2 nanoparticles is competitive with respect to pollutant adsorption and consequent degradation (Hüsken *et al.*, 2009).

The result of the reaction chain of NO_x degradation has drawn much attention and some concern, since the final reaction step involves the dissolution of nitrate ions in rain to form nitric acid, and the consequent acidification of rainwater that reaches the sewers. Nonetheless, the concentration of NO_x in air is in the order of magnitude of tens of ppb (parts per billion), and consequently the possible concentration of HNO_3 that could reach sewers is extremely limited and is not expected to produce any detrimental effect.

Similar tests are performed with VOCs as polluting source, among which propanol, butanol, toluene, formaldehyde and acetone are the most diffuse

model reactants. Also in this case, removal efficiencies are almost 100% in batch conditions and close to 60% in flow conditions. Experimental tests performed in flow conditions are undoubtedly more relevant than batch ones, as they are more representative of the actual working conditions of these materials in service.

13.5.2 Self-cleaning

One of the first studies on the self-cleaning attribute of photoactive materials is that proposed by Cassar in 2004, describing the impregnation of white cement disks with a yellow dye (phenanthroquinone) and the subsequent restoration of the initial white colour in specimens containing TiO_2. Similar works on cement pastes and mortars were carried out with other organic dyes, such as rhodamine B. Aqueous solutions of the dye with a concentration of 0.05 g/L were spread on the surface of mortars and allowed to dry, then colour variations during irradiation were monitored with a spectrophotometer (Ruot *et al.*, 2009).

This method allows an easy evaluation of the self-cleaning property. The spectrophotometer measures the colour of the surface, and converts it into a set of chromatic coordinates (usually the CIELab colour system, defined by the Commission Internationale de l'Éclairage, where L^* is brightness, a^* varies from green to red, and b^* from blue to yellow). In this space, colour changes can be measured as geometric distance between two points, which correspond to two different colours to be compared (for example, A and B in Fig. 13.9). It is possible to calculate the overall colour change (Δcol), or to analyse only the changes in hue (Δhue), or to identify changes in the saturation of a single hue (Δsat). The latter parameter is exploited in dye degradation measurements: since dyes lose their colour when the molecular structure is degraded, colour saturation can be used as a representative parameter of dye concentration. In the case of rhodamine B, which exhibits a strong magenta colour, a decreased intensity of red component of colour indicates that the dye is being degraded.

Yet, it is important to keep in mind that colour changes do not necessarily mean complete degradation, and the organic molecule can still be partially integer even after the colour has disappeared, since it is sufficient to break the molecule chromophore groups to induce the colour loss. This is why these tests often refer to dye 'decolourization' rather than 'mineralization', since the latter can only be measured by TOC (total organic carbon) or spectrometric measurements.

Another important experimental path that can be chosen to test the self-cleaning attribute of cement-based materials is their exposure to a polluted environment and monitoring of surface colour, which is performed with the same colour measurements described for dye decolourization. The polluted

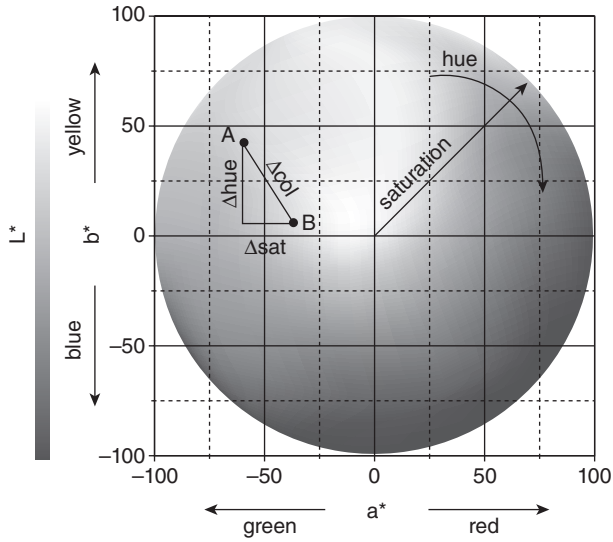

13.9 Colour measurements in CIELab colour space.

environment can be created artificially or it is possible to expose some specimens directly to urban atmosphere. In the latter case, since experimental conditions (humidity, temperature, irradiation) cannot be chosen and regulated, it is fundamental to have a monitoring station close to the exposure site, from where atmospheric data can be obtained. It is then possible to correlate them with the colour measurements, the most relevant parameters being the amount of radiation reaching the surface during the day and the time of wetness, which is closely correlated to the number of rainy days. As for the interpretation of data, a lower colour change in time is expected from a self-cleaning material. Moreover, if the soiled surface of a photoactive material returns towards its original colour right after a rainy event, and the same trend is not observed in a similar 'blank' material (without TiO_2), then this behaviour will be due to the onset of self-cleaning (Diamanti *et al.*, 2008).

13.5.3 A case study of life cycle assessment

A life cycle assessment (LCA) of TiO_2-containing coatings for concrete pavements was performed by Hassan in 2010. The author assumed that an improvement in air quality cannot be used as the only criterion for the complete evaluation of a material that should be considered sustainable, as critical environmental factors may be omitted. Therefore, a life-cycle inventory (LCI) was performed to quantify the energy, abiotic raw material inputs and emission from cradle to grave. A Building for Environmental

and Economic Sustainability (BEES) impact assessment model (Lippiat, 2007) was applied to analyse the inventory.

The reduction of the environmental impact of the material was found to act on four main categories: acidification, eutrophication, air pollutants and smog formation. Parallel increases in global warming, fossil fuel depletion, water intake, ozone depletion and impacts on human health were also assessed, caused mainly by the production phase and fossil energy consumption. Yet, the total environmental performance of the product led to the conclusion that the titanium dioxide coatings tested have an overall beneficial effect on the environment.

13.6 Pilot projects and field tests

The confused mass of information described in the previous sections surely shows the usefulness of TiO_2 in decreasing environmental pollution, and more broadly in improving the quality of materials where it is contained. Nonetheless, it implies at the same time great difficulties in understanding the actual behaviour of photocatalytic materials and in classifying them on the basis of their efficiencies.

These aspects are probably better investigated through large-scale experimental setups, which are fundamental to define the actual behaviour of materials modified with titanium dioxide in real practice. In this frame, Dylla *et al.* (2010) proposed a new laboratory setup to evaluate the influence of various parameters (humidity, pollutant flow rate, mix design) on the efficiency of photocatalytic coatings for concrete pavements, as well as on their resistance to abrasion and wear, given the critic application. A photoreactor with fluorescent lamps was built with a surrounding circuit providing the contaminant source (NO) and desired humidity. Particularly interesting are the dimensions of the photoreactor, 25 cm × 30 cm × 2.5 cm, which allows the evaluation of large samples, up to real-size paving slabs.

Besides large-scale tests, which still belong to the class of laboratory experiments, higher relevance must be given to pilot projects, as the most realistic way to measure the working efficiency directly on site. This is the scenario from which the project PICADA (Photocatalytic Innovative Coverings Applications for Depollution Assessment) took its first steps. In this project, a consortium of eight industries and research laboratories was created, aimed at developing and optimizing industrial formulations of innovative façade coatings with de-soiling and de-polluting properties including titanium dioxide, and at establishment of a local behaviour model under different exposure conditions and in a realistic urban environment.

The biggest pilot test in Europe is probably the 'street canyon' site that was built in France, near Guerville, in the frame work of the PICADA project (Guerrini *et al.*, 2007). The methodology consisted in testing the

effectiveness of photocatalytic properties on a 1:5 scale model reproducing the environmental conditions of a street located between two buildings, in a generic urban context. Two 18 m long lanes were built, and walls were covered with normal plaster in one case and photocatalytic plaster in the other; the atmosphere within the canyons was modified by flowing engine exhaust gases. Both air composition and environmental parameters were monitored, and the efficiency of photocatalytic plaster in keeping air cleaner was proved, with an up to fourfold decrease of contaminants compared to normal plaster in favourable weather conditions (wind, mainly).

Nowadays, examples of TiO_2-containing building materials can be found almost anywhere: some of them are just pilot projects, like the 'street canyon', others are the final product of this technology. One early example of the use of photocatalytic TiO_2 in the European built environment, and probably the most renowned, is the already cited church Dives in Misericordia, designed by Richard Meier and built with precast blocks of photocatalytic concrete produced by the Italcementi group (Fig. 13.7b). This building is often used as reference for the introduction and development of the use of photocatalytic concrete in Europe. It was finished in 2003, and for 7 years a constant monitoring of its colour was performed on the three 'sails' that form its architecture, showing no change in brightness in the areas analysed and only slight changes in the colour coordinates a* and b* on the panels facing south, which was ascribed to the deposition of African sand carried by the sirocco wind.

A demonstration project was carried out in Bergamo, Italy, where photocatalytic slabs were installed on a road and related pavement. Two periods of constant monitoring of NO_x in the surrounding air, lasting 10 days each, showed that in the presence of photocatalytic paving slabs, the pollutant concentration decreased by almost 45%, being the average concentration in that area in the order of ppbv (Guerrini and Peccati, 2007). Other works on photocatalytic roads were performed in laboratory and field conditions by Ballari *et al.* (2010) and in large-scale application by Beeldens (2006) in Antwerp, Belgium, where a road was paved with photocatalytic building blocks, revealing again a decrease in NO_x concentration.

Several other projects have been realized and are still monitored, such as tunnels, airports and schools, whose exterior walls were either built with photocatalytic materials or coated with TiO_2-containing products, such as mortars, plasters, or just paints.

13.7 Existing patents and standards relating to photocatalytic cementitious materials

Although the attention of a large part of the scientific community has been devoted to titanium dioxide for decades, practical applications are more

recent, and have found a worldwide diffusion only in the last few years. The market for photocatalytic construction materials is expected to grow from a volume of $800 million to $1.5 billion by 2014, as proposed in the market report 'Photocatalysts: Technologies and Global Markets' by BCC Research (2010). Commercial products focus mainly on the application of coatings on other materials, in spite of the problems connected to the durability of such products due to environmental factors, or just wear. TOTO Ltd was one of the first companies to notice the economic and innovation implications of the use of TiO_2 in building materials, and collaborated closely with Fujishima and its research group when TiO_2 photocatalysis and self-cleaning were still in their infancy.

An idea of the maturity of a product that still attracts so much basic and applied research is given by market volumes, but also the growing number of patent applications and standards promulgated is indicative of a massive passage from laboratory to real applications.

13.7.1 Overview of current patents

Nowadays, hundreds of patents exist on photocatalytic materials for air purification, self-cleaning surfaces, antibacterial surfaces, and many other sub-categories. Just as an example, in 2009 approximately 60 patent applications were submitted to the WIPO (World Intellectual Property Organization) based on a keyword search of the concept 'photocatalysis', among which 41% come from Japan: the major players are TOTO Ltd (Japan) and Carrier Corp. (USA), followed by Saint Gobain Glass (France) and Italcementi (Italy). Air purification is by far the most popular, and includes air purification devices and photocatalytic filters, which are beyond the scope of this chapter. A short list, surely not comprehensive, of some patents related to photocatalytic cementitious materials is reported in Table 13.1.

13.7.2 Standards for materials testing

Japan was undoubtedly the first country to appreciate the potential of photocatalytic materials, to invest in their application nationwide and to formulate appropriate standards to evaluate their efficiency. All standards that have been, or are being, developed are therefore based on Japanese experience, and often refer to the corresponding JIS (Japanese Industrial Standard), which include the test methods of photocatalytic materials for air purification performance (JIS R 1701), antibacterial activity (JIS R 1702), self-cleaning performance (JIS R 1703), water-purification performance (JIS R 1704) and antifungal activity (JIS R 1705).

In fact, every single outcome of the photoactivation of titanium dioxide requires a different standard, and also the type of supporting material

Table 13.1 Examples of patents on TiO_2 in building materials

Year	Code	Country	Title
2009	13337	United Nations	Coatings based on hydraulic binders with an optimal rheology and high photocatalytic activity
2008	17934	United Nations	New precast cementitious products with photocatalytic activity
2008	236450	USA	Photocatalytic granular mixture for mortar and concrete and its use
2007	1752429 A1	Europe	Bituminous road surface with a photocatalytic effect and a procedure for the preparation of said road surface
2006	565	United Nations	High durability photocatalytic paving for reducing urban polluting agent
2006	2425075 A	UK	Concrete roof tile or wall cladding element
2005	1609910	Europe	A pavement with photocatalytic effect
2004	74202	United Nations	Cement-based paving blocks for photocatalytic paving for the abatement of urban pollutants
2002	2002242113	Japan	Coating method of photocatalyst layer to pavement for air purification
2002	6409821	USA	Hydraulic binder and cement composition containing photocatalyst particles
1999	5861205	USA	NO_x cleaning paving block
1998	10219920	Japan	Extrusion-molded building materials for removal of nitrogen oxide and their manufacture

strongly influences the test methods and the expected results: porous cementitious materials will necessarily undergo a different procedure with respect to compact ceramics, and further differences will characterize the testing of coatings. This short survey will only focus on standards referring to cement-based, and therefore intrinsically porous, photocatalytic materials.

The formulation of such standards in Europe was entrusted to an official working group of CEN (European Committee for Standardization), who was asked to define technical specifications and guidelines: the activity is not closed yet, and the group is still working on it. In the meanwhile, some documents were produced by the ISO (International Standards Organization) working group on photocatalytic materials, starting in 2007, focusing on photocatalytic fine ceramics (Table 13.2). Other standards are under evaluation and will be published probably in the next few years. These

Table 13.2 ISO standards on photocatalytic fine ceramics

Year	Code	Topic
2011	ISO22197-2	Photocatalytic removal efficiency of acetaldehyde
2011	ISO22197-3	Photocatalytic removal efficiency of toluene
2011	ISO10677	Definition of standard UV light source for testing photocatalytic performances
2010	ISO10676	Water purification performances through the forming ability of active oxygen
2010	ISO10678	Photocatalytic degradation of methylene blue
2009	ISO27447	Evaluation of antibacterial activity of photocatalytic surfaces
2009	ISO27448	Self-cleaning performances through the measurement of water contact angle
2007	ISO22197-1	Photocatalytic removal efficiency of nitric oxide

documents will surely become a reference to assess product performances for both public and private building contractors.

13.8 References

Akpan UG, Hameed BH (2009), 'Parameters affecting the photocatalytic degradation of dyes using TiO_2-based photocatalysts: a review', *J. Hazard. Mater.*, 170, 520–529.

Ballari MM, Hunger M, Hüsken G, Brouwers H (2010), 'NO_x photocatalytic degradation employing concrete pavement containing titanium dioxide', *Appl. Catal. B*, 95, 245–254.

Beeldens A (2006), 'Environmental friendly concrete pavement blocks: air purification in the centre of Antwerp', *Proceedings of 10th International Symposium on Concrete Roads*, Brussels.

Bellardita M, Addamo M, Di Paola A, Marcì G, Palmisano L, Cassar L, Borsa M (2010), 'Photocatalytic activity of TiO_2/SiO_2 systems', *J. Hazard. Mater.* 174, 707–713.

Carp O, Huisman CL, Reller A (2004), 'Photoinduced reactivity of titanium dioxide', *Progr. Solid State Chem.*, 32, 33–177.

Cassar L (2004), 'Photocatalysis of cementitious materials: clean buildings and clear air', *MRS Bull.*, 29, 328–331.

Castellote M, Fernandez L, Andrade C, Alonso C (2009), 'Chemical changes and phase analysis of OPC pastes carbonated at different CO_2 concentrations', *Mater. Struct.*, 42, 515–525.

Ceukelaire LD, Nieuwenburg DV (1993), 'Accelerated carbonation of a blast-furnace cement concrete', *Cem. Concr. Res.*, 23, 442–452.

Chai SY, Kim YJ, Lee WI (2006), 'Photocatalytic WO_2/TiO_2 nanoparticles working under visible light', *J. Electroceram.*, 17, 909–912.

Chen J, Poon CS (2009a), 'Photocatalytic cementitious materials: influence of the microstructure of cement paste on photocatalytic pollution degradation', *Environ. Sci. Technol.*, 43, 8948–8952.

Chen J, Poon CS (2009b), 'Photocatalytic construction and building materials: from fundamentals to applications', *Build. Environ.*, 44, 1899–1906.

Clean Air Act Amendments of 1990 §101–131, 42 U.S.C. §7401–7431.

Demeestere K, Dewulf J, De Witte B, Beeldens A, Van Langenhove H (2008), 'Heterogeneous photocatalytic removal of toluene from air on building materials enriched with TiO_2', *Build. Environ.*, 43, 406–414.

Diamanti MV, Ormellese M, Pedeferri MP (2008), 'Characterization of photocatalytic and superhydrophilic properties of mortars containing titanium dioxide', *Cem. Concr. Res.*, 38, 1349–1353.

Doerffler W, Hauffe K (1964), 'Heterogeneous photocatalysis I. The influence of oxidizing and reducing gases on the electrical conductivity of dark and illuminated zinc oxide surfaces', *J. Catal.*, 3, 156–170.

Drelich J, Chibowski E, Meng DD, Terpilowski K (2011), 'Hydrophilic and superhydrophilic surfaces and materials', *Soft Matter*, 7, 9804–9828.

Dylla H, Hassan MM, Mohammad EN, Rupnow T, Wright E (2010), 'Evaluation of environmental effectiveness of titanium dioxide photocatalyst coating for concrete pavement', *Transport. Res. Record*, 2164, 46–51.

Frank SN, Bard AJ (1977a), 'Heterogeneous photocatalytic oxidation of cyanide ion in aqueous solutions at titanium dioxide powder', *J. Am. Chem. Soc.*, 99, 303–304.

Frank SN, Bard AJ (1977b), 'Heterogeneous photocatalytic oxidation of cyanide and sulfite in aqueous solutions at semiconductor powders', *J. Phys. Chem.*, 81, 1484–1488.

Health Perspectives, 109, A174–A177.

Fujishima A, Honda K (1972), 'Electrochemical photolysis of water at a semiconductor electrode', *Nature*, 238, 37–38.

Fujishima A, Zhang XT (2006), 'Titanium dioxide photocatalysis: present situation and future approaches', *Cr. Chim.*, 9, 750–760.

Fujishima A, Ohtsuki J, Yamashita T, Hayakawa S (1986), 'Behavior of tumor cells on photoexcited semiconductor surface', *Photomed Photobiol*, 8, 45–46.

Fujishima A, Zhang X, Tryk DA (2007), 'Heterogeneous photocatalysis: from water photolysis to applications in environmental cleanup', *Int. J. Hydrogen Energy*, 32, 2664–2672.

Gerrity D, Ryu H, Crittenden J, Abbaszadegan M (2008), 'Photocatalytic inactivation of viruses using titanium dioxide nanoparticles and low-pressure UV lamp', *J. Environ. Sci. Health A*, 43, 1261–1270.

Goodeve CF, Kitchener JA (1938), 'Photosensitisation by titanium dioxide', *Trans. Farad. Soc.*, 34, 570–579.

Guerrini GL, Peccati E (2007), 'Photocatalytic cementitious roads for depollution', in Baglioni P, Cassar L, *RILEM Int. Symp. on Photocatalysis, Environment and Construction Materials*, Italy, RILEM, 179–186.

Guerrini GL, Plassais A, Pepe C, Cassar L (2007), 'Use of photocatalytic cementitious materials for self-cleaning applications', in Baglioni P, Cassar L, *RILEM Int. Symp. on Photocatalysis, Environment and Construction Materials*, Italy, RILEM, 219–226.

Hamal DB, Haggstrom JA, Marchin GL, Ikenberry MA, Hohn K and Klabunde KJ (2009), 'A multifunctional biocide/sporocide and photocatalyst based on titanium dioxide (TiO_2) codoped with silver, carbon, and sulfur', *Langmuir*, 26, 2805–2810.

Han F, Kambala VSR, Srinivasan M, Rajarathnam D, Naidu R (2009), 'Tailored titanium dioxide photocatalysts for the degradation of organic dyes in wastewater treatment: a review', *Appl. Catal. A*, 359, 25–40.

Hansen E, Doehne E, Fidler J, Larson J, Martin B, Matteini M, Rodriguez-Navarro C, Pardo ES, Price C, de Tagle A, Teutonico JM, Weiss N (2003), 'A review of selected inorganic consolidants and protective treatments for porous calcareous materials', *Rev. Conserv.*, 4, 13–25.

Hassan MM (2010), 'Quantification of the environmental benefits of ultrafine/nanotitanium dioxide photocatalyst coatings for concrete pavement using hybrid life-cycle assessment', *J. Infrastruct. Sys.*, 16, 160–166.

Hüsken G, Hunger M, Brouwers H (2007), 'Comparative study on cementitious products containing titanium dioxide as photo-catalyst', in Baglioni P, Cassar L, *RILEM Int. Symp. on Photocatalysis, Environment and Construction Materials*, Italy, RILEM, 147–154.

Hüsken G, Hunger M, Brouwers H (2009), 'Experimental study of photocatalytic concrete products for air purification', *Build. Environ.*, 44, 2463–2474.

Irie H, Sunada K, Hashimoto K (2004), 'Recent developments in TiO_2 photocatalysis: novel applications to interior ecology materials and energy saving systems', *Electrochemistry*, 72, 807–812.

Ji T (2005), 'Preliminary study on the water permeability and microstructure of concrete incorporating nano-SiO_2', *Cem. Concr. Res.*, 35, 1943–1947.

Jo BW, Kim CH, Tae G, Park JB (2007), 'Characteristics of cement mortar with nano-SiO_2 particles', *Construct. Build. Mater.*, 21, 1351–1355.

Karatasios I, Katsiotis MS, Likodimos V, Kontos AI, Papavassiliou G, Falaras P, Kilikoglou V (2010), 'Photo-induced carbonation of lime-TiO_2 mortars', *Appl. Catal. B*, 95, 78–86.

Kato S, Masuo F (1964), 'Titanium dioxide-photocatalyzed oxidation. I. Titanium dioxide-photocatalyzed liquid phase oxidation of tetralin', *Kogyo Kagaku Zasshi*, 67, 42–50.

Keidel E (1929), 'Die Beeinflussung der Lichtechtheit von Teerfarblacken durch Titanweiss [Influence of titanium white on the fastness to light of coal-tar days]', *Farben-Zeitung*, 34, 1242–1243.

Konstantinou IK, Albanis TA (2004), 'TiO_2-assisted photocatalytic degradation of azo dyes in aqueous solution: kinetic and mechanistic investigations – a review', *Appl. Catal. B: Environ.*, 49, 1–14.

Kreutler B, Bard AJ (1978), 'Heterogeneous photocatalytic synthesis of methane from acetic acid – new Kolbe reaction pathway', *J. Am. Chem. Soc.*, 100, 2239–2240.

Kurth JC, Giannantonio DJ, Allain F, Sobecky PA, Kurtis KE (2007), 'Mitigating biofilm growth through the modification of concrete design and practice', in Baglioni P, Cassar L, *RILEM Int. Symp. on Photocatalysis, Environment and Construction Materials*, Italy, RILEM, 195–202.

Kwon JM, Kim YH, Song BK, Yeom SH, Kim BS, Bin I (2006), 'Novel immobilization of titanium dioxide (TiO_2) on the fluidizing carrier and its application to the degradation of azo-dye', *J. Hazard. Mater.*, 134, 230–236.

Lackhoff M, Prieto X, Nestle N, Dehn F, Niessner R (2003), 'Photocatalytic activity of semiconductor-modified cement – influence of semiconductor type and cement ageing', *Appl. Catal. B*, 43, 205–216.

Li H, Zhang M, Ou J (2007), 'Flexural fatigue performance of concrete containing nano-particles for pavement', *Int. J. Fatigue*, 29, 1292–1301.

Linkous CA, Robertson RH (2006), 'Effect of photocatalytic coatings on the weathering of elastomeric roofing membrane', *Proceedings of the 15th Symposium on Improving Building Systems in Hot and Humid Climates*, Orlando, FL, ESL-HH-06-07-33.

Linkous CA, Carter GJ, Locuson DB, Ouellette AJ, Slattery DK, Smitha LA (2000), 'Photocatalytic inhibition of algae growth using TiO_2, WO_3, and cocatalyst modifications', *Environ. Sci. Technol.*, 34, 4754–4758.

Linsebigler AL, Lu G, Yates JT (1995), 'Photocatalysis on TiO_2 surfaces: principles, mechanisms, and selected results', *Chem. Rev.*, 95, 735–758.

Lippiat B (2007), 'Building for environmental and economic sustainability (BEES)', Technical manual and user guide, National Institute of Standards and Technology, Springfield, VA.

Matsunaga T, Tomato R, Nakajima T, Wake H (1985), 'Photoelectrochemical sterilization of microbial cells by semiconductor powders', *FEMS Microbiol. Lett.*, 29, 211–214.

Matthews RW (1987), 'Photooxidation of organic impurities in water using thin films of titanium dioxide', *J. Phys. Chem.*, 91, 3328–3333.

McLintock S, Ritchie M (1965), 'Reactions on titanium dioxide; photoadsorption and oxidation of ethylene and propylene', *Trans. Faraday Soc.*, 61, 1007–1016.

Mellott NP, Durucan C, Pantano CG, Guglielmi M (2006), 'Commercial and laboratory prepared titanium dioxide thin films for self-cleaning glasses: photocatalytic performance and chemical durability', *Thin Solid Films*, 502, 112–120.

Mills A, Lee SK (2002), 'A web-based overview of semiconductor photochemistry-based current commercial applications', *J. Photochem. Photobiol. A*, 152, 233–247.

Nazari A, Riahi S (2010), 'The effects of TiO_2 nanoparticles on properties of binary blended concrete', *J. Compos. Mater.*, 45, 1181–1188.

O'Regan B, Gratzel M (1991), 'A low-cost, high-efficiency solar cell based on dye-sensitized colloidal TiO_2 films', *Nature*, 353, 737–740.

Ohtani B (2010), 'Environmental applications of photocatalysis', in Special Lectures on Environmental Science II. Available at: pcat.cat.hokudai.ac.jp/class/es2012/20120405b_BO_Sapporo.pdf (accessed August 2012).

Page K, Palgrave RG, Parkin IP, Wilson M, Savin SLP, Chadwick AV (2007), 'Titania and silver–titania composite films on glass – potent antimicrobial coatings', *J. Mater. Chem.*, 17, 95–104.

Palmisano G, Augugliaro V, Pagliaro M, Palmisano L (2007), 'Photocatalysis: a promising route for 21st century organic chemistry', *Chem. Commun.*, 3425–3437.

Paz Y (2010), 'Application of TiO_2 photocatalysis for air treatment: patents' overview', *Appl. Catal. B*, 99, 448–460.

Polo A, Diamanti MV, Bjarnsholt T, Høiby N, Villa F, Pedeferri MP, Cappitelli F (2011), 'Effects of photoactivated titanium dioxide nanopowders and coating on planktonic and biofilm growth of *Pseudomonas aeruginosa*', *Photochem. Photobiol.*, 87, 1387–1394.

Riahi S, Nazari A (2011), 'Physical, mechanical and thermal properties of concrete in different curing media containing ZnO_2 nanoparticles', *Energy Build.*, 43, 1977–1984.

Ruot B, Plassais A, Olive F, Guillot L, Bonafous L (2009), 'TiO_2-containing cement pastes and mortars: Measurements of the photocatalytic efficiency using a rhodamine B-based colourimetric test', *Sol. Energy* 83, 1794–1801.

Sanchez F, Sobolev K (2010), 'Nanotechnology in concrete – a review', *Construct. Build. Mater.*, 24, 2060–2071.

Schiavello M (1988), 'Basic concepts in photocatalysis', in Schiavello M, *Photocatalysis and Environment: Trends and Applications*, Dordrecht, Kluwer, 351–360.

Schrauzer GN, Guth TD (1977), 'Photocatalytic reactions. 1. Photolysis of water and photoreduction of nitrogen on titanium dioxide', *J. Am. Chem. Soc.*, 99, 7189–7193.

Shapovalov VI (2010), 'Nanopowders and films of titanium oxide for photocatalysis: a review', *Glass Phys. Chem.*, 36, 121–157.

Shibata T, Irie H, Hashimoto K (2003), 'Enhancement of photoinduced highly hydrophilic conversion on TiO_2 thin films by introducing tensile stress', *J. Phys. Chem. B*, 107, 10696–10698.

Sievers M (2011), 'Advanced oxidation processes', in Wilderer P, *Treatise on Water Science, vol. 4*, Oxford, Elsevier, 377–408.

Toma FL, Bertrand G, Klein D, Coddet C (2004), 'Photocatalytic removal of nitrogen oxides via titanium dioxide', *Environ. Chem. Lett.*, 2, 117–121.

Wang R, Hashimoto K, Fujishima A, Chikuni M, Kojima E, Kitamura A, Shimohigoshi M, Watanabe T (1997), 'Light-induced amphiphilic surfaces', *Nature*, 388, 431–432.

Watanabe T, Kojima E, Norimoto K, Saeki Y (1995), 'Fabrication of TiO_2 photocatalytic tile and practical applications', *Fourth Euro Ceramics*, 11, 175–180.

Wysocka-Krol K, Wieliczko A, Podbielska H (2011), 'Silver doped nanomaterials and their possible use for antibacterial photodynamic activity', in Mohseni H, Agahi MH and Razeghi M, *Biosensing and Nanomedicine IV – Proceedings of SPIE, Bellingham, SPIE-Int Soc Optical Engineering*, 809915.

Yu CM (2003), *Deactivation and Regeneration of Environmentally Exposed Titanium Dioxide (TiO_2) Based Products*, Department of Chemistry, Chinese University of Hong Kong.

14

Self-cleaning tiles and glasses for eco-efficient buildings

D. SYNNOTT, N. NOLAN, D. RYAN, J. COLREAVY and S. C. PILLAI, FOCAS Institute, Republic of Ireland

DOI: 10.1533/9780857098832.3.327

Abstract: Self-cleaning and anti-bacterial activities of the photocatalyst titanium dioxide make it a superior compound for use in the ceramics and glass industry. Photocatalytic products have been on the market since 2001. Photocatalysis is a photochemical process that semiconductor materials such as titanium dioxide undergo when irradiated by light of a certain wavelength. A major drawback in commercializing conventional TiO_2 photocatalysts for ceramic applications is the large band gap of these materials which restricts its usefulness to outdoor environments. Titanium dioxide can only be activated upon irradiation with a photon of light <390 nm in the ultraviolet region. Ultraviolet light makes up less than 5% of the solar spectrum, whereas the spectrum consists of ~40% visible light. Therefore, in order to utilize TiO_2 to its full potential and use it in an indoor environment, it is necessary to decrease the band gap size facilitating visible light absorption. In this chapter recent developments in the preparation of visible light activated catalysts are provided. A brief outline of various commercial photocatalytic tiles and glass products are listed. A general scientific mechanism of anti-bacterial action and self-cleaning activity of photocatalysts are also explained in detail. Finally, projected market growth, future trends and recommendations to improve the photocatalytic properties for the applications of tile and glass are described.

Key words: self-cleaning tiles, glass, anti-bacterial activity, solar and visible light.

14.1 Introduction

In 1972, Japanese researchers Fujishima and Honda demonstrated the powerful semiconductor capabilities of titanium dioxide, TiO_2, in the splitting of water in a photoelectrochemical cell. Their work ignited a revolution in the world of semiconductor research with Frank and Bard going on to demonstrate titanium dioxide's unique properties for environmental remediation through the reduction of CN^- in water[1–4] in 1977, and Ollis using TiO_2 for the mineralization of organic pollutants in 1983.[5–7] In the 1990s, following Graetzel's paper on the dye-sensitized solar cell,[8,9] TiO_2 became one of the most internationally researched semiconductor materials. The

increase in TiO_2 publications per year demonstrates the growth in the area.[10,11]

14.1.1 Photocatalysis

The term photocatalysis implies that light is acting as a catalyst in a reaction, which is not the case.[12,13] However, the term photocatalysis will always be used to describe the process that semiconductor materials such as TiO_2 undergo when irradiated by light of a certain wavelength. It is a term that implies photon-assisted generation of catalytically active species.

In photocatalysis light of energy greater than the band gap of the semiconductor excites an electron from the valence band to the conduction band (Fig. 14.1) by the following reaction:.

$$\text{Semiconductor} + h\nu \rightarrow h^{+}_{VB} + e^{-}_{CB} \qquad \text{Scheme 14.1}$$

The excited electron leaves a positive hole in the valence band and these charge carriers can migrate to the catalyst surface and initiate redox reactions on absorbents such as water and oxygen. Positive holes generated by light become trapped by surface adsorbed H_2O. The H_2O becomes oxidized by h^{+}_{VB}, producing H^{+} and OH• radicals (Eq. [14.1]), which are extremely powerful oxidants (Table 14.1). The hydroxyl radicals subsequently oxidize organic species from the surrounding environment to CO_2 and H_2O (Eq. [14.3])[14] and in most cases these are the most important radicals formed in TiO_2 photocatalysis.

Electrons in the conduction band can be rapidly trapped by molecular oxygen adsorbed on the particle. Trapped molecular oxygen will be reduced by excited electrons to form superoxide (O^{2-}•) radicals (Eq. [14.2]) that

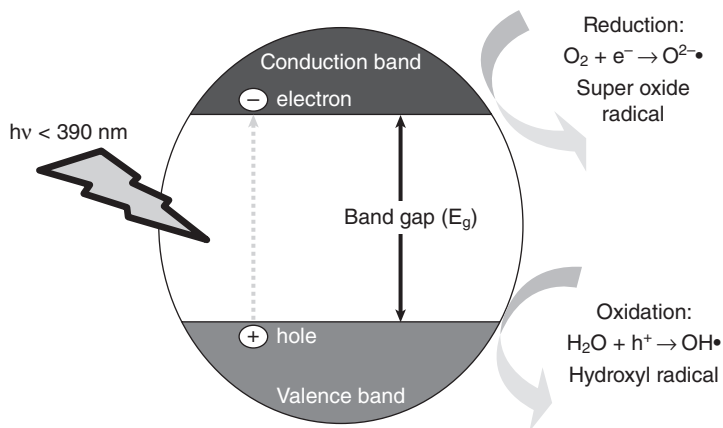

14.1 Schematic of photocatalytic mechanism.

Table14.1 Oxidation potentials of various oxidants relative to normal hydrogen electrode (NHE)

Oxidant	Oxidation potential (V)
OH• (hydroxyl radical)	2.80
O_3 (ozone)	2.07
H_2O_2 (hydrogen peroxide)	1.77
HClO (hypochlorous acid)	1.49
Cl (chlorine)	1.36

may further react with H^+ (Eq. [14.4]), to generate peroxide radicals (•OOH) and hydrogen peroxide, H_2O_2 (Eq. [14.5]).[15,16]

Recombination of the excited electron and the photo-generated hole is a major limitation in semiconductor photocatalysis as it reduces the overall quantum efficiency of the photocatalyst because of the high recombination rate of photoinduced electron-hole pairs at the surface of the photocatalyst.[17] The photocatalytic efficiency can be significantly enhanced if recombination is reduced. Doping with ions,[18–20] heterojunction coupling[21] and nanosized crystals[22] have all been reported to promote separation of the electron-hole pair, reducing recombination and therefore improving the photocatalytic activity of the semiconductor material.

When recombination occurs, the excited electron reverts to the valence band without reacting with adsorbed species (Scheme 14.2).[23] Radiation may be emitted when an excited electron recombines with the valence band. As such, photoluminescence may be successfully employed to monitor recombination and, in general, low intensity photoluminescence signals indicate lower recombination rates.[17]

$$e^-_{CB} + h^+_{VB} \rightarrow \text{energy} \qquad \text{Scheme 14.2}$$

$$H_2O + h^+_{VB} \rightarrow \bullet OH + H^+ \qquad [14.1]$$

$$O_2 + e^-_{CB} \rightarrow O_2^{-}\bullet \qquad [14.2]$$

$$\bullet OH + VOC \rightarrow H_2O + CO_2 \qquad [14.3]$$

$$O_2^{-}\bullet + H^+ \rightarrow \bullet OOH \qquad [14.4]$$

$$\bullet OOH + \bullet OOH \rightarrow H_2O_2 + O_2 \qquad [14.5]$$

$$O_2^{-}\bullet + VOC \rightarrow CO_2 + H_2O \qquad [14.6]$$

$$\bullet OOH + VOC \rightarrow CO_2 + H_2O \qquad [14.7]$$

Equations [14.1]–[14.7] schematize the whole process.[14,24,25] Hydroxyl radicals produced by the photocatalytic process will oxidize the majority of volatile organic compounds (VOC) until complete mineralization.

Recombination competes strongly with the photocatalytic process. It may occur on the surface in the bulk and is in general catalysed by impurities, defects, or all factors which introduce bulk or surface imperfections into the crystal.[26] The fact that the process can only be initiated by UV light is also a limiting factor in the process. It is desirable to produce a photocatalyst that can be activated by visible light to make full use of the solar spectrum.

14.1.2 Practical use of photocatalysts for tiles and glasses

A major drawback in commercializing conventional TiO_2 photocatalysts for community care applications is the large band gap. Titanium dioxide can only be activated upon irradiation with a photon of light <390 nm, limiting its use on commodity materials such as tiles and glasses.[27–29] Ultraviolet light makes up only 3–5% of the solar spectrum, whereas the spectrum consists of ~40% visible light. Therefore, in order to utilize TiO_2 to its full potential it is necessary to decrease the band gap size facilitating visible light absorption.

Non-metal doping has shown great promise in achieving visible light activated photocatalysis, with nitrogen being the most effective dopant. Asahi *et al.* were the first to show visible light absorption through N doping. They reported nitrogen-doped TiO_2 promoted photocatalytic activity up to $\lambda = 520$ nm.[30] The nitrogen substitutional doping of TiO_2 was initially claimed as a method for narrowing the band gap by exclusively changing the valence band structure; fine electronic details of this are, however, under discussion. Asahi *et al.* claimed that the presence of nitrogen narrows the band gap of TiO_2, thus making it capable of performing visible light-driven photocatalysis.[30] However, Ihara *et al.* suggested that it is the oxygen vacancies that contributed to the visible light activity, and the doped nitrogen only enhanced the stabilization of these oxygen vacancies.[31] They also confirmed this role of oxygen vacancies in plasma-treated TiO_2 photocatalysts.[31]

In addition, that the structural oxygen vacancy caused visible light photocatalytic activity was also reported by Martyanov *et al.*[32] Currently there appears to be some agreement on the mechanism of nitrogen-doped visible light absorption explained by Irie *et al.*[33] and Nakamura *et al.*[34] They explained that TiO_2 oxygen lattice sites substituted by nitrogen atoms form an occupied midgap (N-2p) level above the (O-2p) valence band. Irradiation with UV light excites electrons in both the valence band and the narrow (N-2p) band, but irradiating with visible light only excites electrons in the narrow (N-2p) band.[33,34]

It has also been shown that F doping improves both UV and visible light photocatalytic activity. However, their mechanisms are still under discussion. Previous studies have shown that N-F-co-doped TiO_2 powders demonstrated excellent photocatalytic activity no matter what kind of light

source was used. This seems to be a consequence of the perfect combination of some beneficial effects induced by both N and F dopants.[35]

Carbon, phosphorous and sulphur have also shown positive results for visible light responsive TiO_2.[36,37] The non-metal dopants effectively narrow the band gap of TiO_2 (<3.2 eV).[38] Change of the lattice parameters and the presence of trap states within the conduction and valence bands from electronic perturbations give rise to band gap narrowing.[27] Not only does this allow for visible light absorption, but the presence of trap sites within the TiO_2 bands increases the lifetime of photoinduced charge carriers.

Doping of TiO_2 with transition metals such as Cr, Co, V and Fe has extended the spectral response of TiO_2 well into the visible region, also improving photocatalytic activity.[27,39] However, transition metals may also act as recombination sites for the photoinduced charge carriers, thus lowering the quantum efficiency. Transition metals have also been found to cause thermal instability to the TiO_2 nanomaterials.[15] Even though a decrease in band gap energy has been achieved by many groups through metal doping, photocatalytic activity has not been remarkably enhanced because the metals introduced were not incorporated into the TiO_2 framework. In addition, metals remaining on the TiO_2 surface cover photo reaction sites.

14.1.3 Applications of titanium dioxide for tiles and glasses

Despite the great promise shown by the self-cleaning abilities of TiO_2 surfaces, there are certain limitations. Because TiO_2 is a wide band gap (3.2 eV) semiconductor material, the self-cleaning process can only be initiated by light of wavelength ~390 nm or less. This causes substantial reduction in the efficiency of the product as light of such energy, ultraviolet light (UV), makes up only 3–5% of the solar spectrum. Therefore, in order to improve the efficiency of these materials, it is necessary to either reduce the band gap or to introduce mid-band gap energy levels that act as a stepping stone between the energy levels, facilitating visible light absorption.

Titanium dioxide can be incorporated into construction materials such as glasses and tiles to produce anti-bacterial surfaces.[12,13] It can be used to coat hospital surfaces and provide anti-bacterial protection against harmful bacteria such as *E. coli* and MRSA.[40] By applying TiO_2 to roadside partitions and lights, the surfaces can be kept clean while having the added advantage of reducing harmful exhaust gases such as NO_x and VOCs.

14.1.4 Commercial photocatalytic tiles and glass

Pilkington Glass have utilized titanium dioxide technology to develop a range of self-cleaning windows known as Pilkington Activ.[41] Self-cleaning glass clearly displays the benefits of titanium dioxide's self-cleaning and

superhydrophilic properties. In 2001 Pilkington started to develop photocatalytic glass, which has been available in the market since then. The Pilkington Activ was successfully trialled in many countries such as the UK, Ireland and North America. The product is currently available worldwide and is applied in many commercial and private buildings. This is one of the most successful photocatalytic products available in the market. The coating is composed of a 15 nm layer of titanium dioxide deposited by chemical vapour methods.

Saint Gobain Glass's Bioclean is another significant photocatalytic glass product available in the market. These glasses were produced by coating a transparent layer of photocatalytic or hydrophilic material on the glass. An Italian manufacturer, Gambarelli, has developed photocatalytic tiles using titanium dioxide ceramic particles.

TOTO's (Japan) HYDROTECT tiles, with a photocatalytic antibacterial function, has been available since 1993. HYDROTECT finds applications in TOTO's own tile building materials, paints, and coatings. They also licensed the technology to over 100 companies in Japan and overseas. About 270 patents have been registered in the photocatalytic technology domain by TOTO Ltd.[42] Their representative products are white ceramic tiles for exterior walls and home environments. They are fabricated by spraying a liquid suspension containing TiO_2 powder or gel on the surface and then heated to 600–800°C. Through the heat treatment, the TiO_2 is sintered and strongly attached to the tile surface, forming a micrometer thick layer.[43]

Turkish-based ceramic tile manufacturer VitrA has launched a photoactive tile (http://www.vitratilescpd.com/faq/whats-photoactivity-2) to inhibit bacterial growth and eliminate microorganisms through oxidation. Air pollutants such as oxides of nitrogen and sulphur can also be removed using this technology.

14.2 Important production parameters

14.2.1 Temperature stability of the photocatalyst

One of the key issues with using titanium dioxide as a photocatalytic material in tiles and glass is the transition of the photocatalytically active phase, anatase, to the non–photocatalytically active phase, rutile, which typically occurs at 600–700°C. This is 300°C below the typical processing temperatures for tiles.

The retention of a high stable anatase phase with visible light active photocatalytic properties up to a temperature as high as ≥1000°C has not yet been published or patented. Many proposed innovative and commercial applications for photocatalytically active stable titania-coated materials such as bathroom tiles, sanitary wares, and self-cleaning glass for the control

of organic contaminants require high processing temperatures and hence high-temperature stability.2.[4,17] High consumer demand is projected for these materials.

The second area to investigate is the stability of the anatase at high temperature. This can be investigated in many ways. Previous X-ray photoelectron spectroscopy (XPS) studies by the authors' group have indicated that only 0.3 at% F of doping has achieved when 16 mole time (1:16) F precursors trifluoroacetic acid (TFA). This 0.3% F doped sample showed stability up to 900°C and a small increase in dopant content is expected to give even higher temperature stability. Adding dopants above 0.5% by addition of high-temperature stable dopant precursors should be developed. Therefore both the levels of dopants (e.g., N-F, S-F, S-N, C-F, C-N, C-F, etc.) and various precursors (e.g., TFA, $TiCl_4$) should be looked at and incorporated into the titania matrix.

The solid state chemistry at high temperature can also be tuned by changing precursors or employing various annealing schedules such as step heating without grain growth. Step annealing was previously employed successfully to sinter Y_2O_3 materials without significant grain growth. A similar heating strategy can be designed to produce anatase materials with less or little grain growth at higher temperatures (≥1000°C) thus preventing rutile formation. New sintering techniques such as ramp-sustain-decay can be applied. The development of photocatalysts (with lower band gap) which can be activated under visible light (>400 nm) is desired in order to make use of the main part of the solar spectrum, and to extend their applications to room interiors where there is relatively poor lighting illumination.

The anatase-to-rutile phase transformation in TiO_2 is an area of both scientific and technological interest.[44,45] The anatase-to-rutile transformation (ART) is kinetically defined and the reaction rate is determined by parameters such as particle shape/size,[46] purity,[47] source effects,[48] atmosphere[49] and reaction conditions.[50] It is agreed that the mechanism for phase transformation of titania is one of nucleation and growth.[51,52] Anatase nanocrystals coarsen, grow and then transform to rutile only when a critical size is reached.[53] Therefore, phase transformation is dominated by effects such as defect concentration,[54] grain boundary concentration[55] and particle packing.[49] Rutile is the thermodynamically stable phase, while anatase and brookite are both metastable, transferring to rutile under heat treatment at temperatures typically ranging between 600 and 700°C.[56] Anatase is widely regarded as the most photocatalytically active of the three crystalline structures.[57,58]

The generally accepted theory of phase transformation is that two Ti–O bonds break in the anatase structure, allowing rearrangement of the Ti–O octahedra, which leads to a smaller volume, forming a dense rutile phase. The removal of oxygen ions, which generate lattice vacancies, accelerates

the transformation. The transition follows first order kinetics, with an activation energy of ~418 kJ mol^{-1}. The breaking of these bonds can be affected by a number of factors, including the addition of dopants, synthesis method and thermal treatment.[52]

Table 14.2 presents the results of a patent search using the relevant terms, for photocatalytic tiles and glass. There are many patents which relate to high temperature stable anatase titania such as WO2009061707 (A1), but they do not indicate visible light active photocatalytic properties or their intended use in building materials, for example. Most disclosures relate to a process for making titanium dioxide in an anatase crystalline form which is stable at temperatures above 1000°C. Another invention (CN 101205083 (A)) relates to a technology for preparing a nanometre-scale material, in particular to a preparation method in which, after a high temperature (above 700°C) process, nanometre crystal titanium oxide with small crystal size and high surface area, the main anatase phase can still be retained, something that has proved hard to obtain. The invention can realize large-scale preparation at high temperatures (700–1,500°C) and produces the nanometre crystal titanium oxide which is characterized by the main anatase phase, the small crystal size, the high surface area, high crystallinity, low surface state distribution, etc. The nanometre titanium oxide grains prepared by the invention are expected to be applied in photocatalysis fields such as a sensitized solar energy battery, and hydrogen prepared by water splitting.

Table 14.2 Patent search for photocatalytic tiles and glass

Search terms	No. of patents	Patents relevant	Brief description
High temp, stable, anatase	1	1	Precipitating a halide salt and a hydrolysed compound comprising Ti from a reaction mixture
Photocatalytic, titanium dioxide	85	2	See text
Ceramic building material, photocatalytic	1	1	To form a strong photocatalytic layer taking advantage of remaining heat immediately after burning by directly spraying a photocatalyst liquid on a ceramic substrate in a cooling stage immediately after burning
Photocatalytic, TiO_2 antibacterial	3	1	See text
High temperature anatase, ceramic, antibacterial	3	1	See text

There are not many reported patents on materials that are stable, antibacterial and can be activated by visible/room light. The CREST-DIT, Ireland patented materials are the first to claim anti-microbial visible light photocatalytic action and it is believed that they could represent the best available technology to deal with the persistent problems of *E. coli* and MRSA.

There are some interesting reports that tackle the problem of the high temperature stable anatase titania, and spraying the solution directly onto the ceramic surfaces. One such report (JP 2001031483 (A)) set out to solve the following problem: to form a strong photocatalytic layer taking advantage of the remaining heat immediately after burning by directly spraying a photocatalyst liquid on a ceramic substrate during cooling immediately after burning. The reported solution is that the ceramic substrate is a ceramic building material necessitating high-temperature burning such as tile, brick, ceramic plate or roofing tile. Preferably, a mixture of anatase TiO_2 sol and SiO_2 sol is used as the photocatalyst liquid for a ceramic substrate having coarse porous surface, and a photocatalyst liquid containing peroxotitanic acid is used for a ceramic substrate having a smooth surface. The surface temperature suitable for the formation of the photocatalytic layer is preferably 350–500°C. The photocatalytic layer formed on a coarse porous surface of a substrate is resistant to the peeling from the substrate because the TiO_2 particles are fixed to the pore of the porous surface of the substrate to semi-permanently exhibit an excellent effect. The photocatalyst liquid containing peroxotitanic acid preferably forms fine particles of anatase TiO_2 by heat treatment to form a photocatalytic film having high activity. The product has air-cleaning, stain-proofing and antibacterial characteristics.

Another report (KR 20020043133 (A)) provides a novel method of making photocatalytic titanium oxide sol by improving the existing hydrolysis process of the sol-gel method. It is a method for making acidic titanium oxide sol and basic titanium oxide sol, inducing the crystal growth of anatase type at high temperature and pressure. The above titanium oxide sol for the photocatalyst has excellent properties of dispersion and coating and photocatalytic ability to decompose various organic materials.

It can be seen that there are numerous reports/patents that deal with high temperature stable anatase titania, but no such reports include activation due to visible light and photocatalytic properties at high temperatures and that are also used in the application area of anti-bacterial ceramic tiles.

14.3 Mechanism of self-cleaning glasses and tiles

14.3.1 Self-cleaning properties

It is known that titanium dioxide surfaces display excellent anti-fogging and self-cleaning abilities because of the superhydrophilic attributes of TiO_2

surfaces.[54] Wang *et al.* have reported that the transition between the hydrophobic and hydrophilic states could possibly be connected to photoactive electronic transition across the energy gap, i.e., the conversion of Ti^{4+} sites into Ti^{3+} on the surface under UV illumination.[59,60] Therefore in terms of UV activation, there are common features between the photocatalytic mechanism and hydrophilicity.[61]

Recently, however, there has been some consensus that the basic mechanism of these two phenomena may not be the same. According to Watanabe *et al.*,[62] the existence of sodium ions in TiO_2 showed very different effects on these photoinduced reactions, suggesting two different photoinduced defect reaction mechanisms on the surface. The essential photocatalytic mechanism could be explained in terms of bulk properties, such as the charge transfer efficiency of a wide gap semiconductor. Therefore it seems photocatalysis of TiO_2 is more dependent on bulk properties, while the hydrophilicity of TiO_2 is an inherently interfacial property, limited to the interface between TiO_2 surface (solid) and water (liquid).

The hydrophilic mechanism is believed to be as follows; electrons reduce the Ti (IV) cations to the Ti (III) state, and the holes oxidize the O^{2-} anions. In the process, oxygen atoms are ejected and oxygen vacancies are created (Fig. 14.2). Water molecules can then occupy these oxygen vacancies, producing adsorbed OH groups, which tend to make the surface hydrophilic.[63]

14.3.2 Anti-bacterial action

There are two principal ways to realize self-cleaning material surfaces: the development of superhydrophobic or superhydrophilic materials. By trans-

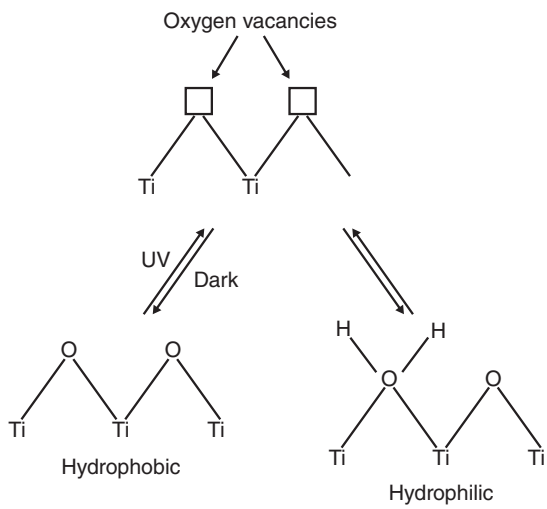

14.2 Mechanism of photo-induced hydrophilicity.

ferring the microstructure of selected plant surfaces to practical materials like tiles and façade paints, superhydrophobic surfaces were obtained (Lotus effect). Superhydrophilic materials were developed by coating glass, ceramic tiles or plastics with the semiconducting photocatalyst titanium dioxide (TiO_2). If TiO_2 is illuminated by light, grease, dirt and organic contaminants are decomposed and can easily be swept away by water (rain).

TiO_2-coated ceramic tiles are considered to be very effective against organic and inorganic materials, as well as against bacteria. There is general interest in the application of these tiles in hospitals and care facilities to reduce the spread of infections and the threat to patients whose immune system has been weakened, in public and commercial facilities and schools to improve the hygienic conditions and in residential kitchens, baths and floors to promote family hygiene and to reduce housework. Furthermore, these tiles show superhydrophilic behaviour. Grease, dirt and other staining materials can easily be swept away with a stream of water. Superhydrophilicity, combined with the strong photocatalytic oxidizing properties, makes this tile self-cleaning in exterior applications.

With the increasing concern for human health and quality of life, the use of TiO_2 for disinfection becomes more and more important. In the ceramic and building industries, there is a special interest in the photoinduced bactericidal effect of TiO_2.[49] This is particularly true when the ceramic is going to be placed in microbiologically sensitive environments, such as medical facilities, and food industries where biological contamination must be prevented.[50]

Applying antibacterial TiO_2 building materials to indoor furnishings has been shown to be an effective way to decrease bacterial counts to negligible levels. It was reported that in an operating room in a hospital the number of bacteria on the wall surface was reduced to zero and the bacteria in the air was also decreased significantly after installing photocatalytic tiles. The longer term effect was much better than the spraying of disinfectants.[51] Several companies, such as TOTO, Karpery and Biocera, have commercialized the concept of a deposited thin film semiconductor photocatalyst on ceramics as an antimicrobial agent. Their semiconductor photocatalyst thin film ceramic products exhibit both UV light-induced antimicrobial agent and deodorizing properties.[54] The light-induced bactericidal activity of TiO_2 can also be used to control biological growth on concrete surfaces. A schematic mechanism of photocatalytic anti-bacterial action is given in Fig. 14.3. Unsightly stains due to the growth of biofilm may cause the loss of aesthetic beauty, particularly in places where design features or maintenance faults result in frequent wetting of the building surface.[53] This could also trigger chemical changes of concrete surfaces and decrease their durability.[55] Photosynthetic algae can only grow where sunlight is available, so that photocatalytic technology is an ideal control method.

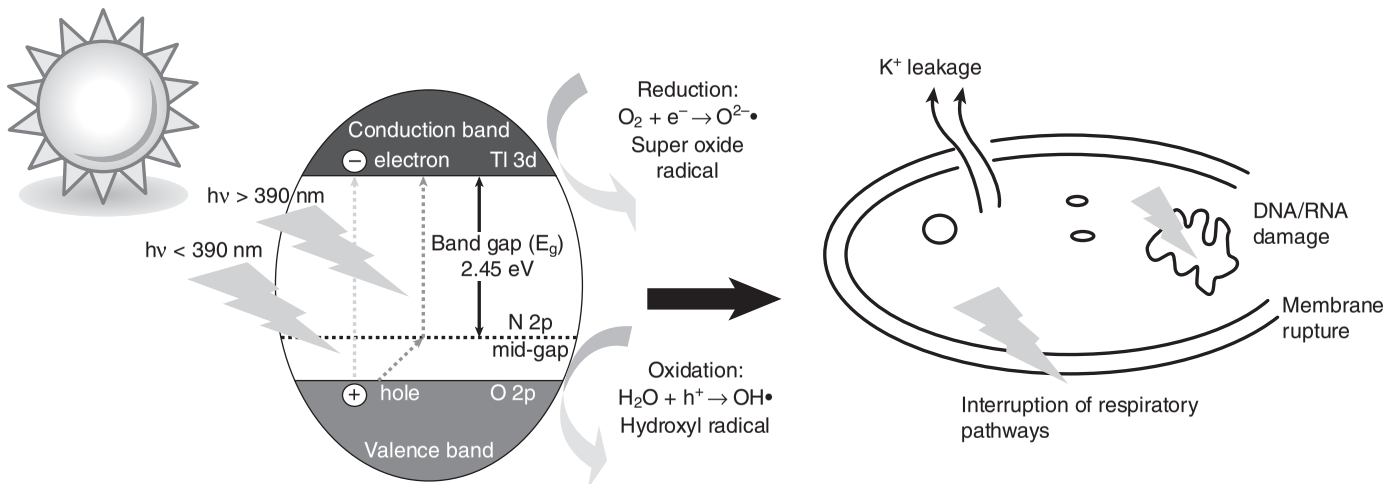

14.3 Mechanism of solar light activated anti-microbial photocatalysts.

Besides self-cleaning cementitious materials, TiO_2-based self-cleaning exterior building products including tiles and glass have been widely commercialized and applied. The self-cleaning and stain-free performance are confirmed by samples suspended outdoors for six months.[59] For interior tiles used in washrooms or bathrooms, soilage and dirt are always a problem. The fatty acids from soap can form chemical bonds with calcium and magnesium in hard water and adhere to the tile surface, which are difficult to clean after the accumulation of dirt. Tiles with a TiO_2 film surface can break the binding between the organic compounds and the ceramic tiles, which make the washing process easier. Compared with the other two major applications, less research work has been conducted in the area of antimicrobial building materials. So far, standardized protocols for evaluating the light-induced anti-bacterial activity have not been established. The stated efficiency of different self-disinfecting products cannot be verified and compared. Moreover, effective and reliable coating techniques are needed to anchor the nano-photocatalysts to interior building surfaces in the event that the dispersion of fallen nanoparticles causes potential health threats.

14.4 Future trends

The sale of photocatalytic products in the world market began to gain momentum since 2001 after the successful commercialization of Pilkington glass. According to the technical market research report (2010), by BCC Research (35 Walnut Street, Suite 100, Wellesley, MA 02481), the global market value for photocatalysts is expected to increase to $1.7 billion in 2014, for a five-year compound annual growth rate (CAGR) of 14.3%. BCC also analysed that the photocatalytic products for the construction sector currently accounts for the largest share of the market. A need to improve the photocatalytic anti-bacterial efficiency is required to implement these materials in the commodity market. In addition, the potential deterioration of photocatalytic efficiency of TiO_2 photocatalysts over time has proven to be an inherent obstacle for the commercialization of photocatalytic coatings on glass and tiles. Research is currently underway in many universities and large companies to tackle these problems. The development of highly efficient visible light activated photocatalysts has been found to be effective compared to conventional TiO_2. The current results on the visible light induced photocatalysts are promising for further development for tiles and glasses driven by solar light as a renewable source of energy.

14.5 Acknowledgement

The authors wish to thank Science Foundation Ireland (SFI grant number 10/US/I1822; US-Ireland R&D partnership) funding. The authors would

like to acknowledge Enterprise Ireland funded projects (IP/2009/0310, IP/2010/0353, IR/2008/0004 and ARE/2008/0005) for financial support. The authors would also like to thank Mr Robert Hickson (VitrA Ireland Ltd), Mr John Browne (Smartglass International) and Dr Hugh Hayden (Radical Coatings) for useful discussions. Thanks to Dr Donal Keane for the technical drawings and Rachel Fagan for proof reading.

14.6 References

1. Pelaez, M.; Nolan, N.T.; Pillai, S.C.; Seery, M.K.; Falaras, P.; Kontos, A.G.; Dunlop, P.S.M.; Hamilton, J.W.J.; Byrne, J.; O'Shea, K.; Entezari, M.H.; Dionysiou, D.D. (2012) *Applied Catalysis B* 125, 331.
2. Kamat, P.V. (2007) *J. Phys. Chem. C* 111, 2834.
3. Parkin, I.P.; Palgrave, R.G. (2005) *J. Mater. Chem*. 15, 1689.
4. Pillai, S.C.; Periyat, P.; George, R.; McCormack, D.E.; Seery, M.K.; Hayden, H.; Colreavy, J.; Corr, D.; Hinder, S.J. (2007) *J. Phys. Chem. C* 111, 1605.
5. Chen, X; Mao, S.S. (2007) *Chem. Rev*. 107, 2891.
6. Yamagishi, M.; Kuriki, S.; Song, P.K.; Shigesato, Y. (2003) *Thin Solid Films* 442, 227.
7. Bach, U.; Corr, D.; Lupo, D.; Pichot, F.; Ryan, M. (2002) *Adv. Mater*. 14, 845.
8. Wang, X.; Yu, J.C.; Ho, C.; Hou, Y.; Fu, X. (2005) *Langmuir* 21, 2552.
9. Graetzel, M. (2001) *Nature* 414, 338.
10. Hoffmann, M.R.; Martin, S.T.; Choi, W.; Bahnemann, D.W. (1995) *Chem. Rev.* 95, 69.
11. Yang, S.W.; Gao, L.J. (2005) *Am. Ceram. Soc*. 88, 968.
12. Bokhimi, X.; Morales, A.; Lopez, T.; Gomez, R.; Navarrete, J. (2004) *J. J. Sol-Gel Sci. Tech.* 29, 31.
13. Bokhimi, X.; Morales, A.; Novaro, O. (1997) *Chem. Mater.* 9, 2616.
14. Cozzoli, P.D.; Comparelli, R.; Fanizza E.; Curri, M.L.; Agostiano A. (2003) *Mat. Sci. Eng. C* 23, 707.
15. Hoffman, A.: Carraway E.R.; Hoffman, M. (1994) *Environ. Sci. Technol. 28*, 776.
16. Mahdavi, F.; Burton T.C.; Li, Y. (1993) *J. Org. Chem.* 58, 744.
17. Liqiang, J.; Yichun, Q.; Baiqi, W.; Shudan, L.; Baojiang, J.; Libin, Y.; Wei. F.; Hinggang, F.; Jiazhong, S. (2006) *Solar Energy Materials & Solar Cells* 90, 1773.
18. Choi, W.; Termin, A.; Hoffman, M.R. (1994) *J. Phys. Chem. B* 98, 13669.
19. Soria, J.; Conesa, J.C.; Augugliaro, V.; Palmisano, L; Schiavello, M.; Sclafani, A. (1991) *J. Phys. Chem.* 95, 274.
20. Yu, J.C.; Yu, J.G.; Ho, K.W.; Jiang, Z.T.; Zhang, L.Z. (2002) *Chem. Mater.* 14, 3808.
21. Vinodgopal, K.; Kamat, P.V. (1995) *Environ. Sci. Technol.* 29, 841.
22. Maira, A.J.; Yeung, K.L.; Lee. C.; Yue, P.L.; Chan, C.K. (2000) *J. Catal.* 192, 185.
23. Li, Y.; Hwang, D.S.; Lee, N.H.; Kim, S.J. (2005) *Chem. Phys. Lett.* 404, 25.
24. Testino, A.; Bellobono, I.R.; Buscaglia, V.; Canevali, C.; D'Arienzo, M.; Polizzi, S.; Scotti, R.; Morazzoni, F. (2007) *J. Am. Chem. Soc.* 129, 3564.
25. Sclafani, A. (1996) *J. Phys. Chem.* 100, 13655.
26. Emilio, C.A.; Litter, M.I.; Kunst, M.; Bouchard, M.; Colbeau-Justin, C. (2006) *Langmuir* 22, 3606.
27. Hamal, D.B.; Klabunde, K.J.J. (2007) *Colloid Interface Sci.* 311, 514.

28. Kuo, Y.-L.; Chen, H.-W.; Ku, Y. (2007) *Thin Solid Films*, 515, 3461.
29. Luo, H.; Takata, T.; Lee, Y.; Zhao, J.; Domen, K.; Yan, Y. (2004) *Chem. Mater*, 16, 846.
30. Asahi, R.; Morikawa, T.; Oikawa, K.; Aoki, K.; Taga, Y. (2001) *Science* 293, 269.
31. Ihara, T.; Miyoshi, M.; Iriyama, Y.; Matsumoto, O.; Sugihara, S. (2003) *Appl. Catal. B* 42, 403.
32. Martyanov, I.N.; Uma, S.; Rodrigues, S.; Klabunde, K.J. (2004) *Chem. Commun.* 7, 2476.
33. Irie, H.; Watanabe, Y.; Hashimoto, K. (2003) *J. Phys. Chem. B* 107, 5483.
34. Nakamura, R.; Tanaka, T.; Nakoto, Y. (2004) *J. Phys. Chem. B* 108, 10617.
35. Li, D.; Ohashi, N.; Hishita, S.; Kolodiazhnyi, T.; Haneda, H. (2005) *J. Sol. State Chem.* 178, 3293.
36. Irie, H.; Watanabe, Y.; Hashimoto, K. (2003) *Chem. Lett.* 32, 772.
37. Sakthivel, S.; Kisch, H. (2003). *Angew. Chem. Int. Ed.* 42, 4908.
38. Morikawa, T.; Asahi, R.; Ohwaki, T.; Aoki, K.; Taga, Y. (2001) *Jpn. J. Appl. Phys.* 40, L561.
39. Borgarello, E.; Kiwi, J.; Gratzel, M.; Pelizzetti, E.; Visca, M. (1982) *J. Am. Chem. Soc.* 104, 2996.
40. Machida, M.; Norimoto, W.K.; Kimura, T. (2005). *J. Am. Ceram. Soc.* 88, 95.
41. Riegel, G.; Bolton, J.R. (1995) *J. Phys. Chem.* 99, 4215.
42. TOTO Ltd. (2008) Patent licensing of super hydrophilic photocatalyst technology. Hydrotech. Available at: http://www.toto.co.jp/docs/hyd_patent_en/case_001.htm
43. Shimohigoshi, M; Saeki, Y. (2007) Research and application of photocatalyst tiles. In: Baglioni P, Cassar L (eds) *RILEM Int. Symp. on Photocatalysis, Environment and Construction Materials*, Italy, 291.
44. Takahaschi, Y.; Matsuoka, Y. (1988) *J. Mater. Sci* 23, 2259.
45. Takahaschi, Y.; Kiwa, K.; Kobayashi, K.; Matsuki, M. (1991) *J. Am. Ceram. Soc.* 74, 67.
46. Sanchez, C.; Livage, J.; Henry, M.; Babonneau, F. (1988) *J. Non-Cryst. Solids* 100, 65.
47. Guilment, J.; Pencelot, O.; Rigola, J.; Truchet, S. (1996) *Vib. Spectrosc.* 11, 37.
48. Nolan, N.T.; Seery, M.K.; Pillai, S.C. (2009) *J. Phys. Chem. C* 113, 16151.
49. Chen J., Poon C.-S. (2009) *Building and Environment* 44, 1899.
50. Amézaga-Marid, P.; Nevárez-Moorillón, G.V.; Orrantia-Borunda, E.; Miki-Yoshida, M. (2002) *FEMA Microbiology Letters* 211, 183.
51. Fujishima, A.; Hashimoto, K.; Watanabe, T. (1999) *TiO_2 Photocatalysis: Fundamentals and Applications*. Japan: BKC, Inc.
52. Mills, A.; Lee, S.K. (2002) *Photochem Photobiol A* 152, 233.
53. Dubosc, A.; Escadeillas, G.; Blanc, P.J. (2001) *Cem Concr Res* 31, 1613.
54. Reidy, D.J.; Holmes, J.D.; Nagle, C.; Morris, M.A. (2005) *J. Mater. Chem.* 15, 3494.
55. Kurth, J.C.; Giannantonio, D.J.; Allain, F.; Sobecky, P.A.; Kurtis, K.E. (2007) Mitigating biofilm growth through the modification of concrete design and practice. In: Baglioni P and Cassar L (eds) *RILEM Int. Symp. on Photocatalysis, Environment and Construction Materials*, Italy, 195.
56. Padmanabhan, S.C.; Pillai, S.C.; Colreavy, J.; Balakrishnan, S.; McCormack, D.E.; Perova, T.S.; Gun'ko, Y.; Hinder, S.J.; Kelly, J.M. (2007) *Chem. Mater*. 19, 4474.
57. Wang, H.; Miao, J.J.; Zhu, J.M.; Ma, H.M.; Zhu, J.J.; Chen, H.Y. (2004) *Langmuir*, 20, 11738.

58. Baiju, K.V.; Sibu, C.P.; Rajesh, K.; Pillai, P.K.; Mukundan, P.; Warrier, K.G.K.; Wunderlich, W. (2005) *Mater. Chem. Phys.* 90, 123.
59. Wang, R.; Hashimoto, K.; Fujishima, A.; Chikuni, M.; Kitamura, A.; Shimohigoshi, M.; Watanabe, T. (1998) *Adv. Mater.* 2, 135.
60. Wang, R.; Hashimoto, K.; Fujishima, A.; Cjikuni, M.; Kojima, E.; Kitamura, A.; Shimohigoshi, M.; Watanabe, T. (1997) *Nature*, 388, 431.
61. Lee, Y.C.; Hong, Y.P.; Lee, H.Y.; Kim, H.; Jung, Y.J.; Ko, K.H.; Jung, H.S.; Hong, K.S. (2003) *J. Colloid and Interface Science* 267, 127.
62. Watanabe, T.; Fukayama, S.; Miyauchi, M.; Fujishima, A.; Hashimoto, K. (2000) *J. Sol-Gel Sci. Technol* 19, 71.
63. Misook, K. (2005) *Mat. Lett.* 59, 3122.

15

Nanotechnology in manufacturing paints for eco-efficient buildings

C. DEL CACHO, O. GEISS, P. LEVA, S. TIRENDI and J. BARRERO-MORENO, European Commission, Joint Research Centre, Institute for Health and Consumer Protection, Italy

DOI: 10.1533/9780857098832.3.343

Abstract: The addition of a photocatalyst provides decontamination properties to a paint. It is capable of continuously oxidizing both organic and inorganic pollutants and microorganisms under the influence of light during its lifetime. Photocatalytic paints are useful for degrading air pollutants, reducing the costs of maintenance of the exterior aspect and sterilizing the environment. TiO_2 is by far the most widely used photocatalyst, but is only active under UV (e.g., solar) irradiation, thus limiting its applicability. In this sense, in order to use photocatalytic paints also in indoor environments, new photocatalysts with a higher activity under visible irradiation is needed. Aspects such as the formation of potentially harmful by-products should also be considered in order to keep the purifying benefits of photocatalytic paints.

Key words: Photocatalytic paints, indoor, outdoor, indoor air quality, by-products.

15.1 Introduction

Photocatalytic paints are characterized by the addition of a photocatalyst which, when irradiated, favours the oxidation of both inorganic and organic air pollutants, and provides self-cleaning properties to the paint and presents bactericidal and antimicrobial properties.

With a production of more than 3,500 million tonnes worldwide in 2011, the paint industry is one of the largest chemical industries, being the biggest markets located in Asia, Europe and North America. The 4,500 paint companies in Europe employ around 175,000 people (WPCIA, 2011).

Basically, photocatalysis is based on the creation of holes on the electronic structure of the photocatalyst surface by the absorption of light of the appropriate wavelength (generally, UV-A):

$$\text{Photocatalyst} \xrightarrow{h\nu} h^+_{vb} + e^-_{cb}$$

where h^+_{vb} and e^-_{cb} represent the hole and the electron created on the catalyst surface as a consequence of the excitation of an electron present in the

valence band of the photocatalyst to the conducting band during the absorption of the incident light.

The optimum wavelength for the activation of a certain photocatalytic material depends on its band gap, as the electrons must, under excitation by absorption of incident radiation, pass into the conducting band. Table 15.1 presents the optimum wavelength of the most commonly used photocatalysts.

The creation of such holes provides a highly reactive and oxidizing material which is thus able to catalyse the oxidation of chemicals deposited or adsorbed on the photocatalyst surface. Particular attention should be paid to the case of adsorbed water and oxygen molecules. These molecules can react with the holes and excited electrons of the photocatalyst, and are transformed into highly reactive compounds such as hydroxyl radicals ($OH^{\bullet}$) and superoxide anions (O_2^-):

$$h^+_{vb} + H_2O \rightarrow OH\bullet + H^+$$

$$e^-_{cb} + O_2 \rightarrow O_2^-$$

The most commonly used photocatalyst is TiO_2. In nature, TiO_2 can be present in three different crystalline structures: rutile, anatase and brookite. TiO_2, and especially rutile TiO_2, has been extensively used since the nineteenth century as a white pigment in the formulation of paints. Even if the chemical reactions induced by irradiated TiO_2 had already been observed, it was not until 1938 that Dooedeve and Kitchener understood the photocatalytic mechanism by which TiO_2 was capable of producing the photo-

Table 15.1 Band gap and optimum excitation wavelength of different photocatalysts

Photocatalyst	Band gap (eV)	Optimal wavelength (nm)
ZnS	3.6	345
SnO_2	3.6	345
Anatase TiO_2	3.2	390
$SrTiO_3$	3.2	390
ZnO	3.2	390
α-Fe_2O_3	3.1	400
$CaBi_2O_4$	3.1	400
Rutile TiO_2	3.0	415
Brookite TiO_2	3.0	415
In_2O_3	2.9	430
WO_3	2.8	445
CdS	2.5	495
V_2O_5	2.2	565
CdSe	1.8	690

bleaching of organic dyes and solvents when irradiated with UV light from a mercury lamp (Dooedeve and Kitchener, 1938). Further experiments demonstrated that the anatase crystalline structure of TiO_2 possessed a considerably higher photoactivity than that of rutile and brookite TiO_2 (Hashimoto *et al.*, 2005).

Different protocols have been described in the literature for the preparation of TiO_2 photocatalysts involving sol-gel processes, vapour decomposition of titanium alkyloxides and $TiCl_4$ and calcination of titanium oxysulphate at 400–600°C (Kaneko and Okura, 2002; Wang *et al.*, 2004; Sun *et al.*, 2008; Akpan and Hameed, 2010).

Once prepared, the photocatalyst is added to the paint formulation, in a concentration typically ranging from 5 to 40% which, depending on the type of application of the paint, is equivalent to a critical pigment volume concentration (CPVC) of around 10% w/v (US Patent, 2009). The CPVC represents the maximum amount of pigment that can be used for a certain amount of non-volatile solvents in the paint formulation without causing a deterioration of the paint properties.

Paints are homogeneous mixtures which contain the following:

- *Binder or resin:* The resin imparts adhesion and binds the pigments together. It has a direct influence on properties such as gloss, durability, flexibility and toughness. Typical binders include alkyl-, chloride-, vinyl-, epoxy- and polyurethane resins. The paint is often named after the main binder used in its formulation. In most cases, the resin is cured after the application of the paint, which generally involves the polymerization of its constituents.
- *Pigments:* Pigments are the materials responsible for the colour and opacity of the paint, and they have a direct influence on its mechanical resistance. Pigments include compounds such as minerals (e.g., mica, talc), inorganic salts (Fe, Cr, Cd, Mo, Ti or Pb oxides and hydroxides, calcium carbonate, zinc phosphate, etc.) and organic dyes (toluidines, phthalocyanines). Some pigments confer antioxidant properties on the paint, thereby increasing its stability towards the degradation of paint constituents.
- *Solvents and diluents:* The appropriate mixture of solvent and diluents is selected in terms of both their volatility and the time required for the curing process of the resin. In this sense, an inappropriate match between these two parameters would result in paints drying rapidly on their surface, but remaining wet in the interior coating. Additionally, solvents have a crucial role in controlling the viscosity of the paint and, thus, the ease of the painting process. The most commonly used solvents are aliphatic solvents, aromatic solvents, alcohols, ketones and esters, which in some cases (e.g., low or zero–VOC paints) are mixed with water.

- *Additives:* A wide range of additives are added to the formulation of the paint in order to favour the drying and curing process, remove the bubbles formed during painting, increase the chemical and mechanical resistance, etc.

Several parameters have been observed to affect the photocatalytic efficiency of paints for the oxidation of air pollutants under irradiation of the photocatalytic paint (Mo *et al.*, 2009). The most critical parameters are:

- *Wavelength of incident radiation:* The wavelength of the incident radiation has to be appropriate in order to excite the electrons of the photocatalyst and initiate the photocatalytic process.
- *Light intensity:* The reaction rate increases with increasing light intensity.
- *Effective surface area of the photocatalyst:* A higher surface area of the photocatalyst increases the photocatalytic rate.
- *Paint constituents and interaction with the photocatalyst:* It has recently been observed that paint constituents (e.g., binder) have a considerable influence on the performance of the photocatalytic paint (Aguia *et al.*, 2010). In this sense, it has been observed that the nature and proportion of the different paint constituents can have a significant effect in terms of enhancing or diminishing the photocatalytic efficiency of the catalyst. Further research is still needed in order to understand the mechanism by which each of the single paint constituents affects the photocatalytic efficiency of photocatalytic paints, in order to better optimize their formulation.
- *Relative humidity:* Water molecules adsorbed on the photocatalytic paint seem to enhance the photocatalytic efficiency of TiO_2 through the formation of hydroxyl radicals which, in turn, oxidize the air pollutants. However, an excessive relative humidity (>70%) inhibits the photocatalytic degradation of air pollutants, due to the competition for adsorption sites on the photocatalyst surface (Pichat, 2010).
- *Temperature:* A rise in the temperature speeds up the kinetics of the reaction between the pollutants and the photocatalyst, while at the same time decreasing the adsorption of the pollutants on the surface of the photocatalytic paint. Since the net photocatalytic reaction rate is a combination of both processes, a maximum photocatalytic oxidation rate is obtained at the optimum temperature (Obee and Hay, 1997).
- *Concentration of the pollutant:* The relationship between the concentration of the pollutant and the photocatalytic rate is generally governed by the Langmuir–Hinselwood model (Shiraisi *et al.*, 2007), according to which the reaction rate increases with the concentration as described in the equation:

$$r = \frac{kK[\text{Pollutant}]}{1 + K[\text{Pollutant}]}$$

where r represents the reaction rate, k the rate constant, K the adsorption coefficient of the pollutant on the photocatalytic paint and [Pollutant] the concentration of the pollutant of concern.

- *Presence of mixtures of pollutants:* Due to the competition on the adsorption of the different pollutants on the surface of the photocatalyst, the photocatalytic reaction rate for a single component is normally lower in the presence of different kinds of pollutants (Ao *et al.*, 2004; Chen and Zhang, 2008).

The present chapter describes the different fields in which photocatalytic paints are used, providing a critical overview of both their advantages and drawbacks, and outlining the areas in which further research is still needed, such as the evaluation of the potential loss in the catalytic efficiency during the lifecycle of photocatalytic paints.

15.2 Application of photocatalytic paints in an outdoor environment

15.2.1 Investigation into the photocatalytic efficiency of active outdoor paints at the laboratory scale

Several experiments corroborated the initial observations carried out by Fujishima and Honda (1972), and demonstrated that TiO_2 powder, and more particularly anatase TiO_2, was capable of degrading air pollutants (e.g., N_2O, NO, NO_2, SO_2, BTEX, carbonyl compounds, alcohols, CO, CH_4, CFCs, etc.) (Wang *et al.*, 2007; Mo *et al.*, 2009; Laufs *et al.*, 2010; De Richter and Caillol, 2011) when exposed to solar-like radiation. Considering the promising results obtained in laboratory-scale experiments, TiO_2 has since been incorporated into building materials, such as concrete, glass or paint (Allen *et al.*, 2009; Pacheco-Torgal and Jalali, 2011; PICADA n.d.).

The typical experimental set-up consists of a chamber test in which a controlled atmosphere with a known concentration of pollutant is created (Fig. 15.1). The paint, installed inside the chamber, is irradiated with a light source of a well characterized emission spectra, while the pollutant is flushed through the chamber and its concentration is monitored at both the entrance (before the photocatalysis) and the exit (after the photocatalysis) of the chamber.

In order to quantify the photocatalytic efficiency of the paint accurately, it is necessary to assess for influence of competitive depletion mechanisms that could affect the concentration of the pollutant of concern inside the chamber. Thus, the experiments involve the evaluation of:

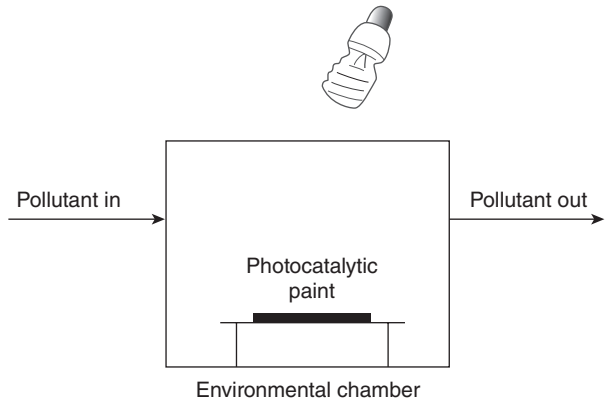

15.1 Schematic experimental set-up for the evaluation of photocatalytic paints.

- the adsorption of the pollutant on the chamber surface
- the adsorption of the pollutant on the photocatalytic paint itself in the absence of irradiation
- the photolytic degradation of the pollutant through decomposition under UV radiation
- the photocatalytic degradation of the pollutant.

Photocatalytic paints are generally activated by irradiating the paint in the test chamber and flushing clean air (i.e., without pollutant) through it for at least 12 hours (Aguia *et al.*, 2011). It is important to stress that, when evaluating the photocatalytic efficiency of paints, the activation conditions are the critical parameters affecting the time required to reach the steady state, after which the photoactivity of the paint either remains constant or diminishes in the event of inactivation by the adsorption of intermediate products on the active catalytic sites.

Aguia *et al.* (2010, 2011) evaluated the photocatalytic efficiency and selectivity towards the photodegradation of NO of 10 different anatase-based photocatalytic paints using a typical outdoor base paint to which they added different commercial TiO_2 photocatalysts in a concentration of 9% w/v. They were quite surprised to observe that there was no direct correlation between the photocatalytic activity of the pure photocatalyst and the corresponding derived photocatalytic paint, in the sense that the most efficient photocatalyst did not yield the optimum photocatalytic paint. Even if further research is needed in order to understand the mechanism by which paint components have such a critical influence on the activity of a photocatalytic paint, this result suggests that the paint components and the way in which the photocatalyst is mixed in the paint matrix play a crucial role in the photoactivity of the final product.

15.2.2 Real-life examples of the use of outdoor photocatalytic paints

Photocatalytic paints possess several properties, the most attractive of which are the following:

- photocatalysis of both inorganic and organic pollutants
- self-cleaning of building materials, reducing the maintenance costs and enabling a longer pristine view of the building
- antimicrobial and antifungal properties, as photocatalytic paints avoid bacterial and fungal growth on their surface
- anti-fogging properties: the contact angle with water decreases to nearly 0° when the photocatalyst is irradiated, avoiding the formation of droplets on the photocatalyst surface.

Some real-life examples of the applications of photocatalytic paints include:

- Music and Art City Hall (Chambery, France)
- Via Porpora (Milan, Italy)
- Umberto I tunnel (Rome, Italy) (Fig. 15.2)
- Charles de Gaulle Airport (Paris, France)
- Camden Council (London, UK)
- Toyota Tsunami plant (Saitama, Japan)

A significant reduction of both inorganic pollutants (NO, NO_2, SO_2) and organic pollutants (benzene, toluene) in the surrounding outdoor air has been observed as a result of the application of photocatalytic paint (Marolt *et al.*, 2011; Guerrini, 2012).

15.2 Umberto I tunnel in Rome.

15.3 Application of photocatalytic paints in an indoor environment

On average, people in Europe and North America spend 90% of their time in confined indoor environments (Leech *et al.*, 2002; Brasche and Bischof, 2005). Indoor air pollutants are either emitted from numerous indoor sources (e.g., furniture, building materials, cleaning agents, electronic equipment), originate from human activities (e.g., cooking) or enter from the outdoor environment by the ventilation system and doors or windows that are insufficiently airtight. Depending on peoples' sensitivity, inappropriate indoor air quality can present several health risks, generically referred to as 'sick building syndrome' symptoms, such as irritation of the eyes, nose and throat, headaches, dizziness, fatigue, asthma, hypersensitivity, pneumonitis, etc. (EPA, 1991). The basic strategies to improve indoor air quality involve the monitoring and eventual substitution of the emission sources, improvement of the ventilation scheme and purification of the air.

Photocatalytic degradation of air pollutants therefore appears to be a promising technique for air purification. As already mentioned, the most widely used photocatalyst is TiO_2, which is only activated by means of UV-A light, the intensity of which is generally low in an indoor environment. Thus, the development of other types of photocatalysts activated by visible light is of the utmost importance in order to apply photocatalytic paints effectively as a methodology for the efficient purification of indoor air.

Apart from the general parameters already mentioned in Section 15.1, the photocatalytic efficiency of indoor paints is greatly influenced by both the nature and the concentration of the photosensitizer that is used to enable the activation of the photocatalyst by visible light. Here, the nature of the photosensitizer used has a direct influence on the change in the band gap of TiO_2 and the wavelength required for the activation of the photocatalyst. The concentration of the photosensitizer, on the other hand, needs to be carefully optimized, in order to fine tune the wavelength required for the activation of the modified photocatalyst. Finally, the photodecomposition of the sensitizer itself should be considered.

15.3.1 Strategies for the preparation of visible light active photocatalytic materials

TiO_2 photocatalytic materials activated by visible light

Two different alternatives have been employed to prepare TiO_2-based photocatalytic materials that can be activated by visible light: sensitization and doping.

The *sensitization* approach consists of the anchoring of an organic coloured dye (e.g., rhodamine B, eosin, erythrosin B, thionine, chlorophyllin or

methylene blue) (Abe *et al.*, 2000; Chatterjee and Mahata, 2001, 2002; Mele *et al.*, 2003; Moon *et al.*, 2003; Kaur and Singh, 2007), a polymer (e.g., polyfluorine-co-thiophene) (Song *et al.*, 2007; Qiu *et al.*, 2008) or a narrow band gap semiconductor (e.g., Bi_2S_3, CdS, CdSe or V_2O_5) (Bessekhouad *et al.*, 2004; Ho and Yu, 2006; Jianhua *et al.*, 2006; Wu *et al.*, 2006) to the TiO_2 surface. The sensitizer acts as an intermediary and, by enhancing the absorption of visible light, it enables the activation of the photocatalyst by electron transfer between the excited sensitizer and TiO_2.

TiO_2 sensitized with meso-tetrakis(4-sulfonatephenyl) porphyrin has been applied successfully to the photo-oxidation of acetaldehyde in indoor air under visible light irradiation (Ismail and Bahnemann, 2010).

The *doping* approach involves the modification of the electronic structure of TiO_2 by adding a dopant that modifies the band structure either by increasing the energy of the valence band or by minimizing the energy of the conduction band. The ultimate effect is a minimization of the band gap, thus enabling the doped photocatalyst to be activated by means of visible radiation.

Doped TiO_2 photocatalysts prepared by doping with either non-metals (e.g., N, C or S) (Ao *et al.*, 2009; Jo and Kim, 2009; Rockafellow *et al.*, 2009) or transition metals (e.g., Fe, Co, Cu, Au or Mn) (Andronic *et al.*, 2009; Bengtsson *et al.*, 2009; Kafizas *et al.*, 2009; Song *et al.*, 2009; Cacho *et al.*, 2011) have been applied successfully for the degradation of indoor air pollutants when activated by visible light.

Non-TiO_2 photocatalytic materials activated by visible light

Only a few attempts at the development of non-TiO_2-based photocatalytic materials that can be activated directly by visible light have been successful, due to their narrower band gap. In this sense, metal calcogenides (e.g., CdS, CdSe) (Reutergardh and Iangphasuk, 1997; Green and Rudham, 2003), metal oxides (α-Fe_2O_3, In_2O_3 SnO_2, WO_3, ZnO) (Faust *et al.*, 1989; Kormann *et al.*, 1989; Pulgarin and Kiwi, 1995; Mazellier and Bolte, 2000; Bandara *et al.*, 2001) and mixed metal oxides ($SrTiO_3$, $CaBi_2O_4$) (Rothenberger *et al.*, 1985; Tang *et al.*, 2004) have been evaluated as potential photocatalysts. However, the formation of short lived metal-to-ligand and ligand-to-metal charge transfer states, and the narrower band gap, make these materials considerably less stable towards their own photocorrosion.

15.3.2 Investigation into the efficiency of photocatalytic indoor paints at the laboratory scale

Photocatalysis of NO and NO_2

Photocatalytic decomposition of NO and NO_2 has been widely investigated using pure TiO_2 film surfaces, photocatalytic paints, photocatalytic concrete

and photocatalytic glass surfaces (Ohko *et al.*, 2009; Huang *et al.*, 2010; Laufs *et al.*, 2010).

In 1998, Negishi *et al.* (1998) proposed a mechanism by which NO is photochemically oxidized into NO_2, and NO_2 is either further oxidized to HNO_3 on a generally slower step or photolytically reverts into the formation of NO and hydroxyl radicals:

$$NO \underset{h\nu, TiO_2(e^-_{cb})}{\overset{h\nu, TiO_2(h^+_{vb})}{\rightleftarrows}} NO_2 \xrightarrow{OH\bullet} HNO_3$$

Such a mechanism was further confirmed by two different kinds of experiments. Thus, Dalton *et al.* (2002) evaluated the adsorption of nitric acid and nitrate ions on the surface of the photocatalyst. Ohko *et al.* (2009), on the other hand, confirmed the formation of a mixture of NO and NO_2 in the gaseous phase when the photocatalysis of either pure NO or NO_2 was tested.

Photooxidation of volatile organic compounds

It is well known that volatile organic compounds (VOCs) are photocatalytically oxidized by TiO_2 when exposed to UV radiation. The potential for cleaning indoor air has been demonstrated for pollutants such as formaldehyde, acetaldehyde, acetone, benzene or toluene in photochemical reactors using UV radiation and anatase TiO_2 powdered films and building materials (Obee and Brown, 1995; Stevens *et al.*, 1998; Pichat *et al.*, 2000; Strini *et al.*, 2005; Everaert and Baeyens, 2004; Maggos *et al.*, 2007). Furthermore, doping of TiO_2 photocatalyst with N has proved valuable for the degradation of acetaldehyde, 2-propanol, acetone, toluene and ethylene under visible irradiation (Asahi *et al.*, 2001; Ihara *et al.*, 2003; Miyauchi *et al.*, 2004; Irokawa *et al.*, 2006). As we will show in Section 15.4.2, the use of photocatalytic paints is more complex than the use of powdered films due to the potential formation of secondary emissions from photocatalytic paint constituents.

One of the parameters that critically affects the performance of photocatalytic paints is the interaction between the paint components and the photocatalyst. Thus, when incorporated into the paint matrix, the photocatalyst loses around 90% of its overall photocatalytical efficiency (Aguia *et al.*, 2011) which, in the case of the degradation of volatile organic compounds, can be critical.

Salthammer and Fuhrmann (2007) have recently evaluated the efficiency of different photocatalytic indoor paints in terms of their degradation of organic and inorganic air pollutants. In general, all the evaluated photocatalytic paints showed the same pattern. In this sense, even if NO_2 abatement was satisfactory when irradiating the photocatalytic paints with a typical

tungsten light bulb, the efficiencies obtained for the degradation of volatile organic compounds were very low. Thus, degradation of formaldehyde and terpene compounds (pinene, limonene) was possible only at high concentration levels, while CO was not observed to be significantly degraded under any of the evaluated conditions.

Antimicrobial and antifungal effect

Hochmannova and Vytrasova (2010) demonstrated the inhibition of the potential cell growth on plates coated with photocatalytic paints prepared using ZnO and TiO_2 Degussa as photocatalysts. ZnO-based photocatalytic paints were able to completely inhibit cell growth for *Escherichia coli*, *Pseudomonas aureaginosa*, *Staphylococcus aureus*, *Aspergillus niger* e *Penicillium chrysogenum*, and were therefore suggested as optimum photocatalysts for the preparation of antimicrobial photocatalytic paints, where a highly sterile environment (e.g., in hospitals) is required.

This antimicrobial effect may be due to the attack of the microorganisms by the hydroxyl radicals and superoxide anions created during the irradiation of the photocatalyst surface (Section 15.1).

15.4 Potential formation of by-products

By-products formed during the photocatalysis can be either intermediate products or secondary emissions. Some of these by-products might even be more harmful compared to the original pollutant degraded by the photocatalytic paint, and their formation should therefore be avoided wherever possible.

- *Intermediate products* are formed due to the incomplete photocatalysis of a certain pollutant.
- *Secondary emissions* are formed due to the photo-oxidation of the supporting material in which the photocatalyst is embedded. Previous studies indicate that various compounds are released due to the oxidation of the organic constituents of the material supporting the photocatalyst during the photocatalytic process.

15.4.1 Formation of intermediate products

Recent studies have shown that the reactions achieved by the degradation of pollutants on photocatalytic paints are generally not complete, and the reaction stops along the way, giving rise to the formation of intermediate products. It is known that NO_2 is formed as an intermediate product by the

incomplete degradation of NO to nitrate (Ohko *et al.*, 2009), while degradation of organic pollutants gives rise to the formation of aliphatic compounds, aromatic compounds, carbonyl compounds, alcohols, alkoxyalcohols and carboxylic acids (Huang and Li, 2011), which may even be more harmful than the original pollutant. In this sense, the formation of compounds such as benzaldehyde, phenol, formic acid, acetic acid, hexamethylene, heptane or benzene as intermediate products during the photocatalytic degradation of toluene has been observed (Sun *et al.*, 2010).

Some of these intermediate products (e.g., carboxylic acids) are strongly adsorbed on the photocatalyst surface (Huang and Li, 2011), and reduce the number of active catalyst sites in the photocatalytic paint, which can in critical cases considerably minimize its efficiency.

The photocatalytic surface can be regenerated by washing the surface with water or irradiating it with UV light. However, these methodologies are not easy to apply in the case of indoor usage, and further research will be needed in order to develop new methodologies to remove adsorbed intermediate products from indoor photocatalytic paints.

15.4.2 Secondary emissions from paint constituents

Formation of carbonyls while irradiating photocatalytic paints under either UV or visible light has been repeatedly observed as part of a set of investigations to assess the decontamination efficiency of photocatalytically active paints in the past. The main source of such carbonyl compounds was assumed to be the photoinduced decomposition of paint binders (Salthammer and Fuhrmann, 2007; Auvinen and Whirtanen, 2008; Pichat, 2010; Geiss *et al.*, 2012).

An exhaustive investigation has recently been carried out in order to evaluate the impact of the different paint components on the formation of carbonyl compounds when irradiating photocatalytic paints. Thus, both the photocatalytic paint and each of its individual components was irradiated in the presence of 5% pure anatase TiO_2 (Geiss *et al.*, 2012). The components evaluated included cohesion agents, super plasticizers, defoaming agents and redispersable resins.

Figure 15.3 shows the amount of the secondary emission of carbonyl compounds during the irradiation of the different paint components in the presence of pure anatase TiO_2 as photocatalyst. As can be observed, formaldehyde, acetaldehyde and acetone appear to be the main degradation compounds for all the paint components evaluated. Lower amounts of longer chain carbonyl compounds such as propanal, butanal or hexanal were formed in the initial stages. A radical mechanism based on the β-scission has been proposed for the degradation of longer-chain carbonyl compounds (Geiss *et al.*, 2012).

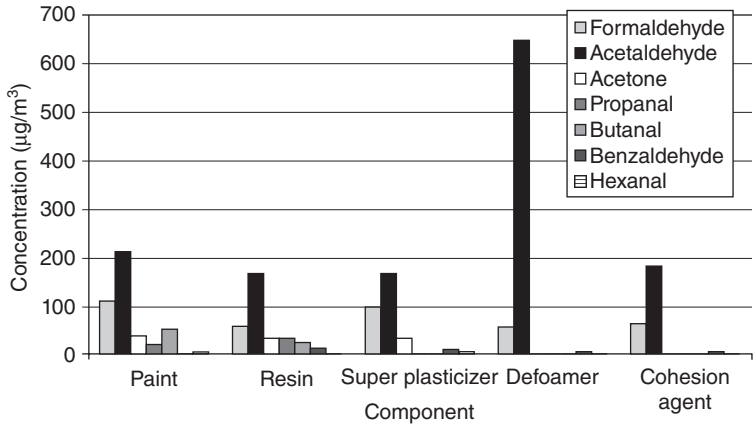

15.3 Formation of carbonyl compounds as secondary emissions during the irradiation of paint constituents mixed with anatase TiO_2.

15.4.3 Possible solutions to diminish the accumulation of by-products during photocatalysis

Indoor environments are characterized by the coexistence of multiple emission sources responsible for overall indoor air pollution. Formaldehyde is a well-known and ubiquitous indoor pollutant emitted from a wide variety of indoor sources, such as household products, furniture or smoke. Similarly, NO_2 is commonly found in indoor environments and originates mainly from combustion and gas appliances. Reported indoor concentrations of formaldehyde and NO_2 in dwellings range from 15 to 30 μg m^{-3} and from 15 to 50 μg m^{-3}, respectively (WHO, 2010).

The formation of NO_2 and/or carbonyl compounds as by-products is an undesirable effect, contributing to the chemical load in indoor environments, and should therefore be eliminated or minimized as far as possible, as they might contribute as a relevant additional source which might exceed the guideline values.

Two different approaches are commonly used to improve indoor air quality and avoid the accumulation of indoor pollutants: they are source control and eventual substitution of the emission sources, and increasing the ventilation.

Studies carried out on the formation of by-products during the photocatalytic degradation of both inorganic and organic pollutants indicate that a relatively large amount of by-products is accumulated, even under the realistic conditions of an air exchange rate of 0.5 h^{-1} and typical indoor concentration levels of the various pollutants. In this sense, experiments carried out on exposure chambers with a synthetic atmosphere containing 50 μg m^{-3} NO, in order to simulate an indoor environment, resulted in the

formation of up to 12 μg m^{-3} NO_2. Similarly, the formation of 30 and 7.5 μg m^{-3}, respectively, of formaldehyde and acetaldehyde was observed, as a result of the decomposition of the paint components.

In order to minimize the formation of intermediate products during the photocatalytic degradation of indoor air pollutants by photocatalytic active paints, the parameters affecting the photocatalytic process need to be optimized, in order to achieve the maximum possible rate of photocatalytic oxidation. Thus, particular attention should be paid to the development of more active photocatalysts in order to optimize the nature and concentration of the sensitizers/dopants used to enable activation by visible light.

Two possible alternative approaches that attempt to minimize the secondary emission of potentially harmful compounds from the degradation of paint constituents during the photocatalytic process have been proposed.

Development of more stable supporting materials

An increase in the stability of the supporting material towards the photocatalytic oxidation should considerably diminish the amount of carbonyl compounds released. In order to increase this stability, a careful selection of the ingredients used in the preparation of the supporting materials should be made. As an example, Fig. 15.4 presents the reduction obtained for the formation of carbonyl compounds during the irradiation of photocatalytic paints, following the appropriate selection of the paint components.

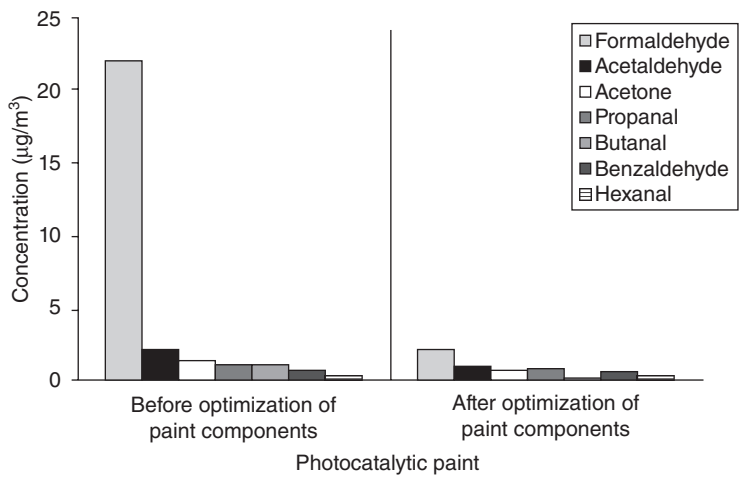

15.4 Reduction in the secondary emissions of photocatalytic paints with an appropriate selection of paint constituents.

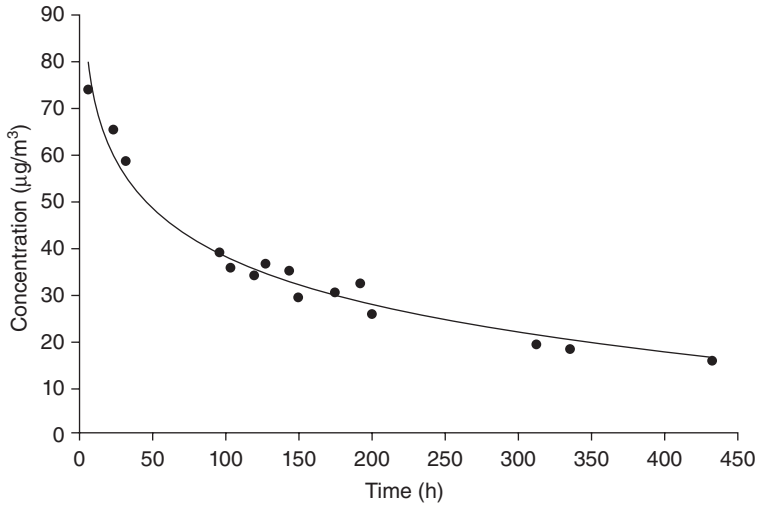

15.5 Secondary emission of formaldehyde in a photocatalytic paint during long-term irradiation.

Pretreatment of the photocatalytic paint prior to commercial distribution

It has been repeatedly observed that the amount of carbonyl compounds emitted diminishes with repeated uses of the photocatalytic material, indicating that the emitted carbonyl compounds depend on the extent of the previous irradiation of the supporting material. In order to confirm this effect, the photocatalytic paint has been irradiated for a long period of time, during which periodic measurements have been taken of the amount of carbonyl compounds. As can be observed in Fig. 15.5, the amount of emitted formaldehyde diminished exponentially with the irradiation time. A similar effect was found for all the carbonyl compounds.

As a consequence of this effect, it would be possible to minimize the amount of emitted carbonyl compounds by pre-treating the photocatalytic paint. It could therefore be irradiated with UV light prior to its commercial distribution, given the emission of carbonyl compounds. Recent experiments carried out under controlled conditions indicate that the secondary emission of carbonyl compounds after continuous irradiation of 3 weeks can be considered to be negligible (Geiss *et al.*, 2012).

15.5 Future trends

The present chapter has outlined the current state of the art in the development of photocatalytic paints. Further research is still needed in order to achieve a breakthrough, in the following areas:

- The incorporation of the nano-catalysts into photocatalytic paints, which would theoretically enhance the photocatalytic efficiency by drastically increasing the specific catalyst surface. Special attention should be attached to the evaluation of the potential health risks derived from the usage of such reactive nano-materials.
- The development of more active catalysts that can be activated by visible radiation.
- The increase in the stability of paint components to minimize the formation of secondary emissions during photocatalysis.

15.6 References

Abe R, Hara K, Sayamaa K, Domen K and Arakawa H, Steady hydrogen evolution from water on eosin Y–fixed TiO_2 photocatalyst using a silane coupling reagent under visible irradiation, *Journal of Photochemistry and Photobiology*, 2000, 137, 63–69.

Aguia C, Angelo J, Madeira LM and Mendes A, Influence of photocatalytic paint components on the photoactivity of P25 towards NO abatement, *Catalysis Today*, 2010, 151, 77–83.

Aguia C, Angelo J, Madeira LM and Mendes A, Photo-oxidation of NO using an exterior paint. Screening of various commercial titania in powder pressed and paint films, *Journal of Environmental Monitoring*, 2011, 92, 1724–1732.

Akpan UG and Hameed BH, The advancements in sol-gel method of doped TiO_2 photocatalysts, *Applied Catalysis A*, 2010, 375, 1–11.

Allen NS, Edge M, Verran J, Caballero L, Abrusci C, Stratton J, Maltby J and Bygott C, Photocatalytic surfaces: environmental benefits of nanotitania, *The Open Materials Science Journal*, 2009, 3, 6–27.

Andronic L, Hristache B, Enesca A, Visa M and Duta A, Studies on titanium dioxide catalyst doped with heavy metals (cadmium, copper and nickel), *Environmental Engineering Management*, 2009, 8, 747–751.

Ao CH, Lee SC, Yu JZ and Xu JH, Photodegradation of formaldehyde by TiO_2 photocatalyst. Effect of NO, SO_2 and VOCs, *Applied Catalysis B*, 2004, 54, 41–50.

Ao Y, Su D, Fu C and Yuan S, Synthesis of C,N,S-tridoped mesoporous titania with enhanced visible light induced photocatalytic activity, *Microporous and Mesoporous Materials*, 2009, 122, 1–6.

Asahi R, Morikawa T, Ohwaki T, Aoki K and Taga Y, Visible light photocatalysis in nitrogen-doped titanium dioxides, *Science*, 2001, 293, 269–271.

Auvinen J and Whirtanen L, The influence of photocatalytic interior paints on indoor air quality, *Atmospheric Environment*, 2008, 42, 4101–4112.

Bandara J, Mielczarski JA, Lopez A and Kiwi J, Sensitized degradation of chlorophenols on iron oxides induced by visible light – comparison with titanium dioxide, *Applied Catalysis B*, 2001, 34, 321–333.

Bengtsson N, Castellote M, López-Muñoz MJ and Cerro L, Preparation of co-doped TiO_2 for photocatalytic degradation of NOx in air under visible light, *Journal of Advanced Oxidation Technologies*, 2009, 12, 55–64.

Bessekhouad Y, Robert D and Weber JV, Bi_2S_3/TiO_2 and CdS/TiO_2 heterojunctions as an available configuration for photocatalytic degradation of organic pollutant, *Journal of Photochemistry and Photobiology A*, 2004, 163, 569–580.

Brasche S and Bischof W, Daily time spent indoors in German homes – baseline data for the assessment of indoor exposure of German occupants, *International Journal of Environmental Health and Hygiene*, 2005, 208, 247–253.

Cacho C, Geiss O, Barrero-Moreno J, Binas VD, Kiriakidis G, Bottalico L and Kotzias D, Studies on photo-induced NO removal by Mn-doped TiO_2 under indoor-like illumination conditions, *Journal of Photochemistry and Photobiology A*, 2011, 222, 304–306.

Chatterjee D and Mahata A, Photosensitized detoxification of organic pollutants on the surface of modified TiO_2 semiconductor particulate system, *Catalysis Communications*, 2001, 2, 1–3.

Chatterjee D and Mahata A, Visible light induced photodegradation of organic pollutants on dye adsorbed TiO_2 surface, *Journal of Photochemistry and Photobiology A*, 2002, 153, 199–204.

Chen WH and Zhang JS, Photocatalytic oxidation of multi-component systems. An investigation using toluene/ethylbenzene, octane/decane/dodecane and formaldehyde/acetaldehyde, *Journal of Advanced Oxidation Technologies*, 2008, 11, 163–173.

Dalton JS, Janes PA, Jones NG, Nicholson JA, Hallam KR and Allen GC, Photocatalytic oxidation of NOx gases using TiO_2: a surface spectroscopic approach, *Environmental Pollution*, 2002, 120, 415–422.

De Richter R and Caillol S, Fighting global warming: the potential of photocatalysis against CO_2, CH_4, N_2O, CFCs, tropospheric O_3, BC and other major contributors to the climate change, *Journal of Photochemistry and Photobiology C*, 2011, 12, 1–19.

Dooedeve CF and Kitchener A, The mechanism of photosensitization by solids, *Transactions of the Faraday Society*, 1938, 34, 902–908.

Environmental Protection Agency, 1991. Indoor Air Facts no. 4: Sick Building Syndrome, available at: http://www.epa.gov/iaq/pdfs/sick_building_factsheet.pdf (accessed August 2012).

Everaert K and Baeyens J, Catalytic combustion of volatile organic compounds, *Journal of Hazardous Materials*, 2004, 109, 113–139.

Faust BC, Hoffamnn MR and Bahnemann DW, Photocatalytic oxidation of sulphur dioxide in aqueous suspensions of α-iron oxide (Fe_2O_3), *Journal of Physical Chemistry*, 1989, 93, 6371–6381.

Fujishima A and Honda K, Electrochemical photolysis of water at a semiconductor electrode, *Nature*, 1972, 238, 37–38.

Geiss O, Cacho C, Barrero-Moreno J and Kotzias D, Photocatalytic degradation of organic paint constituents – formation of carbonyls, *Building and Environment*, 2012, 48, 107–112.

Green KJ and Rudham R, Photocatalytic oxidation of 2-propanol by semiconductor–zeolite composites, *Journal of the Chemical Society Faraday Transactions*, 2003, 89, 1867–1870.

Guerrini GL, Photocatalytic performances in a city tunnel in Rome: NOx monitoring results, *Construction and Building Materials*, 2012, 27, 165–175.

Hashimoto K, Irie H and Fujushima A, TiO_2 photocatalysis: a historical overview and future prospects, *Japanese Journal of Applied Physics*, 2005, 44, 8269–8285.

Ho W and Yu JC, Sonochemical synthesis and visible light photocatalytic behaviour of CdSe and CdSe/TiO_2 nanoparticles, *Journal of Molecular Catalysis A*, 2006, 247, 268–274.

Hochmannova L and Vytrasova J, Photocatalytic and antimicrobial effects of indoor paints, *Progress in Organic Coatings*, 2010, 67, 1–5.

Huang CH, Wang IK, Lin YM, Tseng YH and Lu CM, Visible light degradation of nitric oxides on PtO_x-modified TiO_2 via sol-gel and impregnation method, *Journal of Molecular Catalysis A*, 2010, 316, 163–170.

Huang H and Li W, Destruction of toluene by ozone–enhanced photocatalysis: performance and mechanism, *Applied Catalysis B*, 2011, 102, 449–453.

Ihara T, Miyoshi M, Iriyama Y, Matsumoto O and Sugihara S, Visible light active titanium dioxide photocatalyst realized by an oxygen-deficient structure and by nitrogen doping, *Applied Catalysis B*, 2003, 42, 403–409.

Irokawa Y, Morikawa T, Aoki K, Kosaka S, Ohwaki T and Taga Y, Photodegradation of toluene over TiO_2-xN_x under visible light irradiation, *Phys Chem Chem Phys*, 2006, 8, 1116–1121.

Ismail AA and Bahnemann DW, Metal–free porphyrin–sensitized mesoporous titania films for visible light indoor air oxidation, *Chemical and Sustainability Energy and Materials*, 2010, 3, 1057–1062.

Jianhua L, Rong Y and Songmei L, Preparation and characterization of the TiO_2/V_2O_5 photocatalyst with visible light activity, *Rare Metals*, 2006, 25, 636–642.

Jo WK and Kim JT, Application of visible light photocatalysis with nitrogen-doped or unmodified titanium dioxide for control of indoor-level volatile organic compounds, *Journal of Hazardous Materials*, 2009, 164, 360–366.

Kafizas A, Kellici S, Darr JA and Parkin LP, Titanium dioxide and composite metal/metal oxide titania films on glass: a comparative study of photocatalytic activity, *Journal of Photochemistry and Photobiology A*, 2009, 204, 183–190.

Kaneko M and Okura I, *Photocatalysis: Science and Technology*, Springer, New York, 2002.

Kaur S and Singh V, Visible light induced sonophotocatalytic degradation of reactive red dye 198 using dye sensitized TiO_2, *Ultrasonics Sonochemistry*, 2007, 14, 531–537.

Kormann C, Bahnemann DW and Hoffmann MR, Environmental photochemistry: is iron oxide (hematite) an active photocatalyst? A comparative study: α-Fe_2O_3, ZnO, TiO_2, *Journal of Photochemistry and Photobiology A*, 1989, 34, 161–169.

Laufs S, Burgeth G, Duttlinger W, Kurtenbach R, Maban M, Thomas C, Wiesen P and Kleffmann J, Conversion of nitrogen oxides on commercial photocatalytic dispersion paints, *Atmospheric Environment*, 2010, 44, 2341–2349.

Leech JA, Nelson WC, Burnett RT, Aaron S and Raizenne ME, It's about time: a comparison of Canadian and American time–activity patterns, *Journal of Exposure Analysis and Environmental Epidemiology*, 2002, 12, 427–432.

Maggos T, Bartzis JG, Leva P and Kotzias DK, Application of photocatalytic technology for NO_x removal, *Applied Physics A*, 2007, 89, 81–84.

Marolt T, Sever A, Bernard J, Zivec P and Gaberscek M, Photocatalytic activity of anatase-containing façade coatings, *Surface & Coatings Technology*, 2011, 206, 1355–1361.

Mazellier P and Bolte M, Heterogeneous light induced transformation of 2,6-dimethylphenol in acqueous suspensions containing goethite, *Journal of Photochemistry and Photobiology A*, 2000, 132, 129–135.

Mele G, del Sole R, Vasapollo G, Lopez EG, Palmisano L and Schiavello M, Photocatalytic degradation of 4-nitrophenol in aqueous suspension using

polycrystalline TiO_2 impregnated with Cu(II)-porphyrin and Cu(II)-phthalocyanine, *Journal of Catalysis*, 2003, 217, 334–342.

Miyauchi M, Ikezawa A, Tobimatsu H, Irie H and Hashimoto K, Zeta-potential and photocatalytic activity of nitrogen–doped TiO_2 thin films, *Phys Chem Chem Phys*, 2004, 6, 865–870.

Mo J, Zhang Y, Xu Q, Joaquin Lamson J and Zhao R, Photocatalytic purification of volatile organic compounds in indoor air: a literature review, *Atmospheric Environment*, 2009, 43, 2229–2246.

Moon J, Yun CY, Chung KW, Kang MS and Yi J, Photocatalytic activation of TiO_2 under visible light using acid red 44, *Catalysis Today*, 2003, 87, 77–86.

Negishi N, Takeuchi K and Ibusuki T, Surface structure of the TiO_2 thin film photocatalyst, *Journal of Materials Science*, 1998, 33, 5789–5794.

Obee TN and Brown RT, TiO_2 photocatalysis for indoor air applications. Effects of humidity and trace contaminant levels on the oxidation rates of formaldehyde, toluene and 1,3-butadiene, *Environmental Science and Technology*, 1995, 29, 1223–1231.

Obee TN and Hay SO, Effects of moisture and temperature on the photooxidation of ethylene on titania, *Environmental Science and Technology*, 1997, 31, 2034–2038.

Ohko Y, Nakamura Y, Negishi N, Matsuzawa S and Takeuchi K, Photocatalytic oxidation of nitrogen monoxide using TiO_2 thin films under continuous UV light illumination, *Journal of Photochemistry and Photobiology A*, 2009, 205, 28–33.

Pacheco-Torgal F and Jalali S, Nanotechnology: advantages and drawbacks in the field of construction and building materials, *Construction and Building Materials*, 2011, 25, 582–590.

PICADA, n.d. Photocatalytic Innovative Coverings Applications for Depollution Assessment (PICADA Project), Available at: http://www.picada-project.com/domino/SitePicada/Picada.nsf?OpenDataBase (accessed August 2012).

Pichat P, Some views about indoor air photocatalytic treatment using TiO_2: conceptualization of humidity effects, active oxygen species, problem of C_1-C_3 carbonyl pollutants, *Applied Catalysis B*, 2010, 99, 428–434.

Pichat P, Disdier J, Hoang-Van C, Mas D, Goutailler G and Gaysse C, Purification/deodorization of indoor air and gaseous effluents by TiO_2 photocatalysis, *Catalysis Today*, 2000, 63, 363–369.

Pulgarin C and Kiwi J, Iron oxide mediated degradation, photodegradation and biodegradation of aminophenols, *Langmuir*, 1995, 11, 519–526.

Qiu R, Zhang D, Mo Y, Song L, Brewer E, Huang X and Xiong Y, Photocatalytic activity of polymer modified ZnO under visible light irradiation, *Journal of Hazardous Materials*, 2008, 156, 80–85.

Reutergardh LB and Iangphasuk M, Photocatalytic decoloration of reactive azo dye: a comparison between TiO_2 and US photocatalysis, *Chemosphere*, 1997, 35, 585–596.

Rockafellow EM, Stewart LK and Jenks WS, Is sulphur-doped TiO_2 an effective visible light photocatalyst for remediation?, *Applied Catalysis B*, 2009, 91, 554–562.

Rothenberger G, Moser J, Gratzel M, Serpone N and Sharma DK, Charge carrier trapping and recombination dynamics in small semiconductor particles, *Journal of the American Chemical Society*, 1985, 107, 8054–8059.

Salthammer T and Fuhrmann F, Photocatalytic surface reactions on indoor wall paint, *Environmental Science and Technology*, 2007, 41, 6573–6578.

Shiraisi F, Nomura T, Yamaguchi S and Ohbuchi Y, Rapid removal of trace HCHO from indoor air by an air purifier consisting of a continuous concentrator and photocatalytic reactor and its computer simulation, *Chemical Engineering Journal*, 2007, 127, 157–165.

Song HM, Ko JM and Park JH, Hybrid photoreactive magnet obtained from Fe_3O_4/TiO_2 composite nanoparticles, *Chemical Letters*, 2009, 38, 612–613.

Song L, Qiu R, Mo Y, Zhang D, Wei H and Xiong Y, Photodegradation of phenol in a polymer-modified TiO_2 semiconductor particulate system under the irradiation of visible light, *Catalysis Communications*, 2007, 8, 429–433.

Stevens L, Lanning JA, Anderson LG, Jacoby WA and Chomet N, Investigation of the photocatalytic oxidation of low level carbonyl compounds, *Journal of Air and Waste Management Association*, 1998, 48, 979–984.

Strini A, Cassese S and Schiavi L, Measurement of benzene, toluene, ethylbenzene and o-xylene gas phase photodegradation by titanium dioxide dispersed in cementitious materials using a mixed flow reactor, *Applied Catalysis B*, 2005, 61, 90–97.

Sun H, Wang C, Pang S, Li X, Tao Y, Tang H, Liu M, Photocatalytic TiO_2 films prepared by chemical vapour deposition at atmospheric pressure, *Journal of Non Crystalline Solids*, 2008, 354, 1440–1443.

Sun L, Li G, Wan S and An T, Mechanistic study and mutagenicity assessment of intermediates in photocatalytic degradation of gaseous toluene, *Chemosphere*, 2010, 78, 313–318.

Tang J, Zou Z and Ye J, Efficient photocatalytic decomposition of organic contaminants over $CaBi_2O_4$ under visible light irradiation, *Angewandte Chemie International Edition*, 2004, 43, 4463–4466.

US Patent 2009/0061246 A1, Photocatalytic content, 2009.

Wang S, Ang HM and Tade MO, Volatile organic compounds in indoor environment and photocatalytic oxidation: state of the art, *Environment International*, 2007, 33, 694–705.

Wang W, Gu B, Liang L, Hamilton WA and Wesolowski DJ, Synthesis of rutile nanocrystals with highly controlled size and shape by low temperature hydrolysis: effects of solvent competition, *Journal of Physical Chemistry B*, 2004, 108, 14789–14792.

WHO, 2010. WHO guidelines for indoor air quality: selected pollutants, chapters 3 (formaldehyde) and 5 (nitrogen dioxide). Available at: http://www.euro.who.int/__data/assets/pdf_file/0009/128169/e94535.pdf (accessed August 2012).

WPCIA, 2011. World's Top Ten Paint Companies 2011 Annual Report. Available at: http://www.wpcia.org/News/2011report.html (accessed August 2012).

Wu L, Yu JC and Fu X, Characterization and photocatalytic mechanism of nanosized CdS coupled TiO_2 nanocrystals under visible light irradiation, *Journal of Molecular Catalysis A*, 2006, 244, 25–32.

15.7 Appendix: acronyms and definitions

Bi_2S_3	Bismuth sulphide
BTEX	Mixture of benzene, toluene, ethylbenzene and xylenes
$CaBi_2O_4$	Calcium bismuthate
CdS	Cadmium sulphide
CdSe	Cadmium selenide
CFCs	Chlorofluorocarbon compounds
CH_4	Methane
CO	Carbon monoxide
CPVC	Critical pigment volume concentration
e^-_{cb}	Excited electron in the conducting electronic band of the catalyst as a consequence of the absorption of incident radiation
$h\nu$	Radiation (nm)
h^+_{vb}	Hole created in the valence electronic band of the catalyst due to the excitation of an electron as a consequence of the absorption of the incident radiation
H_2O	Water
HNO_3	Nitric acid
In_2O_3	Indium oxide (III)
k	Photocatalytic rate constant
K	Adsorption coefficient, μg (adsorbed compound)/g (sorbent)
N_2O	Nitrous oxide
NO	Nitric oxide
NO_2	Nitrogen dioxide
O_2^-	Superoxide anion
$OH^\bullet$	Hydroxyl radical
r	Photocatalytic reaction rate, (μg/m^3 catalyzed compound)/h
SnO_2	Tin oxide (IV)
SO_2	Sulphur dioxide
$SrTiO_3$	Strontium titanium oxide
$TiCl_4$	Titanium chloride (IV)
TiO_2	Titanium dioxide
UV	Ultraviolet radiation with wavelengths ranging from 1 to 400 nm
UV-A	UV radiation with wavelengths ranging from 320 to 400 nm
V_2O_5	Vanadium oxide (V)
VOCs	Volatile organic compounds
WO_3	Tungsten oxide (VI)
ZnO	Zinc oxide
ZnS	Zinc sulphide
α-Fe_2O_3	α-ferric oxide

16

Nanotechnology for domestic water purification

S. KAR and P. K. TEWARI, Bhabha Atomic Research Centre, India

DOI: 10.1533/9780857098832.3.364

Abstract: Water, a nonsubstitutional natural resource, is best described by Leonardo Da Vinci as 'the vehicle of nature' ('vetturale di natura'). This is the single most essential commodity responsible for the existence and sustenance of life on the planet earth. It is not at all an exaggeration to state that water is primarily responsible for the restoration of health, environment and prosperiy of human civilization. Unfortunately, this most precious natural resource is becoming increasingly scarce day by day. Water scarcity is among the main problems facing many societies around the world in the twenty-first century. Water use has been growing at more than twice the rate of population increase in the last century. According to a report from the United Nations, by 2025, 1800 million people will be living in countries or regions with absolute water scarcity, and two-thirds of the world's population could be under stress conditions. As emphasized in one of the UN's Millenium Development Goals (MDGs), water scarcity calls for strengthened international cooperation in the fields of technologies for enhanced water productivity. Recent years have witnessed impressive breakthroughs towards application of nanostructured materials such as carbon nanotubes (CNTs), metal/metal-oxide nanoparticles, zeolites, and dendrimers in the field of water purification. The present chapter aims to give an overview of the developments in the application of nanotechnology in water treatment, with a special emphasis on domestic water purification. The focus is oriented to the fact that the ultimate practical realization of this new technology is based on the assessment of the risks as well as benefits posed by nanostructured materials. The challenges involved in producing a well-defined integrated nano-based water purification device are discussed.

Key words: nanotechnology, domestic water purification, nanomaterials, nanotoxicity, carbon nanotube, dendrimers, water quality, nanoparticles.

16.1 Introduction

Water resources are becoming increasingly scarce worldwide. Global water consumption is increasing at more than double the rate of the world's population growth. Population growth, pollution and climate change, which are all accelerating, are likely to combine to produce a drastic decline in water supply in the coming decades. At present 1.1 billion people lack

access to safe drinking water and 2.4 billion people lack access to proper sanitation, nearly all of them in developing countries. At present, a third of the world's population live in water-stressed countries, and by 2025, this is expected to rise to two-thirds. Table 16.1 (Gleick, 2000; Hillie *et al.*, 2007a) shows that water consumption is greatest in irrigated agriculture, accounting for 70% of global water withdrawals in 2000, while the respective shares of industrial and domestic usage were 20% and 10%. Agricultural use dominated globally (70%) and in developing countries (88%). Meanwhile, the share of industrial and domestic use has increased with rising country incomes, while agricultural use has declined.

Figure 16.1 shows the percentage of the population without access to reliable water sources, by region, and the predicted values for 2015 (World

Table 16.1 Relative water withdrawals by sector in 2000 (adapted from Gleick, 2000)

	Water consumption as share of total use		
Country group	Domestic	Agriculture	Industry
Low income	6%	88%	5%
Middle income	10%	70%	20%
High income	15%	41%	44%
World	10%	70%	20%

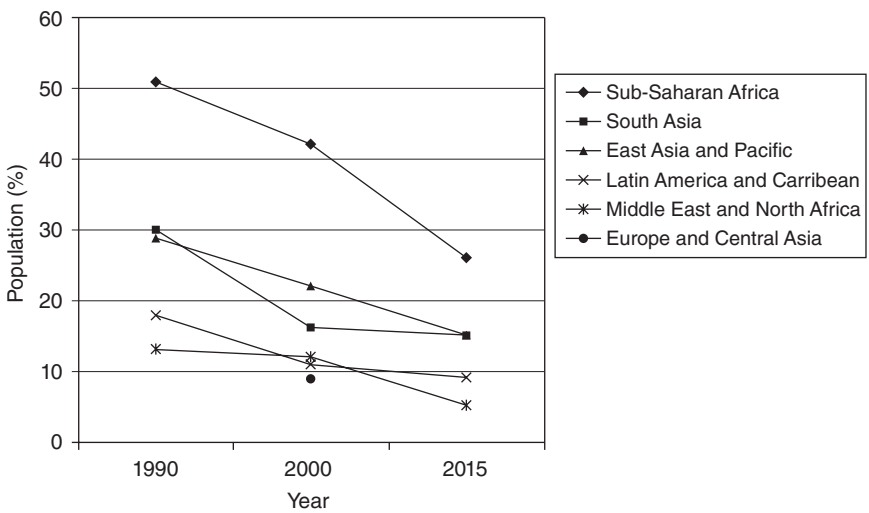

16.1 Population without access to reliable water sources (actual values 1990, 2000; estimated 2015). Source: World Bank (2005).

Bank, 2005). Lack of drinking water and sanitation kills about 4,500 children a day. Many children are missing school because neither their homes nor schools have adequate drinking water and sanitation facilities. Sustainable water management is therefore a critical aspect in addressing poverty, equity and related issues. The UN Millennium Development Goal of *ensuring environmental sustainability* commits governments to 'reduce by half the proportion of people without sustainable access to safe drinking water' by 2015, a goal closely linked with the separate goal of access to sanitation and basic hygiene education.

Different countries and regions face different environmental, social and economic conditions and have different needs with regard to water use, water quality, access to technology, field conditions, and the types of technologies that may be appropriate in different circumstances. Water treatment technologies include filtration using membranes, chemical treatment, heat and ultraviolet treatment and distillation. They seek to remove solid and other contaminants, or to neutralize them, and many treatments have a long history of use in systems for producing water for domestic, industrial and agricultural use (OECD, 2011). Most current approaches are materials intensive, have a large ecological footprint and are not in a position to comply with the increasing water quality standards of developing industrialized nations. The conventional methods of disinfection such as chlorination and ozonation can produce harmful byproducts due to reactions with various constituents of wastewater, which may call for a tradeoff between optimum disinfection and harmful byproduct formation.

The possibility of having ready access to safe drinking water is becoming increasingly rare because of over-exploitation of existing water resources, alarming effects of global warming (causing highly uneven rainfall patterns in particular places, which in turn disturbs the tendency for water harvesting), increasing levels of contamination as a result of rapid industrialization, leaky water distribution systems and deterioration of water quality upon ageing (though water has been treated at the point of entry, POE). On the other hand, funding, governance, trained engineers and skilled labour are commonly recognized obstacles to establishing regional and national-scale water treatment systems.

The difficulty and lack of success in overcoming obstacles to regional and national water supplies has led, in part, to increased interest in point-of-use (POU) water treatment methods at the household and community level (Hillie *et al.*, 2007b). Community and household level POU water treatment methods avoid many of the barriers associated with large-scale water supply projects because they are relatively inexpensive, can be purchased by the unit, and/or constructed using readily available materials. For these reasons, POU technologies avoid the need for large capital investments, management systems and governance structures.

Nanotechnology is increasingly being identified as an area of science and technology that could play a role in addressing some of the shortcomings of conventional POU devices. Studies by Brame *et al.* (2011), Theron *et al.*, (2008) and Watlington (2005) suggest that nanotechnology-based materials could lead to cheaper, more durable, and more efficient water treatment technologies that meet the needs of developing countries. Several water treatment methods and devices that incorporate nanoscale materials are already commercially available, and others are being developed. These nanotechnology-based products include water filters, filtration membranes, catalysts, and nanoparticles for groundwater remediation. However, a well-defined and well-engineered nano-based product needs to address significant challenges before a suitable POU device for household use can be commercialized to take care of the safe-water needs of the poor as well as the rich.

The present chapter aims to provide readers with a review of the practical applications of nanomaterials in the water sector. In the following sections, an overview of the different types of nanomaterials (e.g., metal and metal oxide nanoparticles, carbon nanotubes, zeolites, dendrimers, etc.) presently in use for water treatment applications is provided along with the different methods of nanomaterials synthesis. Subsequent sections discuss the environmental and health implications of the use of nanomaterials. Finally, the chapter focuses on the challenges associated with development of practical nano-based water purification systems.

16.2 Nanomaterials and water purification

There are a number of studies (Diallo *et al.*, 2009; Cloete *et al.*, 2010; Hotze and Lowry, 2010) highlighting the importance of nanostructured materials in the field of water purification, desalination, wastewater treatment, water recycle and reuse. Nanomaterials have shown their potential not only in water treatment, but also in water quality monitoring through sensing and detection. However, we shall restrict our discussion to water treatment applications within the confinement of water purification only. The specific issues regarding application modalities with respect to a household (domestic) scale are addressed in Section 16.7.

16.3 The need for nanomaterials in water purification

The variation in the quality and quantity of water available across the globe is drastically different and hence it is mandatory to have different kinds of region-specific solutions. The already scarce water resource is becoming increasingly scarce because of rapid population growth and ceaseless

industrialization. Coupled to this is the alarming issue of global warming and climate change which is potentially responsible for uneven distribution of rainfall. All these factors in turn lead to increasing levels of contamination and, moreover, newer types of contamination than encountered previously. The permissible limits of contaminants in a proposed safe drinking water are becoming less and less with the passage of time (e.g., the recommended maximum permissible value for arsenic in drinking water according to WHO international standards has been reduced from 200 ppb to 10 ppb through a number of revisions in the last 50 years. The case is the same with lead, where the limits have been brought down to 10 ppb from 50 ppb).

Given the deteriorating water resource situation, it is inevitable that newer, more efficient and more selective water purification technologies are required to take care of the specific contaminants at a very low level. The technology to remove these contaminants should also reach molecular limits so that capture can be highly efficient in a minimum residence time. On the other hand, such a process should be environmentally friendly, economically feasible and with minimum or no use of electricity for rural adaptability.

'Nanotechnology' has a tremendous role to play in such a precarious situation, where the reactions can take place at ionic/atomic/molecular scale in a very selective manner with amazingly high efficiency. Because of the significant increase in surface-to-volume ratio in a nano-dimension, the contaminant uptake capacity becomes many fold. Compared to the conventional water treatment technologies such as membrane-based treatment, activated carbon, UV-based filtration, electrodialysis and distillation, the nano-based systems would provide the following advantages (Pradeep and Anshup, 2009a):

- higher efficiency of removal even at low concentration of adsorbents
- functionalization capability of nanomaterials leads to specific uptake
- low waste generation.

Two of the major distinctions that define types of conventional remediation technologies also apply to nanotechnologies for remediation: adsorptive versus reactive and *in situ* versus *ex situ*. Absorptive remediation technologies remove contaminants (especially metals) by sequestration, whereas reactive technologies affect degradation of contaminants, sometimes all the way to harmless products (e.g., CO_2 and H_2O in the case of organic contaminants). *In situ* technologies involve treatment of contaminants in place, whereas *ex situ* refers to treatment after removing the contaminated material to a more convenient location (e.g., pumping contaminated groundwater to the surface and treatment above ground). *In situ* degradation of contaminants, when feasible, is often preferred over

other approaches because it has the potential to be more cost effective (Tratnyek and Johnson, 2006). However, *in situ* remediation requires delivery of the treatment to the contamination and this has proven to be a major obstacle to expanded development of *in situ* remediation technologies. With respect to this issue, nanotechnology has special relevance because of the potential for injecting nanosized (reactive or absorptive) particles into contaminated water. In this manner, it should be possible to create either: (i) *in situ* reactive zones with nanoparticles that are relatively immobile; or (ii) reactive nanoparticle plumes that migrate to contaminated zones if the nanoparticles are sufficiently mobile.

The current understanding of the basic processes involved in this technology is still evolving and incomplete. In addition to making it difficult to move forward with the engineering of full-scale implementations, these uncertainties make it very difficult to assess the risks that this technology might bear to human and/or ecological health. Recognizing this, some groups have adopted the 'precautionary' position that *in situ* applications of nanoparticles for remediation should be prohibited (The Royal Society and The Royal Academy of Engineering, 2004), whereas others have recommended, in effect, that research on all fronts should proceed in parallel (EPA, 2005).

16.4 Types, properties and uses of nanomaterials in water purification

Nanoparticles have two key properties that make them particularly attractive as sorbents. On a mass basis, they have much larger surface areas than bulk particles. Nanoparticles can also be functionalized with various chemical groups to increase their affinity towards target compounds. It has been found that the unique properties of nanoparticles enable the development of high capacity and selective sorbents for metal ions and anionic contaminants. To make the discussion on the application of nanomaterials in the field of water purification easy to comprehend and follow, the nanomaterials can be categorized under four different classes:

1. zeolites
2. dendrimers
3. metal-containing nanoparticles including metal oxides
4. carbon nanotubes.

The literatures encompassing the research and development work involving these nanomaterials are cited very briefly in the sub-sections that follow. To make the discussion meaningful and somewhat exhaustive, at different places (application of nanomaterials like TiO_2 nanoclays and magnetic nanoparticles), excerpts from the *Annual Review of Nano Research* (Mansoori *et al.*, 2008) are reproduced.

16.4.1 Zeolites

Zeolites are microporous crystalline solids with well-defined structures. Generally they contain silicon, aluminium and oxygen in their framework and cations, water and/or other molecules within their pores. Many occur naturally as minerals and they are extensively mined in many parts of the world. Others are synthetic and are made commercially for specific uses. Synthetic zeolites are usually made from silicon-aluminium solutions or coal fly ash, and are used as sorbents in column filters. Zeolites are widely used as ion-exchange beds for domestic and commercial water purification, and water softening where alkali metals such as sodium or potassium prefer to exchange out of the zeolite, being replaced by the 'hard' calcium and magnesium ions from the water. Commercial wastewater containing heavy metals can also be cleaned up using such zeolites. Zeolites are generally used for the removal of metal contaminants. Natural zeolites from Mexico and Hungary have been shown to reduce arsenic from drinking water sources to levels deemed acceptable by the World Health Organization (Elizalde-González *et al.*, 2001).

Zeolites made from coal fly ash can adsorb a variety of heavy metals including lead, copper, zinc, cadmium, nickel, and silver from wastewater. Under some conditions, fly ash zeolites can also adsorb chromium, arsenic and mercury. NaP1 zeolites ($Na_6Al_6\ Si_{10}O_{32}, 12H_2O$) have a high density of Na (I) ion exchange sites. They can be inexpensively synthesized by hydrothermal activation of fly ash with low Si/Al ratio at 150°C in 1.0–2.0 M NaOH solutions. NaP1 zeolites have been evaluated as ion exchange media for the removal of heavy metals from acid mine wastewaters. Alvarez-Ayuso *et al.* (2003) reported the successful use of synthetic NaP1 zeolites to remove Cr (III), Ni (II), Zn (II), Cu (II) and Cd (II) from metal electroplating wastewater. The adsorptive capacity of zeolites is influenced by several factors including their composition, the water pH, and the concentrations and types of contaminants. For example, the water pH influences whether the ash surface is positively or negatively charged. Also, because lead and copper are more easily adsorbed by fly ash, high concentrations of these metals decrease the amount of cadmium and nickel removed (Wang *et al.*, 2004).

Zeolite-silver compound has been proven effective against microorganisms, including bacteria and mould. Additionally, the silver in this compound provides residual protection against regrowth of these biological contaminants. Zeolites do not adequately remove organic contaminants. Also, air moisture contributes to zeolites' saturation and makes them less effective. Zeolites were reported to result in high flux reverse osmosis nanocomposite membrane (the utilities of having a membranous structure have been discussed in the last section) without compromise in selectivity (Jeong *et al.*, 2007).

16.4.2 Dendrimers

Dendrons are dendritic wedges that comprise one type of functionality (such as chemical bonding) at their core and another at the periphery. To obtain a dendrimer structure, several dendrons are reacted with a multifunctional core to yield a dendrimer. Using different synthetic strategies, over 100 compositionally different dendrimer families have been synthesized and over 1000 differentiated chemical surface modifications have been reported (Bosman *et al.*, 1999; Fischer and Vögtle, 1999; Tomalia and Majoros, 2003). One such dendrimer structure is shown in Fig. 16.2 (Jang *et al.*, 2009).

Dendritic polymers exhibit many features that make them particularly attractive as functional materials for water purification. These 'soft' nanoparticles, with sizes in the range of 1–20 nm, can be used as high capacity and recyclable water soluble ligands for toxic metal ions, radionuclide and inorganic anions (Ottaviani *et al.*, 2000). The environmental applications of dendrimers were first explored by Diallo *et al.* (2005). They reported the effective removal of copper from water via different generations of poly(amidoamine) (PAMAM) dendrimers. Later, Diallo *et al.* (2005) studied the feasibility of using dendrimer improved ultrafiltration to recover Cu (II) from aqueous solution. The dendrimer-Cu (II) complexes can be efficiently separated from aqueous solutions by ultrafiltration. Dendritic polymers can also be used as (i) recyclable unimolecular micelles for recovering organic solutes from water (Arkas *et al.*, 2003) and (ii) scaffolds and templates for the preparation of redox and catalytically active nanoparticles. Dendritic polymers have also been used successfully as delivery vehicles or scaffolds for antimicrobial agents such as Ag (I) and quaternary ammonium chlorides (Balogh *et al.*, 2001).

PAMAM-based silver complexes and nanocomposites have proved to be effective antimicrobial agents *in vitro*. Rether and Schuster (2003) made a water-soluble benzoylthiourea modified ethylenediamine core-polyamidoamine dendrimer for the selective removal and enrichment of toxicologically relevant heavy metal ions. They studied complexation of Co (II), Cu (II), Hg (II), Ni (II), Pb (II) and Zn (II) by the dendrimer ligand and using the polymer-supported ultrafiltration process.

One of the novel systems for encapsulating organic pollutants is crosslinked dendritic derivatives. In the research carried out by Arkas *et al.* (2005) for the preparation of ultra pure water, the amino groups of polypropyleneimine dendrimer and hyperbranched polyethylene imine were interacted under extremely mild conditions with 3-(triethoxysilyl) propyl isocyanate. They produced porous ceramic filters and employed these dendritic systems for water purification. In this experimental work, the concentration of polycyclic aromatic compounds in water was reduced to a few

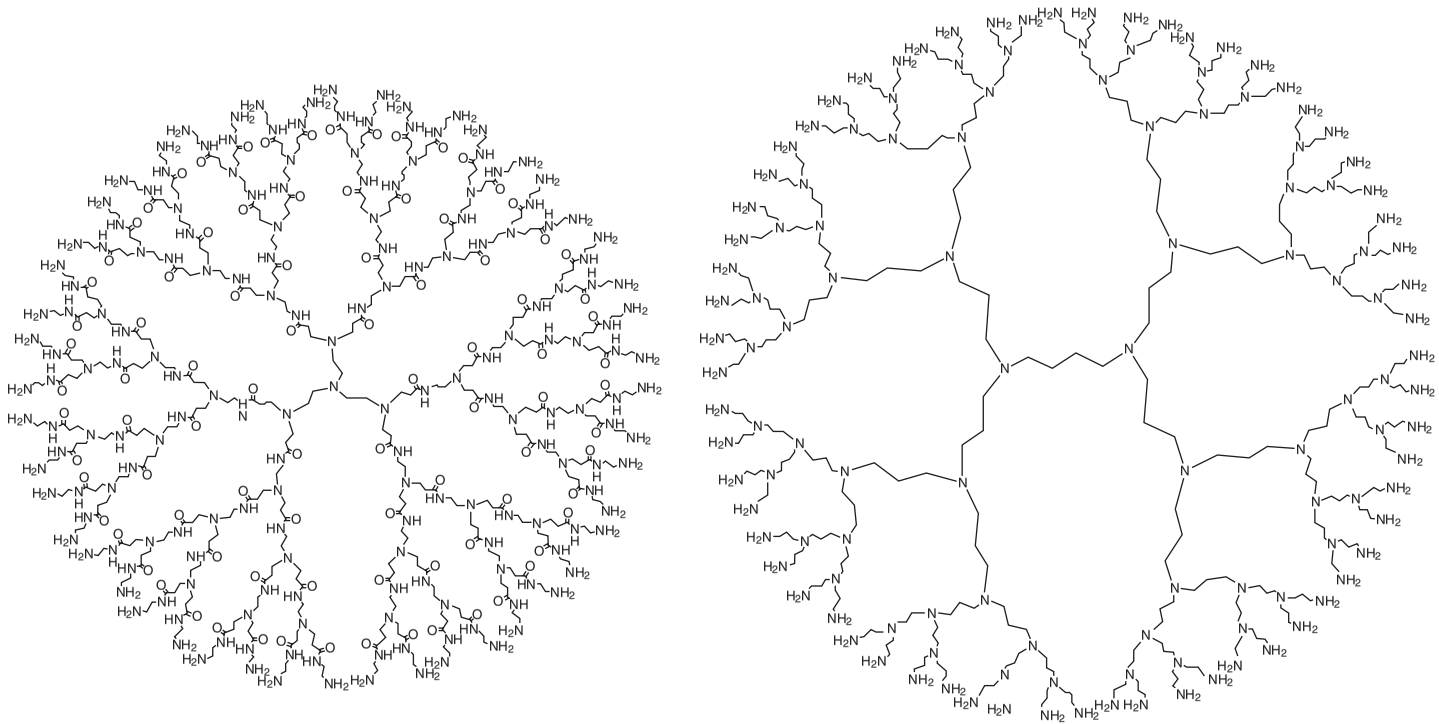

(a) (b)

16.2 Commercially available G5 PAMAM (a) and G4 PPI (b) dendrimers (adapted with permission from Jang *et al.*, 2009).

ppb's by continuous filtration of contaminated water through these filters. Then, the filters loaded with pollutants were effectively regenerated by treatment with acetonitrile.

In another work, Arkas *et al.* (2006) developed a method that permits removal of organic pollutants by employing a simple filtration step, which can be easily scaled up. They used the long-alkyl chain functionalized polypropylene imine dendrimers, polyethylene imine hyperbranched polymers and β-cyclodextrin derivatives which are completely insoluble in water.

16.4.3 Metal-containing nanoparticles

Metal and metal oxide nanoparticles have been studied extensively for water treatment applications. Most notable among the metal nanoparticles are the noble metals (such as silver and gold which are treated as famous biocides) and nano zero-valent iron (NZVI) used for treatment of water containing pesticides. Among metal oxides, oxides of iron, aluminium, zinc, magnesium and titanium have been made use of significantly in groundwater remediation. We first discuss the category of metals and then case studies pertaining to metal oxides are discussed.

Zero-valent iron (ZVI)

Among the popular nanosorbents at the present time, the most exploited is the nano ZVI having applications ranging from removal of halogenated organics, arsenic, nitrate and heavy metals. Nanoparticles could provide very high flexibility for both *in situ* and *ex situ* remediations. They can also be anchored onto a solid matrix such as carbon, zeolite or membrane for enhanced treatment of water. ZVI removes aqueous contaminants by reductive dechlorination, in the case of chlorinated solvents or by reducing them to an insoluble form, in the case of aqueous metal ions.

Different material and engineering aspects of ZVI nanoparticles used for removal of environmental pollutants were discussed by Li *et al.* (2006b). These nanoparticles were used for separation and immobilization of Cr (VI) and Pb (II) from aqueous solution by reduction of chromium to Cr (III) and Pb to Pb (0) (Ponder *et al.*, 2000). Nanopowder of ZVI was used for the removal of nitrate in water (Choe *et al.*, 2000). Nanoscale ZVI was employed by Lowry and Johnson (2004) for dechlorination of polychlorinated biphenyl (PCB) to lower-chlorinated products under ambient conditions. It was demonstrated that nano-sized ZVI oxidizes organic compounds in the presence of oxygen (Feitz *et al.*, 2005). The high surface area of nanoscale ZVI may allow for more efficient generation of oxidants. A decrease in reactivity is expected with the build-up of iron oxides on the surface, particularly at high pH.

The EZVI (emulsified zero-valent iron) technology with nanoscale or microscale iron was enhanced to address this limitation associated with the conventional use of ZVI. Quinn *et al.* (2005) evaluated the performance of nanoscale emulsified zero-valent iron (nEZVI) to improve *in-situ* dehalogenation of dense, non-aqueous phase liquids (DNAPLs) containing trichloroethene (TCE) from groundwater. One of the applications of ZVI is the removal and sorption of arsenic contamination from groundwater (Kanel *et al.*, 2006). Nanopowder of ZVI as a fine powder cannot be used in fixed-bed columns unless they have granular shape (Guo and Chen, 2005).

Xu and Zhao (2007) used carboxy methyl cellulose (CMC) stabilized ZVI nanoparticles to reduce Cr (VI) in aqueous media through batch and continuous flow column study. They found that the stabilized ZVI nanoparticle is more effective than the non-stabilized one for the removal of Cr (VI). In the batch experiments, the reduction of Cr (VI) was improved from 24% to 90% as the dosage of ZVI increased from 0.04 to 0.12 g/L. In another work, Xiong *et al.* (2007) studied the degradation of perchlorate in water and illustrated the stabilized ZVI nanoparticles could increase perchlorate reduction rate by 53% in saline water (with concentration of NaCl up to 6% w/w).

Giasuddin *et al.* (2007) investigated the removal of humic acid (HA) with ZVI nanoparticles and also their interaction with As (III) and As (V). Cheng *et al.* (2007) also applied ZVI nanoparticle and commercial form of ZVI powder with different mesh sizes for the dechloronation of p-chlorophenol from water. Comparison between those particles indicated that the nanoscale was more effective for the reduction process.

Noble metal nanoparticles

The first detailed report on the interaction of noble metal nanoparticles with halocarbons appeared in 2003 (Nair and Pradeep, 2003). It was found that noble metals at nanodimensions react with halocarbons in a manner similar to other metals (i.e., reductive dehalogenation) leading to the formation of metal halide with no reaction byproducts. The reaction was later extended to several halocarbons and was found to be completely efficient at room temperature.

The reaction of noble metal nanoparticles was studied with widely used pesticides such as endosulfan (Nair *et al.*, 2003), malathion (Nair and Pradeep, 2007) and chlorpyrifos (Nair and Pradeep, 2007). The noble metal nanoparticles supported on alumina were very effective for the removal of pesticides from solution. Realizing the fact that a number of pesticides found in drinking water are organochlorine (e.g., simazine, lindane, atrazine, etc.) or organosulfur pesticides (e.g., triazophos, quinalphos, etc.) or contain nitrogen-based functional groups (e.g., carbaryl,

carbofuran, monochrotofos, etc.), the chemistry of supported noble metal nanoparticles can comfortably be utilized for the complete removal of such pesticides from drinking water. This aspect of complete removal of a wide variety of pesticides makes the chemistry of supported noble metal nanoparticles unique for drinking water purification.

Noble metal nanoparticles are also found extremely important for ultra-low concentration sensing of pesticides. Overall, there are two approaches followed for ultra-low concentration detection of pesticides using gold nanoparticles:

- changes in the signature properties of a functional group attached to noble metal nanoparticle surface in the presence of organic molecules: reported to reach a detection limit in ppt level (T. J. Lin *et al.*, 2006; Rajan *et al.*, 2007; Sun *et al.*, 2008);
- changes in the optical properties of noble metal nanoparticles upon interaction with pesticides (Burns *et al.*, 2006; Dubas and Pimpan, 2008).

Another interesting application area of noble metal nanoparticles in drinking water purification is the sequestration of heavy metals (Henglein, 1998). Also the functionalized noble metal nanoparticle surfaces can be exploited for the detection of heavy metals (Ono and Togashi, 2004; Lee *et al.*, 2007; Lu and Liu, 2007).

The anti-microbial effects of silver, in zerovalent and ionic form, have been widely studied in great detail (Aymonier *et al.*, 2002; Sondi and Sondi, 2004; Jain and Pradeep, 2005; Sambhy *et al.*, 2006). Due to the numerous scientific investigations published on this topic and its consequences in different applications, review articles may be consulted for a detailed understanding (Silver, 2003; Silver *et al.*, 2006; Neal 2008; Rai *et al.*, 2009; Sharma *et al.*, 2009). The chemistry behind the biocidal activity of silver nanoparticles, and the way silver ions act against micro-organisms are discussed in the review by Pradeep and Anshup (2009a). While the precise details are not yet elucidated, protein inactivation and loss of replication ability of DNA are suggested. A few important observations are highlighted by Pradeep and Anshup (2009a).

Metal oxide nanoparticles

Wang *et al.* (2007) investigated the effect of size, fabrication method, and morphology of ZnO nanoparticles as photocatalysts on the decomposition of methyl orange. It was found that the preparation method was the most important step and ZnO nanoparticle, 50 nm in diameter synthesized via thermal evaporation method, provided the highest photocatalyst activity.

Alumina nanoparticles have been utilized for the removal of heavy metals from drinking water (Kasprzyk-Hordern, 2004). The suggested

mechanism involves the metal ion induced flocculation of negatively charged alumina nanoparticles (alkaline pH conditions). Alumina is used as support for heterogeneous catalysis (Nair and Pradeep, 2007). The major reasons behind the use of oxides for water purification are: high surface area for adsorption, mesoporous structure, presence of surface charge, stability and low solubility in water.

Titanium dioxide (TiO_2) is one of the most important materials used in water treatment applications because of its photocatalytic properties. Two different types of photocatalytic applications can be distinguished in water treatment: solar photocatalysis and photocatalytic systems equipped with artificial ultraviolet (UV) light. Both systems can be applied at ambient temperature to degrade various chemical and microbiological pollutants in water and air. As it makes use of sunlight, solar photocatalysis technology is inexpensive, environmentally friendly and universally applicable. The equipment needed is minimal and also appropriate for developing countries or remote sites with no access to electricity. Nanoparticles that are activated by light, such as the large band-gap semiconductors titanium dioxide (TiO_2) and zinc oxide (ZnO), are frequently studied for their ability to remove organic contaminants from various wastewater. These nanoparticles have the advantages of ready availability, being inexpensive, and having low toxicity. The rapid recombination of photo-generated electron hole pairs and the non-selectivity of the system are the main problems that limit the application of photocatalysis processes. The specific chelating agents such as arginine, lauryl sulfate and salicylic acid can modify the surface properties of nanocrystal TiO_2 and inhibit rapid recombination of photo-generated electron hole pairs. A comprehensive review of photocatalytic nano-TiO_2 for environmental applications is found in Kwon *et al.*, (2008).

Conventional TiO_2 photocatalysts are utilized only under UV light due to its wide bandgap of 3.2 eV and, therefore, cannot be used indoors or inside vehicles. In order to obtain the photocatalytic activity under visible light, various types of TiO_2-based photocatalysts have been created (Sato, 1986; Kisch *et al.*, 1998; Zang *et al.*, 1998; Asahi *et al.*, 2001; Umebayashi *et al.*, 2002; Irie *et al.*, 2003; Sakthivel and Kisch, 2003; Miyauchi *et al.*, 2004); and nitrogen-doped TiO_2 ($TiO_{2-x}N_x$) is regarded as one of the most effective and practical catalysts (Irie *et al.*, 2003; Miyauchi *et al.*, 2004; Irokawa *et al.*, 2006). Nitrogen doping has extended the photoactive wavelengths up to 520 nm as a result of bandgap narrowing, realizing the equivalent photoactivity in conventional TiO_2 under UV light since the number of carrier-recombination centres was minimized. The change in band gap and generation of free radicals are shown in Fig. 16.3.

Synthesized titanium dioxide nanoparticles of both anatase and rutile forms were used for wet oxidation of phenols by hydrothermal treatment (Andersson *et al.*, 2002). In another study, a novel composite reactor with

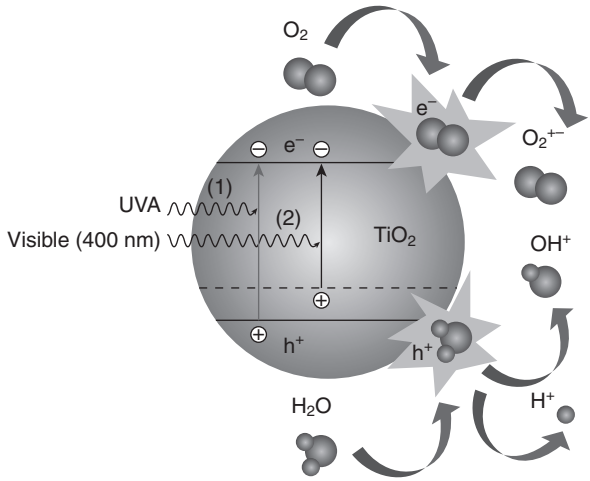

16.3 Change in band gap and generation of free radicals in TiO_2 photocatalyst.

combination of photochemical and electrochemical system was used for the degradation of organic pollutant such as Rhodamine 6G (R-6G) (Chen *et al.*, 2003). Fine TiO_2 particles have shown better efficiency than the immobilized catalysts, but complete separation and recycling of fine particles (less than 0.5 μm) from the treated water, are very expensive. Therefore, from an economical point of view, this method is not suitable for the industrial scale. This problem was solved by fixing the carbonblack-modified nano-TiO_2 (CB-TiO_2) on aluminium sheet as a support (L. Li *et al.*, 2003). The photocatalytic activity of CB-TiO_2 thin films was observed to be 1.5 times greater than that of TiO_2 thin films in the degradation of reactive Brilliant Red X-3B.

Decomposition of parathion with the nanometer rutile titanium dioxide (TiO_2) powder as the sonocatalyst after treatment of high-temperature activation was carried out by Wang *et al.*, (2006). In the study by Li *et al.* (2006a), carbon grain coated with activated nano-TiO_2 (20–40 nm) (TiO_2/AC) was prepared and used for the photodegradation of methyl orange (MO) dyestuff in aqueous solution under UV irradiation. Mahmoodi *et al.* (2007) immobilized TiO_2 nanoparticles for the degradation and mineralization of two agricultural pollutants (Diazinon and Imidacloprid as *N*-heterocyclic aromatics).

The photocatalytic efficiency of immobilized TiO_2 nanoparticle with 6 nm diameter (supported by glass substrate) as well as conventional suspended catalysts has been investigated recently by Mascolo *et al.* (2007) for the degradation of methyl red dye. Although the mechanism for dye degradation was found to be the same for both cases (suspended as well as

immobilized nanoparticles), lowering of photodegradation performance in the immobilized case was due to reduction in active surface area for adsorption and subsequent catalyst action. However, the recovery of nanoparticles is easy when the particles are immobilized.

Degradation of nitrobenzene by using nano-TiO_2 and ozone was studied by Yang *et al.* (2007). They compared the effect of nano-TiO_2 catalysed plus ozone and ozone only and found that the catalysed ozonation was more efficient than ozone alone. Sobana *et al.* (2006) prepared silver nanoparticles doped with TiO_2 and used them for the photodegradation of direct azo dyes.

16.4.4 Carbon nanotubes

A carbon nanotube (CNT) is a one-atom thick sheet of graphite (called graphene) rolled up ino a seamless cylinder with diameter of the order of a nanometer and capped at both ends by hemispheres of fullerene. This results in a nanostructure where the length-to-diameter ratio exceeds 10,000. CNTs can be categorized by their structures as single-walled nanotubes (SWNT) and multi-walled nanotubes (MWNT). In the most general way, the CNT can be shown as composed of a concentric arrangement of several cylinders (Fig. 16.4). The high curvature of the graphene sheets increases the total energy of the tubules per carbon atom, but this is more

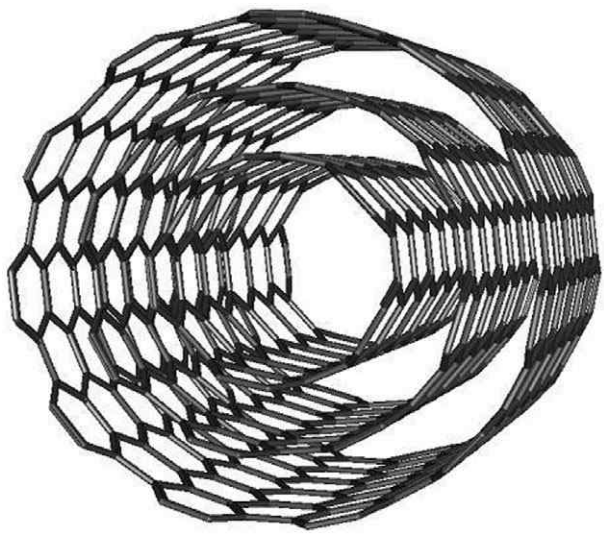

16.4 Multi-walled carbon nanotube shown as composed of a concentric arrangement of several graphene cylinders.

than offset by a lowering of the energy because of the absence of dangling bonds at the edges of the graphene sheets. Such cylindrical carbon molecules have novel properties that make them potentially useful in a wide variety of applications in water and health care.

The as-grown or acidified CNTs have shown potential as a sorbing media for removal of various contaminants from water. The as-grown CNTs have got defect sites (originated during synthesis), which make them a suitable adsorbent for uptake of contaminants. However, it is noteworthy that such CNTs do not pose any selectivity towards uptake of specific contaminants. On the other hand, the surface area of as-grown CNTs lies in the range of 50–100 m^2/g, which is not significant in comparison to activated charcoal or activated alumina (where the surface area is up to 1000 m^2/g), which are being extensively used in water decontamination because of being cheaper and having easy availability. However, some of the work carried out by researchers using as-grown and functionalized CNTs are cited below.

Peng *et al.* (2005) developed a novel adsorbent, ceria supported on CNTs (CeO_2-CNTs), for the removal of arsenate from water. Under natural pH conditions, an increase from 0 to 10 mg/L in the concentration of Ca (II) and Mg (II) results in an increase from 10 to 81.9 and 78.8 mg/g in the amount of As (V) adsorbed, respectively. The adsorption was shown to be pH-dependent. The efficient regeneration of the loaded adsorbent was carried out and the adsorption mechanism was suggested.

Y. H. Li *et al.* (2003a) used aligned carbon nanotubes (ACNTs) for the removal of fluoride from water. The adsorption slightly depends on the solution pH value. The highest adsorption capacity of ACNTs occurs at pH 7 and reaches 4.5 mg/g at equilibrium fluoride concentration of 15 mg/L. Y. H. Li *et al.* (2003b) studied the removal of cadmium (II) with as-grown and surface-oxidized CNTs. Cadmium (II) adsorption capacities for three kinds of oxidized CNTs increase owing to the functional groups introduced by oxidation compared with the as-grown CNTs. The cadmium (II) adsorption capacity of the as-grown CNTs is only 1.1 mg/g, while it reaches 2.6, 5.1 and 11.0 mg/g for the H_2O_2-, HNO_3- and $KMnO_4$-oxidized CNTs, respectively, at the cadmium (II) equilibrium concentration of 4 mg/L. Adsorption of cadmium (II) by CNTs was strongly pH-dependent and the increase of adsorption capacities for HNO_3- and $KMnO_4$-oxidized CNTs is more obvious than that of the as-grown and H_2O_2-oxidized CNTs at lower pH regions. Analysis revealed that the $KMnO_4$-oxidized CNTs hosted manganese residuals, and these surely contributed to cadmium sorption to a yet-undefined extent.

Li *et al.* (2002) found that CNTs show exceptional adsorption capability and high adsorption efficiency for lead removal from water. The adsorption is significantly influenced by the pH value of the solution and the nanotube surface status, which can be controlled by their treatment processing. The

adsorption isotherms are well described by both the Langmuir and Freundlich models.

The first data on multi-wall nanotubes (MWNTs) as sorbent for dioxin removal was reported by Long and Yang (2001). A technique based on temperature-programmed desorption (TPD) was used to study dioxin adsorption. The amount adsorbed on CNTs is 1034 higher than on activated carbon. Hence, significantly higher dioxin removal efficiency is expected with CNTs than with activated carbon. The strong interaction between dioxin and CNTs may be attributed to the unique structure and electronic properties of CNTs. The CNTs consist of hexagonal arrays of carbon atoms in graphene sheets that surround the tube axis. Strong interactions between the two benzene rings of dioxin and the surface of the CNTs are expected.

Srivastava *et al.* (2004) reported the fabrication of freestanding macroscopic hollow cylinders having radially aligned CNT (ACNT) walls, with diameters and lengths up to several centimetres. These cylindrical membranes are used as filters in the elimination of multiple components of heavy hydrocarbons from petroleum – a crucial step in post-distillation of crude oil – with a single-step filtering process, and the filtration of bacterial contaminants such as *Escherichia coli* or the nanometre-sized poliovirus (~25 nm) from water. These macro filters can be cleaned for repeated filtration through ultrasonication and autoclaving.

Techniques have been developed to synthesize CNTs in significant quantities using three different methods:

1. arc discharge,
2. laser ablation and
3. chemical vapour deposition (CVD).

An overview of these different routes is summarized in Table 16.2 (Balasubramanian and Burghard, 2005).

Of the various methods of CNT synthesis, CVD has got tremendous potential for scaleup. In addition, the growth of CNTs can take place without having patterned substrate (with impregnation of catalyst particles). A special case of CVD is called spray pyrolysis, where liquid precursors like mixture of benzene and ferrocene can be used. The experimental setup is shown in Fig. 16.5 (Dasgupta *et al.*, 2008). It consists of a sprayer, a container for the liquid precursor and a quartz tube (inner diameter 10 mm). The sprayer is made up of a pyrex nozzle (inner diameter 0.4 mm) and an outer pyrex tube with an exit diameter of 2 mm. The inner nozzle carries the liquid precursor and the outer one carries the nitrogen gas. The sprayer is attached to the quartz tube kept inside a resistive furnace. An optimized combination of composition and the flow rate of liquid precursor solution, the carrier gas flow rate, the diameter of inner and outer nozzles of sprayer and the temperature of growth helps in the synthesis of CNTs

Table 16.2 Overview of the important synthesis procedures for CNTs (adapted with permission from Balasubramanian and Burghard, 2005)

Synthesis method	Principle	Type of CNT with yield	Maximum production rate
Arc discharge	Carbon atoms are generated through an electric arc discharge at $T > 3000$°C between two graphite rods. Catalyst metal particles (Fe, Co, Ni) required	Both SWNT and MWNT can be produced; yield: about 30% by weight	120 g per day
Laser ablation	Generation of atomic carbon at $T > 3000$°C through laser irradiation of graphite containing catalyst metal particles (Fe, Co, Ni)	Mainly SWNT can be formed; yield: about 70% (expensive method)	50 g per day
Chemical vapour deposition	Decomposition of gaseous hydrocarbon source is catalysed by catalyst metal particles (Fe, Co, Ni). Spray pyrolysis method with liquid precursor such as benzene + ferrocene can be used directly where patterned substrate with catalyst impregnation is not required. Temperature of synthesis is about 750–1000°C	Both SWNT and MWNT can be formed; yield: about 60%	50 kg per day

with particular length, diameter and alignment. Each of the parameters is critical toward the nature as well as yield of CNTs (Dasgupta *et al.*, 2008). This synthesis route provides CNTs with a high degree of alignment because the catalyst particle (iron in the case of ferrocene precursor) is generated *in situ*. Also the method is economical with no requirement of substrate preparation as well as less involvement of trained manpower compared to the other two synthesis routes.

A self-standing tubular macrogeometry of aligned carbon nanotubes with very high surface area (~90 m^2/g) was developed with optimization of spray pyrolysis parameters. The macrogeometry of aligned CNTs is shown in Fig. 16.6, and Fig. 16.7 shows the scanning electron microscope (SEM) image depicting the highly aligned CNTs along the thickness of cylinder. It has the usual advantages of a membrane where, based upon the principle of size exclusion, the water purification can take place.

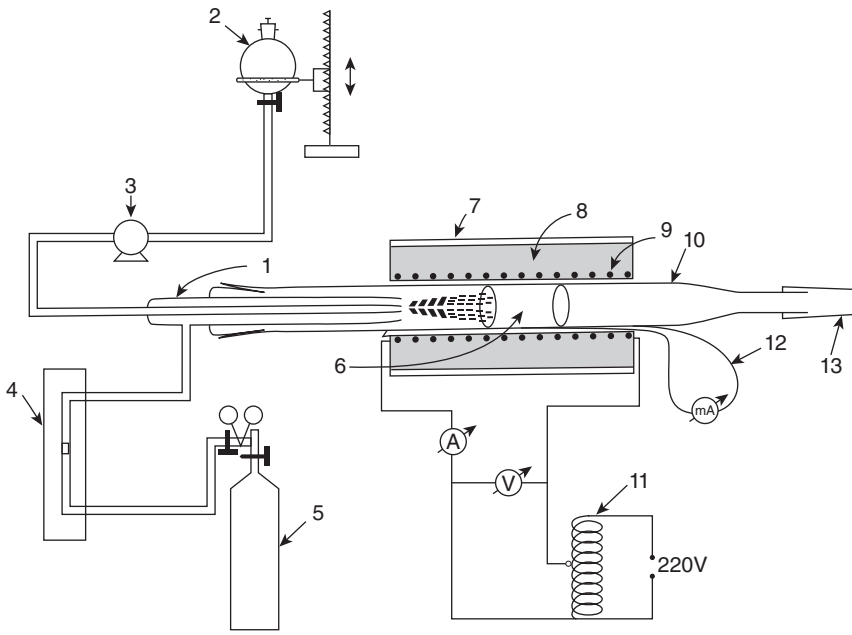

16.5 Schematic of the spray pyrolysis setup: (1) pyrex sprayer, (2) container for ferrocene-benzene solution, (3) peristaltic pump, (4) nitrogen gas flow meter, (5) nitrogen gas cylinder, (6) quartz template, (7) furnace outer shell, (8) thermal and electrical insulation, (9) heating element, (10) quartz tube, (11) power supply, (12) thermocouple, (13) outlet to exhaust (adapted with permission from Dasgupta *et al.*, 2008).

A noteworthy breakthrough in the area of development of nanotube chemistry is the oxidation of CNT in concentrated nitric acid (Rosca *et al.*, 2005). Such a drastic condition helps in opening of the CNT tips as well as oxidative etching along the sidewalls enabling the decoration of walls with various oxygen-containing groups (mainly carboxyl group). The incorporation of carboxyl group exposes various useful sites in CNTs for further modification as per requirements (ester or amide bond formations can take place). In addition, the formation of anhydride at the tube ends can take place through which the rings of CNTs are accessible (Sano *et al.*, 2001). The most important implication of the introduction of a carboxyl group lies in the fact that the van der Waals forces existing between the individual CNTs are reduced and hence the CNTs can be made water soluble (as-grown CNTs are not soluble in any solvent) by addition/substitution of new moieties.

On the other hand, addition reactions help in direct coupling of functional groups onto the π-conjugated carbon framework. A series of addition

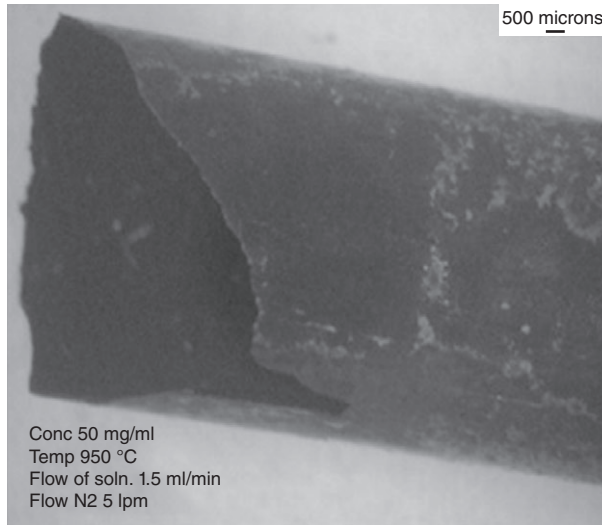

16.6 The stereoscopic micrograph of the self-standing macrotube made up of aligned carbon nanotubes (adapted with permission from Dasgupta *et al.,* 2008).

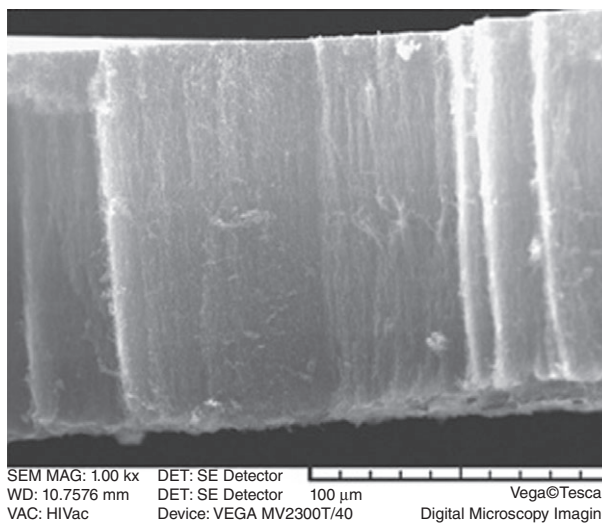

16.7 SEM image of the self-standing tube showing the alignment of CNT in the radial direction (adapted with permission from Dasgupta *et al.,* 2008).

reactions like fluorination, hydrogenation and cycloaddition can be possible. The fluorine atoms of fluorinated CNTs can be replaced through nucleophilic substitution reaction, and thus, functional groups of alcohols, amines and Grignard reagent, etc., can be successfully incorporated onto the CNT sidewall.

So far we have been concerned mainly with the functionalization of the sidewall and tip of CNTs. But the inner hollow cavity of CNTs offers tremendous opportunity to materials scientists, chemists and engineers to do excellent R&D in the nanoscale test tube. The critical issue is the wetting properties of the CNTs. The wettability determines what liquid would fill the tube by capillary action and cover the inner surface. The Young–Laplace relation relates the pressure difference ΔP across the liquid–vapour interface in a capillary to the surface tension of the liquid (γ) and contact angle (θ) between the solid and the liquid as shown by:

$$P = 2\gamma r^{-1} \cos\theta \qquad [16.1]$$

where r is the radius of curvature of the meniscus. The contact angle θ is an indicator of the strength of the interaction between the liquid and the solid interface relative to the cohesive forces in the liquid. If θ is smaller than 90°, the contact between the liquid and the surface is said to be wetting and ΔP is positive. Therefore the liquid will be pulled into the capillary spontaneously, as there is an energy gain in the wetting process. If θ is larger than 90°, the contact angle is said to be non-wetting and ΔP will be negative. Therefore, when $\theta > 90°$, the only way to introduce liquid into a capillary is to apply pressure larger than ΔP.

Extremely high aspect ratios, molecularly smooth hydrophobic graphitic walls, and nanoscale inner diameters of carbon nanotubes give rise to the unique phenomenon of ultra-efficient transport of water through these ultra-narrow tubes. The idea of water occupying such confined hydrophobic channels is somewhat difficult to comprehend, though experimental evidence has confirmed that water can indeed occupy these channels (Naguib *et al.*, 2004; Kolesnikov *et al.*, 2006). The proposed water transport mechanism has a distinct similarity to the transport mechanisms of biological ion channels. In recent years, numerous simulations (Hummer *et al.*, 2001; Kalra, 2003) of water transport through SWNT have suggested that fast molecular transport takes place, far in excess of what continuum hydrodynamic theories would predict if applied on this length scale. There have been many efforts to define the boundary between bulk water and confined water transport, and it was found sensible to set a threshold for the continuum treatment of liquid as around 7.5 nm.

A no slip boundary condition is typically used in continuum fluid dynamics. It constrains a fluid closest to a solid boundary to obtain the same tangential velocity as the solid. When the tangential velocity of the fluid

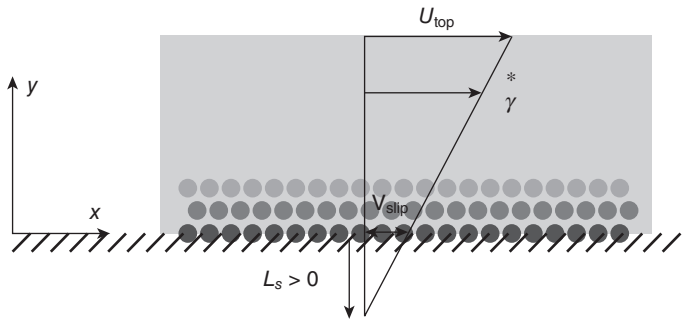

16.8 Hydrodynamic slip flow profile characterized by slip length L_s (adapted from Choi *et al.*, 2011).

differs from that of the solid, we usually say the surface imposes a slip boundary condition as depicted in Fig. 16.8 (Choi *et al.*, 2011). The slip boundary condition helps us describe non-continuum behaviour of water transport inside the CNT in the framework of continuum dynamics. For example, slip length, L_s, may serve as a good indicator for the molecular interaction between water molecules and CNT via provision of information about the degree of departure the transport innately has from the hydrodynamic Hagen–Poiseuille flow. Also, the slip length indicator can compare with results of molecular dynamics (MD) simulations often used for the exact prediction of water flow under the CNT nanoconfinement.

Slip length, L_s, is convenient to explain the hydrodynamic boundary condition at the interface of fluid and wall, which is defined according to the Navier boundary condition:

$$L_s \left.\frac{\partial v_t}{\partial n}\right|_{wall} = v_{t,wall} - v_{wall}, \qquad [16.2]$$

where n and t denote normal and tangential directions of the wall, v_t is the velocity of a fluid tangential to the wall, and v_{wall} is the velocity of the wall. $v_{t,wall} - v_{wall}$ is denoted as a slip velocity.

The solutions for the velocity and the corresponding volume flow rate in the flow direction, z, with respect to the distance from the centre, r, have a parabolic profile given by:

$$U_s = -\frac{dp}{dz}\frac{R^2}{4\mu}\left(1 - \frac{r^2}{R^2} + \frac{2L_s}{R}\right) \qquad [16.3]$$

$$Q_{Hagen-Poiseuille} = -\frac{dp}{dz}\frac{\pi R^4}{8\mu} \qquad [16.4]$$

$$Q_s = Q_{Hagen-Poiseuille}\left(1 + \frac{4L_s}{R}\right) \qquad [16.5]$$

where μ, p and R represent viscosity, pressure, and tube radius, respectively.

There are two primary reasons a continuum theory of a molecular scale slip is investigated. On the one hand, it helps to understand the behaviour of a flow in a nanoscale tube. On the other hand, the slip length theory can serve as a reference to explain large water flow enhancements, compared with no-slip Hagen–Poiseuille formalism, observed by several experimental studies (Majumder *et al.*, 2005a; Holt *et al.*, 2006; Whitby *et al.*, 2008) using CNT membranes.

Although the ultrafast water transport in the CNT could be explained by the slip length model to some extent, results of MD simulations, especially on the water configuration, are investigated as an effective way to understand many fundamental nanofluidic characteristics. In fact, lots of physical properties of water depend on the coherence and the number of hydrogen bonds. The hydrogen bond is useful in explaining water configuration or properties inside CNT, since water has a dipole and an electrostatic interaction via hydrogen bonding.

The effect of CNTs on bacteria and viruses has not received particular attention, probably due to the difficulty of dispersing CNTs in water. Surfactants or polymers such as polyvinylpyrolidone (PVP) or Triton-X are generally used to facilitate the dispersion. The few studies available credited SWNTs with antimicrobial activity towards Gram-positive and Gram-negative bacteria, and the damage inflicted was attributed to either a physical interaction or oxidative stress that compromise cell membrane integrity (Narayan *et al.*, 2005; Kang *et al.*, 2008). However, the degre of aggregation and the bioavailability of the nanotube will have to be considered to exploit the antimicrobial properties effectively.

It is noteworthy here that CNTs are the only nanostructured material bestowed with so many unusual (however essentially interesting) attributes which can serve as a wonderful global water filter. The critical factor is to put the CNTs in a membranous structure to exploit all their potential benefits, which are discussed in Section 16.7.

16.4.5 Other nanomaterials (nanoclays, micelles, magnetic nanoparticles)

Clays are alumino silicates with a planar silicate structure. There are three main categories of clay: kaolinite, montmorillonite–smectite and illite, amongst which the first two are the most widely studied (Pradeep and Anshup, 2009b). Usually the structure contains silicate sheets (Si_2O_5) bonded to aluminium oxide/hydroxide layers ($Al_2(OH)_4$) called gibbsite layers. The primary structural unit of this group is a layer composed of one octahedral sheet with one tetrahedral sheet (kaolinite is 1:1 clay mineral).

The condensation of two sheets happens by coordination of an oxygen atom with one silicon atom in the tetrahedral sheet and two aluminium atoms in the octahedral sheet. Clays undergo exchange interactions of adsorbed ions with the outside too.

Although clays are very useful for many applications, they have one main disadvantage, they lack permanent porosity. To overcome this problem, researchers have been looking for a way to prop and support the clay layers with molecular pillars. Most of the clays can swell and thus increase the space in between their layers to accommodate the adsorbed water and ionic species. Ding *et al.* (1999) and Ooka *et al.* (2004) prepared different kinds of TiO_2 pillared clays from different raw clays and the adsorption and photocatalytic-decomposition performance were evaluated. It was found that surface hydrophobicity of pillared clays (especially TiO_2) largely varied with the host clay. Since the TiO_2 particles in the pillared clays are too small to form a crystal phase, they presented poor photocatalytic activity.

Nanocomposite of iron oxide and silicate was also synthesized for degradation of azo-dye orange (II) (Feng *et al.*, 2003). A new class of nano-sized large porous titanium silicate (ETAS-10) and aluminium-substituted ETAS-10 with different Al_2O_3/TiO_2 ratios were successfully synthesized by Choi *et al.* (2006) and applied to the removal of heavy metals, in particular Pb (II) and Cd (II).

Micelles are self-assembled surfactant materials in a bulk solution. Surfactants or 'surface active agents' are usually organic compounds that are amphipathic, meaning they contain both hydrophobic groups (tails) and hydrophilic groups (heads). Therefore, they are typically soluble in both organic solvents and water. Surfactant-enhanced remediation techniques have shown significant potential in their application for the removal of polycyclic aromatic hydrocarbon (PAHs) pollutants. Molecular self-assembly is gathering of molecules without guidance or management from an outside source. There are two types of self assembly: intramolecular and intermolecular. Attaching a monolayer of molecules to mesoporous ceramic supports gives materials known as self-assembled monolayers on mesoporous supports (SAMMS). The highly ordered nanostructure of SAMMS is the result of three molecular self-assembly stages. SAMMS of silica-based materials are highly efficient sorbents for target species, such as heavy metals, tetrahedral oxometalate anions and radionuclides (Mansoori *et al.*, 2008).

Magnetic nanoparticles are generally studied as adsorbents and nanocatalysts for water treatment. One of the major applications of magnetic particles is in the area of magnetic separation. In this case, it is possible to separate a specific substance from a mixture of different other substances, called 'magnetically assisted chemical separation' (MACS). Hu *et al.* (2005) developed an innovative process combining nanoparticle adsorption and

magnetic separation for the removal and recovery of Cr (VI) from wastewater. Chang *et al.* (2006) prepared the magnetic chitosan nanoparticles with an average diameter of 13.5 nm as a magnetic nano-adsorbent. Magnetic chitosan nano-adsorbent was shown to be quite efficient for the fast removal of Co (II) ions at the pH range of 3–7 and the temperature range of 20–45°C.

Ngomsik *et al.* (2006) have studied the removal of nickel ions from the aqueous solution using magnetic alginate microcapsules. Also, magnetic particles in the microcapsules allowed easy isolation of the microcapsule beads from aqueous solutions after the sorption process. Mayo *et al.* (2007) also studied the effect of particle sizes in the adsorption and desorption of As (III) and As (VI). Different kinds of magnetic nanoparticles were also employed for the removal of organic pollutants, such as sorption of methylene blue on polycyclic acid-bound iron oxide from an aqueous solution (Mak and Chen, 2004).

16.5 Synthesis of nanomaterials

There are a number of techniques available to fabricate different nanomaterials (Tiwari *et al.*, 2008). Nanoparticles can be produced from larger structures (top-down) by use of ultrafine grinders, lasers and vapourization followed by cooling. For complex particles, nanotechnologists generally prefer to synthesize nanostructures by a bottom-up approach by arranging molecules to form complex structures with new and useful properties. The detailed views on different synthesis routes is beyond the scope of this chapter and hence they are listed below with references:

- layer-by-layer deposition (Philips *et al.*, 2006)
- self-assembly (Graveland and Kruif, 2006; Lorenceau *et al.*, 2005)
- gas phase synthesis and sol-gel processing (Siegel, 1991, 1994; Uyeda, 1991)
- crystallization (Boanini *et al.*, 2006)
- microbial synthesis (Bhainsa and Souza, 2006; Bhattacharya and Gupta, 2005)
- other methods (sonochemical processing, cavitation processing, microemulsion processing and high-energy ball milling).

16.6 Nanotechnology: health, safety and environment

Nanotechnology is a potential provider of unprecedented technological solutions to many environmental problems including climate change, pollution and clean drinking water. It is claimed that it enables economic

growth through more efficient and durable products and new markets. However, the applicability of such a system has to be perceived after due consideration of the process and product in its entirety, with serious attention being paid to the probable health and environmental risks.

While it is perceived that nanotechnology will deliver cleaner production (e.g., through green chemistry, synthesis and processing of nanoscale materials that will reduce consumption of raw materials and natural resources such as water and energy, and improved chemical reactions and catalysis), in reality it is very difficult to ensure these propositions unless there is a proper life cycle analysis of the nanomaterials through validated nano-specific risk assessment methodologies.

Although there are now only a limited number of products in the marketplace that contain engineered nanomaterials, the pace of nanotechnology development assures that the market soon is going to be flooded with nano-based products. In such a case, it is essential to have a grasp of the attribute-related concerns, associated health and environment risks and the extent of the population going to be affected.

The following attributes of nanoparticles create a number of unknown exposures:

- size of particles: the size of nanoparticles necessitates usage of sophisticated analytical tools.
- increased reactivity and conductivity: nanoparticles are more reactive and conductive than the same material in bulk.
- routes of exposure: because of their very small size, nanoparticles can be inhaled or ingested; in addition, they are capable of crossing the blood-brain barrier, which protects the brain against contamination (Oberdörster *et al.*, 2004).

16.6.1 Evidence for toxicity of nanomaterials

Nanoparticles have the ability to induce lung injuries because of their small size, a large surface area, and an ability to generate reactive oxygen species (ROS).[1] The short-term pulmonary toxicity studies in rats with ultrafine and fine carbon black, nickel and TiO_2 particles have established enhanced lung inflammatory strength of the ultrafine particles in comparison to fine-sized particulates of similar composition (Warheit *et al.*, 2006; Grassian *et al.*, 2007; Pettibone *et al.*, 2008). Low toxicity nanoparticles such as carbon black and polystyrene stimulate the macrophages via reactive oxygen species and calcium signalling, to make proinflammatory cytokines such as

[1] Section 16.6.1 is adapted from Wani *et al.*, 2011: Nanotoxicity: dimensional and morphological concerns, *Advances in Physical Chemistry*, Volume 2011, doi:10.1155/2011/450912.

tumour necrosis factor alpha (Brown *et al.*, 2004). The cationic nanoparticles, including gold and polystyrene, have shown to cause haemolysis and blood clotting, while usually anionic particles are quite non-toxic. High exposures to diesel exhaust particles (DEPs) by inhalation caused altered heart rate in hypertensive rats interpreted as a direct effect of DEP on the pacemaker activity of the heart (Hansen *et al.*, 2007). Exposure to single-walled carbon nanotubes has also resulted in cardiovascular effects (Li *et al.*, 2007). The nanoparticles inhaled can gain access to the brain by means of two different mechanisms, namely, transsynaptic transport after inhalation through the olfactory epithelium and uptake through the blood-brain barrier (Lockman *et al.*, 2004; Jallouli *et al.*, 2007). *In vitro* studies have shown that multiwalled carbon nanotubes are capable of localizing within and initiating an irritation response in human epidermal keratinocytes, which are a primary route of occupational exposure (Baroli *et al.*, 2007; Zvyagin *et al.*, 2008).

The change in the structural and physicochemical properties of nanoparticles with a decrease in size could be responsible for numerous material interactions that could lead to toxicological effects (Nel *et al.*, 2006); for example, shrinkage in size may create discontinuous crystal planes that increase the number of structural defects as well as disrupt the electronic configuration of the material and give rise to altered electronic properties (Fig. 16.9). These changes could establish specific surface groups that could function as reactive sites. Chemical composition of the materials is particularly responsible for these changes and their importance. The surface groups can make nanoparticles hydrophilic or hydrophobic, lipophilic or lipophobic, or catalytically active or passive. These surface properties can lead to toxicity by the interaction of electron donor or acceptor active sites (chemically or physically activated) with molecular oxygen (O_2), and electron capture can lead to the formation of the superoxide radical, which generates additional reactive oxygen species (ROS) through Fenton chemistry (Fig. 16.9).

Various studies have been carried out to investigate the adverse effects of nanoparticle on the biological systems (N. Li *et al.*, 2003; Hoshino *et al.*, 2004; Li *et al.*, 2007; Baker *et al.*, 2008; Lyon *et al.*, 2006; Peters *et al.*, 2006) and the interaction of nanoparticles with biological systems is represented in Fig. 16.10. It has been demonstrated that carbon black nanoparticles produce their increased inflammatory effects via mechanisms other than the leaching of soluble components from the particle surface. Transition metals are an important source of free radicals, which are important in PM10-stimulated lung inflammation. Therefore, it is clear that nanoparticles may exert their increased proinflammatory effects, at least in part, by modulating intracellular calcium.

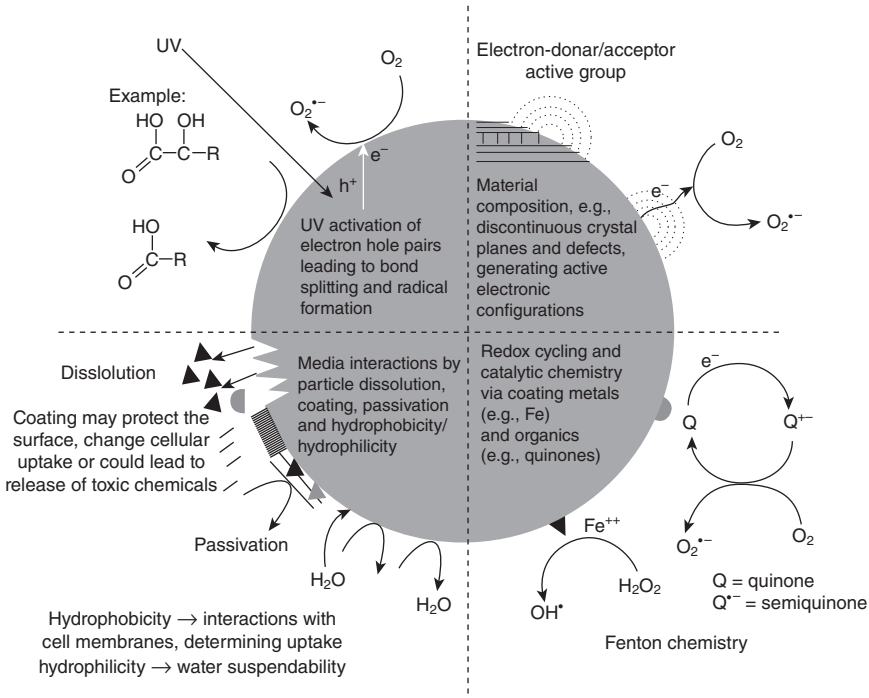

16.9 Effect of reactive oxygen species in cells (adapted from Wani *et al.,* 2011).

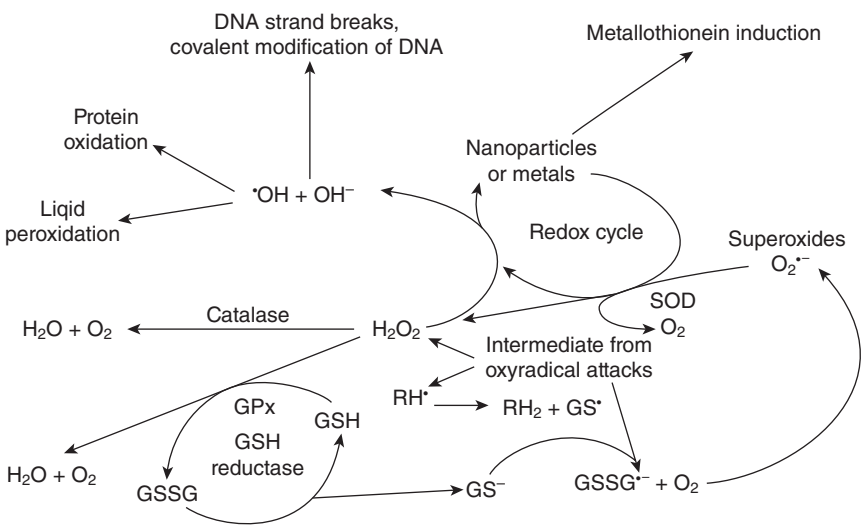

16.10 Interaction and the adverse effects of nanoparticles on biological systems (adapted from Wani *et al.,* 2011).

Nanomaterials themselves constitute a new generation of toxic chemicals. As particle size decreases, in many nanomaterials the production of free radicals increases, as does toxicity. Studies have shown that nanomaterials now in commercial use can damage human DNA, negatively affect cellular function and even cause cell death. There is a small but growing body of scientific studies (termed as nanotoxicology) showing that some nanomaterials are toxic to commonly used environmental indicators such as algae, invertebrate and fish species (Hund-Rinke and Simon, 2006; Lovern and Klaper, 2006; Templeton *et al.*, 2006; Federici *et al.*, 2007; Lovern *et al.*, 2007). There is also evidence that some nanomaterials could impair the function or reproductive cycles of earthworms which play a key role in nutrient cycling that underpins ecosystem function (Fordsmand *et al.*, 2008).

Studies demonstrated that when introduced into the lungs of rodents, certain carbon nanotubes cause inflammation, granuloma development, fibrosis, artery 'plaque' responsible for heart attacks and DNA damage (Donaldson *et al.*, 2006; Lam *et al.*, 2006; Muller *et al.*, 2006). Two independent studies have shown that some carbon nanotubes can also cause the onset of mesothelioma – cancer previously thought to be only associated with asbestos exposure (Poland *et al.*, 2008; Takagi *et al.*, 2008). We now discuss in brief the toxicity of those nanomaterials (such as silver, CNT, TiO_2 and silica) that are being used substantially in water purification applications.

16.6.2 Toxicity of silver nanoparticles

Silver nanoaprticles (Ag NPs) are, due to their antimicrobial properties, the most widely used NPs in commercial products. Ag NPs are incorporated into medical products like bandages as well as textiles and household items. The toxicity of Ag NPs has also been shown by a number of *in vitro* studies (Kawata *et al.*, 2009; Kim *et al.*, 2009; Foldbjerg *et al.*, 2009, 2011). Toxicological investigations of NPs imply that, for example, size, shape, chemical composition, surface charge, solubility, their ability to bind and affect biological sites as well as their metabolism and excretion influence the toxicity of NPs (Schrand *et al.*, 2010; Castranova, 2011). The high surface area of metal-based NPs increases the potential that metal ions are released from these NPs (Bian *et al.*, 2011; Mudunkotuwa and Grassian, 2011), yet it is not clear to what degree the toxicity of Ag NPs results from released silver ions and how much toxicity is related to the Ag NPs themselves. It is quite possible that free silver ions in Ag NP preparations play a considerable role in the toxicity of Ag NP suspensions. While the contribution of free silver ion to the measured toxicity of Ag NP suspensions is an important determinant for the toxicity, a combined effect of Ag ion and Ag NP appears for lower concentrations of Ag ions.

16.6.3 Toxicity of carbon nanotubes

Despite their many advantages, CNTs represent a hazard to the environment and human health. Like asbestos, the aspect ratio (length:diameter) and metal components of CNTs are known to have an effect on the toxicity of carbon nanotubes. Kim *et al.* (2011) evaluated the toxic potential of CNTs in relation to their aspect ratio and metal contamination, *in vivo* and *in vitro* genotoxicity tests were conducted using high aspect ratio (diameter: 10–15 nm, length: ~10 μm) and low aspect ratio multi-wall carbon nanotubes (MWCNTs, diameter: 10–15 nm, length: ~150 nm) according to OECD test guidelines 471 (bacterial reverse mutation test), 473 (*in vitro* chromosome aberration test), and 474 (*in vivo* micronuclei test). High aspect ratio MWCNTs were found to be more toxic than the low aspect ratio MWCNTs. Thus, while high aspect ratio MWCNTs do not induce direct genotoxicity or metabolic activation-mediated genotoxicity, genotoxicity could still be induced indirectly through oxidative stress or inflammation.

A recent *in vivo* cancer therapy study using CNTs originally designed as drug delivery enhancers was able to demonstrate that tumour cells respond to toxicity differently than do wild type cells (Liu *et al.*, 2008). Lam *et al.* (2004) tested a variety of SWCNT samples with varying amounts of metal impurities and concluded that all SWCNT preparations induced dose-dependent lung granulomas in mice. Warheit *et al.* (2004) reported a mild and transient pulmonary inflammatory response in rats instilled intratracheally with SWCNTs, with subsequent development of multifocal granulomas in the lungs after 1 month in a mouse instillation study using highly purified SWCNTs.

Shvedova *et al.* (2005) found granulomas, lung fibrosis and a significant elevation in markers of toxicity in bronchoalveolar lavage (BAL) fluid and concluded that SWCNTs exerted greater toxicity on a mass basis than crystalline silica. A critical review of carbon nanotube toxicity and assessment of potential occupational and environmental health risks was provided by Lam *et al.* (2006), where the toxicological hazard assessment of potential human exposures to airborne CNTs and occupational exposure limits for these novel compounds are discussed in detail.

16.6.4 Toxicity of titanium dioxide and silica (SiO_2) nanoparticles

Studies with fine and ultrafine (<100 nm) TiO_2 particles demonstrate some respiratory toxicity and epithelial inflammation of the lung in rodents (Ferin and Oberdörster, 1985; Ferin *et al.*, 1991; Oberdörster *et al.*, 1992; Bermudez *et al.*, 2002, 2004; Warheit *et al.*, 2005, 2006). Silica nanoparticles have been shown to have a low toxicity when administered in moderate doses (W Lin

et al., 2006; Chang *et al.*, 2007; Jin *et al.*, 2007). Unfortunately, silica nanoparticles also tend to agglomerate and have been demonstrated to lead to protein aggregation *in vitro* at a dose of 25 μg/mL (Barik *et al.*, 2008). Oxidative stress has been implicated as an explanation behind silica nanoparticles cytotoxicity both *in vitro* and *in vivo* (Chen and von Mikecz, 2005; Yang *et al.*, 2009; Wang *et al.*, 2009). All these studies have reported cytotoxicity and oxidative stress, as determined by increasing lipid peroxidation (LPO), reactive oxygen species (ROS), and decreasing cellular glutathione (GSH level), but no similarity exists regarding dose response.

Very little is known about the safety risks presented by engineered nanomaterials. Given their unique properties, particularly their increased reactivity and electrical conductivity, safety concerns are focusing on whether nanomaterials could cause fires or explosions. Because nanoparticles behave differently from larger particles, questions have arisen about whether they can pollute the water supply or damage crops during processes that release these particles into the air, soil or water. Again, studies in this area are in their infancy.

In the short term, the major health and safety risks will be to researchers in laboratories and production staff exposed during the manufacture of nanomaterials. People in these occupations must be aware of the potential hazards of using materials that have unknown properties, and they must take measures to mitigate their risks. However, their activities are contained and generally do not pose a threat to the public or to the environment.

Owing to the highly interdisciplinary nature of nanotechnology, it can be viewed as an enabling technology that is a sincere augmentation of the existing technologies in the field of water purification, textile, aerospace, health care and electronics. Keeping in view the unknown behaviour and fate of nanomaterials in the environment, nanotechnology may pose tremendous challenges to the existing waste management systems. Knowledge on the mobility, persistence and bioaccumulation potential in the environment is hardly available. Hence risk assessment on the possible impact of nanowastes is critical and needs to be made.

Regulators in the United States, the European Union and elsewhere around the world believe that nanoparticles represent an entirely new risk and that it is necessary to carry out an extensive analysis of the risk. Such studies then can form the basis for government and international regulations. As a proper and comprehensive risk and life cycle analysis, encompassing production, application and waste management strategies of nanomaterials, is of urgent need for a successful commercialization of a technology with proven societal benefits, otherwise environmental costs could be high and the technology as a whole could be distrusted or rejected by the public.

16.7 Domestic water purification: challenges to bring about an integrated system

According to a WHO (2007) report on 'combating waterborne disease at the household level' by (The International Network to Promote Household Water Treatment and Safe Storage):

- 1.1 billion lack access to an 'improved' drinking water supply; many more drink water that is grossly contaminated.
- 4 billion cases of diarrhoea occur annually, of which 88% is attributable to unsafe water, and inadequate sanitation and hygiene.
- 1.8 million people die every year from diarrhoeal diseases, the vast majority children under 5.
- Lack of safe water perpetuates a cycle whereby poor populations become further disadvantaged, and poverty becomes entrenched.
- WHO estimates that 94% of diarrhoeal cases are preventable through modifications to the environment, including through interventions to increase the availability of clean water, and to improve sanitation and hygiene.

The major drinking water contaminants are shown in Table 16.3 (Daniels and Mesner, 2005). The most serious amongst them are microbiological contamination. WHO guidelines make reference to the water supply situation common in many countries where water must be collected from a well or standpipe, transported home and then stored for domestic use. In such circumstances: 'Water that is transported or stored unhygienically may be recontaminated, which represents a public health risk. Most recontamination is the result of behavioural patterns; if these can be changed, the health risk can be reduced or eliminated' (WHO, 1997). In their *Water Handbook*, UNICEF observe: 'There are many cases of water which is bacteria-free at the source becoming contaminated during transportation, storage and consumption. Any water supply project that neglects this aspect will be ineffective' (UNICEF, 1999).

There is now conclusive evidence that simple, acceptable, low-cost interventions at the household and community level are capable of dramatically improving the microbial quality of household stored water and reducing the attendant risks of diarrhoeal disease and death. Treating water at the household level has been shown to be one of the most effective and cost-effective means of preventing waterborne disease in development and emergency settings. Promoting household water treatment and safe storage (HWTS) helps vulnerable populations to take charge of their own water security by providing them with the knowledge and tools to treat their own drinking water (UNICEF, 2008). Household-level approaches to drinking water treatment and safe storage are also commonly referred to

Table 16.3 Common water contamination problems (adapted from Daniels and Mesner, 2005)

Contaminant or problem	Possible cause of problem	Solutions
The following pollutants are health hazards and must be treated for the safety of your family. If you cannot successfully remove these pollutants, you should find an alternative source of water		
Arsenic	Naturally occurring in water in some areas	Reverse osmosis, ion exchange
Bacteria	Well not sealed; sewage, manure or surface runoff	Remove source of bacteria; chlorination; ozonation; UV disinfection
Lead	Corrosive water, lead pipes or lead solder	Replace plumbing, reverse osmosis, anion exchange (water softener)
Nitrate	Well not sealed; faulty septic system; animal waste; fertilizers	Remove source of nitrate; distillation; reverse osmosis; anion exchange (water softener)
Pesticides and organic chemicals	Use of pesticides, chemicals near water source	Activated carbon filter; reverse osmosis; distillation
The contaminants below are not health hazards, but you may choose to treat because of aesthetic reasons		
Bad odour, colour, taste	Variety of sources	Ion exchange; activated carbon filter; chlorination
Cloudy or dirty water	Fine sand, clay, or other particles	Mechanical filter
Hardness	Naturally occuring minerals in water	Ion exchange (water softener)
Rotten eggs odour	Hydrogen sulphfide gas	Chlorination and activated carbon filter
Staining of sink and/or laundry from iron or manganese	Naturally occurring in water, especially deep wells	Ion exchange or green sand filters (0–10 ppm); chlorination and filtration (if over 10 ppm)

as managing the water at the 'point-of-use'. This term or its abbreviation 'POU' typically describes the same procedures as other abbreviations derived from household water treatment, like 'HHWT' or 'HWT' or 'HWTS'. (The 'S' in 'HWTS' refers to safe storage.) 'Household water management' is also commonly used, and can encompass both treatment and storage. All these terms can refer to a variety of treatment procedures, for example, with chlorine or other chemical disinfectants, sunlight or UV lamps, various filters, or flocculation-disinfection formulations (WHO, 2007).

A comparison of POU conventional water filtration technologies is shown in Table 16.4. It compares the performance of the ceramic-based filters with that of activated carbon, granular media. From all perspective (efficiency of decontamination, capacity and ease of use), activated carbon has been found to be the best conventional household water treatment method.

Table 16.5 provides a comparative chart of conventional UV treatment and chemical treatment technologies. It has been observed that coagulation-flocculation outweighs UV-based and chemical-based water treatment options in terms of type and range of contaminants that can be addressed. However, it requires the involvement of trained manpower.

A comparison of POU nanotechnology-based water purification technologies is given in Table 16.6. It is evident from the table that nanoparticle embedded membranes have all the essential features that can be tuned to address the specific contaminant. In addition, it is scalable and widely deployable.

16.7.1 Sustainability of a water purification technology

There are thousands of types of water filters that have the capability to purify contaminated water. However, most filters are too expensive for the nations with the greatest need for potable water. Technologically advanced filters have no real application in countries without the capability to sustain them, which is why more basic filtering methods are needed to truly have an impact on the global clean water shortage. Such organizations as the UN and WHO are currently pushing the water filter industry to develop sustainable solutions to empower many rural nations with the ability to filter their own water in cheaper, more environmentally friendly ways. These sustainable technologies are innovative, simple, and incorporate combinations of basic science and local materials to create usable and efficient filters. Sustainable, or appropriate, technology is defined as, 'Technology that can be made at an affordable price by ordinary people using local materials to do useful work in ways that do the least possible harm to both human society and the environment' (Cunningham *et al.*, 1999).

The following guidelines are suggested based on an evaluation of the sustainable technology definition, the ethical standards, and information from sustainable development of technologies (Skye McAllister, 2005). It is important to keep in mind that these steps are to be used in addition to traditional engineering standards and ethics.

- limit non-renewable energy consumption
- lessen environmental impact
- readily available, easy to manufacture materials

Table 16.4 Comparison of POU conventional water filtration technologies (adapted from Hillie *et al.*, 2007b)

		Contaminants removed			Amount of water		Cost (US$)		Ease of use		
Filter type		Biological	Organic	Inorganic	Flow rate	Useful life	Unit	Filter	Labour demands	Setup and use	Maintenance
Ceramic	Disk	• Bacteria • Cysts • Coliform • Fecal Coliform	No	• Asbestos • Iron	1–11 L/hr	5 yrs	$3.50	$0.49–$1.02	Unskilled	Easy	Monthly scrubbing
	Candle				0.3–0.8 L/hr	6–12 mos	$2.29	$0.46			
Biosand		• Coliform • Fecal Coliform • Protozoa • Helminthes	No	• Arsenic • Cadmium • Copper • Iron • Lead • Zinc	30 L/hr	Indefinite	$12.00–$30.00	n/a	Unskilled	Moderate – biolayer must be established	Sporadic sand agitation and cleaning

Activated Carbon	Granular Solid block	• Bacteria • Cysts (bacteria within the filter can cause recontamin.)	Most all; incl: Pest-, herb- and insecticides Industrial Chemicals PCBs PAHs VOCs MTBE	• Arsenic • Chlorine • Chromium • Mercury (organic complex forms only)	V** – Unit size	9–12 mos 12 mos	$100/yr $10-Carafe $330–$2500	$3.00 $0.02/L	Unskilled and trained	Easy	Regular cleaning by trained person
Granular Media	Bucket Drum and filter Roughing Cistern	• Bacteria • Cysts • Coliform • Parasites • Protozoa	No	No	500 L/day 40–200 L/day V – Unit size	V – Media	$50.00 <$0.001/L $01/L U – Low	$20.00 U*** – Low	Unskilled Unskilled and trained	Easy Easy	Biweekly filter cleaning Backwashing by trained person
Fibre and Fabric		• Pathogenic Larvae • Larva hosting crustaceans • Bacteria with large copepods • Zooplankton	No	No	V – No. of material layers	Limited	≈$0.00	≈$0.00	Unskilled	Easy	None

*Cysts: Giardia and cryptosporidium cysts.
**V: Variable depending on.
***U: Exact amount unspecified.

Table 16.5 Comparative chart of POU conventional UV and chemical treatment technologies (adapted from Hillie *et al.*, 2007b)

		Contaminants removed			Amount of water treated			Ease of use		
Technology type		Biological	Organic	Inorganic	Flow rate	Useful life/ chem. quant.	Cost (US$)	Labour demands	Setup and use	Maintenance
UV radiation	UV lamps	• Bacteria • Bact. Spores • Coliform • Enteric • Viruses	No	No	>1 L/min	1 yr/bulb	$10–$100/yr	Unskilled	Easy	Regular cleaning
	Sodis				10 L/bottle	Indefinite	≈$0.00			Regular bottle cleaning
Coagulation-flocculation	Synthetic polymer	• Bacteria • Coliform • Fecal Coliform • Viruses	No	• Arsenic • Asbestos • Cadmium • Chromium • Selenium	n/a	V** – Source water quality	>$100/yr/hh***	Unskilled and trained	Moderate – Trained person must determine necc. dosage	Chemical storage and preparation by trained person
	Alum and Iron Salt						$10–$100/yr/hh		Moderate – Powder crushed before each use	n/a
	Natural polymer						<$10/yr/hh			

Chemical disinfection	Sodium hypochlorite	• Bacteria • Coliform • Fecal Coliform • Viruses	No	No	n/a	25 mL/mo.	$700–$2500 – Generator $4.80–$9.60/yr/hh	Unskilled and trained	Moderate – Trained person must generate chemical	Chemical storage and preparation by rained person
	Bleaching powder						$10/yr/hh		Easy	
PuR® Flocculant-Disinfectant		• Bacteria • Cysts* • Coliform • Fecal Coliform • Parasites • Protozoa • Viruses	No	Arsenic	10 L/sachet	n/a	$.10/sachet	Unskilled	Easy	none

*Cysts: Giardia and cryptosporidium cysts.
**V: Variable depending on.
***HH: Household (4–5 people).

Table 16.6 Comparison of POU nanotechnology-based water purification technologies (adapted from Hillie *et al.*, 2007b)

		Contaminants removed			Amount of water treated		Cost (US$)*		Ease of use		
Technology type		Biological	Organic	Inorganic	Flow rate/ water quantity	Useful life	Unit	Filter/media	Labour demands	Setup and use	Maintenance
Nano- Ceramics, Clays, and Adsorbents	Cell pore	Bacteria	U	• Arsenic • Lead • Other U	U – 100X > other organic membranes	U	U- retrofitted	U – competitive	Unskilled	Moderate – biolayer must be established	Biweekly filter cleaning
	Nanopore	• Bacteria • Coliform • Fecal Coliform • Fungi • Viruses	U	U	V*** – source water quality and membrane size	U			Unskilled	Easy	Infrequent steam sterilization
	SAMMS	No	No	• Arsenic • Cadmium • Chromium • Lead • Mercury • Radionuclides • Other U	U – 13X > other adsorbents	Indefinite		$150/kg	Unskilled and trained	Moderate	Occasional regeneration by trained person

ArsenX	No	No	• Arsenic • Chromium • Molybdenum • Uranium • Vanadium	38 mg arsenic per gram media	Indefinite	$0.07–$0.20 per 1000 L			
Cyclodextrin Polymer	No	Most all	U	22 mg organ. contamin. per gram media	Indefinite	U – competitive			
Polypyrrole Polymer	U	U	• Sea Salt • Calcium • Cesium • Chromium • Magnesium • Perchlorate • Other U	U	Indefinite		Trained	Moderate	Occasional regeneration with electrical current by trained person

*Costs assume mass production.
**Biological contaminants: Bacteria, Bacterial Spores, Giardia & Cryptosp. Cysts, Coliform, Fecal Coliform, DNA & RNA, Fungi, Mold, Parasites, Protozoa, and Viruses Organic contaminants: Pest-, Herb-, & Insecticides, Industrial Effluents, MTBE, PAHS, PCBs, VOCs, and others. Inorganic contaminants: Heavy Metals, Nitrites, Salts, Asbestos, Radionuclides, Calcium, Magnesium, and others.
***V: Variable depending on.
****U: Exact amount unspecified.

Table 16.6 Continued

	Contaminants removed			Amount of water treated		Cost (US$)*		Ease of use		
Technology type	Biological	Organic	Inorganic	Flow rate/ water quantity	Useful life	Unit	Filter/ media	Labour demands	Setup and use	Maintenance
CNT membranes	Most all**	U****	• sea salt • Arsenic • Cadmium • Mercury • Selenium	U – > reverse osmosis membranes	U	U – 75% < reverse osmosis		Use comparable to reverse osmosis membranes Requires less frequent maintenance		
Nanomesh Filters	Most all	• Pest-, Herb-, & Insecticides • Industrial Effluents (Almost all org. cont. can be removed through functionalizing the material)	• Arsenic • Lead (Almost all inorg. cont. can be removed through functionalizing the material)	6 l/ hr – prototype	U	U – competitive		Unskilled	Easy	n/a
Nanomesh Waterstick				0.67 L/min	200–300 L per stick	U – competitive	n/a			

Nanofibrous filters Nanofiltration	Membranes	Most all	U	Most all	V – membrane size	U	U – <reverse osmosis		Use comparable to reverse osmosis membranes Requires less frequent maintenance		
	Devices				1–3.5 L/min	U			Unskilled	Easy	n/a
	Nanoceram	Most all	U	• Sea Salt • Arsenic • Chromium • Lead • Radionuclides • Other U	1–1.5 L/min/ cm^3 media	U – 10X > other fiber filters	U-retrofitted	$3.00/$m^2$ media $75-20–200 filters dep. on size	Unskilled	Easy	Infrequent cleaning
	World filter	• Bacteria • Parasites • Viruses		U	4–6 L/hr – HH unit 336 L/hr – Village unit	378 L – HH unit 95,000 L per filter – Village unit	$6.00–$11 – HH unit $100–$150 – Village unit	$0.80–$0.90			n/a

*Costs assume mass production.
**Biological contaminants: Bacteria, Bacterial Spores, Giardia & Cryptosp. Cysts, Coliform, Fecal Coliform, DNA & RNA, Fungi, Mold, Parasites, Protozoa, and Viruses Organic contaminants: Pest-, Herb-, & Insecticides, Industrial Effluents, MTBE, PAHS, PCBs, VOCs, and others. Inorganic contaminants: Heavy Metals, Nitrites, Salts, Asbestos, Radionuclides, Calcium, Magnesium, and others.
***V: Variable depending on.
****U: Exact amount unspecified.

Table 16.6 Continued

		Contaminants removed			Amount of Water Treated		Cost (US$)*		Ease of use		
Technology type		Biological	Organic	Inorganic	Flow rate/ water quantity	Useful Life	Unit	Filter/media	Labour demands	Setup and use	Maintenance
Zeolites	Coal Fly Ash AgION	NO • Bacteria • Mould • Other U	NO	• Arsenic • Cadmium • Chromium • Copper • Lead • Mercury • Nickel • Zinc • Other U	V- source water quality	U		retrofitted $0.50-$4.50/kg	Unskilled and trained	Moderate	Occasional regeneration and hazardous spent waste disposal by trained person
Nanocatalysts	NZVI Pd-Coated NVZI	NO	Most all	• Arsenic • Mercury • Nickel • Nitrates • Silver • Radioactive Metals • Other U	V – source water quality and membrane size	U – some% capacity lost per regen.	U-retrofitted	$40–$50/kg $68- $146/kg	Trained and skilled	Difficult	Maintenance must be conducted by skilled and trained persons
	Nano-Titanium Dioxide	Most all – U	Most all	• Arsenic • Other U	V – membrane size	Indefinite		$1.10–>$100/ kg			
	Adsorbsia	• Bacteria • Viruses	U	• Arsenic	40–400 L/min/ m^2 filter	25–38 L/g media		$14/L media	Unskilled	Easy	n/a
	AD33	U	U	• Arsenic • Chromium • Copper • Lead • Zinc • Other U	16–38 L/min – systems 2 L/min – cartridges	2–4 yrs – media 3,800–11,400 L – cartridges		$8–$13/L media $50 – cartridges	Unskilled	Easy	n/a
Magnetoferritin		V – dep. on membrane			U		U		U		

*Costs assume mass production. **Biological contaminants: Bacteria, Bacterial Spores, Giardia & Cryptosp. Cysts, Coliform, Fecal Coliform, DNA & RNA, Fungi, Mold, Parasites, Protozoa, and Viruses Organic contaminants: Pest-, Herb-, & Insecticides, Industrial Effluents, MTBE, PAHS, PCBs, VOCs, and others. Inorganic contaminants: Heavy Metals, Nitrites, Salts, Asbestos, Radionuclides, Calcium, Magnesium, and others. ***V: Variable depending on. ****U: Exact amount unspecified.

- safe and efficient manufacturing processes
- scalability
- easy to operate and maintain the product
- no disregard to cultural principles, practices or customs.

16.7.2 Challenges with development of integrated nano-based systems for water purification

There are three different categories of challenges associated with development of successful nano-based technologies and products:

- availability of nanomaterials
- integration of nanomaterials into water purification systems
- societal implications because of health and environment risks.

Availability of nanomaterials

From the databank on different routes of production and usage of nanomaterials, it is strongly believed that there will not be any dearth of nanomaterials either in present day or in the near/far future. As demand rises, the production would automatically try to cope up with the demand. The Freedonia Group has completed a study of the nanomaterials industry (Freedonia Group Inc., 2005). The study provides data on the demand for nanomaterials in the US for the years 2000 and 2003. It also includes forecasts of demand to the years 2008, 2013 and 2020 by classes of materials (e.g., metal oxides, clays, metals, polymers and chemicals, nanotubes, dendrimers, etc.) and by applications (e.g., abrasives; coatings, thin films, sunscreens; biocides; pharmaceutical fillers and reinforcements; catalysts; structural materials, etc.). These forecasts anticipate that most nanomaterials will be nanoscale versions of established products such as silica, titanium dioxide, clays and metal powders. Larger quantities of carbon nanotubes, fullerenes and dendrimers will also be available as these nanomaterials become key components of several application industries in water, electronics and health care.

Integration of nanomaterials into water purification systems

This is the most serious challenge that has to be overcome for exploiting the potential benefits of nanomaterials with exposition of minimum health and environment risks. Most of the usage of nanomaterials at present is based on the applications identified with fine powders. As we have discussed in the previous section regarding the sustainability of a technology/product, the nanoparticles have to be impregnated in a chemically compatible and physically suitable host matrix so that a robust device can emerge with the

potential for global applicability. The embedding of nanopowders in a host matrix would have the following advantages:

- The agglomeration of the nanoparticles can be minimized and hence better utilization of the desirable properties can be possible.
- The support can provide a high concentration environment of target contaminant species around the loaded nanoparticles by adsorption. Therefore, the rate of reaction/sorption is enhanced.
- The contaminants, after being reacted/oxidized on the nano surfaces, the resulting toxic intermediates can also get adsorbed on the support and as a result, they are not released in the air atmosphere to cause secondary pollution.
- The potential sorption capability of the nanoparticle–support hybrid can be maintained for a long time.
- Most important, the recovery of nanoparticles would be easy from the host matrix and therefore their reusability can be improved.
- The possibility of secondary contamination of purified product water with the nanomaterials can be minimized.

Another most important property that can be incorporated in a hybrid matrix is the option for treatment of contaminants of different kind by a single system instead of addressing the contaminant sequentially. Here the challenge will be to develop cost-effective and environmentally acceptable separation and reactive media that can be deployed in composite packed-bed reactors (Savage and Diallo, 2005) as shown in Fig. 16.11 for purification of water contaminated by mixtures of metal ions, organic solutes and bacteria.

When we discuss the incorporation of nanomaterials onto a host matrix, the immediate process/technology that comes to our mind is 'membranes'. Membranes have gained an important place in chemical technology and are used in a broad range of applications. The key property that is exploited is the ability of a membrane to control the permeation rate of a chemical species through the membrane. In separation applications, the goal is to allow one component of a mixture to permeate across the membrane freely, while hindering permeation of other components. A membrane system separates an influent stream into two streams known as the permeate and the concentrate. The permeate is the portion of the fluid that has passed through the semi-permeable membrane, whereas the concentrate stream contains the constituents that have been rejected by the membrane. Membrane separation processes enjoy numerous industrial applications with the following advantages:

- appreciable energy savings
- environmentally benign

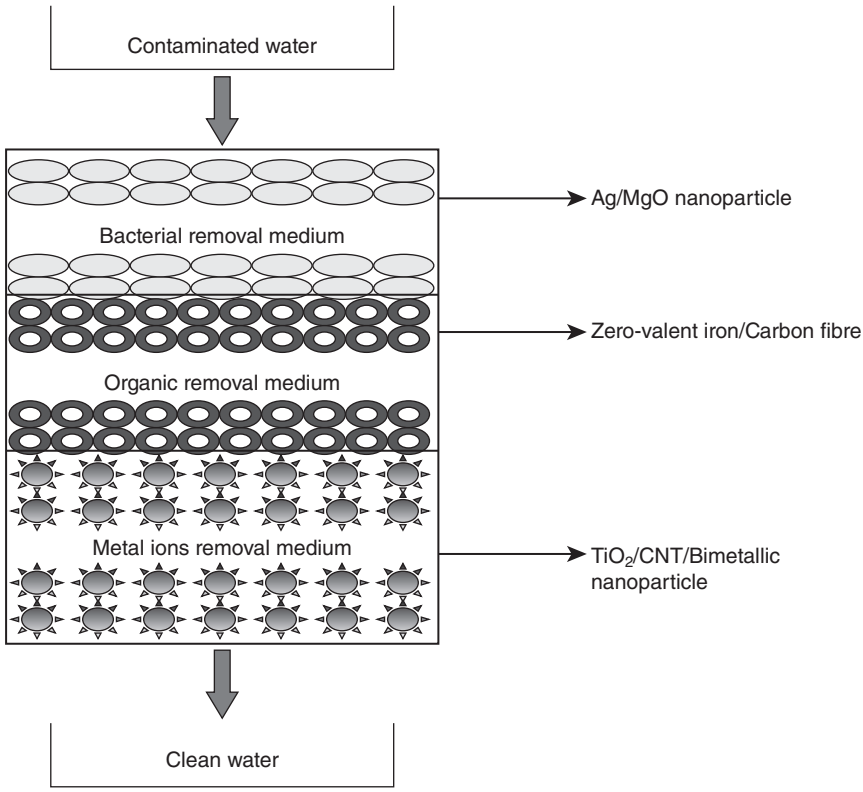

16.11 Schematic of composite nanomaterial packed-bed reactor for water purification (adapted with permission from Savage and Diallo, 2005).

- clean technology with operational ease
- replaces conventional processes like filtration, distillation, ion exchange and chemical treatment systems
- produces high-quality products
- greater flexibility in designing systems.

Pressure driven membrane processes such as reverse osmosis (RO), nanofiltration (NF) and ultrafiltration (UF) are becoming the 'standard' water purification technologies for public utilities and industry because they are flexible, scalable, modular and relatively easy to operate and maintain.

The impregnation of nanomaterials onto polymeric membrane host matrix would help fabrication of a nanocomposite membrane having synergistic effects on water purification performances in the manner that membrane by the principle of size exclusion would take care of the unwanted

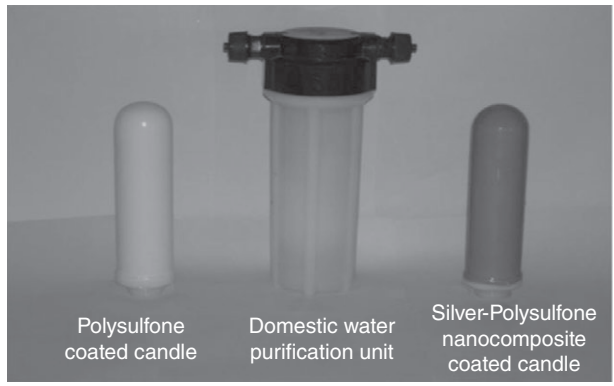

16.12 Domestic water purification candles showing the silver coating for disinfection. The white candle is without silver coating and the grey one with silver coating.

contaminants, while the nanomaterials can add on selectivity to the system. This can be illustrated by the following real research examples being carried out in the workplace of the authors.

Take the case of a domestic polysulfone ultrafiltration membrane candle with polysulfone membrane which takes care of the suspended solids, colour, odour and most importantly microbial contamination. The impregnation of silver nanoparticles into it would assure the product water totally disinfected and in addition help in restoring the life of the membrane by making the membrane surface biofouling resistant. Fig. 16.12 shows the domestic water purification candle with and without silver coating. Using a similar approach, nanocomposite membrane coatings can be provided for removal of arsenic using zero-valent iron and removal of pesticides using titanium dioxide nanoparticles. Also the membranes can be impregnated with multiple nanoparticles to ensure removal of multiple contaminants and in turn the system can be designed for region- or field-specific water conditions.

Kar *et al.* (2011) focused on development of nanoparticle embedded membrane with better biofouling resistant behaviour to be used in wastewater treatment. Nanocomposite polysulfone (PS) membranes with incorporation of nanoparticles of silver (Ag), copper (Cu) and silver-copper mixture (Ag + Cu) were synthesized (as per the composition shown in Table 16.7) and characterized. Representative cross sections were punched from each membrane after they are flushed with bacteria culture, and placed on Luria agar plates and incubated at 37°C overnight. The results (Fig. 16.13) showed growth of bacteria in PS and PS+Cu while no bacterial growth was detected in PS+Ag and PS+Ag+Cu. This confirmed that the impregnation of silver on to the polysulfone host matrix make the membrane surface less

Table 16.7 Composition of nanocomposite membranes

Membrane	PS (g)	NMP (g)	Nanoparticle (g)
Polysulfone	18	82	Nil
Polysulfone + Ag	14.8	82	3.2 (silver)
Polysulfone + Cu	14.8	82	3.2 (copper)
Polysulfone + Ag + Cu	14.8	82	3.2 (silver-copper)

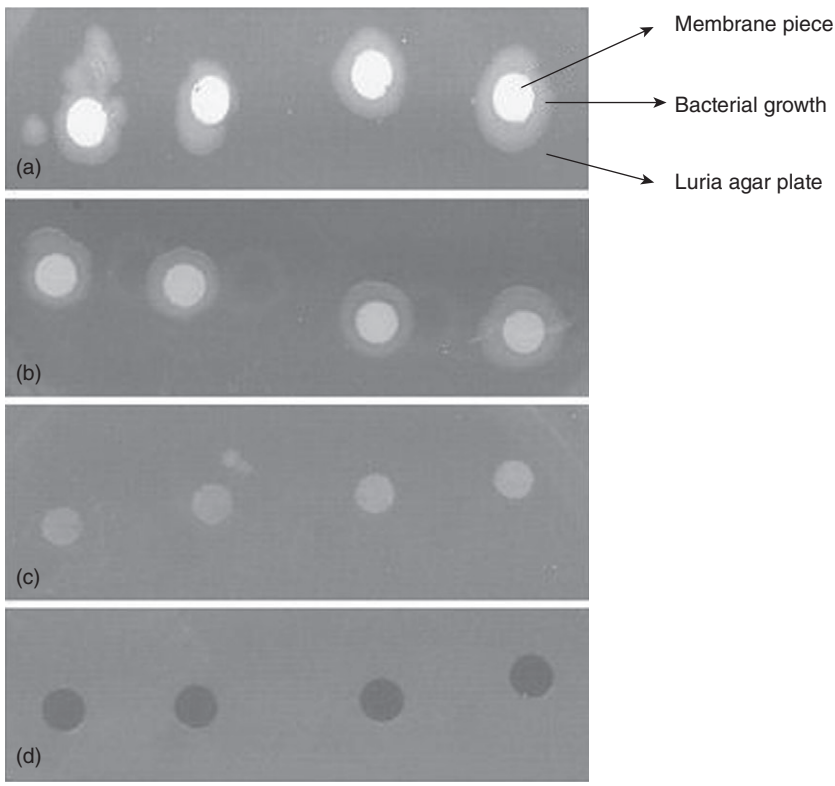

16.13 Biofouling-resistant property of membrane surfaces showing no bacterial growth in the silver impregnated nanocomposite membranes: (a) polysulfone; (b) polysulfone+copper; (c) polysulfone+silver+copper; (d) polysulfone+silver.

prone to biofouling, and hence an anti-biofouling membrane was developed.

The potential attributes of CNTs were discussed previously. Again the emphasis is upon the fact that CNT is the only nanostructured material which, on impregnation onto a membrane host matrix (Hinds *et al.*, 2004;

Holt *et al.*, 2006), can help in the formulation of the next generation of membranes with improved flux, slectivity and anti-fouling. The fast mass transport of water through CNT would ensure high flux (Majumder *et al.*, 2005a). The functionalization of the CNT tip, as shown in Fig. 16.14, would confirm the gate-keeper controlled chemical separation (Majumder *et al.*, 2005b). In addition to the foregoing, the CNT itself or appropriately functionalized CNTs would make the membrane surface anti-biofouling (Kang *et al.*, 2008; Narayan *et al.*, 2005). However, there are numerous challenges associated with each step of membrane making, starting from growth of CNTs to membrane performance evaluation and scale up. Primarily, there are four approaches (Majumdar and Ajayan, 2010) to the synthesis of membranes based on CNTs as shown in Fig. 16.15.

1. Deposition of carbonaceous materials inside pre-existing ordered porous membranes, such as anodized alumina, also known as the template synthesized CNT membranes (Miller *et al.*, 2001).
2. Membranes based on the interstice between nanotubes in a vertical array of CNTs, subsequently referred to as the dense-array outer-wall CNT membrane (Srivastava *et al.*, 2004).
3. Encapsulation of as-grown vertically aligned CNTs by a space-filling inert polymer or ceramic matrix followed by opening up of the CNT tips using plasma chemistry, or the open-ended CNT membrane (Hinds *et al.*, 2004; Holt *et al.*, 2006).
4. Membranes composed of nanotubes as fillers in a polymer matrix, also known as mixed-matrix membranes.

Although CNT-based membranes possess excellent properties to emerge as next generation membranes, still a significant number of challenges remain to be tackled. To grow 12–13 order of magnitude CNTs per square centimetre is a real technological challenge, though chemical vapour deposition methodology offers excellent parameters to achieve this objective. It is very difficult to obtain the yield of CNTs in a particular batch of synthesis beyond 90% reproducibly. Tedious purification steps to remove the sooty deposits and to make the CNT wall defect free make things more complicated. The nanocomposite membrane fabrication route has to confirm that CNTs are well dispersed and well aligned, which is highly challenging. It may require functionalization of CNTs to have better dispersion. Functionalization of CNTs with desired functional groups requires substantial knowledge of Chemistry, for CNT is not soluble in any solvent. The most critical step, that is opening of the CNT tips with either acid treatment or plasma-based oxidation, is not that trivially simple to be adopted. Moreover, the tip-opening step may cause thinning of the CNT wall and disruption of tube integrity and subsequent failure of membrane channels. Finally, scale-up with respect to CNT growth, CNT alignment, nanocomposite formation,

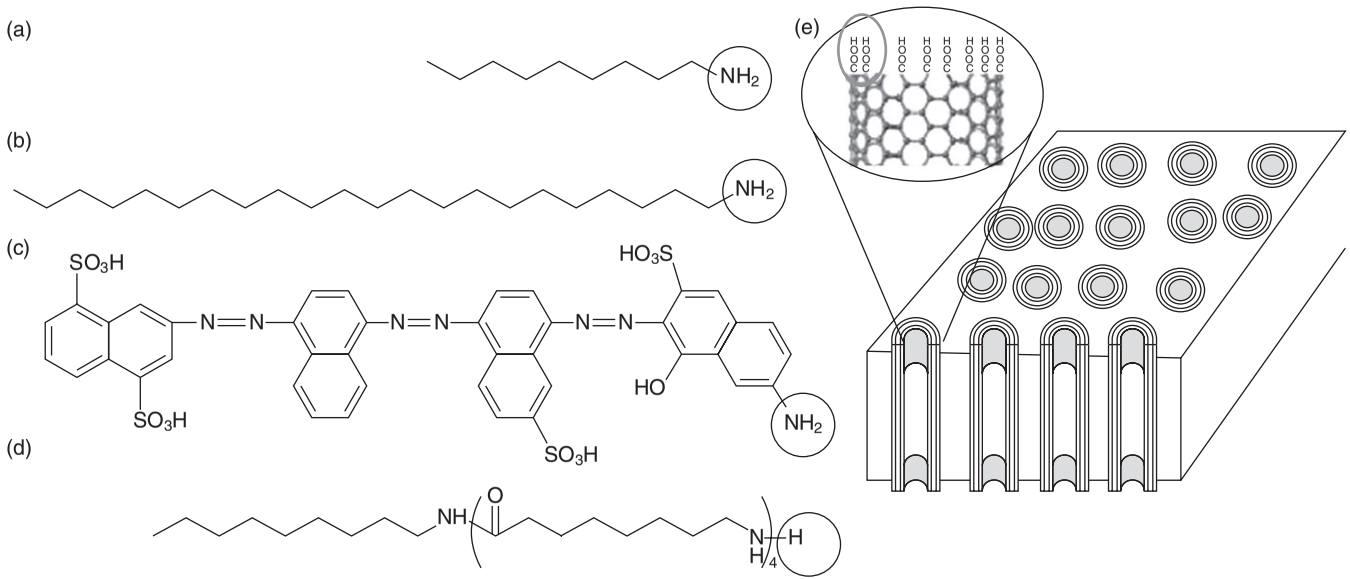

16.14 Functionalization of the CNT membrane via coupling chemistry between amine groups (circled) of the functional molecule and the carboxylic acid with (a) short (C9)-chain amine, (b) long (C22)-chain amine, (c) charged dye molecule with SO_3^{2-} groups, and (d) long-chain polypeptide resulting in change of transport properties through the CNT membrane (e). Figures (a)–(e) adapted with permission from Majumder *et al.*, (2005a). These experiments indicate the feasibility of functionalizing CNT membranes and should offer avenues for imparting antifouling, biocompatible, molecular recognition or selective adsorption properties, whenever desired.

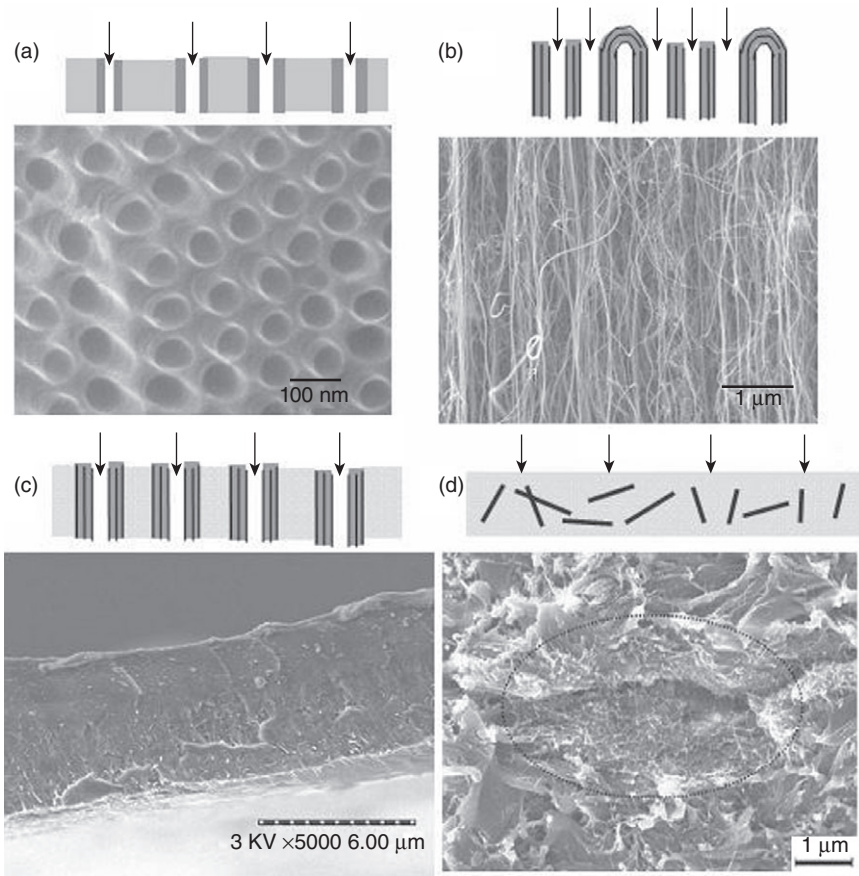

16.15 Different approaches to carbon nanotube (CNT) membrane synthesis. (a) Template synthesis approach – carbonaceous material deposited inside anodized alumina template; (below) scanning electron micrograph (SEM) of the nanotubes after dissolution of the template. (b) Dense-array outer-wall CNT membrane; (below) SEM image demonstrating the dense array of CNTs. The fluid transport is through the interstice between the nanotubes, although some transport can occur through some open-ended tubes (Srivastava *et al.*, 2004). (c) Open-ended CNT membrane; (below) SEM image showing the cross section of the membrane with aligned CNTs in an impervious polymer matrix; transport in this membrane structure occurs through the inner core of the CNT (Hinds *et al.*, 2004). Image taken with permission from Majumder *et al.* (2007). (d) Mixed-matrix membrane composed of CNTs in a polymer matrix; (below) SEM image of the composite membrane structure. Image taken with permission from Geng *et al.* (2007).

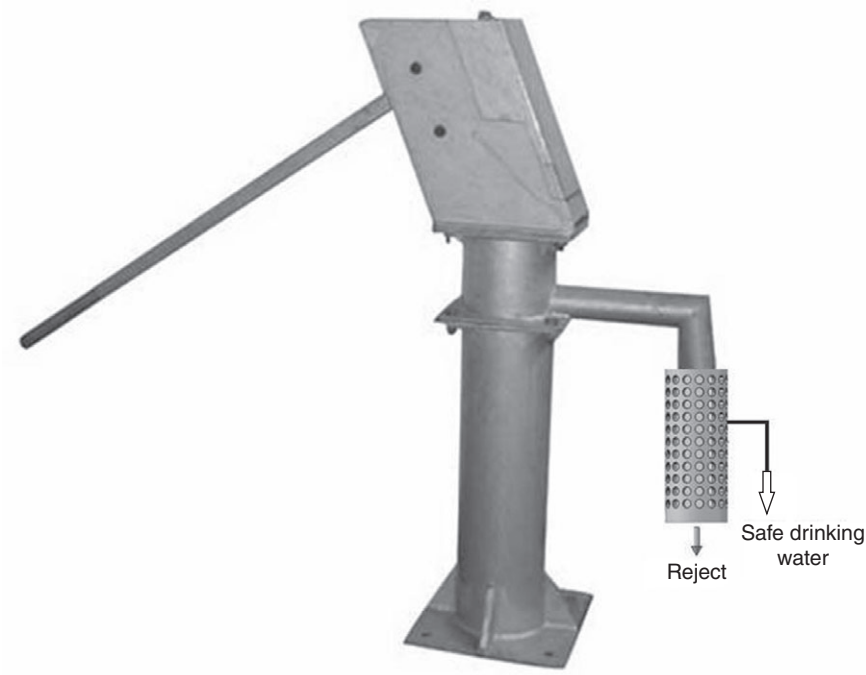

16.16 A schematic of application of CNTs on a household scale showing cross flow filtration of contaminated water through macrogeometry of aligned CNTs.

CNT tip or side-wall functionalization, are all highly complex and many material as well as process challenges are involved. It is proposed that aligned CNTs may be grown in cylindrical macrogeometry instead of growth of CNTs on rectangular supports. The former path seems to be technically a more efficient means of finding a durable CNT-based device bearing in mind the conditions prevalent in the actual field as shown in Fig. 16.16.

Societal implications

As yet the potential for nanomaterials to exert deleterious effects on humans or the environment is poorly understood, but data on their possible effects are needed so that expanded development and use of nanotechnology can proceed. The environmental fate and toxicity of a material are critical issues in materials selection and design for water purification. There are no systematic investigations of the hydrolytic, oxidative, photochemical and biological stability of nanomaterials (e.g., dendrimers, carbonaceous nanoparticles, metal oxides, etc.) in natural and engineered environmental systems. Assessing the risk of using nanomaterials presents some unique

challenges because there is little published research on which to base conclusions and recommendations. As with any new technology that offers significant benefits to humankind, there are also risks of adverse and unintended consequences with nanotechnology. Interdisciplinary discussions of ethical and social dimensions of nanotechnology must be respected. Investment in nanotechnology by governments as well as careful attention to consequences to human health and the environment are both necessary for the public to accept and benefit from commercial products with nanomaterials. Nanotechnology will present opportunities to integrate science and technology with social science and humanities. Education must provide mechanisms for updating scientists and engineers on new technologies as well as helping to organize intelligent debates about societal effects of nanotechnology (Doyle, 2006).

16.8 Acknowledgments

The authors would like to thank Mr Nitesh Goswami, Scientific Officer C, Bhabha Atomic Research Centre, India for providing sincere assistance toward careful editing of this chapter.

16.9 References

Alvarez-Ayuso E, Sánchez A G and Querol X (2003), 'Purification of metal electroplating waste waters using zeolites', *Water Res*, 37, 4855–4862.

Andersson M, Osterlund L, Ljungstrom S and Palmqvist A (2002), 'Preparation of nanosize anatase and rutile TiO_2 by hydrothermal treatment of microemulsions and their activity for photocatalytic wet oxidation of phenol', *J Phys Chem B*, 106, 10674–10679.

Arkas M, Tsiourvas D and Paleos C M (2003), 'Functional dendrimeric "nanosponges" for the removal of polycyclic aromatic hydrocarbons from water', *Chem Mater*, 14, 2844–2847.

Arkas M, Tsiourvas D and Paleosc M (2005), 'Organosilicon dendritic networks in porous ceramics for water purification', *Chem Mater*, 17, 3439–3444.

Arkas M, Allabashi R, Tsiourvas D, Mattausch E M and Perfler R (2006), 'Organic/inorganic hybrid filters based on dendritic and cyclodextrin "nanosponges" for the removal of organic pollutants from water', *Environ Sci Technol*, 40, 2771–2777.

Asahi R, Morikawa T, Ohwaki T, Aoki K and Taga Y (2001), 'Visible-light photocatalysis in nitrogen-doped titanium oxides', *Science*, 293, 269–271.

Aymonier C, Schlotterbeck U, Antonietti L, Zacharias P, Thomann R, Tiller J C and Mecking S (2002), 'Hybrids of silver nanoparticles with amphiphilic hyperbranched macromolecules exhibiting antimicrobial properties', *Chem Comm*, 24, 3018–3019.

Baker G L, Gupta A, Clark M L, Valenzuela B R, Staska L M, Harbo S J, Pierce J T and Dill J A (2008), 'Inhalation toxicity and lung toxicokinetics of C60 fullerene nanoparticles and microparticles', *Toxicol Sci*, 101(1), 122–131.

Balasubramanian K and Burghard M (2005), 'Chemically functionalized carbon nanotubes', *Small*, 1, 180–192.

Balogh L, Swanson D R, Tomalia D A, Hagnauer G R and McManus A T (2001), 'Dendrimersilver complexes and nanocomposites as antimicrobial agents', *Nano Lett*, 1, 18–21.

Barik T K, Sahu B and Swain V (2008), 'Nanosilica – from medicine to pest control', *Parasitol Res*, 103, 253–258.

Baroli B, Ennas M G, Loffredo F, Isola M, Pinna R and López-Quintela M A (2007), 'Penetration of metallic nanoparticles in human full-thickness skin', *J Invest Dermatol*, 127, 1701–1712.

Bermudez E, Mangum J B, Asgharian B, Wong B A, Reverdy E E, Janszen D B, Hext P M, Warheit D B and Everitt J I (2002), 'Long-term pulmonary responses of three laboratory rodent species to subchronic inhalation of pigmentary titanium dioxide particles', *Toxicol Sci*, 70, 86–97.

Bermudez E, Mangum J B, Wong B A, Asgharian B, Hext P M, Warheit D B and Everitt J I (2004), 'Pulmonary responses of mice, rats, and hamsters to subchronic inhalation of ultrafine titanium dioxide particles', *Toxicol Sci*, 77, 347–357.

Bhainsa K C and Souza S F (2006), 'Extracellular biosynthesis of silver nanoparticles using the fungus *Aspergillus* fumigates', *Colloids Surfaces B: Biointerfaces*, 47, 160–164.

Bhattacharya D and Gupta R K (2005), 'Nanotechnology and potential of microorganisms', *Crit Rev Biotechnol*, 25, 199–204.

Bian S W, Mudunkotuwa I A, Rupasinghe T and Grassian V H, (2011), 'Aggregation and dissolution of 4 nm ZnO nanoparticles in aqueous environments: influence of pH, ionic strength, size, and adsorption of humic acid', *Langmuir*, 27, 6059–6068.

Boanini E, Torricelli P, Gazzano M, Giardino R and Bigi A (2006), 'Nanocomposites of hydroxyapatite with aspartic acid and glutamic acid and their interaction with osteoblast-like cells', *Biomaterials*, 27, 4428–4433.

Bosman, A W, Janssen H M and Meijer E W (1999), 'About dendrimers: structure, physical properties and applications', *Chem Rev*, 99, 1665–1688.

Brame J, Li Q and Alvarez P J J (2011), 'Nanotechnology enabled water treatment and reuse: emerging opportunities and challenges for developing countries', *Trends Food Sci & Tech*, 22, 618–624.

Brown D M, Donaldson K, Borm P J, Schins R P, Dehnhardt M, Gilmour P, Jimenez L A and Stone V (2004), 'Calcium and ROS-mediated activation of transcription factors and TNF-α cytokine gene expression in macrophages exposed to ultrafine particles', *Am J Physiol*, 286, L344–L353.

Burns C, Spendel W U, Puckett S and Pacey G E (2006), 'Solution ionic strength effect on gold nanoparticle solution color transition', *Talanta*, 69, 873–876.

Castranova V (2011), 'Overview of current toxicological knowledge of engineered nanoparticles', *J Occup Environ Med*, 53, S14–S17.

Chang J S, Chang K L B, Hwang D F and Kong Z L, (2007), '*In vitro* cytotoxicitiy of silica nanoparticles at high concentrations strongly depends on the metabolic activity type of the cell line', *Environ Sci Technol*, 41, 2064–2068.

Chang Y C, Chang S W and Chen D H (2006), 'Magnetic chitosan nanoparticles: studies on chitosan binding and adsorption of Co (II) ions', *Reactive Func Poly*, 66, 335–341.

Chen J, Liu M, Zhang L, Zhang J and Jin L (2003), 'Application of nano TiO_2 towards polluted water treatment combined with electro-photochemical method', *Water Res*, 37, 3815–3820.

Chen M and von Mikecz A (2005), 'Formation of nucleoplasmic protein aggregates impairs nuclear function in response to SiO_2 nanoparticles', *Experimental Cell Res*, 305, 51–62.

Cheng R, Wang J L and Zhang W X (2007), 'Comparison of reductive dechlorination of p-chlorophenol using FeO and nanosized FeO', *J Hazard Mater*, 144, 334–339.

Choe S, Chang Y Y, Hwang K Y and Khim J (2000), 'Kinetics of reductive denitrification by nanoscale zero-valent iron', *Chemosphere*, 41, 1307–1314.

Choi J H, Kim S D, Noh S H, Oh S J and Kim W J (2006), 'Adsorption behaviors of nano-sized ETS-10 and Al-substituted-ETAS-10 in removing heavy metal ions, Pb^{2+} and Cd^{2+}', *Micro Meso Mater*, 87, 163–169.

Choi J W, Alexandrova M A and Park H G (2011), 'Carbon nanotube nanofluidics', Available at. http://cdn.intechopen.com/pdfs/17301/InTech-Carbon_nanotube_nanofluidics.pdf

Cloete T E, de Kwaadsteniet M, Botes M and López-Romero J M (2010), *Nanotechnology in Water Treatment Applications*, Norfolk, Caister Academic Press.

Cunningham W P, Cunningham M A and Saigo B W (1999), *Environmental Science: A Global Concern*, 7th edn, New York, McGraw-Hill.

Daniels B and Mesner N (2005), 'Drinking water treatment systems', Water Quality, Utah State University Extension. Available at: http://extension.usu.edu/smac/files/uploads/DW_Bacteria_Jan2011.pdf

Dasgupta K, Kar S, Ramani V, Bindal R C, Prabhakar S, Tewari P K, Bhattacharya S, Gupta S K and Sathiyamoorthy D (2008), 'Self-standing geometry of aligned carbon nanotubes with high surface area', *Mater Lett*, 62, 1989–1992.

Diallo M, Christie S, Swaminathan P, Johnson J H Jr and Goddard W A (2005), 'Dendrimer enhanced ultrafiltration. 1. Recovery of Cu (II) from aqueous solutions using PAMAM dendrimers with ethylene diamine core and terminal NH_2 groups', *Environ Sci Technol*, 39, 1366–1377.

Diallo M, Duncan J, Savage N, Street A and Sustich R (2009), 'Nanotechnology solutions for improving water quality'. In Savage N, Diallo M, Dancan J, Street A, Sustich R (eds) *Nanotechnology Applications for Clean Water*, Norwich, NY, William Andrew, pp. 585–588.

Ding Z, Zhu H Y, Lu G Q and Greenfield P F (1999), 'Photocatalytic properties of titania pillared clays by different drying methods', *J Colloid Interf Sci*, 209, 193–199.

Donaldson K, Aitken R, Tran L, Stone V, Duffin R, Forrest G and Alexander A (2006), 'Carbon nanotubes: a review of their properties in relation to pulmonary toxicology and workplace safety', *Toxicol Sci*, 92(1), 5–22.

Doyle M E (2006), FRI Briefings: 'Nanotechnology: A Brief Literature Review'. Available at: http://fri.wisc.edu/docs/pdf/FRIBrief_Nanotech_Lit_Rev.pdf

Dubas S T and Pimpan V (2008), 'Humic acid assisted synthesis of silver nanoparticles and its application to herbicide detection', *Mater Lett*, 62, 2661–2663.

Elizalde-González M P, Mattusch J and Wennrich R (2001), 'Application of natural zeolites for preconcentration of arsenic species in water samples', *J Environ Monit*, 3, 22–26.

EPA (2005), Nanotechnology Workgroup: 'Nanotechnology White Paper', Science Policy Council, US EPA. Available at: http://www.epa.gov/osa/pdfs/nanotech/epa-nanotechnology-whitepaper-0207.pdf

Federici G, Shaw B and Handy R (2007), 'Toxicity of titanium dioxide nanoparticles to rainbow trout (*Oncorhynchus mykiss*): gill injury, oxidative stress, and other physiological effects', *Aquatic Toxicol*, 84, 415–430.

Feitz A J, Joo S H, Guana J, Suna Q, Sedlak D L and Waite T D (2005), 'Oxidative transformation of contaminants using colloidal zero-valent iron', *Colloids Surf A: Physicochem Eng Aspects*, 265, 88–94.

Feng J, Hu X, Yue P L, Zhu H Y and Lu G Q (2003), 'Degradation of azo-dye orange II by a photoassisted fenton reaction using a novel composite of iron oxide and silicate nanoparticles as a catalyst', *Ind Eng Chem Res*, 42, 2058–2066.

Ferin J and Oberdörster G (1985), 'Biological effects and toxicity assessment of titanium dioxides: anastase and rutile', *Am Ind Hyg Assoc J*, 46, 69–72.

Ferin J, Oberdörster G, Soderholm S C and Gelein R (1991), 'Pulmonary tissue access of ultrafine particles', *J Aerosol Med*, 4, 57–68.

Fischer M and Vögtle F (1999), 'Dendrimers: from design to application: a progress report', *Angew Chem Intl Ed Engl*, 38, 884–905.

Foldbjerg R, Olesen P, Hougaard M, Dang D A, Hoffmann H J and Autrup H (2009), 'PVP-coated silver nanoparticles and silver ions induce reactive oxygen species, apoptosis and necrosis in THP-1 monocytes', *Toxicol Lett*, 190, 156–162.

Foldbjerg R, Dang D A and Autrup H, (2011), 'Cytotoxicity and genotoxicity of silver nanoparticles in the human lung cancer cell line, A549', *Arch Toxicol*, 85, 743–750.

Fordsmand J C, Krogh P, Schaefer M and Johansen A (2008), 'The toxicity testing of double-walled nanotubescontaminated food to *Eisenia veneta* earthworms', *Ecotoxicol Environ Safety*, 71, 616–619.

Freedonia Group, Inc. (2005), 'Nanomaterials – market size, market share, market leaders, demand forecast, sales, company profiles, market research, industry trends'. Available at: www.freedoniagroup.com

Geng H Z, Kim K K, So K P, Lee Y S, Chang Y and Lee Y H (2007), 'Effect of acid treatment on carbon nanotube-based flexible transparent conducting films', *J Am Chem Soc*, 129, 7758–7759.

Giasuddin A B M, Kanel S R and Choi H (2007), 'Adsorption of humic acid onto nanoscale zerovalent iron and its effect on arsenic removal', *Environ Sci Technol*, 47, 2022–2027.

Gleick P H (2000), *The World's Water 2000–2001: The Biennial Report on Freshwater Resources*, Washington, DC, Island Press.

Grassian V H, O'Shaughnessy P T, Adamcakova-Dodd A, Pettibone J M and Thorne P S (2007), 'Inhalation exposure study of titanium dioxide nanoparticles with a primary particle size of 2 to 5 nm', *Environ Health Perspect*, 115, 397–402.

Graveland B J F and Kruif C G (2006), 'Unique milk protein based nanotubes: food and nanotechnology meet', *Trends Food Sci Technol*, 17, 196–203.

Guo X and Chen F (2005), 'Removal of arsenic by bead cellulose loaded with iron oxyhydroxide from groundwater', *Environ Sci Technol*, 39, 6808–6818.

Hansen C S, Sheykhzade M, Møller P, Folkmann J K, Amtorp O, Jonassen T and Loft S (2007), 'Diesel exhaust particles induce endothelial dysfunction in apoE–/– mice', *Toxicol Appl Pharmacol*, 219, 24–32.

Henglein A (1998), 'Colloidal silver nanoparticles: photochemical preparation and interaction with O_2, CCl_4, and some metal ions', *Chem Mater*, 10, 444–450.

Hillie T, Munasinghe M, Hlope M and Deraniyagala Y (2007a), 'Nanotechnology, water and development, Global Dialogue on Nanotechnology and the Poor: Opportunities and Risks', Meridian Institute's project website. Available at: http://www.merid.org/nano/waterpaper

Hillie T, Munasinghe M, Hlope M and Deraniyagala Y (2007b), 'Overview and comparison of conventional water treatment technologies and nano-based water treatment technologies. Global Dialogue on Nanotechnology and the Poor: Opportunities and Risks', Meridian Institute's project website. Available at: http://www.merid.org/nano/watertechpaper

Hinds B J, Chopra N, Andrews R, Gavalas V and Bachas L (2004), 'Aligned multi-walled carbon nanotube membranes', *Science*, 303, 62–65.

Holt J K, Park H G, Wang Y, Stadermann M, Artyukhin A B, Grigoropoulos C P, Noy A and Bakajin O (2006), 'Fast mass transport through sub-2-nanometer carbon nanotubes', *Science*, 312, 1034–1037.

Hoshino A, Fujioka K, Oku T, Nakamura S, Suga M, Yamaguchi Y, Suzuki K, Yasuhara M and Yamamoto K (2004), 'Quantum dots targeted to the assigned organelle in living cells', *Microbiol Immunol*, 48, 985–994.

Hotze M and Lowry G (2010), 'Nanotechnology for sustainable water treatment', in Hester R E and Harrison R M, *Sustainable Water*, London, RSC, 138–164.

Hu J, Lo I M C and Chen G (2005), 'Fast removal and recovery of Cr (VI) using surface-modified jacobsite ($MnFe_2O_4$) nanoparticles', *Langmuir*, 21, 11173–11179.

Hummer G, Rasaiah J C and Noworyta J P (2001), 'Water conduction through the hydrophobic channel of a carbon nanotube', *Nature*, 414(6860), 188–190.

Hund-Rinke K and Simon M (2006), 'Ecotoxic effect of photocatalytic active nanoparticles (TiO_2) on algae and daphnids', *Environ Sci Poll Res*, 13(4), 225–232.

Irie H, Watanabe Y and Hashimoto K (2003), 'Nitrogen-concentration dependence on photocatalytic activity of $TiO_{2-x}N_x$ powders', *J Phys Chem B*, 107, 5483–5486.

Irokawa Y, Morikawa T, Aoki K, Kosaka S, Ohwaki T and Taga Y (2006), 'Photodegradation of toluene over $TiO_{2-x}N_x$ under visible light irradiation', *Phys Chem Chem Phys*, 8, 1116–1121.

Jain P and Pradeep T (2005), 'Potential of silver nanoparticle-coated poly-urethane foam as an antibacterial water filter', *Biotechnol Bioeng*, 90, 59–63.

Jallouli Y, Paillard A, Chang J, Sevin E and Betbeder D (2007), 'Influence of surface charge and inner composition of porous nanoparticles to cross blood-brain barrier *in vitro*', *Int J Pharm*, 344, 103–109.

Jang W D, Selim K M K, Lee C H and Kang I K (2009), 'Bioinspired application of dendrimers: from bio-mimicry to biomedical applications', *Prog Polym Sci*, 34, 1–23.

Jeong B-H, Hoek E M V, Han Y, Subramani A, Huang X, Hurwitz G, Ghosh A K and Jawor A (2007), 'Interfacial polymerization of thin film nanocomposites: a new concept for reverse osmosis membranes', *J Membr Sci*, 294, 1–7.

Jin Y, Kannan S, Wu M and Zhao J X (2007), 'Toxicity of luminescent silica nanoparticles to living cells', *Chem Res Toxicol*, 20, 1126–1133.

Kalra A (2003), 'From the cover: osmotic water transport through carbon nanotube membranes', *Proceedings of the National Academy of Sciences,* 100, 10175–10180.

Kanel S R, Greneche J M and Choi H (2006), 'Arsenic(V) removal from groundwater using nano scale zero-valent iron as a colloidal reactive barrier material', *Environ Sci Technol*, 40, 2045–2050.

Kang S, Herzberg M, Rodrigues D F and Elimelech M (2008), 'Antibacterial effects of carbon nanotubes: size does matter', *Langmuir*, 24, 6409–6413.

Kar S, Subramanian M, Ghosh A K, Bindal R C, Prabhakar S, Nuwad J, Pillai C G S, Chattopadhyay S and Tewari P K (2011), 'Potential of nanoparticles for water purification: a case-study on anti-biofouling behaviour of metal based polymeric nanocomposite membrane', *Desl Water Treat*, 27, 224–230.

Kasprzyk-Hordern B K (2004), 'Chemistry of alumina, reactions in aqueous solution and its application in water treatment', *Adv Colloid Interface Sci*, 110, 19–48.

Kawata K, Osawa M and Okabe S (2009), '*In vitro* toxicity of silver nanoparticles at noncytotoxic doses to HepG2 human hepatoma cells', *Environ Sci Technol*, 43, 6046–6051.

Kim S, Choi J E, Choi J, Chung K H, Park K, Yi J and Ryu D Y (2009), 'Oxidative stress dependent toxicity of silver nanoparticles in human hepatoma cells', *Toxicol InVitro*, 23, 1076–1084.

Kim J S, Lee K, Lee Y H, Cho H S, Kim K H, Choi K H, Lee S H, Song K S, Kang C S and Yu I J, (2011), 'Aspect ratio has no effect on genotoxicity of multi-wall carbon nanotubes', *Arch Toxicol*, 85, 775–786.

Kisch H, Zang L, Lange C, Maier W F, Antonius C and Meissner D (1998), 'Modified amorphous titania – a hybrid semiconductor for detoxification and current generation by visible light', *Angew Chem Int Ed*, 37, 3034–3036.

Kolesnikov A I, Loong C K, De Souza N R, Burnham C J and Moravsky A P (2006), 'Anomalously soft dynamics of water in carbon nanotubes', *Physica B: Condensed Matter*, 385–386(Part 1), 272–274.

Kwon S, Fan M and Cooper A (2008), 'Photocatalytic applications of micro- and nano-TiO_2 in environmental engineering', *Crit Rev Environ Sci Technol*, 38, 197–226.

Lam C W, James J T, McCluskey R and Hunter R L (2004), 'Pulmonary toxicity of single-wall carbon nanotubes in mice 7 and 90 days after intractracheal instillation', *Toxicol Sci*, 77, 126–134.

Lam C W, James J, McCluskey R, Arepalli S and Hunter R (2006), 'A review of carbon nanotube toxicity and assessment of potential occupational and environmental health risks', *Crit Rev Toxicol*, 36, 189–217.

Lee J S, Han M S and Mirkin C A (2007), 'Colorimetric detection of mercuric ion (Hg2+) in aqueous media using DNA-functionalized gold nanoparticles', *Angew Chem Int Ed*, 46, 4093–4096.

Li L, Zhu W, Zhang P, Chen Z and Han W (2003), 'Photocatalytic oxidation and ozonation of catechol over carbon-black-modified nano-TiO_2 thin films supported on Al sheet', *Water Res*, 37, 3646–3651.

Li N, Sioutas C, Cho A, Schmitz D, Misra C, Sempf J ,Wang M, Oberley T, Froines J and Andre Ne (2003), 'Ultrafine particulate pollutants induce oxidative stress and mitochondrial damage', *Environ Health Perspect*, 111, 455–460.

Li Y, Li X, Li J and Yin J (2006a), 'Photocatalytic degradation of methyl orange by TiO_2-coated activated carbon and kinetic study', *Water Res*, 40, 1119–1126.

Li X Q, Elliott D W and Zhang, W X (2006b), 'Zero-valent iron nanoparticles for abatement of environmental pollutants: materials and engineering aspects', *Crit Rev Solid State Mater Sci*, 31, 111–122.

Li Y H, Wang S, Zhang X, Wei J, Xu C, Luan Z and Wu D (2003a), 'Adsorption of fluoride from water by aligned carbon nanotubes', *Mater Res Bull*, 38, 469–476.

Li Y H, Wang S, Luan Z, Ding J, Xu C and Wu D (2003b), 'Adsorption of cadmium (II) from aqueous solution by surface oxidized carbon nanotubes', *Carbon*, 41, 1057–1062.

Li Y H, Wang S, Wei J, Zhang X, Xu C, Luan Z, Wu D and Wei B (2002), 'Lead adsorption on carbon nanotubes', *Chem Phys Lett*, 357, 263–266.

Li Z, Hulderman T, Salmen R, Chapman R, Leonard S S, Young S H, Shvedova A, Luster M I and Simeonova PP (2007), 'Cardiovascular effects of pulmonary exposure to single-wall carbon nanotubes', *Environ Health Perspect*, 115(3), 377–382.

Lin T J, Huang K T and Liu C Y (2006), 'Determination of organophosphorous pesticides by a novel biosensor based on localized surface plasmon resonance', *Biosens Bioelectron*, 22, 513–518.

Lin W, Huang Y W, Zhou X D and Ma Y (2006), '*In vitro* toxicity of silica nanoparticles in human lung cancer cells', *Toxicol Appl Pharmacol*, 217, 252–259.

Liu Z, Chen K, Davis C, Sherlock S, Cao Q, Chen X and Dai H (2008), 'Drug delivery with carbon nanotubes for *in vivo* cancer treatment', *Cancer Res*, 68, 6652–6660.

Lockman P R, Koziara J M, Mumper R J and Allen D (2004), 'Nanoparticle surface charges alter blood-brain barrier integrity and permeability', *J Drug Targ*, 12, 635–641.

Long R Q and Yang R T (2001), 'Carbon nanotubes as superior sorbent for dioxin removal', *J Am Chem Soc*, 123, 2058–2059.

Lorenceau E, Utada A S, Link D R, Cristobal G, Joanicot M and Weitz D A (2005), 'Generation of polymerosomes from double-emulsions', *Langmuir*, 21, 9183–9186.

Lovern B and Klaper R (2006), 'Daphnia magna mortality when exposed to titanium dioxide and fullerene (C60) nanoparticles', *Environ Toxicol Chem*, 25(4), 1132–1137.

Lovern S, Strickler J and Klaper R (2007), 'Behavioural and physiological changes in daphnia magna when exposed to nanoparticle suspensions (titanium dioxide, nano-C60, and C60HxC70Hx)', *Environ Sci Technol*, 41, 4465–4470.

Lowry G V and Johnson K M (2004), 'Congener-specific dechlorination of dissolved PCBs by microscale and nanoscale zerovalent iron in a water/methanol solution', *Environ Sci Technol*, 38, 5208–5216.

Lu Y and Liu J (2007), 'Smart nanomaterials inspired by biology: dynamic assembly of error-free nanomaterials in response to multiple chemical and biological stimuli', *Acc Chem Res*, 40, 315–323.

Lyon D Y, Adams L K, Falkner J C and Alvarez P J J (2006), 'Antibacterial activity of fullerene water suspensions: effects of preparation method and particle size', *Environ Sci Technol*, 40, 4360–4366.

Mahmoodi N M, Arami M, Yousefi L N and Gharanjig K (2007), 'Photocatalytic degradation of agricultural N-heterocyclic organic pollutants using immobilized nanoparticles of titania', *J Hazard Mater*, 145, 65–71.

Majumder M and Ajayan P M (2010), 'Carbon nanotube membranes: a new frontier in membrane science', in Drioli E and Giorno L, *Comprehensive Membrane Science and Engineering (Volume 1)*, Oxford, Elsevier, 291–310.

Majumder M, Chopra N and Hinds B J (2005a), 'Effect of tip functionalization on transport through vertically oriented carbon nanotube membranes', *J Am Chem Soc*, 127, 9062–9070.

Majumder M, Chopra N, Andrews R and Hinds B J (2005b), 'Nanoscale hydrodynamics – enhanced flow in carbon nanotubes', *Nature*, 438, 44.

Majumder M, Zhan X, Andrews R and Bruce H J (2007), 'Voltage gated carbon nanotube membranes', *Langmuir*, 23, 8624–8631.

Mak S Y and Chen D H (2004), 'Fast adsorption of methylene blue on polyacrylic acid-bound iron oxide magnetic nanoparticles', *Dyes and Pigments*, 61, 93–98.

Mansoori G A, Bastami T R, Ahmadpour A and Eshaghi Z (2008), 'Environmental application of nanotechnology', *Annual Review of Nano Research*, 2, 1–73.

Mascolo G, Comparelli R, Curri M L, Lovecchio G, Lopez A and Agostiano A (2007), 'Photocatalytic degradation of methyl red by TiO_2: comparison of the efficiency of immobilized nanoparticles versus conventional suspended catalyst', *J Hazard Mater*, 142, 130–137.

Mayo J T, Yavuz C, Yean S, Cong L, Shipley H, Yu W, Falkner J, Kan A, Tomson M and Colvin V L (2007), 'The effect of nanocrystalline magnetite size on arsenic removal', *Sci Technol Adv Mater*, 8, 71–75.

Miller S A, Young V Y and Martin C R (2001), 'Electroosmotic flow in template-prepared carbon nanotube membranes', *J Am Chem Soc*, 123, 12335–12342.

Miyauchi M, Ikezawa A, Tobimatsu H, Irie H and Hashimoto K (2004), 'Zeta potential and photocatalytic activity of nitrogen doped TiO_2 thin films', *Phys Chem Chem Phys*, 6, 865–870.

Mudunkotuwa I A and Grassian V H (2011), 'The devil is in the details (or the surface): impact of surface structure and surface energetics on understanding the behavior of nanomaterials in the environment', *J Environ Monit*, 13, 1135–1144.

Muller J, Huaux F and Lison D (2006), 'Respiratory toxicity of carbon nanotubes: how worried should we be', *Carbon*, 44, 1048–1056.

Naguib N, Haihui Y, Yury G, Almila G Y, Constantine M M and Yoshimura M (2004), 'Observation of water confined in nanometer channels of closed carbon nanotubes', *Nano Lett*, 4, 2237–2243.

Nair A S and Pradeep T (2003), 'Halocarbon mineralization and catalytic destruction by metal nanoparticles', *Curr Sci*, 84, 1560–1564.

Nair A S and Pradeep T (2007), 'Extraction of chlorpyrifos and malathion from water by metal nanoparticles', *J Nanosci Nanotechnol*, 7, 1871–1877.

Nair A S, Tom R T and Pradeep T (2003), 'Detection and extraction of endosulfan by metal nanoparticles', *J Environ Monit*, 5, 363–365.

Narayan R J, Berry C J and Brigmon R L (2005), 'Structural and biological properties of carbon nanotube composite films', *Mater Sci Eng B*, 123, 123–129.

Neal A L (2008), 'What can be inferred from bacterium–nanoparticle interactions about the potential consequences of environmental exposure to nanoparticles?', *Ecotoxicology*, 17, 362–371.

Nel A, Xia T, Madler L and Li N (2006), 'Toxic potential of materials at the nanolevel', *Science*, 311, 622–627.

Ngomsik A F, Bee A, Siaugue J M, Cabuil V and Cote G (2006), 'Nickel adsorption by magnetic alginate microcapsules containing an extractant', *Water Res*, 40, 1848–1856.

Oberdörster G, Ferin J, Gelein R, Soderholm S C and Finkelstein J (1992), 'Role of the alveolar macrophage in lung injury: studies with ultrafine particles', *Environ Health Perspect*, 97, 193–199.

Oberdörster G, Sharp Z, Atudonrei V, Elder A, Gelein R, Kreyling W and Cox C (2004), 'Translocation of inhaled ultrafine particles to the brain', *Inhalation Toxicol*, 16, 453–459.

OECD (2011), 'Fostering nanotechnology to address global challenges: water', Available at: http://www.oecd.org/dataoecd/22/58/47601818.pdf

Ono A and Togashi H (2004), 'Highly selective oligonucleotide-based sensor for mercury (II) in aqueous solutions', *Angew Chem Int Ed*, 43, 4300–4302.

Ooka C, Yoshida H, Suzuki K and Hattori T (2004), 'Highly hydrophobic TiO_2 pillared clay for photocatalytic degradation of organic compounds in water', *Micro Meso Mater*, 67, 143–150.

Ottaviani M F, Favuzza P, Bigazzi M, Turro N J, Jockusch S and Tomalia D A (2000), 'A TEM and EPR investigation of the competitive binding of uranyl ions to starburst dendrimers and liposomes: potential use of dendrimers as uranyl ion sponges', *Langmuir*, 19, 7368–7372.

Peng X, Luan Z, Ding J, Di Z, Li Y and Tian B (2005), 'Ceria nanoparticles supported on carbon nanotubes for the removal of arsenate from water', *Mater Lett*, 59, 399–403.

Peters A, Veronesi B, Calderón-Garcidueñas L, Gehr P, Chen L C, Geiser M, Reed W, Rothen-Rutishauser B, Schürch S and Schulz H (2006), 'Translocation and potential neurological effects of fine and ultrafine particles: a critical update', *Part Fiber Toxicol*, 3, 13.

Pettibone J M, Adamcakova-Dodd A, Thorne P S, O'Shaughnessy P T, Weydert J A and Grassian V H (2008), 'Inflammatory response of mice following inhalation exposure to iron and copper nanoparticles', *Nanotoxicology*, 2(4), 189–204.

Phillips K S, Han J H, Martinez M, Wang Z Z, Carter D and Cheng Q (2006), 'Nanoscale glassification of gold substrates for surface plasmon resonance analysis of protein toxins with supported lipid membranes', *Anal Chem*, 78, 596–603.

Poland C, Duffin R, Kinloch I, Maynard A, Wallace Q, Seaton A, Stone V, Brown S, MacNee S W and Donaldson K (2008), 'Carbon nanotubes introduced into the abdominal cavity of mice show asbestos like pathogenicity in a pilot study', *Nat Nanotechnol*, 3, 423–428.

Ponder S M, Darab J G and Mallouk T E (2000), 'Remediation of Cr (VI) and Pb (II) aqueous solutions using supported nanoscale zero valent iron', *Environ Sci Technol*, 34, 2564–2569.

Pradeep T and Anshup (2009a), 'Noble metal nanoparticles for water purification', *Thin Solid Films*, 517, 6441–6478.

Pradeep T and Anshup (2009b), 'Detection and extraction of pesticides from drinking water using nanotechnologies', in Savage N, Diallo M, Duncan J, Street A and Sustich R, *Nanotechnology Applications for Clean Water*, New York, William Andrew.

Quinn J, Geiger C, Clausen C, Brooks K, Coon C, O'Hara S, Krug T, Major D, Yoon W S, Gavaskar A and Holdswoth T (2005), 'Field demonstration of DNAPL dehalogenation using emulsified zero-valent iron', *Environ Sci Technol*, 39, 1309–1318.

Rai M, Yadav A and Gade A (2009), 'Silver nanoparticles as a new generation of antimicrobials', *Biotechnol Adv*, 27, 76–83.

Rajan, Chand S and Gupta B D (2007), 'Surface plasmon resonance based fiber-optic sensor for the detection of pesticide', *Sensor Actuator B Chem*, 123, 661–666.

Rether A and Schuster M (2003), 'Selective separation and recovery of heavy metal ions using water-soluble N-benzoylthiourea modified PAMAM polymers', *React Func Poly*, 57, 13–21.

Rosca I D, Watari F, Uo M and Akasaka T (2005), 'Oxidation of multiwalled carbon nanotubes by nitric acid', *Carbon*, 153124–153131.

Sakthivel S and Kisch H (2003), 'Daylight photocatalysis by carbon-modified titanium dioxide', *Angew Chem Int Ed*, 42, 4908–4911.

Sambhy V, MacBride M M, Peterson B R and Sen A (2006), 'Silver bromide nanoparticle/polymer composites: dual action tunable antimicrobial materials', *J Am Chem Soc*, 128, 9798–9808.

Sano M, Kamino A, Okamura J and Shinkai S (2001), 'Ring closure of carbon nanotubes', Science, 293, 1299–1301.

Sato S (1986), 'Photocatalytic activity of NOx-doped TiO_2 in the visible light region', *Chem Phys Lett*, 123, 126–128.

Savage N and Diallo M S (2005), 'Nanomaterials and water purification: opportunities and challenges', *J Nanopart Res*, 7, 5331–5342.

Schrand A M, Rahman M F, Hussain S M, Schlager J J, Smith D A and Syed A F (2010), 'Metal-based nanoparticles and their toxicity assessment', *Wiley Interdiscip. Rev. Nanomed. Nanobiotechnol*, 2, 544–568.

Sharma V K, Yngard R A and Lin Y (2009), 'Silver nanoparticles: green synthesis and their antimicrobial activities', *Adv Colloid Interface Sci*, 145, 83–96.

Shvedova A A, Kisin E R, Mercer R, Ashley R. Murray A R, Johnson V J, Potapovich A I, Tyurina Y T, Gorelik O, Arepalli S, Berry D S, Hubbs A F, Antonini J, Evans D E, Ku B K, Ramsey D, Maynard A, Kagan V E, Castranova V and Baron P (2005), 'Unusual inflammatory and fibrogenic pulmonary responses to singlewalled carbon nanotubes in mice', *Am J Physiol*, 289, L698–L708.

Siegel R W (1991), 'Nanomaterials: synthesis, properties and applications', *Ann Rev Mater Sci*, 21, 559–578.

Siegel R W (1994), 'Physics of new materials', in Fujita F E, *Springer Series in Materials Science, 27*, Berlin, Springer.

Silver S (2003), 'Bacterial silver resistance: molecular biology and uses and misuses of silver compounds', *FEMS Microbiol Rev*, 27, 341–353.

Silver S, Phung L T and Silver G (2006), 'Silver as biocides in burn and wound dressings and bacterial resistance to silver compounds', *J Ind Microbiol Biotechnol*, 33, 627–634.

Skye McAllister (2005), EPD 397 Technical report: 'Analysis and comparison of sustainable water filters'. Available at: http://potterswithoutborders.com/manual-uploads/UploadedDocuments/Studies/analysis-and-comparison-of-sustainable-water-filters.pdf

Sobana N, Muruganadham M and Swaminathan M (2006), 'Nano-Ag particles doped TiO_2 for efficient photodegradation of direct azo dyes', *J Molecular Catalysis A: Chemical*, 258, 124–132.

Sondi I and Sondi B S (2004), 'Silver nanoparticles as antimicrobial agent: a case study on *E. coli* as a model for Gram-negative bacteria', *J Colloid Interf Sci*, 275, 177–182.

Srivastava A, Srivastava O N, Talapatra S, Vajtai R and Ajayan P M (2004), 'Carbon nanotube filters', *Nat Mater*, 3, 610–614.

Sun X, Xia K and Liu B (2008), 'Design of fluorescent self-assembled multilayers and interfacial sensing for organophosphorus pesticides', *Talanta*, 76, 747–751.

Takagi A, Hirose A, Nishimura T, Fukumori N, Ogata A, Ohashi N, Kitajima S and Kanno J (2008), 'Induction of mesothelioma in p53+/- mouse by intraperitoneal application of multi-wall carbon nanotube', *J Toxicol Sci*, 33(1), 105–116.

Templeton R, Ferguson P, Washburn K, Scrivens W and Chandler G (2006), 'Life-cycle effects of single-walled carbon nanotubes (SWNTs) on an estuarine meiobenthic copepod', *Environ Sci Technol*, 40, 7387–7393.

Theron J, Walker J A and Cloete T E (2008), 'Nanotechnology and water treatment: applications and emerging opportunities', *Crit Rev Microbiol*, 34, 43–69.

The Royal Society and The Royal Academy of Engineering (2004), *Nanoscience and Nanotechnologies: Opportunities and Uncertainties*, The Royal Society and The Royal Academy of Engineering, London, Available from URL: http://www.raeng.org.uk/news/publications/list/reports/Nanoscience_nanotechnologies.pdf

Tiwari D K, Behari J and Sen P (2008), 'Application of nanoparticles in waste water treatment', *World Applied Sciences Journal*, 3, 417–433.

Tomalia D A and Majoros I (2003), 'Dendrimeric supramolecular and supramacromolecular assemblies', *J Macro Sci*, 43, 411–477.

Tratnyek P G and Johnson R L (2006), 'Nanotechnologies for environmental clean up', *Nano Today*, 1, 44–48.

Umebayashi T, Yamaki T, Itoh H and Asai K (2002), 'Band gap narrowing of titanium dioxide by sulfur doping', *Appl Phys Lett*, 81, 454–456.

UNICEF (1999), 'Towards better programming: a water handbook', *Water, Environment and Sanitation Technical Guidelines Series – No. 2*, United Nations Children's Fund, New York. Available at: http://www.scribd.com/doc/34473748/A-Water-Handbook

UNICEF (2008), 'Promotion of household water treatment and safe storage in UNICEF wash programmes'. Available at: http://www.unicef.org/wash/files/Scaling_up_HWTS_Jan_25th_with_comments.pdf

Uyeda R (1991), 'Studies of ultrafine particles in Japan: crystallography, methods of preparation and technological applications', *Prog Mater Sci*, 35, 1–96.

Wang F, Gao F, Lan M, Yuan H, Huang H and Liu J (2009), 'Oxidative stress contributes to silica nanoparticle-induced cytotoxicity in human embryonic kidney cells', *Toxicol InVitro*, 23, 808–815.

Wang H, Xie C, Zhang W, Cai S, Yang Z and Gui Y (2007), 'Comparison of dye degradation efficiency using ZnO powders with various size scales', *J Hazard Mater*, 141, 645–652.

Wang J, Teng X, Wang H and Ban H (2004), 'Characterizing the metal adsorption capability of a class F coal fly ash', *Environ Sci Technol*, 38, 6710–6715.

Wang J, Ma T, Zhang Z, Zhang X, Jiang Y, Dong D, Zhang P and Li Y (2006), 'Investigation on the sonocatalytic degradation of parathion in the presence of nanometer rutile titanium dioxide (TiO_2) catalyst', *J Hazard Mater*, 137, 972–980.

Wani M Y, Hashim M A, Nabi F and Malik M A (2011), 'Nanotoxicity: dimensional and morphological concerns', *Adv Phys Chem*, 2011, 450912.

Warheit D B, Laurence B R, Reed K L, Roach D H, Reynolds G A M and Webb T R (2004), 'Comparative pulmonary toxicity assessment of single-wall carbon nanotubes in rats', *Toxicol Sci*, 77, 117–125.

Warheit D B, Brock W J, Lee W J, Webb K P and Reed K L (2005), 'Comparative pulmonary toxicity inhalation and instillation studies with different TiO_2 particle formulations: impact of surface treatments on particle toxicity', *Toxicol Sci*, 88, 514–524.

Warheit D B, Webb T R, Sayes C M, Colvin V L and Reed K L (2006), 'Pulmonary instillation studies with nanoscale TiO_2 rods and dots in rats: toxicity is not dependent upon particle size and surface area', *Toxicol Sci*, 91, 227–236.

Watlington K (2005), 'Emerging nanotechnologies for site remediation and wastewater treatment'. Available at: http://nepis.epa.gov/Adobe/PDF/P1003FG4.pdf

Whitby M, Cagnon L, Thanou M and Quirke N (2008), 'Enhanced fluid flow through nanoscale carbon pipes', *Nano Lett*, 8, 2632–2637.

WHO (1997), *Guidelines for Drinking Water Quality, Surveillance and Control of Community Supplies*, 2nd edn. Vol. 3. WHO, Geneva. Available at: www.who.int/water_sanitation_health/dwq/2edaddvol2a.pdf

WHO report (2007), 'Combating waterborne disease at the household level', The International Network to Promote Household Water Treatment and Safe Storage. Available at: www.who.int/water_sanitation_health/publications/combating_diseasepart1lowres.pdf

World Bank (2005), *World Development Indicators*. Available at: http://data.worldbank.org/products/data-books/WDI-2005

Xiong Z, Zhao D and Pan G (2007), 'Rapid and complete destruction of perchlorate in water and ion-exchange brine using stabilized zero-valent iron nanoparticles', *Water Res*, 41, 3497–3505.

Xu Y and Zhao D (2007), 'Reductive immobilization of chromate in water and soil using stabilized iron nanoparticles', *Water Res*, 41, 2101–2108.

Yang H, Liu C, Yang D, Zhang H and Xi Z (2009), 'Comparative study of cytotoxicity, oxidative stress and genotoxicity induced by four typical nanomaterials: the role of particle size, shape and composition', *J Appl Toxicol*, 29(1), 69–78.

Yang Y, Ma J, Qin Q and Zhai X (2007), 'Degradation of nitrobenzene by nano-TiO_2 catalyzed ozonation', *J Molec Catal A: Chem*, 267, 41–48.

Zang L, Lange C, Abraham I, Storck S, Meier W H and Kisch H (1998), 'Amorphous microporous titania modified with platinum(IV) chloride: a new type of hybrid photocatalyst for visible light detoxification', *J Phys Chem B*, 102, 10765–10771.

Zvyagin A V, Zhao X, Gierden A, Sanchez W, Ross J A and Roberts M S (2008), 'Imaging of zinc oxide nanoparticle penetration in human skin *in vitro* and *in vivo*', *J Biomed Opt*, 13, 064031.